Loughborough University

This item is held in Loughborough University's Institutional Repository (https://dspace.lboro.ac.uk/) and was harvested from the British Library's EThOS service (http://www.ethos.bl.uk/). It is made available under the following Creative Commons Licence conditions.

creative commons

COMMONS DEED

Attribution-NonCommercial-NoDerivs 2.5

You are free:

- to copy, distribute, display, and perform the work

Under the following conditions:

Attribution. You must attribute the work in the manner specified by the author or licensor.

Noncommercial. You may not use this work for commercial purposes.

No Derivative Works. You may not alter, transform, or build upon this work.

- For any reuse or distribution, you must make clear to others the license terms of this work.
- Any of these conditions can be waived if you get permission from the copyright holder.

Your fair use and other rights are in no way affected by the above.

This is a human-readable summary of the Legal Code (the full license).

Disclaimer

For the full text of this licence, please go to:
http://creativecommons.org/licenses/by-nc-nd/2.5/

THE EARLY AGE BEHAVIOUR OF CONCRETE INDUSTRIAL GROUND FLOOR SLABS

Jonathan William Bishop

A Doctoral Thesis Submitted in partial fulfilment of the requirements for the award of

Doctor of Philosophy of Loughborough University

13th December 2001

© Jonathan William Bishop 2001

ABSTRACT

This thesis is concerned with the early-life behaviour of concrete industrial ground floors. Advances in construction methods are placing increased demands on the performance of industrial floors and pushing the limits of the current design guidance. Uncertainties about the true behaviour of industrial floors have been addressed by a programme of in-situ monitoring.

An in-situ instrumentation methodology has been developed to monitor the slab and the local climate. Vibrating wire strain gauges and demecs were used to collect concrete shrinkage and joint performance data, whilst thermocouple arrays and thermistors in the strain gauges recorded the slab temperature. This allowed the effects of the cement hydration and the impact of ambient conditions on the slab to be assessed. The use of an automated data collection system allowed the timing as well as the magnitude of the movements to be measured helping identify cause and effect. Floor slabs covering long strip and large area pour construction, jointed and jointless detailing and mesh fabric and fibre reinforcement have been investigated.

The data has shown the strong thermal influence on the behaviour of the slabs. Initial joint opening was found to be triggered by the cooling of the slab, whilst the effects of seasonal temperature changes in the first couple of months after construction could be as large if not larger than the drying shrinkage. Frictional resistance was found to reduce the measured movement, whilst the restraint arising from adjacent pours was also found to be significant.

Finite element models of the temperature development have been produced using material property data found in the literature. Calibration and verification were carried out using the temperature data collected from site with good agreement.

Structural models were then developed using the temperature and degree of hydration output from the thermal analysis as input. These models were used to determine the theoretical stress distribution in slabs at early-ages, and to conduct a parametric study. This demonstrated that the warping stresses present in a slab are generally greater than those from frictional restraint. The thesis concludes with recommendations for the design and construction of industrial ground floors.

Concrete industrial floors, Ground floor slab, In-situ instrumentation, Performance monitoring, Early-age, Joint behaviour, Restraint, Cracking, Finite element modelling.

ACKNOWLEDGEMENTS

I would first like to thank my two research supervisors, Professor Simon Austin and Dr. Peter Robins, without whose guidance and encouragement this thesis would never have been possible.

I would also like to thank the laboratory technicians in the Department of Civil & Building Engineering at Loughborough University for their invaluable help in carrying out the site instrumentations. I am especially grateful to Mr David Spendlove for his knowledge of concrete and music, and his patience with a survey staff!

My thanks go to the Engineering and Physical Sciences Research Council for funding this research and to the following companies and associations for their assistance in facilitating the work:

The ACIFC	Amazon.co.uk
ANC Ltd.	ASDA
The British Atmospheric Data Centre	Burks Green
The Concrete Society	Face Consultants Ltd.
Gazeley Properties Ltd.	Somero Enterprises Ltd.
Sprigg-Little Partnership	Stanford Industrial Concrete Flooring Ltd.
Stuarts Industrial Flooring Ltd.	Wincanton Logistics

and in particular, Mr. Stephen Meller of Gage Technique International for his interest and willingness to work unsociable hours to help instrument floors.

Finally, I would like to thank my parents for their support and encouragement, and Linda Griffiths for loving me despite my preoccupation.

CONTENTS OF THESIS

DECLARATION i

ABSTRACT ii

ACKNOWLEDGEMENTS iii

CONTENTS OF THESIS iv

LIST OF FIGURES viii

LIST OF TABLES xiii

NOTATION xiv

1. INTRODUCTION 1

1.1. BACKGROUND 1

1.2. AIMS AND OBJECTIVES OF THE RESEARCH 2

1.3. RESEARCH METHODOLOGY 3

1.4. RESEARCH OUTPUTS 5

1.5. THESIS STRUCTURE 5

2. LITERATURE REVIEW 8

2.1. INTRODUCTION 8

2.2. CURRENT DESIGN GUIDANCE 8

2.3. DETAIL DESIGN 8

2.3.1. Slab aspect ratios 9

2.3.2. Joints 9

2.3.3. Free movement joints 9

2.3.4. Restrained movement joints 10

2.3.5. Jointless construction 10

2.3.6. Crack control reinforcement and joint spacing 11

2.3.7. Placement of Reinforcement 12

2.3.8. Summary of detail design guidance 13

2.4. STRUCTURAL DESIGN 14

2.4.1. Elastic design method 14

2.4.2. Plastic design method 16

2.4.3. Structurally reinforced 17

2.4.4. Summary of structural design guidance 18

2.5. INVESTIGATIONS INTO THE INFLUENCE OF CONSTRUCTION VARIABLES 18

2.5.1. Subgrade and sub-base support 18

2.5.2. Slip membrane 20

2.5.3. Reinforcement *20*
2.5.4. Joints *21*
2.5.5. Restraint *24*
2.5.6. Temperature *25*
2.6. IN-SITU INSTRUMENTATION AND MONITORING 26
2.6.1. General concrete structures *26*
2.6.2. Slabs and pavements *28*
2.6.3. Relative humidity *30*
2.7. MODELLING OF MATERIAL PROPERTIES 30
2.7.1. Compressive strength *31*
2.7.2. Tensile strength *32*
2.7.3. Elastic modulus *33*
2.7.4. Poisson's ratio *35*
2.7.5. Creep *36*
2.7.6. Shrinkage *38*
2.7.7. Plastic shrinkage *38*
2.7.8. Drying shrinkage *39*
2.7.9. Cracking *44*
2.7.10. Thermal properties *45*
2.7.11. Thermal expansion and contraction *45*
2.7.12. Thermal conductivity, λ_c *47*
2.7.13. Specific heat capacity *47*
2.7.14. Boundary conditions *47*
2.8. MATHEMATICAL MODELLING OF SLAB BEHAVIOUR 49
2.8.1. Introduction *49*
2.8.2. Thermal changes *49*
2.8.3. Curling and warping *51*
2.8.4. Restraint *54*
2.8.5. Frictional ground restraint *55*
2.8.6. Warping restraint *57*
2.8.7. Internal restraint *59*
2.8.8. Age adjusted effective modulus method *59*
2.9. SUMMARY 60

3. EXPERIMENTAL PROGRAM 70

3.1. INTRODUCTION 70
3.2. CHOICE OF INSTRUMENTATION 71
3.2.1. Ambient conditions *71*
3.2.2. Concrete and sub-base *71*
3.2.3. Datalogger *73*
3.2.4. Laboratory testing *73*

3.2.5. Trial site instrumentation *74*
3.3. DEVELOPMENT OF THE METHODOLOGY 75
3.3.1. Gauge support *75*
3.3.2. Interface box and cabling system *76*
3.3.3. Instrumentation layout / planning *77*
3.3.4. Long strain gauges *78*
3.3.5. Day joint gauges *78*
3.3.6. Demec gauge joint monitoring *79*
3.3.7. Gauge pairs *79*
3.4. FINAL SITE INSTRUMENTATION METHODOLOGY 80
3.4.1. Pre-site preparation *80*
3.4.2. Site practices *81*
3.5. SITE PROGRAMME 81
3.6. CONCLUSIONS 82

4. DETAILED SITE INFORMATION 89

4.1. INTRODUCTION 89
4.2. NORTHAMPTON: MESH REINFORCED LONG STRIP 89
4.3. CHEPSTOW: MESH REINFORCED JOINTED LARGE AREA POUR 90
4.4. LEEDS: MESH REINFORCED JOINTED LARGE AREA POUR 91
4.5. DAVENTRY: STEEL FIBRE REINFORCED JOINTED LARGE AREA POUR 92
4.6. BEDFORD: STEEL FIBRE REINFORCED JOINTLESS LARGE AREA POUR 93
4.7. MARSTON: STEEL FIBRE REINFORCED JOINTLESS LARGE AREA POUR 93

5. ANALYSIS OF DATA 102

5.1. INTRODUCTION 102
5.2. ANALYTICAL METHODOLOGY 103
5.2.1. Zero correction of strains *103*
5.2.2. Thermal correction of strain readings *104*
5.2.3. Determination of creep effects on restraint stresses *105*
5.2.4. Justification of joint gauge strain readings *106*
5.2.5. Analysis of daily strain change *106*
5.3. THERMAL BEHAVIOUR 107
5.4. STRUCTURAL BEHAVIOUR 110
5.4.1. Restrained movement joints *111*
5.4.2. Free movement joints *116*
5.4.3. Restraint *120*
5.4.4. Longitudinal restraint *120*
5.4.5. Warping restraint *131*
5.4.6. The effect of ambient temperature *133*
5.4.7. Comparisons with predictive models *137*

5.5. SUMMARY OF RESULTS 139
5.5.1. Thermal behaviour *139*
5.5.2. Restrained movement joints *139*
5.5.3. Free movement joints *140*
5.5.4. Restraint effects *140*
5.5.5. Effect of ambient temperature *140*
5.5.6. Comparison with predictive models *141*

6. FINITE ELEMENT MODELLING 176

6.1. INTRODUCTION 176
6.2. THERMAL MODELLING 177
6.3. STRUCTURAL MODELLING 181
6.4. SUMMARY 187

7. CONCLUSIONS AND RECOMMENDATIONS FOR FURTHER WORK 199

7.1. CONCLUSIONS 199
7.1.1. Introduction *199*
7.1.2. Instrumentation methodology *199*
7.1.3. Data interpretation *201*
7.1.4. Implications for design *204*
7.2. RECOMMENDATIONS FOR FURTHER WORK 206
7.2.1. Introduction *206*
7.2.2. Site Instrumentation *207*
7.2.3. Finite element modelling *207*

8. REFERENCES 209

APPENDIX A. STRAIN GAUGE INFORMATION 209

APPENDIX B. CONCRETE MIX DESIGNS AND FURTHER SITE INFORMATION 232

APPENDIX C. BEDFORD DETAIL SURVEY RESULTS 252

LIST OF FIGURES

FIGURE 1.1 – SITE INSTRUMENTATION PROGRAMME 7

FIGURE 2.1 - TYPES OF FREE MOVEMENT JOINT 61

FIGURE 2.2 - TYPES OF RESTRAINED MOVEMENT JOINT 61

FIGURE 2.3 - YIELD LINE FAILURE PATTERN FOR AN INTERNAL LOAD (MEYERHOF, 1962) 61

FIGURE 2.4 - STRESS VERSUS CRACK SEPARATION CURVES FOR FRC (WANG ET. AL.,1990) 61

FIGURE 2.5 – JOINT EFFECTIVENESS WITH DIFFERENT LOAD APPLICATIONS (ZOLLINGER & BARENBERG, 1990) 62

FIGURE 2.6 - ACTIVE JOINTS IN A PLAIN CONCRETE PAVEMENT (POBLETE ET. AL., 1988A) 62

FIGURE 2.7 - INSTRUMENTATION TO MONITOR JOINT DEFLECTION (POBLETE ET. AL., 1988A) 63

FIGURE 2.8 - MOISTURE DISTRIBUTION IN A CONCRETE SLAB (PARROTT, 1990) 63

FIGURE 2.9 - MOISTURE PROFILES IN A LABORATORY DRIED CONCRETE SLAB (PARROTT, 1990) 64

FIGURE 2.10 - COMPARISON OF THE DIFFERENT ELASTIC MODULI 64

FIGURE 2.11 - COMPARISON OF DIFFERENT METHODS OF PREDICTING ELASTIC MODULUS DEVELOPMENT WITH TIME (BAZANT & PANULA, 1978B) 65

FIGURE 2.12 - KELVIN MODEL FOR A VISCOELASTIC SOLID 65

FIGURE 2.13 - DRYING SHRINKAGE BEHAVIOUR FOR SEVERAL DIFFERENT CONCRETES (BAZANT & BAWEJA, 1995B) 66

FIGURE 2.14 – THEORETICAL DAILY TEMPERATURE CHANGE AT DIFFERENT DEPTHS UNDER A SLAB (AFTER THOMLINSON) 66

FIGURE 2.15 – CURLED SHAPE OF A SLAB SHORTER THAN THE CRITICAL LENGTH 67

FIGURE 2.16 – CURLED SHAPE OF A SLAB LONGER THAN THE CRITICAL LENGTH 67

FIGURE 2.17 – RELATIONSHIP BETWEEN SLAB THICKNESS, TEMPERATURE DIFFERENCE AND THE CRITICAL SLAB LENGTH 67

FIGURE 2.18 - THREE WAYS TO EXPRESS THE INTERFACIAL LINEAR SHEAR STIFFNESS, K_s (PETTERSSON, 1998) 68

FIGURE 2.19 – SLAB MOVEMENTS OBSERVED AT STILLESVILLE FOR 19- AND 23 °F TEMPERATURE CHANGE IN LONG SLAB AND MOVEMENTS COMPUTED FOR CONSTANT FRICTION (FRIBERG, 1954) ... 68

FIGURE 2.20 - VARIATION OF STRESS DUE TO FULL RESTRAINT 69

FIGURE 2.21 - STRESSES WITH FULL WARPING RESTRAINT BUT NO END RESTRAINT 69

FIGURE 2.22 - CREEP STRAIN RESULTING FROM A CONSTANT AND A GRADUALLY APPLIED STRESS (KOVLER, 1997) 69

FIGURE 3.1 - STRAIN GAUGES TESTED FOR USE IN SITE INSTRUMENTATION 84

FIGURE 3.2: LAB TESTING TO DETERMINE THE EARLY AGE APPARENT STRAINS MEASURED BY THE DIFFERENT GAUGES 84

FIGURE 3.3 - CLOSE UP OF THE GAUGE FIXING METHOD FOR THE TRIAL SITE 85

FIGURE 3.4 – STRAIN GAUGES SUSPENDED FROM THE REINFORCEMENT CHAIRS 85

FIGURE 3.5 – GAUGE FIXING METHOD FOR FIBRE REINFORCED FLOORS 85

FIGURE 3.6 – GAUGE FIXING METHOD FOR FABRIC REINFORCED FLOORS 85
FIGURE 3.7 - SCHEMATIC OF GAUGE CLUSTERS AND DIRECTLY CONNECTED GAUGES 85
FIGURE 3.8 - CRIMP CONNECTION WITH STRAIN RELIEF PRIOR TO WATERPROOFING 86
FIGURE 3.9 - PROTECTING THE EXPOSED PART OF A STANDARD 10" STRAIN GAUGE 86
FIGURE 3.10 – MODIFIED DAY-JOINT GAUGE WITH DUMMY END BLOCK 87
FIGURE 3.11 – BEFORE REMOVAL OF POLYSTYRENE 87
FIGURE 3.12 - AFTER ATTACHMENT OF EXTENSION ARM 87
FIGURE 3.13 - DRILLING HOLES TO LOCATE THE DEMEC PIPS 87
FIGURE 3.14 - LABORATORY DEMONSTRATION OF THE GAUGE PAIRS 88
FIGURE 3.15 – COMPLETED CLUSTER BOX 88
FIGURE 3.16 - MARKING THE LOCATION OF GAUGES AFTER EMBEDMENT 88
FIGURE 4.1 – NORTHAMPTON: LONG STRIP GAUGE LAYOUT AND LOCATION 95
FIGURE 4.2 – NORTHAMPTON: SECTION VIEW OF THE SLAB SHOWING THE STRAIN GAUGE LOCATIONS 96
FIGURE 4.3 – NORTHAMPTON: INSTRUMENTATION AT THE CONTRACTION JOINT 96
FIGURE 4.4 – NORTHAMPTON: DATALOGGER INSTALLATION 96
FIGURE 4.5: CHEPSTOW: INSTRUMENTATION DETAILS FOR THE MESH REINFORCED JOINTED LARGE AREA POUR 97
FIGURE 4.6: LEEDS: INSTRUMENTATION DETAILS FOR THE MESH REINFORCED JOINTED LARGE AREA POUR 98
FIGURE 4.7 – DAVENTRY: INSTRUMENTATION DETAILS FOR THE FIBRE REINFORCED JOINTED LARGE AREA POUR 99
FIGURE 4.8 – BEDFORD: INSTRUMENTATION DETAILS FOR THE FIRST FIBRE REINFORCED JOINTLESS LARGE AREA POUR 100
FIGURE 4.9 – MARSTON: INSTRUMENTATION DETAILS FOR THE SECOND FIBRE REINFORCED JOINTLESS LARGE AREA POUR 101
FIGURE 5.1 - EFFECT OF VARYING THE ZERO TIME ON THE CALCULATED STRAIN 142
FIGURE 5.2 – COMPARISON OF APPARENT AND CORRECTED STRAINS 142
FIGURE 5.3 – APPARENT AND THERMALLY CORRECTED STRAINS 142
FIGURE 5.4 - SCHEMATIC OF JOINT GAUGE BEHAVIOUR 143
FIGURE 5.5 - REPRESENTATIVE LINEAR FIT OF DAILY TEMPERATURE AND STRAIN CHANGES 143
FIGURE 5.6 - MEASURED CONCRETE INTERNAL TEMPERATURES 144
FIGURE 5.7 - MEASURED CONCRETE INTERNAL TEMPERATURES 145
FIGURE 5.8 – LEEDS: EFFECTS OF CONCRETE HYDRATION ON THE UNDERLYING LAYERS OF GROUND 146
FIGURE 5.9 –SINE CURVE APPROXIMATION TO MEASURED TEMPERATURES (DATA FROM THE MET. OFFICE WEATHER STATION LEEDS_W_C) 146
FIGURE 5.10 – LEEDS: THEORETICAL ANNUAL TEMPERATURE VARIATION AT DIFFERENT DEPTHS 147
FIGURE 5.11 – LEEDS: COMPARISON OF THE THEORETICAL AND THE MEASURED TEMPERATURE DISTRIBUTIONS 147
FIGURE 5.12 - CHEPSTOW: FORMED RESTRAINED MOVEMENT JOINT BEHAVIOUR 147
FIGURE 5.13 - CHEPSTOW: POUR 11 SAWN RESTRAINED MOVEMENT JOINT BEHAVIOUR 148

FIGURE 5.14 - CHEPSTOW POUR 13: BEHAVIOUR OF EMBEDMENT STRAIN GAUGES 148
FIGURE 5.15 - CHEPSTOW POUR 13: BEHAVIOUR OF SAWN RESTRAINED MOVEMENT JOINTS 148
FIGURE 5.16 - DAVENTRY POUR 8: BEHAVIOUR OF SAWN RESTRAINED MOVEMENT JOINTS 149
FIGURE 5.17 – LEEDS POUR 4: BEHAVIOUR OF SAWN RESTRAINED MOVEMENT JOINT 36 149
FIGURE 5.18 - LEEDS POUR 1: BEHAVIOUR OF EMBEDMENT STRAIN GAUGES 149
FIGURE 5.19 – LEEDS POUR 1: BEHAVIOUR OF SAWN RESTRAINED MOVEMENT JOINTS 20 & 23 150
FIGURE 5.20 – LEEDS POUR 4: BEHAVIOUR OF SAWN RESTRAINED MOVEMENT JOINT 34 150
FIGURE 5.21 – LEEDS POUR 1:BEHAVIOUR OF SAWN RESTRAINED MOVEMENT JOINT 21 & 22 150
FIGURE 5.22 – LEEDS POUR 2: BEHAVIOUR OF SAWN RESTRAINED MOVEMENT JOINTS 27 & 28 151
FIGURE 5.23 – LEEDS POUR 4: BEHAVIOUR OF EMBEDMENT STRAIN GAUGES 151
FIGURE 5.24 – LEEDS POUR 1: DEMEC READINGS ALONG SECTION A-A 152
FIGURE 5.25 – LEEDS POUR 2: DEMEC READINGS ALONG SECTION B-B 152
FIGURE 5.26 – LEEDS POUR 4: DEMEC READINGS ALONG SECTION C-C 152
FIGURE 5.27 – LEEDS POUR 2: BEHAVIOUR OF EMBEDMENT STRAIN GAUGES 153
FIGURE 5.28 – MARSTON: MEASURED MOVEMENT FROM THE SLAB EDGES 153
FIGURE 5.29 – MARSTON: MEASURED MOVEMENT AT THE DAY JOINTS 154
FIGURE 5.30 – BEDFORD: COMPARISON OF JOINT MOVEMENTS FROM EACH SIDE OF THE CENTRAL POUR 154
FIGURE 5.31 - LEEDS: BEHAVIOUR OF THE FORMED FREE MOVEMENT JOINT BETWEEN POURS ONE AND TWO 155
FIGURE 5.32 - LEEDS: BEHAVIOUR OF THE FORMED FREE MOVEMENT JOINT BETWEEN POURS ONE AND FOUR 155
FIGURE 5.33 - LEEDS: BEHAVIOUR OF THE FORMED FREE MOVEMENT JOINT BETWEEN POURS TWO AND FOUR 155
FIGURE 5.34 - LEEDS POUR 2: PRECISION LEVEL SURVEY 1 MONTH AFTER CONSTRUCTION 156
FIGURE 5.35 – NORTHAMPTON: LONG STRIP FREE MOVEMENT JOINT BEHAVIOUR 156
FIGURE 5.36 - DAVENTRY: POUR 5 SAWN FREE MOVEMENT JOINT BEHAVIOUR 156
FIGURE 5.37 - DAVENTRY: MEASURED JOINT WIDTHS ALONG SECTION B-B 15 MONTHS AFTER CONSTRUCTION 157
FIGURE 5.38 - NORTHAMPTON: INCREMENTAL CONTRACTION OVER THE FIRST MONTH AFTER CONSTRUCTION 157
FIGURE 5.39 – BEDFORD POUR 2: MEASURED MOVEMENT FROM THE EMBEDMENT STRAIN GAUGES 158
FIGURE 5.40 – MARSTON POUR 6: MID-SLAB CONTRACTION AGAINST POSITION 159
FIGURE 5.41 – MARSTON POUR 7: MID-SLAB CONTRACTION AGAINST POSITION 159
FIGURE 5.42 – MARSTON POUR 9: MID-SLAB CONTRACTION AGAINST POSITION 159
FIGURE 5.43 - MARSTON: VARIATION OF THE THERMAL COEFFICIENT OF EXPANSION 160
FIGURE 5.44 – CHEPSTOW: CRACK LOCATIONS AS AT 19TH NOVEMBER 1999 161
FIGURE 5.45 - CHEPSTOW: CONCRETE CONTRACTION WITH LOCATION 162
FIGURE 5.46 – CHEPSTOW: DISJOINTED CRACKING ACROSS A SAW-CUT JOINT 163
FIGURE 5.47 – NORTHAMPTON: MEASURED STRAIN CHANGES AT THE FIRST OPENING OF THE FM JOINT 163

FIGURE 5.48 - MARSTON: JOINT WIDTH MEASUREMENTS 140 DAYS AFTER CONSTRUCTION..... 164
FIGURE 5.49 – NORTHAMPTON: PRECISION LEVEL SURVEY RESULTS 24 HOURS AFTER CONSTRUCTION. 165
FIGURE 5.50 – NORTHAMPTON: SURFACE PROFILE OF THE LONG STRIP SLAB 10 MONTHS AFTER CONSTRUCTION 165
FIGURE 5.51 – NORTHAMPTON: SLAB PROFILES NEAR TO JOINTS 10 MONTHS AFTER CONSTRUCTION.... 166
FIGURE 5.52 - NORTHAMPTON: DIFFERENTIAL MOVEMENT WITH TIME..... 167
FIGURE 5.53 - BEDFORD 2 POUR 9: WARPING MOVEMENT FROM A JOINTLESS LARGE AREA POUR 168
FIGURE 5.54 - LEEDS POUR 4: CONCRETE SHRINKAGE STRAIN 169
FIGURE 5.55 - LEEDS POUR 1: CONCRETE SHRINKAGE STRAIN 169
FIGURE 5.56 - BEDFORD: LONG TERM CONCRETE STRAINS..... 170
FIGURE 5.57 - BEDFORD: AMBIENT TEMPERATURE FROM BEDFORD SAWS (DATA COURTESY OF THE BADC) 170
FIGURE 5.58 - BEDFORD: LONG TERM SHRINKAGE STRAINS 170
FIGURE 5.59 – CHEPSTOW: PLAN ELEVATION OF THE PRECISION LEVEL SURVEY RESULTS SHOWING CRACK A..... 171
FIGURE 5.60 – CHEPSTOW: 3D PLOT OF THE SLAB AROUND CRACK A 171
FIGURE 5.61 – CHEPSTOW: SECTIONAL VIEWS ACROSS CRACK A..... 172
FIGURE 5.62 – CHEPSTOW: SECTIONAL VIEWS ACROSS CRACK A..... 173
FIGURE 5.63 - CHEPSTOW POUR 11: CONCRETE SHRINKAGE STRAIN..... 174
FIGURE 5.64 - CHEPSTOW POUR 10: CONCRETE SHRINKAGE STRAIN..... 174
FIGURE 5.65 – LEEDS POUR 1: DRYING SHRINKAGE BEHAVIOUR 175
FIGURE 5.66 - LEEDS POUR 2: CONCRETE SHRINKAGE STRAIN 175
FIGURE 6.1 – A FINITE ELEMENT MODEL OF THE SLAB-GROUND SYSTEM. 189
FIGURE 6.2 – LEEDS: COMPARISON OF THE BEST MODEL WITH MEASURED DATA..... 189
FIGURE 6.3 - MEASURED AND FINITE ELEMENT CALCULATED SLAB TEMPERATURES FOR NORTHAMPTON 190
FIGURE 6.4 - MEASURED AND FINITE ELEMENT CALCULATED TEMPERATURES FOR MARSTON..... 190
FIGURE 6.5 – COMPARISON OF EARLY-AGE MEASURED AND PREDICTED TEMPERATURES FROM CHEPSTOW 190
FIGURE 6.6- THEORETICAL AND MEASURED TEMPERATURES FROM CHEPSTOW 191
FIGURE 6.7 - COMPARISON OF FINITE ELEMENT AND PREDICTED TEMPERATURES FOR BEDFORD 191
FIGURE 6.8 - COMPARISON OF FINITE ELEMENT AND MEASURED TEMPERATURES FROM LEEDS 191
FIGURE 6.9 - THERMAL PROFILE THROUGH THE SLAB SYSTEM..... 192
FIGURE 6.10 – DEFORMED SHAPE OF A FINITE ELEMENT MODEL OF A SLAB EXPOSED TO A NEGATIVE THERMAL GRADIENT 192
FIGURE 6.11 - SHEAR STRESS DISTRIBUTION ALONG THE SLAB/SUB-BASE INTERFACE..... 192
FIGURE 6.12 - DISTRIBUTION OF THE GROUND PRESSURE UNDER THE SLAB..... 193
FIGURE 6.13 – RESTRAINT STRESSES AT THE LINE OF SYMMETRY 193
FIGURE 6.14 – NORTHAMPTON: COMPARISON OF THE JOINT MOVEMENT FROM THE FINITE ELEMENT MODEL AND THE SITE DATA FOR POSITION 2..... 194

FIGURE 6.15 – NORTHAMPTON: COMPARISON OF STRAINS FROM THE FINITE ELEMENT MODEL WITHOUT DRYING SHRINKAGE AND THE SITE DATA (INTERFACE SHEAR STIFFNESS, K_s = 24 MN/M^3) 195
FIGURE 6.16 – NORTHAMPTON: COMPARISON OF STRAINS FROM THE FINITE ELEMENT MODEL WITH DRYING SHRINKAGE AND THE SITE DATA (INTERFACE SHEAR STIFFNESS, K_s = 24 MN/M^3) 196
FIGURE 6.17 – FE MODEL OF NORTHAMPTON: THEORETICAL STRESS DISTRIBUTION IN THE SLAB 197
FIGURE 6.18 - FE MODEL OF NORTHAMPTON: WARPING STRESSES 198
FIGURE 6.19 - FE MODEL OF NORTHAMPTON: STRESS DISTRIBUTIONS 198

LIST OF TABLES

TABLE 1.1 - INSTRUMENTATION DETAILS OF THE INVESTIGATED FLOORS 4

TABLE 2.1 - DETAIL DESIGN GUIDANCE ON JOINT SPACING 11

TABLE 2.2 - RELATIONSHIP BETWEEN ERRORS IN *K* VALUE AND ERRORS IN SLAB THICKNESS (SOURCE: NCHRP REPORT 372, 1995) 19

TABLE 2.3 - HYPOTHETICAL JOINT DEFLECTIONS AND EFFICIENCIES (GULDEN AND BROWN, 1985) 22

TABLE 2.4 – SUMMARY OF MATERIAL THERMAL PROPERTIES 48

TABLE 2.5 - COMPARISON OF COEFFICIENTS OF FRICTION, μ 56

TABLE 3.1 – PROPERTIES OF THE AVAILABLE STRAIN GAUGE TYPES. 72

TABLE 3.2 - STRAIN GAUGE DETAILS 74

TABLE 5.1 - COMPARISON OF EARLY AGE TEMPERATURE CHANGES 108

TABLE 5.2: LEEDS - COMPARISON OF THE LONGITUDINAL BEHAVIOUR OF THE FIRST TWO POURS 115

TABLE 5.3 - NORTHAMPTON: STATISTICAL COMPARISON OF DAILY STRAIN CHANGES 121

TABLE 5.4 – BEDFORD: MEAN EARLY LIFE INCREMENTAL MOVEMENT 122

TABLE 5.5 - BEDFORD: STATISTICAL COMPARISON OF DAILY STRAIN CHANGES 123

TABLE 5.6 – MARSTON: INCREMENTAL MOVEMENT 124

TABLE 5.7 - MARSTON: STATISTICAL COMPARISON OF DAILY STRAIN CHANGES 126

TABLE 5.8 – LEEDS: LONGITUDINAL AND TRANSVERSE CONTRACTION FROM THE FIRST TWO POURS 128

TABLE 5.9 – NORTHAMPTON: COMPARISON OF CALCULATED AND MEASURED JOINT OPENING 129

TABLE 5.10 – MARSTON: COMPARISON OF CALCULATED AND MEASURED JOINT OPENING 129

TABLE 5.11 : THEORETICAL DRYING SHRINKAGE, ε_T, AND CALCULATED DRYING SHRINKAGE, ε_M 138

TABLE 6.1 - MATERIAL PROPERTIES FOR THE FIRST THERMAL FINITE ELEMENT MODEL 179

TABLE B.1 – NORTHAMPTON: LOCATION OF STRAIN GAUGES AND THEIR TYPES 233

TABLE B.2 – CHEPSTOW: LOCATION OF STRAIN GAUGES AND THEIR TYPES 233

TABLE B.3 – LEEDS: LOCATION OF STRAIN GAUGES AND THEIR TYPES 234

TABLE B.4 – BEDFORD: LOCATION OF STRAIN GAUGES AND THEIR TYPES 234

TABLE B.5 – DAVENTRY: LOCATION OF STRAIN GAUGES AND THEIR TYPES 235

TABLE B.6 – MARSTON: LOCATION OF STRAIN GAUGES AND THEIR TYPES 236

TABLE B.7 - LEEDS: CONCRETE MIX DESIGN 237

TABLE B.8 - NORTHAMPTON: CONCRETE MIX DESIGN 238

TABLE B.9 - DAVENTRY: CONCRETE MIX DESIGN 239

TABLE B.10 - MARSTON: CONCRETE MIX DESIGN 240

TABLE B.11 - CHEPSTOW: CONCRETE MIX DESIGN 241

TABLE B.12 - BEDFORD: CONCRETE MIX DESIGN 242

TABLE B.13 - BEDFORD CUBE TEST RESULTS 243

TABLE B.14 - MARSTON CUBE TEST RESULTS 244

TABLE B.15 - NORTHAMPTON CUBE TEST RESULTS 244

TABLE B.16 - CHEPSTOW CUBE TEST RESULTS 245

TABLE B.17 - DAVENTRY CUBE STRENGTH RESULTS 245

NOTATION

a/c	Aggregate/cement ratio
a/g	Aggregate/gravel ratio
a	Material parameter; Radius of equivalently loaded area
a_t	Temperature induced deflections
a_s	Shrinkage induced deflections
A	Active length of slab for thermal movements
A_s	Required area of steel to carry frictional restraint force
b	Material parameter; Special theory radius of equivalently loaded area
c	Material parameter
C_0	Specific creep
C_d	Drying creep
C_p	Decrease in creep after drying
d_x	Actual movement at any point in a slab
D	Effective thickness of drying member
E_0	Asymptotic modulus
$E_c(t)$	Concrete modulus of elasticity at time t.
E_{28}	Concrete 28 day elastic modulus
E_g	Effective strain gauge stiffness
E_{max}	Maximum allowable evaporation rate
E_T	Linear softening modulus
f	Resonant frequency of the vibrating wire strain gauge; Load factor
f_{ck}	Characteristic design strength
f'_c	Mean compressive strength of standard test cylinders
f_{ct}	Uniaxial tensile strength
$f_{ct,spl}$	Cylinder splitting tensile strength
$f_{ct,fl}$	Flexural strength
f_{cu}	Compressive strength of standard test cubes

f_y	Steel characteristic strength
F_t	Maximum frictional restraint force per metre width of slab
g	Acceleration due to gravity
G_f	Fracture energy
G.F.	Gauge factor relating resonant frequency to strain
h	Slab thickness
h_d	Depth to which drying assumed to occur
h^2	Thermal diffusivity
JE_δ	Joint effectiveness
k	Modulus of Subgrade Reaction; Material strength reduction factor; Material parameter
k_h	Humidity dependence of drying shrinkage
k_e	End restraint factor
k_s	Shrinkage shape function
k_t	Time dependence of drying shrinkage
k_w	Warping restraint factor
K	Boundary conduction coefficient
K_{s1}	Initial tangent shear stiffness
K_{s2}	Secant shear stiffness
K_{s4}	Mean shear stiffness
l	Radius of relative stiffness
l_{ch}	Characteristic length
L	Distance between free movement joints
LTE_δ	Load transfer efficiency
m	Material parameter
M_n	Negative moment at failure
M_p	Positive moment at failure
M_o	Ultimate moment capacity
M_y	Ultimate moment capacity of an unreinforced slab
n	Material parameter

P	Total applied load
P_o	Ultimate load
qn	Specific flux vector in direction **n** outwards normal to a surface
$Q(t)$	Cumulative heat of hydration at time t
Q_{max}	Total cumulative heat of hydration
r	Sample correlation coefficient
r_o	Critical degree of hydration
$r(t)$	Degree of hydration
$R_{e,3}$	Equivalent flexural ratio
RH	Relative humidity
s/c	Sand/cement ratio
s	Exposed surface area of drying member
$S(t)$	Shrinkage time curve
t	Age of concrete; Time
t'	Age of concrete when loading applied
t_0	Age of concrete when drying began
t_{max}	Age of concrete when maximum temperature obtained
T	Measured temperature
T_{grad}	Temperature gradient in a member
T_h	Period of variation of ambient relative humidity
v	Volume of drying member
w_o	Initial water content
w/c	Water cement ratio
z	Distance from a free movement joint; Slab deflection

α_c	Thermal coefficient of expansion for concrete
$\alpha_{c\ eff}$	Effective thermal coefficient of expansion for concrete
α_{sg}	Thermal coefficient of expansion for the strain gauge wire

α_1	Parameter related to cement type
α_2	Parameter related to method of curing
δ_l	Deflection of loaded side of a joint
δ_u	Deflection of unloaded side of a joint
δT	Temperature change
Δ	Unit weight
Δ_J	Joint opening
ΔT	Temperature difference between opposite faces of a member
ε	Strain
ε_{app}	Apparent strain (as measured by strain gauges)
ε_{sh}	Mean shrinkage strain in a cross section
$\varepsilon_{s\infty}$	Ultimate shrinkage potential
$\varepsilon_{sh\infty}$	Ultimate shrinkage strain
ε_{corr}	Corrected strains accounting for the gauge thermal effects
ε^e	Elastic strain
ε^{cr}	Crack strain
ϕ	Free boundary potential
ϕ_E	Environmental potential
γ	Eulers constant (0.5772); Thickness coefficient
φ_l	Material parameter
μ	Friction coefficient
ν	Poisson's ratio
θ_0	Theoretical periodic temperature variation (daily or annual)
$\theta(t,x)$	Theoretical temperature at time, t and a depth x from the slab surface
ρ_c	Concrete density
ρ_{sb}	Sub-base density
σ	Stress
σ_c	Maximum stress under a corner load

σ_e	Maximum stress under an edge load
σ_i	Maximum stress under an internal load
τ	Elapsed time from maximum temperature zero point
τ_{sh}	Shrinkage square half time
ω	Joint width

1. Introduction

1.1. Background

The concrete ground floor of many buildings is one of it's prime assets. If the floor, for reasons of structural or surface irregularity or integrity, cannot sustain the business operation of the facility then the capital value of the structure is at risk.

Much of the existing stock of industrial floors is unsuitable for modern applications and it is being redeveloped or replaced. In 2000 the market was estimated at 7 million square metres of floor per year, representing an estimated 6% (around £50m) of the total UK consumption of concrete and a turnover of approximately £110m (Figures: ACIFC and DETR). Many industries are reliant on the ground floor industry and are placing growing demands on ground floor performance in terms of flatness, joint integrity, reduced cracking and resistance to wheel wear. For example, the last five years has seen the adoption of machine laid floors for the majority of close tolerance heavy duty floors for the distribution industry. However, there is a lack of understanding of concrete floor slab construction materials and their behaviour, reflected in current design practice, and improvements are needed if effective and economic engineering solutions to these demands are to be achieved.

Engineers have to make assumptions and idealise behaviour when designing any structure. This is because design techniques are approximations which simplify the problem to the point where it can be solved relatively simply and quickly. A quick, and thus simplified, analysis is also required to meet the economic demands of having a structure designed, constructed and in use as quickly as possible. However, assumptions and simplifications can introduce errors, particularly if they are applied in situations for which they were not intended.

For industrial floors the main design guidance available to engineers in the UK is the Concrete Society Technical Report 34 (Barnbrook *et. al.*, 1994), which gives advice on the detail and structural design of concrete ground floor slabs. Most of the detail design guidance contained in TR34 is empirical and based on out-of-date construction methods and the limited theory is largely unsubstantiated. New construction forms (specifically fibre-reinforced and large area pours) and greater performance requirements from clients have resulted in the need for a better theoretical understanding and revised design guidance to be made available to engineers if uneconomic solutions and costly failures are to be avoided. This cannot be achieved without

some form of in-situ monitoring of the behaviour of the slabs, coupled with performance modelling.

In-situ instrumentation provides useful performance data which can be compared with predictions to verify design methods. Industrial floor slabs can benefit greatly from in-situ instrumentation as the designs fall into several generic categories allowing findings from one floor to be applicable to the design of another floor in the same category.

1.2. Aims and Objectives of the Research

The research presented here was undertaken with funding from the Engineering and Physical Sciences Research Council to monitor and model the behaviour of concrete industrial ground floors, in order to address some of the gaps which have become apparent in the design guidance. **More specifically, the project aimed to improve the understanding of how the early-age development of the concrete's material properties interacts with the climate and curing, along with the form of construction (joints, reinforcement and slab restraint), to produce a suitably low stressed concrete that can efficiently carry the subsequent stresses due to the imposed loads.**

The objectives were:

1. to conduct field monitoring of selected new floor constructions, combined with small sample tests (located on site and in the lab) to help characterise material properties, to quantify the extent and timing of early movements and the associated climatic conditions;
2. to develop and refine – in light of the above – a material performance model, using currently available information, which takes account of appropriate parameters of: the concrete mix; the bay geometry, joints and subgrade restraint; and the exposure and climatic conditions;
3. to inform practising engineers and researchers of the findings and make recommendations on the principles, content and use of an appropriate design approach.

The project was designed to focus on the early-age slab behaviour, which was defined as the 28 day period following construction before the slab was loaded. However, once the instrumentation had been installed, monitoring was still possible in some cases for longer than this initial period, although not necessarily through automatic collection with a datalogger. Where available, the long-term data has also been presented and discussed in this thesis, allowing the affects of seasonal temperature changes and drying on the behaviour of the slab to be assessed.

1.3. Research Methodology

An extensive literature review identified: little work on the early-age behaviour of industrial floors; a range of relevant information on thermal and moisture induced concrete movements; and several material models already in existence which were suitable for incorporation in either finite element or spreadsheet based models of concrete behaviour. Although there was little information available on the early-age behaviour of industrial floors, a relevant body of work on the design and performance monitoring of rigid pavements was identified.

Initially the ambient temperature, relative humidity (RH) and wind speed were identified as the parameters most likely to affect the behaviour of the slabs. Instrumentation was chosen to monitor these ambient characteristics as well as the internal temperature of the slab, and in some cases the internal RH, and dew point of the slab. The movement of the concrete and of the saw-cut joints were recorded by several types of vibrating wire (vw) strain gauges, which were chosen for their long-term stability, precision and sensitivity. The instruments were connected to dataloggers which stored the results until they were downloaded into a portable computer.

An iterative procedure was used to develop the techniques required to locate the strain gauges correctly in the slab and to connect them reliably and efficiently to the datalogger. This was developed in the laboratory and then further refined on a trial instrumentation before embarking on a full-scale site instrumentation. Initial problems were quickly overcome leading to the development of a methodology which is flexible, reliable and sufficiently robust to stand the rigours of site.

Based on data from the Association of Concrete Industrial Flooring Contractors (ACIFC) on relative proportions of floors under construction in the UK, and after consultation with specialist flooring contractors, consultants and material suppliers, four floor types were identified that represent the majority of current and future construction:

- Long strip
- Fibre reinforced jointed large area pour
- Mesh reinforced jointed large area pour
- Fibre reinforced jointless large area pour

A programme was developed to instrument these floor types whilst also encompassing some variety in the environmental variables previously identified. Anecdotal evidence suggested that most problems were encountered when floors were constructed in spring and autumn, due to the large difference between day and night-time temperatures.

The types of floors which have been investigated can be seen in Table 1.1 together with the type of data collected. Laboratory testing of cube samples to determine compressive strength has been carried out, together with drying shrinkage tests, where a shrinkage-reducing

admixture was used in one of the pours. No other testing of site samples was carried out because of the difficulties in carrying out temperature matched curing on site, and the availability of extensive published data which was sufficient to determine the early-age material properties based on the concrete constituents.

Table 1.1 - Instrumentation details of the investigated floors

Floor	Type	No of embedment gauges	No of joint gauges	No of concrete temperature sensors	Duration of initial readings
1	Mesh reinforced long strip	12	6	24	8 weeks
2	Fibre reinforced jointed large area pour (LAP)	35	25	10	3 weeks
3	Fibre reinforced jointless LAP	5	8	5	4 weeks
4	Mesh reinforced jointed LAP	12	14	8	4 weeks
5	Fibre reinforced jointless LAP	41	16	19	3 weeks
6	Mesh reinforced jointed LAP	19	40	26	12 weeks

Precision level surveys were carried out on some of the floors to allow comparison of floor shape immediately after construction and at later dates in order to try and identify curling. Where permission was obtained from the client, demec pips were also placed across saw-cut joints. This allowed more joints to be monitored, and over a greater movement range than was possible with vibrating wire strain gauges.

Meteorological Office weather data was made available to the research team by the British Atmospheric Data Centre allowing the impact of the ambient conditions on the long-term strains to be analysed when data logging of temperatures was suspended or had ceased.

Data collection was carried out on most sites for at least one month after construction resulting in over 40,000 data points per slab. Monitoring was continued on some sites either by replacing the data logger or one-off site visits, as shown in Figure 1.1. Macros were written to process the data before analysis was carried out in Matlab, Origin and MS Excel. A common set of graph templates was developed to enable the comparison of results from different sites.

Finite element and spreadsheet based models were used to compare theoretical predictions of behaviour with that actually measured by the instruments. These used established constitutive models of concrete taking into account the prevalent ambient conditions, the mix proportions of the concrete, the dimensions of the structure itself, and the material which the floor was cast upon. Using concrete hydration data, the finite element models can determine the thermal changes in the slab, based on the mix constituents, and use this information to predict the concrete material properties with time. This data provides the input for the structural analyses designed to identify the residual stresses in floor slabs before they enter service.

The finite element models were calibrated and verified against the site data before investigations of some of the construction variables were carried out in accordance with objective two.

The research findings have been disseminated into and beyond the academic community as provided for in objective three. This has been, and continues to be undertaken by publication in conferences and seminars (Bishop, 1998; Austin *et. al.*, 1999; Austin & Bishop, 2000;), academic and professional journals (Austin *et. al.*, 1998, Austin *et. al.*, 2001) and through the maintenance of a project web site (http://www-staff.lboro.ac.uk/~cvjwb/index.html). Several further journal papers are currently in preparation.

1.4. Research Outputs

The research has produced new insights in our understanding of the behaviour of concrete industrial floor slabs. A number of site instrumentations have been carried out providing a large amount of performance data, which was previously unavailable. This information is being made available in the form of a Guidance Document to be published by the Concrete Society and the ACIFC, which will allow engineers to explore the early-age behaviour of the different types of industrial floor.

Finite element models have been developed and calibrated using the site data, which will allow the further study of the behaviour of industrial floors. It has also been demonstrated that the simple spreadsheet based predictions of drying shrinkage and curling deformation give good agreement with the more complicated and expensive to run finite element calculations.

The author has also made significant contributions to the ongoing rewrite of TR34: Concrete Industrial Ground Floors – A guide to their design and construction (2002), which is the main guidance document available to engineers for the design of industrial ground floors in the UK.

1.5. Thesis structure

Chapter 1 is an introduction to the thesis. It describes the current challenges facing the flooring industry and outlines the aims and objectives of the research.

Chapter 2 presents the current design guidance and state of the art research in slabs and pavements. Mathematical models of material properties and their implementation in spreadsheet and finite element models are then discussed.

Chapter 3 describes the selection and development of the instrumentation used to monitor the early-age behaviour of concrete industrial floors, and the production of an in-situ instrumentation methodology. The full process has not been presented for brevity, rather the

key stages of development required before arriving at a methodology which was practicable, reliable and robust. This is done in the context of industrial ground floor slabs, although the final method can be applied to any concrete structural member.

Chapter 4 contains detailed information on the layout of the sites and the location of the instrumentation. The instrumentation layouts have been produced on A3 pages, which can be folded out to provide the reader with quick reference to gauge locations when looking at the results presented in the later chapters.

Chapter 5 initially presents the methods used to analyse the site data before the results from the site instrumentation programme are discussed. In order to be of most use, the data has been divided into two sections covering free and restrained movement joint behaviour, followed by two sections discussing the effects of restraint and temperature changes on the slab behaviour. Finally the drying shrinkage movement is compared with the predictions from a numerical model.

Chapter 6 describes the mathematical modelling process used for comparison with the site data presented in chapter 5. A brief overview of the finite element method is first given, before the development of the thermal and structural models used to predict the behaviour of ground supported slabs is discussed. The results from these models are then compared with the site data, allowing some further behavioural trends to be identified.

Chapter 7 brings together the summaries and conclusions from chapters 3 to 6. Several recommendations are made for changes to the guidance given to floor slab designers, along with recommendations for further work.

The Early Age Behaviour of Concrete Industrial Ground Floor Slabs

Research programme

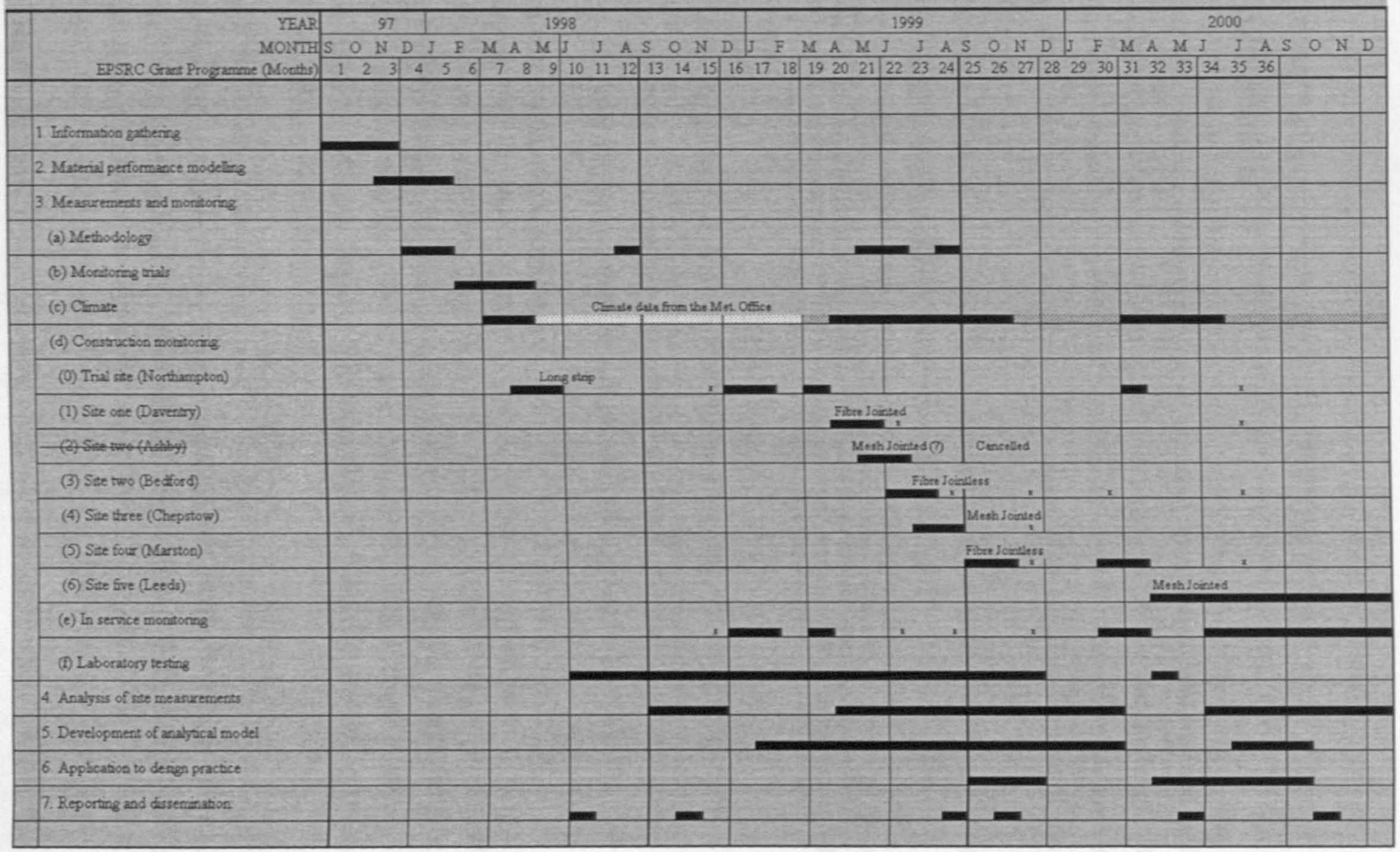

Figure 1.1 – Site instrumentation programme

2. Literature review

2.1. Introduction

This chapter reviews the literature relating to industrial floor design, behaviour and modelling. Current design guidance will be introduced with emphasis on the detail design, which is concerned with controlling the early age behaviour of the slab. Where possible the historical context of this current design guidance will be expounded to highlight the lack of theoretical grounding. Although the structural design does not fall directly within the remit of this research it will briefly be covered so as to allow the reader to understand the significance of the detail design in determining the useful life of the structure.

The methods and techniques used for monitoring structures, slabs and, in particular, pavements are introduced, and the results of these studies are then compared with theoretical predictions of behaviour.

Finally the mathematical modelling of concrete properties and the incorporation of these constitutive models in larger scale spreadsheet or finite element models of structural behaviour are discussed.

2.2. Current design guidance

The design of ground bearing flat slabs is usually divided into two stages, namely: structural design and detail design. Structural design is concerned with sizing the slab so that it can carry the stresses generated by the imposed loads, whilst detail design attempts to ensure that the slab maintains its structural integrity during the concrete hardening and drying processes so that it can withstand the imposed loading.

Although the structural design of the slab falls outside the scope of this research it will be briefly discussed, as this will show some of the anomalies which are present in the currently available design guidance, and also allow the reader to understand better the importance of the detail design process.

2.3. Detail design

The purpose of detail design is to ensure that the slab maintains its structural integrity during the concrete hardening and drying processes so that it can withstand the subsequently applied

service loading and vehicular trafficking. Long established empirical rules which govern the form of construction, bay sizes, reinforcement selection and joint detailing are currently applied to achieve this aim. Steel fabric or steel fibre reinforcement is used to distribute the shrinkage induced tensile forces in the slab, whilst the bay length/width ratio is chosen to keep the stresses at some acceptable but undetermined level. The joints must be spaced to prevent cracks forming elsewhere in the slab but they must not open to such a degree that aggregate interlock is lost, thereby losing the shear transfer effect. Fibre reinforcement is assumed to assist the transformation of tensile forces in a similar manner to fabric reinforcement, but its effect is small scale and localised.

2.3.1. Slab aspect ratios

Neal (1996) recommends slab aspect ratios should not exceed 1:1.5 to avoid uneven opening of joints, although no mention of slab or panel aspect ratios is made by Ringo & Anderson (1996) or TR34.

2.3.2. Joints

Joints are provided in concrete slabs to act as controlled cracks thus reducing the likelihood of random cracking at other locations. Stresses are increased at the desired location by saw-cutting a groove between 1/4 and 1/3 of the slab thickness to reduce the cross-sectional area. This is generally done about 24 hours after the slab is constructed although the Soff-cutt™ system, which is widely used it the USA, allows the joints to be cut before the concrete has reached final set.

The terminology used to refer to the joint types has been revised and simplified for the new version of TR34 currently being produced. This new terminology has been adopted here, although where relevant, for clarity, the old classification under TR34 (1994) will also be mentioned.

The joints in an industrial ground floor can be divided in to two main types, namely those which allow movement – *free movement joints* – and those which do not – *restrained movement joints*.

2.3.3. Free movement joints

This joint type is designed to allow free opening in order to prevent the build up of longitudinal restraint stresses, whilst ensuring that effective load transfer is maintained. The formed free movement joint (Figure 2.1a) used between adjacent pours is not very common because of constructability issues – it is very difficult to get the levels of the two slabs perfectly matched leading to increased wear and risk of breakdown of the joint under trafficking.

Sawn free movement joints (Figure 2.1b) are commonly used in long-strip construction, where their spacing allows the determination of the crack control reinforcement according to the frictional restraint theory. They are also sometimes used to divide pours in jointed large area floors, although this is much less common due to the difficulties in locating and aligning the joint, and the lack of clarity in the design guidance on how these floors should be designed.

2.3.4. Restrained movement joints

As their name suggests, the reinforcement used across these joints is expected to control the joint width. The reinforcement is continuous across the joint, to control the width, but is generally located in the bottom of the slab. These joints can be formed using bonded bars or fabric reinforcement across a joint (Figure 2.2), although no differentiation is made in the current design guidance for the effect these different reinforcement types may have on the performance of the joint.

These joints are generally used to provide relief to stresses due to warping, although they are also used mid-way between free movement joints, where the frictional restraint stresses will be greatest, to reduce the risk of random cracking.

Most day joints are currently constructed as formed restrained movement joints with another joint, which can either be a sawn free or restrained movement joint, about 900mm away.

In nominally reinforced large area pours the reinforcement is laid continuously across the pour resulting in the formation of restrained movement joints at all of the saw cuts. Although technically under the new definitions these are restrained movement joints, the weight of fabric reinforcement provided must be kept light (generally A142) in order to allow the joints to open – for this reason they were referred to as special induced contraction joints in TR34 (1994).

Although warping restraint is mentioned briefly in TR34 Section 5.4, no guidance is given as to the magnitude of the stresses which could be expected due to this restraint, nor is any specific guidance given on the optimum spacing for sawn restrained movement joints to alleviate these warping stresses.

2.3.5. Jointless construction

The latest development is the jointless floor. As long as the construction joints can be well protected the lack of saw-cut joints can enhance the long-term serviceability of this floor type. Although jointless floors have been undertaken in the UK since the 1980's the available detail design guidance is still limited. Neither TR34 (1994) nor Knapton (1999) cover this form of construction, even though the latter reference deals specifically with large area pours. Experience has shown that >35kg/m^3 fibres seem to be required to prevent noticeable cracking in these floors, but this has yet to be incorporated in any design guidance.

2.3.6. Crack control reinforcement and joint spacing

Recommendations for joint spacing in the current design guidance varies widely, and in some cases the advice appears contradictory. Knapton (1999) recommends maximum joint spacing dependent on the concrete type, with increases allowable for higher dosages of fibre reinforcement, whilst no mention is made of fabric reinforcement. Neal (1996) only gives two recommended joint spacings – one for fabric reinforcement and one for fibre reinforcement – whilst the cross-sectional area of crack control reinforcement to be used varies from A142 to A252 based solely on the slab thickness (150-200mm and greater than 275mm respectively). No dosage information is given for fibre reinforced slabs, though the joint spacing is recommended not to exceed 7m. The joint spacing recommended in TR34 varies from 6m for unreinforced slabs to a designed distance where reinforcement areas are calculated to allow for subgrade friction effects.

Table 2.1 - Detail design guidance on joint spacing

Reference:	Design criteria	Joint spacing
Single Pour Industrial Floor Slabs, Knapton (1999)	Plain C40 concrete	6m
	20kg/m^3 ZC 60/1.00 steel fibre reinforcement C40 concrete	6m
	30kg/m^3 ZC 60/1.00 steel fibre reinforcement C40 concrete	10m
	40kg/m^3 ZC 60/1.00 steel fibre reinforcement C40 concrete	12m
TR34 (1994)	Plain concrete (>160mm thick)	<6m
	Nominal fabric reinforcement	6-8m
	Reinforced against sub-base friction	See equation 2.1
	Fibre reinforcement (20kg/m^3) [1]	6-8m
ICE Good Practice Guide, Neal (1996)	Fabric reinforcement (amount dependant on slab thickness)	5m
	Fibre reinforcement	7m
Designing Floor Slabs on Grade, Ringo & Anderson (1996)	Plain concrete (spacing in ft between 2 and 3 times slab thickness in inches)	3-9m according to slab thickness
	Reinforced concrete	See equation 2.1

[1] Joint spacing for fibre reinforced slabs is not specifically covered. They should be treated as nominally reinforced.

Although both TR34 and Knapton give joint spacing for unreinforced slabs, this form of construction is highlighted as being risky, since if cracks do form there is nothing to control their width.

Where joint spacing and reinforcement areas are explicitly designed according to TR34 (1994) the assumption is made that the only restraint to movement in a ground-supported slab is that due to friction between the slab bottom and the subgrade/sub-base or slip membrane. Neglecting the eccentricity of this restraint leaves a triangular stress distribution between free movement joints (TR34 Section 5.4.2) with the maximum resulting force on a unit width of slab given by:

$$F_t = \mu \cdot \Delta \cdot h \cdot \frac{L}{2} \qquad \text{equation 2.1}$$

Where F_t is the theoretical maximum tensile force (kN per m width of slab), μ is the friction coefficient, Δ is the unit weight of the concrete (24 kN/m^3) and h and L are the slab thickness and distance between free movement joints respectively (m). Reinforcement is then detailed to carry this frictional load, giving a required area of steel, A_s according to equation 2.2 where f_y *is* the steel characteristic strength (460N/mm^2) and k is the material strength reduction factor (usually 0.85).

$$A_s = \frac{\mu \cdot \Delta \cdot h \cdot L}{2 \cdot k \cdot f_y} \qquad \text{equation 2.2}$$

Although the additional restraint which could be present under a slab when the service loading is applied is briefly mentioned in TR34 and engineers are advised to account for this, no guidance is given as to how this should be done in practice. As will be shown later, experimental evidence has shown that the coefficient of friction depends strongly on the applied load, reducing as the load increases. Therefore, if engineers attempt to predict the additional restraint once service loading has been applied and design reinforcement accordingly, the design could be very conservative.

The spacing of joints and the methods used to determine the reinforcement required to control cracking is confusing when considering jointed large area pours. The guidance suggests that nominal reinforcement can be used to control cracking with joints at 6 to 8m centres, but no advice is given on the use of contraction joints. Following the frictional restraint theory reinforcement would have to be designed to carry the stresses from one end of the slab to the other unless contraction joints were included, although this is obviously excessive. Neal (1996) takes a slightly more pragmatic approach by relating the reinforcement to the thickness of the slab, ignoring the joint spacing, although a joint spacing of 5m is recommended.

The very light fabrics used in this approach are not strong enough to control joint opening, and indeed TR34 (1994) states that heavier fabrics must not be used because of the risk of cracking away from the joints that this could cause.

2.3.7. Placement of Reinforcement

Several different recommendations can be found in the literature for the most effective placement of crack control reinforcement, which in some cases appear related to issues of constructability. TR34 recommends placing the fabric 50mm from the top surface of the slab (Section 5.1.6) where it will be most effective in controlling crack widths, although in some cases this could interfere with wire guidance systems for mechanical handling equipment. In a later section (5.4.1b) nominally reinforced slabs are discussed, where it is stated that these are

often constructed with reinforcement placed 50mm from the bottom of the slab. Although no justification for this is given the author believes this is related to constructability. Reinforcement near the top of the slab is most effective in controlling crack widths, but cannot be continuous across saw-cut joints. Because of the difficulty in locating sawn restrained movement joints in large area pours, placing the fabric reinforcement in the bottom of the slab allows unimpeded cutting of the joints.

Although TR34 recommends placing the fabric with 50mm cover it is acknowledged that the exact placement of the reinforcement is not critical giving a tolerance of +/-10mm. Wire supports should be used to locate the reinforcement at the correct depth, whilst weak concrete or wooden supports are not suitable.

Knapton (1999) generally agrees with the recommendations in TR34 for the placement of the reinforcement, although the only method shown for locating the reinforcement involves the fabric being trodden into the concrete. Even though the exact location of the reinforcement in the slab may not be critical, this method for locating the reinforcement can not be recommended, as there is liable to be significant variation in the final location of the reinforcement. Whatever position is specified for the reinforcement, consistency must be achieved in order to prevent some areas of the slab behaving differently to others.

Neal (1996) recommends placing all of the reinforcement at mid-depth in the slab. This avoids interference problems with wire guidance systems and for large area pours avoids problems with saw-cut joints, whilst providing better crack control than reinforcement near the bottom face of the slab.

Kiamco (1997) concluded that as the frictional restraint is an eccentric load applied to the bottom face of the slab, reinforcement placed near this face would be *proactive* in preventing cracking from propagating through the slab. Additionally, if sufficient reinforcement is used to offer post crack structural strength, the lever arm from the centroid of this reinforcement to the concrete compression zone in the top of the slab would allow the slab to carry load after cracking. Reinforcement placed near the top face of the slab will be *reactive* in controlling the width of cracks which have already propagated through the slab. However, because of the small lever arm, this reinforcement would offer no structural advantage once the slab has cracked.

2.3.8. Summary of detail design guidance

The available design guidance is mainly empirical and does not reflect the construction techniques currently being widely used in the UK. There is contradictory advice offered by different publications with no real theoretical justification to any of the figures proposed.

Because construction methods have evolved based on experience of previous failures, contradictions appear in the guidance. For example, TR34 states that to be most effective in controlling cracking, reinforcement should be placed near the upper surface of a slab. However, this cannot practically be applied in a large area pour, so the reinforcement is placed lower down in the slab even though it's crack controlling properties may then be negligible.

Advice on joint spacing, especially in large area pours, is also confusing. The joint spacing is decided to keep joint widths within acceptable limits. Reducing the joint spacing should reduce the joint width – assuming all joints open. However, as the frictional restraint is proportional to the joint spacing this also reduces, making it less likely that all joints open, and more likely that those which do will become dominant and lose load transfer.

2.4. Structural design

The structural design of ground supported slabs is a problem which was first addressed early in the 20th century for the design of road pavements and runways. In the intervening period two fundamentally different design theories have become widely accepted. Namely:

- an elastic approach as proposed by Westergaard (1926)
- a plastic approach as typified by Meyerhof (1962)

In both cases the structural design of ground supported slabs differs fundamentally from the approach taken for the design of concrete structures in other design codes, e.g. BS8110, in that the flexural strength of the concrete is the limiting design variable. Simple bending theory shows that increasing the thickness of a member in flexure reduces the tensile stresses in the outermost fibres, hence reducing this problem to one of sizing the slab to accommodate the applied loading. Both of the following design approaches assume the slab to be free of stresses and deformations before the application of the load.

Although fabric reinforcement is often used in ground supported slabs, this is designed solely for the purpose of crack control and is currently assumed not to alter the structural behaviour.

2.4.1. Elastic design method

The elastic design methodology pioneered by Westergaard in the 1920's predicts the yield or first cracking load for a perfectly elastic, homogeneous slab supported on a dense liquid type subgrade. This load is predicted for three loading conditions, namely internal, edge and corner. Westergaard (1926) detailed how to accommodate combinations of loads in his original paper whilst further empirical developments to this approach by Kelley (1939) and Pickett (1951) allowed the loss of support caused by curling of the slab or deterioration in the sub-base to be accounted for. This design approach has featured in almost every design guide published since;

however, since their first appearance in the 1920's these equations have often been misquoted and misapplied, prompting Ioannides *et. al.* (1985) to carry out a review of this design approach.

The internal load and corner load is considered to be applied over an equivalent circular area of radius a, although for internal loads this was further modified using Westergaard's Special Theory to account for shear stresses in the vicinity of the load. Using this theory for a slab of thickness h the radius of equivalent area becomes b found according to:

$$b = \left(1.6a^2 + h^2\right)^{0.5} - 0.675h \quad \text{if } a < 1.724h$$

$$b = a \quad \text{if } a > 1.724h \qquad \text{equation 2.3}$$

Ioannides *et. al.* (1985) found maximum stress under an internal load to be:

$$\sigma_i = \left[\frac{3P(1+\nu)}{2 \cdot \pi \cdot h^2}\right] \cdot \left[\ln\left(\frac{2l}{b}\right) + 0.5 - \gamma\right] + \left[\frac{3P(1+\nu)}{64h^2}\right] \cdot \left[\left(\frac{b}{l}\right)^2\right] \qquad \text{equation 2.4}$$

Where P is the total applied load, ν is the slab Poisson's ratio (0.15), h is the slab thickness and γ is Euler's constant (0.5772). Westergaard defined the dimensionless relationship between the stiffness of the slab and the sub-base as the *radius of relative stiffness*, l.

$$l = \left(\frac{E_c h^3}{12\left(1-\nu^2\right)k}\right)^{1/4} \qquad \text{equation 2.5}$$

where k is the modulus of subgrade reaction and E_c is the slab elastic modulus.

The edge load is considered to be uniformly applied over a semi-circular area of radius a_2 centred at the slab edge, although later modifications allowed for circular, elliptical and square load areas to be considered. Ioannides *et. al.* (1985) found the differences to be very small (<1%) and related to the distance of the centroid of the equivalent area from the slab edge. The following equation for edge stress was found to give very good agreement with finite element predictions:

$$\sigma_e = \left[\frac{3P(1+\nu)}{\pi(3+\nu)h^2}\right] \cdot \left[\ln\left(\frac{E \cdot h^3}{100k \cdot a_2^4}\right) + 3.84 - 4 \cdot \frac{\nu}{3} + 0.5(1+2\nu)\left(\frac{a_2}{l}\right)\right] \qquad \text{equation 2.6}$$

Corner loads have proved to be the most difficult load case to analyse, with many revisions and modifications suggested over the years to try to match theoretical predictions to observed behaviour. Treating the load as uniformly applied over a circular area, radius a, on an unsupported cantilever (Goldbeck,1919; Older, 1924) gives:

$$\sigma_c = \frac{3P}{h^2} \qquad \text{equation 2.7}$$

This takes no account of subgrade support and can be considered a lower bound to the solution. Westergaard proposed equation 2.8 which has good agreement with the finite element predictions.

$$\sigma_c = \frac{3P}{h^2} \cdot \left[1 - \left(\frac{a \cdot \sqrt{2}}{l} \right)^{0.6} \right] \qquad \text{equation 2.8}$$

However, load testing has shown there to be a greater degree of variation in results from the corner position, leading to the recommendation that a conservative approach be taken. The equation proposed by Picket (1951) seems overly conservative, especially for *a/l* ratios less than 0.14 where it predicts lower failure loads than for a cantilevered slab. Kelley (1939) suggested a relationship, which converges to Pickett's values at higher *a/l* ratios, but is closer to the cantilevered beam solution at small *a/l* ratios.

$$\sigma_c = \frac{3P}{h^2} \cdot \left[1 - \left(\frac{a \cdot \sqrt{2}}{l} \right)^{1.2} \right] \qquad \text{equation 2.9}$$

2.4.2. Plastic design method

Whereas the elastic design method predicts the load required to cause cracking in the slab, the plastic design approach uses the yield line theory to establish the collapse load of the slab. This ultimate load is much higher than the crack load as the slab has to form a mechanism, which for the internal and edge condition requires not only radial cracking on the bottom of the slab, but also circumferential tension cracks on the upper slab surface (Figure 2.3). Meyerhof (1962) stated that this collapse load was about twice the yield or cracking load for plain concrete slabs for the internal and edge conditions, with an increased difference for structurally reinforced slabs. Because the failure mechanism of corner loads is the same in both approaches, the predicted failure load is similar.

As the slab fails, the ultimate moment capacity of the slab will have been reached at all points along the yield lines. In an unreinforced section, per unit length of yield line this will be:

$$M_y = \frac{f_{ct} \cdot h^2}{6} \qquad \text{equation 2.10}$$

In an unreinforced section the ultimate moment, $M_0 = M_y$. However, if the post crack behaviour of the slab is ductile, moment redistribution can occur giving an ultimate moment capacity equal to the sum of the negative (M_n) and positive moments (M_p) at failure:

$$M_0 = M_n + M_p \qquad \text{equation 2.11}$$

Although load testing at the University of Greenwich (Beckett, 1990 & 1999) has demonstrated that mesh fabric reinforced slabs can exhibit ductile post crack behaviour, there

is currently no recognised test allowing this to be quantified. For fibre reinforced concrete the change to the post crack behaviour depends on the dosage and the type of fibre used. Thus, not only do the fibres control cracking, but the enhanced post crack properties of the concrete can be accommodated in the design, making for thinner slabs. The property used in design is the equivalent flexural ratio, otherwise known as the $R_{e,3}$ value, and can be determined from a third point beam test carried out in accordance with the JSCE-SF4 standard.

Meyerhof looked at the same three loading conditions previously used by Westergaard, namely internal, edge and corner. For unreinforced slabs with $a/l > 0.2$ he proposed the following formulas, whilst a similar series of equations were proposed for slabs with structural reinforcement.

Internal
$$P_0 = \frac{4\pi \cdot M_0}{1 - \frac{a}{3 \cdot l}}$$ equation 2.12

Edge
$$P_0 = \frac{(\pi + 4) \cdot M_0}{1 - \frac{2 \cdot a}{3 \cdot l}}$$ equation 2.13

Corner
$$P_0 = \frac{4 \cdot M_0}{1 - \frac{a}{l}}$$ equation 2.14

The equations determined by Meyerhof (1962) to calculate the ultimate load capacity of ground supported slabs were quite complicated, resulting in the simpler equations from the appendix of his paper being adopted in TR34 (1994). These revised equations developed after looking at the approach taken by Losberg (1960) are much more conservative than his original equations.

There is no serviceability check inherent in the plastic design approach, but Meyerhof advised that if global safety factors of between 2 and 3 were used, serviceability requirements should be met. No recommendation on safety factors was made for the revised equations given in the appendix to his paper. TR34 (1994) uses a global safety factor of 1.5 with these conservative equations, which gives very similar results to Meyerhof's original equations using a load safety factor of 2. Nevertheless, if a crack free floor is essential this design approach may not be suitable.

2.4.3. Structurally reinforced

This method of design is an extension of the plastic design approach just mentioned. However, this time the reinforcement content of the slab is increased to carry the flexural stresses arising under the load, whilst the concrete slab is sized to carry the much smaller negative moment arising away from the load (Kiamco, 1998; Losberg, 1978). The cross-sectional area of reinforcement required to carry the positive moment will be greater than currently provided for

crack control, but the reduction in the thickness of slab required to carry the negative moment will partially compensate for this increased cost.

2.4.4. Summary of structural design guidance

There appears to be little understanding of the two structural design methods currently used in the UK, with the differences in approach not explained in the design guidance. The elastic approach gives a yield load which can be applied with a low global safety factor because of the residual strength above this load, whereas the plastic design method gives the collapse load for the slab. When using Meyerhof's original equations good agreement is obtained between theory and site tests for most loading conditions; however, this method does not ensure that the slab will be crack free or within acceptable deflection limits under service loading. Additionally because a collapse load is predicted higher global safety factors are required than for the Westergaard method, although this is currently not done in TR34.

With both methods a proliferation of different equations are in use and in many cases ranges of applicability are not defined and guidance is not forthcoming to explain which equations should be applied in which circumstance. Hopefully, the revision to TR34 currently in progress will address all of these issues.

2.5. Investigations into the influence of construction variables

The constructional variables affecting the early-age behaviour of floors, which are common to all floor types, are briefly covered in this section. Although some of these parameters are beyond the control of the designer, it is important that the influence that they have on the behaviour of the finished slab is understood. As no experimental work on the behaviour of industrial floors with respect to these variables could be found, the investigations reported here are generally from pavements.

2.5.1. Subgrade and sub-base support

There is scope for infinite variation in the material properties of subgrade, which may be natural ground or some form of man-made fill. The latter is increasingly the case as redevelopment of so-called 'brown field' sites becomes more prevalent.

Both elastic and plastic structural design methods model the subgrade support as perfectly elastic, with reactions proportional to the vertical displacement. Westergaard introduced the concept of the *modulus of subgrade reaction*, k, as the factor which when multiplied by the deflections, z, would give the subgrade reaction. This was an empirical value assumed to be constant at all points and independent of deflection and load area, although it was acknowledged that these factors would alter its value. No test method for determining k was

ever proposed by Westergaard, who suggested testing completed slabs on given subgrade types and adjusting *k* in the equations until the deflections predicted by the formulas matched those measured on the slabs. The reconciliation of these back calculated *k* values with those from plate tests directly on the subgrade was never addressed, although plate tests and CBR's are now commonly carried out to determine the *k* value used in design. Alternatively if this information is not available it can be estimated from soil classification information. However, as the slab thickness is not very sensitive to the *k* value (Westergaard, 1927; NCHRP Report 372, 1995) this does not have to be estimated with great accuracy (Table 2.2).

Table 2.2 - Relationship between errors in *k* value and errors in slab thickness (Source: NCHRP Report 372, 1995)

Error in *k*-value [%]	Typical maximum error in slab thickness [%]
10	1.0
25	2.5
50	5.0
100	10.0

Because of the confusion over the determination of *k*, an *enhanced* top-of-base modulus of subgrade reaction arose when sub-bases began to be used to improve the trafficking properties of the subgrade and combat pumping at joints in America in the 1950's. Although site testing of pavements in the 1930's and 40's to try and verify Westergaards equations and determine reliable ways of measuring the design value of *k* had concluded that there was no correlation between top of base *k* values and slab deflections, this practice has since become widely accepted (NHCRP Report 372). Based on these and more recent tests several authors (Teller and Sutherland, 1943; Sale, 1977; Ahlvin, 1991) have concluded that the top-of-base *k* values are artificially high and not justified for design. The recommendation from the NCHRP Report 327 was that the enhanced top of base *k* value should no longer be used in the design of pavements in the USA.

Although TR34 and other design guidance allows the use of enhanced *k* values, modern computing techniques allow a full analysis of the slab, sub-base and subgrade system to be undertaken. This means there is no longer any need, or justification, for designers to continue simplifying the problem to one of a slab on a modified subgrade.

Ozbeki *et. al.* (1985) used finite element techniques to carry out a parametric study of rigid slab behaviour. They found that increasing the modulus of subgrade reaction decreased the corner deflection of a pavement slab significantly, although the tensile stresses in the x-

direction were not reduced in the same way. They recommended a minimum value of k of $54N/cm^3$ in order to prevent breakdown of the joints, however, this was only sufficient when load transfer was provided by dowels.

2.5.2. Slip membrane

The primary purpose of this membrane is to reduce the coefficient of friction under a slab, thus reducing the stresses arising due to this restraint. The different coefficients measured with different friction reducing mediums are covered in Chapter 2.8.5 along with the techniques used to model friction.

In most cases the plastic slip membrane will also act as a moisture barrier and this can affect the performance of the slab. Although Roper and Anderson (1982) found that construction on a sand sub-base reduced the initial plastic and drying shrinkage compared to construction on a slip membrane, Ytterberg (1987c) found in a series of experimental studies that exposing the bottom of a slab to moist ground can actually accentuate problems with curl. In the laboratory tests a 7.6m long slab was allowed to stand on a dry sub-base and gave vertical deflections of 3.3mm. Drying the slab completely and then wetting the bottom gave a vertical deflection of 4.6mm (a 38% increase). Eisenmann and Leykauf (1990) report on similar slab wetting experiments conducted at the Munich Technical University where a 39% increase in upward deflection was measured in laboratory tests. Despite water treatment over a period of weeks these readings could not be repeated when the same experiment was conducted on site. This difference in behaviour was believed to be caused by a higher ambient RH and rain falling on the surface of the external slabs. Aïtcin *et. al.* (1997) also recommended placing floor slabs on a draining substrate or constructing on an impervious membrane to prevent the ingress of moisture from under the slab causing excessive curling.

2.5.3. Reinforcement

A 3.5 mile test section of road was constructed (Spigolon, 1963) to assess the effects of varying pavement thickness and steel percentage, the size and spacing of transverse reinforcement and the use of a cement treated base. The ends of the pavement sections were anchored with cast-in-place concrete piles to prevent seasonal longitudinal movements. All reinforcement was located at mid-slab depth. Longitudinal movements relative to fixed observational points at the side of the test sections were made in addition to measurement of crack widths and spacing. Initially the sections constructed in October to December showed more cracking than those sections constructed in the spring of the following year. However, after several years the crack spacing in both sections had stabilised and differences between the sections were hard to determine. No significant behavioural differences related to the constructional variation could be found, although the authors pointed out that the variations in

the constructional parameters were small in relation to the normal distribution of the crack widths and spacing. Crack widths were found to vary significantly with temperature and to increase with time, although it was not known whether the latter trend would continue.

Crawford and Anderson (1963) varied the depth of cover to the reinforcing steel between 64mm and 94mm and tried various methods of controlling the end movement on two sections of interstate highway totalling almost 1.5 miles in length in North Dakota. The pavement thickness (203mm) and quantity of reinforcement (0.646% longitudinal steel) was held constant in the trial sections. All of the measured crack widths were found to be small; however, the section with the reinforcement steel at 64mm showed almost 25% less opening, although the average crack frequency was 700mm as opposed to over 900mm for the sections with the reinforcement at nearly mid-depth.

2.5.4. Joints

Saraf and McCullough (1986) studied the relationship between the depth of saw-cut at joints and the concrete properties and the occurrence of longitudinal cracks in concrete pavements. A statistical analysis of variation showed that a reduction in the variability of concrete strength could lead to a significant reduction in the depth of saw-cut required. Investigations on two sections of pavement, one with limestone aggregate and the other with river gravel, confirmed the theoretical evaluation, showing that the concrete with the least variation in tensile strength had the greatest proportion of cracks within the saw-cut joints.

Teller and Sutherland (1936) determined the load transfer, now generally referred to as the joint effectiveness as:

$$JE_{\delta} = \frac{2\delta_u}{\delta_u + \delta_l} \times 100 \qquad \text{equation 2.15}$$

Where JE_{δ} is the load transfer as a percentage and δ_u and δ_l are the deflections of the unloaded and loaded slabs respectively. Similarly the load transfer efficiency, which is a measure of the slab discontinuity caused by a joint, is defined as (Ioannides & Korovesis, 1990):

$$LTE_{\delta} = \frac{\delta_u}{\delta_l} \times 100 \qquad \text{equation 2.16}$$

Gulden and Brown (1985) showed that these equations can be misleading when applied to real situations, although confusingly they used joint efficiency instead of load transfer efficiency, and load transfer instead of joint efficiency. Even though the magnitude of the difference in joint movement is identical for all locations in Table 2.3 the calculated joint efficiency and load transfer for location 1 is the worst, however, the performance of this joint is actually

closer to the real life ideal. They recommend simply comparing the magnitude of the deflections and their differences.

Table 2.3 - Hypothetical joint deflections and efficiencies (Gulden and Brown, 1985)

Test location	Deflection (mils)		Joint efficiency (%)	Load transfer (%)
	Loaded side	Unloaded side	$(\delta_u/\delta_l \times 100)$	$2\delta_u/(\delta_u+\delta_l) \times 100$
1	6	1	17	29
2	10	5	50	87
3	35	30	86	92

Ozbeki *et. al.* (1985) carried out finite element and site investigations to determine the sensitivity of slab deflections and joint efficiency to the following parameters:

- Dowel size
- Modulus of subgrade reaction
- Modulus of dowel-concrete interaction
- Joint width
- Dowel modulus of elasticity
- Concrete modulus of elasticity

They found that only the modulus of subgrade reaction and the modulus of dowel-concrete interaction had a significant effect with respective minimum recommended values of 54.4 N/cm^3 and 54.3 kN/cm^3 to keep slab deflections and joint efficiency within levels which will prevent deterioration and eventual failure of the joint system. Zollinger and Barenberg (1990) also found that improvements in the foundation strength improved the long-term joint efficiency.

Initially when joints crack and open the load is transferred by aggregate interlock and reinforcement dowel action. The load transfer efficiency due to aggregate interlock decreases as the joint opens, with Ioannides & Korovesis (1990) proposing the following relation:

$$LTE_{\delta}\ (\text{percent}) = 100 - 25\omega \qquad \text{equation 2.17}$$

where ω is the joint opening in millimetres, thus giving zero joint efficiency once the opening is 4mm. The joint efficiency also decreases as the number of load repetitions increases. It was noticed, however, that this only occurred once the load had exceeded some critical value, with no deterioration of the joint being caused by lighter loads, although angular aggregates were found to maintain load transfer longer under repetitive loading conditions.

Wang *et. al.* (1990) have developed a new testing method for carrying out uni-axial direct tensile testing of concrete specimens. They used this to analyse the behaviour of various artificial fibre reinforced concretes. Tensile failures were found to occur with applied stress between 1.7 and 3.7 MPa depending on the fibres used. Residual stresses were still between 1.0 and 2.5 MPa when the joint had opened by 0.4mm and in the case of the longer high-strength polyethylene fibres were still over 0.6 MPa when the joint had opened by 4mm

(Figure 2.4). This clearly demonstrates that joint performance in fibre reinforced slabs is dependent not only on the fibre dosage, but also on the fibre type.

Zollinger and Barenberg (1990) tested 9-in (230mm) and 7-in (180mm) thick continuously reinforced slabs subjected to repetitive loading of 9kip (40kN - equivalent to a lorry at 30mph). The joint effectiveness was found to level off after 700,000 to 800,000 load applications (Figure 2.5) with the joint effectiveness after 1million load applications giving a useful indication of likely performance for design guidance. For the 9-in thick slab joint widths of 0.6mm were found to have an efficiency of over 90%, although this same joint width had an efficiency of only 50% for the 7-in slab. Joint widths exceeding 1.1mm were needed before the efficiency dropped below 50% for the 9-in slab, with this still requiring ¼ million load applications. The 7-in slab had zero joint efficiency with joint widths of 1.7mm after 120,000 load applications, whilst the joint width was able to exceed 2.1mm for the 9-in slab, and still required ½ million load applications before all load transfer was lost.

Ioannides *et al.* (1990) showed how using thicker dowel bars at closer spacing can reduce joint deflection and increase the joint efficiency, however, this must be done judiciously as this may also cause a detrimental increase of restraint to longitudinal warping or curling. This in turn may cause more distress in the pavement than if the dowels were omitted completely. Friberg (1940) was the first author to suggest that the load transfer decreased linearly with increasing distance from the point of application of the load, reaching zero at a distance of 1.8 times the radius of relative stiffness (equation 2.5). This was in agreement with the original work by Westergaard (1928), although more recently a finite element study of slab-dowel systems by Tabatabaie (1978) found that this effective length should really be equal to the radius of relative stiffness. The study also found the dowel diameter and the concrete elastic modulus altered the maximum dowel deflection and concrete bearing stress, whilst the slab thickness and subgrade modulus were found to have a much lesser effect.

Knapton (1999) states that experience indicates that significant load transfer occurs when joints open by up to 1mm, but when joint opening exceeds 2mm there is little or no load transfer. No further justification for these figures is given.

Poblete *et. al.* (1988a) measured how joint opening in a plain concrete pavement was non-uniform as the pavement aged. At early ages this was in the order of one open joint every three or more panels. After 2 years the joints had all opened, but it was still possible to identify the joints which opened earliest because of the greater opening (Figure 2.6). Joint opening was found to be less in pavements which had been constructed during cold and humid ambient conditions, thus providing better load transfer.

Minkarah *et. al.* (1981) carried out a statistical analysis of slab movements with joint spacings between 5.2m and 12.4m. They found that the short-term movements were of greater magnitude than the long-term seasonal changes, regardless of the slab length, although the long-term movements were directly proportional to the slab length. Not all joints were found to move; in particular some joints showed large movement with adjacent joints not moving at all, although the joints which moved were found to vary over time.

Free thermal contraction of concrete is related to the temperature change and the thermal coefficient of expansion. By multiplying by the distance between the joints the expected joint movement can be determined (equation 2.18). However, this relationship was not found to be valid for the measured joint movements.

$$\text{Movement} = \alpha_c \,.\, \delta T.\, L \qquad \text{equation 2.18}$$

Possible reasons for this may lie in the indeterminacy of the variables in the equation. α_c varies for each concrete mix, and because some of the joints do not always move, the length parameter could contain large errors.

Bodocsi *et. al* (1993) carried out further studies on the test sections investigated by Minkarah *et. al.* twenty years after they were constructed and found that the joint movement gave good agreement with the theoretically predicated movements using equation 2.18. The researchers found that all of the joints moved equally and that the movement was most closely related to the mean slab temperature. A statistical analysis showed there was no relationship between the type of sub-base or the joint reinforcement and the movement measured at the joint. Additionally there was no significant difference in the behaviour of the joints at 40ft (12.2m) and 20ft (6.1m) spacings. This was because the 40ft sections all contained active cracks midway between the joints making them behave like 20ft sections. Although the 20ft sections also contained similar cracks none of these were found to be active.

2.5.5. Restraint

Bloom and Bentur (1995) developed a laboratory testing rig to determine the restraint stresses in normal and High Performance concrete at early ages. Concrete with a *w/c* ratio of 0.5 exposed to drying at 40°C and 40%RH had measured stresses of 1.5MPa after 5 days when the tensile strength was 2.2MPa. Even sealed specimens were found to have restraint stresses of 1.0MPa after the same time. The stresses were found to be higher in concrete with a low *w/c* ratio - 0.33 gave tensile stresses of 2.5MPa after 5 days. The presence of silica fume did not alter the magnitude of the 5 day stresses, but they occurred more rapidly.

Kovler (1994) also developed a laboratory test method using 'dog bone' shaped samples to measure the mechanical behaviour of free and restraint concrete. The arrangement of the test

rig allowed the separation of the creep effects from the sample shrinkage by testing two specimens simultaneously – one of which is restrained, whilst the other is free. Stresses of 1.5 MPa were found to develop in the 40mm x 40mm specimens within 24 hours of exposure to the drying environment (30% RH). This stress increased with time remaining just below the tensile strength of the concrete.

Nagataki (1970) cast a trial slab 23¼ ft (7m) long to determine the shrinkage effects under external exposure conditions. The results showed that the mean shrinkage at all sections was the same although the warping strains were found to decrease nearly linearly with distance from the end of the slab, with no warping strain at the middle section. This showed that frictional restraint was insufficient to prevent movement whilst warping restraint increased with distance from the end of the slab.

The unrestrained section of CRC pavement monitored by Crawford and Anderson (1963) showed reduced cracking 120ft (37m) from the East end and 500ft (152m) from the West end with no cracking at all within 100ft (30m) of the ends of the slab. The second section of CRC pavement with fully restrained ends also showed a slight reduction in cracking within 100ft of the ends, which is believed to be related to the slight movement of the anchoring lugs, however, cracking was still present up to the ends of the slab.

Ytterburg (1987c) reported unpublished work by Schrader (1987) where the risk of cracking in slabs cast against older slabs with protruding reinforcement was highlighted. In order to minimise this restraint the use of square dowels with spacers was recommended. ACI 325 Subcommittee IV (in Ytterburg, 1987c) concluded that longitudinal and transverse dowels may result in a restraint stress of 0.17 MPa, which would increase the stresses at all other sections in the slab by the same amount.

2.5.6. Temperature

When analysing the temperature effects in pavements several studies [Poblete *et. al.* (1988b), Rollings (1993) and Armaghani *et. al.* 1987) have found that a permanent upward curl exists in the slabs such that a positive temperature gradient is required to establish full sub-base support. This was believed to be caused by the presence of a positive thermal gradient, caused by solar warming of the slab surface, when the concrete hardened. As the slab cooled this initial gradient resulted in the slab surface contracting more than the rest of the slab leading to the development of upwards curling. The magnitude of these gradients was found to be between 5 and 10°C.

Many of the instances of vertical movement occurred within the first few days or weeks in the life of the slabs. This ruled out drying shrinkage as a mechanism for the movement and led Rollings (1993) to conclude that frictional restraint of autogeneous or related shrinkage of

hydrating cement and thermal gradients resulting from the exothermal hydration of the cement were the main causes of this early curling. Although these effects were only small the relatively thin slabs studied meant that this differential movement was sufficient to cause curling. Drying shrinkage may have been ruled out as a cause of the early-age curling, however, it was identified as being contributory to the continued movement as the slab aged.

Spigolon (1963) found visible transverse cracks started forming in an instrumented highway pavement constructed in October about 3 days after construction. The West pavement section constructed in October had average crack spacing of 5 to 10ft, whilst the East pavement constructed the following spring had a much slower rate of crack formation, although after two or more years the difference was hard to distinguish. In a second instrumented pavement most sections had cracks forming after 2 to 3 days although one section poured in cold weather had several thousand feet of slab with no cracks even after 60 days.

2.6. In-situ instrumentation and monitoring

No details of previous in-situ early-age monitoring of concrete industrial floor slabs could be found. Kim and Lee (1998) carried out laboratory tests on the differential drying shrinkage of external concrete slabs using embedment strain gauges, whilst long-term monitoring of joints in concrete pavements (Nagataki, 1970; Poblete *et. al.*, 1988b) has been carried out using both Carlson and vw strain gauges. In all cases no readings were taken earlier than 24 hours after construction was completed. Similarly readings only began after 24 hours in the long-term testing of a suspension bridge reported by Lachemi *et. al.*(1996a). Although readings were then taken every two hours the authors felt that the readings during the first 24 hours would not be useful.

2.6.1. General concrete structures

Instrumentation of buildings is an area which has become more topical in recent years with interest in intelligent structures. More information is required in order to determine the true performance of structures, which in turn allows assessment of the reliability and accuracy of the assumptions made in the design codes. Wright and Lloyd (1992) carried out an instrumentation of a multi-storey building to monitor loads and deflections during construction and in service. They installed 200 sensors, including vibrating wire pressure cells and inclinometers to monitor foundation performance and vibrating wire strain gauges cast into concrete members and welded to steelwork to monitor the structural behaviour. Cost limitations restricted them to manual recording of data on a weekly basis as opposed to the automatic logging system originally foreseen. However, this was still sufficient to allow significant differences between designed and actual behaviour to be seen. They identified the

difficulty in defining the actual loads on a building in service without carrying out controlled loading tests, and highlighted the fragility of most available instrumentation. This is not a problem when carrying out laboratory work, but presents problems for protecting the equipment on site. The Federal Highway Administration of the US Department of Transportation (FHWA, 1996) recommends using at least three strain gauges at each location to provide redundancy in case a gauge is damaged.

Scott and Gill (1987) describe a technique for instrumenting concrete using wire resistance strain gauges. These gauges can be much smaller than vibrating wire strain gauges, however, the grid of support wires required to locate them generally makes them unsuitable for use on site. Additionally because of long term stability problems the FHWA recommends the use of vibrating wire strain gauges for the measurement of long term strains instead of electrical resistance strain gauges (FHWA, 1996).

Shahawy and Arockiasamy (1996a) carried out a comprehensive study of the Sunshine Skyway Bridge in Florida. A total of 259 A-10 Carlson strain meters were used to monitor the concrete strains and temperatures in 17 of the pre-cast bridge segments, three sections of the bridge pylons and 11 sections of the two main bridge piers. These strain meters were cast directly into the concrete with all cables routed through conduit to an automatic data acquisition system. Samples of the concrete used in the construction were also subject to a large-scale field and laboratory testing process. Test cylinders were cured on site for three days before being removed for testing. Compressive strength, elastic modulus, Poisson's ratio, and the coefficient of thermal expansion were determined at approximate ages of 3, 7, 28, 90, 180 and 365 days. Further cylinders with embedded vibrating wire strain gauges were subject to creep and shrinkage tests on site. Six of the pre-cast bridge segments also had 28 thermocouples embedded in them to record the thermal profiles, whilst an additional 14 thermocouples were used to measure the temperature distribution across the major and minor axes of the bridge pylon. Manual readings were taken initially but all of the instrumentation was then connected to a computer controlled data logger to allow automated readings to be taken.

Lachemi *et. al.* (1996a) also monitored the behaviour of a high performance air entrained concrete bridge with thermocouples and vibrating wire strain gauges embedded in the deck slab and one of the bridge abutments. All of the instruments were connected to a remote data acquisition system connected by modem to a computer. Temperatures and strains were taken every 2 hours although instrument failure meant that no strain readings were taken during the first 2 days following construction. In any case the authors stated that strain readings taken during the first 24 hours whilst the concrete hardened would not have been valid.

A laboratory and numerical study (Boulay and Paties, 1993) of the interaction between early-age concrete and a vibrating wire strain gauge found that once the concrete modulus had exceeded 1.5 GPa the errors between the measured and imposed deformations due to thermal or structural loads were less than 5%. It was found that the thermal deformations were over-indicated by the gauges at early ages, whilst the structural deformations were under-indicated. This was believed to be because the concrete was not sufficiently strong to transfer structural loads to the gauges or to restrain the gauge under applied thermal loads. The results were found to be dependent on the geometry of the specimen and of the gauge.

One way of avoiding the problem of the interaction between the strain gauges and the concrete at early ages would be the use of fibre-optic sensors. For examples of methods for implementing fibre-optic sensors in the monitoring of concrete structures, and explanations of what can be measured using this technology see The First European Conference on Smart Structures and Materials (1992). The drawback of this method of structural monitoring is the extremely high cost. Approximate costs at November 1997 were £1000 per installed meter of fibre-optic cable.

2.6.2. Slabs and pavements

Instrumentation of slabs and pavements has been carried out to determine the behaviour of joints with respect to thermal changes, both on a seasonal and a daily scale, or to assess restraint, joint efficiency and curling.

Several investigators have used mechanical gauges located in plugs set into the concrete to monitor the horizontal movement of joints and cracks [Mandel *et. al.* (1990); Crawford & Anderson (1963); Gulden & Brown (1985)]. Because of the low cost involved these can be installed across many joints and cracks in a pavement, although automatic readings are not possible. Spigolon (1963) also monitored the horizontal movement of several points along a section of CRC highway relative to concrete monuments embedded 10ft (3m) into the ground.

Gulden and Brown (1985) monitored vertical deflections relative to fixed reference points using dial gauges mounted on a frame which rested on the shoulder of the pavement. A similar technique was employed by Poblete *et. al.* (1988b), who instead used LVDTs attached to a deep reference base (Figure 2.7) to measure the absolute vertical movement of joints as well as the faulting. Periodic monitoring of these joint movements, as well as the slab temperature, was carried out with a portable PC. On each occasion the position of a test vehicle was also recorded as it travelled down the instrumented section of pavement to allow the joint movements to be correlated to the loading.

Minkarah *et. al.*(1981) instrumented almost 1km of highway pavement. Electrical linear motion transducers and temperature sensors connected to strip-chart recorders were placed

across some of the joints, giving continuous readings for up to 1 week, whilst the other joints were monitored by hand using dial gauges on a monthly basis. Vertical joint deflection readings were also taken electronically four times a year. Bodocsi *et. al.*(1993) continued the monitoring of joint movements, although a 16 channel datalogger replaced the strip-chart recorders, many joint readings were still taken by hand with a Demec gauge.

Barenberg and Zollinger (1990) instrumented pavements to monitor shrinkage, curl and load effects. They used wire resistance strain gauges sealed in a polyester resin which was coated in a gritty substance to promote bonding to the concrete. In order to eliminate local effects a gauge length greater than three times the maximum aggregate size was chosen. 'Dummy' gauges were installed in parallel with each active gauge because the resistivity of the lead wires changes with temperature and the thermal coefficient of expansion of the gauge itself is modified once it is bonded to the concrete. These dummy gauges were sealed in PVC tubing to isolated them from the concrete allowing a zero load effective strain to be obtained. This method worked well for the load strains but problems were encountered when trying to analyse thermal strains. In order to guarantee the accurate placement of the strain gauges the bottom gauges were fixed to a u-shaped metal bar which was located in holes drilled in the sub-base. No satisfactory method of supporting the top strain gauges was developed so the authors tried three different approaches to locate the gauges once the pavement had been laid. Firstly grooves were cut in the hardened pavement with the gauges being grouted in place. Secondly wooden blanks were placed in the slab during construction. Once the concrete had set these were removed and the gauges grouted into place. The long-term durability of the grout was a concern for these first two methods and neither allowed very early strains to be obtained, although the second method was better in this respect. The third method involved working the gauge into the fresh concrete. This solved both problems just mentioned, though accurate placement for both depth and direction were difficult to achieve. It was felt that with practice this method would be the preferred for any future installations. Interference from nearby electrical sources also caused problems when monitoring the gauges. This situation was improved by the use of high quality lead wires and connectors, but improved grounding of the logging instrumentation and a high frequency filtering system were required to significantly improve the signal to noise ratio.

Nishizawa *et. al.* (1997) instrumented two sections of CRC pavement in Japan to identify the magnitude of thermal stresses. Three strain gauges with internal thermocouples were embedded at each measurement point, recording stresses at the top, mid-depth and the bottom of the slab. No readings were taken until the slab was three months old at which time two time periods each lasting two weeks were monitored with readings of temperature and strain taken every hour. Readings were taken in late winter and late spring of 1996.

Most recently, the Federal Aviation Authority installed a fully automated instrumentation system at Denver International Airport as part of an ongoing research effort into runway behaviour. Carlson meters and electrical resistance strain gauges have been embedded in the runways and taxiways of the airport to allow real-time data on movements to be collected. This instrumentation along with additional sensors monitoring ambient air and ground conditions is linked to an Oracle7™ database with a Java™ web interface[1] enabling the database to be queried from anywhere in the world.

2.6.3. Relative humidity

The internal moisture is one of the parameters which plays a critical role in determining the material properties and performance of concrete. For example, durability of the surface and corrosion of reinforcement is linked to the moisture exposure history of the concrete. Under most exposure conditions moisture is lost from the concrete into the environment causing the internal moisture distribution to vary both with location and time (Figure 2.8 and Figure 2.9).

Andrade *et. al.* (1999) investigated the distribution of relative humidity in concrete exposed to natural and artificial weathering, demonstrating that under conditions of variable ambient temperature and relative humidity the temperature is the most important parameter in determining the long-term moisture profile. Furthermore, Bazant and Baweja (1995b) demonstrated that a periodic humidity variation of length T_h did not affect the pore humidity at the centre of a cross section if $\tau_{sh} \geq 2T_h$. This justified the use of constant humidity test data when deriving models of creep and drying shrinkage for application on 'real' structures. For typical concretes this can be restated in terms of the effective thickness, D, as:

$$D \geq 25.4 \cdot \left(\frac{T_h}{10days} \right)^{0.5} \text{ [mm]} \qquad \text{equation 2.19}$$

Therefore, daily variations in the ambient RH would only affect the pore moisture content to a depth of 4mm, and annual changes would only affect it to a depth of about 75mm.

2.7. Modelling of material properties

In order to carry out any form of numerical modelling the behavioural characteristics of all of the construction materials must be mathematically described. In the case of an industrial ground floor slab, the system which must be modelled for both thermal and structural analyses involves the slab, the sub-base, the subgrade and all of the interfaces between these materials.

---

[1] http://www.airtech.tc.faa.gov/pavement/diaip.htm

This section of the literature review describes the various methods available to model these elements of the system.

The material properties of the sub-base and subgrade have been assumed constant[2], whilst nearly all of the properties of the concrete change with time e.g. elastic modulus and thermal conductivity. Instead of linking the development of material properties to time, the degree of hydration can be used. This is a fundamental property of the maturing concrete and allows a continuous function to describe the changing material behaviour. In contrast, linking the material behaviour to the concrete age would not take account of accelerated or delayed hydration due to variability in site conditions, or the differential development of properties in a slab as hydration progressed. Several different measures of the degree of hydration are discussed in *Properties of set concrete at early ages* (Rilem Commission 42-CEA, 1981) and Byfors (1980). The degree of hydration, *r*, defined as the momentary cumulative proportion of the heat of hydration at time *t*, *Q(t)*, compared to the total cumulative heat at full hydration, Q_{max} (equation 2.20) is described here more fully.

$$r(t) = \frac{Q(t)}{Q_{max}} \qquad \text{equation 2.20}$$

This expression assumes that the production of heat during hydration is concurrent with the degree of hydration, which is not unreasonable given the good correlation between the amount of cement that has reacted and the amount of liberated heat for ordinary Portland cements (van Breugal, 1998). More research is needed on the relationship between evolved heat and degree of reaction in non-Portland and blended cements as although the evolved heat gives an indication of the degree of reaction the relationship may not be a linear one.

Because of the changing material properties, and because some of the changes experienced are partly irreversible, the stress and strain state in concrete is history dependant (Philjavaara, 1982).

2.7.1. Compressive strength

For a detailed discussion of the methods used in the determination of the compressive strength the reader is referred to Neville (1995). As for many concrete material properties the compressive strength has been found to vary with the concrete age and can, in turn, be related to the degree of hydration. This relationship between compressive strength and degree of hydration has been found to be linear (Byfors, 1980; Rilem Commission 42-CEA, 1981).

---

[2] The thermal properties of soils are dependent on the moisture content. However, for the purposes of this investigation, constant values from the literature have been used.

Using this relationship De Schutter & Taerwe (1996) used equation 2.21 to relate the compressive strength at a given degree of hydration $f_c(r)$ to the compressive strength at full hydration $f_c(r = 1)$. Here r_0 reflects the fact that a critical degree of hydration must be reached before the concrete has a compressive strength, whilst a is a parameter to fit the experimental data.

$$\frac{f_c(r)}{f_c(r=1)} = \left(\frac{r-r_0}{1-r_0}\right)^a \qquad \text{equation 2.21}$$

Values of r_0 tabulated by De Schutter and Taerwe ranged from 0.15 to 0.6, although most fell in the range 0.15 to 0.22. This agrees with Rostasy *et. al.* (1993) who found r_0 and a to be 0.17 and 1.5 respectively. Byfors (1980) found a relationship between the water cement ratio of the concrete and the critical degree of hydration following a regression analysis of data from Taplin (1959).

$$r_0 = k\frac{w_0}{c} \qquad \text{equation 2.22}$$

Where w_0 is the initial water quantity, c is the cement content and k is a material parameter which varied between 0.4 and 0.46.

2.7.2. Tensile strength

Oluokun (1991) identifies the difficulty of obtaining the true tensile strength of concrete by stating *the tensile strength of concrete is a physical property that has no absolute meaning; it is always expressed in terms of a specific test procedure.*

Various test methods are discussed in Neville (1995) although these are generally only applicable for the testing of mature concrete. Rilem Commission 42-CEA (1981) produced a series of guidelines for the tensile testing of early-age concrete.

Uniaxial tensile testing by Hannant (1994), Ziegeldorf *et. al.* (1982), and Kasai *et. al.* (1971) shows that there is a rapid increase in the tensile strength of concrete between 5 and 7 hours after casting. This rate of growth slowed after about 10 to 15 hours with the data showing an almost linear relationship between the compressive strength and the tensile strength of the concrete, especially at very early ages - $0 < t < 2$days. After this the relationship diverges slightly, showing a more rapid development of tensile strength.

Oluokun (1991) assembled the published data from 11 investigations into the splitting strength development carried out over a period of 20 years. They covered different curing regimes (time and temperature), *w/c* ratios, age at testing, and cement types, with the results indicating that none of these have an effect on the compressive/tensile strength ratio. The relationship between the splitting tensile and compressive strengths was proposed to take the form:

$$f_{ct,spl} = k(f'_c)^n \qquad \text{equation 2.23}$$

Where k and n are material parameters determined from laboratory tests. Values of n between 0.5 and 0.75 have been suggested (Neville, 1995). For all concretes over 12 hours old ($f'_c > 6.9$ MPa) Oluokun *et. al.* (1991b) found the following relationship to be valid:

$$f_{ct,spl} = 0.206(f'_c)^{0.79} \qquad \text{equation 2.24}$$

In a later study Oluokun (1991) found the best fit of the combined database of published data to be with $k = 0.214$ and $n = 0.69$.

The British Code of Practice BS8007: 1987 gives the following relationship between the direct tensile strength and the cube strength:

$$f_{ct} = 0.12(f_{cu})^{0.7} \qquad \text{equation 2.25}$$

De Schutter and Tearwe (1996) show how the relative development of the splitting, flexural and uniaxial tensile strength with maturity is similar, whilst Neville (1995) highlights that there is little difference between the different relationships.

Taking equation 2.24 and again assuming the relationship between compressive strength and maturity in equation 2.21 it can be shown that the tensile strength relates to the maturity according to:

$$\frac{f_{ct}(r)}{f_{ct}(r=1)} = \left(\frac{r - r_0}{1 - r_0}\right)^c \qquad \text{equation 2.26}$$

Parameter c is found from $a.n$. Using $a = 1.5$ from before and $n = 0.69$ gives 1.035 which agrees with Rostasy *et. al.* (1993) who found it to be equal to 1.

2.7.3. Elastic modulus

The elastic, or Young's modulus, is a measure of the ratio of stress to strain in a sample. In the case of concrete this ratio is not constant, being itself a function of material age, temperature and relative humidity as well as of the constituent parts of the concrete and the rate and duration of application of the stress.

There are several different elastic moduli commonly used for concrete (Figure 2.10). They are the *initial tangent modulus*, the *tangent modulus*, and the *secant modulus*. The initial tangent modulus is the tangent to the stress-strain curve at the origin. This is, however, of limited practical importance as it fails to take into account the creep of the concrete. The tangent modulus can be determined at any point on the stress-strain curve for concrete, but as it is a tangent it is only valid for stresses near the point for which the modulus was determined. The secant modulus is the gradient of the line from the origin to a defined point on the stress-strain

curve. This can be used to account for the elastic and the creep deformations of the concrete. As the modulus decreases with increasing stress, the stress at which it is determined must be stated with the modulus. For comparisons between concrete according to BS 1881:Part121:1983 the maximum stress applied to the samples should be 33% of the ultimate strength.

The Young's modulus for concrete increases as the compressive strength increases, although in general it tends to increase at a progressively slower rate as the compressive strength increases (Rilem Commission 42-CEA, 1981). For this reason the equations for predicting the elastic modulus of concrete tend to relate it to the compressive strength, as this is also a function of the variables previously mentioned. Because of the dependence of the concrete elastic modulus on the elastic modulus of the aggregate and on the aggregate content of the concrete the precise relationship between the compressive strength and the elastic modulus is unclear. ACI 318-89 (Revised 1992) gives the relationship as:

$$E_c = 4.73(f_c')^{0.5} \qquad \text{equation 2.27}$$

where f'_c is the compressive strength of standard test cylinders in MPa and E_c is in GPa.

The elastic modulus can also be related to the density of the concrete, which should help to account for the different aggregate proportions. ACI 318-89 (Revised 1992) states this relationship as:

$$E_c = 43\rho_c^{1.5}(f_c')^{0.5} \times 10^{-6} \qquad \text{equation 2.28}$$

where ρ_c is the density of the concrete (kg/m^3). Oluokon *et. al.* (1991a) found this relationship to be valid for all concretes from 12hrs after casting.

More recently, methods treating concrete as a multi-phase composite have been introduced. Li *et. al.* (1999) describe how elastic theory and the rule of mixture method can be combined to allow not only the relative proportion of each phase but also the maximum size and gradation of the elements in the aggregate phase to be used to determine the elastic modulus. Although this latter method gives good agreement with test data it will not be used here. This is because designers specify concrete performance in terms of concrete compressive strength and cube samples are regularly taken on site to measure this in order to test for compliance.

There is little data available from tensile testing of concrete, but according to Neville (1995, p.419) *the best assumption which can be made about the modulus of elasticity in tension is that it is equal to the modulus in compression.*

ACI 209 shows the elastic modulus to vary with respect to the 28-day elastic modulus according to equation 2.29 where $E(t)$ is the predicted elastic modulus, E_{28} is the 28 day elastic modulus and t is the age of the concrete in days.

$$E(t) = E_{28} \times \left(\frac{t}{4 + 0.85 \times t} \right)^{0.5} \qquad \text{equation 2.29}$$

Bazant & Osman (1976) proposed a more accurate description of the variation of the modulus with time, which also allowed the effects of the duration of the loading on the modulus to be predicted. The conventional elastic modulus can be determined according to equation 2.30 using a load test duration of 0.1 days (Bazant and Panula, 1978b). The four material parameters required for solution of this equation, E_0, m, n and φ_1 are defined and discussed in Chapter 2.7.5.

$$\frac{1}{E_c(t')} = \frac{1}{E_0} + \frac{\varphi_1}{E_0} \cdot 10^{-n} (t')^{-m} \qquad \text{equation 2.30}$$

Bazant and Panula (1978b) recommended using this expression instead of equation 2.29 when carrying out creep calculations - the increased accuracy can be seen in Figure 2.11 where the two models are compared.

The long-term growth of the elastic modulus according to equation 2.30 is much higher than predicted by equation 2.29. This is because it relates to a condition of constant water content, whereas the ACI expression is applicable only for drying concrete specimens of standard dimensions; the hydration reaction stops in these specimens relatively soon, whereas in concrete which is not drying the hydration continues for much longer (Bazant & Osman, 1976).

A final relationship between the degree of hydration and the elastic modulus - in line with the other concrete properties - was proposed by De Schutter and Taerwe (1996) in order to simplify its use in modelling applications.

$$\frac{E_{co}(r)}{E_{co}(r = 1)} = \left(\frac{r - r_0}{1 - r_0} \right)^b \qquad \text{equation 2.31}$$

Parameter b is again found from a x n, this time giving 0.75 using the ACI formula for E_c (equation 2.27). For comparison Rostasy *et. al.* (1993) proposed 2/3.

2.7.4. Poisson's ratio

The ratio of lateral strain to longitudinal strain is the Poisson's ratio. For concrete in compression in the range where longitudinal strain is linearly proportional to the applied stress then the Poisson's ratio is approximately constant. It has been found to vary between 0.1 and 0.3, although generally values of about 0.15 to 0.22 are used in calculations (Neville, 1995). No generally applicable mathematical formulas relating any variables to this behaviour have yet been determined so if high accuracy is required testing should be carried out on a particular concrete.

Several different opinions appear in the literature on the relationship between Poisson's ratio and time. Oluokun *et. al.* (1991a) concluded that the Poisson's ratio was insensitive to both the age and the richness of the concrete mix and that it did not change appreciably with the compressive strength development, although the data they based this on showed an increase of between 20 and 40% between 6 and 12 hours after casting for all samples.

2.7.5. Creep

Creep of concrete is a time dependant viscoplastic response under the influence of stress, which can either result in a reduction of stress under conditions of constant strain, or it can manifest as an increase in strain under conditions of constant stress. Rheologically speaking the former is defined as relaxation, although for the purposes of this discussion it will be referred to as creep relaxation.

A description of the main processes involved in creep and their modelling will be given here. For further information and a more detailed description of these processes the reader is referred to Bazant and Wittman (1982), Bazant (1988), Gilbert (1988) and Bazant and Carol (1993).

The creep behaviour itself comprises two components, namely:

- basic creep
- drying creep

Basic creep is a delayed elastic strain in the material, which is reversible on removal of the load. The time over which this strain occurs (and recovers on removal of the load) varies from material to material and, in the case of concrete, is strongly dependent on the age at loading. The predominant cause of basic creep is seen as the property of delayed elasticity as well as the viscous deformation of the hydrated cement gel (Rüsch *et. al.*, 1983).

Drying creep (also known as the Pickett effect) is the strong increase in creep of a specimen exposed to drying when compared to a sealed specimen (Bazant *et. al.*, 1988). It is ascribed to an accelerated movement of water molecules in the pore system of the hydrated cement paste caused by the external load (Rüsch *et. al.*, 1983).

There are many mathematical formulas in the literature for predicting creep (see Bazant & Osman, 1976). Van Breugel (1982) described how the early hardening process of concrete can be likened to a Taylor series, where an increase in hydration and hence stiffness is represented by the addition of further Kelvin units (Figure 2.12). The double power law is discussed further here because it has been shown to be accurate for specimens loaded after only one day (Bazant & Osman, 1976) and also it's ease of conversion into a Taylor series for numerical implementation.

Assuming that the creep law of concrete is linear and that the principle of superposition is valid the creep compliance function $J(t,t')$ applies. This function represents strain (including elastic strain but excluding shrinkage) in time t caused by a constant unit stress that has been acting since time t'. The specific creep $C_0(t,t')$ is the creep strain produced at time t produced by a unit stress acting since time t'. Time t' is measured from the setting of the concrete and represents its age. According to Bazant *et. al.* (1976) the basic creep compliance function takes the form of equation 2.32.

$$J(t,t') = \frac{1}{E_0} + C_0(t,t') \qquad \text{equation 2.32}$$

$$C_0(t,t') = \frac{\varphi_1}{E_0} t'^{-m}(t-t')^n \qquad \text{equation 2.33}$$

Where E_0, m, n and φ_1 are material constants. E_0 is defined as the left side asymptote of the creep curve in the log-time plot. This asymptote is reached only at ultra short times which lie outside the range of validity of equation 2.33. This time period is even smaller than for the dynamic modulus, leading to this modulus being called the asymptotic modulus. It can be found from equation 2.34 (Bazant & Panula, 1978b) where ρ_c is the concrete density (kg/m^3), f'_c is the 28 day cylinder strength (N/mm^2) and $1/E_0$ is in 1/MPa.

$$\frac{1}{E_0} = \left[0.01305 + \frac{0.0853}{z_1^2}\right] \times 10^{-3} \qquad \text{equation 2.34}$$

$$z_1 = \frac{0.00005}{1769.1} \cdot \rho_c{}^2 \cdot f'_c$$

Constants m and n are found according to equation 2.35 and equation 2.36, although Bazant & Osman (1976) carried out extensive curve fitting of published data finding values of constants m and n to be 1/3 and 1/8 respectively if no specific test data is available.

$$m = 0.28 + \frac{47.541}{(f'_c)^2} \qquad \text{equation 2.35}$$

$$\text{for } x > 4: \quad n = 0.12 + \frac{0.07x^6}{5130 + x^6}$$

$$\text{for } x \le 4: \quad n = 0.12 \qquad \text{equation 2.36}$$

$$x = \left[2.1\frac{a/c}{(s/c)^{1.4}} + \frac{(f'_c)^{1.5}}{181.05}\left(\frac{w}{c}\right)^{1/3}\left(\frac{a}{g}\right)^{2.2}\right]a_1 - 4$$

Where a/c is the total aggregate to cement ratio, s/c is the sand to cement ratio, w/c is the water to cement ratio and a/g is the total aggregate to gravel ratio, all by weight. The remaining constant φ_1 can be found from:

$$\varphi_1 = \frac{10^{3n}}{2\left(28^{-m} + \alpha\right)}; \quad \alpha = \frac{1}{40\,w/c} \qquad \text{equation 2.37}$$

To allow for the effects of simultaneous drying equation 2.32 can be extended (Bazant and Panula, 1978c) as shown in equation 2.38:

$$J(t,t') = \frac{1}{E_0} + C_0(t,t') + C_d(t,t',t_0) - C_p(t,t',t_0) \qquad \text{equation 2.38}$$

Where C_d represents the increase in creep due to drying, C_p represents the decrease in creep after drying and t_0 is the age of the concrete at the start of drying (days). Except in very thin specimens C_p is rarely reached in practice and C_d is only reached after a long time (Bazant *et. al.*, 1978). As these additional terms represent only a slight modification of equation 2.32 they can safely be ignored when considering the early age behaviour of an industrial floor.

2.7.6. Shrinkage

Shrinkage is defined as the reduction in volume of unloaded concrete at constant temperature (Rüsch *et. al.*, 1983). This process is primarily caused by a loss of water during the drying process, resulting in a shrinkage strain, ε_{sh}. The inverse process, which is of little significance in practice for internal slabs, is called swelling.

The only length change that can directly be linked to the hygral mechanisms involved is unrestrained shrinkage. Experimentally this situation is very difficult to attain, as even in thin specimens a hygral gradient exists as soon as drying begins. In larger specimens depending on the geometry and the diffusion coefficient this gradient can exist for many years. The measured length change under these conditions is, therefore, also a function of the internal stress distribution (Wittman, 1982).

2.7.7. Plastic shrinkage

Plastic shrinkage occurs before the concrete has set, as moisture is lost into the environment. Water moving out of a porous body which is not fully rigid causes contraction as a result of capillary tension. During the plastic phase in concrete this is a simple volumetric change caused by the loss of water from the system due to evaporation and the accompanying compaction of the particles in the paste. The magnitude of this shrinkage is affected by the rate of water loss from the concrete (and hence by ambient temperature, RH and wind speed) and by the stiffness of the hydrating cement paste (Uno, 1998). The rate of moisture loss itself is not an indication of plastic shrinkage cracking as much depends on the stiffness of the concrete mix itself.

Turton (1989) stated that plastic shrinkage cracking does not appear to be a major problem in industrial floors in the UK because of the power floating processes used, although occasionally

on removal of floor surfaces in preparation for another floor finish plastic shrinkage cracks have been apparent. This highlights how power-trowelling operations can close over cracks in the surface of the concrete giving the appearance of a perfect slab, whilst cracks remain through the majority of the slab depth. This may not always be the case however, as Shaeles and Hover (1988) investigated the occurrence of plastic shrinkage cracking in thin panels exposed to forced drying. They found there was no direct correlation between the rate of moisture loss and the severity of cracking, although in all cases slabs with a finished surface experienced less cracking.

Several authors have tried to relate plastic shrinkage cracking to the evaporation rate (Kohler *et. al.*, 1955; Menzel, 1954; Uno, 1998). However, as different concrete mixes bleed at different rates and other variables such as the rate and method of finishing also seem to affect the formation of plastic shrinkage cracks the use of a constant value seems erroneous (Shaeles and Hover, 1988). In most cases for a given mix type there does appear to be a critical evaporation rate, which was acknowledged by Uno (1998). The critical evaporation rate for different concretes based on a further analysis of data presented by Samman *et. al.* (1996) was suggested.

$$E_{\max} = 1.6 - 0.016 f_c \qquad \text{equation 2.39}$$

Where E_{max} is the maximum allowable evaporation rate (kg/m^2/hr) and f_c is the compressive strength of concrete (MPa). For C40 concrete equation 2.39 gives a critical rate of 1 kg/m^2/hr which equals the rate given in the ACI report (305R-96) "Hot Weather Concreting."

Interestingly Anderson and Roper (1982) found that construction on a plastic membrane as opposed to on an absorbent sub-base increased the bleed rate, which made the concrete less susceptible to plastic shrinkage cracking.

The plastic shrinkage of a porous media has been modelled by Radocea (1994), but the number of variables involved in modelling the concrete in this semi-fluid state at very early age make accurate modelling very difficult. As plastic shrinkage cracking can be prevented by controlling the environmental conditions under which concrete is cast, it will not be considered further here, however, the maximum evaporation rates given in equation 2.39 must not be exceeded.

2.7.8. Drying shrinkage

Once the paste has begun to set any subsequent loss of moisture from the system will cause internal stresses to be set up which in turn lead to strains. If the stresses exceed the instantaneous strength of the cement paste then cracking occurs. According to Grzybowski and Shah (1989) the drying of porous materials can proceed by 3 mechanisms:

- capillary stress theory, according to which an internal hydrostatic stress increases as the capillary pores become smaller
- disjoining pressure theory, according to which water which is in a micropore must be in equilibrium with the surrounding relative humidity; to reach equilibrium water has to diffuse out of the pore
- diffusion of water, which uses step-by-step integration in time to link moisture loss at a prescribed point to temperature, diffusivity of the material, the pore moisture content and the effect of hydration on the moisture content.

Early drying shrinkage in concrete is believed to be largely due to surface tension in the capillary pore water, whilst long term drying shrinkage is believed to be due to the loss of water adsorbed on the surfaces of hydrated cement paste (Perenchio, 1997). However, at no time is the change in volume of the concrete equal to the volume of water removed (Neville, 1995).

Powers (1968) mentions the role of capillary water in explaining the hysteresis exhibited by concrete under changing humidity, or for the dependence of volume change on the capillary porosity. This latter dependence is also modelled by Shimomura and Maekawa (1997) who relate the shrinkage of concrete to a distribution function of porosity. Care must be taken, however, as Power's definition of capillary pore water also includes some of the water which is held in the gel pores. Any possible effect which may be caused by the water in these pores should be expected to be larger due to the smaller radius and hence the greater hydrostatic force.

Powers (1968) also noted that the drying shrinkage was greater than predicted by the capillary stress theory, introducing the concept of disjoining effects. This was later given a more rigorous mathematical justification based on irreversible surface thermodynamics by Bazant (1970, 1971, 1972a & b).

When the humidity level in concrete drops to low levels, further drying shrinkage is caused by the loss of adsorbed water from the cement particles (Powers, 1968). Solids, as well as liquids, have a surface tension, although the effects of this are normally negligible. However, in the case of very small particles ($r = 1 \times 10^{-6}$ cm), such as the colloidal cement particles found in the cement paste, the change in volume caused by this surface tension can become very large relative to the particles size ($\Delta V/V = 5800 \times 10^{-6}$). The adsorption of water by these particles during hydration reduces the surface tension and allows them to expand. Thus, on drying the particles are once more able to shrink, causing a reduction in the volume of the paste

Many factors control the ultimate shrinkage potential of concrete according to the mechanisms described above. For example, Kasai *et. al.* (1982) have shown that the free shrinkage potential

of concrete made with high early strength cement is greater than for ordinary Portland cement, although super high early strength cements had the lowest shrinkage potential. Concretes with high water/cement ratios have more redundant water which causes increased shrinkage on evaporation (Kasai *et. al.*, 1982; Neville, 1995), whilst reducing the aggregate content or using aggregates which are weak or shrink will also increase the shrinkage (Neville, 1995)

A simple empirical model proposed by Hillerborg was cited in Thelandersson *et. al.* (1998) where the drying shrinkage for an indoor slab can be determined according to equation 2.40 where w_0 is the original water content of the concrete mix in l/m^3.

$$\varepsilon_s = 3.75 \times (w_0 - 50) \times 10^{-6} \qquad \text{equation 2.40}$$

Many models have been developed to provide predictions of the mean shrinkage across structural members, with varying degrees of complexity to account for ambient, material and dimensional effects. Whilst this makes them suitable for determining the long-term behaviour of a structure where the interaction of different elements is considered this approach does not allow the deformation and resultant stress profile in individual sections to be modelled.

McDonald and Roper (1993) carried out a study of the accuracy of several theoretical models of concrete drying shrinkage. They looked at seven theoretical models including ACI 209R-82, Bazant-Panula (1978a-d) and CEB-FIP (1978) comparing the results of predictions with laboratory tests on more than 46 Australian concretes. They found that the more complicated models (Bazant-Panula) did not necessarily give the most accurate results when the concrete mix parameters were not well known. The results show much better agreement between the test data and the Australian code predictions than those from the European or American codes. The authors describe methods of parameter optimisation which can be used to improve the fit of code predictions, although whilst this could be justified for a particular project it is warned that strict relationships to code concepts cannot then be claimed.

Hansen and Almudaiheem (1987) investigated the influence of elastic modulus and aggregate content on the ultimate drying shrinkage of concrete. At their time of writing the most accurate model was by Bazant and Panula (1978a-d) and this still only claimed +/- 31% when predicting creep and shrinkage. An alternative approach using the theory of elasticity and composite theory was suggested. This accounts for the significant influence of the cement paste shrinkage and the aggregate content on the concrete shrinkage. This model predicts that increasing the aggregate content decreases the drying shrinkage. Critically increasing this from 65% to 70%, which is the range for most normal strength concretes, the predicted shrinkage was found to decrease by 18%, although this had yet to be verified by tests.

The Bazant-Panula model was further developed under the auspices of RILEM Technical Committee 107 and published in a series of papers (Bazant and Baweja, 1995a, b & c). This model, B3, will briefly be described to show how the ambient conditions, geometrical and material properties interact to control the drying shrinkage of concrete.

The mean shrinkage in a cross-section at any time t, when drying began at time t_0 is predicted as:

$$\varepsilon_{sh}(t,t_0) = -\varepsilon_{sh\infty} \cdot k_h \cdot S(t) \qquad \text{equation 2.41}$$

Where $\varepsilon_{sh\infty}$ is the ultimate drying shrinkage, k_h is the humidity dependence, and $S(t)$ is a time curve to describe the progression of the shrinkage.

$$S(t) = \tanh\left(\frac{t-t_0}{\tau_{sh}}\right)^{0.5} \qquad \text{equation 2.42}$$

Extending the period of wet curing diminishes the shrinkage on subsequent drying exposure. This is due to the increased stiffness and reduced moisture diffusivity of the concrete (Bazant *et.al.*, 1976). Because of this the value of the shrinkage strain should be inversely proportional to the elastic modulus at the time when the moisture content begins to drop appreciably. Additionally as there is a hygral gradient in all but the thinnest of sections, a delay will be introduced between the beginning of drying and a reduction in the water content at the centre of the sample. This is accounted for by the shrinkage square half-time, τ_{sh}, in the denominator, which is related to the square of the specimen's effective thickness and its shape, and the time at which the shrinkage started as shown in equation 2.44. The addition of 600 to 7 in the numerator of equation 2.43 is supposed to make the constant $\varepsilon_{sh\infty}$ represent the final shrinkage of a 150mm thick slab.

$$\varepsilon_{sh\infty} = \varepsilon_{sh}\frac{E(7+600)}{E(t_0+\tau_{sh})} \qquad \text{equation 2.43}$$

$$\tau_{sh} = k_t(k_s D)^2 \qquad \text{equation 2.44}$$

where the effective cross-sectional thickness, D (in cm), is related to the volume, v and exposed surface area, s according to $D = 2v/s$, whilst k_s is a shape factor equal to 1.00 for an infinite slab. Although an industrial floor is not an infinite slab, the ratio of thickness to plan dimension is sufficiently large for this approximation to be valid.

The time dependence of the shrinkage is reflected in the time coefficient:

$$k_t = 54.98 \cdot t_0^{-0.08} f_c'^{-0.25} \qquad \text{equation 2.45}$$

where t_0 is the time when drying began (days) and f'_c is the mean compressive strength (MPa).

The ultimate drying shrinkage potential, $\varepsilon_{s\infty}$ is dependent on the composition of the concrete as shown in equation 2.46 and also on the time at which the drying began t_0.

$$\varepsilon_{s\infty} = \alpha_1 \cdot \alpha_2 \cdot \left[0.019 \cdot w^{2.1} \cdot (f_c')^{-0.28} + 270\right] \quad \left(\text{in } 10^{-6}\right) \qquad \text{equation 2.46}$$

where α_1 and α_2 relate to the type of cement used and the method of curing - for type I cement and sealed curing these parameters are 1.0 are 1.2 respectively, w is the water content (kg) and f'_c is the mean 28 day cylinder compressive strength (MPa). If only the characteristic design strength f_{ck} is known then $f'_c = f_{ck} + 8.3$ MPa.

Finally the humidity dependence for relative humidity $h \leq 0.98$ is given by:

$$k_h = 1 - h^3 \qquad \text{equation 2.47}$$

Model B3 does not describe well the autogeneous shrinkage in concrete, but this is considered acceptable as at the water/cement ratios used in industrial floor slabs ($w/c \approx 0.5$) this amounts to only around 5% of the drying shrinkage (Bazant *et. al.*, 1988).

Whilst discussing the sensitivity and theoretical basis of the B3 model (Bazant and Baweja, 1995c), the largest source of error in the model predictions was identified as the dependence of the model parameters on the composition of the concrete. Although short-term measurements can be used to update the creep model, this same procedure cannot be applied to the shrinkage model until the final stages of drying, when the curve of ε_{sh} versus log (t-t_0) has begun to level off (Figure 2.13). If testing was ceased before the divergence of the two curves began then it could be wrongly concluded that both samples behaved in the same way.

Because of the uncertainties involved in modelling concrete material properties the authors of the model B3 recommended generating test data using the following coefficients of variation (Bazant & Baweja, 1995a):

$$\begin{aligned} \omega(\varphi_1) &= 23\% \text{ for creep, with or without shrinkage} \\ \omega(\varphi_2) &= 34\% \text{ for shrinkage} \end{aligned} \qquad \text{equation 2.48}$$

As the ambient relative humidity and the concrete compressive strength are also not constant the following coefficients of variation are suggested:

$$\begin{aligned} \omega(\varphi_3) &= 20\% \text{ for relative humidity } h \rightarrow \varphi_3 h \\ \omega(\varphi_4) &= 15\% \text{ for compressive strength } f'_c \rightarrow \varphi_4 f'_c \end{aligned} \qquad \text{equation 2.49}$$

Therefore assuming Gaussian distribution the 95% confidence limits for the drying shrinkage would be given by $1 \pm 1.96 \times 0.34 = 1 \pm 0.67$. The structure should be designed using the 95% confidence limits and not the mean values as this means that only 1 in 20 structures might fail as opposed to 1 in 2 were the mean values to be used for design.

2.7.9. Cracking

The required approach when modelling cracking in concrete is dependant on the application. Smeared cracking is most suitable when load deflection behaviour is required without completely realistic crack patterns, whereas if detailed local behaviour is required then adaptations of the discrete cracking model are more appropriate (Al-Nasra and Wang, 1994).

In the smeared cracking model, tensile failure of an element does not lead to a physical crack, rather the element is still modelled as a continuum. However, the post crack strain is decomposed into two parts, the elastic strain and the crack strain.

$$\varepsilon = \varepsilon^{e} + \varepsilon^{cr} \qquad \text{equation 2.50}$$

The stiffness is reduced to accommodated the presence of cracks. This process is carried out according to the post-crack stress-strain relationship adopted for the concrete. Thelandersson (1998) proposed the following linear softening modulus (equation 2.51).

$$E_T = \frac{E_c}{1 - \left(\frac{2l_{ch}}{l}\right)} \qquad \text{equation 2.51}$$

Where E_c is the elastic modulus of the concrete, l is the length of the structure and l_{ch} is the characteristic length as defined in equation 2.52.

$$l_{ch} = \frac{G_f \cdot E}{f_{ct}^2} \qquad \text{equation 2.52}$$

where G_f is the fracture energy, and f_{ct} is the tensile strength of the concrete. Generally in a finite element application the length l is the element length, chosen to be less than twice the characteristic length. This ensures that the stiffness of a cracked element will always be a negative number (Nagy, 1997).

de Borst and van den Boogaard (1994) carried out a similar analysis to that required here looking at the risk of cracking at early ages in concrete tetrapods used in sea defences. As data which can be used in this sort of analysis is very sparse they detailed an approach which allows the derivation of a consistent formulation accounting for creep and creep fracture of early age concrete.

The early-age concrete material properties are very non-linear in time being related to the degree of hydration, which is dependent on the relationship between evolved heat and the cumulative heat produced. This second function can be modelled in a separate thermal analysis using the same meshed domain as the structural model, although in order to prevent inconsistencies in the stress profile the thermal elements must be of a lower order than the structural elements.

The development of the young's modulus was modelled using equation 2.53, which accounts for its time and temperature dependence.

$$E(t) = E_0 \int_0^t (T/T_0)^7 \left\{1 - \exp\left[(-\beta(t-\tau))/(T/T_0)^6\right]\right\} \dot{r}\, d\tau \qquad \text{equation 2.53}$$

The double power law (equation 2.32 and equation 2.33) was then used to model the development of stresses with time accounting for creep losses.

The fracture energy of concrete increases with maturity, but there is currently insufficient information on this relationship at early ages. For this reason de Borst and van den Boogaard (1994) used a constant value of G_f for all their models.

2.7.10. Thermal properties

A thorough review of the literature has been carried out to identify the thermal parameters to be used in the finite element models. Many investigations into the early-age thermal behaviour of mass-concrete structures have been carried out in order to assess the probability of cracking. Various material parameters have been determined which will be of use in the current investigation. These are discussed briefly below whilst the values found are summarised in Table 2.4.

Some of the concrete properties can be determined using a commercial computer program (Hymostruc). This takes the chemical composition of the cement and the concrete mix design and produces output of the adiabatic hydration curve for the concrete and the maturity dependant thermal properties (van Breugel, 1991).

2.7.11. Thermal expansion and contraction

Thermal expansion and contraction is the change in length of concrete purely as a result of an increase or a reduction in the temperature, although the latter is sometimes incorrectly referred to as thermal shrinkage. In order to prevent confusion with hygral effects here, the terminology contraction and expansion will be used for thermal effects, whilst shrinkage and swelling will be reserved for hygral effects.

Thermal movement can occur during the early life of a concrete structure as the result of two different effects. Firstly, thermal gradients can arise in the structure as the heat generated by the hydrating cement is lost to the environment. As the concrete hardens and the thermal gradients dissipate, stresses arise. Generally this is not problematic for industrial ground floors as they are not directly exposed to sunlight, thus limiting the temperature of the upper surface of the slab. Additionally the limited thickness of the slabs keeps the gradient between the middle and the surfaces of the concrete small. The second process by which thermal movement occurs arises from uniform thermal change. This affects concrete at early ages when the

temperature reduces after cement hydration, and also in the long term due to seasonal ambient temperature changes.

Low heat cements have often been used in the past for mass concrete pours to try and combat these problems. Most contained granulated slag and often less than 50% Portland Cement clinker. In such cases, despite a moderate temperature rise, cracking may still occur because the Young's modulus develops too slowly in the early hardening phase (Springenschmid and Breitenbücher, 1998). Nagy (1997) carried out finite element studies on the stresses at early ages in hydrating concrete concluding that an early development of the elastic modulus was beneficial in preventing tension cracking, whilst concrete which developed high temperatures during hydration caused more cracking. This is because without a rapid growth of the stiffness the concrete cannot develop compressive stress during the heating phase. Therefore, when it cools down the tensile stresses will be greater than the control case.

Temperature changes in concrete cause strains according to equation 2.54, where α_c is the coefficient of thermal expansion for concrete, and δT is the temperature change.

$$\varepsilon_{ct} = \alpha_c \cdot \delta T \qquad \text{equation 2.54}$$

The coefficient of thermal expansion has been found to be largely time dependent (Byfors, 1980) with values reducing by a factor of 7 over the first 128 hours after mixing. A rapid drop was recorded over the first 8 hours from about $70x10^{-6}$ to $20x10^{-6}$ /°C with a further slow reduction until the value of $12x10^{-6}$ /°C was obtained after about 28 hours. This remained constant for the duration of the test (128 hours).

Jonasson and Emborg (1996) and several other investigators discussed by Emborg (1998) also found that the coefficient of thermal expansion and contraction for concrete is significantly different for the first heating and the cooling cycle, although for mature concrete the values converge. Initial coefficients of thermal expansion and contraction of around 9.5-10.5 μstrain/°C and 7.0-8.0 μstrain/°C respectively were found for concrete with a w/c ratio of 0.5. For this reason it was recommended that thermal deformations at early ages should be defined in terms of a coefficient of expansion and a separate coefficient of contraction.

The coefficient of thermal expansion also has a direct dependence on the relative humidity, on the change in temperature, and on aggregate type and content. (Byfors, 1980). The latter dependence accounts for the range of values from about $7x10^{-6}$ to $13x10^{-6}$ given by Neville (1995). Experiments by Powers & Brownyard (1946) have shown the value of α_c to be at a minimum when the concrete is fully saturated or fully dried, but to have a larger value for intermediate moisture contents.

A value of 10 μstrain/°C is generally used for concrete in the absence of specific test data.

2.7.12. Thermal conductivity, λ_c

This property of concrete depends on the moisture content, content and type of aggregate, porosity, density and temperature. Byfors (1980) concluded that there was no relationship between concrete maturity and the thermal conductivity, with any measured changes being due to changes in moisture content. For ordinary concrete he suggested a value of 2.4 W/m.K, whilst (van Breugel, 1998) suggested values in the range 1.0 to 3.0 W/m.K were typical.

2.7.13. Specific heat capacity

This property of concrete is also affected by the moisture content, although unlike the thermal conductivity the aggregate type tends to have little effect. Neville (1995) suggested values in the range of 840 to 1170 J/kg.K.

2.7.14. Boundary conditions

The same values quoted by Thelanderson *et. al.*(1998) were also used by Nagy (1997) and quoted in Pettersson (1998). Truman *et. al.* (1991) didn't quote an actual wind speed, but for a condition with wind crossing exposed concrete surface suggested 23 $W/m^2 \cdot K$. Ayotte *et. al.* (1997) gave the same value for exposed concrete, but recommending a reduced value when formwork was still in place. Truman *et. al.* (1991) carried out a parameter study to find suitable values for the interfaces between materials below surface level. In order to obtain free heat transfer between layers, thus making the rate dependant on the thermal properties of both sides of the boundary, they found a value in excess of 173 $W/m^2.K$ was necessary.

Table 2.4 – Summary of material thermal properties

Material Property	Concrete	Sub-base	Subgrade	Reference
Thermal conductivity, λ (W/m.K)	1.37	2.22	1.5	Rees *et. al.* (1995)
	1.76	-	-	Khan *et. al.* (1998)
	1.3-1.7	-	-	Mirambell (1990)
	2.0	2.6[1]	-	Ayotte *et. al.* (1997)
	2.1	-	-	Thelandersson *et. al.* (1998)
	2.0	2.6[2]	1.37	Truman *et. al.*(1991)
	1.5	-	-	Pettersson (1998)
	2.4	-	-	Byfors (1980)
	1.9	1.8	1.28	CIBSE (1999)
Specific heat capacity, *c* (J/kg.K)	880	930	2000	Rees *et. al.* (1995)
	770	-	-	Khan *et. al.* (1998)
	1006	670	-	Ayotte *et. al.* (1997)
	1000	-	-	Thelandersson *et. al.* (1998)
	880	-	1886	Truman *et. al.*(1991)
	1000	-	-	Pettersson (1998)
	1000	-	-	Byfors (1980)
	1006	-	-	Neville (1995)
	840	840	880	CIBSE (1999)
Density, ρ (kg/m^3)	2400	2000	1500	Rees *et. al.* (1995)
	2480	-	-	Khan *et. al* (1998).
	2370	2760	-	Ayotte *et. al* (1997).
	2350	-	-	Thelandersson *et. al* (1998)
	2400	-	2098	Truman *et. al* (1991).
	2350	-	-	Pettersson (1998)
	2300	2240	1460	CIBSE (1999)
Thermal coefficient of expansion, α (x 10^{-6} /°C)	7-11.5	-	-	Mirambell (1990)
	10	-	-	Thelandersson *et. al.*(1998)
	8-15	-	-	Neville (1995)
	10	-	-	Pettersson (1998)
Concrete air boundary (W/m^2.K)	8.3 (side) 9.3 (bottom) 6.2 (top)			Khan *et. al.* (1998)
	4.8 (with formwork) 23 (exposed)			Ayotte *et. al.*(1997)
	5.0 (wind speed < 0.1 m/s)			CIBSE (1999)
	7.7 (wind speed 0.5 m/s) 13.5 (wind speed 2 m/s)			Thelandersson *et. al.*(1998)
	20.0			Faraggi *et. al* (1987).
Interfaces under slab (W/m^2.K)	173 [3]			Truman *et. al.*(1991)

[1] Rock foundation not granular aggregate

[2] Rhodes (cited in Truman)

[3] This value was found by Truman *et. al.* to allow free heat flow across the boundary. Thus the thermal gradient is controlled by the thermal properties of the materials on either side of the boundary.

2.8. Mathematical modelling of slab behaviour

2.8.1. Introduction

> Obviously, the usefulness of the data generated by these [finite element] programs is determined by how well the critical parameters are predicted, modelled and implemented into a numerical method since reliable experimental data on a mass-concrete structure is hard to find. Truman *et. al.* (1991)

The modelling of the slab-on-grade problem should be approached using non-linear, viscoplasticity concepts accounting for numerous random discontinuities. Such an approach, however, is quite unfeasible, and given the complexity of the problem and the uncertainties inherent in its definition only the simplest of idealisations can really be justified (Ioannides & Khazanovich, 1998).

For each of the properties under investigation the simplified approaches suitable for implementation in spreadsheets will first be discussed before more complicated numerical implementations are presented. In many cases the simplified approaches can be justified. However, their application at early ages when the concrete material properties are changing rapidly is often very difficult.

2.8.2. Thermal changes

Analyses have been carried out on mass concrete structures to assess the likelihood of thermal cracking due to the heat of hydration (Trueman *et. al.*, 1991; de Borst & van den Boogaard, 1994). However, only one study could be found on the on the effects of frictional restraint on slabs as they hardened (Eierle & Schikora, 1999), and this looked at two cases – firstly the edge of the slab and secondly a fully restrained section in the middle of the slab.

Choubane and Tia (1995) compared the stresses in a slab resulting from a linear and a non-linear temperature distribution. The tensile stresses resulting from the linear distribution were found to be higher for the daytime condition and lower for the night-time condition than those determined using a non-linear temperature distribution. As the critical tensile stresses were found to occur during the daytime (Richardson & Armaghani, 1987) this would result in a linear temperature distribution underestimating the load carrying capacity of the slab, therefore making this approach a conservative one.

Thompson *et. al.* (1987), Armaghani *et. al.* (1987) Venkatasubramanian (1963), Liang and Niu (1998) and Thomlinson (1940a & b) all studied the periodic nature of temperature variations in concrete slabs. Thomlinson proposed a method for predicting the temperature distribution in a

semi-infinite slab system subject to a periodic surface temperature variation. The shortcomings of this approach were identified by Liang and Niu. (1998) as:

- It assumed that the pavement and the subgrade had the same thermal properties, and
- It ignored the difference in temperature between the air and the slab surface due to gas phase resistance.

Although the simplified approach results in a linear temperature distribution Lang (1941) and Liang and Niu (1998) have shown that the differences between the linear and non-linear temperature distributions are minimal unless the thermal changes in the slab are very rapid.

As the non-linear methods often involve very analytical closed-form solutions, which are time consuming and complicated to solve for every case, and the differences between the non-linear and linear solutions will be minimal for indoor slabs, the following techniques will be used for comparison with the site data.

Two periodic cycles control the ambient temperature; namely the annual seasonal change and the daily diurnal change. Hulsey and Powell (1993) proposed an equation of the form of equation 2.55 to predict the annual air temperature variation, where t is the number of days into the year. Liang and Niu (1998) suggested values for the variables of 13.9°C, 12.8°C and 201.5 days for A, B and γ' respectively.

$$T_a = A\cos\left(2\pi\left(t-\gamma'\right)/365\right)+B \qquad \text{equation 2.55}$$

The daily temperature variation can be predicted using an equation of the same form but with 24 in the denominator replacing the 365. Assuming this form of variation Thomlinson's method allows the temperature distribution at different depths to be calculated.

$$\theta = \theta_0 e^{-\frac{x}{h}\sqrt{\frac{\pi}{T}}} \sin\left(\frac{2\cdot\pi}{T}t - \frac{x}{h}\sqrt{\frac{\pi}{T}}\right) \qquad \text{equation 2.56}$$

where θ is the temperature on a plane distance x from the slab surface, at time t, θ_0 is the amplitude of the temperature variation at the slab surface, h^2 is the diffusivity of the material and T is the time period of the temperature cycle. De Schutter and Tearwe (1995) determined the thermal diffusivity of concrete after 7 days to be $0.029 m^2/h$., thus giving a theoretical daily thermal distribution for depths up to 2m below the slab surface as shown in Figure 2.14.

Zero times for the daily variation were found to be 08:00 and 09:30 by Thomlinson and Mirambell(1990) respectively, whilst the corresponding time for the annual variation was found to be the end of April by Thomlinson and mid-April by Liang & Niu.

Lachemi and Aïtcin (1997) monitored the temperatures in a concrete viaduct during construction to validate a finite element model. This model was then used to perform a

parametric study on the influence of ambient and fresh concrete temperature on the maximum temperature obtained and the thermal gradient within the structure. They found that for the same ambient temperature the higher the fresh concrete temperature the faster the peak temperature is reached. However, the influence of the ambient environment appears to be less significant as for a given initial temperature the peak is reached at the same time irrespective of the ambient temperature. A high ambient temperature and a low concrete temperature were both found to minimise the thermal gradient within the structure. Another way of minimising the thermal gradients within concrete structures was investigated by Loo *et. al.* (1995). They used computer models to assess the effects of cooling layers of concrete on the maximum temperatures obtained in thick concrete pours. When analysing the effects of different material parameters they noted the much higher rate of heat loss with a wet soil subgrade than a dry soil subgrade. The dry soil subgrade acts as an insulator, but the high specific heat capacity of the water means the wet soil requires a large amount of heat to warm up.

When modelling the temperature distribution in slab, sub-base and subgrade systems Pufahl *et. al.* (1990) also found that the analysis was very sensitive to the properties of the boundary between the base course and the subgrade. It was found that the predicted temperature distribution could be made to match the measured distribution by adjusting the flux across this boundary. Although the authors used this technique to get a very good fit for this set of data, there is no guarantee that the values arrived at will be of any use for other data sets.

Alivazadeh-Farhang and Silfwerbrand (1998) tested beams exposed to thermal gradients and mechanical loads and combinations of the two. The results can be confusing because, although it was demonstrated that the individual stresses can be superimposed to accurately determine the resultant stress state in the test beams, the tests which were conducted do not replicate ground supported slabs and pavements. The test samples were simply supported and were loaded until they cracked, with the failure occurring in the bottom of the beams, whereas the majority of the failures of ground supported slabs and pavements are due to curled edges cracking from the top face under load. The sensitivity of the structural analysis to the boundary conditions, which in turn depend strongly on the thermal load in the slab, was emphasised by Faraggi *et al.* (1987) and Mirambell (1990). They showed that it is not possible to analyse thermal effects and applied loading separately with the results added using superposition.

2.8.3. Curling and warping

Before describing these effects the terms curling and warping will first be defined. According to ACI Publication SP-19 (1978) 'Cement and Concrete Terminology' :

curling – the distortion of an originally essentially linear or planar member into a curved shape such as the warping of a slab due to creep or differences in temperature or moisture content in the zones adjacent to its opposite faces.

warping – a deviation of a slab or wall surface from its original shape, usually caused by temperature or moisture differentials or both within the slab or wall. (See also curling).

Therefore, as floor slabs are initially essentially linear, these terms can be used interchangeably.

Eisenmann and Leykauf (1990) identified the three possible causes of slab curling as being:

1. Negative temperature gradient (surface colder than the bottom of the slab);
2. Hardening of the paved concrete at a positive temperature gradient (higher zero stress temperature at the top of the slab than the bottom); and
3. Shrinkage at the slab surface and/or moisture expansion at the slab bottom

The first cause of curling, where the surface of the slab is cooler than the bottom of the slab, occurs at night. However, as industrial floors are enclosed and, therefore, not exposed to direct sunlight, they are not subjected to the large daily temperature variations required to develop this form of curling. Furthermore, by constructing the floor slab inside a completed building, the top surface of the slab cannot be warmed by direct sunlight. This prevents the concrete hardening with an elevated surface temperature, which is the second cause of curling. This leaves non-uniform drying shrinkage as the main cause of curling in industrial ground supported slabs.

As a slab begins to dry from its top surface, the differential strain causes the slab to take on a dished shape, resulting in the end sections of the slab rising off the sub-base. At some length, defined as the critical length, L_{cr}, the internal stresses arising from the non-uniform shrinkage are equal and opposite to the stresses resulting from the self-weight of the unsupported end section of the slab. If the slab length does not exceed the critical length, then its entire length will be curled (Figure 2.15); however, if the critical length is exceeded, the end sections to a length of $L_{cr}/2$ will be curled, and the middle section of the slab will be flat (Figure 2.16).

For a given slab, the critical length is related to the size of the non-uniform strain, the slab thickness and the concrete elastic modulus. Eisenmann and Leykauf calculated that the critical length of slab which is liable to curl due to a negative thermal gradient is:

$$L_{cr} = 167 \cdot h \cdot \sqrt{\alpha_c \cdot T_{grad} \cdot E_c} \qquad \text{equation 2.57}$$

And due to hygral gradients caused by non–uniform shrinkage from the upper surface of the slab:

$$L_{cr} = 409.6 \cdot \sqrt{\frac{t \cdot \varepsilon_s \cdot (h - h_d) \cdot E_c}{h}} \qquad \text{equation 2.58}$$

where L_{cr} is the critical length (mm), T_{grad} is the temperature gradient (K/mm), h is the slab thickness (mm), α_c is the thermal coefficient of expansion (assumed to be 10 μstrain/°C), h_d is the thickness of slab over which the drying shrinkage, ε_s, is assumed to take place (mm) – normally assumed less than 50mm - and E_c is the elastic modulus (N/mm^2). Because this theory is based on beams resting on a rigid base it over predicts the actual warping deflections seen in slabs. However, the authors found good agreement between theoretical prediction and observations.

Several months after construction, drying shrinkage will affect the whole of the slab, and not just the surface region. This can be approximated by a linear shrinkage profile through the full depth of the slab. Although, as previously stated, industrial floors are generally not exposed to thermal gradients that are able to cause warping, equation 2.57 can be used to give a better approximation of the long-term drying shrinkage effects than equation 2.58. This can be done by converting the drying shrinkage into an equivalent thermal gradient (ETG), according to equation 2.59, which is then substituted for T_{grad} in equation 2.57.

$$ETG = \frac{\varepsilon_{sh}}{\alpha_c \cdot h} \qquad \text{equation 2.59}$$

Leonards and Harr (1958) used equivalent thermal gradients to represent the effects of the moisture and temperature differentials in concrete slabs assuming that the effects of both were linearly distributed. They found gradients of between 0.66 and 1.31 °C/cm for enclosed ground floor slabs.

Pettersson (1998) considered the case of a ground-supported slab exposed to positive thermal gradients, determining the critical length to be as shown in equation 2.60. L_{cr}, h, and α_c are as defined above, whilst ΔT is the temperature difference between the top and bottom faces of the slab. ρ_c is the density of the concrete (assumed 24.000 x 10^{-6} kg/mm^3), g is the acceleration due to gravity (9.81 m/s^2) and f is a load factor (taken as 1 in this case as only self weight is considered).

$$L_{cr} = \sqrt{\frac{4 \cdot \alpha_c \cdot E_c \cdot \Delta T \cdot h}{5 \cdot \rho_c \cdot g \cdot f}} \qquad \text{equation 2.60}$$

These equations are very similar and rearranging equation 2.60 into the form of equation 2.57 gives:

$$L_{cr} = \sqrt{\frac{4 \cdot h^2}{5 \cdot \rho_c \cdot g \cdot f}} \cdot \sqrt{\alpha_c \cdot E_c \cdot \frac{\Delta T}{h}} \qquad \text{equation 2.61}$$

Equating the first group of terms in each equation to solve for f gives 1.2 showing that equation 2.57 is a simplified solution to equation 2.60 for the factored dead load used in design. The relationship between the slab thickness, the temperature gradient and the critical slab length can be seen in Figure 2.17.

Eisenmann and Leykauf also determined the vertical deflection resulting from the conditions determined in equation 2.57 and equation 2.58. These equations neglect the influence of Poisson's ratio, which is only applicable for a beam and not for a slab, however, the inaccuracy is only small.

$$a_t = 0.125 \cdot \alpha_c \cdot \Delta T \cdot (L_{cr})^2 - 2.250 \cdot 10^{-6} \frac{(L_{cr})^4}{E \cdot h^2} \qquad \text{equation 2.62}$$

$$a_s = 0.75 \cdot \frac{t \cdot \varepsilon_{sh} \cdot (h-t) \cdot {L_{cr}}^2}{h^3} - 2.25 \cdot 10^{-6} \frac{{L_{cr}}^4}{E \cdot h^2} \qquad \text{equation 2.63}$$

where a_t and a_s are respectively the temperature and drying induced shrinkage and the other parameters are as previously defined. Where the slab length is less than L_{cr} the actual slab length should be used.

Rollings (1997) also calculated the vertical movement due to thermal gradients to be

$$a_t = \frac{\Delta\varepsilon_{sh} \cdot L^2}{8 \cdot h} \qquad \text{equation 2.64}$$

Where $\Delta\varepsilon_{sh}$ is the differential movement between the upper and lower faces of the slab and L and h are the length between joints and slab thickness respectively (m).

Barenberg and Zollinger (1990) concluded that for jointed PCC pavements the combined curl and warping strains can be as large or larger than the anticipated load strains.

Many of the traditional slab analysis formulas assume that the slab remains fully supported by the sub-base as it is loaded. Pernetti (1998) proposed a simplified analysis method which accounts for the loss of sub-base support and does not require complex analyses. However, only loss of support due to a positive thermal gradient is considered. This means that the approach cannot be modified to analyse the loss of support due to curling or initial thermal gradients leading to negative curvature in the slabs.

2.8.4. Restraint

Strains in concrete, irrespective of their cause, do not cause stresses until they are restrained. This can be in the form of internal restraint arising from non-linear strain distributions, or external restraint from supports, adjacent members etc.

Other than the restraint due to friction between the slab and the underlying material, external restraint is not accounted for in design guidance like TR34 when carrying out the detail design.

This will lead to underestimation of the stress state in the concrete before service loads are applied reducing the factor of safety for the structural design, and can lead to unaccounted cracking in the slab.

External restraint at the edges or the ends of the slab is almost always going to be present to some degree in real construction projects.

The models in the previous section deal only with the theoretical free drying shrinkage. However, as a result of this restraint two further classes of stress arise, namely:

- internal restraint stress due to non-linearity in the thermal and hygral gradients, and
- external restraint stress caused by abutment against older structures or frictional ground restraint.

For concrete industrial ground floor slabs the thermal gradient is generally small as the section in not thick enough to allow the build up of significant heat, so the majority of the restraint comes from sub-base friction (as discussed in the following section) or from adjacent pours. The service loads can increase the degree of restraint significantly, although this is also not currently considered in the design guidance.

2.8.5. Frictional ground restraint

The determination of joint spacing and the calculation of reinforcement requirements as provided for in TR34 (Barnbrook *et. al.*, 1994) is done according to a triangular stress distribution proposed by Losberg (1978) amongst others. This assumes that all restraint is caused by frictional interaction between the slab and the sub-base giving a load distribution per meter width of slab as previously given by equation 2.1 (reproduced below). This approach determines the reinforcement based on the maximum expected stresses, leading to an inefficient design for the majority of the slab length. Kunt and McCullough (1990) recommended using reduced friction values to calculate the required reinforcement at sections away from the slab middle. This requires a computational approach to allow for material and environmental variations and is not practical.

$$F_t = \mu \cdot \Delta \cdot h \cdot \frac{L}{2} \qquad \text{equation 2.1 (repeated from before)}$$

Timms (1963) experimented with different friction reducing mediums for use under slabs to establish the variability in restraint. The test slabs were loaded at different rates and under different seasonal conditions establishing that the frictional resistance to the first movement was appreciably higher than for subsequent movements, although neither the seasonally dependant moisture content of the sub-base or the slab thickness had a measurable effect. Friberg (1954), Kunt and McCullough and Pettersson (1998) discovered a reduction in the

friction coefficient with increasing slab thickness, whilst the former also found a reduction with increased slab length. Friberg found maximum values for the coefficient of friction for a slab cast on a paper slip layer of 1.5. All of the authors found similar values for the coefficient of friction as shown in Table 2.5.

Table 2.5 - Comparison of coefficients of friction, μ

Type of sub-base	Reference		
	Timms	Kunt & McCullough	Pettersson
Cement treated granular base	-	52.3	-
Flexible sub-base	3.2	5.0	-
Asphalt-stabilised granular base	2.5	3.8	-
Lime-treated clay	-	2.9	-
Untreated clay	2.1	1.9	-
Granular sub-base	1.7	-	1.5 - 2.9*
Sand	1.0	-	0.85 - 1.2*
Polyethylene sheeting	0.9	-	0.5 – 1.0*

*The higher value is for self-weight only whilst the lower value is for 5 x self-weight.

Pettersson carried out further laboratory tests to determine the rate at which the frictional restraint evolves as this is a function of the shear stiffness of the boundary. Even assuming a constant limiting coefficient of friction, μ_{max}, the rate at which this is achieved can be quite different (Figure 2.18). Values obtained for a crushed aggregate sub-base covered by a polythene slip membrane were $K_{s1} = 3.2$ and $K_{s2} = 15.6$. Using a bilinear approximation based on $K_{s4} = (K_{s1} + K_{s2})/2$ gives a shear stiffness of 9.4 MN/m^3 and $\mu_{max} = 1.0$.

Once the frictional restraint to movement has been determined the actual movement at any point in a slab, d_x , due to a given thermal change can be calculated according to equation 2.65 as shown in Figure 2.19.

$$d_x = \frac{\alpha_c \cdot \delta T}{2A}(A - z)^2, \quad A = \frac{E_c \cdot \alpha_c \cdot \delta T}{\Delta \cdot \mu}, \quad d_x \geq 0 \qquad \text{equation 2.65}$$

where α_c is the thermal coefficient of expansion of concrete, E_c is the concrete elastic modulus, δT is the temperature change and z is the distance from the end of the slab. A is the active length of slab where the thermally induced stresses are greater than the frictional restraint stresses thus allowing movement to occur. Nagataki (1970) found that the measured restrained strain between the free end of a slab and a section 230ft (70m) from the end was 110 x 10^{-6} which was 1.7 times the value calculated using elastic theory, a friction coefficient of 1.2 and an elastic modulus of 4.5 x 10^6 psi (31GPa).

As previously mentioned ACI 325 Subcommittee IV (in Ytterburg, 1987c) concluded that longitudinal and transverse dowels may result in a restraint stress of 0.17MPa. This means that the stress state at the ends of a slab may not be zero as currently assumed in all the design guidance. This will lead to increased stresses at other sections in the slab increasing the risk of cracking. Additionally reinforcement only designed to carry the tensile stresses arising from frictional restraint may be insufficient to control cracks resulting from some other form of restraint.

2.8.6. Warping restraint

A parameter study carried out by Mirambell (1990) showed that the maximum principal stress due to thermal gradients was not significantly altered by the subgrade modulus. Increasing the slab thickness reduced the stresses and, conversely, increasing the slab length up to the critical length increased the stress. Once the critical length was reached the stresses were not increased by further increases in length. The concrete thermal conductivity was not found to alter the temperature or stress distributions significantly, although a linear relationship was found between the thermal coefficient of expansion and the principal stress.

Losberg (1978) showed that the stresses due to warping restraint could be calculated according to equation 2.66, where $\delta\varepsilon_t$ is the difference in shrinkage or temperature strain between both surfaces of the slab. For indoor slabs on grade he predicted uneven shrinkage can give warping stresses, $\sigma_w = 0.34$ N/mm^2.

$$\sigma_w = \frac{E_c}{1-\nu}\frac{\delta\varepsilon_t}{2} \qquad \text{equation 2.66}$$

Nagataki (1970) found that warping strains reduced with distance from the free ends of a test slab, thereby indicating increasing warping restraint. He concluded that warping was almost fully restrained about 10ft (3m) from the end of a slab. Typical stresses resulting from this restraint were 230psi (1.59 N/mm^2) compressive and tensile stresses at the bottom and top faces of the slab respectively. When added to drying shrinkage stresses these form a significant proportion of the concrete tensile strength. Pettersson (1998) showed how the maximum restraint stress in a slab exposed to linear thermal gradients varied as a function of the critical length (equation 2.67).

$$\sigma = 1.2\sigma_w \cdot \left(\frac{L}{L_{cr}}\right)^2, L \le L_{cr} \qquad \text{equation 2.67}$$

Once the critical length is exceeded the maximum stress is treated as a constant with a value of $1.2\sigma_{mo}$.

Curling and warping stresses have been modelled by Thomlinson (1940a & b) for slabs with conditions of no- and full end restraint to both longitudinal and warping movements. Assuming a periodic variation in the daily and annual temperature cycles the internal, warping and end-restraint stresses could be determined as follows.

Resultant stress = Internal stress + Stress due to end restraint + Stress due to warping restraint

$$\sigma_r = A_i \sin\frac{2\pi}{T}(t+t_i) + k_e A_e \sin\frac{2\pi}{T}(t+t_e) + k_w A_w \sin\frac{2\pi}{T}(t+t_w) \qquad \text{equation 2.68}$$

where T is the duration of the time period, t is the time in to the time period and A_i, A_e, A_w, t_i, t_e and t_w are determined according to equations 8 to 10, 12 and 15 in Thomlinson (1940a) which are not repeated here for brevity. The parameters k_e and k_w are restraint factors usually varying between 0 and 1 – with 1 being full restraint – although for some slabs on a deformable sub-base the value of k_w can reach 1.1 (Westergaard, 1929). Once the values for k_e and k_w have been fixed equation 2.68 can be reduced to the form:

$$\sigma_r = A_r \sin\frac{2\pi}{T}(t+t_r) \qquad \text{equation 2.69}$$

where

$$A_r = \left[\left(A_i \sin\frac{2\pi}{T}t_i + k_e A_e \sin\frac{2\pi}{T}t_e + k_w A_w \sin\frac{2\pi}{T}t_w\right)^2 + \left(A_i \cos\frac{2\pi}{T}t_i + k_e A_e \cos\frac{2\pi}{T}t_e + k_w A_w \cos\frac{2\pi}{T}t_w\right)^2\right]^{0.5} \qquad \text{equation 2.70}$$

and

$$\tan\frac{2\pi}{T}t_r = \frac{A_i \sin\frac{2\pi}{T}t_i + k_e A_e \sin\frac{2\pi}{T}t_e + k_w A_w \sin\frac{2\pi}{T}t_w}{A_i \cos\frac{2\pi}{T}t_i + k_e A_e \cos\frac{2\pi}{T}t_e + k_w A_w \cos\frac{2\pi}{T}t_w} \qquad \text{equation 2.71}$$

The solution to these equations can be expressed in dimensionless form (Figure 2.20 and Figure 2.21) using the dimensionless daily stress and the thickness coefficient, γ. The actual stresses are found by multiplying by $\frac{\alpha_c \cdot E_c \cdot \theta_0}{1-\nu_c}$, whilst the thickness, d is found from equation 2.72 where h^2 is the thermal diffusivity of the concrete (thermal conductivity/heat capacity per unit volume) and T is the time period.

$$d = \gamma \cdot h\left(\frac{T}{\pi}\right)^{0.5} \qquad \text{equation 2.72}$$

The time offset from the top surface behaviour is also plotted on the graph for the daily cycle. Thus it is possible to determine not only the magnitude of the maximum stresses, but also the time at which these stresses will occur.

Thomlinson stated that no general recommendations could be made on which size of slab was best as this depended on the magnitude of the applied loads and the thermal and hygral induced stresses. As part of this study the effects of reinforcement in the section were studied. The numerical analysis showed that the warping and end restraint stresses did not vary by

more than 8% from those of the unreinforced slab. As the reinforcement did little to alter the warping and end restraint stresses it was recommended that this 'temperature' reinforcement was best placed at mid-depth in the slab to try and control any large cracks should the concrete be stressed up to its ultimate strength.

Kelley (1939) [Quoted in NHCRP report 372] found that for slabs shorter than 5.2m for k = 27 kPa/mm and less than 4m for k = 81 kPa/mm, temperature curling stresses actually increased with increasing k. This trend was also reported by Al-Nasra and Wang (1994) and reflects the inability of the slab to settle into the sub-base, thus increasing the proportion of the slab which is cantilevered off the ground.

2.8.7. Internal restraint

Internal restraint arises due to non-linearity in the thermal or hygral gradients in the slab. Thomlinson also investigated these effects, however, Liang and Niu (1998) have shown that in concrete slabs the thermal gradients can be approximated well by linear equations as non-linearities are small. Drying of the slab is a long-term process and, although initially this results in non-linearities, many of the finite element analyses of slabs on grade ignore this as the deviation from a linear profile is small (Al-Nasra & Wang, 1994; Kim *et. al.*, 1998 & Al-Nasra, 1997).

2.8.8. Age adjusted effective modulus method

Formulae have already been presented which allow the determination of the elastic modulus at a given time, $E_c(t)$ and the creep effects of a load applied to the concrete at this time. However, these relationships on their own do not allow the analysis of problems where the load is gradually applied, or varies with respect to time. Figure 2.22 (Kovler, 1997) shows the difference in creep strain resulting from a constant stress and a gradually applied stress.

In order to predict these creep effects Trost (1967) and Bazant (1972c) developed the age adjusted effective modulus method (equation 2.73). This uses the creep coefficient $\phi(t,t')$, which is the ratio of the creep strain to the instantaneous elastic strain in a specimen subjected to constant sustained stress, and introduces an ageing coefficient, $\chi(t, t')$ to account for the non-uniformity of the stress over time.

$$\bar{E}_{ce}(t,t') = \frac{E_c(t,t')}{1+\chi(t,t')\cdot\phi(t,t')} \qquad \text{equation 2.73}$$

The creep coefficient is determined according to equation 2.74, whilst the elastic modulus, $E_c(t,t')$ is determined as previously shown in equation 2.30.

$$\phi(t,t') = E_c(t,t')\cdot J(t,t') - 1 \qquad \text{equation 2.74}$$

The ageing coefficient is dependent on the age at first loading, the member geometry, the duration of loading and the drying conditions amongst other factors. Gilbert (1988) shows the range of values to be 0.6 to 0.9. However, for many practical applications this coefficient can be taken as constant and equal to 0.8 (Kovler, 1997).

2.9. Summary

Following this investigation of the literature, it is apparent that the current design guidance available to engineers is inconsistent in its recommendations, and seems fundamentally flawed in its separation of the detail and structural design.

The detail design takes as its starting point the assumption that the concrete is subjected to sufficient restraint to the inherent shrinkage processes to cause cracking. However, the structural design assumes a homogeneous and uncracked section. The empirical modifications to Westergaard's theory account for loss of support but do not allow for residual stresses from restrained longitudinal shrinkage or curling, whilst Meyerhof's formulae account for neither effects.

No published research could be found on the non-structural behaviour of industrial floors; either with respect to their thermal behaviour or the magnitude and timing of concrete shrinkage and joint movements. This may explain why much of the detail design guidance is empirical. The use of the enhanced k value in the structural design is curious, given that in this case there was research – dating back to the 1950s – showing that this was not justified.

A large body of work relating to the instrumentation of concrete pavements in the USA and South America was found, although much of this related to the monitoring of joint movements. Almost all of these studies were carried out after construction, so little guidance on the potential problems of in-situ instrumentation was identified.

A large number of mathematical relationships were found to describe the time and maturity dependant material characteristics of concrete, and the thermal and structural relationships between the concrete and its environment. This thesis does not aim to further develop these relationships; rather they will be used to predict the early-age behaviour of concrete ground floor slabs for verification against site data.

To this end, this study also aims to address the lack of data on the non-structural behaviour of concrete floors, which will in turn allow a better understanding of the intrinsic stresses affecting their structural load capacity.

a – formed free movement joint

b – sawn free movement joint

Figure 2.1 - Types of free movement joint

a – formed restrained movement joint

b – sawn restrained movement joint

Figure 2.2 - Types of restrained movement joint

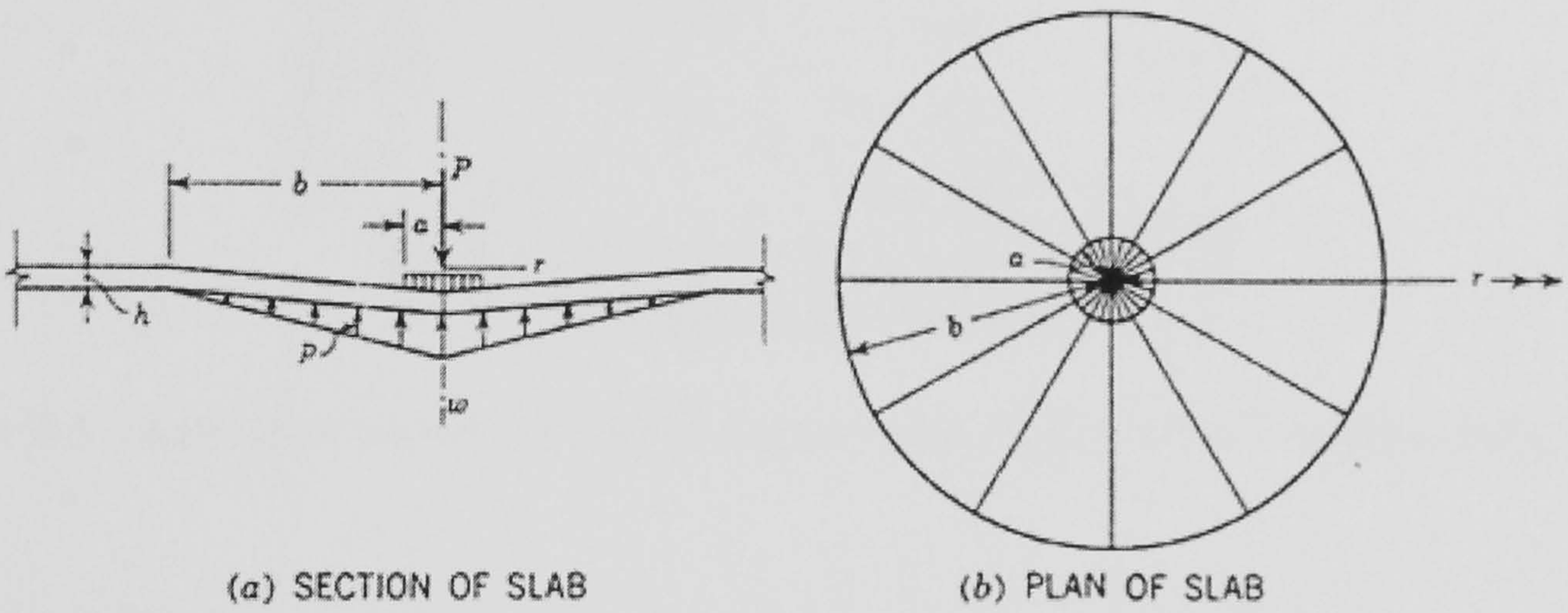

(a) SECTION OF SLAB

(b) PLAN OF SLAB

Figure 2.3 - Yield line failure pattern for an internal load (Meyerhof, 1962)

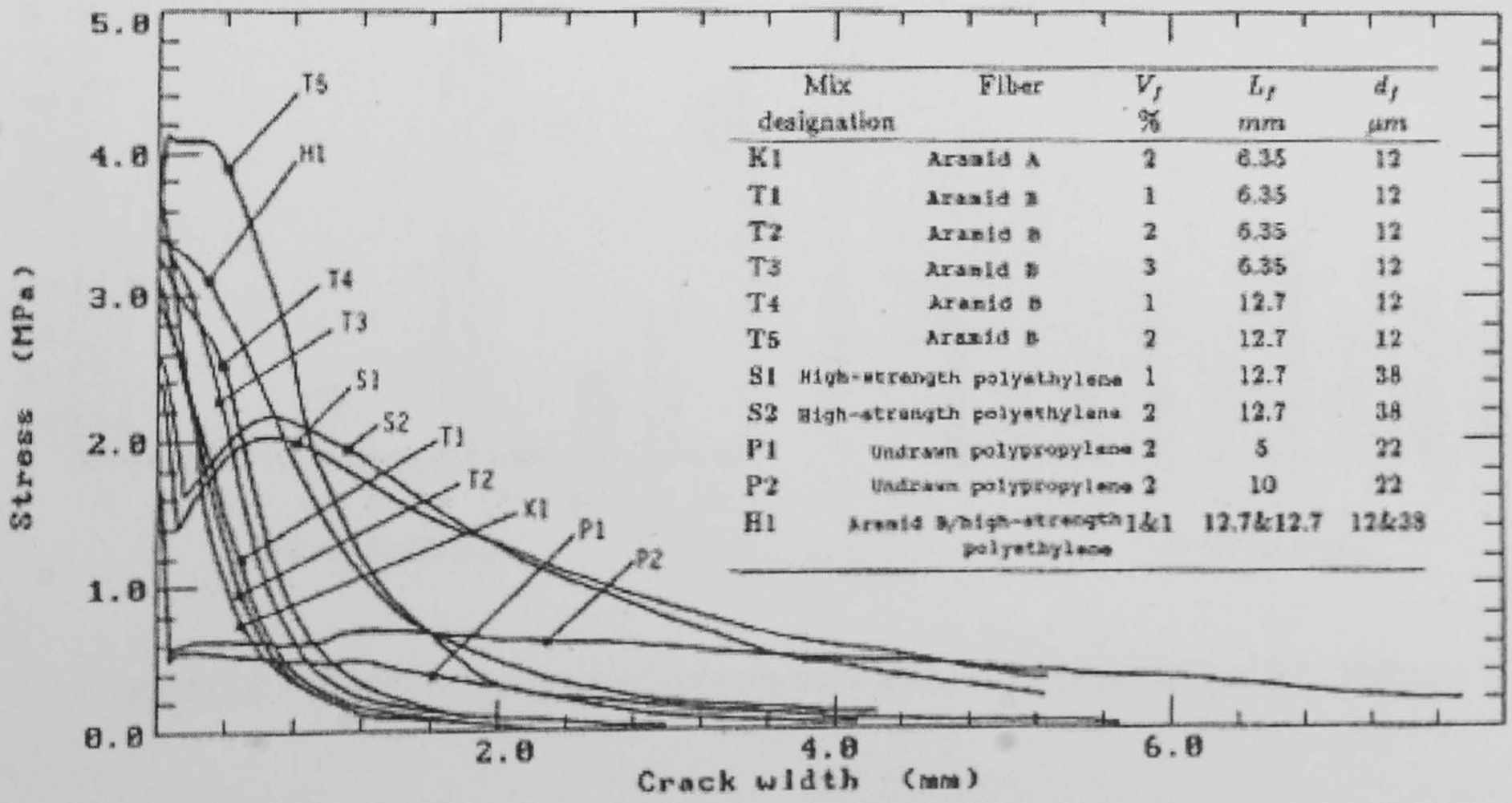

Mix designation	Fiber	V_f %	L_f mm	d_f μm
K1	Aramid A	2	6.35	12
T1	Aramid B	1	6.35	12
T2	Aramid B	2	6.35	12
T3	Aramid B	3	6.35	12
T4	Aramid B	1	12.7	12
T5	Aramid B	2	12.7	12
S1	High-strength polyethylene	1	12.7	38
S2	High-strength polyethylene	2	12.7	38
P1	Undrawn polypropylene	2	5	22
P2	Undrawn polypropylene	2	10	22
H1	Aramid B/high-strength polyethylene	1&1	12.7&12.7	12&38

Figure 2.4 - Stress versus crack separation curves for FRC (Wang et. al.,1990)

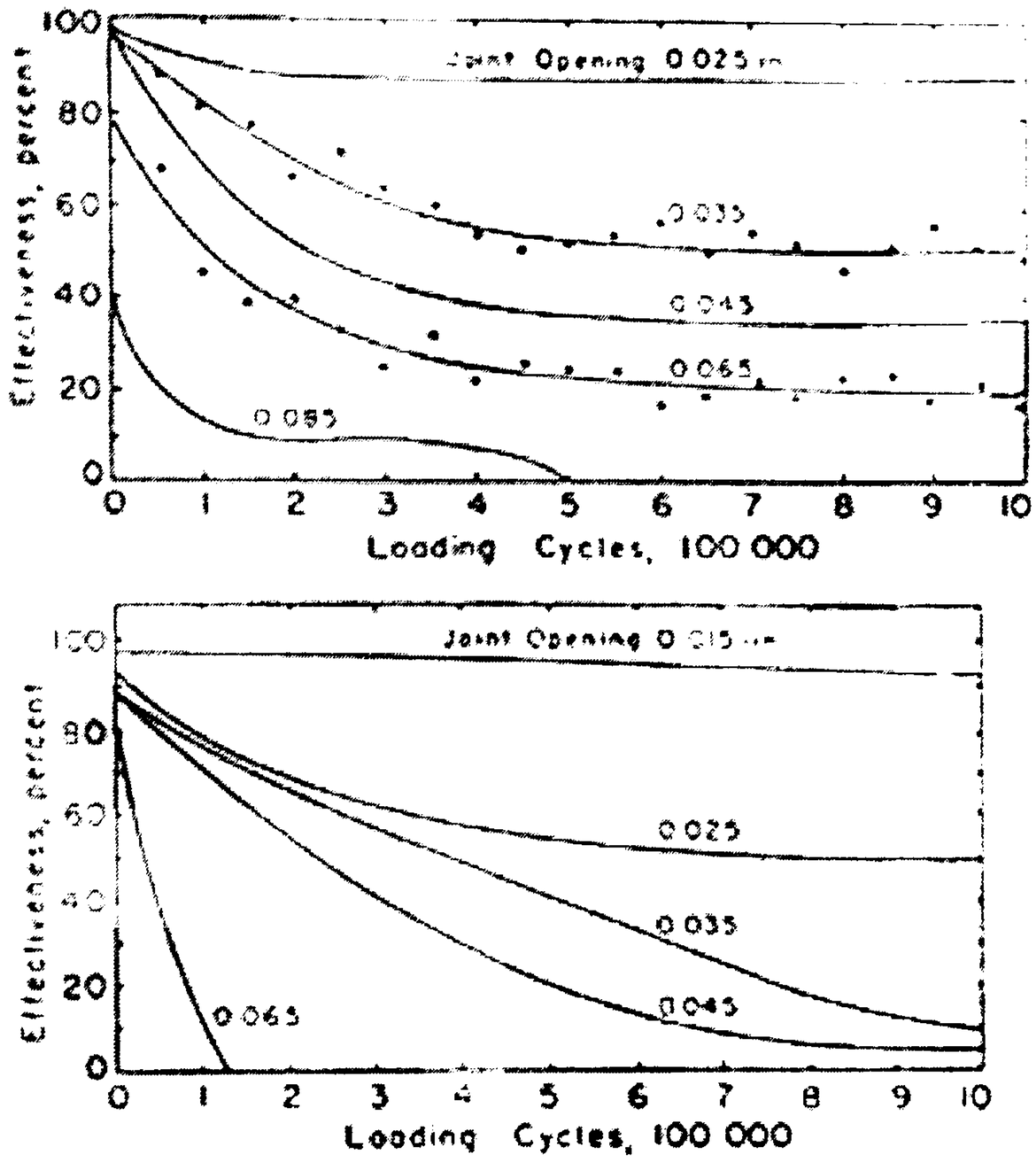

Figure 2.5 – Joint effectiveness with different load applications (Zollinger & Barenberg, 1990)

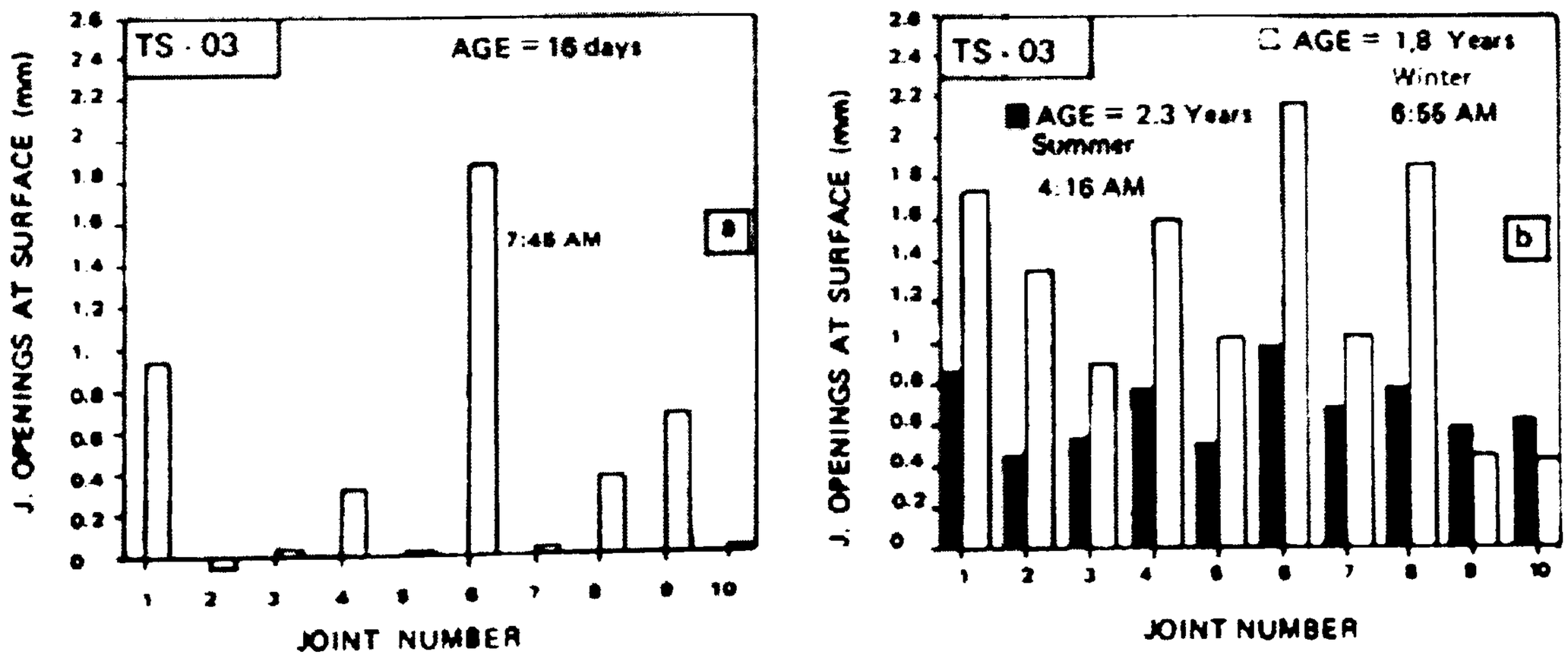

Figure 2.6 - Active joints in a plain concrete pavement (Poblete et. al., *1988a)*

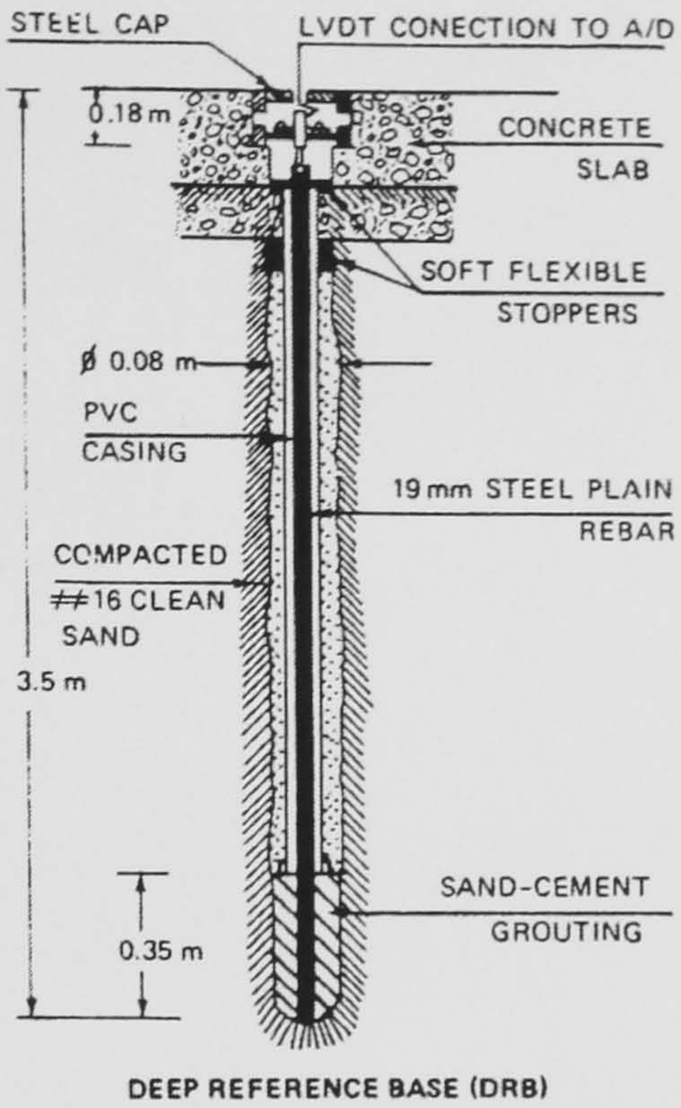

Figure 2.7 - Instrumentation to monitor joint deflection (Poblete et. al.*, 1988a)*

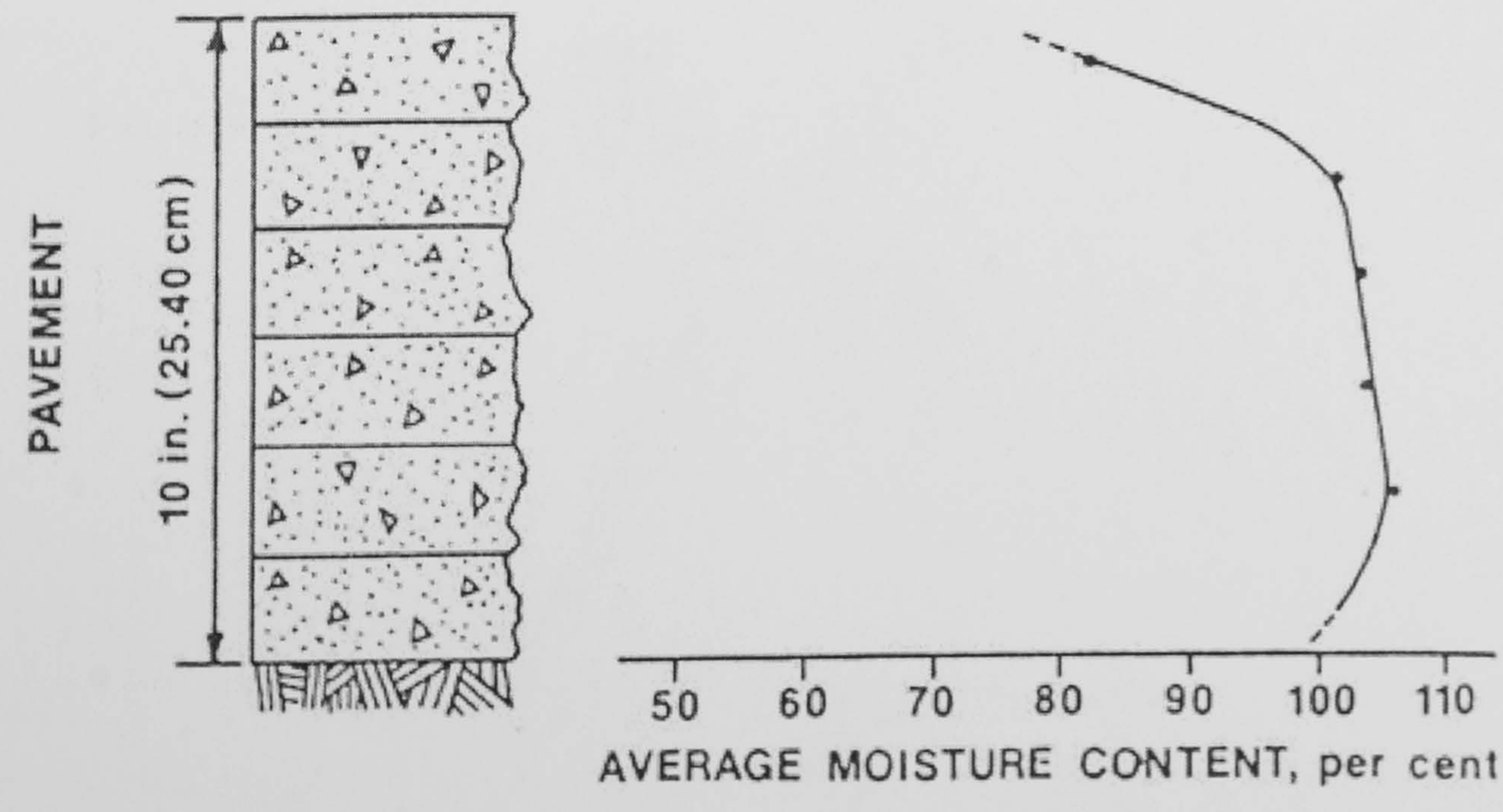

Figure 2.8 - Moisture distribution in a concrete slab (Parrott, 1990)

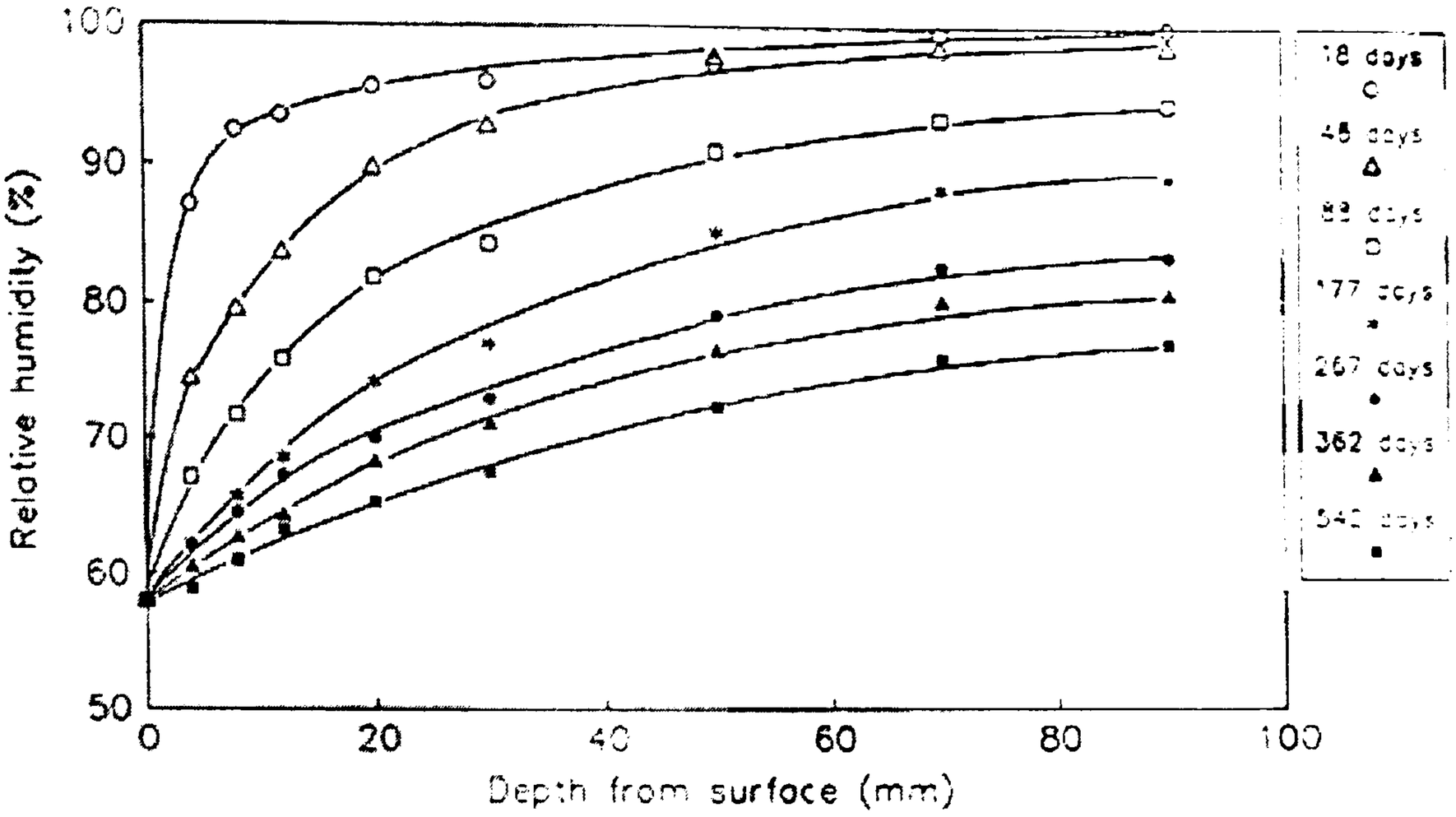

Figure 2.9 - Moisture profiles in a laboratory dried concrete slab (Parrott, 1990)

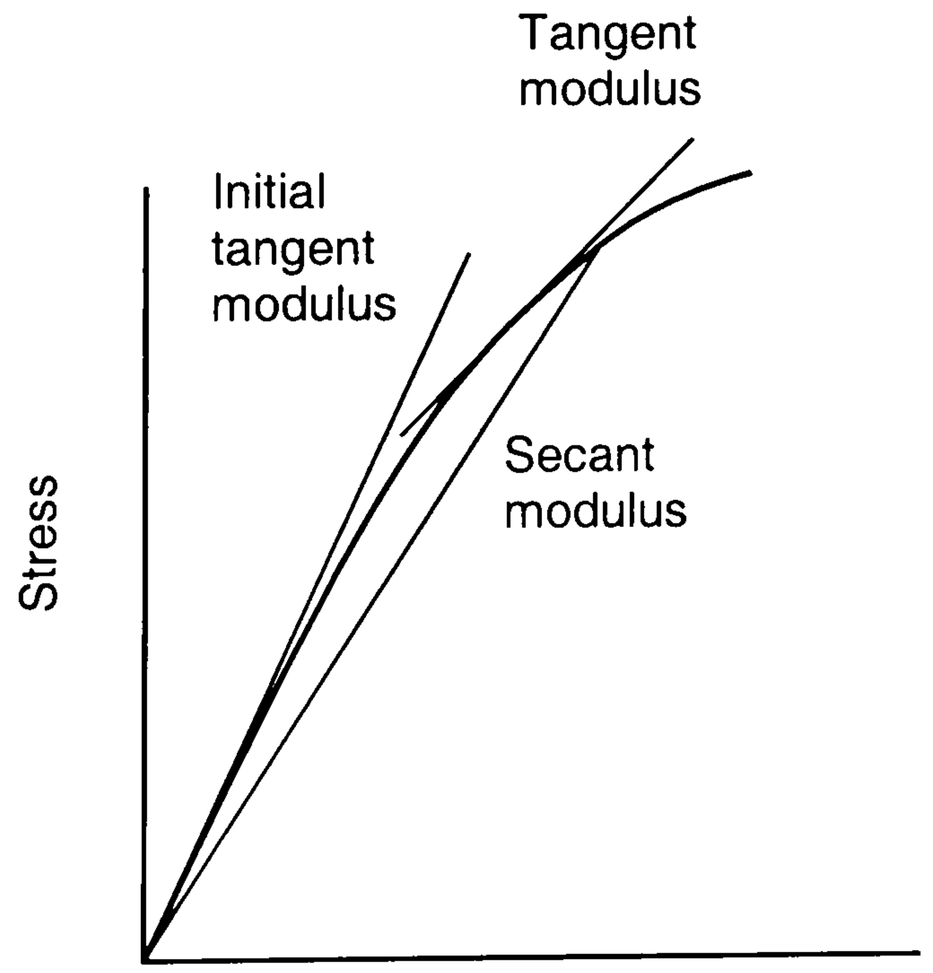

Figure 2.10 - Comparison of the different elastic moduli

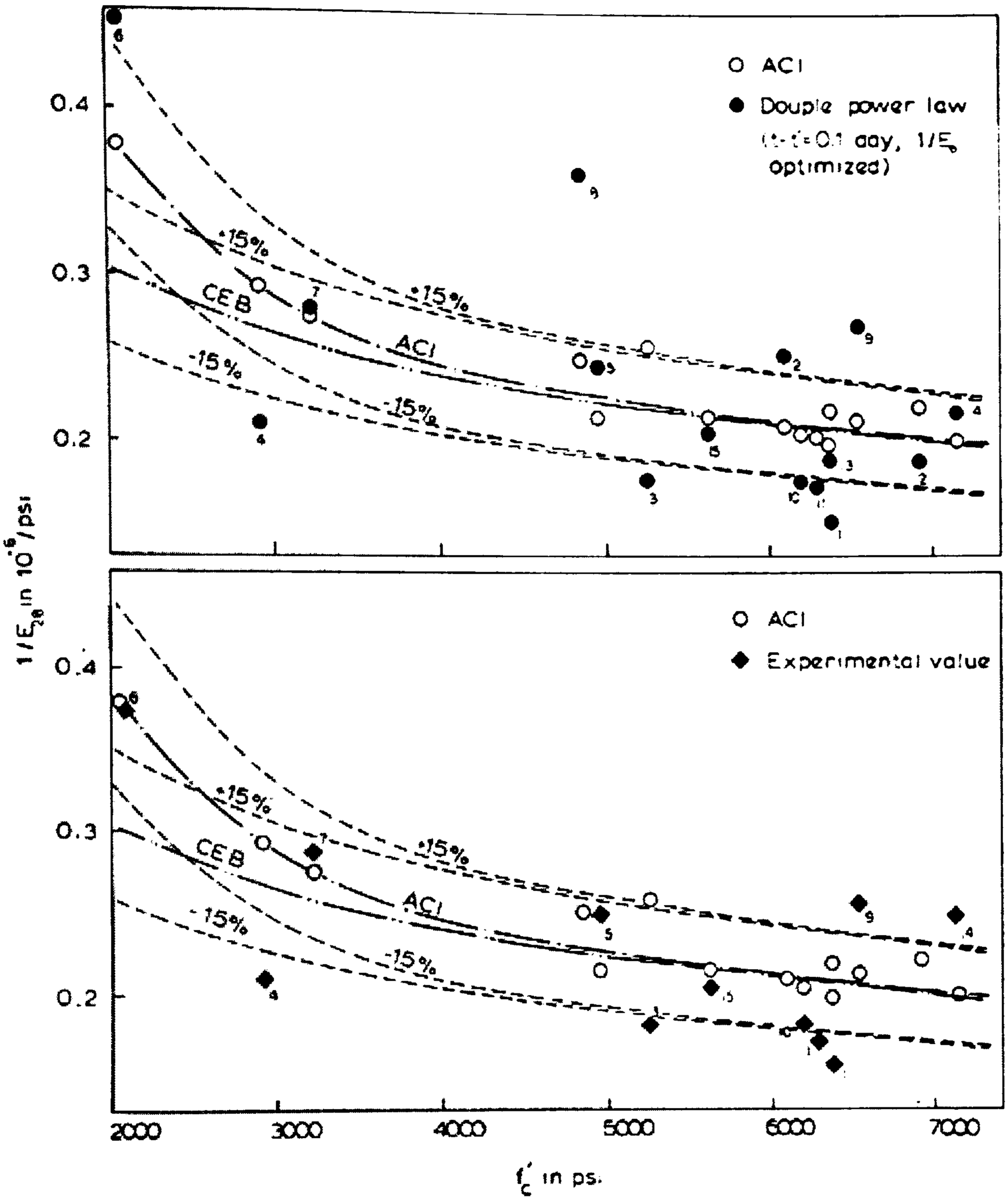

Figure 2.11 - Comparison of different methods of predicting elastic modulus development with time (Bazant & Panula, 1978b)

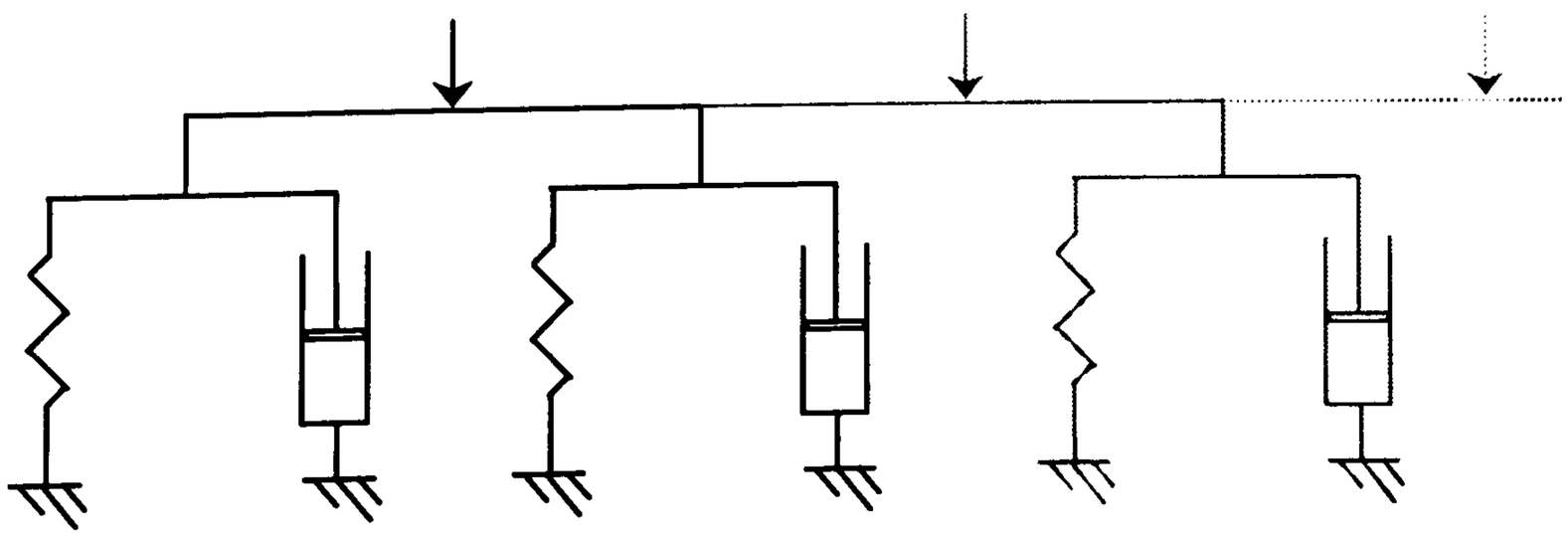

Figure 2.12 - Kelvin model for a viscoelastic solid

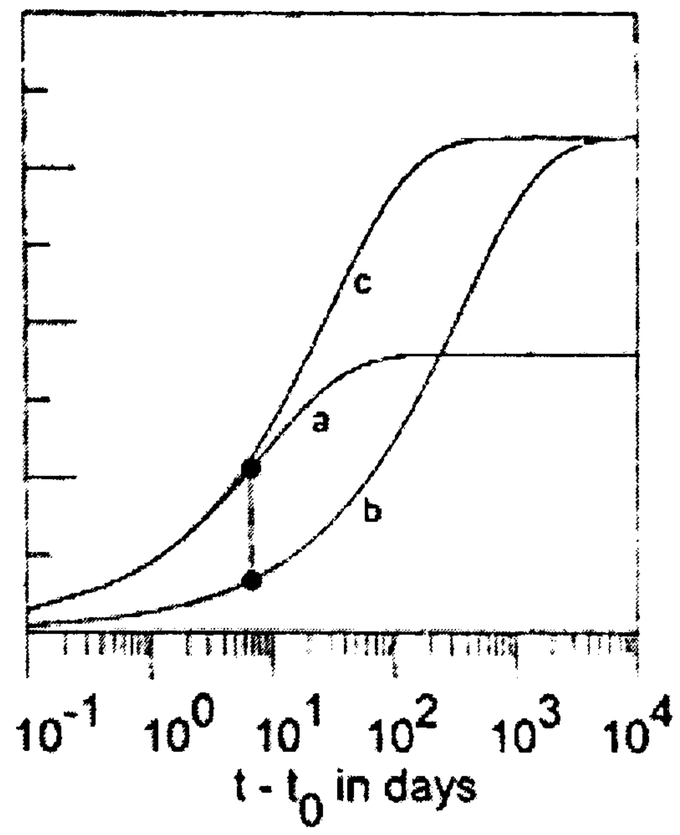

Figure 2.13 - Drying shrinkage behaviour for several different concretes (Bazant & Baweja, 1995b)

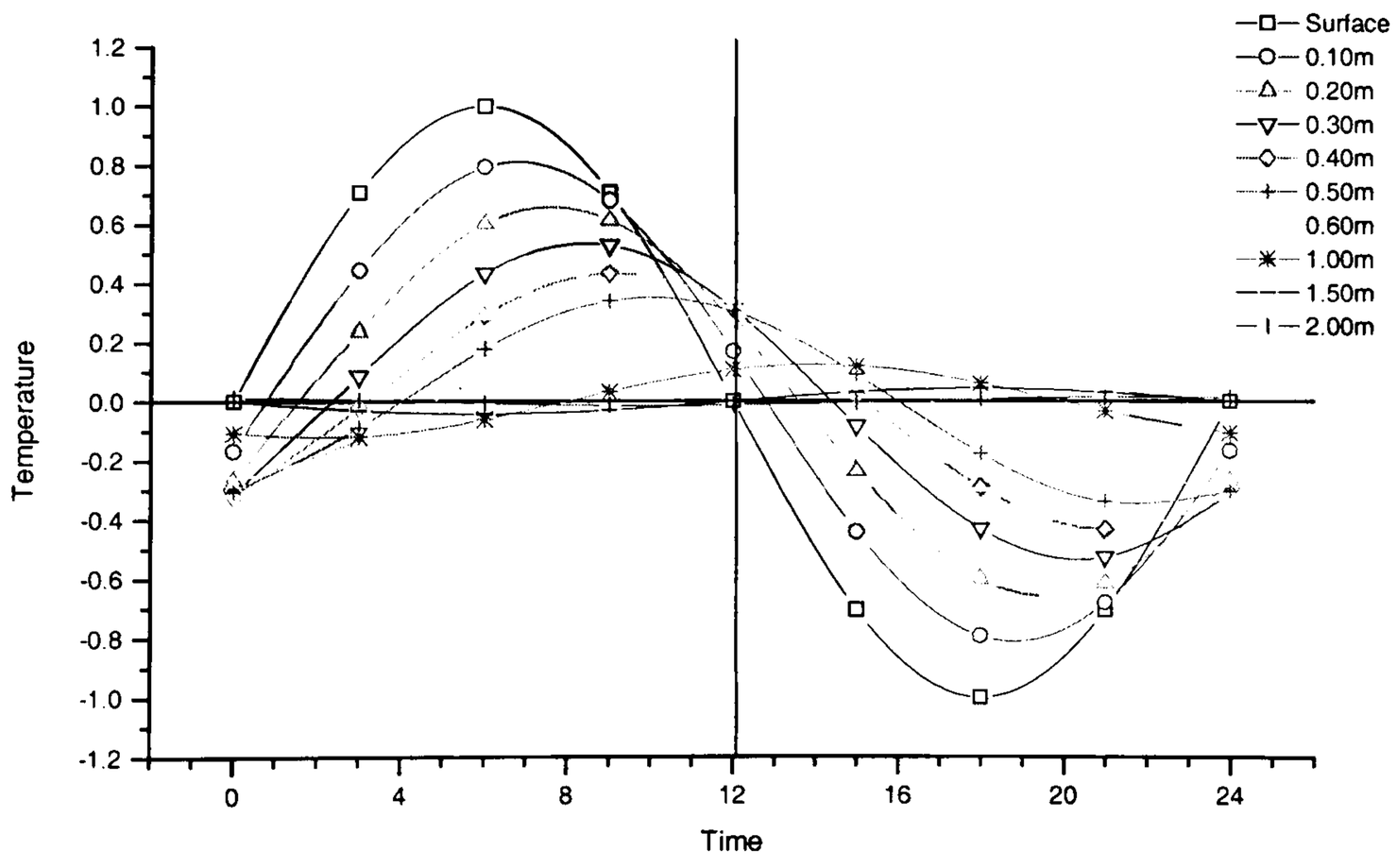

Figure 2.14 – Theoretical daily temperature change at different depths under a slab (after Thomlinson)

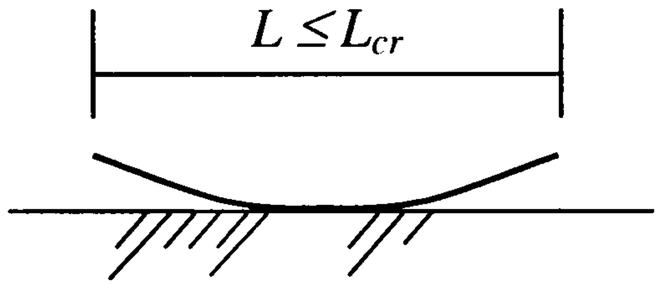

Figure 2.15 – Curled shape of a slab shorter than the critical length

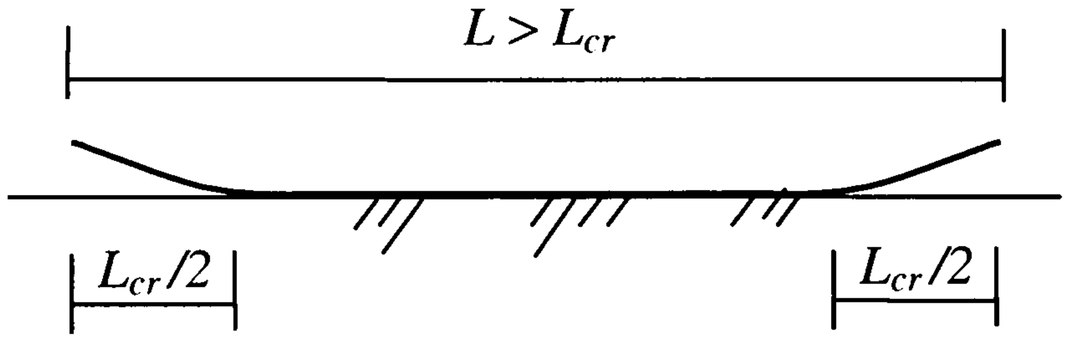

Figure 2.16 – Curled shape of a slab longer than the critical length

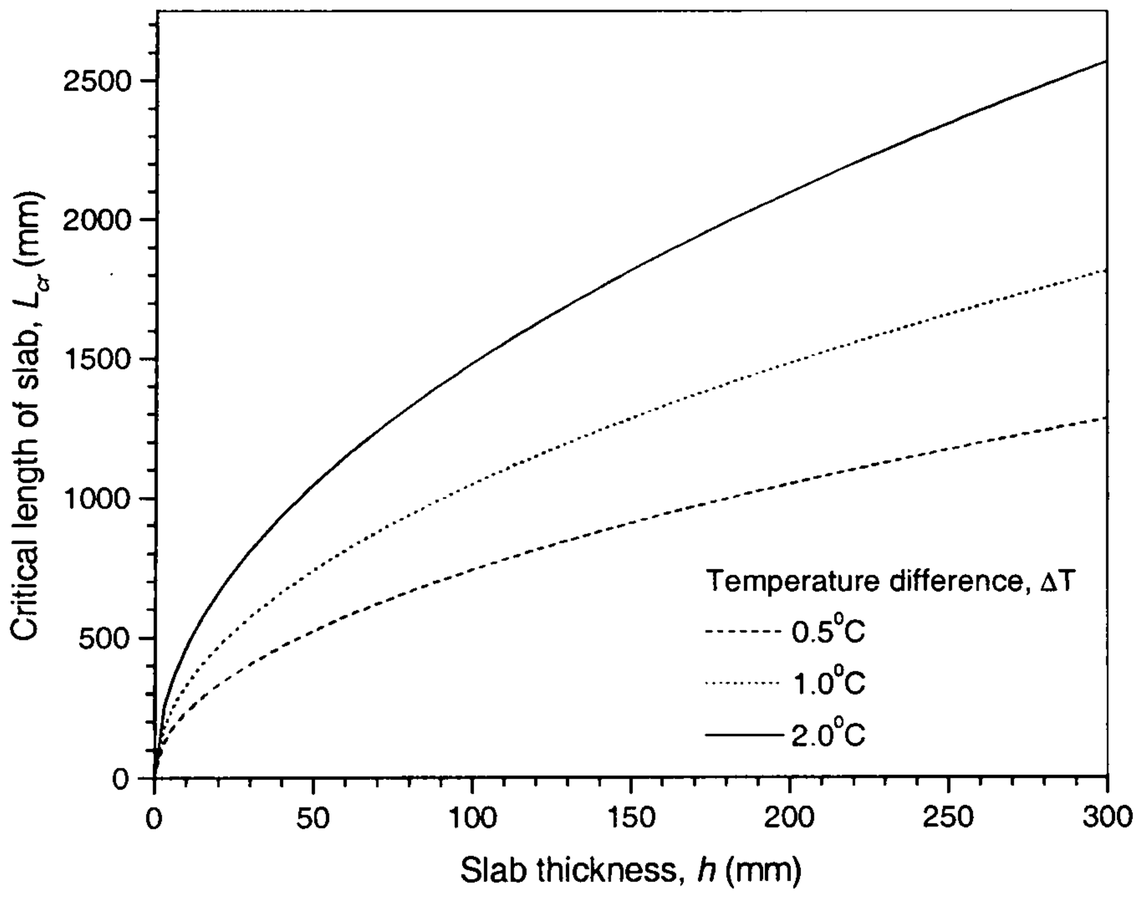

Figure 2.17 – Relationship between slab thickness, temperature difference and the critical slab length

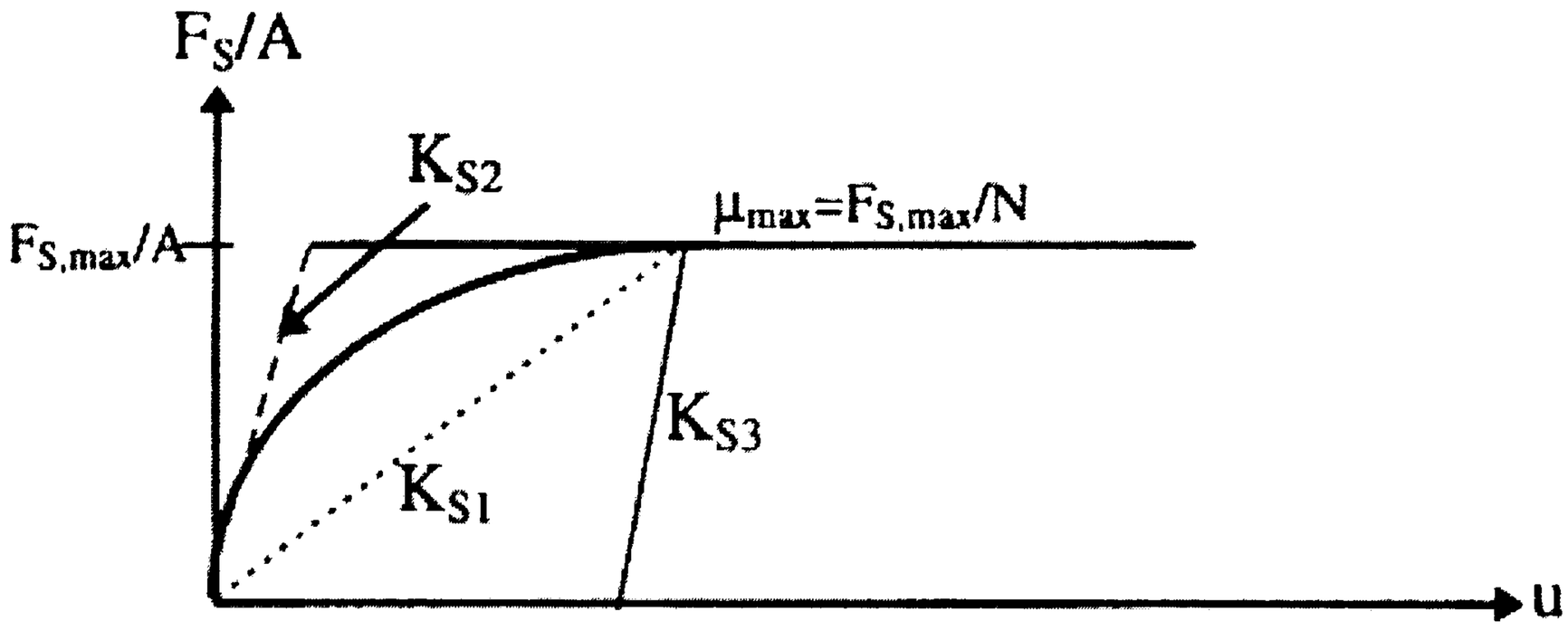

Figure 2.18 - Three ways to express the interfacial linear shear stiffness, K_s (Pettersson, 1998)

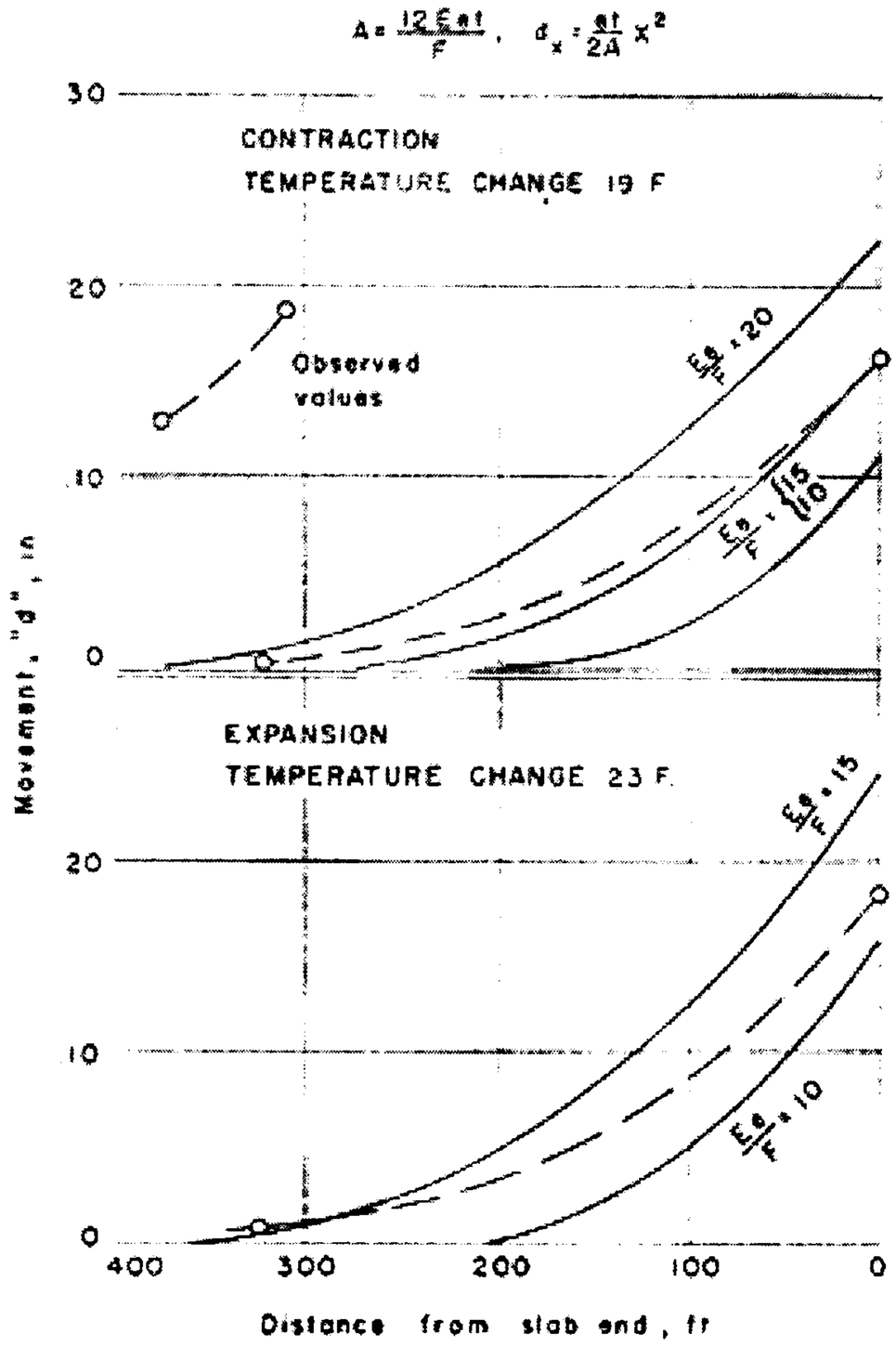

Figure 2.19 – Slab movements observed at Stillesville for 19- and 23 °F temperature change in long slab and movements computed for constant friction (Friberg, 1954).

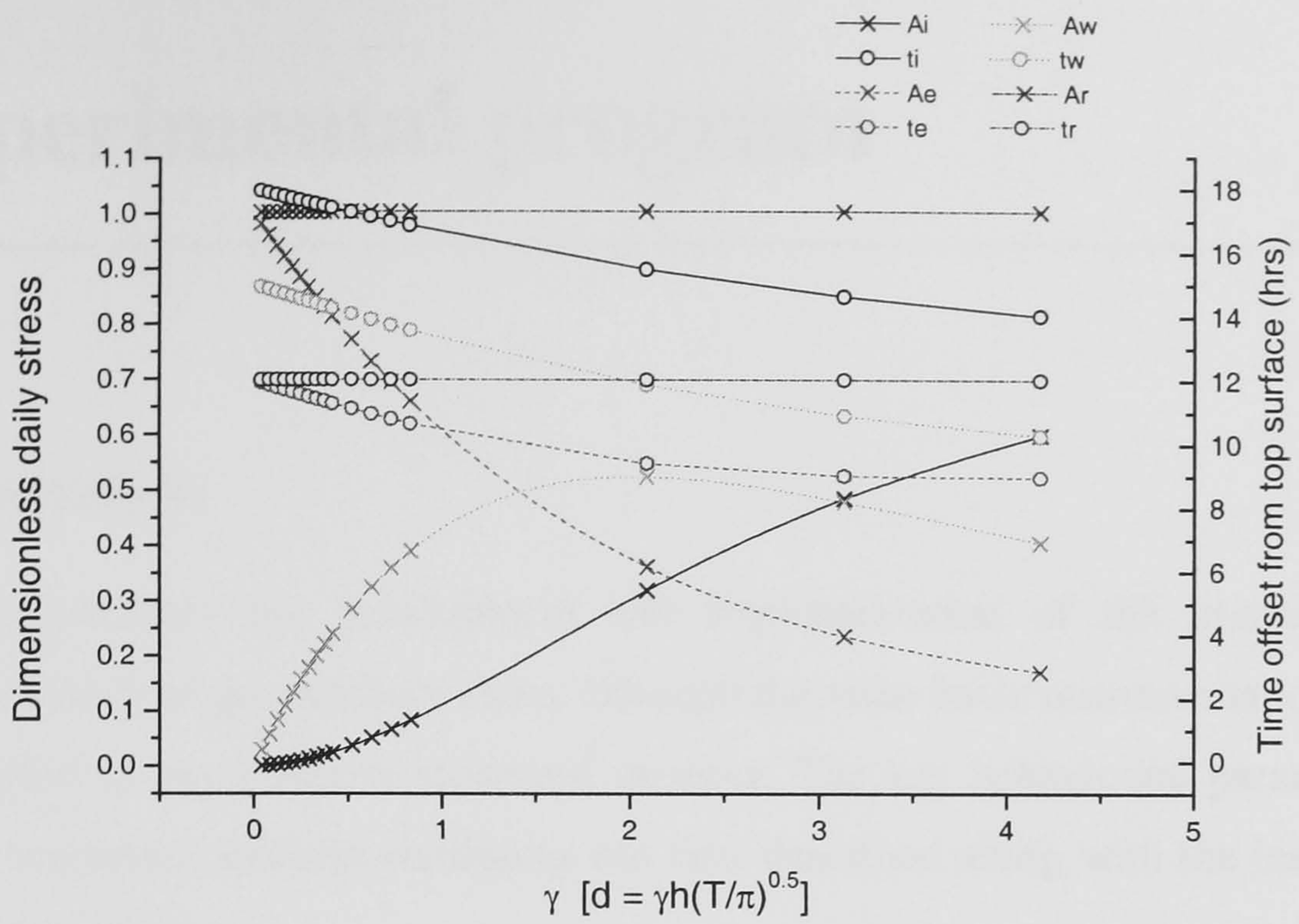

Figure 2.20 - Variation of stress due to full restraint

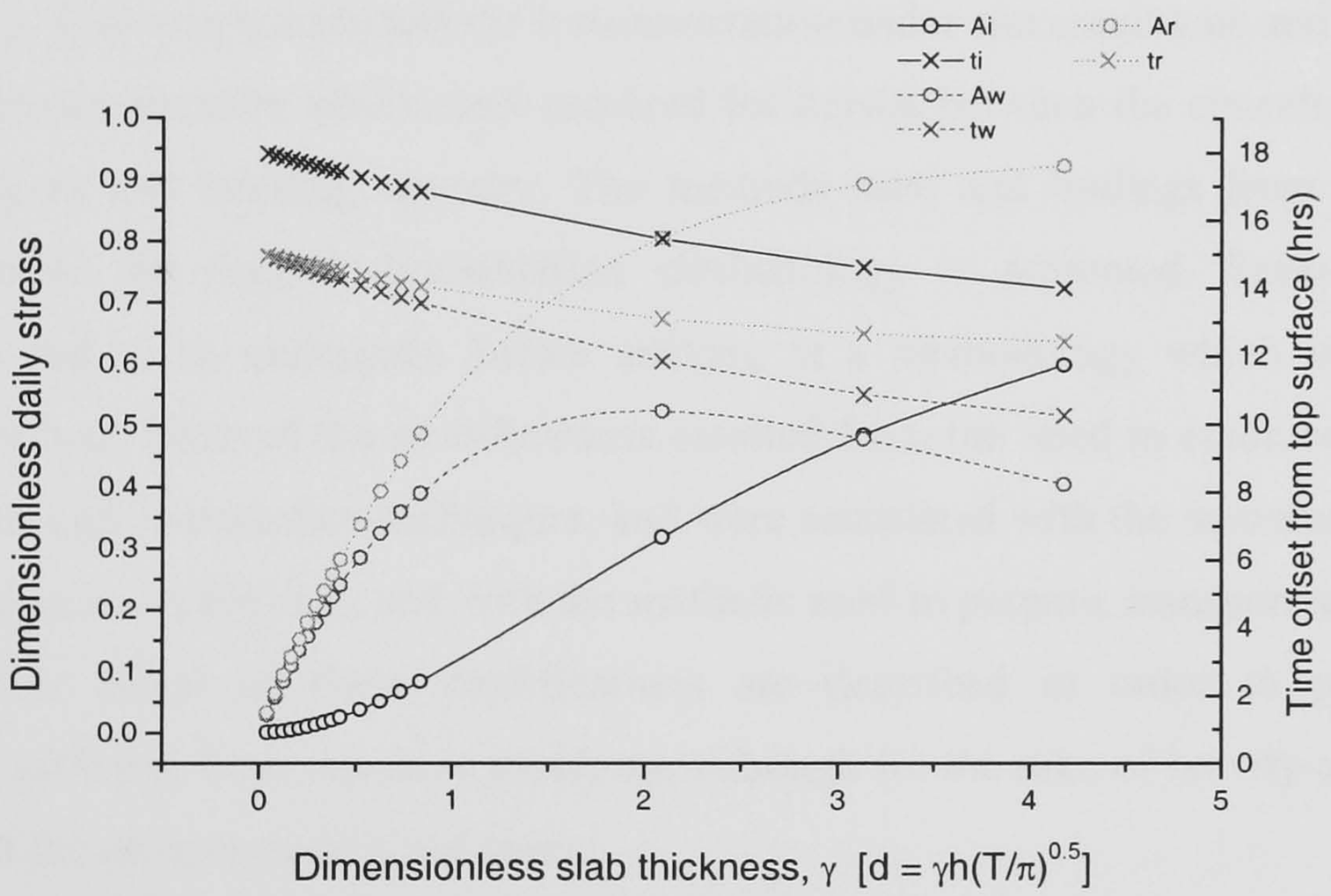

Figure 2.21 - Stresses with full warping restraint but no end restraint

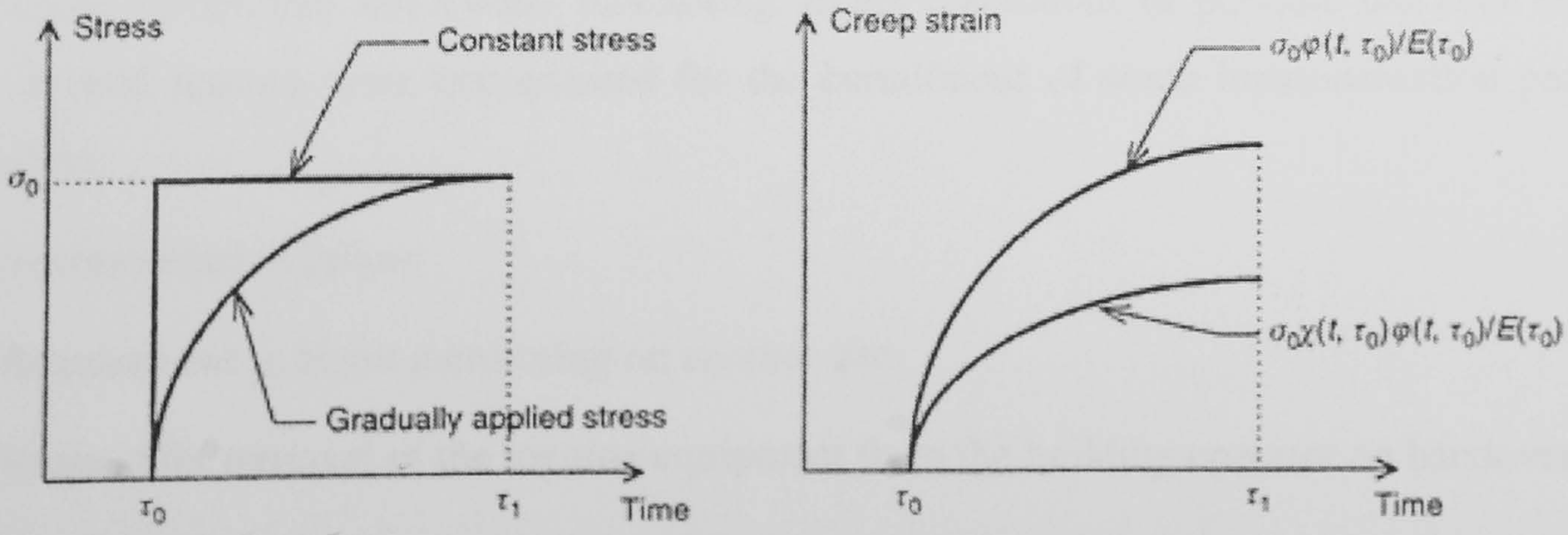

Figure 2.22 - Creep strain resulting from a constant and a gradually applied stress (Kovler, 1997)

3. Experimental program

3.1. Introduction

This chapter describes the development and implementation of the in-situ monitoring technique for industrial ground floor slabs, although the same basic instrumentation techniques could be applied to any concrete structural member. The key behavioural parameters of the slab and the impacting ambient conditions are first described along with the instrumentation chosen to monitor them.

Before any of the full-scale instrumentations were carried out a pilot study was conducted on a long strip slab. This was used to test the instrumentation under site conditions and to determine the lines of communication which were required for liaison between the consultants, flooring contractor, client and building operator. The methods used and findings from this trial are discussed before the final instrumentation methodology is presented. Several stages of development had to be undergone before arriving at a methodology which is practicable, reliable and robust. Most of the modifications resulted from the need to embrace a variety of site conditions and construction techniques, and were associated with the instrumentation used at specific locations in the slab, and with the methods used to prepare, transport and install the instrumentation. Some of these modifications are described in order to prevent other investigators suffering from the same problems, although for the sake of brevity a step-by-step description of the development is not given.

Finally the experimental programme is presented, showing the periods of instrumentation for the various floor types. In most cases at least the first 4 weeks after construction were monitored completely and further monitoring, either continuous or periodic has been carried out. Several reasons were encountered for the curtailment of some instrumentation periods, including:

- Instrumentation failure
- Requirement to begin monitoring on another site
- Request for removal of the logging equipment from the building operator on handover.

3.2. Choice of instrumentation

A number of key features were identified as being of relevance to the study of the early age behaviour of concrete structures, namely:

1. Information on the movement of the concrete was of prime interest, particularly that associated with the shrinkage and creep of the slab. Key locations such as joints, points of restraint, and openings were identified and instrumented. This involved instrumenting construction joints and induced joints as well as concrete within bays to determine the effects of restraint;
2. the measured movements in the concrete are dependent on the concrete's internal relative humidity and temperature, therefore sensors were used to determine the internal profiles of these parameters; whilst
3. the effect of the atmospheric environment (air speed, ambient temperature and relative humidity), which controls the rate of moisture loss from the slab and is the driving function of the internal temperature changes, was also measured.

The sensors had to be capable of being monitored automatically by a computer-controlled datalogger. This allowed them to be sampled at different frequencies to suit the rate of change of their readings. Site access was then only required periodically to download the stored data onto a laptop computer.

3.2.1. Ambient conditions

The choice of instrumentation for the ambient conditions was relatively straightforward as these parameters are routinely monitored in weather stations. A Vaisala type temperature and relative humidity (RH) probe housed in a radiation shield was used. This probe had an accuracy of ±1% RH compared to a factory reference and had a long-term stability of better than 1% RH per year. The temperature readings were made to an accuracy of ±0.2°C at 20°C. Air movement was recorded by two digital switched anemometers which were fixed to a column at right angles to each other to prevent wind shadow, caused by the supporting column, from affecting the readings.

3.2.2. Concrete and sub-base

Type T thermocouples were chosen to monitor the thermal profile through the slab and into the sub-base because they were well suited to the temperature ranges encountered during the hydration and service life of the slabs and they are the only thermocouple type which is suited to a damp environment. Additionally they were cheap to install over relatively large distances and the small size and low specific heat capacity of a thermocouple meant there was virtually

no latency in the measured temperature response. They were initially used to assess the accuracy of the built-in thermistors in the strain gauges. However, on later sites thermocouple arrays measured the temperature distribution through the depth of the slab and for the last instrumentation through the sub-base and into the subgrade.

Chilled mirror probes were chosen to monitor the concrete internal RH, dew-point and temperature because of their high degree of accuracy and long-term stability. By optically measuring the formation of dew on a mirror, which is alternately heated and cooled, these sensors are both very precise and resistant to contamination giving good long-term stability. As a result of the technology involved in the sensor head these instruments are fragile and expensive, which does not make a good combination for site work. Because of difficulties in protecting these sensors they were not used on site as much as would have been ideal. However, some readings were obtained for comparison with existing data.

Several strain gauge types are available to monitor the strains in concrete and their properties are compared in Table 3.1. A low gauge stiffness is important as this allows readings to be obtained early in the life of the concrete slab, whilst long-term stability is essential to eliminate systematic drift affecting the measurements. Differential movements between the top and bottom of the slab were of the order of several microstrains so high resolution and stability of the readings were also required.

Table 3.1 – Properties of the available strain gauge types.

	VW strain gauges	Electrical wire resistance strain gauges
Stiffness	Very low (~ 40 N/mm^2)	High (~14.7 kN/mm^2) [1]
Affected by cable lengths	No	Yes
Resolution	< 1 μstrain	Dependent on lead length
Thermal effects	11 μs/°C [2]	Complicated to account for
Long term stability	Excellent (< 1 μs/year)	Excellent
Dynamic readings	No	Yes
Automatic monitoring	Yes	Yes
Manual monitoring	Yes	Yes

[1] An embedment strain gauge of type EGP-5-120 was tested as described in Chapter 3.2.4.

[2] Additional thermal effects are apparent at early ages in the acrylic gauges as described later, but this can be accounted for in the analysis.

Vibrating wire (vw) strain gauges were chosen because they fulfilled all of the above criteria, but additionally, and crucially for carrying out in-situ investigations, the readings were independent of the length and the type of the lead wire between the gauge and the datalogger. This enabled last minute changes of instrumentation location and lead length to be carried out

without affecting the gauge readings. Manual readings could also be taken quickly and easily on site to confirm the correct operation of the gauges before they were embedded in concrete. This ability to take manual readings also allows visits to be made to sites to gather long-term movement data once the data logging equipment has been removed.

The choice of vw strain gauges is also in agreement with guidance from the American Federal Highway Authority (FHWA, 1996), which recommends vw strain gauges and Carlson gauges for long term readings.

The monitoring of service loading effects fell outside the remit of this research, which was only intended to monitor the slabs before they went into service, although it was still intended to produce instrumentation layouts which would be flexible enough to provide useful long-term performance data.

Thermistors located in the strain gauge coil housing recorded the temperature in the slab and allowed thermal corrections to be applied to the readings, whilst also providing more thermal data to be added to that collected by the thermocouples.

3.2.3. Datalogger

The datalogger formed the heart of the instrumentation and had to provide flexibility of use whilst being easy and intuitive to program and wire up. The chosen datalogger had 6 double or 12 single ended channels, which could be expanded by adding multiplexers allowing up to 32 instruments to go to a single datalogger channel. The multiplexers could also be daisy-chained to increase the monitoring capacity.

The datalogger control programs were written using MS Windows® based software. Control flags, set manually using a laptop computer connected to the datalogger, were used to control the activation of different parts of the program, in addition to time dependant controls. In this way it was possible to activate the monitoring of gauges in several phases corresponding to the construction sequence. It was also possible to reduce the sample frequency incrementally as the slab aged. As the datalogger only had a finite storage space, decreasing the frequency of readings, to match the slowing rate of shrinkage with time, allowed a greater period of time between site visits to download the data.

3.2.4. Laboratory testing

Although vibrating wire (vw) strain gauges had been chosen as the most suitable instrument for the site instrumentations, several different types of vw gauge were available. Gage Technique International supplied two embedment gauge types, the TES 5.5 and the TEAB 5.5, which were both 5.5 inches (140mm) long. The TES used a thin walled steel tube for the barrel, whilst the TEAB used an acrylic tube reducing its stiffness - this gauge had only

previously been used for laboratory testing because of its fragility. Geokon supplied the other embedment strain gauge, the 4200x, which also had a barrel made from a thin walled steel tube. This strain gauge had the excitation/pickup coil in a removable housing to simplify the installation process. Images of the three strain gauges can be seen in Figure 3.1.

Laboratory investigations were carried out to establish how early reliable data could be obtained from the sensors and to identify any possible problems in their use. The strain gauges were tested for sensitivity, robustness and reliability by casting them in an 800x500x180 mm concrete specimen and subjecting it to forced drying. Reliable and repeatable readings were obtained from all of the gauges after only two hours (Figure 3.2). However, these early strain readings must be interpreted with care as at very early ages the stiffness of the concrete relative to the gauge is low and, therefore, the effect of the gauge stiffness on the measured strains could be large (Boulay and Paties, 1993).

Laboratory testing to determine the stiffness of the strain gauges was carried out by suspending them rigidly and applying small loads to the free end. Dividing the load by the surface area of the flange plates allowed an equivalent applied stress to be determined and plotting this against the strains provided an effective elastic modulus, E_g, for each of the strain gauges. The gauge dimensions and the results of this testing are summarised in Table 3.2, whilst full specification information for the strain gauges is in Appendix A.

Table 3.2 - Strain gauge details

Gauge type	*TEAB*	*4200x*	*TES*
Gauge length (mm)	140	152	140
Area of flange plates (mm^2)	1075	284	1075
Effective stiffness, E_g (N/mm^2)	68	49	1740

The much greater stiffness of the *TES* gauge as a result of its sturdier construction explains why it is the least sensitive during the early age of the concrete.

3.2.5. Trial site instrumentation

As each of the gauges had performed satisfactorily in the laboratory trial a site trial was carried out to assess how each gauge type would stand up to the construction methods used. This also gave an opportunity to investigate the gauge fixing technique and the different methods for connecting the gauges to the datalogger, whilst allowing the collection of some early performance data on one of the slab types.

The strain gauges in the laboratory trial and in this site trial were suspended from piano wire, which was passed through holes drilled in the flange plates of the gauges (Figure 3.3). This

method of attachment imposed negligible longitudinal restraint, and minimised the amount of additional reinforcement in the area around the gauge, thus causing the least modification to the concrete being monitored. As the reinforcement was located in the top of the slab (with 50mm cover) it was possible to attach the piano wire carrying the gauges to the chairs supporting the reinforcement at a range of depths and orientations (Figure 3.4).

The three types of strain gauge used in the laboratory trial were again used in the site trial, with some of them grouped in clusters with one run of multi-core cable connecting them to the datalogger. This technique, which proved successful, allowed the number of cables to be reduced which consequently dramatically reduced the cost of the instrumentation.

It became apparent in the planning for this trial that large numbers of cables would require connecting to the datalogger, and for this reason an interface box was designed. The interface box provided a neat and waterproof termination to the cables and allowed the quick and easy connection or removal of the datalogger using 4no. 25-way RS232 connectors. Because the interface box was wired up and tested in the laboratory, the risk of wiring mistakes being made on site was also removed. Where the cables between the datalogger and the gauges had to cross the line of an earlier pour they were passed through a length of scaffold tube, which was buried in the sub-base to prevent damage due to the vehicular trafficking during the construction process.

3.3. Development of the methodology

The development of the instrumentation methods and of new sensors took place over four full site instrumentations over a period of 18 months. Because of the differences in site conditions and construction techniques encountered on these sites this development work was carried out in an iterative fashion, with each change improving the reliability of the instrumentation methodology and reducing the risk of damage to the strain gauges.

3.3.1. Gauge support

One of the most major developments required was in the method used to support the strain gauges. Although the method using piano wire worked well for the long strip slab, the extra force of the flowing concrete in the first large area pour caused the gauges to move excessively. This resulted in several of the joint gauges missing the joint they were supposed to be crossing. The solution was to cable-tie the strain gauges to reinforcement chairs with a length of silicone tubing between the gauge barrel and the chair to prevent movement and damage to the gauge. The chairs were then taped to the slip membrane Figure 3.5, or in the case of fabric reinforced floors, were cable-tied to the reinforcement Figure 3.6.

3.3.2. Interface box and cabling system

It became apparent during the planning stage for the trial instrumentation that a large number of cables would require connecting to the datalogger. For simplicity, and in order to save time in preparing for future site instrumentations, a standard datalogger set up was devised which allowed up to 80 vw strain gauges to be monitored (including 12 with internal thermistors), as well as the ambient probes, and an array of thermocouples. This standardisation meant that the dataloggers were interchangeable between sites, only requiring the correct control program to be loaded.

In order to allow this standardisation and enable the dataloggers to be removable, an interface box was designed. This provided a neat, waterproof and inconspicuous termination to the multi-core cables and also facilitated their re-ordering to accommodate the common datalogger set-up. In order to simplify the control program all of the strain gauges with thermistors were sampled first, followed by all of the acrylic barrelled gauges and finally the steel barrelled gauges. As the gauge layout for each site was different the numbers and locations of these gauges changed each time, but by re-ordering the cables in the interface box the impact on the datalogger was minimised. By preparing this box in the laboratory, testing was carried out on the finished wiring loom under controlled conditions, making faults easier to spot and rectify.

Early interface boxes used 15-way RS 232 connectors to attach the cables from the gauge clusters. However, problems with these terminations led to the adoption of a hardwiring system, where all of the wires were fixed into terminal strips inside the interface box. Though this made transportation slightly more difficult this modification reduced the time required to produce the interface box, and because the terminal strips were quick and convenient to connect to the vw strain gauge manual read-out box, the process of taking manual readings was simplified.

After the site trial, which had only used 4no. 25-way RS232 connectors to link the interface box to the datalogger, the monitoring capacity was increased and so 6no. 25-way RS232 connectors were required. A spreadsheet was developed to keep track of the gauge numbers and locations as well as the colours of the large numbers of wires connecting them to the logger. Once the spreadsheet had been completed it was also used when programming the datalogger, as it provided a complete record of how every gauge was connected.

Two options for connecting the strain gauges to the interface box were identified (Figure 3.7), namely:

- Individual cable runs for all gauges
- Clusters of gauges connected with multi-core cable

Individual cable runs cost £1.15/m compared to £0.70/m for 12-core cable capable of carrying the signals from up to 6 strain gauges. The cost of cabling a typical instrumentation layout using 20 gauges over a 40m length using individual cable runs would have been about £500 as opposed to less than £100 using multi-core cable, even allowing for the cost of the cluster boxes. Thus, given the large areas to be monitored, the economic argument in favour of gauge clusters and multi-core cable runs was overwhelming.

This method for connecting the strain gauges to the interface box was verified on the trial site. However, an unacceptable number of gauges were lost in the first large area pour because the force of the moving concrete as it was poured broke some of the wiring connections. This problem was solved by using cable glands in the cluster boxes and by cable-tying a loop into the leads at all connections to keep the crimps free of stress (Figure 3.8). The joints were then taped up to prevent the ingress of moisture from the concrete.

Some strain gauges were also lost during saw cutting on several sites and investigation revealed that the leads had been severed. This occurred on the first large area pour where cables had not been secured and on subsequent mesh reinforced slabs where the cables had been tied to the bottom of the reinforcement. It is believed that non-uniformity in the location of the reinforcement may have led to both this and the leads being cut as the joints were formed. In order to prevent sub-base level variation and changes in the depth of the reinforcement causing this problem the cables should all be taped securely to the slip membrane.

Various methods were tried to protect the multi-core cables connecting the cluster boxes to the interface box, though burying the cables in the sub-base proved to be the most efficient. Once the cables had been protected none of the cables were damaged by the normal trafficking of the floor.

3.3.3. Instrumentation layout / planning

Various different layouts of gauges were used to attempt to measure differential movement through the thickness of the slab, at different distances from the joints, at the joints themselves and in different directions. The gauge layout also reflected the type of floor being constructed. For example the increased distances between joints in a jointless pour required the use of a greater number of embedment gauges in order to monitor any behaviour related to the distance from a movement joint. In contrast a jointed floor might use an equal number of joint and embedment gauges to relate joint movement to the concrete shrinkage at different locations in the pour.

Arrays of thermocouples were embedded in several of the floors to monitor the thermal profile through the slab and into the sub-base more precisely than was possible using the thermistors

in the strain gauges. These sensors were attached to reinforcement chairs to control their position within the slab, whilst a spike was driven through the sub-base and into the subgrade to allow sensors to monitor temperature changes up to 1m below the finished slab surface. All of the sensors were covered with tape to prevent contact with reinforcement from affecting the readings.

The chilled mirror probes could not be placed into wet concrete, requiring the use of removable blanks made from 25mm ∅ metal bars inside a length of tight fitting plastic conduit. Once the bar was removed the conduit sealed the sides of the hole preventing moisture loss and allowing the probes to measure the RH at a specific depth. The plastic tube also extended above the surface of the slab and provided some support for the probes. Real support and protection for the probes was difficult to provide without damaging the surface of the floor, and for this reason the probes could not be used for long, having to be removed before the building became operational.

3.3.4. Long strain gauges

Once the most suitable type of sensor had been determined, the locations which were to be instrumented then had to be identified. As the range of movement which a vw strain gauge can measure is dependent on it's length, locations where larger movements could reasonably be expected were instrumented using longer strain gauges. Standard vw strain gauges were 140mm long, and had a quoted range of at least 3000 μstrain, which equated to a measurable movement of 0.42mm. In order to measure across joints, 254mm long strain gauges were developed. These gauges had an increased frequency response because of their increased length and, additionally, any strain reading represented a larger movement than for a small gauge because of the increased gauge length. Thus these 254mm strain gauges had a quoted range in excess of 1mm, although readings from these gauges exceeded 10,000 μstrain (2.5mm) before failure. The additional length of these joint gauges also gave a greater margin for error in locating the gauges across the intended position of the saw-cut joints.

3.3.5. Day joint gauges

Monitoring across induced joints - such as saw-cut joints in concrete slabs - proved possible with the 254mm gauges. However, trying to monitor across day-joints was difficult as part of the gauges was left exposed once the slab had been cast (Figure 3.9). After several gauges were damaged because it proved difficult to protect them adequately, a new gauge with a removable extension arm was developed in association with Gage Technique International (GTI) (Figure 3.10).

The vibrating wire part of the gauge was embedded in the first pour with the end block attachment for the extension arm protected by polystyrene (Figure 3.11). Once the formwork had been removed the polystyrene could be broken out leaving the end block ready for connection of the extension arm just prior to the commencement of the second pour (Figure 3.12).

This newly developed gauge can be used in any situation where monitoring is required across day joints, or indeed in any situation where phased construction is being used and a part of the gauge might otherwise be left exposed for any period of time.

3.3.6. Demec gauge joint monitoring

Excluding the cost of the datalogging equipment the cost of installing strain gauges was about £100 /gauge. This made monitoring large areas of a floor and large numbers of joints prohibitively expensive. In order to monitor extra joints in a floor or to carry out ad-hoc monitoring on floors where a data logger was not present a Demec gauge was used. A steel template was used to locate two shallow 10mm drill holes 200mm apart on either side of the joint (Figure 3.13). Demec pips were glued into these holes allowing subsequent movements to be measured. Recessing the pips into shallow holes in the floor protected them from traffic in the building and effectively hid them from view. Several building operators objected to the installation of these pips because of concerns about the damage caused to the surface of the floor. However, on the floors where they were installed even the research team occasionally had problems locating the pips for subsequent readings to be taken and no adverse effects due to trafficking were observed.

3.3.7. Gauge pairs

A further method was developed with GTI to enable the larger movements occurring at the edges of jointless floors to be monitored. Two strain gauges were used in parallel, with one gauge initially having it's wire slack, whilst the other gauge was set up as normal. Before the first gauge reached the end of its movement range the wire in the second gauge became taught and continued to monitor the movement once the first gauge had broken (Figure 3.14). This technique is more complicated and expensive than using Demec pips to monitor joint movement, but it can be applied in situations where permission is not given for Demec pips to be installed. Although these proved to be successful the additional cost did not realise much additional range of movement, and if the first gauge is damaged the readings from the second gauge are of no use.

It is therefore recommended that, where possible, a joint gauge is used to get the magnitude and timing of the early joint movements, whilst Demec pips are installed to record the longer term openings.

3.4. Final Site Instrumentation methodology

3.4.1. Pre-site preparation

Once the areas to be instrumented had been chosen, a location for the datalogger had to be found. Ideally the datalogger should be fairly central in the area of interest, yet also away from frequently trafficked areas, unless some form of protection can be assured. Once the position of the datalogger had been determined, the strain gauge locations were then chosen - generally all joints were instrumented and at least one gauge was placed between each pair of joints to measure the concrete shrinkage. Where possible more than one gauge was placed at each location to provide a degree of redundancy. This allowed performance data to be gathered from two different depths in the slab when both gauges worked, and if one gauge failed there was still data from the remaining gauge. Once the gauge locations and types were finalised they were grouped into clusters of up to six gauges for connection to the interface boxes. The gauge positioning information was entered into a spreadsheet to allow the wires from each cluster box to be identified. This spreadsheet was then used to produce the wiring plan for the interface box allowing for the rearrangement of the gauges to suit the standardised datalogger. The decision to use this standard datalogger arrangement meant that the multiplexers only had to be wired-up to the datalogger and connected to 25-way RS232 connectors once. This was time consuming and care had to be taken to avoid errors, which could lead to sensors being misidentified or misread by the logger.

The datalogger control programs were written to allow automatic sampling of the gauges at predetermined rates depending on the number of gauges, the age of the slab and the expected time between site visits. Normal time scales were every half hour for the first 24 hours, hourly for the first week and then 3 or 4 hourly thereafter. A manual override activated by a control flag was also provided to increase the sampling frequency of the gauges to once every 2 minutes. This was used when the logger program and wiring loom were being tested and debugged before transportation to site and to check the correct operation of the gauges before embedment in the concrete. Once the system had been verified as working correctly the cluster boxes were filled with silicone sealant to fully waterproof the connections and closed (Figure 3.15).

Part of the pre-site preparation also involved visiting the site to discuss the instrumentation programme with all affected personnel. The placement of the gauges did not disrupt the construction process. Because of the fragility of the gauges, the assistance and co-operation of the flooring workers had to be obtained.

3.4.2. Site practices

On arrival on site the datalogger, battery, interface box and ambient probes were first attached to their column before burying the gauge cluster boxes and their multi-core connecting leads in the top of the sub-base. The strain gauges were transported to site in their packaging to reduce the risk of damage. However, once on site they were connected to pre-cut sections of reinforcement chair and tested for correct operation with the manual gauge readout box before being stored safely. After placement of the slip membrane the locations of the gauges were marked and the cable to connect the gauges to the cluster boxes was cut. These leads were connected, cable-tied to provide strain relief and waterproofed as early as possible, but the strain gauges were not attached until just before they were required, to avoid the risk of accidental damage. Although precautions were taken to provide strain relief to all of the connections it was still felt necessary to reduce the possible movement in the cable runs. This was achieved by taping the cables to the slip membrane.

Once the gauges had been fixed in place and connected to the datalogger, they were checked for correct operation as at this stage faulty gauges could still be replaced. When the time came to embed the gauges in the concrete they were first surrounded with concrete by hand, before concrete was allowed to flow gently around the gauges as it was discharged and spread from the ready-mix truck. At all times care was taken to ensure that no concrete fell directly on top of the gauges, as this sudden pressure could have been sufficient to damage them. After embedment the location of the gauges was clearly marked, either by placing a road cone on top of the concrete (Figure 3.16) or by having a technician stand over the gauge. This was done until the slab was finished by the LaserScreed™ when the risk of accidental damage ended.

In some cases precision level surveys were carried out on the slabs after they had been cast and at subsequent intervals to assess the vertical movement of the slab's surface. These surveys were carried out using a Leica Wild NA3003 digital level, which (when used in conjunction with an Invar digital staff) has a standard deviation on repeated readings to the same point 30m away of 0.05mm. The results obtained are only used to a precision of 0.1mm, but this gives a good indication of the variations in the slab surface. The surveys were carried out on 1 x 1m or 2 x 2m grids to suit the floor area. Detail surveys were also carried out on all of the floors on subsequent data collection visits to locate and quantify any cracking in the floor.

3.5. Site programme

As previously mentioned, the duration of the monitoring on each site varied according to the operational requirements of the building owners/operators and the demands of the instrumentation schedule (Figure 1.1). Where possible monitoring was carried out for at least

the first 4 weeks following construction, though in several cases monitoring was only possible for two weeks before the logger had to be removed. Subsequent manual readings were obtained for these and all of the other sites to allow the long-term effects to be established

3.6. Conclusions

Following the instrumentation and early-age monitoring of floor slabs in six buildings recommendations have been made which could be applied to the early-age monitoring of any concrete structure. The following bullet points identify the main activities to be carried out for a structural instrumentation:

- Obtain drawings of the structure - identify key locations for instrumentation
- Select suitable sensors
- Design wiring loom and write logger program
- Wire up interface box and gauge cluster boxes
- Test wiring set-up and logger program
- Transport to site
- Fix logger and ambient instrumentation in place
- Install and protect cables from interface box to gauge cluster boxes
- Mark the gauge locations and fix the leads from the cluster boxes in place
- Fix the gauges rigidly in place and connect leads - the gauges should be connected in place as they are needed; the crimp connections should be looped and cable tied to provide strain relief before being waterproofed with tape; the correct functioning of the gauge should be verified
- Embed the gauge in concrete - concrete should be placed all around the gauge with care being taken to prevent concrete from dropping directly onto the gauge
- Performance monitoring - the datalogger is left on site recording data; periodic access is required to download data.

The recommended methodology provides a robust and reliable method for locating the strain gauges which should not disrupt the construction process. Mounting the gauges on reinforcement chairs enables them to be placed quickly and once these chairs have been taped or tied down there is little chance of movement. The newly developed gauges have worked well, although special care is required when installing the 254mm steel strain gauges as their additional length makes them more vulnerable to damage. The gauges for monitoring across

day joints are an important development and open up many new possibilities for engineers wanting to monitor across construction joints in all kinds of structures.

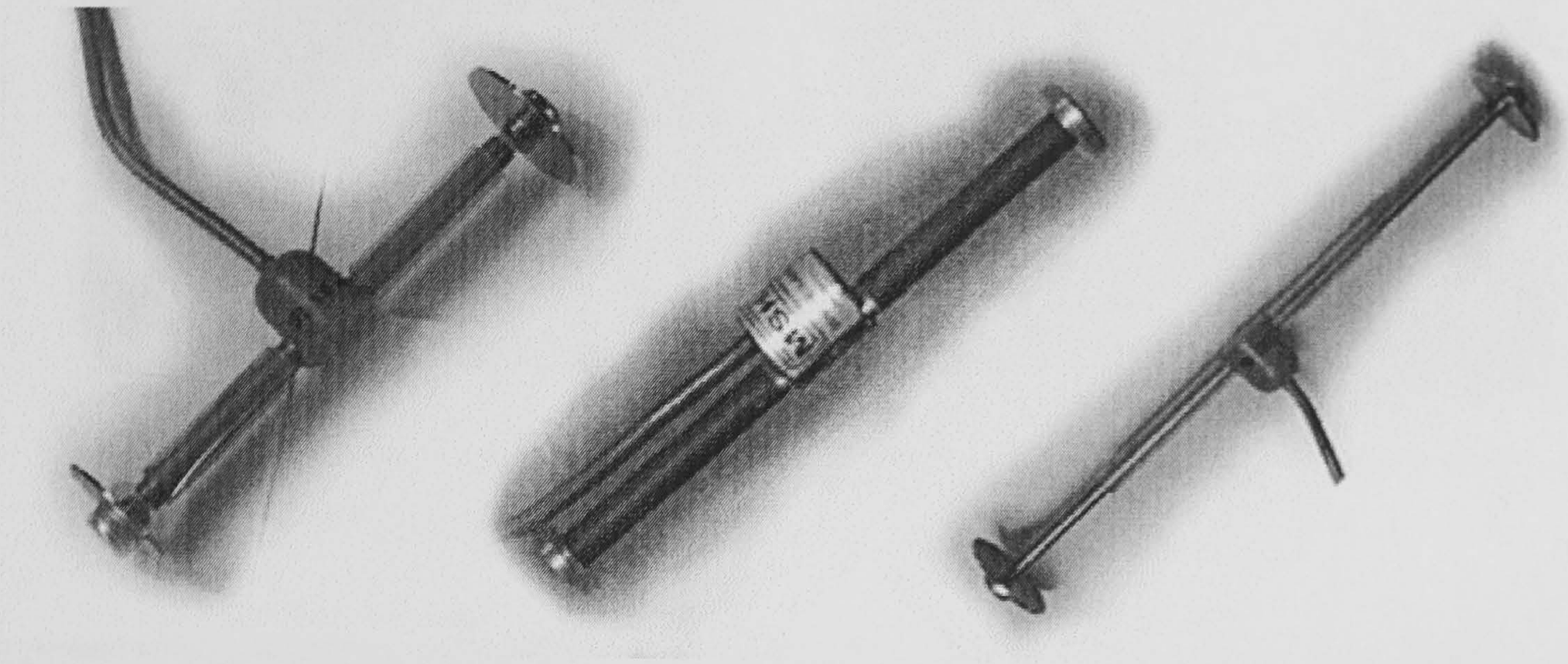

a) TEAB 5.5 b) 4200x c) TES 5.5

Figure 3.1 - Strain gauges tested for use in site instrumentation

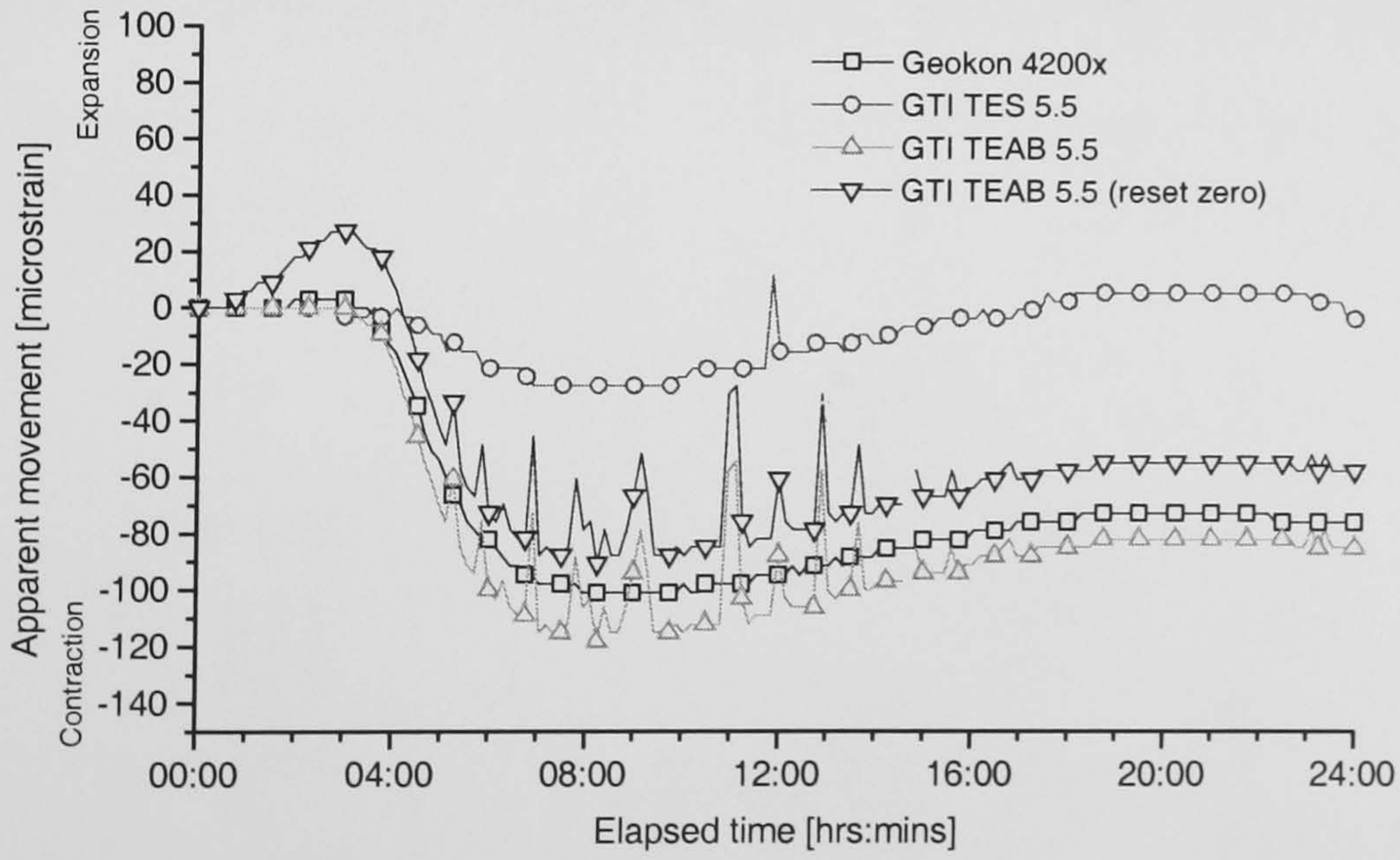

Figure 3.2: Lab testing to determine the early age apparent strains measured by the different gauges

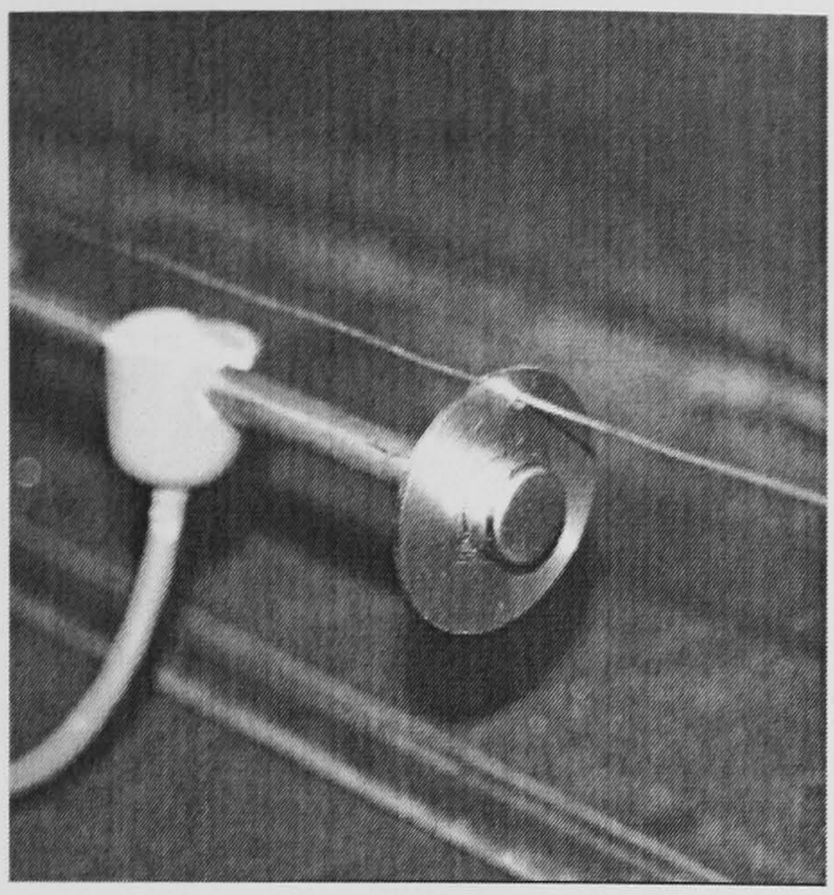

Figure 3.3 - Close up of the gauge fixing method for the trial site

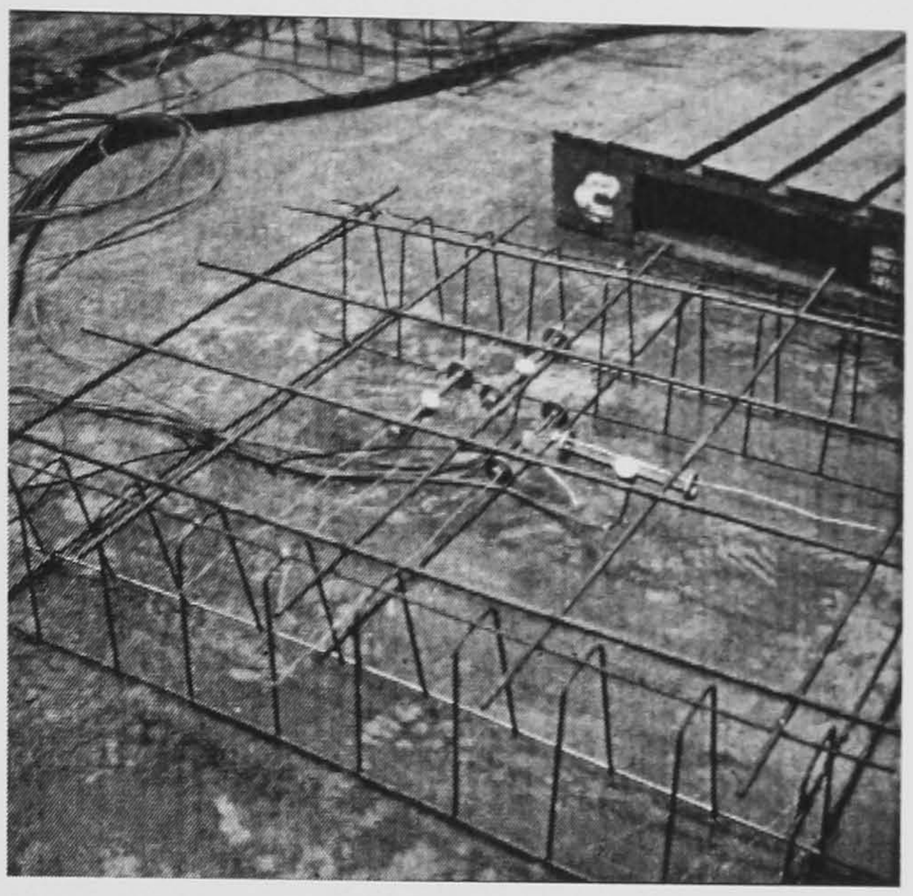

Figure 3.4 – Strain gauges suspended from the reinforcement chairs

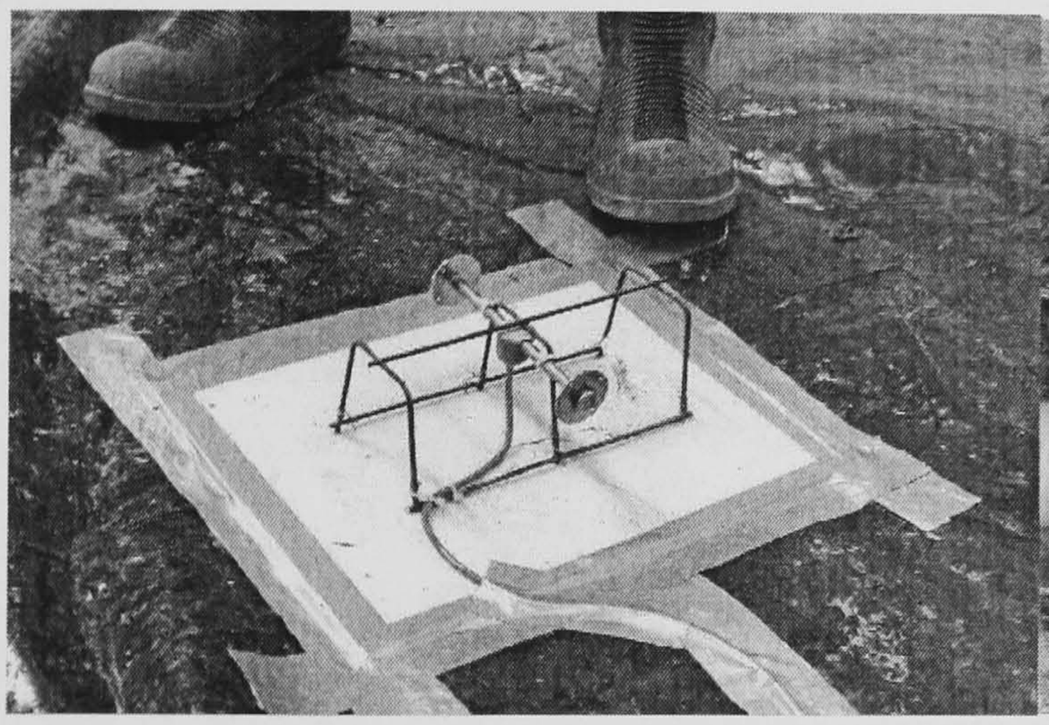

Figure 3.5 – Gauge fixing method for fibre reinforced floors

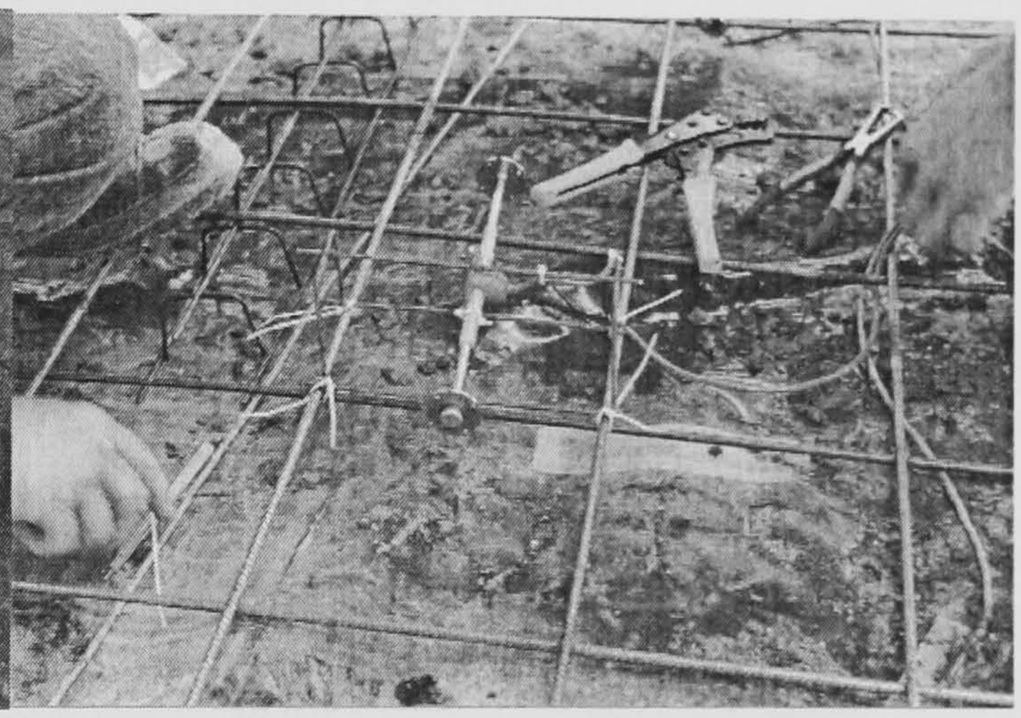

Figure 3.6 – Gauge fixing method for fabric reinforced floors

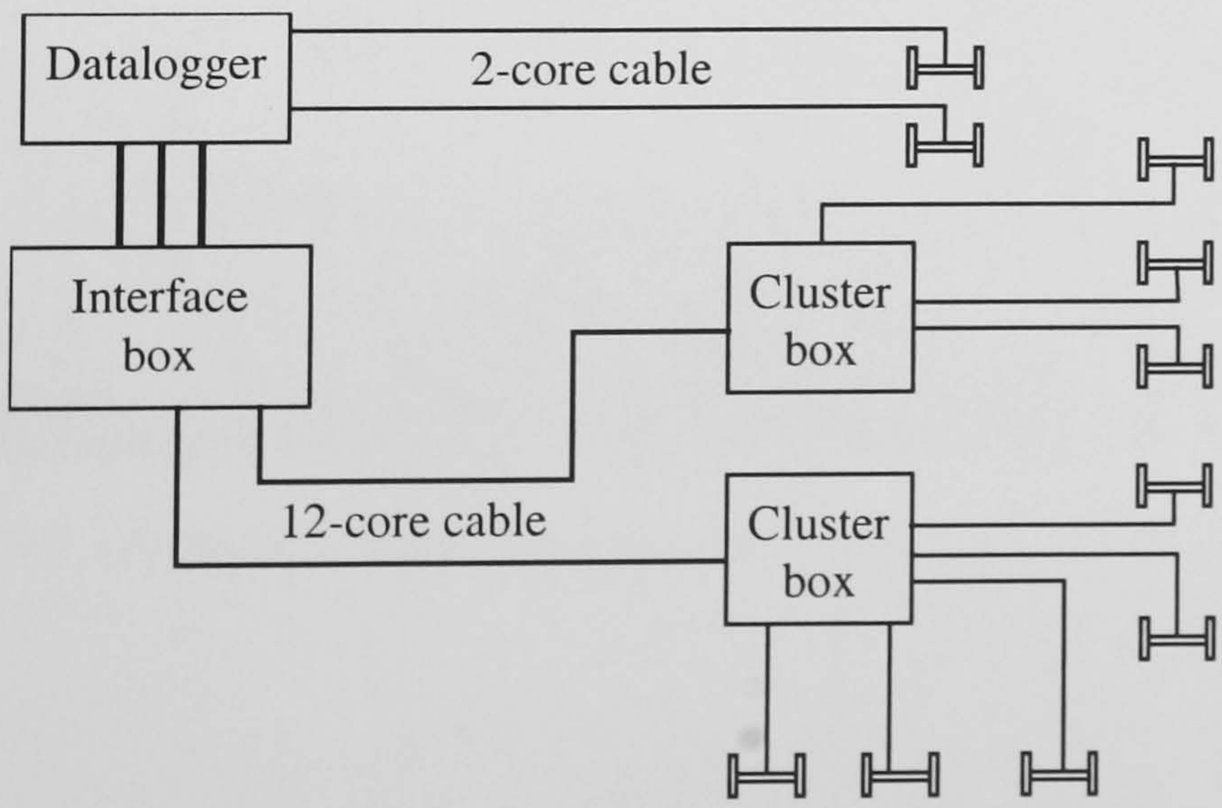

Figure 3.7 - Schematic of gauge clusters and directly connected gauges

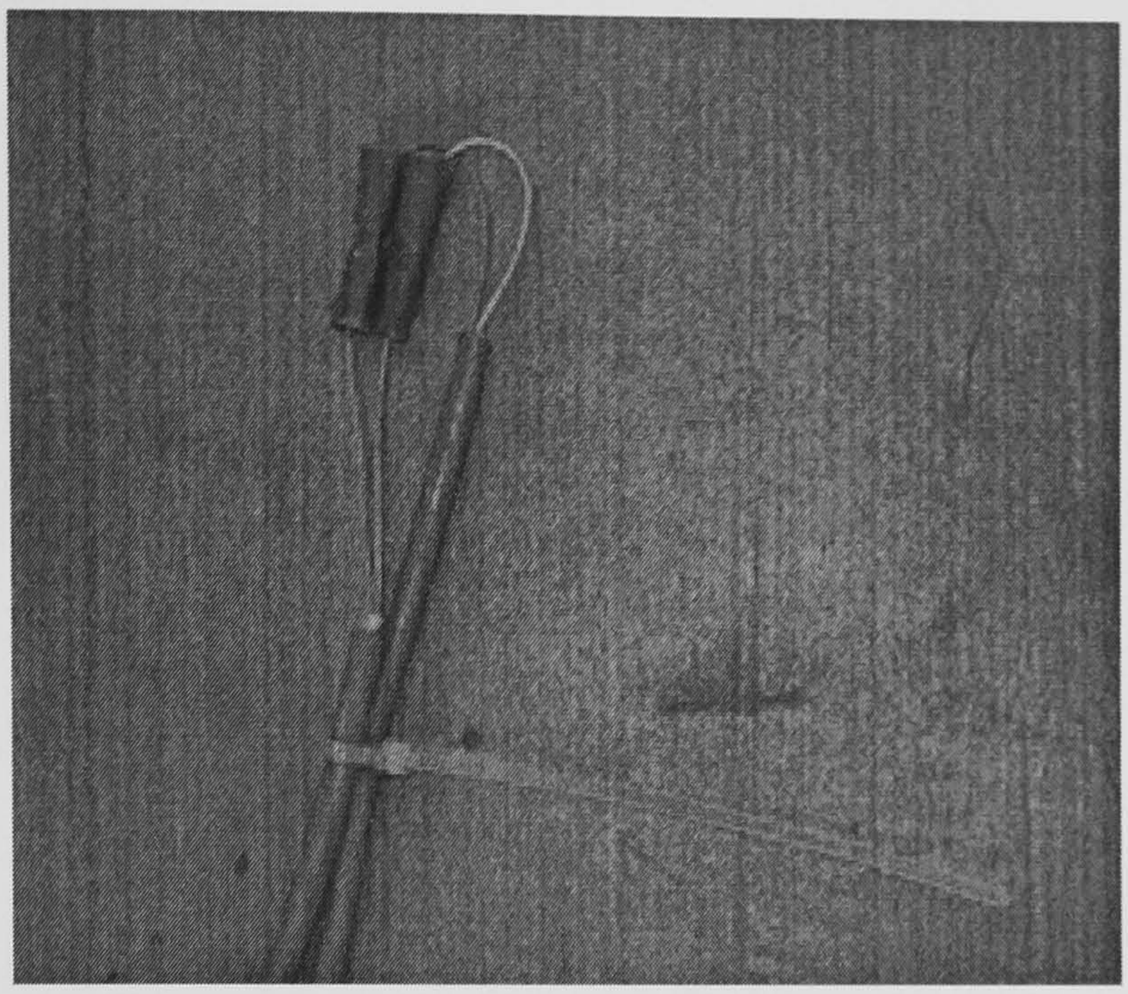

Figure 3.8 - Crimp connection with strain relief prior to waterproofing

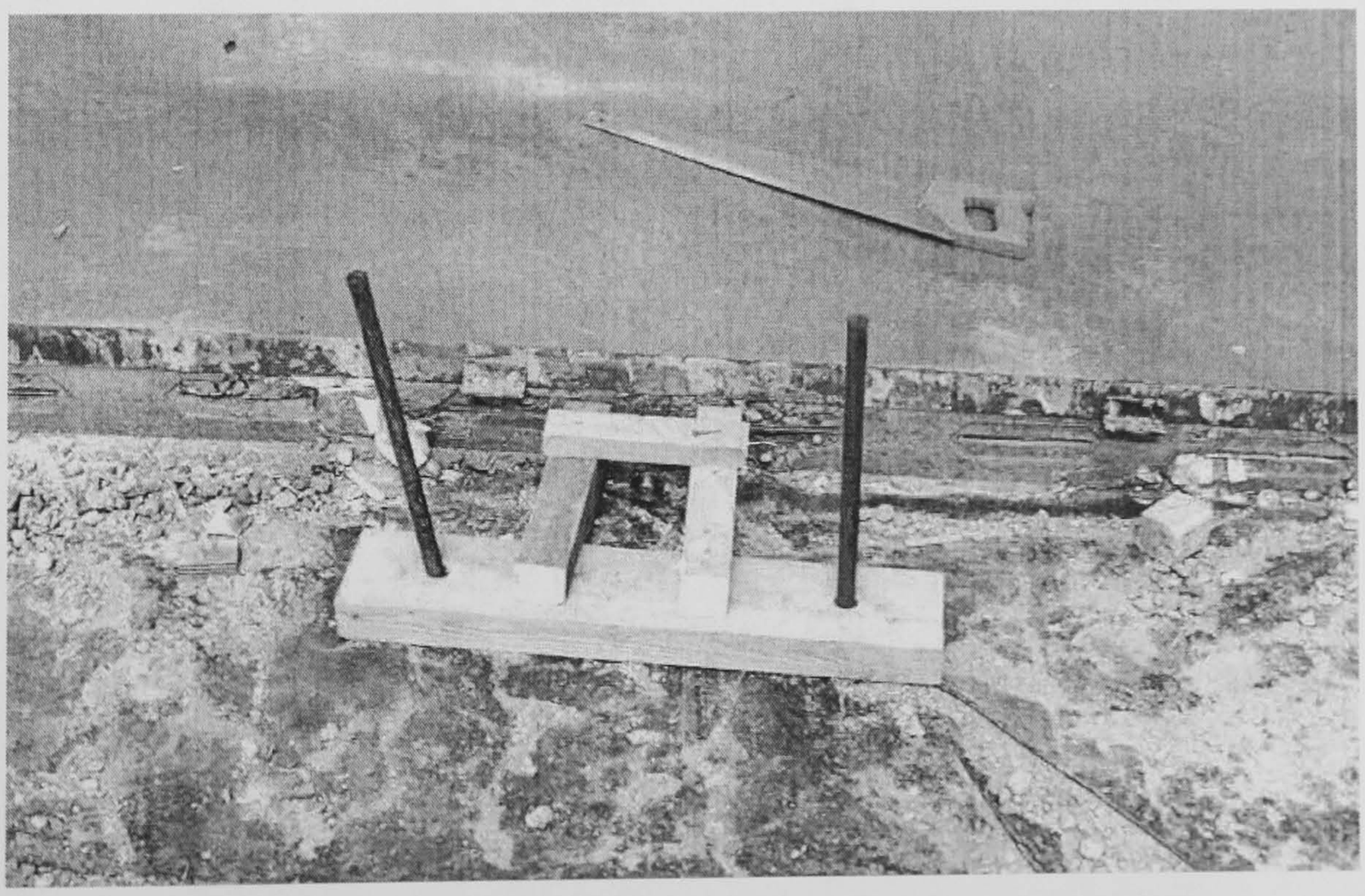

Figure 3.9 - Protecting the exposed part of a standard 10" strain gauge

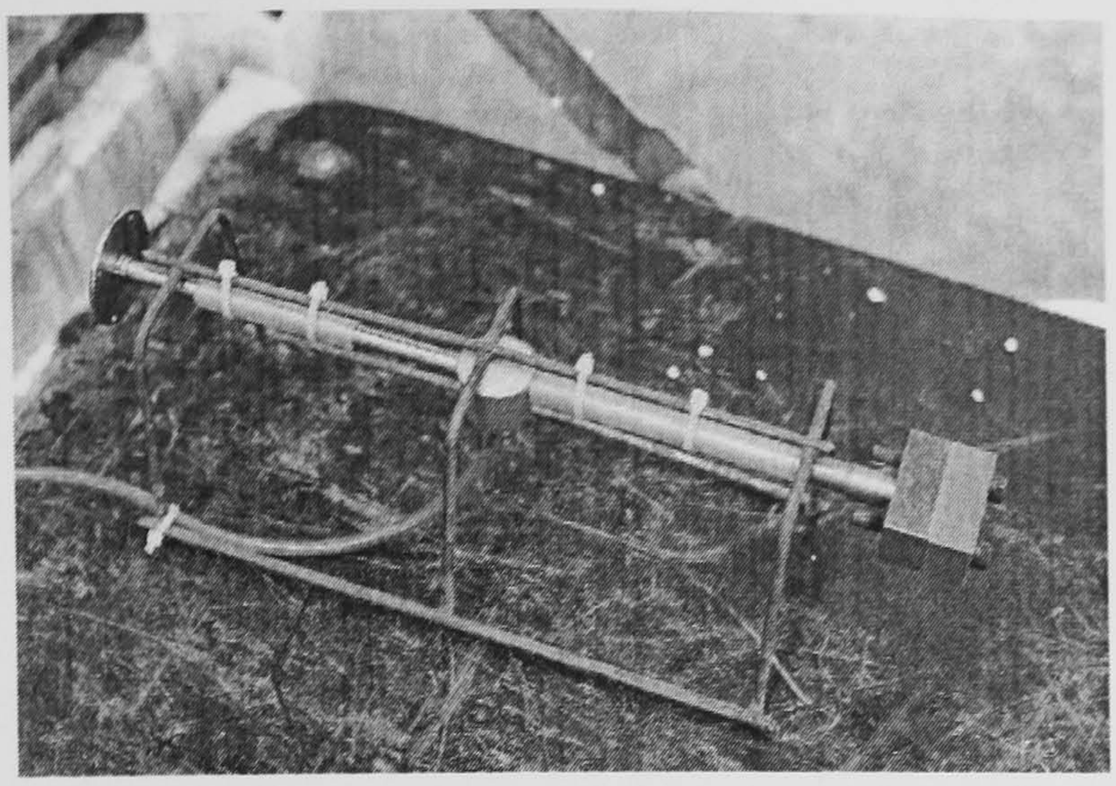

Figure 3.10 – Modified day-joint gauge with dummy end block

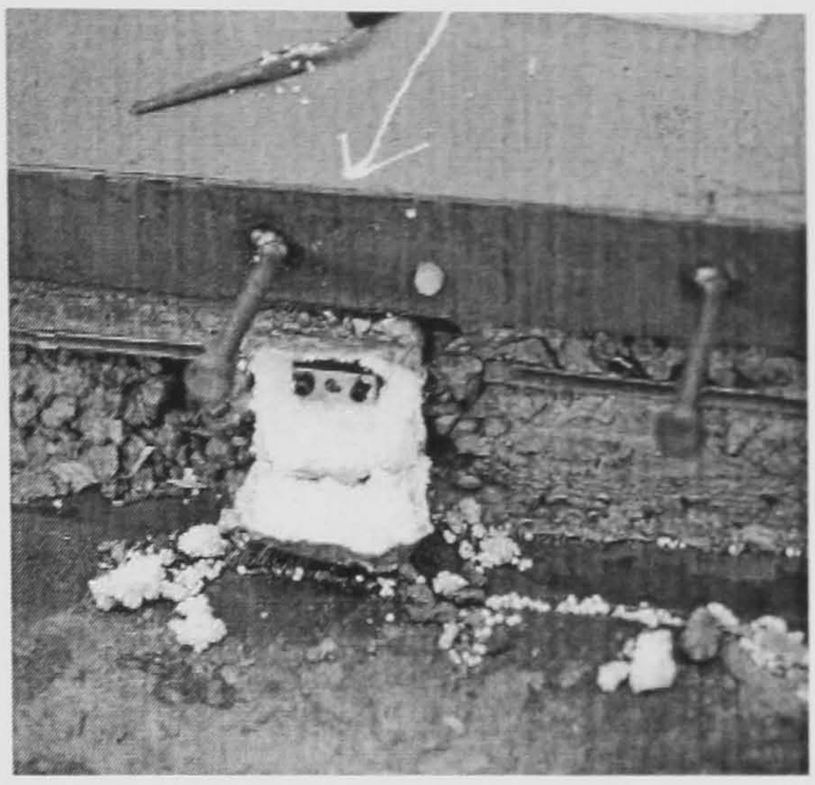

Figure 3.11 – Before removal of polystyrene

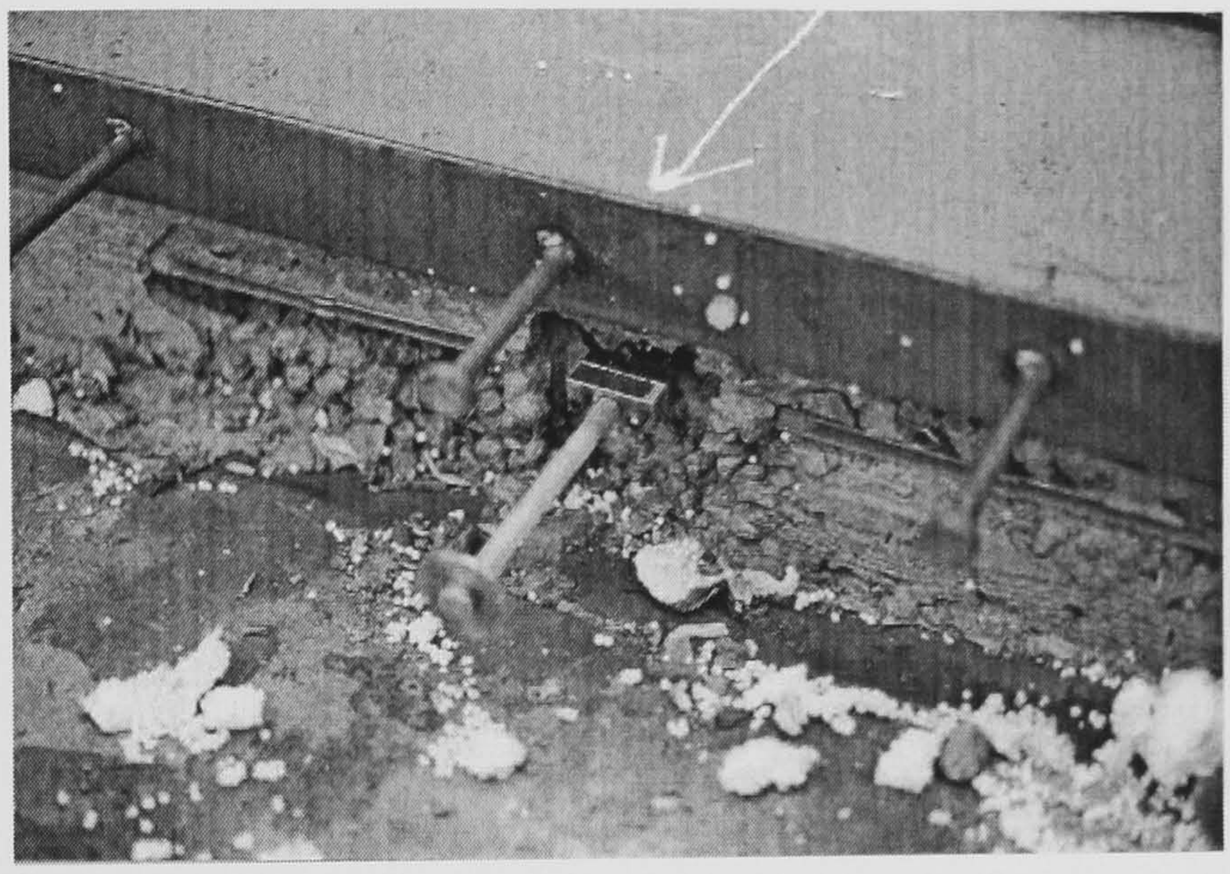

Figure 3.12 - After attachment of extension arm

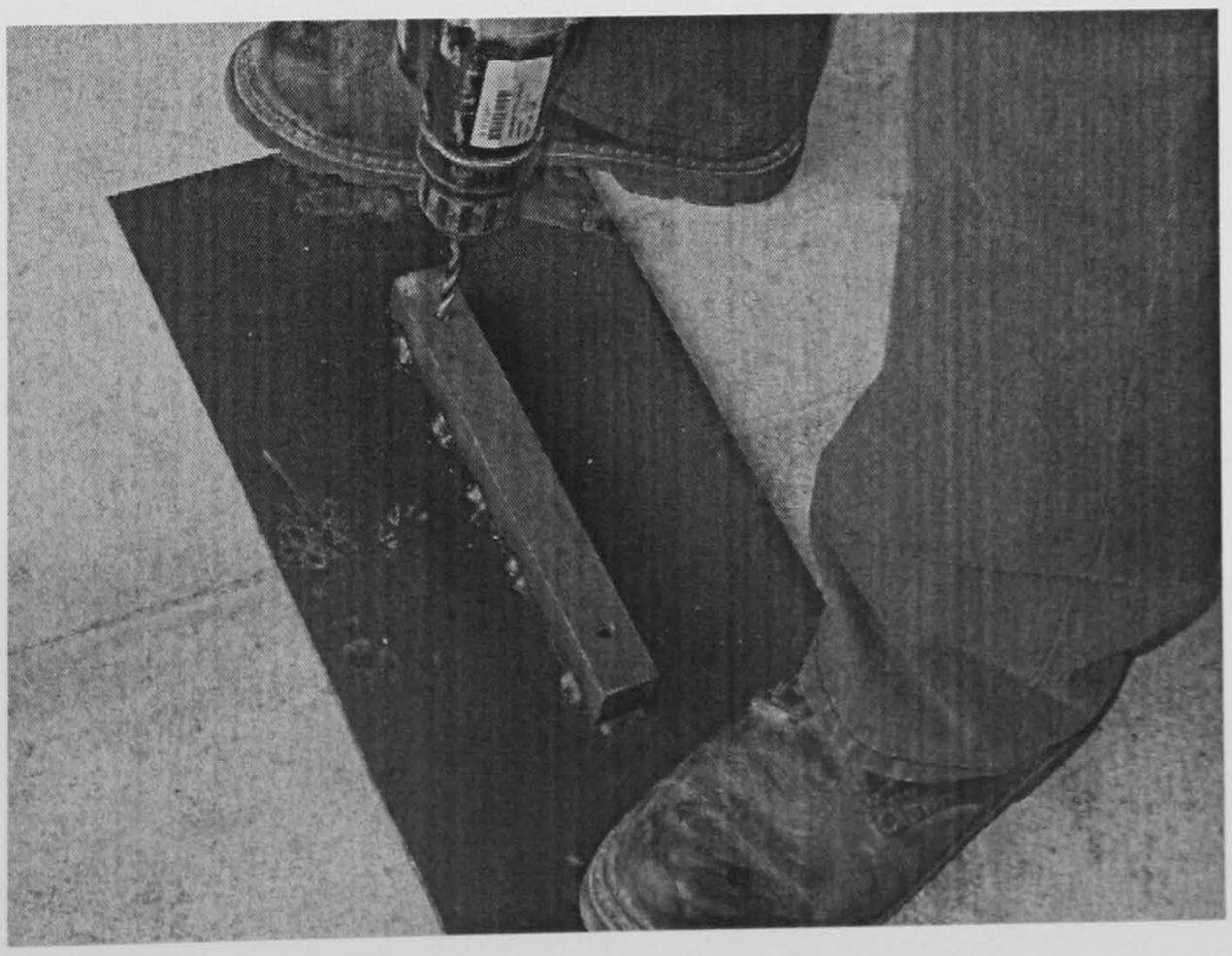

Figure 3.13 - Drilling holes to locate the Demec pips

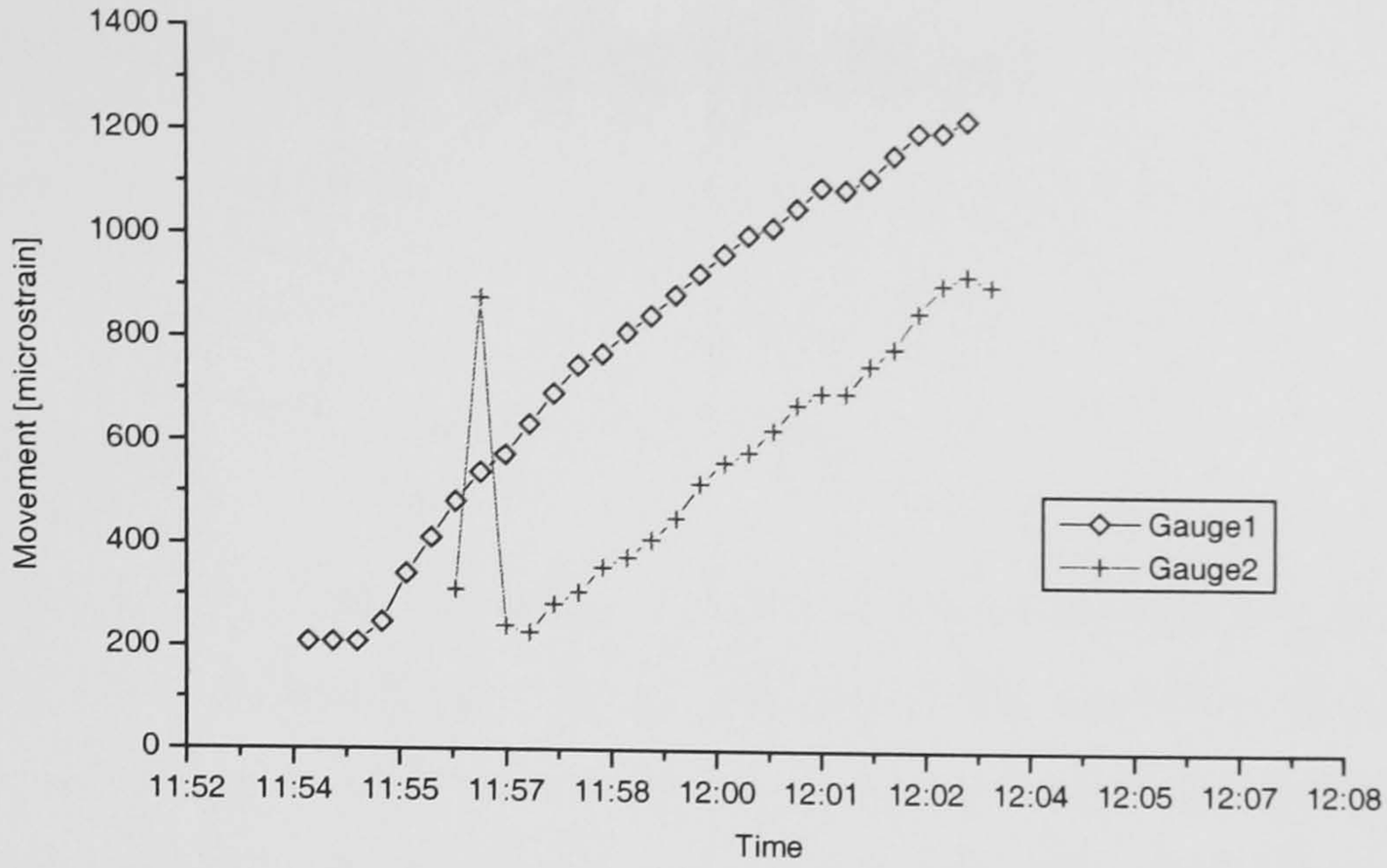

Figure 3.14 - Laboratory demonstration of the gauge pairs

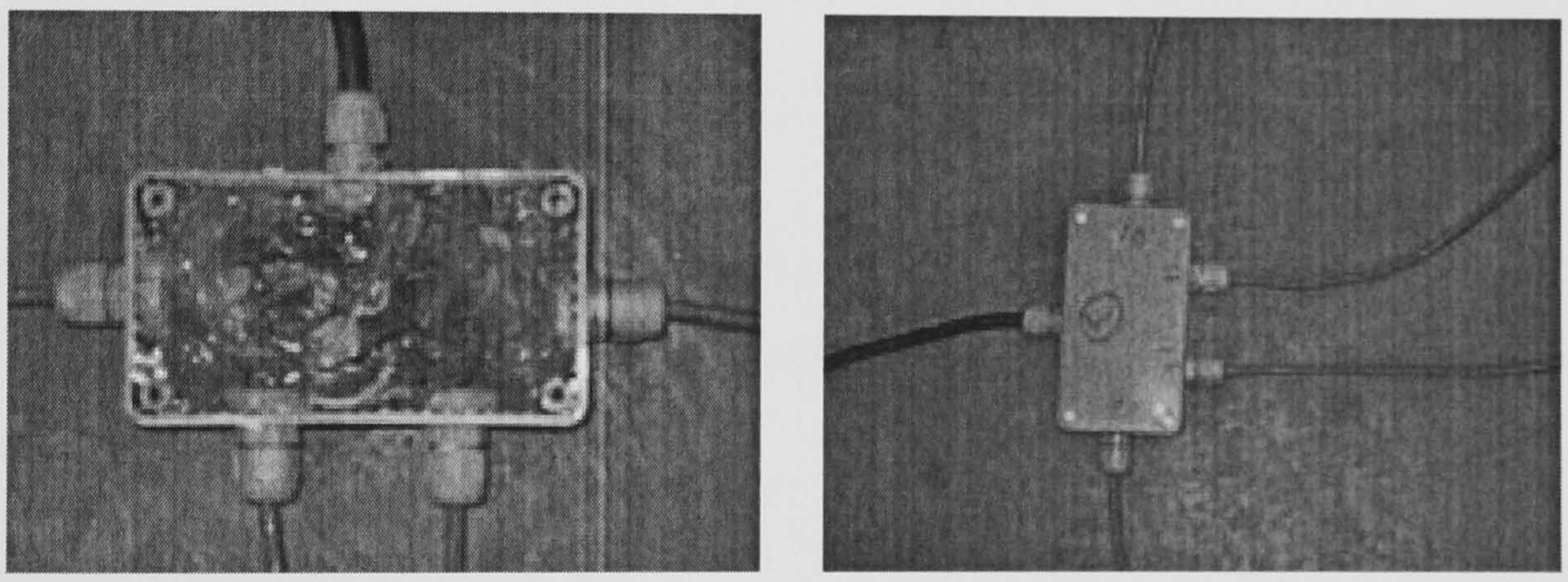

Figure 3.15 – Completed cluster box

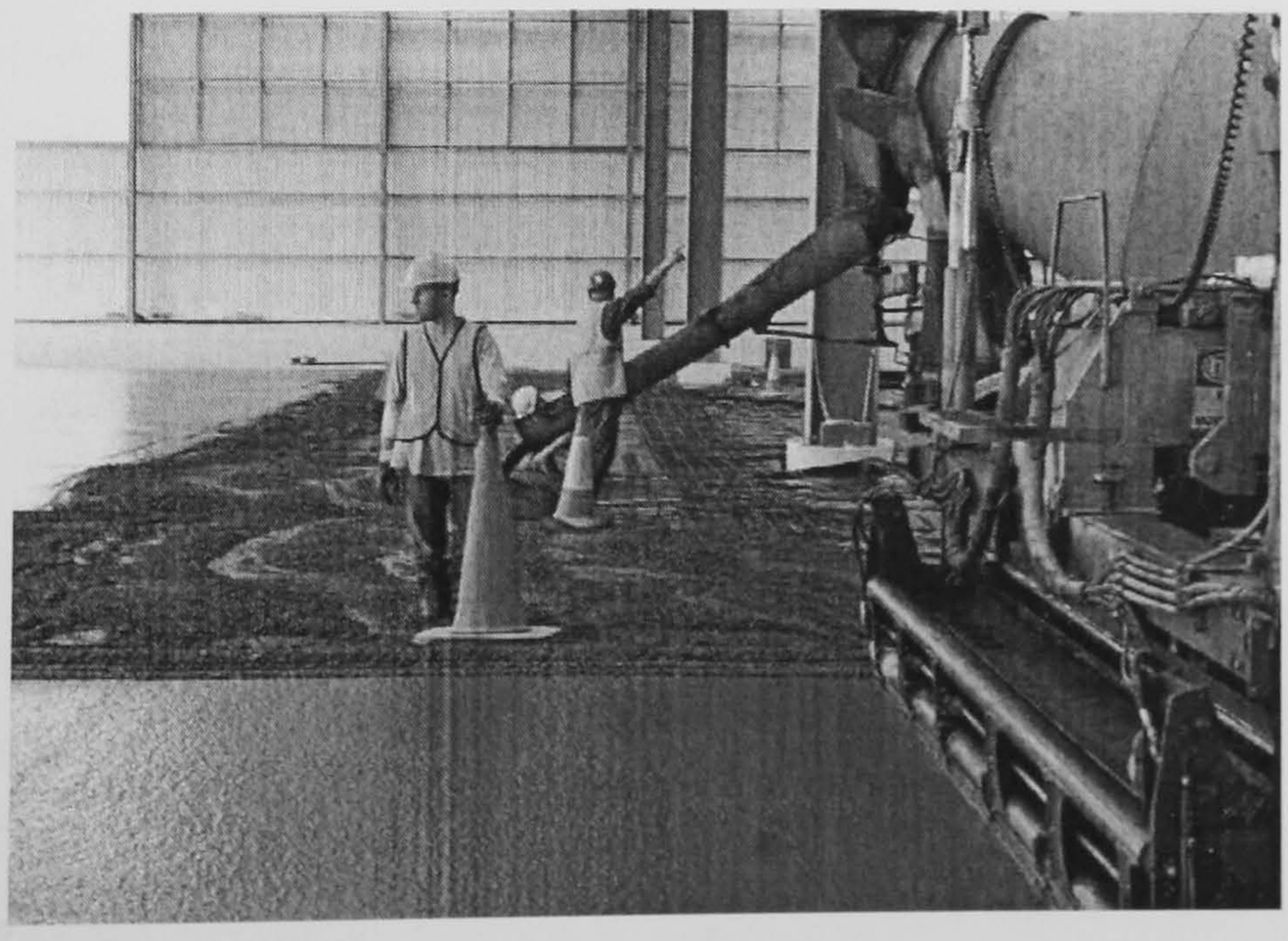

Figure 3.16 - Marking the location of gauges after embedment

4. Detailed site information

4.1. Introduction

Information about the size, instrumentation location and identification of each of the sites is given in this chapter. Confidentiality requires the sites not be identified by name, but a full description of the building layout and the instrumentation locations is provided, along with a general description of the geographical location of the building. The floors are described according to their category and not in the order, in which they were instrumented.

The concrete mix designs, cube test results and further instrumentation location information for each floor are presented in Appendix B. This appendix also contains information about the Meteorological Office weather stations that were used for ambient weather data when site monitoring was not being carried out.

All the plans of gauge locations and identifications have been provided on A3 paper to allow them to be folded out of the thesis for easy reference in the later chapters where the results are presented and discussed.

4.2. Northampton: Mesh reinforced long strip

This floor slab was constructed in a distribution warehouse located on the M1 corridor in the Midlands. Flooring work was carried out from the end of January until the end of March 1998, although the discovery of soft spots in the subgrade meant that work was not continuous during this period. Long strip construction was chosen for this floor in order to meet the Category 1 defined movement flatness tolerances.

Instrumentation was included in a section of the third phase of this floor (Figure 4.1), which was constructed on 23rd March 1998.

The placement of the instrumentation in the slab allowed the effects of depth and the distance from joints and adjacent strips to be monitored, as well as the performance of the two different types of joint. The strain gauges were fixed at two different levels in the slab (three at position 6) to allow any depth related effects to be monitored. The gauges were 80mm and 60mm from the slab top and bottom respectively, with the third gauge 120mm from the slab bottom at position 6. The gauge layout and instrumentation positioning with respect to the rest of the building was as shown in Figure 4.1and Figure 4.2.

This long strip slab was constructed on top of a 1200 gauge polythene damp proof membrane (lapped and taped to prevent the passage of Radon gas) which in turn was laid on a 150mm thick Type 1 sub-base. The slab was 260mm thick and reinforced with A193 crack control mesh reinforcement supported on chairs giving 50mm top cover. The instrumented strip was tied along the longitudinal edges to the adjacent strips with formed restrained movement joints using 900mm long 12mm ∅ mild steel dowel bars at 300mm centres. Two types of joint were monitored, namely a sawn restrained movement joint and a sawn free movement joint. The sawn free movement joints were reinforced at mid-depth with 500mm long, 20mm ∅ mild steel dowel bars at 300mm centres. A tight fitting plastic sleeve was used to debond half of each of these dowels to allow free opening of the joint (Figure 4.3). The sawn restrained movement joints had 900mm wide strips of A193 mesh placed 50mm from the bottom of the slab, which was intended to carry longitudinal stresses across the joint controlling joint opening, whilst reducing the risk of cracking mid-way between free movement joints and alleviating warping stresses (TR34, 1994). The longitudinal joints were saw-cut to a depth of 20mm 24 hours after construction of the slab, whilst all of the other joints were saw-cut 75mm deep.

The installed data logger and interface box can be seen connected to a laptop computer in Figure 4.4. This allows the progress of the strain gauge embedment to be monitored in real time.

After the ambient probes had been removed from site, ambient temperature information was obtained from the Moulton Park Meteorological Office weather station located at OS grid reference SP 765644.

4.3. Chepstow: Mesh reinforced jointed large area pour

The first mesh reinforced jointed large area pour floor to be instrumented was constructed in a distribution warehouse alongside the M4 near to Chepstow. Construction of the floor was carried out between 7th and 27th July 1999 with the instrumented sections of floor, pours 10, 11 and 13, being cast on 21st, 22nd and 26th July. The instrumentation layout and relation of these pours to the building can be seen in Figure 4.5.

This large area pour floor was constructed on top of a 200mm layer of Type 1 hardcore covered with a 1200-gauge polythene slip membrane. The slab was 225mm thick and reinforced with A193 nominal crack control reinforcement 50mm from the slab bottom. Joint spacing was to suit the column layout and was on 8.200m centres down the length of the building and 5.900m centres across the building in the instrumented pours. The concrete used was of grade C40 and specified to have a shrinkage of less than 0.045%.

The day-joints between pours were formed restrained movement joints with 1.500m long T12 dowels at 200mm centres. The sawn restrained movement joints consisted of a saw-cut groove 75mm deep and 3mm wide, which was cut 24 hours after placement of the slab. The crack control reinforcement was continuous across these joints.

Instrumentation was only placed at mid-depth in this slab in order to maximise the area of floor which could be monitored. Once the ambient probes were removed from the site, ambient temperature information was obtained from the Penhow Met. Office weather station located at OS grid reference ST 413906.

4.4. Leeds: Mesh reinforced jointed large area pour

A second mesh reinforced jointed large area construction floor was constructed just off the M62 near Leeds (Figure 4.6). This floor formed the working platform in a combined chilled, frozen and ambient food distribution building. Construction of the floor for the ambient and chilled storage areas was carried out between 10th and 20th April 2000, with the instrumented pours - 1, 2 and 4 - constructed on the 10th, 11th and 13th.

Pours 1 and 2 form an ambient storage area, which is operated between 12 and 14°C, whilst the chilled storage in the remainder of the building operates at 2 - 4°C. The building was taken down to its operating temperature 14 weeks after construction work finished on the floor.

Formed free movement joints were used in the day-joints between the ambient and chilled storage areas to prevent differential thermal movement induced stresses. These joints were also used to isolate the second pour, which contained a shrinkage-reducing admixture, from the first pour. Diamond dowels 6mm thick and 125mm square were used at 500mm centres to provide load transfer across these joints, whilst leaving the joint free to move horizontally.

The 225mm thick floor slab was cast on a 1200 gauge polythene slip membrane laid on top of 150mm of well-compacted Type 1 granular hardcore. Crack control reinforcement was provided by A193 mesh placed 50mm from the bottom of the slab.

The remaining day-joints were of the formed restrained movement type with 1.500m long T12 bars at 200mm centres. Sawn free movement joints were placed 900mm from these joints with 600mm long R30 dowels at 300mm centres to provide load transfer. Half of each dowel was sleeved to debond it and allow free joint opening. Further sawn free movement joints were provided in the floor to allow stresses due to thermal contraction and drying shrinkage to be accommodated.

Sawn restrained movement joints were used at all other locations, with the A193 mesh running continuously across them. All of the saw cuts were 75mm deep and 3mm wide.

Two joint gauges were installed across half of the joints in pours 1, 2 and 3 (Figure 4.6) to monitor depth related joint movements and provide redundancy in the case of failure, whilst single embedment gauges were located at mid-depth in the slab mid-way between the instrumented joints. All of the joints in these three pours were also monitored with Demec pips to allow a complete picture of joint movement to be obtained.

Two arrays of thermistors were installed in pours 1 and 2 to measure the temperature variation up to 0.8m below the surface of the slab, whilst two chilled mirror probes were used to record the relative humidity at different depths in the slab.

Once the ambient probes were removed from the site, ambient temperature information was obtained from the Leeds Met. Office weather station located at OS grid reference SE 290339.

4.5. Daventry: Steel fibre reinforced jointed large area pour

This floor slab was constructed in a distribution warehouse close to the M1 corridor near Daventry. The floor was constructed between the 22nd and 31st March 1999, with the instrumented sections of floor constructed on the 26th and 31st March 1999 (Figure 4.7).

The floor was 160 mm thick and contained 25kg/m^3 Dramix RC 45/50 steel fibres for crack control. It was constructed on a 1200 gauge polythene slip membrane placed on 200mm well compacted Type 1 granular sub-base.

Day joints were of the formed restrained movement type with 1500mm long T12 bars at 200mm centres. Sawn free movement joints 900mm from these joints were reinforced with 400mm long T16 bars at 300mm centres; the bars were sleeved over half their length to debond them from the concrete. The same reinforcement was used at the other sawn free movement joints in the slab. All of the joints were saw-cut 3mm wide and to a depth of 50mm.

Instrumentation was placed in two lines down the length of pour 5, and in one line across it, to assess if the distance from the edge of the building affected the movement. The spacing of the embedment gauges was varied in order monitor any differences in behaviour related to distance from the sawn restrained movement joints.

All of the strain gauges were placed at mid-depth in both pours. Demec pips were also fixed above the gauges along section A-A, allowing larger joint movements to be measured and also giving some indication of differential movements at the joints.

Once the ambient probes were removed from the site, ambient temperature information was obtained from the Church Lawford Saws Meteorological Office weather station located at OS grid reference SP 456736

4.6. Bedford: Steel fibre reinforced jointless large area pour

A jointless large area pour was used for a distribution warehouse located on the M1 corridor near Bedford (Figure 4.8). The 165mm thick floor was constructed on top of a 1200 gauge polythene slip membrane in three pours on the 24th, 28th and 29th June 1999. Dramix RC – 60/65–BN steel fibre reinforcement was used at a dosage of 35 kg/m^3 to control cracking, whilst also providing improved post crack ductility allowing the slab thickness to be reduced according to the ultimate load design method.

Diamond dowels 125mm square and 6mm thick were used at the free movement joints between the pours at 300mm centres. These provide shear load transfer between the two slabs but do not prevent horizontal joint movement.

Instrumentation was placed across the free movement joints between both pours, and embedment gauges monitored longitudinal movements down the length of the building and transverse movements across its width in the second pour. This was the first jointless floor and the second large area pour to be monitored. Large numbers of gauges had been lost in the first large area pour, so a revised instrumentation methodology was used. Because of uncertainty about the floor behaviour (and in order to reduce risks with the instrumentation until the instrumentation methodology had been proven), a smaller number of gauges was used compared to the previous floor.

Newly developed joint gauges were also installed alongside the 10" long steel gauges used previously across day joints without success.

Only one gauge was used at each location so no depth related effects could be monitored. However, the effects of distance from a free movement joint and restraint were investigated.

Local weather data was provided by the Meteorological Office weather stations at Bedford Saws and Woburn. These are located at OS grid references TL 049597 and SP 964360

4.7. Marston: Steel fibre reinforced jointless large area pour

This second jointless large area pour construction floor was also located on the M1 corridor near Marston (Figure 4.9). The 175mm thick slab was constructed on a 1200 gauge polythene slip membrane and reinforced with 35kg/m^3 Dramix type RC-65/60-BN steel fibres. Construction work was carried out from 15th to 28th September 1999, with the instrumented sections of floor cast on 22nd, 23rd and 27th September. Diamond dowels were again used between the pours to provide shear load transfer.

Each of the joints between the pours was monitored as was the movement between the edge of pours 7 and 9 and the walls of the building. Embedment strain gauges were installed at

different depths and distances from the free movement joints down the length of the building, although gauges were also installed part way across the building in pour 9. This distribution of instrumentation was chosen to make it possible to assess the influence of the free length on both the longitudinal and the warping behaviour of the slab.

Local weather data was provided by the Bedford Saws and Woburn Meteorological Office weather stations located at OS grid references TL 049597 and SP 964360.

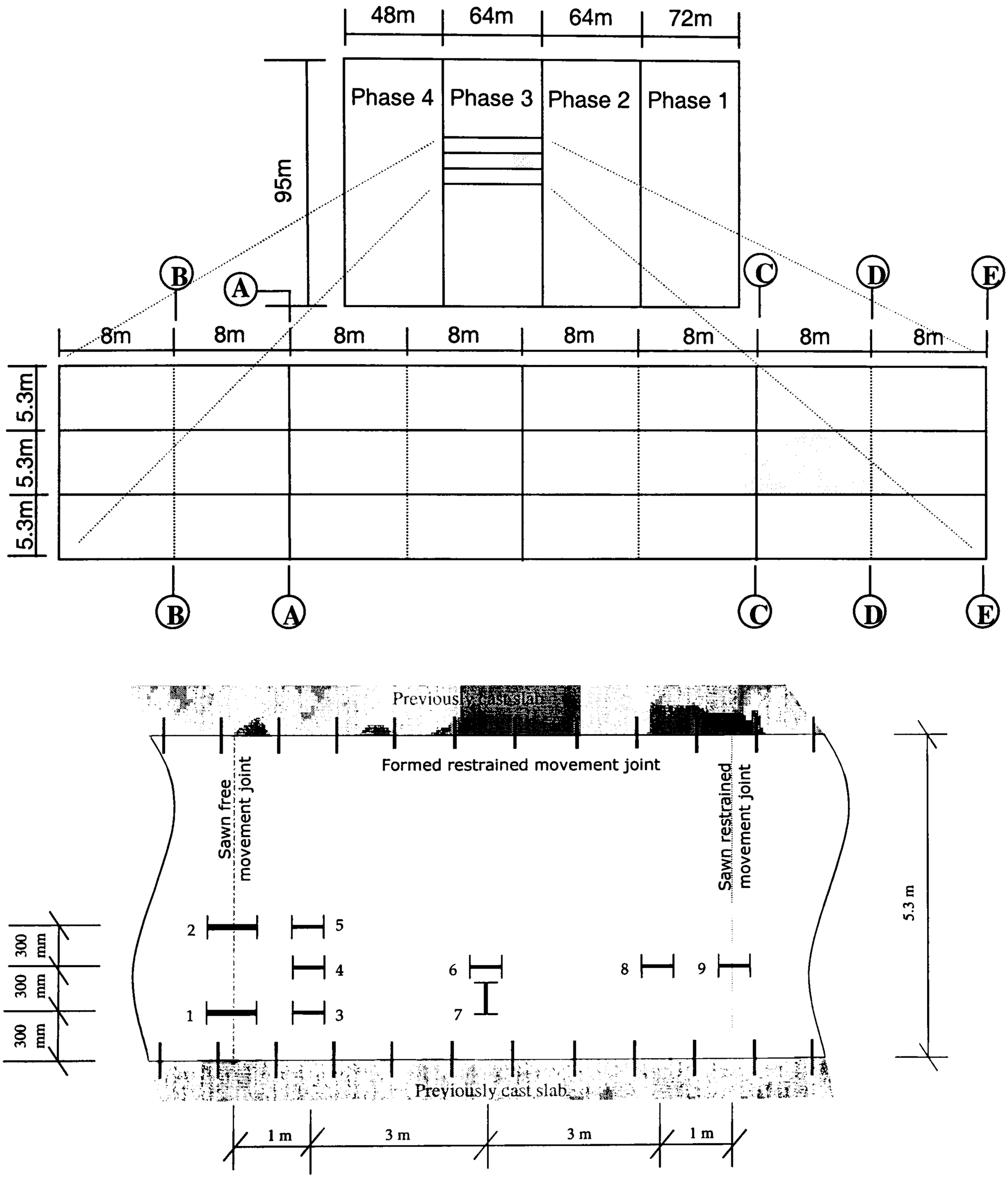

Figure 4.1 – Northampton: Long strip gauge layout and location

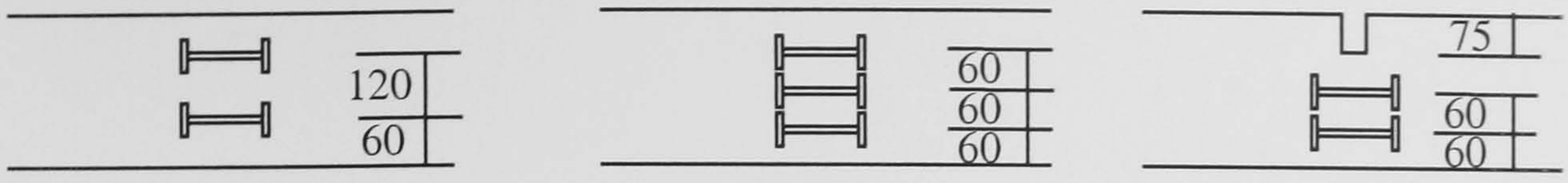

a – double gauges b – triple gauges c – joint gauges

Figure 4.2 – Northampton: Section view of the slab showing the strain gauge locations

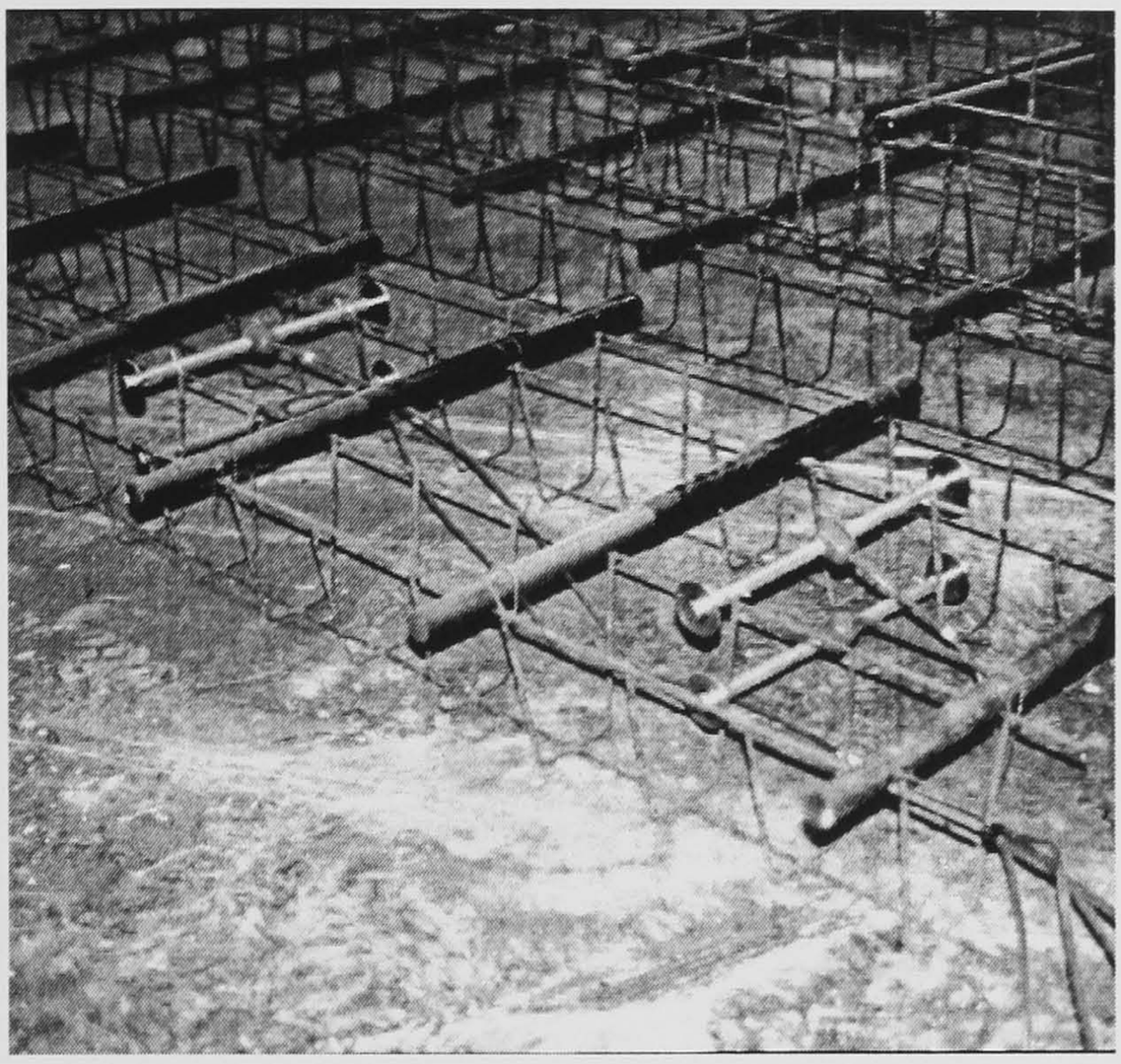

Figure 4.3 – Northampton: Instrumentation at the contraction joint

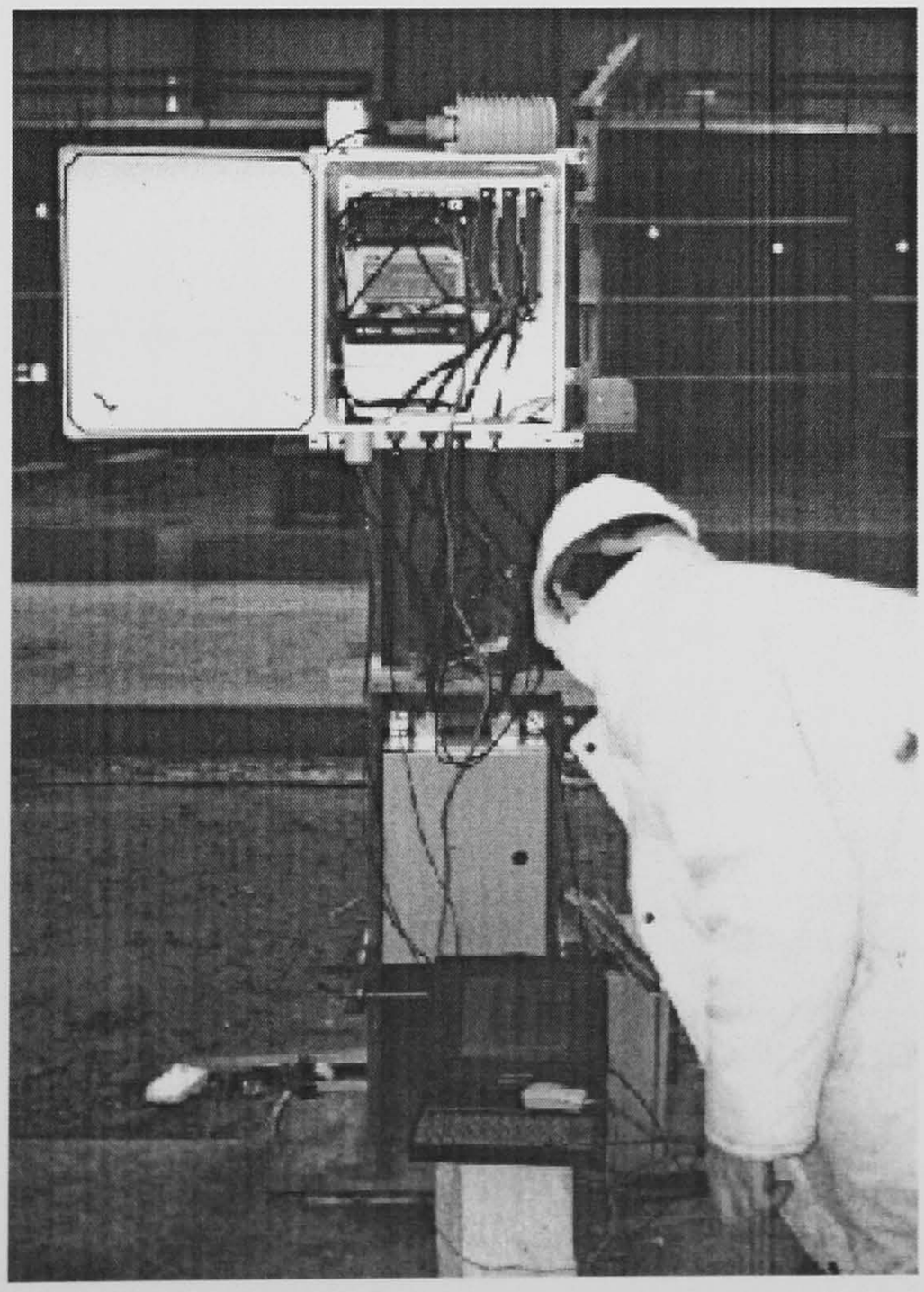

Figure 4.4 – Northampton: Datalogger installation

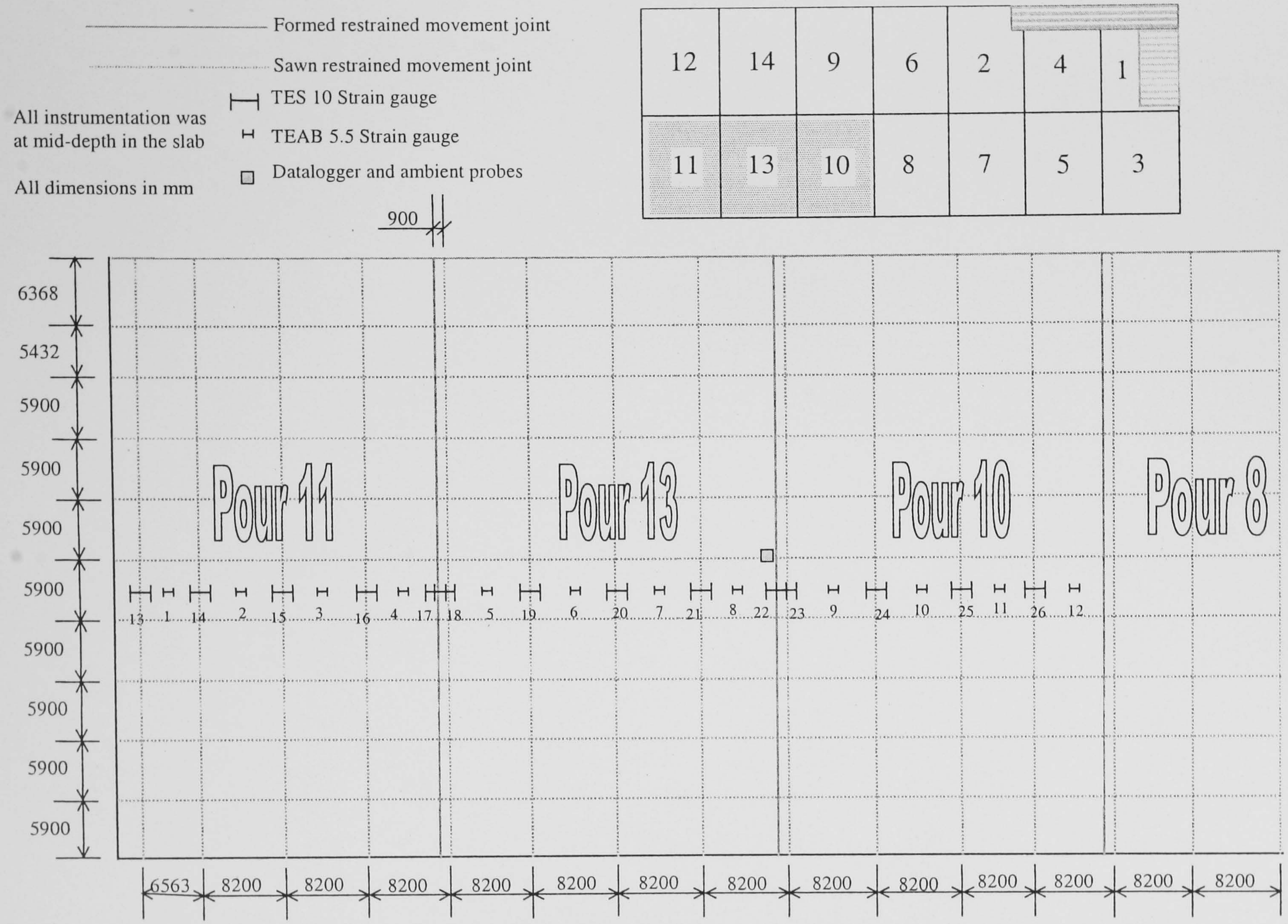

Figure 4.5: Chepstow: Instrumentation details for the mesh reinforced jointed large area pour

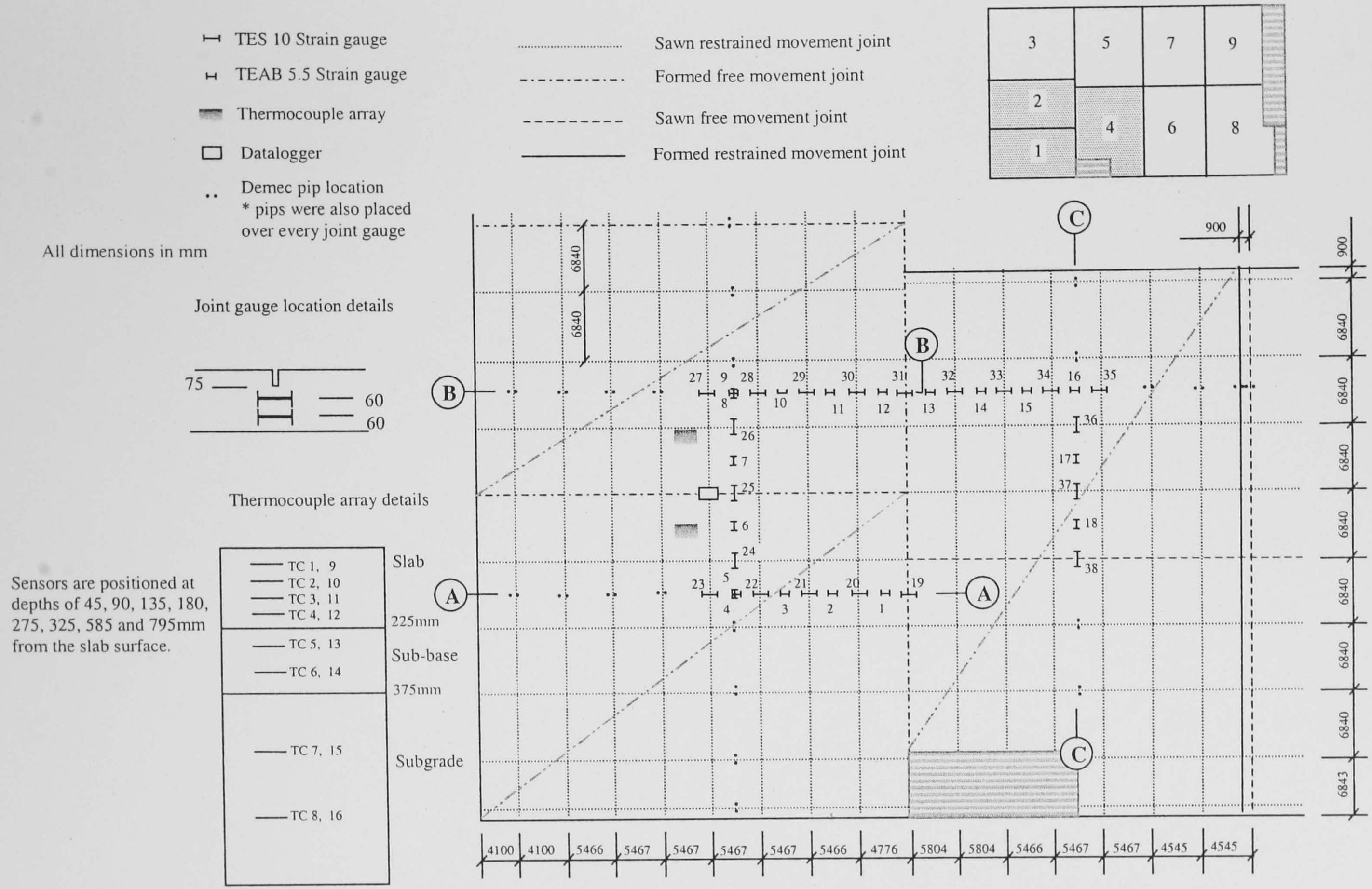

Figure 4.6: Leeds: Instrumentation details for the mesh reinforced jointed large area pour

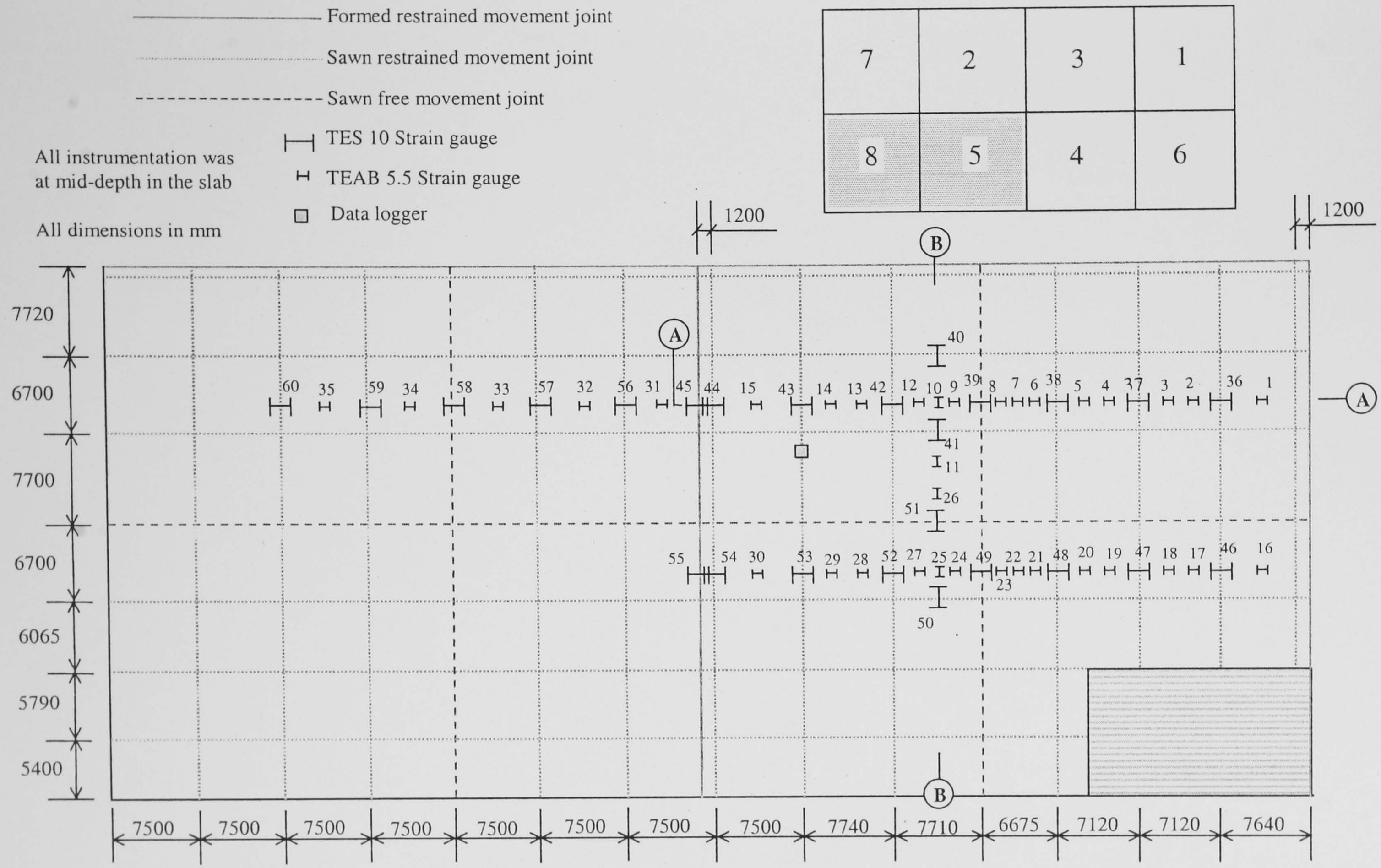

Figure 4.7 – Daventry: Instrumentation details for the fibre reinforced jointed large area pour

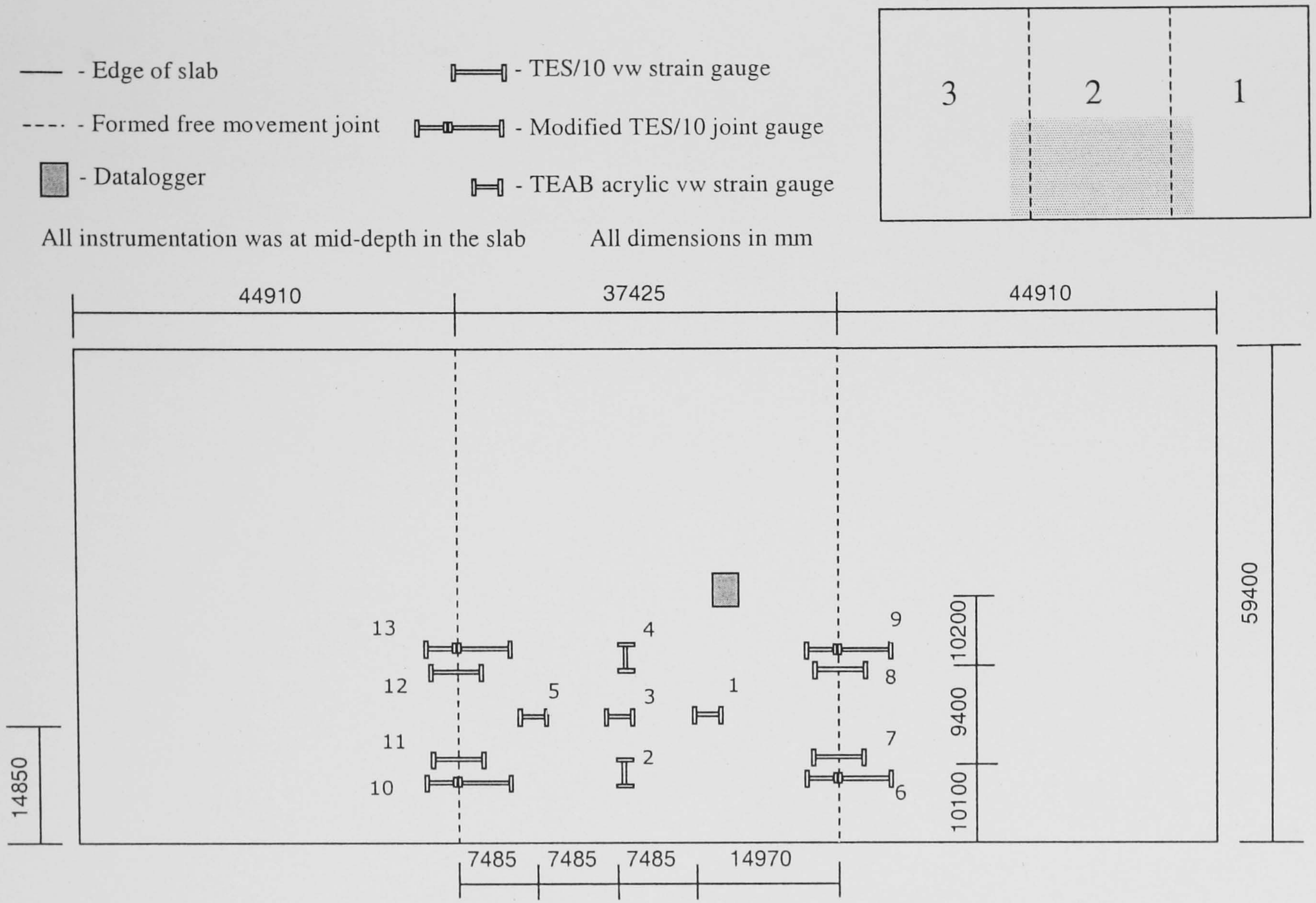

Figure 4.8 – Bedford: Instrumentation details for the first fibre reinforced jointless large area pour

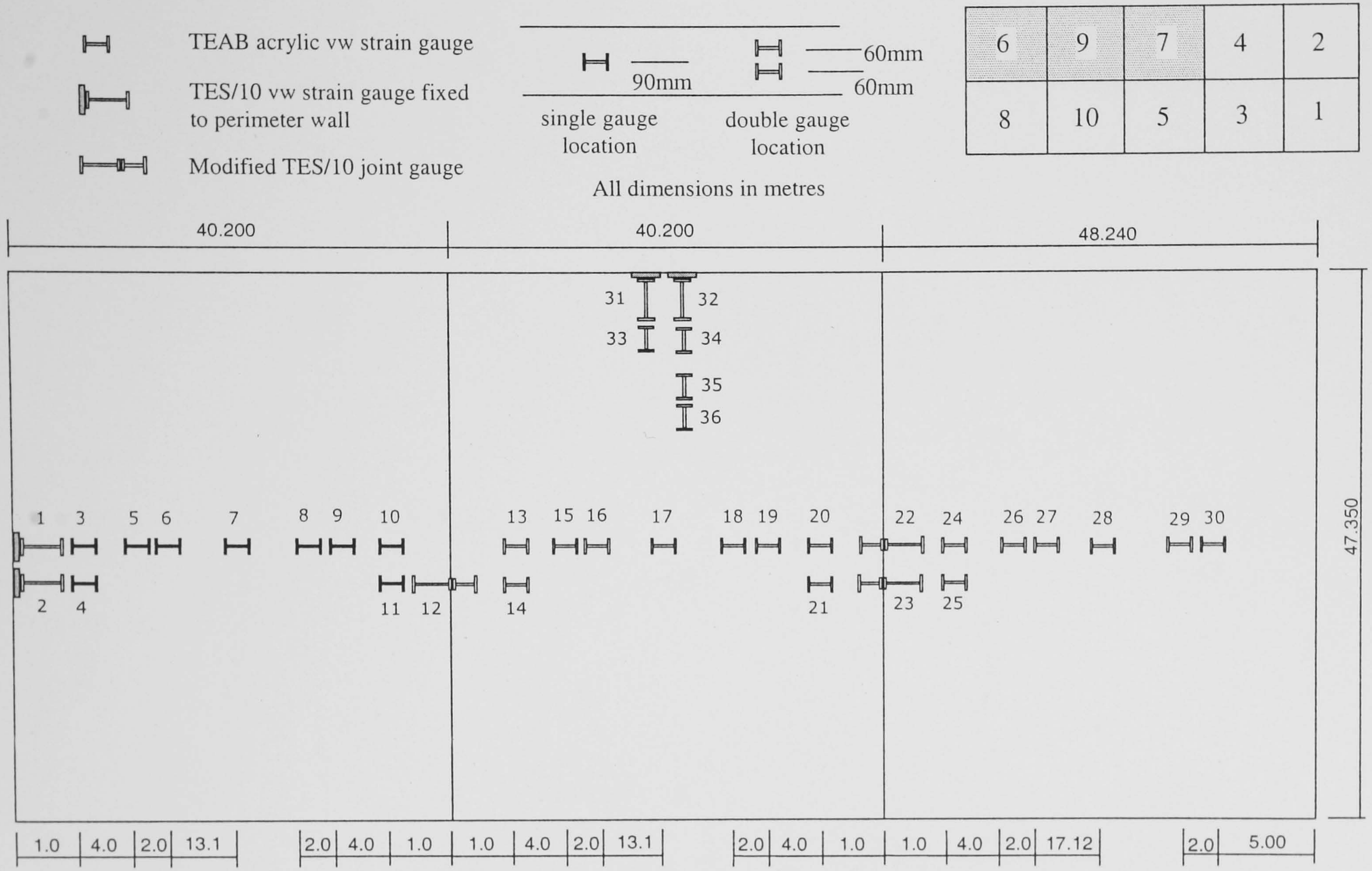

Figure 4.9 – Marston: Instrumentation details for the second fibre reinforced jointless large area pour

5. Analysis of data

5.1. Introduction

This chapter presents the data from the sites which have already been identified in Chapter 4. Strain data from the concrete and joint movements are presented for all sites, although the monitoring positions were varied in order to try and identify different behavioural patterns. The monitoring periods differ depending on the length of site access allowed following construction, and this along with the distance to some of the sites also affected the ability to carry out additional work such as precision level surveys. It had initially been intended that the different construction methods would be investigated along with the effects of seasonal variations in the ambient conditions. However, because of difficulties in gaining permission from clients and building operators to carry out instrumentations, it became necessary to accept sites which met the floor type criteria for selection, even if they did not necessarily fall within the seasonal periods initially desired. As a result of this it was sometimes necessary to remove a data logging set up from one site in order to begin monitoring on a new site, even though access was still available at the old site.

Strains, joint movements, and internal slab temperatures are presented for all monitored periods, whilst ambient weather data collected either from sensors mounted with the logging set up or from nearby Meteorological Office weather stations is also provided.

The first part of this chapter introduces the techniques which were employed in the analysis of the data. This includes both the justification of the readings obtained, the processing of these readings to arrive at meaningful strain data, as well as the analyses aimed at determining the more general behaviour and the influence of location and environment on the slab performance. The same analyses are carried out for all floor types and could equally be adapted to any concrete specimens. The justification for the interpretation of measured strains as joint movements is also discussed.

A series of generic plots have been developed, which are common to all of the sites and allow the key behavioural patterns to be presented. When referring to gauges throughout this chapter the gauge number refers to the location and the letter refers to the vertical position of the gauge. For example:

Gauge 3B - Bottom gauge at location 3 Gauge 4M - Middle gauge at location 4

The rest of the information in this chapter is presented in several sections covering the behaviour experienced at different locations and due to different causes, namely:

- thermal behaviour
- longitudinal restraint
- relationship between temperature and concrete movement
- joint behaviour
- warping restraint

In each section the behaviour of the different floor types is compared and contrasted, with any implications for designers highlighted.

5.2. Analytical methodology

5.2.1. Zero correction of strains

Strain is defined as the change of length of an object relative to its initial length (equation 5.1). This makes all strain a relative measure, making the choice of zero strain arbitrary.

$$\varepsilon = \frac{\delta L}{L} \qquad \text{equation 5.1}$$

The data logger records the resonant frequency reading from each of the strain gauges within the slab, which are converted into strains according to equation 5.2.

$$\varepsilon_{app} = \left(f_1^{\,2} - f_2^{\,2}\right) \times 10^{-3} \times \text{G.F.} \qquad \text{equation 5.2}$$

where, ε_{app} is the apparent measured strain (in microstrain), f_1 is the initial or Datum frequency of the vibrating wire in Herz, f_2 is a subsequent reading, and G.F. is a gauge factor expressing the relationship between the wire length and resonant frequency. Strains follow the standard convention, with a positive strain change indicating compression.

The very early-age apparent strains will be affected by the interaction of the stiffening concrete and the strain gauge. No strain readings will be obtained until the concrete is stiffer than the strain gauge and even then as the concrete stiffens the thermally induced strains will be overestimated, whilst load induced strains will be underestimated (Boulay and Paties, 1993). The degree of this effect depends on the stiffness of the strain gauge and the rate of strength growth in the concrete.

Testing to determine the effective stiffness of the strain gauges, E_g, was described in Chapter 3.2.4, with the results showing stiffnesses below 100 N/mm^2 for the TEAB and 4200x strain gauges and below 2 kN/mm^2 for the TES gauge.

Because of the sensitivity of the strain gauges, placing the concrete around them sometimes caused a change in the gauge length followed by a period of unsteady readings. The initial large variability in the readings is believed to have several possible causes:

1. Thermal shock caused by the difference in ambient and concrete temperature. (This is a particular problem for the acrylic strain gauges used, due to the high thermal coefficient of expansion of the barrel).
2. Disturbances to the concrete caused by the levelling and finishing of the concrete.
3. The lack of restraint around the flanges of the gauges, which is later provided by the hardened concrete. This particularly affects the acrylic barrelled gauges.

Items 1 and 3 from above are initially interrelated as the lack of restraint allows the thermal expansion of the strain gauges caused by the thermal shock. Once the concrete stiffness has exceeded that of the strain gauge the gauges will measure the concrete strains, albeit with initial interaction between the gauge and concrete stiffness affecting the readings.

The time at which the maximum concrete temperature is reached has been chosen as the zero point for the strain readings as this is repeatable across sites, although it will occur at different elapsed times after construction depending on the concrete mix and the ambient conditions. Additionally, the high creep rates at this early time mean the concrete can be assumed to be in, or near to, a zero stress state before the concrete reaches its maximum temperature (ACI Committee 207, 1987). Using this zero time allows legitimate comparisons to be made between measurements from different sites.

As can be seen from Figure 5.1, because strains are arbitrary and relative the choice of the zero point simply shifts the total strain relative to the ordinate axis and has no effect on the magnitude of the calculated strains between two given points in time.

A second zero point has been used 3 days after construction in order to isolate the drying shrinkage effects. This point was chosen because the initial thermal effects due to hydration have finished, and because with the application of curing membranes little moisture should have been lost from the top surface of the slab by this time. Data generated using this zero point allows the short and long-term drying shrinkage behaviour across different sites to be compared. Comparison with the corrected gauge strains also allows the seasonal thermal influence on the concrete strains to be analysed.

5.2.2. Thermal correction of strain readings

The temperature within the slab was measured by thermistors embedded in the coil housings of the strain gauges and by arrays of thermocouples running through the slab and down into the sub-base and subgrade. This enabled data on the thermal profile in the slab to be gathered both during cement hydration and during the later life of the slab, as well as allowing the thermal correction of the strain gauge readings.

The internal temperature of the slab, as well as causing expansion and contraction of the concrete, also affects the readings obtained from the vibrating wire strain gauges. The thermal

coefficient of expansion of the wire in the strain gauges, α_{sg}, is 11 μstrain/°C, which is very similar to that for unrestrained concrete, α_c, of 10 μstrain/°C (Neville, 1995). The apparent measured strain from the vw gauges is made up of the concrete drying shrinkage, and the thermal expansion and contraction of both the concrete and the vibrating wire.

Of interest are the shrinkage and the thermal effects on the concrete movement; however, the thermal effects on the vibrating wire will partly mask this behaviour. Thus the actual concrete strain taking account of shrinkage and internal thermal effects, but excluding the gauge thermal effects is found from:

$$\varepsilon_{cor} = \varepsilon_{app} + \delta T \cdot \alpha_{sg} \qquad \text{equation 5.3}$$

where ε_{cor} is the strain corrected for gauge thermal effects, ε_{app} is the apparent measured strain from the vw gauge, α_{sg} is the thermal coefficient of expansion of the vibrating wire and δT is the temperature change between the zero and current times.

The effect of this thermal correction can be seen in Figure 5.2 where apparent and corrected strains along with a plot of the slab's internal temperature are given. The relationship between the temperature and the induced strain in an unrestrained specimen is governed by the thermal coefficient of expansion, α_c. Reference to Figure 5.3 shows how the uncorrected strains would give a negative value of the thermal coefficient of expansion for concrete which is clearly incorrect, whilst the corrected strains give a positive value of approximately 8 μstrain/°C. This is a restrained thermal coefficient of expansion and so will always be lower than values obtained from an unrestrained specimen.

Thermal correction of the concrete movement has also been carried out to allow comparison with drying shrinkage models. In this case it has been assumed that due to the application of curing membranes the moisture loss from the top of the slab during the first 3 days was negligible, allowing $t = 3$ days to be used as the zero point t_0.

5.2.3. Determination of creep effects on restraint stresses

Consider two strain gauges embedded in a large area pour at 2m and 20m from a free edge. If subjected to a temperature change of δT over a given time period, the difference in corrected strain readings between the two gauges is $\delta\varepsilon$ - with the gauge nearest the free edge showing greatest contraction. The apparent restraint to the contraction 20m from the free edge will have induced a tensile stress in the slab.

In order to account for the gradual application of the stress and the creep relaxation with time, the age adjusted effective modulus can be used to determine the stresses. Firstly the creep compliance function $J(t,t')$ and the elastic modulus $E_c(t,t')$ are calculated allowing the determination of the creep coefficient $\phi(t,t')$ according to equation 2.74. This is then used in

equation 2.73 to give the age-adjusted modulus, $\bar{E}_{ec}(t,t')$. The restraint stresses at the end of the time period are then given from:

$$\sigma(t) = \delta\varepsilon(t,t') \cdot \overline{E}_{ec}(t,t') \qquad \text{equation 5.4}$$

The implicit assumption in this approach is that there is zero stress at all points at the start of the time period. This will generally not be the case, though given that any stresses will be small this should still allow reasonable estimation of the restraint stress. It should again be emphasised that this calculation attempts to quantify the difference in stress between two points in the slab over a given time period. It does not determine the absolute stress at any point.

5.2.4. Justification of joint gauge strain readings

Strain gauges crossing joints were based on the TES/10 strain gauge, which has a gauge wire length of 254mm (10in.) and a gauge factor for use in equation 5.2 of 10. Movement of the flanges, which are positioned on either side of the joints, causes changes in the length of this wire. Before the formation of any cracks the gauge measures the relative movement of these two flanges and the analysis of the readings assumes that these movements occur uniformly along the gauge length (Figure 5.4a). However, once a crack forms (Figure 5.4b) the assumption of uniform behaviour is no longer valid. The relative movement of the flanges is still measured, but these are now embedded on opposite sides of the joint. The discontinuity in the concrete means that any movement measured by the strain gauge (point *c*) can now be assumed to be concentrated at the joint. As the gauge length is known, the expansion measured by the gauge can be converted directly to a joint opening. This neglects the effect of the free shrinkage movement of the concrete between the flanges and the joint (point *d*), though this has a negligible effect on the joint width.

Where strain gauges have been placed across the construction joint between two pours, their measurements have been zeroed with respect to the later pour. This was done because no relative movement could occur until the concrete on both sides of the joint had been placed.

5.2.5. Analysis of daily strain change

In order to analyse more effectively the effects of the thermal changes on the movements at different locations in the slab a further analysis has been carried out. This involved analysing the strain data acquired at maximum and minimum temperatures over a number of 24 hour periods. As zero temperature change leads to zero strain change, a best fit line can be plotted through the data and the origin (Figure 5.5). This assumes the drying shrinkage, which occurs over a given 24 hour period, is small relative to the thermal strain; this is not an unreasonable assumption even at early ages. The line will have a gradient, *m*, given by:

$$m = \frac{\varepsilon_{max} - \varepsilon_{min}}{T_{max} - T_{min}} \qquad \text{equation 5.5}$$

This is equivalent to the thermal coefficient of expansion, which is defined as the change in length for a unit temperature change. These plots from the embedment gauges return effective thermal coefficients of expansion for the concrete, $\alpha_{c\ eff}$, which allow the differences in restraint to be assessed. To show the quality of the best-fit lines the sample correlation coefficient, r, is determined for each of the plots.

A statistical analysis of the gradients and standard errors of the lines can then be carried out to check that they are discrete. An unpaired Students t-test is carried out as shown in equation 5.6, where m_1 and m_2 are the gradients of the lines and se_1 and se_2 are the standard errors. The H_0 hypothesis that there is no difference between the data recorded by the different strain gauges.

$$t = \left| \frac{m_1 - m_2}{\left(se_1^2 + se_2^2\right)^{0.5}} \right| \qquad \text{equation 5.6}$$

A confidence of 95% is generally taken as the critical value to statistically disprove H_0, i.e. show that there is a significant difference between the data sets.

5.3. Thermal behaviour

Thermal changes in concrete result from interaction with the ambient environment through conduction, radiation and convection, and the release of heat as the cement hydrates. The dominant effect during the first week after construction in all of the slabs was the increase in the concrete temperature caused by the cement hydration and the subsequent thermal losses to the environment as the temperature returned to ambient levels.

Ambient temperature data was collected from each of the sites from before construction commenced, whilst the concrete temperature was obtained from the time of placement. In some cases moisture affected the temperature readings at very early ages. However, as can be seen with reference to Figure 5.6 and Figure 5.7 the absence of this corrupted data does not prevent a full picture of the temperature history from being determined.

Where early age temperature data was collected, an initial period can be identified where heat losses into the ground and to the air exceed the rate of heat generation due to the hydration of the cement. Neville (1995) and Brüll and Komlos (1982) identified the dormant period for concrete as being from about 1 to 2 hours long depending on the chemical composition of the cement. During this period the adiabatic heat gain of the concrete is negligible, which results in a drop in temperature when the concrete is exposed to a cooling environment (Figure 5.6a). This heat loss continues until the rate of heat production exceeds the rate at which the heat is

lost to the environment, which in the case of the site measured data generally occurred after about 2 to 3 hours. The second bay at Leeds, which contained a shrinkage-reducing admixture, was the exception in this respect and the period of heat loss lasted for 7 hours. The other two instrumented bays at this site showed thermal losses lasting for only 3 to 4 hours, despite lower supply temperatures of the monitored sections of concrete. This difference in behaviour of the second bay is believed to have been caused by the addition of the shrinkage-reducing admixture, which according to the manufacturers can have a slight retarding effect.

As a result of the heat loss to the environment during the dormant period, the average temperature of the slab drops, whilst a thermal gradient also becomes apparent with the bottom of the slab being cooler than the top of the slab. This shows that the heat loss to the underlying ground through conduction is higher than the convective loss to the air.

The concrete supply temperature, the magnitude of the temperature drop, the thermal gradient and the duration of the dormant period are all compared for the different sites in Table 5.1.

Table 5.1 - Comparison of early age temperature changes

Site		Supply temp (°C)	Dormant period			Peak temperature	
			Average temp drop (°C)	Temperature gradient[1] (°C/cm)	Duration (hours)	Elapsed time, t_{max} (hours)	Average temp (°C)
Northampton		15.3	0.8	+0.07	2.25	17	24.5
Daventry	Pour 5	16.8	1.5	*	2.5	14.5	21.5
	T6	16.0	0.9	*	2.75	14	19.4
	T27	16.2	0.8	*	2.75	13	18.8
	T12	18.2	1.0	*	2.25	13	21.2
Bedford	Pour 2	21.2	#	#	#	14	24.6
Chepstow	Pour 10	21.9	#	#	#	11	30.0
	Pour 11	21.4	#	#	#	12	28.5
	Pour 12	21.8	#	#	#	11	31.7
Marston	Pour 6	17.9	#	#	#	13	26.8
		21.0	#	#	#	14	30.4
	Pour 7	20.0	#	#	#	14	29.5
	Pour 9	18.6	#	#	#	17	24.8
Leeds	Pour 1	12.4	1.0	+0.08	3.1	22	17.0
	Pour 2	13.5	1.7	+0.06	7.0	27	16.5
	Pour 4	10.3	1.4	*	2.5	24	15.7

[1] The temperature gradient has been determined by dividing the temperature difference between sensors by their separation. Because of cover requirements this does not account for thermal differences at the slab boundaries. A positive gradient means the top of the slab is warmer than the bottom.

* Not possible to determine a gradient as only one gauge present

No temperature data available

Following the dormant period the measured internal temperatures show a rapid rise, although any thermal gradients remain fairly constant. The time at which the maximum heat due to cement hydration is evolved depends on the chemical makeup of the concrete. However, Neville (1995) and Wang and Dilger (1995) agree that in general this occurs at an age of around 10 hours. Once this peak heat rate has been passed the temperature in the concrete will continue to rise, albeit more slowly, until the rate of losses to the environment exceeds the rate of heat production, at which point the temperature will begin to drop. This is in agreement with the measured data where the maximum temperatures generally occurred between 13 and 17 hours after construction. No relationship between the ambient temperature and the duration of the dormant period, or the timing and magnitude of the maximum temperature could be found. This is in agreement with site testing and finite element studies carried out by Lachemi and Aïtcin (1997). There is a clear correlation between the concrete supply temperature and the time at which the maximum temperature was obtained, with reductions in the supply temperature delaying the occurrence of peak temperatures. This is also in agreement with Lachemi and Aïtcin, although their other finding that increased supply temperature increased the peak temperature in the concrete was not confirmed. This difference in behaviour is believed to be related to the increased thermal losses on several of the sites due to air movement across the top of the slab and is examined more fully in the finite element analysis section (Chapter **6.2**).

The conductive heat exchange between the slab and the underlying layers has an effect on the heat development in the slab – in particular in the development of the thermal gradient – but also causes an increase in the temperature of the underlying layers (Figure 5.8). The thermocouples 850mm below the slab surface at Leeds (TC8 and TC16 in Figure 4.6) registered a rise of over 3°C. The underlying layers act as a heat sink during the first couple of days following construction and then return some of this heat energy as the slab cools. This behaviour has important implications for the modelling of the slab system and means that the underlying layers need to be modelled rather than simplifying the system to one of a slab with a prescribed boundary flux along its bottom edge.

In addition temperature readings from several sites showed the heat sink effect of casting against an adjacent pour. Measurements from the Northampton site showed a reduction in the maximum measured temperature of almost 2°C between 300 and 900mm from the slab edge.

The impact of ambient temperatures on the concrete temperature can be clearly seen in all cases after about 48 hours, with changes in the cooling temperature visible after as little as 24 hours in the case of Daventry (Figure 5.6a). From this point onwards diurnal temperature changes are clearly visible on top of the continuing reduction in temperature towards the ambient conditions. The time taken for the internal and ambient temperatures to converge was dependent on the peak concrete temperature and the ambient temperature history, although

generally more than 70 hours were required. After this the slab temperatures followed the ambient temperatures, albeit with a reduced amplitude and a lag of several hours.

Thomlinson (1945a and b) suggested a technique for predicting the temperature distribution in a slab-subgrade system subject to a sinusoidal driving function of temperature, on either a daily or an annual cycle (Chapter 2.8.2). Figure 5.9 shows the accuracy of the sine curve approximation to ambient temperature data.

As no concrete surface temperature data was available (due to the cover requirements) the temperature variation at a depth of 45mm has been used to back-calculate a daily slab surface temperature variation, θ_0, as previously defined in equation 2.56. The temperature variation throughout the slab, sub-base and subgrade at Leeds has then been calculated. This determines the daily effect at the different depths, but does not account for the differences in temperature due to the annual temperature variation. These variations have been calculated, again using equation 2.56 but with the annual time constant and diffusion coefficients (Figure 5.10).

The temperatures at different depths at 15:00 hrs on several different dates from site measurements at Leeds and the theoretical calculations are compared in Figure 5.11. The predictions are generally within 1°C of the measured values with the discrepancies being caused by preceding periods of unusually warm or cold weather. This demonstrates that although the theoretical approximations can give an overall prediction of the temperature distribution, their inability to account for short-term fluctuations (over a couple of days) in the ambient temperature, which characterise natural weather patterns, means that the predictions can rarely be precise.

5.4. Structural Behaviour

At early ages two factors contribute to the strain changes in concrete. Firstly, thermal changes during the first couple of days include the rapid temperature gain as the cement hydrates, followed by a slower drop back to ambient temperatures. These thermal changes cause a corresponding expansion and contraction according to the concrete's thermal coefficient of expansion and the degree of restraint. At the same time moisture begins to be lost from the exposed surface of the slab leading to drying shrinkage.

Various different types of joint are commonly used in industrial floors, and several of these joint types have been instrumented allowing their performance to be evaluated. In order to present and discuss the results the joints have been divided into two groups, namely:

- Restrained movement joints – includes formed and sawn joints (Figure 2.2).
- Free movement joints – includes formed and sawn joints, and free slab edges (Figure 2.1).

These joint types will be discussed in turn and any similarities or differences in behaviour across the floor types will be highlighted. Reference to the concrete strains measured between the joints, and precision level survey information is also used to explain the trends seen at the joints.

The gauge layout information in Chapter 4 has been provided on fold out pages allowing reference to be made to the figures whilst looking at the results presented in this chapter.

5.4.1. Restrained movement joints

The instrumented restrained movement joints (rm) included sawn rm joints in large area pours and a long strip floor, and formed rm joints between adjacent bays.

Only two formed rm joints were successfully instrumented, with the data showing different behaviour for each of these joints, which were at opposite sides of pour 13 in the fabric reinforced jointed large area construction floor at **Chepstow** (Figure 4.5). Although the joint movements were small over the first six days they were closely related to the thermal changes seen in the slab. The initial increase in joint width measured by gauge 22, to a maximum of 0.13mm, corresponded to the falling slab temperature following hydration (Figure 5.12). The falling ambient temperature about 7 days after construction was matched with increased joint opening measured by gauge 22. However, gauge 17 behaved differently showing a reduction in opening. This change in behaviour of gauge 17 coincided with the opening of the adjacent sawn rm joints monitored by gauges 15 and 16. (τ = 12 days in Figure 5.13). The formed rm joints were reinforced with T12 bars at 200 centres providing 566mm^2/m of reinforcement – about three times the steel area provided by the A193 mesh across the sawn restrained movement joints. Therefore, once cracking had occurred at the sawn rm joints their much lower restraint to opening explains why they continued to open rather than the formed joint.

Only gauges 15, 16 and 23 crossing sawn restrained movement joints measured joint opening during the initial monitoring period of 28 days. Gauge 23 only registered an opening at the very end of the period, by which time gauge 22 showed a joint opening of 0.22mm, similar to that measured by gauges 15 and 16 – 0.25 and 0.35mm respectively. When further readings were taken four months later gauge 23 showed a joint opening of 0.13mm, whilst the formed rm joint opening measured by gauge 22 had reduced to 0.12mm. This compared to 0.49 and 0.56mm from gauges 15 and 16. Gauge 17 had stopped recording joint opening and instead showed shrinkage of 261 μstrain, which was almost identical to the adjacent embedment gauges.

Not all sawn restrained movement joints were found to open, and the strain gauges across the joints that remained closed measured similar shrinkage to the embedment strain gauges (Figure 5.14 and Figure 5.15).

Several sawn restrained movement joints were instrumented in the fibre reinforced jointed large area pour floor at **Daventry**. This was the first large area pour to be monitored and the joint gauge location method being used at this time left them free to move under the force of the concrete as it was poured. Additionally, several of the joint gauges were damaged during construction leaving an incomplete picture of the slab behaviour. The only joint gauge that survived embedment and recorded opening in the two weeks following construction before the datalogger had to be removed was gauge 57 in pour 8 (Figure 4.7). This gauge measured an initial opening of 0.7mm overnight following the saw-cutting of the joints (Figure 5.16). No movement was recorded during the next day, although a further movement of 0.52mm occurred that night. The joint width then remained fairly constant until $\tau = 6$ days when another overnight joint movement of 0.45mm was measured.

Gauges 36, 38-42, 48, 52, 56 and 58-60 (Figure 4.7) also survived the construction process, although readings from gauges 41 and 42 stopped as the saw-cutting was carried out. Further investigation revealed that the leads connecting the gauges were on open circuit, indicating that the leads, rather than the gauges, may have been damaged by the saw-cutting. All of these joint gauges measured similar shrinkage to the embedment gauges before the logger was removed.

Manual readings of the joint gauges were made 3 months after construction at which time gauges 40, 52, 58 and 59 had measured openings of 0.7, 0.45, 0.17 & 0.17mm respectively. Joint gauges 36, 48 & 56 still measured shrinkage similar to the adjacent embedment strain gauges.

Further manual readings of the gauges as well as demec measurements of the joint opening were carried out 15 months after construction. At this time joint gauges 38 and 57 also failed to provide readings. However, as gauge 57 had already recorded over 2mm movement during the first two weeks after construction, it is likely that subsequent joint opening had been sufficient to cause failure of the gauge. No demec pips had been placed across the joints in this pour, but visual inspection of this joint showed a width of approximately 9mm, which corresponds to an opening of about 6mm.

Demec readings from the joints crossed by gauges 36, 37, 38, and 42 recorded movements of 1.13, 1.41, 1.11 and 1.74mm respectively. The joint monitored by gauges 39 and 49 is a sawn free movement joint and will be covered in the next section, whilst readings from across the other joints in this pour were not possible because the floor loading rendered the demec pips inaccessible.

Comparison of the demec and joint gauge readings shows greater movement from the slab surface at all joints. For example. gauge 52 recorded an opening of 1.06mm compared to 1.74mm from the demec gauge. This difference in measured joint opening could be expected

due to the difference in drying shrinkage through the cross-section as moisture is lost from the slab surface.

Gauges 36 and 48 continued to show similar shrinkage to the embedment gauges, rather than any joint opening, although the demec reading from these joints were 1.13 and 1.11mm. The lack of any measured joint movement from gauges 36 and 48 could have two causes. Firstly the gauges could have been displaced sufficiently by the concrete during placement to miss the joint they were supposed to cross, and secondly differential movement in the slab could have lead to the joint opening at the surface but not lower down in the slab. This differential movement has already been seen to result in a difference in measured joint widths from the demecs and the joint gauges.

The installation methodology was modified to reduce gauge movement during concreting before pour 8 commenced, but joint gauges 56 and 60 (Figure 4.7) also showed similar behaviour to the embedment gauges. Unfortunately, no surface joint movement readings were possible for this pour, as block stacking covered the joints once the building was in operation.

The large difference in measured joint opening from gauge 52 and the demec gauge adjacent to gauge 42 could be indicative of differential opening of the joint. However, there is also a physical separation of more than 14m between the monitored points on the joint, which also applies to gauge 48 and the associated demec reading. Visual inspections have shown that joint opening is generally not uniform along the length of a joint, which might also account for some of the difference.

Further support for differential movement explaining the differences in joint width measurements comes from the jointed large area pour in **Leeds** (Figure 4.6). Joint gauges at two different depths in the slab were used here, showing that there was a reduction in joint opening as the distance from the slab surface increased; with demec surface readings again showing much greater opening.

Ambient temperatures were low when the first three pours were constructed, retarding the early age strength gain of the concrete and delaying the saw-cutting of the sawn restrained movement (rm) joints for 24 hours.

The only sawn rm joint to open during the first 28 days was position 36, which recorded a small overnight opening of 0.1mm at $\tau = 20$ days (Figure 5.17). This joint continued to open slowly with an inverse relationship between the joint width and the slab temperature, and at all times the top gauge measured greater joint opening than the bottom gauge. Readings from the demec pips crossing this joint continued the trend, showing greater opening than the top gauge at all times. Reductions in the joint opening can be seen from both the joint gauges and the demec readings at position 36 as the ambient temperature increased around $\tau = 63$ days. As the temperature dropped again after this spike around $\tau = 71$ days the reducing temperature caused

a contraction of the slab (Figure 5.18), and joint gauges at positions 20 and 23 also began to measure opening (Figure 5.19). A reduction in joint width and subsequent opening can also be seen in the measurements from position 36 at the same time (Figure 5.17). The top gauge at position 34 also registered a small overnight opening at this time (Figure 5.20), although no movement was recorded from the bottom gauge until $\tau = 87$ days, when the gauges at positions 21 and 22 also first recorded joint opening (Figure 5.21).

Most of the joint gauges recorded movement as the building temperature was adjusted to the operating range around $\tau = 100$ days. With a temperature of 14.6°C pours one and two were initially close to the required temperature range of 10-12°C. On cooling, the slab temperature fell to 10°C before rising back to 12°C and finally stabilising near 11°C. This change in temperature triggered joint movement at positions 27 and 28 (Figure 5.22) and increased joint width where movement had already been seen (Figure 5.19 and Figure 5.21).

Greater joint movement was recorded for pour 4, in the chill store, as this experienced a temperature change 10°C greater than the ambient storage areas. The reduction in air temperature resulted in slab temperatures dropping from 14 to 6°C between $\tau = 102$ and 116 days, although it was a further month before slab temperatures went below 4°C. These changes had a dramatic effect on the concrete strains measured by the embedment gauges (Figure 5.23), which was then reflected by joint opening (Figure 5.17).

The differences in operating temperature also affected the long-term behaviour of the joints in the different pours. Gauges in pours 1 and 2 continued to record slow joint widening, whilst those in pour 4 showed constant width once the floor had reached it's operating temperature. This is unsurprising as the embedment strain gauges show that there was over 40% less contraction in the chill store once it was at operating temperatures. For example from $\tau = 135$ to 195 days the concrete in pours 1 and 4 showed a mean contraction of 21 and 12 μstrain respectively.

There were also significant differences in the behaviour of the two pours kept at ambient temperatures. The mean joint opening and concrete contraction over several time periods can be seen compared in Table 5.2 below. It must be borne in mind that the contractions measured by the embedment gauges are at mid-depth in the slab and only cover one half of the slab length, whilst the joint width readings cover the whole length of each pour and are taken from the demec pips fixed to the slab surface. It has already been demonstrated that differential contraction and joint movement is present through the thickness of slabs, so direct comparisons of the joint widths and measured contractions should not be made based on these readings. This table confirms that there is a definite reduction in concrete contraction and joint widths in pour 2 compared with pour 1, with these differences increasing as the slab aged.

The second pour contained a shrinkage-reducing admixture, but nevertheless the lower contraction and joint opening could have also been due to higher restraint, thus leading to the concrete being more highly stressed. To discount this, free shrinkage tests were carried out on samples taken from all three monitored concrete pours. Two samples from each pour were prepared on site in 100 x 100 x 400mm moulds, with one sample treated with the spray-on curing membrane after finishing. The samples were stripped from the moulds 24 hours after casting, at which time a length reading was taken. The beam with the curing membrane then had the other five faces sealed with bitumen paint to try to replicate the exposure conditions experienced at the surface of the slab, whilst the other beam was left untreated to try and establish the maximum free shrinkage for the concrete mix. All specimens were left in an outside building to approximate the exposure history of the slab. After 28 days the shrinkage from the exposed specimens containing the SRA was less than 40% of that from the normal concrete mixes. There was less difference between the sealed specimens, though again the concrete containing the SRA showed less shrinkage. The difference between the sealed specimens was only about 200 μstrain, whilst for the exposed specimens it exceeded 1000 μstrain.

Table 5.2: Leeds - Comparison of the longitudinal behaviour of the first two pours

	Mean concrete contraction [microstrain]		Mean joint movement [mm]	
	Pour 1	Pour 2	Pour 1	Pour 2
28 days	43	17	0.03	0.02
63 days	61	24	0.10	0.05
106 days	102	59	0.49	0.19
152 days	132	71	0.56	0.23
222 days	166	99	0.77	0.50

Comparison of the mean measured contractions is also slightly misleading because the movement in pour 2 was 25% higher near the middle of the pour (where the joints had opened), than it was at the monitored end of the pour where the joints remained closed for more than 5 months after construction. Despite the non-uniformity of the pour 2 behaviour, even the largest recorded contraction near the middle of the pour, where the joint opening was greatest, was only 50% of the mean pour 1 contraction after 28 days. This increased to 60% of the mean pour 1 contraction as the slab aged to 222 days.

Demec readings showed movement of all of the joints in pours 1, 2 and 4, although the pattern of opening differed (Figure 5.24, Figure 5.25 and Figure 5.26). The joint opening in pour 2 was non-uniform, with no significant movement recorded before the adjustment of the

temperature to the operating range. At this time (τ = 104 days) a difference was observed in the contraction measured by embedment gauges 9 and 12. By τ = 152 days the contraction from the embedment gauges near the centre of the pour in the longitudinal direction (positions 9 and 10T) was almost 20% greater than gauge 12 at the edge of the pour (Figure 5.27). This difference in behaviour was reflected in the demec readings, where only the middle four joints were found to have opened after 152 days.

Neglecting the stresses in the slab before this time interval, the stresses induced by this restraint can be calculated (equation 5.4).

For the period τ = 104 to 152 days the age adjusted modulus is 23.9 GPa, which gives a theoretical restraint stress of 0.36 N/mm^2. This accounts for about 10% of the tensile capacity of the slab, and combined with stresses from service loading this could contribute to the onset of cracking.

Although there was still some variation in the joint widths from pours 1 and 4 during the first 3 months after construction, they were generally more consistent in width. At later times some joints can still be seen to open by more than their neighbours (Figure 5.24 & Figure 5.26), with differences of almost 50% in pour 1 after 222 days, whilst in pour 4 the joint nearest pour 6 had opened by around 2mm more than all of the other joints after the same time, with further smaller differences between the other joints. No significant differences were seen in the behaviour of the joints dependant on their direction.

A sawn restrained movement joint was also instrumented in the long strip slab at **Northampton**, though the gauges crossing this joint didn't record any opening. Conversely they actually showed some of the highest shrinkage of any point in this floor - especially during the first 3 days after construction. This may be because the close proximity to the formed free movement joint at the end of the slab meant that the frictional restraint was reduced.

5.4.2. Free movement joints

A variety of free movement joints were instrumented, including sawn and formed joints. Additionally the movement between the free edge and the adjacent walls of two large area pours at **Marston** (Figure 4.9) has been monitored. Although not strictly a free movement joint, this is still an unrestrained movement of part of the slab.

As previously described for the restrained movement joints, the initial joint opening in every case appeared to be triggered by a drop in the ambient – and hence slab – temperature. The first movement generally happened around 36 hours after construction. The exceptions were the free edges of the slabs at **Marston**, where very slow movement began as soon as the concrete began cooling, with a more rapid opening from 60 hours after construction (τ = 1.75

days in Figure 5.28), and the movement between pours 2 and 3 at **Bedford**. This also began as soon as pour 3 began cooling at 22:00 hours on the day of construction, which was approximately 13 hours after construction, although here the movement was fairly rapid.

Once movement had commenced daily thermal variations were evident in the movement patterns from the edge of the pours at **Marston** (Figure 5.28), but these were much smaller than those which became apparent at the joints between the pours (Figure 5.29). The internal temperature of the slabs was influenced by the ambient temperatures from about 36 hours after construction, with the influence increasing as the slab temperature approached ambient levels. Generally, the only movements seen during the first couple of days after construction relate to thermal changes in the slab. This is because moisture diffusion in concrete is a very slow process and additionally in order to improve the curing near the slab surface, a spray-on membrane was used on all of the investigated slabs. This should have considerably reduced the moisture losses from the slab surface during the first week after construction. Additionally, no moisture will have been lost from the bottom of the slabs as they were all constructed on polythene slip membranes. At the day joints the movement was the sum of the thermal contraction from each bay, whilst at the edges of the pours it related to that bay alone. As the contraction at the day joint was greater, the impact of the daily temperature increase (which actually caused a slight closing of the joint) was also more noticeable.

Although the movement at the free edge of the pour was smaller than the movement at the joint between two pours, the difference was smaller than expected. The mean movement from the edges of pours 6 and 9 at $\tau = 7$ days was 1.03mm and 1.61mm respectively, which was considerably greater than half the movement measured between the pours, with only about 0.75mm (30%) difference between gauges 1, 12 and 23 after 13 days.

As pour 9 (the infill bay) was constructed several days after the other instrumented bays, they had already undergone a significant proportion of the thermal contraction that accompanied the temperature drop following hydration. The joint movement readings are, therefore, the sum of the remaining contraction of the older slabs (pours 6 and 7) and the full thermal movement from pour 9 - the new slab. The temperature of the older slab, although still falling, is influenced by the daily ambient temperature variations at this time, which also explains the greater influence of the temperature variation on the joint opening (compare Figure 5.28 and Figure 5.29).

The joint opening data from the other jointless large area pour at **Bedford** shows a similar pattern. In this case the joint between pours 2 and 3, which were completed on consecutive days, showed much greater movement than that between pours 1 and 2 which were constructed three days apart (Figure 5.30). Both formed free movement joints began to open at the same time, as temperatures dropped overnight on the same day that pour 3 was constructed, and

continued to show the same temperature related trends as the floor aged. Although the initial opening was greater between pours 2 and 3, the temperature related movement as the slab aged was very similar at both free movement joints.

Movement was recorded from the formed free movement joints between pours 1, 2 and 4 at **Leeds** (Figure 4.6). However, with the exception of the gauges between pours 1 and 2, which recorded joint opening of 0.5mm (Figure 5.31), the movement was generally much smaller than at the other sites. The upper gauges between pours 1 and 4, and 2 and 4 recorded joint movements of 0.14 and 0.20mm respectively (Figure 5.32 and Figure 5.33), whilst the bottom of the joints appeared to remain essentially closed with gauge readings of 0.03 and 0.02mm. This difference in behaviour, compared to the formed free movement joints in the other floors, is believed to be related to the much lower maximum concrete temperatures – below 17°C compared to over 24°C for the other floors.

The long-term behaviour of the free movement joints at **Leeds** also differed from the other formed free movement joints. No significant movement of the joints between the ambient and chill storage areas was measured, although it has already been shown that all of the restrained movement joints in these pours opened, which might explain this behaviour. What remains curious, is that the restrained movement joints appear to have opened in preference to the free movement joints.

The top gauge between pours 1 and 2 recorded comparatively large joint opening, with the movement reaching 1.7mm at $\tau = 220$ days. However, the bottom gauge at this point did not record any joint opening. This difference is believed to have been caused by curling of the slab resulting from differential movement in the slab, with further supporting evidence provided by the precision level survey (Figure 5.34), which shows that a 2m wide strip on either side of the joint has curled upwards by up to 4mm.

A further sawn free movement joint was instrumented (Gauges 1T, 1B, 2T & 2B) in the long strip slab, **Northampton**, although an additional formed free movement joint was just adjacent to the instrumented section of slab (Figure 4.1).

Although saw cutting of the free movement joint took place 24 hours after construction no joint movement occurred until 12 hours later ($\tau = 0.92$ days in inset enlargement Figure 5.35)

As for all the other joints differential opening related to the depth in the slab was recorded, with the upper gauges measuring the greatest opening. However, an additional differential opening was seen in the long strip slab at Northampton, which was related to the distance from the edge of the strip. The difference in movement between positions 1 and 2 was 0.1mm 2 hours after the joint began to open and increased to ~0.15mm after 4 days. The difference was similar for the gauges at the bottom of the slab and those at the top of the slab, indicating that the restraint was uniform through the slab section. This restraint is believed to have been

provided by the longitudinal dowel bars tying the adjacent strips together. At early ages as the fresh concrete hydrates the restraint from these dowel bars can be significant. However, as the concrete matures and the strengths and relative movements between the adjacent strips even up, they begin to move uniformly. This is evidenced by the constancy in the difference between readings from the joint gauges at the two positions after early ages have passed.

The differential movement could have been caused by one, or several, of the following factors:

- frictional restraint acting on the bottom surface of the slab;
- differential thermal gradients in the slab as the concrete set; and
- differential hygral gradients due to drying shrinkage causing the upper surface to shrink more than the lower surface.

The last cause of differential movement can be ruled out for the initial difference in movement, as drying shrinkage is a long-term effect and cannot influence behaviour during the first couple of hours after construction. Differential thermal gradients have been shown to be present at early-ages in ground floor slabs. However, because the slabs are enclosed and not exposed to solar radiation the temperature has been shown to be highest in the centre of the slab and not at the surface, which should rule out the second possible cause.

All ground floor slabs undergo a uniform temperature drop as the excess heat from the cement hydration is lost to the environment. Frictional restraint acting on the bottom of the slab reduces the expected movement relative to the upper surface of the slab, with the difference in movement at different points then being attributed to this restraint.

No information on the differential movement of the sawn free movement joint monitored by gauges 39 and 49, in the fibre reinforced jointed large area pour at **Daventry** (Figure 4.7) could be obtained. The joint first opened 7 days after construction (Figure 5.36) and had reached a width of 1.07mm after 3 months when the first manual readings were taken. Unfortunately, at this time loading on the floor prevented surface measurements of the joint opening and when manual readings were next taken after 15 months the joint opening had caused failure of both joint gauges and also exceeded the full range of the demec gauge. Measurement of the joint with a rule found it to be 9mm wide, representing an opening of around 6mm, which was significantly wider than for any of the restrained movement joints in this direction.

This behaviour was not repeated at the longitudinal sawn free movement joint at position 51. This joint width measured after 15 months was 4.5mm, indicating an opening of around 1.5mm, which was less than the opening measured at any of the other joints in this direction (Figure 5.37). This trend was also repeated in pour 4 at **Leeds**, where the sawn free movement joint at position 38, which also behaved in a similar way to the adjacent sawn restrained movement joints (Figure 5.26).

This is perhaps more surprising than in the fibre reinforced floor as, once the joints have cracked, the restraint to movement should be lower at the free movement joint than at the other joints. In the fibre reinforced floor the post crack restraint will still be similar at all of the joints, although as the joints begin to open the load transfer capacity of the dowelled joint will be significantly greater than the other joints.

5.4.3. Restraint

Theoretically as the distance from a free movement joint increases two distinct effects will influence the concrete movement. The longitudinal restraint to movement will increase according to the frictional drag equation (equation 2.1), and the restraint to warping will increase up to a limiting value due to the weight of slab to be cantilevered according to equation 2.60 and equation 2.67.

These two different effects can be separated when looking at the readings from the embedment strain gauges. At locations where gauges have been installed in the top and bottom of the slab the differential movement gives an indication of the warping movement, whilst comparisons between the bottom gauges show the longitudinal movement. The warping movement will result from thermal and hygral gradients arising in the slab. However, moisture loss in concrete is a long-term process, so any movement of the gauges at the bottom of the slab during the first couple of months after construction is likely to be mainly as a result of thermal changes.

In order to try to isolate the different restraint effects the strains at different depths and locations have been compared over successive time periods. At early ages the measured behaviour has been found to be strongly influenced by the slab temperature, but the effects of restraint are also apparent.

The effective thermal coefficients of expansion, $\alpha_{c\ eff}$ for the different gauges within a slab are also compared, as this indicates the degree of restraint to the free thermal movement.

5.4.4. Longitudinal restraint

In the long strip slab at **Northampton** the thermal boundary conditions resulted in temperature gradients both vertically through the slab and across the slab between positions 3 and 5 (see Figure 4.1) as discussed earlier in this chapter.

The maximum temperature recorded at position 3 was almost 2 °C lower than at any other gauge location. Up until $\tau = 3$ days the temperature drops at upper gauge positions 3, 4 and 5 were respectively 9.3, 10.0 and 10.5 °C, whilst the measured contraction was 59, 64 and 82μstrain (Figure 5.38). There was little differential movement at position 3 with the bottom gauge recording a contraction of 55 μstrain. At position 4 the contraction from the bottom gauge was 70 μstrain and exceeded that of the upper gauge, whilst at position 5 the bottom gauge recorded 68 μstrain.

Assuming a concrete thermal coefficient of expansion of 10 μstrain/°C and taking the measured temperature difference of 1.2 °C between positions 3 and 5, the maximum expected difference in thermal contraction should be 12 μstrain. The measured difference of 23 μstrain was almost twice this value. Similar results were found when comparing the vertical differential movement in the slab. At position 6, for example, the temperature drop undergone by the bottom gauge was 0.7 °C less than the upper gauge, but the differential movement was 21 μstrain.

These discrepancies are indicative of restraint to the free contraction of the slab. The edge of the slab is connected to the previous pour by longitudinal dowel bars which hold the two strips together and facilitate load transfer across the formed joint. However, at early ages these also act as a form of restraint to the fresh concrete. The similarity in bottom readings from positions 4 and 5 seems to indicate that the influence of the edge restraint is limited to the length of the dowel bars, which protrude 450mm into each strip.

The age adjusted modulus for loading between $\tau = 0$ and 3 days according to equation 2.73 is 12.4 GPa. Therefore, the edge restraint induces theoretical stresses between positions 3 and 5 of approximately 0.16 N/mm^2, which are insignificant.

The same trend is repeated by the effective thermal coefficient of expansion, $\alpha_{c\ eff}$ (Gradient in Table 5.3). At positions 3, 4 & 5 the value for the upper gauges increases with distance from the edge of the pour, whilst that of the lower gauges remains very similar. At position 3 the difference between the top and bottom gauges was not statistically significant, but at the other two positions the upper gauges had a higher effective coefficient than the lower gauges.

Table 5.3 - Northampton: Statistical comparison of daily strain changes

Gauge	Gradient	standard error	Gauge	Gradient	standard error	Students t	Conclusion
3t	9.83	0.19	3b	9.36	0.25	1.50	Similar
4t	10.39	0.17	4b	9.82	0.23	1.99	Different
5t	10.99	0.17	5b	9.43	0.19	6.12	Different
6t	9.46	0.18	6m	10.59	0.21	7.40	Different
6m	10.59	0.21	6b	11.74	0.25	2.76	Different
8t	11.21	0.65	8b	9.60	0.29	1.12	Similar
9t	10.09	0.60	9b	12.00	0.28	16.82	Different
3t	9.83	0.19	4t	10.39	0.17	0.03	Similar
3b	9.36	0.25	4b	9.82	0.23	5.39	Different
4t	10.39	0.17	5t	10.99	0.17	3.77	Different
4b	9.82	0.23	5b	9.43	0.19	1.23	Similar
4t	10.39	0.17	6t	9.46	0.18	4.47	Different
4b	9.82	0.23	6b	11.74	0.25	2.02	Different
6t	9.46	0.18	8t	11.21	0.65	0.41	Similar
6b	11.74	0.25	8b	9.60	0.29	2.54	Different
8t	11.21	0.65	9t	10.09	0.60	1.12	Similar
8b	9.60	0.29	9b	12.00	0.28	33.10	Different

As the distance from the sawn free movement joint increases, the measured movement from the top gauges at 600mm from the slab edge is very consistent. Positions 4, 6 and 8 recorded 64, 62 and 66 μstrain contraction until $\tau = 3$ days. The bottom gauges, however, show a reduction and then an increase in contraction with 70, 41 and 53 μstrain for the same locations. Thus position 4 recorded 17 μstrain more contraction than position 8, even though the measured temperature drop was almost 1 °C less. As the contraction initially reduces with increased distance from the free movement joint, this trend is believed to be related to the frictional restraint, although the similarity in the effective thermal coefficient of expansion shows that this seems to have very little effect on the daily temperature strains. The increase in contraction recorded by the bottom gauge at position 8 could relate to the proximity of the formed free movement joint at the end of the slab.

Using the previously determined age adjusted modulus this difference in movement between positions 4 and 6 would induce theoretical restraint stresses of 0.36 N/mm^2, which although greater than the effects of the edge restraint should still not be sufficient to cause cracking in the slab.

The measurements from the two jointless large area pours allow the effects of the frictional restraint to be investigated further. As the distances between the movement joints are greater, the effects of the restraint can be seen more easily.

The incremental movement from **Bedford** (Table 5.4) showed that gauges 2 and 5, which were nearest to the edges of the pour and were in the last sections of concrete to be placed, measured the greatest movement during the first three days. They also recorded very similar movement over each of the subsequent time intervals, although gauge 5, which was slightly closer to the edge of the slab, measured marginally more movement each time. The daily thermal movements of these two gauges were also similar (Table 5.5).

Table 5.4 – Bedford: Mean early life incremental movement

Position	Mean movement [microstrain]					
	0-3 days	3-7 days	7-14 days	14-21 days	21-28 days	28-35 days
1	-32	-6	-27	+7	-21	+31
2	-50	-5	-26	+4	-19	+28
3	-38	-6	-29	+4	-26	+25
4	-35	0	-20	+6	-16	+25
5	-48	-6	-28	+5	-23	+28

Over the first three days the magnitude of the measured contraction was found to decrease with distance from the free edges of the slab, although the difference between positions 1 and 3 was only 6 μstrain. The free movement joint between pours 2 and 3 opened more than the joint

between pours 1 and 2, which was reflected in the concrete movement, with gauge 3 recording more rapid contraction than gauge 1 even though they were both the same distance from the free movement joints.

Table 5.5 - Bedford: Statistical comparison of daily strain changes

Gauge	Gradient	standard error	Gauge	Gradient	standard error	Students t	Conclusion
1	8.24	0.25	3	7.27	0.15	3.33	Different
3	7.27	0.15	5	7.33	0.13	0.30	Similar
2	7.17	0.17	4	6.17	0.22	3.60	Different
1	8.24	0.25	2	7.17	0.17	3.54	Different
5	7.33	0.13	2	7.17	0.17	0.75	Similar
1	8.24	0.25	4	6.17	0.22	6.22	Different

The concrete contraction between $\tau = 3$ and 14 days from gauges 2 and 4, monitoring across the slab, was less than from any of the other gauges, although in the short period of rising temperatures between 14 and 28 days the expansion recorded by gauge 4 was greater than elsewhere. This difference in behaviour is believed to relate to the restraint provided across the building because the slab was tied to the concrete perimeter retaining walls. Because the stresses at position 4 will have been larger than at the other gauge locations, the thermal expansion caused by the increase of temperature will have had the greatest effect here.

Because of the restraint the effective thermal coefficients of expansion for positions 2 and 4, although significantly different, were lower than for all of the other positions.

After 28 days the movement recorded by gauges 5 and 1 was 100 and 79 μstrain respectively (Figure 5.39a), although most of the difference in contraction occurred during the first 72 hours following initialisation of the strains. The measured contraction of 96 μstrain across the building recorded by gauge 2 was similar to that from gauge 5, whilst gauge 4 recorded the smallest contraction of only 65 μstrain, with half of this difference occurring during the first 72 hours (Figure 5.39b).

The age adjusted effective modulus for loading from $\tau = 0$ to 3 days is 13.5 GPa. Hence the restraint across the building would induce theoretical stresses of 0.20 N/mm^2 after 3 days, and 0.35 N/mm^2 after 28 days given an age adjusted modulus from $\tau = 0$ to 28 days of 11.2 GPa. Using the relationship in equation 2.24 the predicted 28 day tensile strength is 3.76 N/mm^2. After 3 days the degree of hydration found by the finite element models, discussed in more detail in the next chapter, was around 0.55, giving a 3 day tensile strength of approximately 1.6 N/mm^2 according to equation 2.26. This means that this restraint stress accounts for almost 13% of the tensile capacity of the slab after 3 days dropping to around 9% after 28 days. The calculated stress caused by the restraint down the length of the building was approximately

0.22 N/mm^2 after 3 days and 0.24 N/mm^2 after 28 days, which accounted for between 14 and 6% of the tensile capacity of the concrete as the slab aged.

Crack surveys carried out at periodic intervals once the building was in service have shown that almost all of the cracking which occurred in this floor was perpendicular to the direction of maximum restraint, i.e. across the building (See Appendix C for crack survey results).

The same reduction in longitudinal movement over the first 3 days can be seen in the readings from the embedment gauges in the second jointless large area pour at **Marston**. Where two gauges were located at a monitoring position the readings have been averaged. This assumes a linear strain distribution through the cross section, which may not always be the case, but allows a comparison to be made between the contractions at all of the instrumented points.

Incremental readings over the first 12 days are given in Table 5.6, though the measured strains from pour 6 until $\tau = 3$ days must be interpreted with care. The maximum temperature of the concrete containing gauge positions 1 to 6, which was poured between 8am and 9:30am, was 3.5°C lower than the maximum temperature of the concrete poured later in the day. This demonstrates two trends which are apparent at early ages. Firstly, the magnitude of the strain is strongly dependent on the maximum temperature of the concrete and, secondly, the measured strain decreases with distance from the edge of the pour (see positions 10 and 7 in Table 5.6 and Figure 5.40).

Table 5.6 – Marston: Incremental movement

Position	Mean movement [microstrain]			Position	Mean movement [microstrain]		
	0-3 days	3-7 days	7-12 days		0-3 days	3-7 days	7-12 days
3	-65	-29	-51	19	-76	-58	*
4	-73	-39	-55	20	-78	-63	*
5	-65	-33	-51	21	-83.5	-60	*
6	-63	-33	-50	24	*	*	*
7	-93	-23	-47	25	-97	-27	-40
8	-104	-29	-50	26	-85	-30	-44
9[#]	-110	-30	-56	27	-98	-30	-44
10	-108	-32	-55	28	-75	-25	-41
11	*	*	-48	29	-84	-35	-48
13	-73	-54	*	30	-84	-33	-47
14	-84	-55	*	33	-90	-60	*
15	-78	-58	*	34	-77	-56	*
16	-67	-55	*	35	-74	-59	*
17	-58	-53	*	36	-59	-54	*
18	-61	-53	*				

* No data available for this time

[#] Reading from position 9 is an upper gauge only not a mean reading

The gauges cast in pour 7 recorded a maximum temperature of 28.6°C and produced similar strains to those measured by the later gauges in pour 6. Again the gauges in the middle of the pour showed much less contraction at all times (Figure 5.41). The similarity of the readings from the gauge positions at each side of this pour (30 and 26) indicates that the restraint at the joint with the previous pour is not significant.

Data from pour 9 again demonstrates the effects of frictional restraint, with the measured strain reducing with increasing distance from the edges of the slab (Figure 5.42). The relationship between the maximum temperature and the magnitude of the strains is not seen in this case. The gauges cast in the morning (positions 31-36) recorded a maximum temperature of 25°C, whilst the gauges across the middle of the pour (positions 13-21) recorded a maximum temperature of 30°C. The measured strains, however, were slightly lower for the gauges at positions 13-21. One possible explanation is the possibility of increased restraint in this direction caused by the adjacent pours.

After the first three days the slab temperature generally converged with the ambient temperature, meaning that all of the strain gauges were experiencing the same thermal changes.

A reduction in movement could almost always be seen between the gauges 5m and 7m from the slab edge, though the mean reading 5m from the slab edge was occasionally larger than the reading 1m from the slab edge (see positions 13, 15 and 16).

The difference in movement measured by the gauges 1m from the edge of the slab and mid-slab in pour 9 was 17 μstrain after 1 day and 26 μstrain after 3 days. Using the age adjusted modulus this gives theoretical stresses of around 0.21 N/mm^2 and 0.29 N/mm^2 respectively, which is not sufficient to cause cracking, but nevertheless accounts for around 20% of the tensile capacity of the slab.

For restraint occurring between 7 and 140 days the age adjusted modulus is 12.7 GPa. The movement over this period at positions 16, 17 and 18 was very similar, but around 40 μstrain less than the movement at positions 13 and 20. This results in a theoretical restraint stress away from the edges of the pour of approximately 0.51 N/mm^2, which accounts for approximately 20% of the tensile strength of the concrete in this floor calculated according to equation 2.24.

The effective thermal coefficients of expansion concur with the long-term slab strain measurements (Table 5.7). Pours 6 and 7 show little variation (Figure 5.43a & b), with only gauge 25 being significantly different from all of the other gauges in pour 7. Figure 5.43c shows the variation with distance from the edge of the bay for pour 9. It can clearly be seen that the gradient reduces, and hence the restraint increases, as the distance from the free movement joints increases. This is in agreement with the plot of strain against location, which showed a significant increase near to the free movement joints.

Table 5.7 - Marston: Statistical comparison of daily strain changes

Gauge	Gradient	standard error	Gauge	Gradient	standard error	Students t	Conclusion
3t	11.10	0.15	3b	10.80	0.12	1.56	Similar
4t	10.90	0.14	4b	11.40	0.21	1.98	Similar
5t	10.93	0.09	5b	11.43	0.20	2.28	Different
10t	12.02	0.32	10b	10.88	0.36	2.37	Different
13t	14.43	0.59	13b	13.03	0.42	1.93	Similar
15t	12.47	0.27	15b	13.48	0.31	2.46	Different
17t	9.88	0.33	17b	9.19	0.36	1.41	Similar
20t	15.01	0.54	20b	13.65	0.41	2.01	Different
3t	11.10	0.15	4t	10.90	0.14	0.97	Similar
3b	10.80	0.12	4b	11.40	0.21	2.48	Different
4t	10.35	0.14	5t	10.93	0.09	3.48	Different
4b	10.58	0.21	5b	11.43	0.20	2.93	Different
5t	10.93	0.09	6m	11.45	0.21	2.28	Different
5b	11.43	0.20	6m	11.45	0.21	0.07	Similar
5av	11.18	0.22	6m	11.45	0.21	0.89	Similar
6m	11.45	0.21	7m	11.40	0.22	0.16	Similar
7m	11.40	0.22	8m	10.62	0.18	2.74	Different
8m	10.62	0.18	9b	11.15	0.22	1.86	Similar
9b	11.15	0.22	10b	10.88	0.36	0.64	Similar
10t	12.02	0.32	11m	10.79	0.34	2.63	Different
10b	10.88	0.36	11m	10.79	0.34	0.18	Similar
13t	14.43	0.59	14m	10.88	0.23	5.61	Different
13b	13.03	0.42	14m	10.88	0.23	4.49	Different
13av	13.73	0.72	14m	10.88	0.23	3.75	Different
14m	10.88	0.23	15t	12.47	0.27	4.48	Different
14m	10.88	0.23	15b	13.48	0.31	6.74	Different
14m	10.88	0.23	15av	12.98	0.41	4.45	Different
15t	12.47	0.27	16m	11.78	0.27	1.81	Similar
15b	13.48	0.31	16m	11.78	0.27	4.14	Different
15av	12.98	0.41	16m	11.78	0.27	2.43	Different
16m	11.78	0.27	17t	9.88	0.33	4.46	Different
16m	11.78	0.27	17b	9.19	0.36	5.76	Different
16m	11.78	0.27	17av	9.54	0.49	4.02	Different
17t	9.88	0.33	18m	11.99	0.31	4.66	Different
17b	9.19	0.36	18m	11.99	0.31	5.89	Different
17av	9.54	0.49	18m	11.99	0.31	4.24	Different
18m	11.99	0.31	19m	13.42	0.35	3.06	Different
19m	13.42	0.35	20t	15.01	0.54	2.47	Different
19m	13.42	0.35	20b	13.65	0.41	0.43	Similar
19m	13.42	0.35	20av	14.33	0.68	1.19	Similar
20t	15.01	0.54	21m	11.44	0.30	5.78	Different
20b	13.65	0.41	21m	11.44	0.30	4.35	Different
20av	14.33	0.68	21m	11.44	0.30	3.90	Different
25m	11.00	0.12	26m	10.33	0.17	3.22	Different
26m	10.33	0.17	27m	10.71	0.16	1.63	Similar
27m	10.71	0.16	28m	10.23	0.23	1.71	Similar
28m	10.23	0.23	29m	10.49	0.22	0.82	Similar
29m	10.49	0.22	30m	10.67	0.22	0.58	Similar

The data in the shaded rows are average values for an instrumentation position.

Few of the sawn restrained movement joints in the fabric reinforced jointed large area pour at **Chepstow** opened, which will have induced higher restraint stresses in the floor. Isolated cracking was first reported in this floor in November 1999, almost 3 months after construction, at which time a detail survey was carried out. This identified cracking in several areas of the floor, although pour 4, which had been an in-fill bay was the worst affected area (Figure 5.44). By casting this pour within several other pours the early age thermal movement will have been restrained leading to higher residual stresses in the slab.

Evidence of this form of restraint can be seen with reference to Figure 5.45. The contraction in pour 10 after 1 day measured by gauge 12 at the end cast against pour 8 was 38 μstrain, whilst gauge 9 at the free end measured 55 μstrain. Pour 11 also showed a slight increase in contraction from 22 to 29 μstrain between gauge 1 at the edge of the building and gauge 4, which was a free edge. The contraction from pour 13, which was an in-fill bay, measured by gauges 6 and 7 was around 14 μstrain. Gauge 5 measured 28 μstrain; however, this was 4m from the formed restrained movement joint monitored by gauge 17, which was found to open by 0.04mm during the first 24 hours, possibly accounting for this difference.

Both pours with at least one restrained edge showed a variation in the measured contraction of around 17 μstrain until t = 1 day. The theoretical age adjusted modulus for this period is 13.4 GPa, which leads to theoretical restraint stresses of 0.23 N/mm^2. By comparison, the variation in contraction measured in pour 11, which was unrestrained at both edges, lead to theoretical restraint stresses of only 0.09 N/mm^2.

It is clear that the cracks in this floor did not form within the first 24 hours after construction, as they are not continuous across the saw-cut joints (Figure 5.46).

There was no reduction in the contraction as the distance from the ends of the slabs increased down the length of the building in the first jointed large area pour at **Leeds**, even though none of the joints were found to open during the first couple of weeks after construction, whilst a very slight reduction of 3 μstrain was found across the pour (Table 5.8). The mean contraction across the pour was found to be significantly greater than down the length of the pour, 43 μstrain compared to 52 μstrain in the first week. This pattern was repeated for the second pour, with mean lengthways contraction of 18 μstrain compared to 27 μstrain across the pour. There was also a much clearer difference in contraction measured by the two gauges across the second pour, with gauge 7 measuring 8 μstrain more contraction in the first 3 days.

These trends were not continued in the long term, a factor which appears to be related to the joint opening. Although the gauges in the middle of the pours initially showed the least contraction, this behaviour changed once the joints began to open. For example, the contraction at the centre of pour 2 (Gauges 9 and 10T), where joint widths were greatest, was 20% greater than at the edge of the pour after 4 months.

Table 5.8 – Leeds: Longitudinal and transverse contraction from the first two pours

Position	Movement [microstrain]			Position	Movement [microstrain]		
	0-3 days	3-7 days	7-14 days		0-3 days	3-7 days	7-14 days
2	-32	-12	+5	7	-31	-1	+1
3	-28	-14	+4	8	-23	0	+1
4	-32	-12	+6	9	-11	-4	+5
5	-35	-16	+4	10T	-20	-4	+6
6	-38	-16	+4	12	-17	+1	+4

If no cracking occurs in the slab, the joint movement should be equal to the area under a graph of contraction against location. This is because the integral of strain against length gives a displacement. The inherent assumption when designers determine joint spacing is that all of the concrete between joints will move uniformly. The comparison of the measured joint widths with the measured contractions allows the accuracy of this assumption to be assessed.

For the long strip slab at **Northampton**, analysis of the movements from the embedment gauges when the joint first opened shows that the reduction in strain as the distance from the joint increases is almost linear up to a distance of 7m, as shown in Figure 5.47. However, the measured strains from the embedment gauges over the first few weeks were found to decrease up to 4m from the free movement joint before beginning to increase again, with this change in behaviour attributed to the proximity of the formed free movement joint at the end of the slab.

Therefore, measured contraction has been integrated over two lengths, 7m and 4m, for comparison with the joint movement (Table 5.9). It has been assumed that the concrete contraction on both sides of the joint is similar, giving incremental contractions as shown in Figure 5.38. Calculated joint widths have been given for gauge positions 1B and 2B using the bottom contraction readings from positions 3, 5, 6 and 8. Little difference in behaviour was found between the bottom gauges 900mm and 600mm from the slab edge at positions 4 and 5. This relationship has been assumed to be the same along the length of the strip allowing the contraction from positions 6 and 8 to be used to calculate the joint movements for the 4m and 7m active lengths of slab.

The difference in strains between positions 3 and 5 has also been assumed constant along the strip, with the difference applied to the contraction at position 6 allowing the joint movement 300mm from the slab edge to be determined.

For **Northampton** very good agreement was found for the joint width predictions using the active length of 4m at 7 and 14 days. Reference to Figure 5.35 shows that the joint opening began to flatten off after about 16 days. Calculating the predicted joint opening at position 2

after 28 days using the 4m length gives a width of 0.94mm; this compares to a measured opening of 0.75mm. Further calculations using this length show reasonable agreement with the measured joint opening as the slab ages – after 270 days the predicted opening at position 2 was 1.11mm compared to measured opening of only 1.03mm, whilst after 375 days the predicted movement was 0.90mm compared with measured movement of 0.89mm.

Table 5.9 – Northampton: Comparison of calculated and measured joint opening

	Measured joint width, $\Delta_J(t)$ [mm]		Calculated over 4m length* [mm]		Calculated over 7m length* [mm]	
Elapsed time, t	7	14	7	14	7	14
Position 2B	0.52	0.73	0.50	0.69	0.93	1.33
Position 1B	0.34	0.55	0.36	0.58	0.70	1.12

* As embedment gauges were only located on one side of the sawn free movement joint the calculated joint movement assumes that the concrete contraction was similar on the opposite side of the joint.

The same approach has been applied to the joint movements from the **Marston** jointless large area pour (Table 5.10). As a distinct change in the shrinkage behaviour of each of the pours was seen from the gauges around 7m from the free movement joints, this has been used as one active length, whilst the mid-point of the slab has also been used as another, as is assumed in the design.

Battery failure meant that no readings were taken between 10 and 140 days after construction. For this reason the joint movements and the concrete shrinkage have only been compared at these ages. The joint widths at this later time were determined by visual inspection using a rule, as the opening had exceeded the full range of the joint gauges.

Table 5.10 – Marston: Comparison of calculated and measured joint opening

Gauge position	Measured joint width, Δ_J [mm]		Calculated over 7m length [mm]		Calculated from mid-slab [mm]	
Elapsed time, t	7	140 [1]	7	140	7	140
1	1.11	2.5	0.67	1.62	1.13	4.62
12	2.54	10.0	1.37	2.86	3.52	7.56
23	2.54	9.0	1.29	2.83	3.71	8.01
32	1.67	4.0	0.91	1.56	2.80 [2]	5.43 [2]

[1] Readings were taken optically with a rule as the range of the strain gauges had been exceeded.

[2] Assumes shrinkage at mid-slab is the same as at position 36 – as for the other slab direction.

After 7 days the difference between the predicted movement calculated over the length of 7m and the measured movement was very similar for all of the joints; varying between 54 and

60% over the measured movement. The predictions based on the movement calculated from mid-slab matched the measured movement for position 1, whilst at positions 12 and 23 the width was over predicted by around 40%. The difference being even greater for position 32. although assumptions had to be made about the mid-slab movement at this point, which could account for some of the discrepancy.

After 7 days the movement from pour 6 had been quite uniform, whilst that from pour 9 showed definite non-linearity between 5 and 7m from the day joint. If the movement calculated from mid-slab for pour 6 is added to the movement from the edge 7m from pour 9 the predicted joint width increases to 80% of the measured width.

The difference in the measured joint widths and the predicted widths after 140 days could have two possible causes:

- Errors could have arisen in measuring the joint widths. This is possible because of difficulties in choosing the zero point for edge movements due to unevenness of the building walls, and differential contraction which could have affected all readings.
- The theoretical joint opening calculated from mid-length in the slab assumes that this point of each pour does not move, and that the movement occurs from this point to the two edges. Due to differences in restraint this assumption may be wrong.

This hypothesis could be verified in two ways:

- The relative movement of the slab to the sub-base could be measured at several locations.
- All of the panels in a floor and all of the joints could be instrumented. The sum of the concrete contraction has to be greater than or equal to the sum of the joint movements.

Unfortunately, the data collected as part of this project does not allow either of these two causes to be directly verified. However, joint width measurements were taken across all of the joints at 140 days, showing there was up to 30% variation in the width of the day joints (Figure 5.48). Over the same time period the contraction measured at the middle of the three instrumented pours was 230, 233 and 238 μstrain.

The movement in the three instrumented slabs varied near to the joints, but was very similar over the inner sections. Assuming this behaviour was repeated in all of the other slabs an estimate of the mean contraction for the length of the building can be obtained using the mean contraction from the three instrumented pours of 233.7 μstrain. The total length of floor slab was 209.04m giving a total predicted contraction of 48.8mm. Assuming that the slab remained uncracked this should equate to the total joint opening down the length of the building. Summing the measured joint opening after 140 days gives a total of 43.5mm, which is less than the mean predicted movement.

This makes it most likely that the second possible cause for discrepancies in the joint width predictions is correct – i.e. the slabs do not move about their mid-points, resulting in uneven opening of the day-joints. However, the similarity between the predicted and measured movement over the length of this building indicates that most parts of the floor have moved, leaving a reduced risk of cracking due to restraint. Calculating an approximate mean restraint from the difference in measured and calculated movement gives a value of 25 μstrain.

5.4.5. Warping restraint

The long strip floor at **Northampton** and the jointless large area pour **Bedford2** had strain gauges installed at two different depths in the slab, in order to allow the differential movement to be analysed. Both floors showed evidence of warping with large differential movements near to the joints.

A precision level survey of the instrumented section of the long strip slab (**Northampton**) was carried out 24 hours after construction, which showed the floor to have a slight curvature across its width (Figure 5.49). The occurrence of this profile so soon after construction could have resulted from some of the early differential thermal changes, though it is also believed in part to be caused by 'false curl'. This can occur as a result of the vertical movement of the vibrating beam used to level and compact the floor, and the powerfloats carrying material from the middle of the strip towards the edges.

Further surveys carried out once the building was in service showed that several millimetres of curling deflection had occurred within about 1m of the joints after 10 months. This vertical movement was consistently found to be less near to the sawn free movement joints than at the sawn restrained movement joints (Figure 5.50 and Figure 5.51). This difference in behaviour is believed to be related to the higher moment resistance of the steel dowels crossing the free movement joints compared to the fabric reinforcement crossing the restrained movement joints. This confirms that the restrained movement joints are able to perform as assumed in TR34 (1994) and release moment stresses which have built up in the slab. However, there is an associated risk, particularly to the end user, as increased warping deflections of the slab can affect the operation of the building.

There was little difference in the differential movement at all instrumented sections after 28 days. At later times the differential movement measured near to the sawn restrained movement joint was greater than that measured near the sawn free movement joint, whilst the smallest differential movement was measured mid-way between the two joints (Figure 5.52), which concurs with the slab profile from the level surveys.

Leonards and Harr (1958) used equivalent temperature gradients (ETG) to represent the thermal and hygral length changes in slabs and pavements. The respective maximum differential gradients extrapolated to the full thickness of the slab at positions 4, 6 and 8 after

850 days were 219, 130 and 386 μstrain. Converting these measured strains into ETGs, using α_c = 10 μstrain/°C, gives 0.84, 0.5 and 1.48 °C/cm for positions 4, 6 and 8 respectively. These values compare well to the range of 0.66 to 1.33 °C/cm found by Leonards and Harr for internal slabs exposed to a drying environment. The range cited in NCHRP Report 372 (1995) based on Chilean and German data was 1.1 to 1.5°C/cm.

The warping restraint between positions 6 and 8 is the difference between the strain gradients measured at each point. Over the time period from 28 to 370 days this was 82 μstrain, which when extrapolated to give the difference in strain across the slab thickness gives 178 μstrain, or an ETG of 0.68 °C/cm.

The maximum stresses arising in a slab with thickness, h, under exposure to an ETG whilst fully restrained are given by:

$$\sigma_r = \frac{E_c \cdot \alpha_c \cdot ETG \cdot h}{2 \cdot (1 - \nu)} \qquad \text{equation 5.7}$$

Given that the age adjusted modulus over this time was 13.4 GPa, and using a Poisson's ratio of 0.2 this leads to a warping restraint stress of 1.49 N/mm^2. A further large increase occurred between 370 and 730 days, with the restrained strain between positions 6 and 8 growing by a further 30 μstrain. Extrapolated over the full thickness of the slab, and with an age adjusted modulus of 21.5 GPa this gives an additional warping restraint stress of 0.87 N/mm^2. The residual stress from the earlier restraint can also be calculated using the required age adjusted modulus of 12.1 GPa, leaving 1.35 N/mm^2, and a combined restraint stress of 2.22 N/mm^2. No further significant change in differential movement was seen between 730 and 850 days.

TR34 (1994) uses the following relationship to give the flexural strength of concrete, allowing a 10% increase to give the strength at 90 days.

$$R_{28} = 0.393 f_{cu}^{\ 2/3} \qquad \text{equation 5.8}$$

The cube tests for **Northampton** gave a 28 day compressive strength of 56.9 N/mm^2, giving a 90 day flexural strength of 5.8 N/mm^2. Therefore, the combined warping restraint stresses between 28 and 730 days account for almost 40% of the flexural strength of the concrete.

Warping was also measured in the jointless large area pour at **Marston**. Again the reduction in the measured warping can be seen as the distance from the edge of the slab increased (Figure 5.53 a, b & c).

The approximate stresses resulting from this restraint can be calculated as above. Unfortunately failure of the logging equipment meant that no readings were obtained between 11 and 140 days, so the warping has had to be assumed to have occurred uniformly over this time period. By 140 days the difference in strain gradient between mid-slab and the left-hand edge had reached 265 μstrain, or an ETG of 1.51 °C/cm. This gives an estimated warping

restraint stress of 2.1 N/mm^2 using the age adjusted effective modulus of 12.7 GPa, which again accounts for a significant proportion of the flexural strength of the slab.

The stresses induced in the slabs by warping restraint have been found to be significantly larger than those resulting from longitudinal restraint. Additionally, whereas the longitudinal restraint builds up over a long distance, the warping restraint reaches a constant maximum value at the critical length from the slab edge. This means that the majority of the slab is often exposed to this restraint.

However, warping restraint induces tensile stresses in the top half of the slab and compressive stresses in the bottom half, which is in the opposite sense to the stress distribution under point loads on the slab. Therefore, away from the edges of the slab this restraint could actually be beneficial to the load carrying capacity of the slab, though this will not be the case in aisles where, in combination with the hogging moment, the warping restraint could cause cracking under normal service conditions.

5.4.6. The effect of ambient temperature

The behaviour of all parts of floors has been strongly influenced by its temperature – especially during the first week after construction when the thermal changes are generally at their greatest, being influenced by the ambient conditions and the heat released due to cement hydration. Temperature rises and drops of greater than 10°C were commonly seen during the first 3 or 4 days after construction. Assuming a concrete thermal coefficient of expansion of 10 μstrain/°C and no restraint, this would equate to a thermal expansion and contraction of more than 100 μstrain. As the concrete temperature increases the concrete stiffness is so low and the creep rate so high that stresses generally do not arise. However, as the concrete begins to cool down more than 20 hours after placement, the elastic modulus has developed sufficiently for stresses to arise if restraint is present. Although creep rates are still high at this time, restraint to this thermal contraction could still cause cracking of the concrete as the tensile strength is also not fully developed.

The impact of the reduction in temperature of the chill store on the concrete in pour 4 at **Leeds** was demonstrated in Figure 5.23. Applying the thermal corrections to account for the concrete contraction shows how the resulting drying shrinkage after 220 days is only 60% of the total movement undergone by this floor (Figure 5.54). Comparison with Figure 5.55, which shows pour 1, indicates how the drying shrinkage has also been reduced when the slab has been exposed to the lower ambient temperature.

Long-term data also shows the influence of seasonal temperature variations. Figure 5.56 shows the long term concrete strains measured at **Bedford**, without any correction for the temperature of the concrete. This slab was constructed at the end of June 1999 when ambient temperatures were around 20°C. Local Meteorological Office data shows that the mean daily ambient

temperature dropped from a high at the end of August to a low in mid January 2000, before beginning to rise again (Figure 5.57). The slab temperature at the end of the monitoring period in August 1999 was found to be 22°C. This had dropped to 6°C in November when manual readings were again taken, before rising to 9.5°C by mid February 2000. The final manual readings in July 2000 gave a slab temperature of 21°C, showing an annual temperature variation of around 16°C.

Figure 5.58 has been corrected to allow for the thermal expansion and contraction of the concrete, and therefore, shows the drying shrinkage of the concrete. These strain readings were all taken on an unloaded slab, to avoid differences in imposed loading affecting these readings.

Assuming the thermal coefficient of expansion for concrete to be 10 μstrain/°C, the expected free thermal contraction between August and November would have been 160 μstrain. The maximum difference in measured values over this period, recorded by gauge 3, was 220 μstrain. This gauge also had the largest calculated drying shrinkage of 90 μstrain, leaving a possible restraint of 30 μstrain. The age adjusted modulus for a load applied over this period is 24.8 GPa, giving a theoretical restraint stress of around 0.74 N/mm^2.

As the distance from the edge of the pour increased, both the thermal contraction and the drying shrinkage reduced, with gauge 1 recording a contraction of 206 μstrain. The readings from the gauges across the building were generally lower than from those down the buildings length. The measured changes at gauges 2 and 4 were 197 and 191 μstrain respectively, which would lead to possible restraint stresses of 0.74 N/mm^2 at gauge 4 assuming that the movement at gauge 3 had been totally unrestrained. If the maximum free movement was indeed 250 μstrain, the restraint on gauge 4 was 59 μstrain, which equates to possible restraint stresses of 1.46 N/mm^2.

The free movement joint between pours 1 and 2, which had been around 3mm wide on 3rd August 1999 had opened to 9.5mm by the 18th November, whilst the joint separating pours 2 and 3 had opened from 5mm to 10mm over the same period. The size of these joint openings means that frictional restraint will have been overcome and free movement of the slabs must have occurred.

As the slab temperature increased from November 1999 until July 2000 the expected thermal expansion was 150 μstrain. The drying shrinkage calculated for all of the gauges over this period was around 30 μstrain. Differences in measured strain were still recorded by the embedment gauges, showing that the restraint stresses again vary with location. The measured differences in strain for gauges 3 and 5 were 96 μstrain, whilst gauge 4, with 79 μstrain, again measured the smallest change.

This leaves a difference of 25 μstrain between the calculated and theoretical thermal expansion for gauge 3, which is almost identical to the restrained strain seen during the previous time period. This demonstrates that the frictional restraint was similar for thermal contractions and expansions.

Crack surveys were undertaken on each site visit (see Appendix C), however, no visible cracking was seen in pour 2 until July 2000. The presence of these cracks which had opened by up to 3mm in some places could explain the smaller than expected expansion from gauge 4. If the restraint stresses had been released, then frictional restraint would again first have to be overcome before movement could occur.

The age adjusted modulus for loads applied between November and July was 29.1 GPa, which shows the difference in stress between the concrete at positions 3 and 4 could have been up to 0.5 N/mm^2.

Similar differences in behaviour were measured from the long strip near **Northampton**. This slab was constructed in March 1998 and was continuously monitored for 6 weeks, before the datalogger had to be removed. Further periods of monitoring were carried out from January to March 1999 and in April and July 2000. Over each of these successive time periods the movement measured by the bottom gauge at each location has been strongly influenced by the seasonal changes in the slab temperature, which varied from 11°C to over 20°C. For example, between April and July 2000 the slab temperature increased from 14 to 20°C. At the same time the bottom embedment gauge at position 6 showed an expansion of 40 μstrain, although the calculated drying shrinkage during this period was negligible. The theoretical restraint during this period amounted to approximately 20 μstrain, which using the elastic modulus as before and neglecting creep would give a longitudinal compressive stress or reduction of tensile stress of 0.6 N/mm^2.

Isolated cracking was also seen in the floor slab at **Chepstow** in early November 1999, 4 months after construction. A full detail survey of the floor was carried out to identify the location and size of the cracks and to attempt to classify their type. A precision level survey of one of the main cracks was also carried out with a digital level to ascertain whether there was any curling or faulting across the crack. A complete set of manual readings for all of the embedded vibrating wire strain gauges was also taken, to give an indication of the magnitude of movements which had occurred in the floor - although there was no cracking present in the area which had been instrumented.

The locations of the cracks which were identified in the floor can be seen marked on the full building plan in Figure 5.44. With the exception of crack A, all of the cracks were hairline cracks (i.e. <0.1mm). The results of the precision level survey of this crack can be seen in Figure 5.59 where they have been superimposed on the plan view of the crack survey data. The

grey-scale representation indicates the levels of the floor relative to the top left-hand corner of the plot. A 3-D representation of the results is presented in Figure 5.60.

To allow for an easier visual assessment of the results, the floor profile across crack A has been plotted along the length of the crack in Figure 5.61 and Figure 5.62. The data shows that the maximum fault across the crack is 0.8mm (Figure 5.62e). At the other sections where readings were taken there was either no faulting or it was less than 0.4mm. The crack width (measured with an optical crack microscope) varied between 0.4mm and 1.4mm with one exceptional reading of 2.3mm. No correlation was found between the crack width and the degree of faulting across the crack.

There is no evidence to suggest that there is any curling present in the slab, as the gradient on both sides of the crack is generally similar - it must be borne in mind that the scales on the figures are in the ratio of 1:1000 (i.e. metres on the abscissa and mm on the ordinate axes) - thus the gradients in Figure 5.61d and 5.62e which look quite severe are actually only 1/250 or 0.4%.

Although it is possible for plastic shrinkage or early-age thermal contraction cracks to form within the first 24 hours and remain unnoticed until later in the life of the slab, cracking before saw cutting has been ruled out here. This is because an inspection of the cracks showed that they were not continuous across the saw-cut joints; rather they jumped sideways by as much as 200mm (Figure 5.46). Had the cracks formed before the saw-cutting it would be expected that they would be continuous across the joint location as there would have been no plane of weakness present.

The main causes of long-term strains, which can lead to cracking, are drying shrinkage and thermal contraction. Drying shrinkage is a very long-term process, the magnitude of which is small in comparison with the early-age thermal and plastic shrinkage effects, and indeed with those of the seasonal thermal effects until the concrete has aged for several years. As it occurs over a longer time scale it is also possible for creep to negate some of the effects.

Ambient temperatures peaked around the end of July, with a maximum slab temperature of 24°C, but by mid November when manual readings were taken the slab temperature had dropped to 16°C. Assuming the concrete within the slab had a thermal coefficient of expansion α_c of 10 μstrain/°C, this would equate to a thermal contraction of 80 μstrain. The maximum measured change over this time period was 129 μstrain from gauge 1 by the edge of the building. Of this around 80 μstrain was believed to be due to drying shrinkage (Figure 5.63), meaning that around 30 μstrain of movement was restrained during this period. The age adjusted effective modulus for loading over this time is 19.9 GPa, which gives approximate restraint (i.e. tensile) stresses of 0.6 N/mm^2. The smallest recorded movement was 78 μstrain from gauge 10, of which 59 μstrain was believed to be drying shrinkage (Figure 5.64). The

difference in drying shrinkage between these two points was 21 μstrain, whilst the restrained thermal movement was a further 61 μstrain, giving a total restrained strain of 82 μstrain. Using the same age adjusted effective elastic modulus as before gives a restraint stress of over 1.6 N/mm^2.

Even neglecting the difference in drying shrinkage and the thermal effects, the difference in recorded movement between gauges 1 and 10 was 51 μstrain. Using the age adjusted effective modulus to account for creep effects produces a tensile restraint stress of over 1.0 N/mm^2.

On it's own this is not sufficient to cause failure of the floor. However, at the time of the initial floor survey, the racking over pours 1-8 (Figure 4.5) had been loaded (starting on the 17th September 1999). The cracking was mainly confined to this loaded area of the building and in particular to pour 4, which had been constructed as an infill bay. This could have lead to restraint stresses from a very early age in this slab, if the thermal contraction following hydration was prevented. The seasonal drop in temperature during the autumn, further combined with the application of service loading appears to have combined to cause cracking in this floor.

The measurements from the instrumented sections of floor in November appear to show a large amount of restrained movement, though no cracking was observed at this time. A further site survey was undertaken by the consulting engineers responsible for the floor in March 2000, once all parts of the racking had been loaded. This showed further cracking in the instrumented sections of the floor, with several of these cracks coinciding with embedment gauges which had previously shown the least movement – i.e. greatest restraint. This appears to confirm that the combination of drying shrinkage, seasonal temperature changes and service loading can cause cracking in a floor, where individually they would not.

These seasonal thermal changes will not influence the warping of the slab, as they occur slowly and cause uniform temperature changes. However, they will affect the longitudinal stress state depending on the restraint conditions. This can lead to increased tensile stresses in the slab in the autumn and winter as temperatures drop. Some warehouses will also see a rise in stock levels through the autumn in the run up to Christmas, which can also increase the restraint experienced by the slab, further exacerbating the problem.

5.4.7. Comparisons with predictive models

The trends seen in the site data have been compared with patterns of expected behaviour, in order to identify the validity of applying predictive models to the design of industrial floors. The initial shrinkage curve after the surface has dried has been found (Figure 5.65) to evolve in proportion to $(t-t_0)^{0.5}$, as predicted by Bazant and Kim (1991).

Furthermore once the temperature effects have been accounted for, comparisons between sites show that the shrinkage after the first 28 days can be related to the thickness of the slabs. The smallest drying shrinkage (36 μstrain) was recorded at Northampton, which was also the thickest slab at 260mm; whilst the thinnest slab, Bedford, gave the largest 28 day drying shrinkage of 56 μstrain. The two 225mm thick floors, Leeds and Chepstow, had similar maximum 28 day drying shrinkage of 41 and 48 μstrain respectively, even though the concrete in the latter floor contained a shrinkage reducing admixture.

The sole exception to this thickness related shrinkage behaviour was the second pour at Leeds, which contained a shrinkage-reducing admixture, resulting in a 50% reduction in the 28 day drying shrinkage compared to pour one (Figure 5.66).

After 120 days the drying shrinkage from Chepstow was almost 15% less than that from Leeds pour 1, whilst pour 4 was approximately 30% less. This difference between pours 1 and 4 remained similar until 220 days when the last readings were taken.

The drying shrinkage of concrete is influenced by the ambient relative humidity, although because of the low moisture diffusivity of concrete a mean value can be used, ignoring the daily fluctuations. The mean long-term ambient relative humidity was not measured for any of the slabs in service, as the ambient environment sensors had to be removed because of operational concerns expressed by the building operators.

However, the RH for a building has to be within the range of 20 to 65% in order to provide comfort and prevent mould and unpleasant odours (CIBSE, 1999). In practice it will be towards the drier end of this range, but using a value of 40%, which lies in the middle of the allowable range, the theoretical drying shrinkage ε_t has been calculated for the different floor slabs using the B3 model (Table 5.11).

Table 5.11 : Theoretical drying shrinkage, ε_t, and calculated drying shrinkage, ε_m

	$t-t_0$	ε_t	ε_m	$t-t_0$	ε_t	ε_m	$t-t_0$	ε_t	ε_m	$t-t_0$	ε_t	ε_m
Northampton	28	-37	-36	120	-81	*	240	-114	-128	386	-144	-144
Chepstow	28	-43	-47	120	-92	-96	240	-130	*	386	-164	*
Leeds	28	-49	-41	120	-106	-112	220	-150	-149	386	-189	*
Bedford	28	-68	-54	140	-159	-148	240	-207	-162	386	-259	-179

* No data available

With the exception of Bedford very good agreement is seen at all times between the theoretical and the measured drying shrinkage strains. At Bedford the theoretical shrinkage exceeds the measured shrinkage at all times, although the difference still lies within the 95% confidence limits suggested by Bazant of +/- 67%. Because it is thinner, this floor will be more sensitive to variations in the RH. Using a value of 50% in the shrinkage calculation improves the

correlation with the measured shrinkage. However, it still over-predicts the 386 day drying shrinkage by 30 μstrain (17%).

5.5. Summary of results

The results from all of the different sites will briefly be summarised here before comparisons are made with mathematical models in the next chapter. The behaviour will again be subdivided according to the joint types, the restraint, the effect of temperature changes and the methods of predicting behaviour.

5.5.1. Thermal behaviour

A direct link was found between the delivery temperature of the concrete and the elapsed time before the maximum temperature was achieved, although no correlation was found with the maximum temperature of the concrete. The use of a shrinkage-reducing admixture in one of the pours appeared to retard the initial set of the concrete, which could leave it at risk of plastic shrinkage cracking for longer.

Because of thermal losses to the ground beneath the slab and the air above the slab, the maximum measured temperature was at mid-depth in the slab, whilst thermal gradients were also found across the long strip slab and in other large area pours cast against other bays.

5.5.2. Restrained movement joints

The behaviour of restrained movement joints has been found to be inconsistent, though the behaviour expected from these joints according to the design guidance is also unclear.

In the long strip slab, sawn restrained movement joints were detailed to reduce the risk of cracking mid-way between free movement joints where the restraint stresses were greatest, and to release warping stresses. These joints were found to prevent joint opening, though the vertical deflection at the joints was found to be consistently larger than at dowelled free movement joints. This indicates that they released some of the warping stresses, but the increased vertical movement could have serviceability implications for the end users.

The behaviour of the sawn restrained movement joints in large area pours varied. In all floors some joints were found to remain closed whilst other joints opened. In some cases the opening was sufficient to lose aggregate interlock.

Differential movement lead to surface measurements of joint widths exceeding the measurements at mid-depth and below by more than 1mm. For this reason load transfer across joints based on surface measurements must be treated as a minimum possible value.

If this type of joint is to be used in a floor the designer must accept that there is a risk that load transfer will be lost across these joints. If the floor is only lightly loaded, this may not be of concern, but in other cases some more reliable method of load transfer must be found.

5.5.3. Free movement joints

Free movement joints were generally found to open as soon as the slabs began to cool. Variations of up to 30% in joint width down the length of a building seems to indicate that the bays do not all move about their centre.

5.5.4. Restraint effects

Although warping restraint is not considered in TR34 (1994), the results indicate that warping can induce greater stresses in the slab than frictional restraint. The jointless large area pours allowed the clearest demonstration of both forms of restraint. Whilst the longitudinal movement near the edges of the pours was up to 50 μstrain more than in the middle after 10 months, this is small when compared to the warping restraint of 175 μstrain experienced at the middle sections of this slab at the same time.

Similar warping restraint was measured in the long strip slab, whilst precision level surveys showed that the occurrence of vertical movement was generally restricted to within 1 to 2m of the joints. This is in general agreement with equation 2.60. As with the large area pours, this means that the majority of the floor will be subjected to this maximum warping restraint stress. Away from joints this could increase the point load capacity of slabs as the restraint stresses are opposite in sense to those induced by loading. However, this is not the case in the middle of aisles where the tensile stress in the top of the slab will reduce the negative moment capacity of the slab, and could lead to cracking in the slab surface.

The difference in measured strains (and hence restraint stresses) was noticeably larger in the floors at Bedford and Chepstow, where cracking was observed. At Bedford longitudinal restraint resulting from detailing appears to have caused the cracking, whilst the cracking at Chepstow seems to have resulted from a combination of restrained thermal contraction and warping, combined with load induced stresses.

5.5.5. Effect of ambient temperature

Seasonal temperature changes have been found to significantly affect the measured strains in all floors. A similar change was seen as the temperature was reduced in the chill store at Leeds. Because most industrial floors are in unheated buildings, an annual temperature variation in excess of 15°C was recorded; this corresponds to a thermal movement of 150 μstrain, or more than 30% of the ultimate drying shrinkage specified for most floors. When added to drying shrinkage this can lead to the build up of significant stresses.

The impact of this thermal change is currently not considered in design, leading to a possible underestimation of the contraction potential of the floor. This can lead to excessive joint widths which, particularly in the case of jointed large area pours, could cause load transfer problems.

5.5.6. Comparison with predictive models

The shrinkage response of the floors was found to be proportional to $(t - t_0)^{0.5}$ as predicted by Bazant and Kim (1991). Additionally very good agreement was found between the calculated shrinkage from the instrumented sites and the drying shrinkage predicted according to model B3 (Bazant & Baweja, 1995a, b & c).

As expected the thinner slabs were found to shrink more than the thicker slabs. However, the results seem to indicate that engineers could get good predictions of the shrinkage potential of most slabs using this drying shrinkage model.

The use of a shrinkage-reducing admixture did seem to reduce the joint movement and concrete shrinkage in the second pour at Leeds compared to the other pours. However, it also retarded the initial set of the concrete leaving it more open to plastic shrinkage cracking. If the conditions in the building can be controlled to reduce evaporation, and this admixture were used in warmer ambient conditions, when the concrete hydrated more rapidly, then this could reduce the potential stresses in a restrained slab, and minimise the joint opening in a slab which was able to move freely.

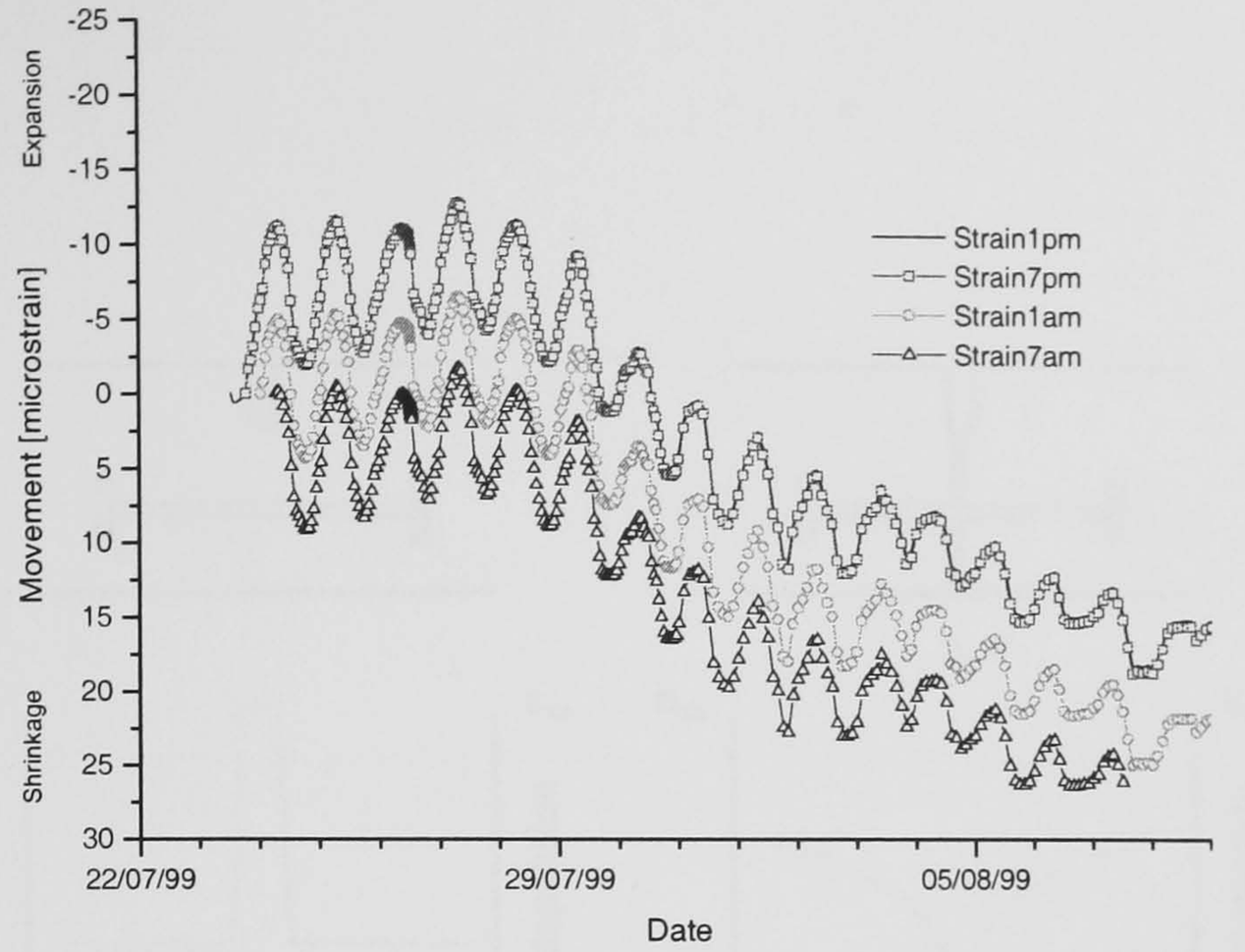

Figure 5.1 - Effect of varying the zero time on the calculated strain

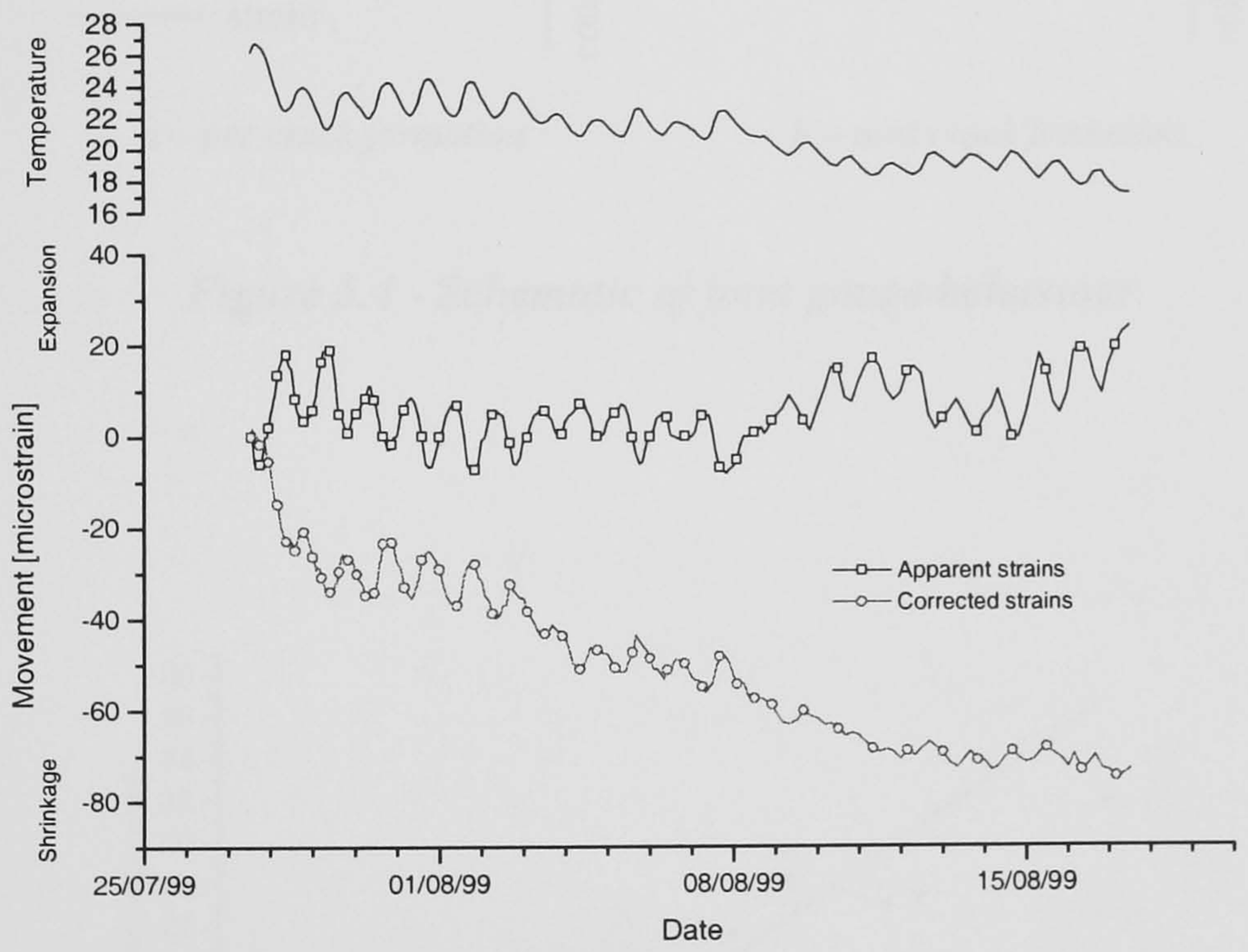

Figure 5.2 – Comparison of apparent and corrected strains

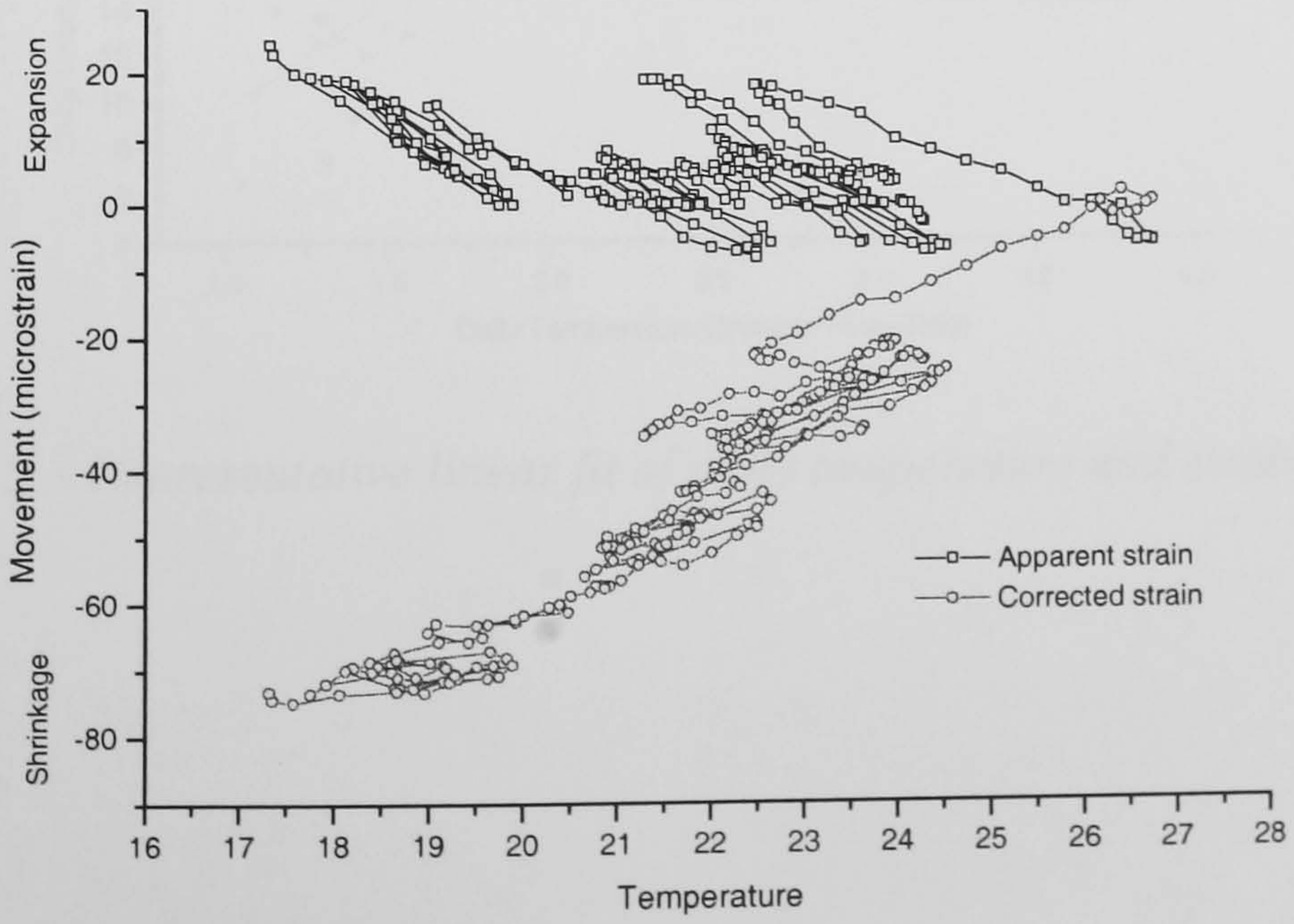

Figure 5.3 – Apparent and thermally corrected strains

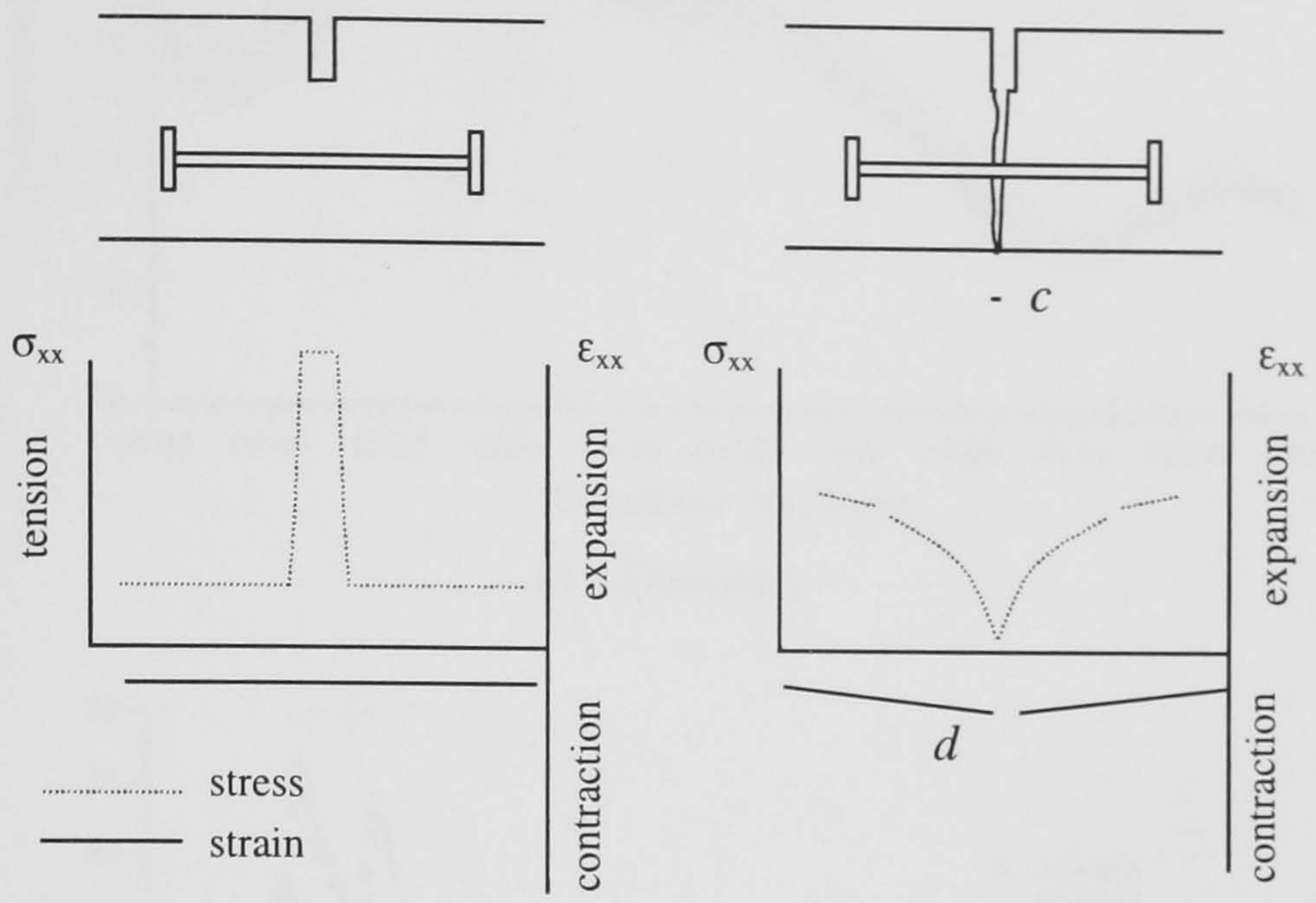

a – pre crack formation *b – post crack formation*

Figure 5.4 - Schematic of joint gauge behaviour

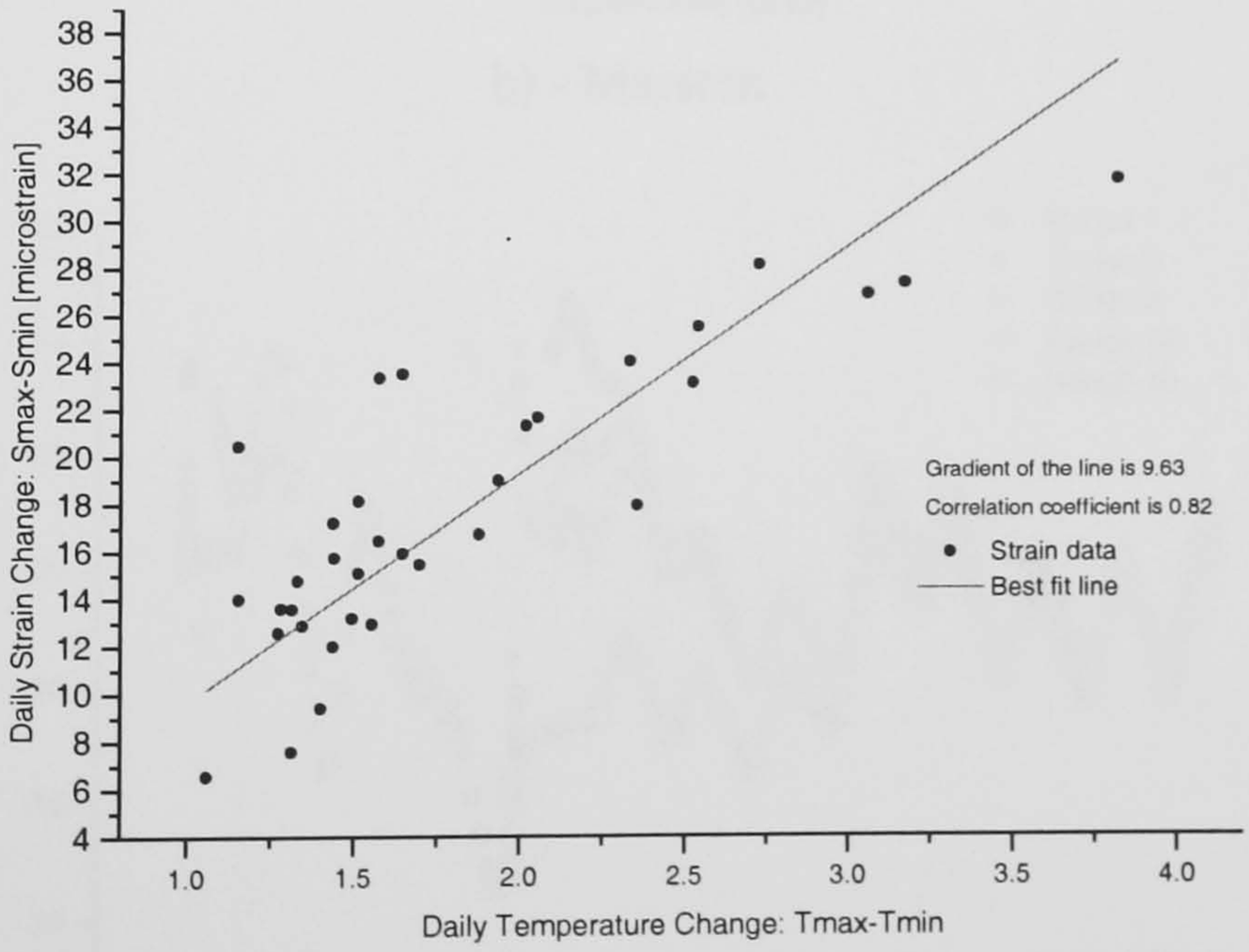

Figure 5.5 - Representative linear fit of daily temperature and strain changes

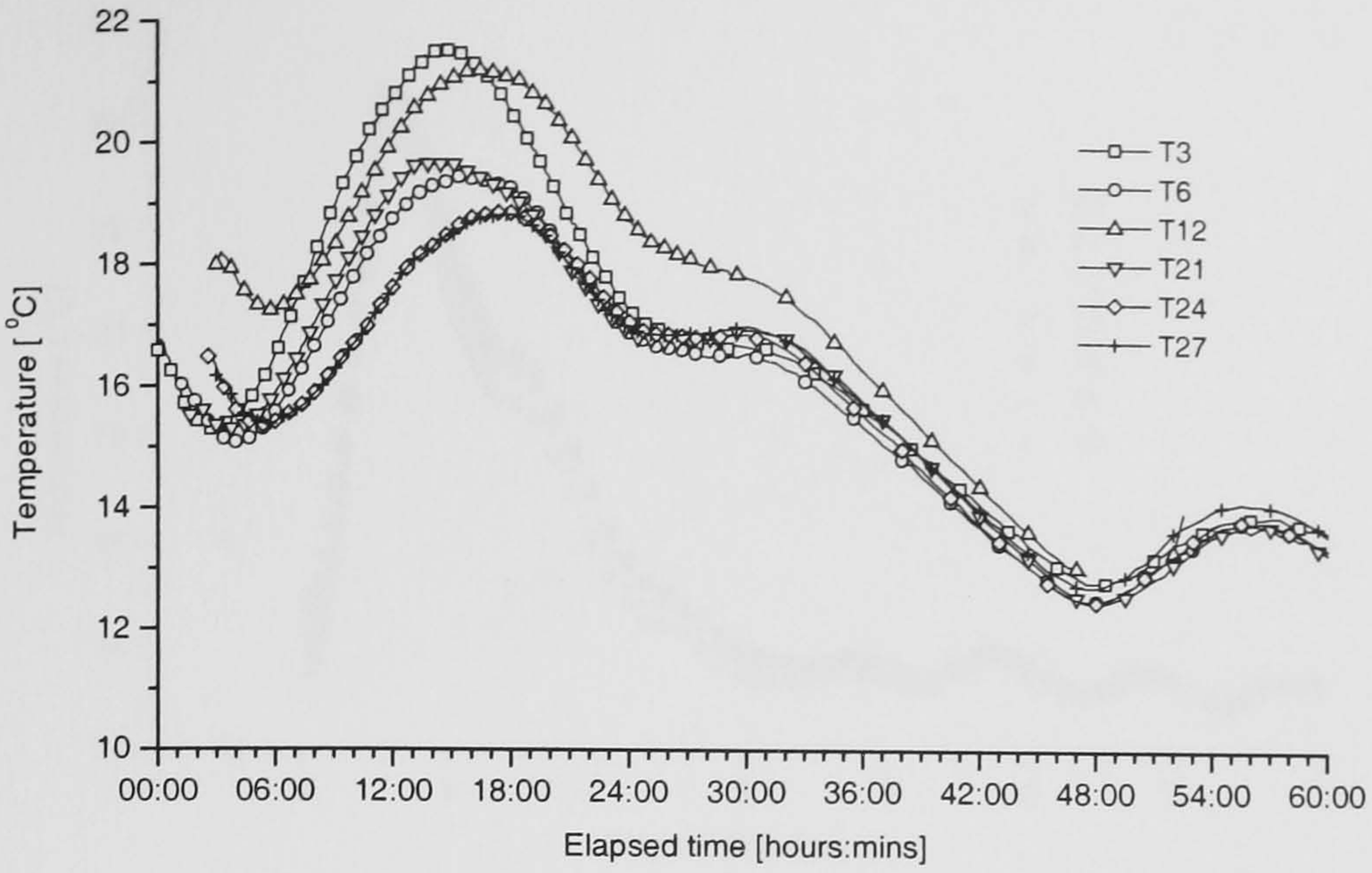

a) - Daventry

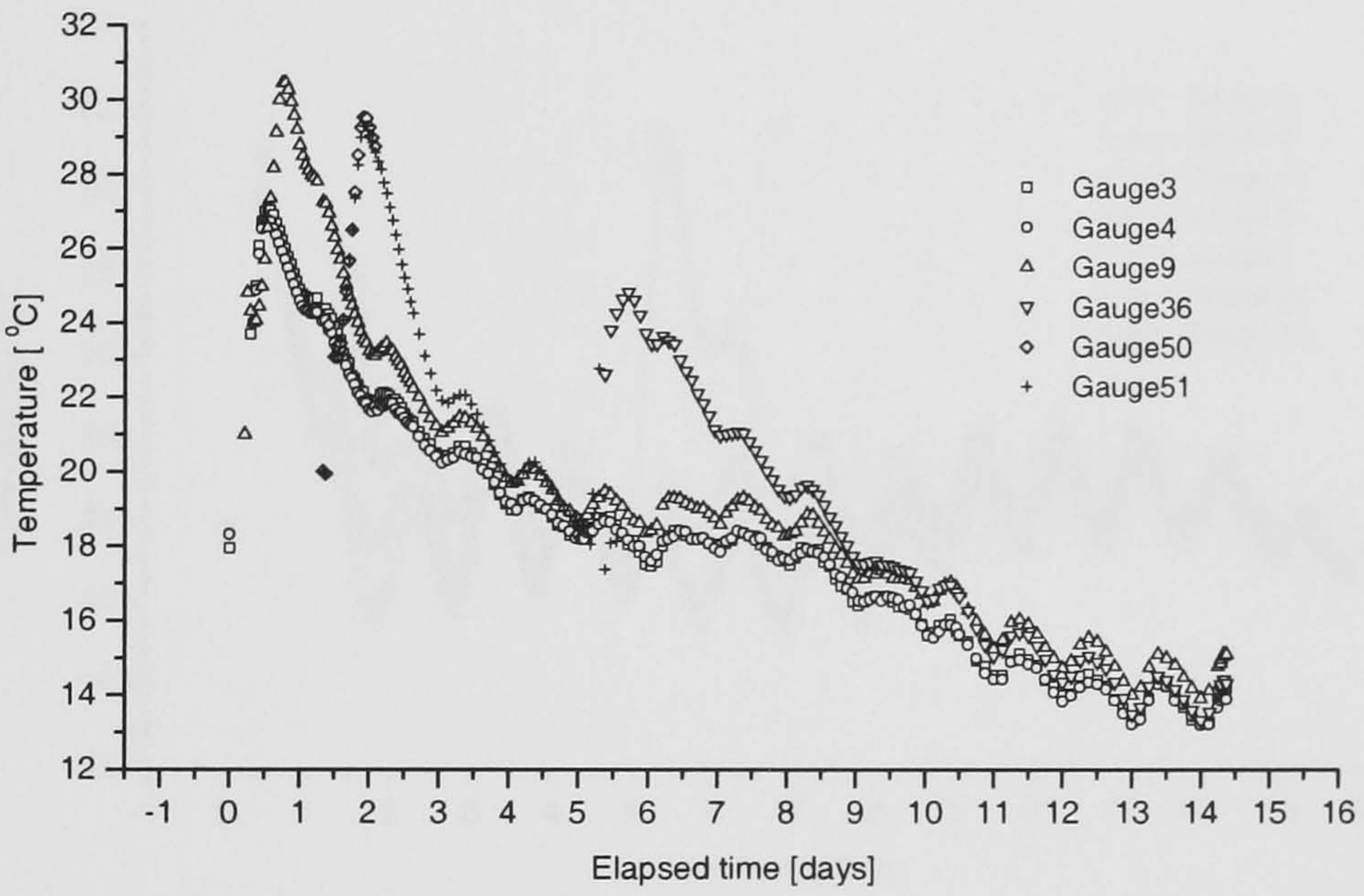

b) - Marston

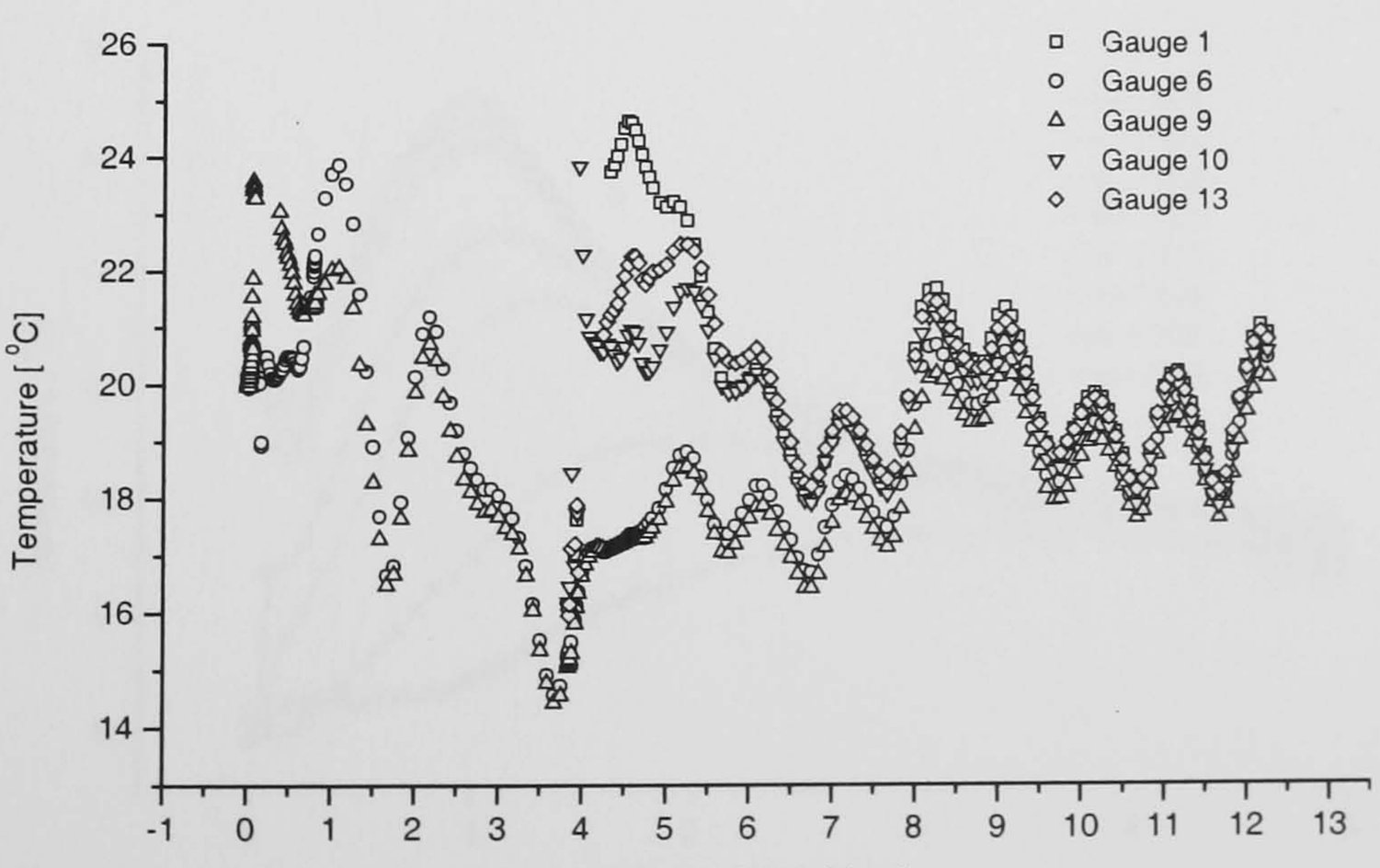

c) – Bedford

Figure 5.6 - Measured concrete internal temperatures

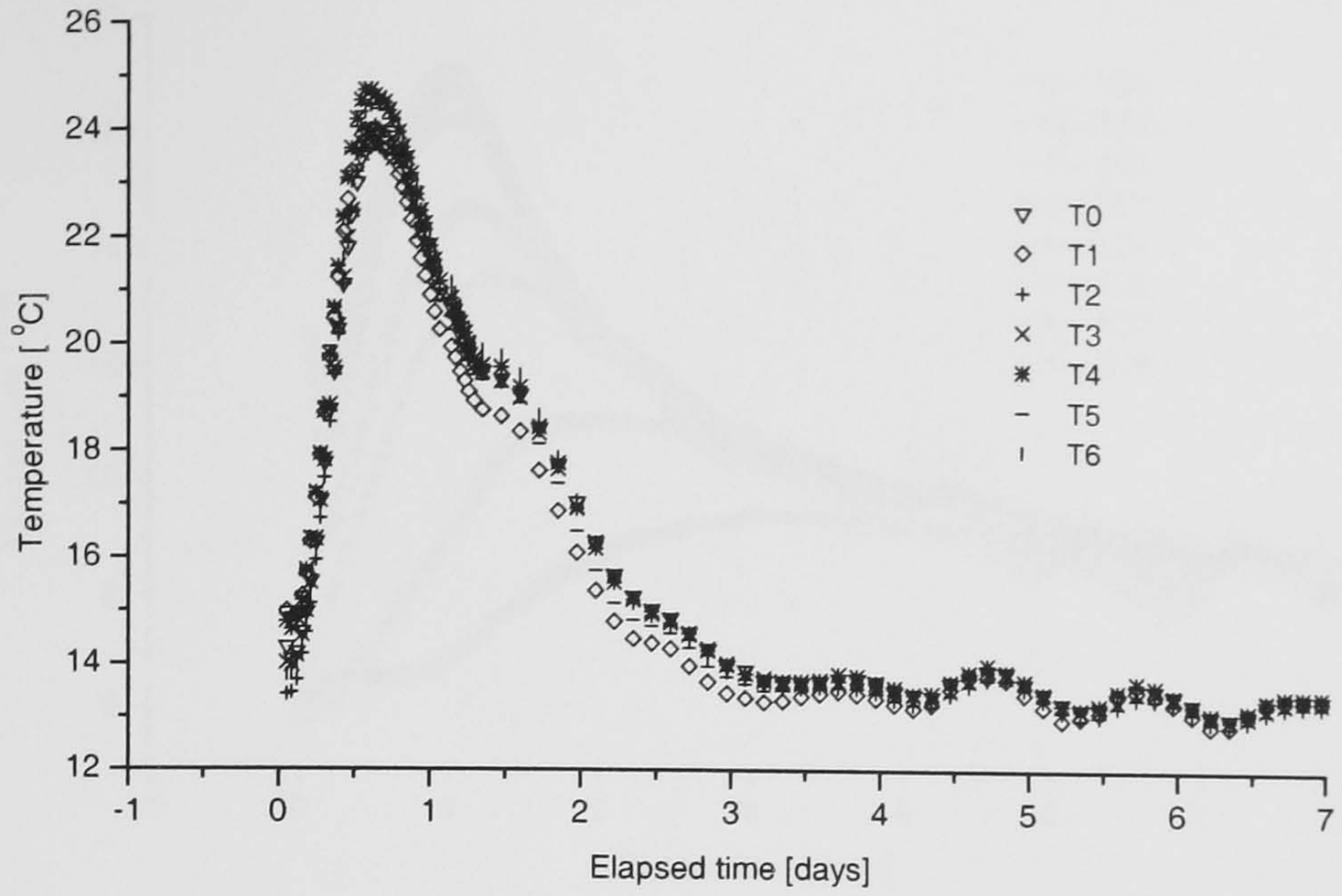

a) - Northampton

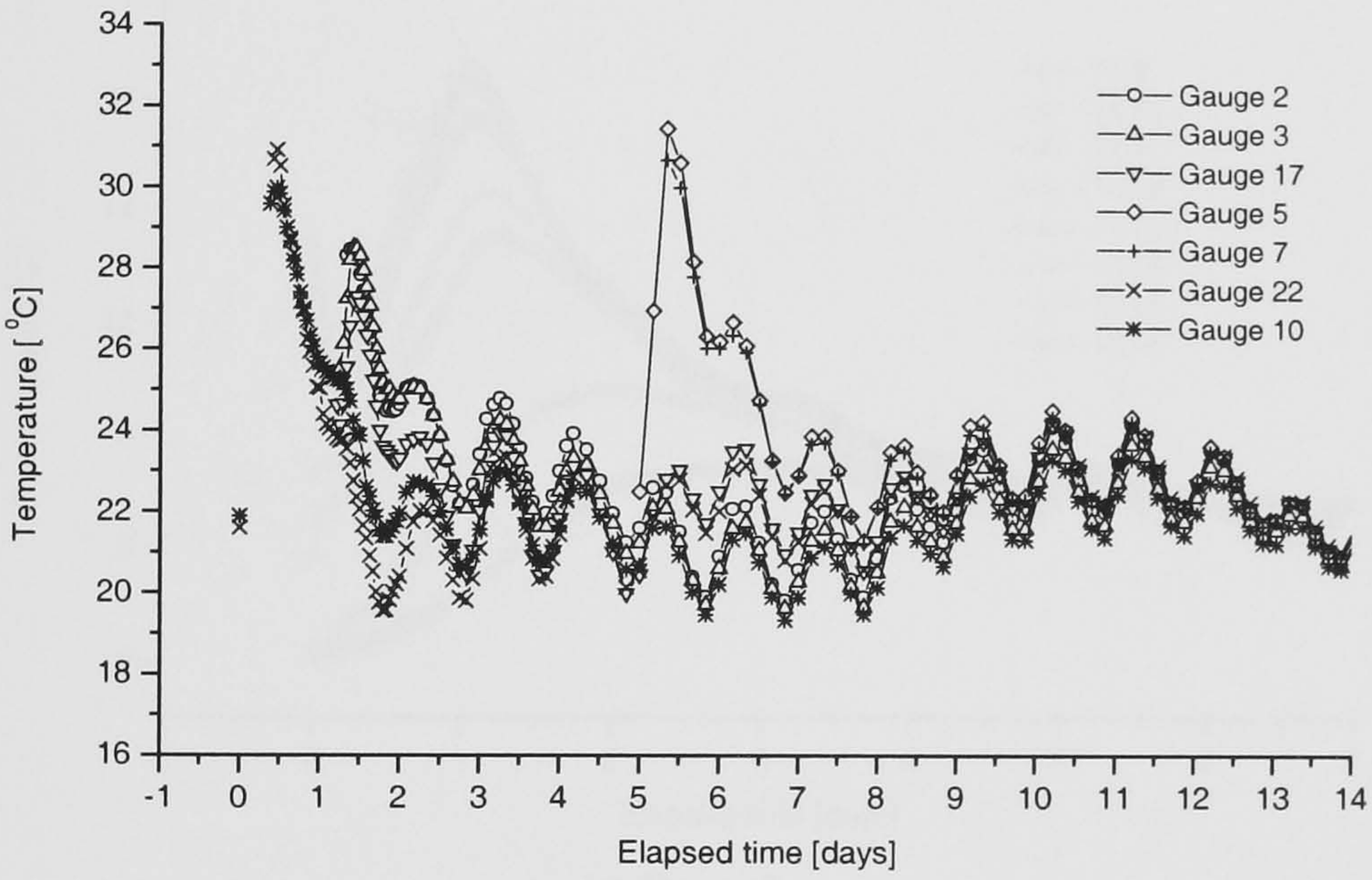

b) - Chepstow

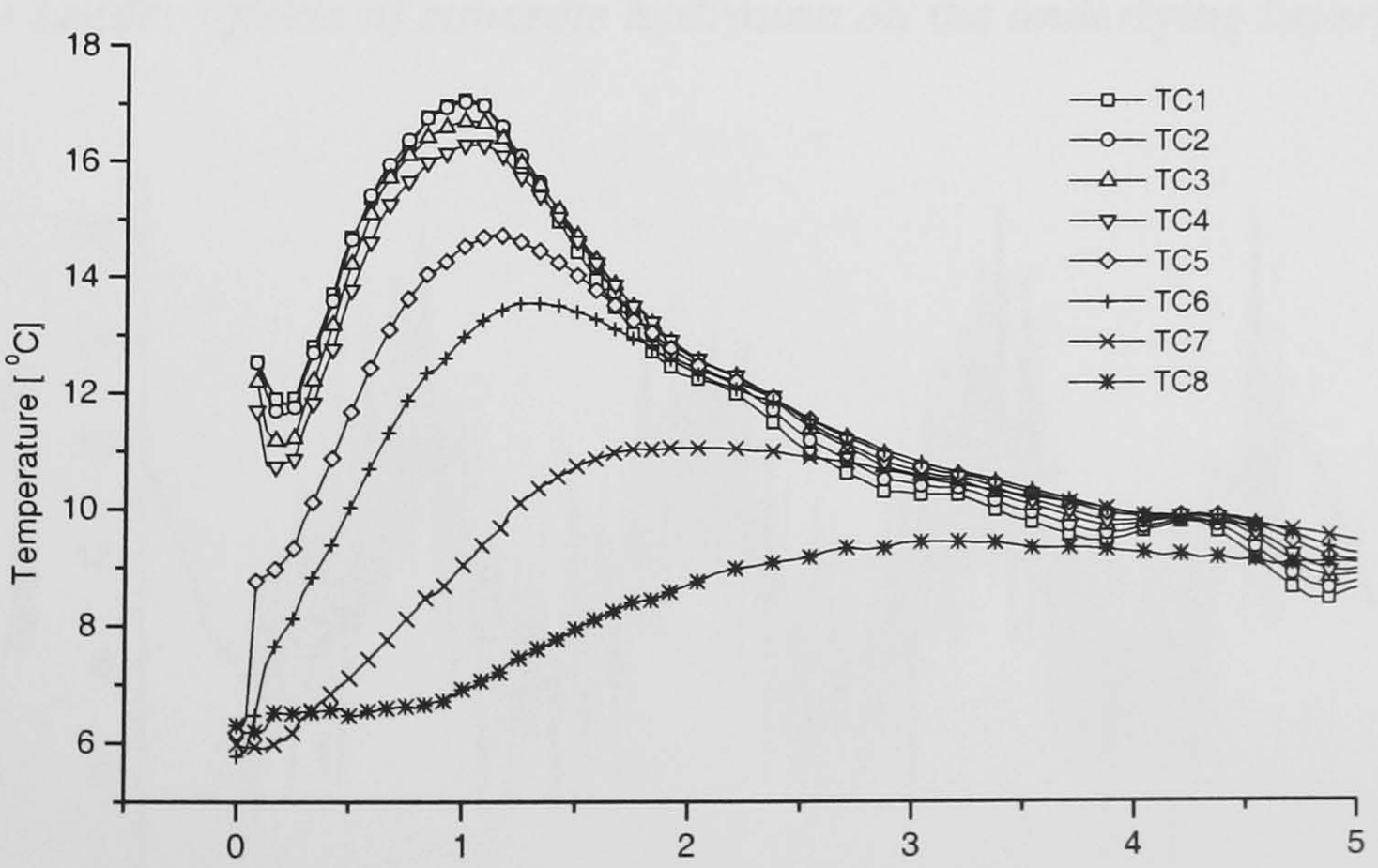

c) - Leeds

Figure 5.7 - Measured concrete internal temperatures

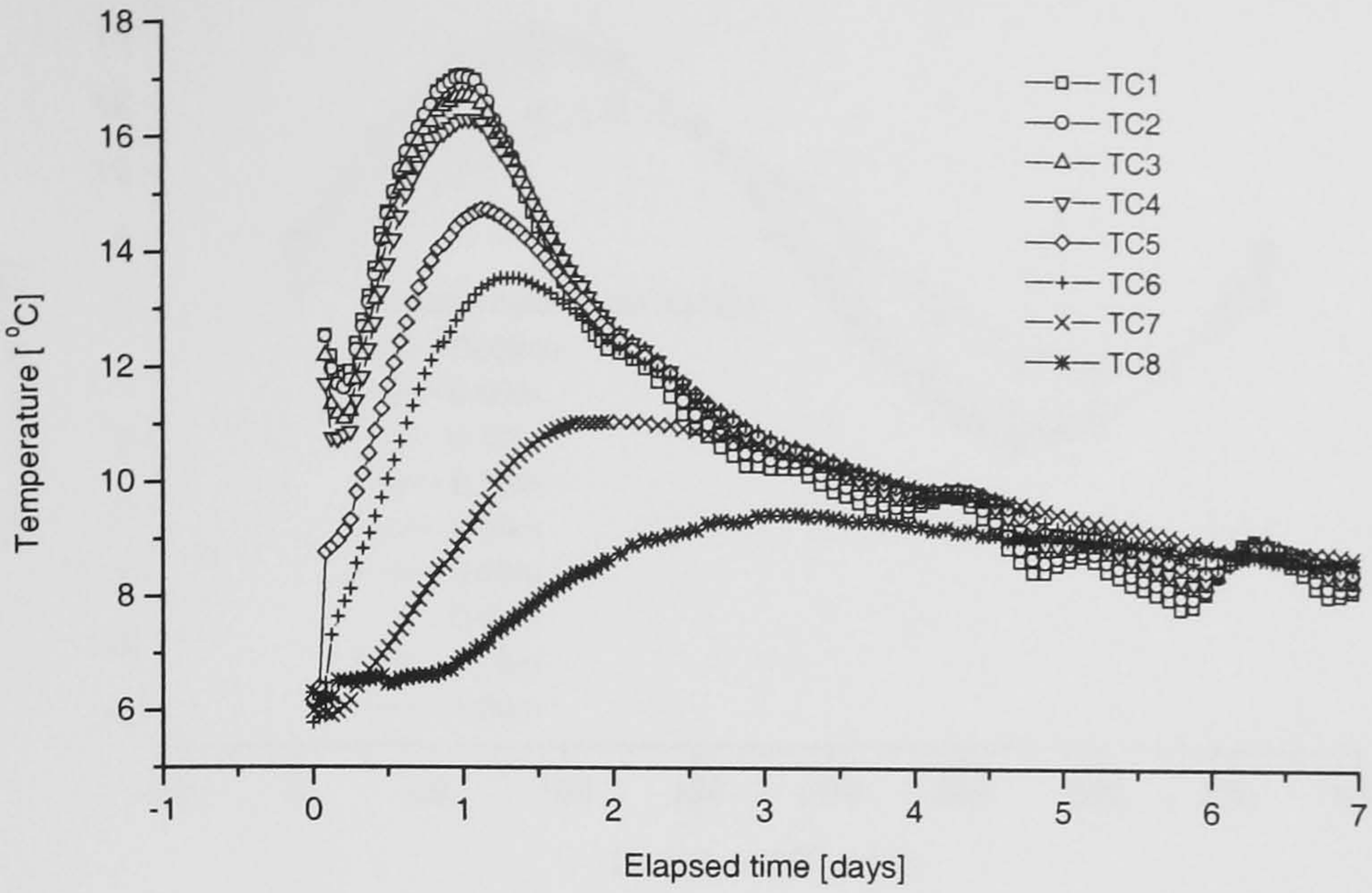

a) Pour 1

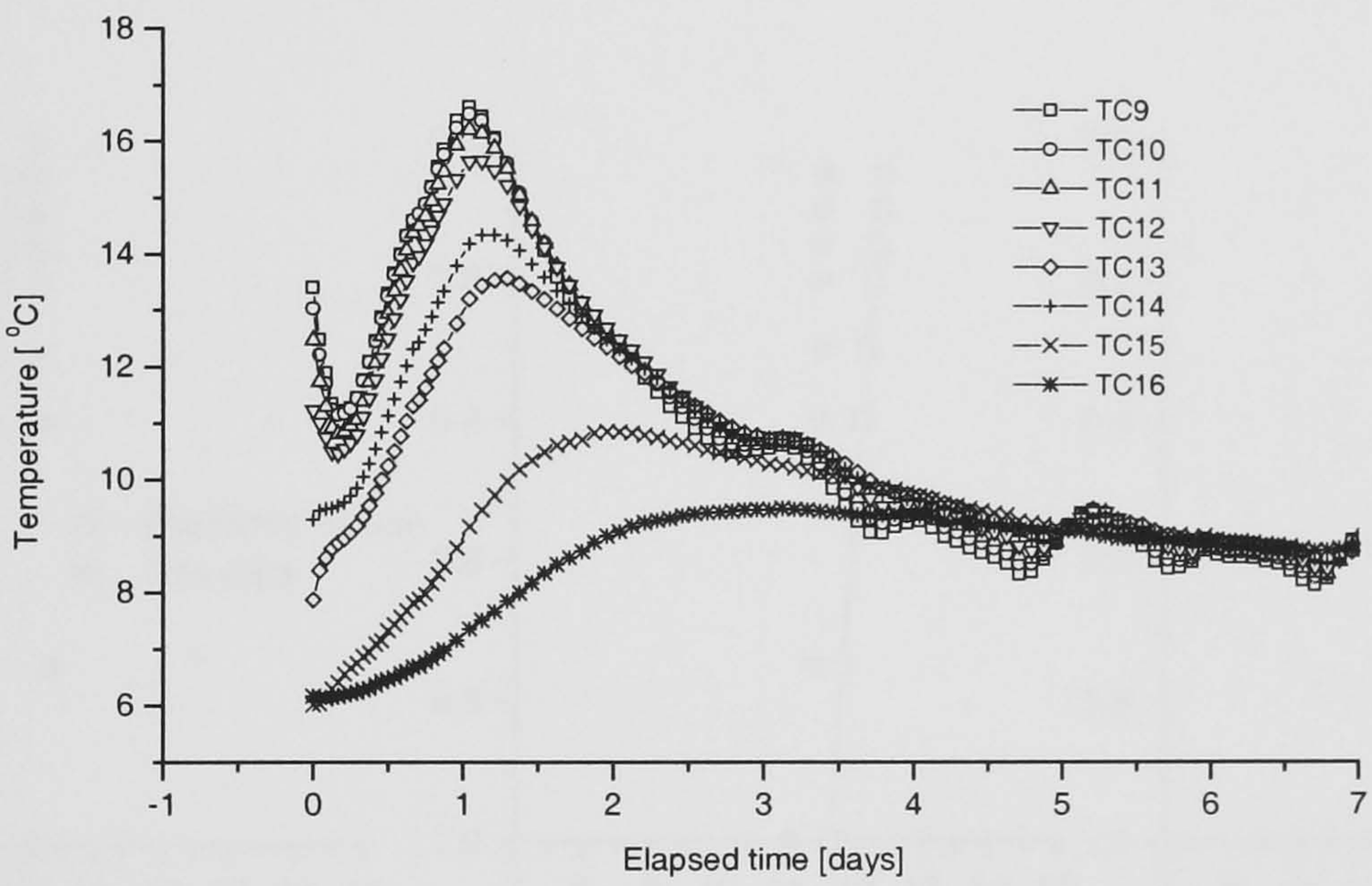

b) Pour 2

Figure 5.8 – Leeds: Effects of concrete hydration on the underlying layers of ground

Figure 5.9 –Sine curve approximation to measured temperatures (Data from the Met. Office weather station Leeds_W_C)

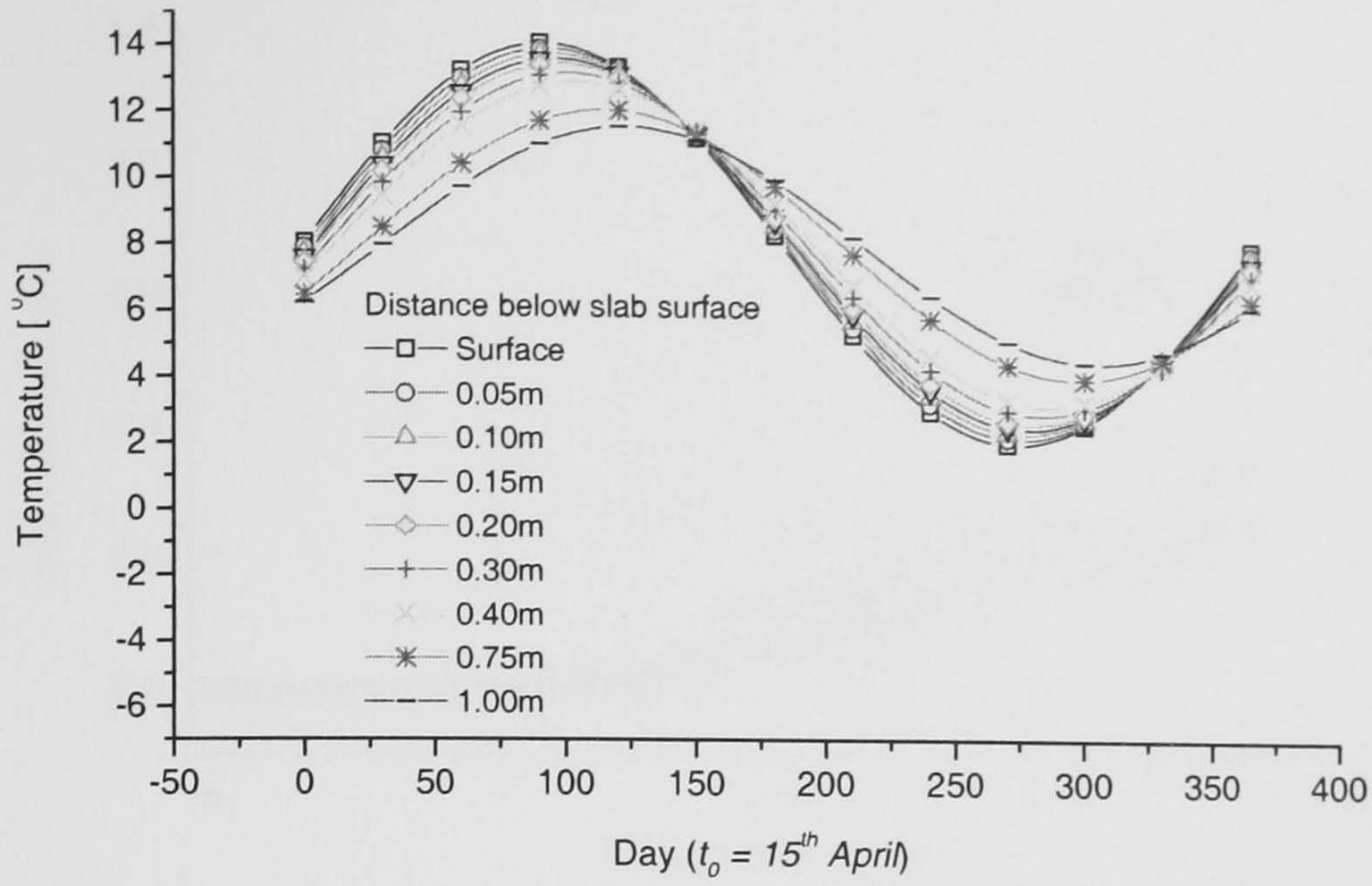

Figure 5.10 – Leeds: Theoretical annual temperature variation at different depths

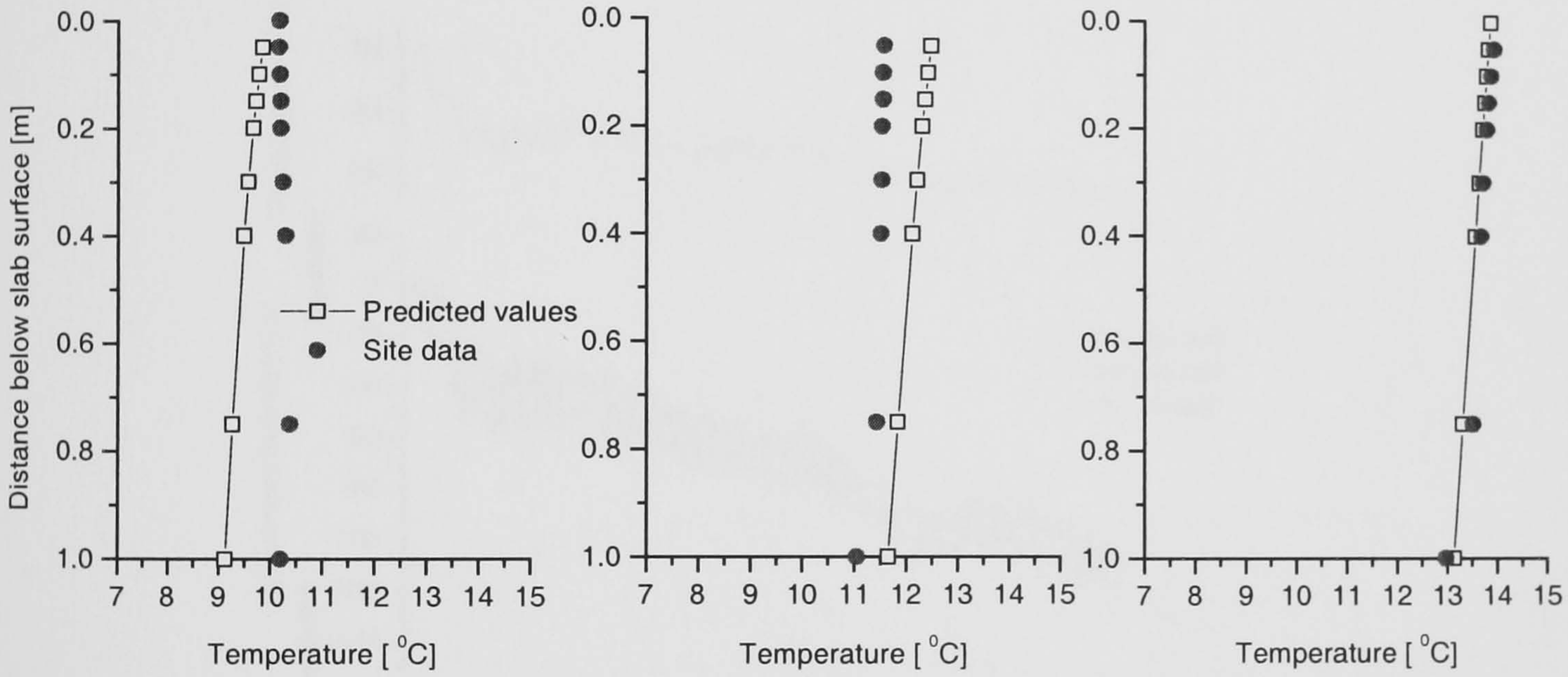

a) 4th May 2000 b) 4th June 2000 c) 4th July 2000

Figure 5.11 – Leeds: Comparison of the theoretical and the measured temperature distributions

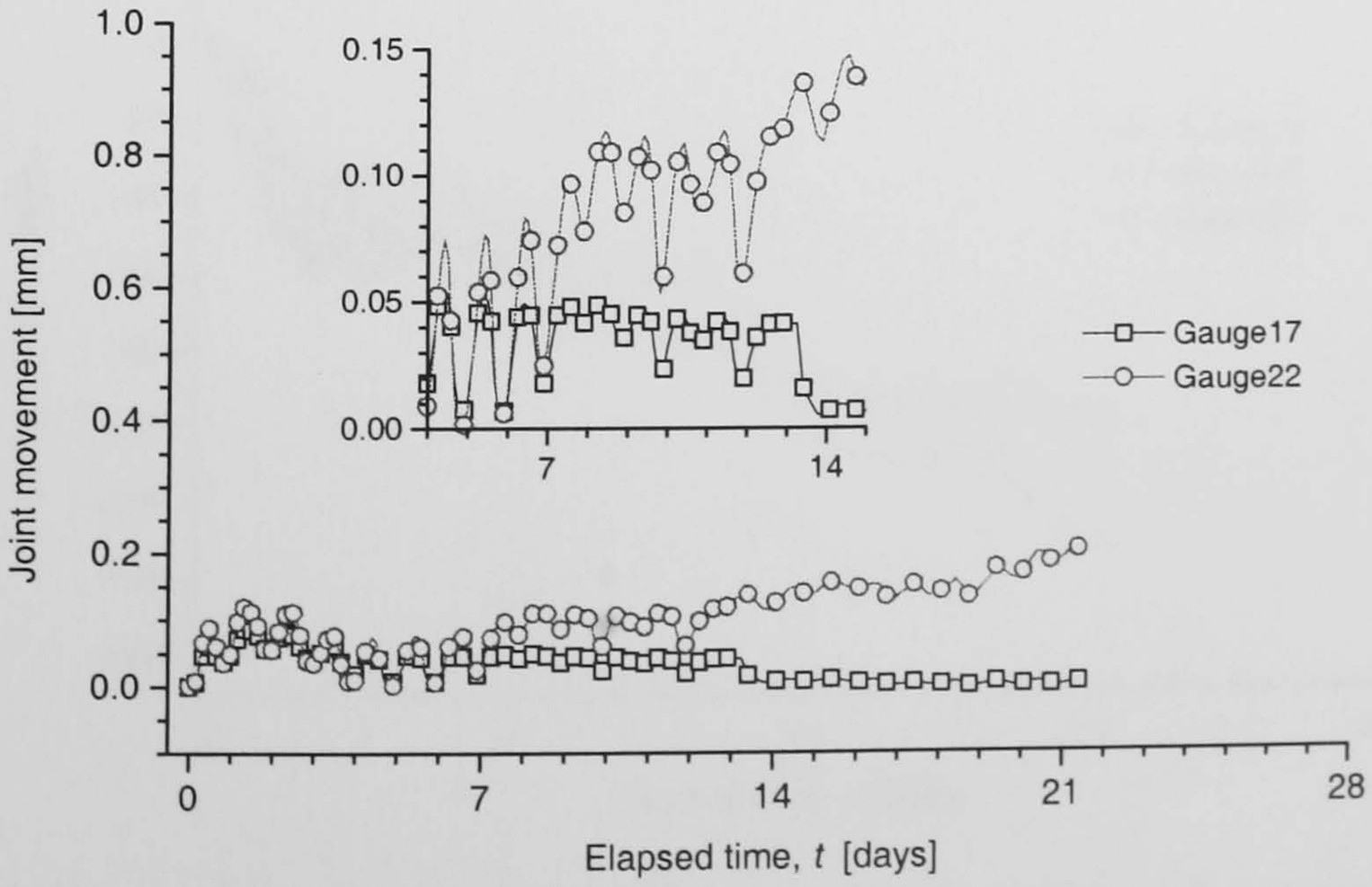

Figure 5.12 - Chepstow: Formed restrained movement joint behaviour

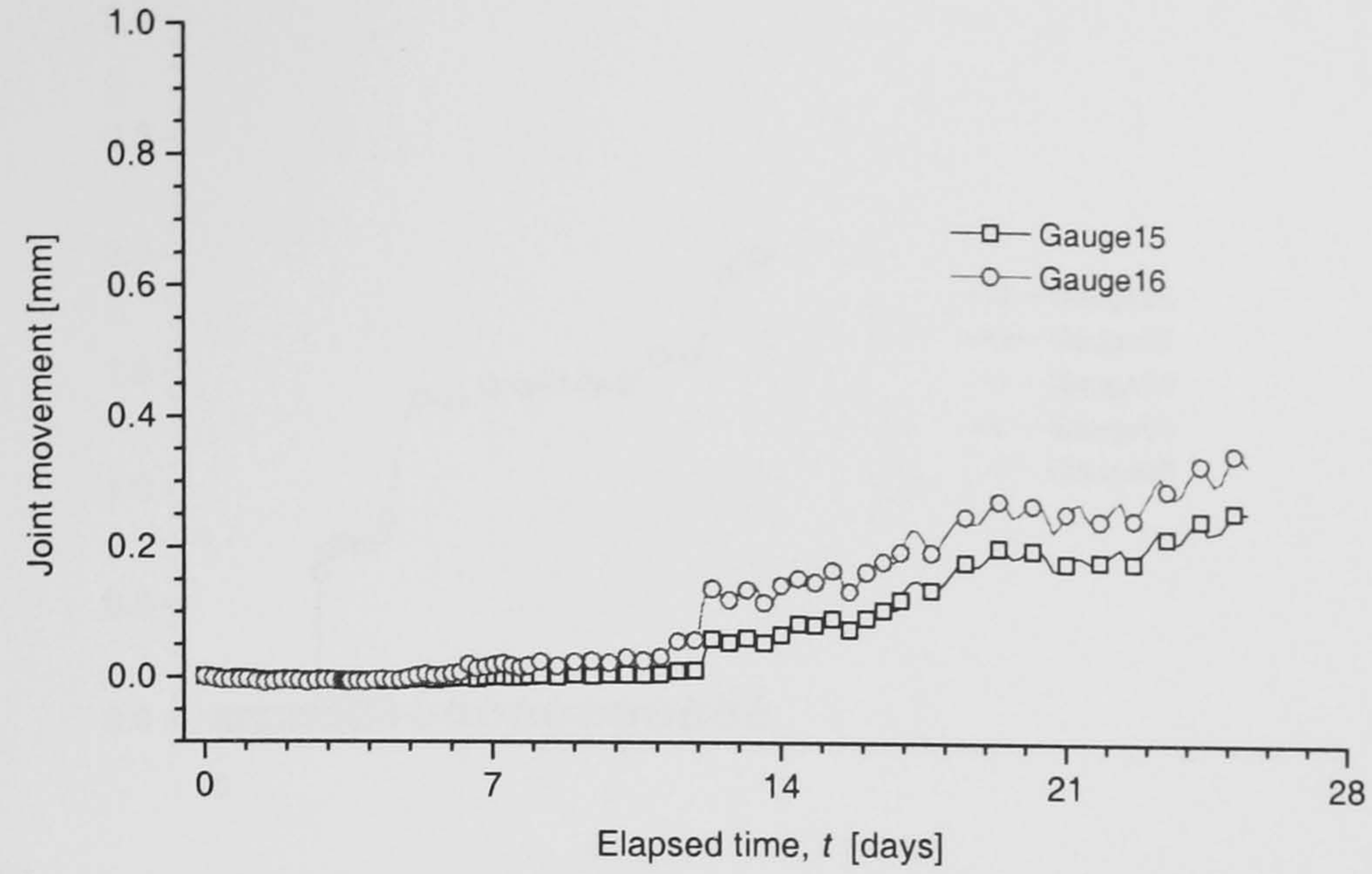

Figure 5.13 - Chepstow: Pour 11 Sawn restrained movement joint behaviour

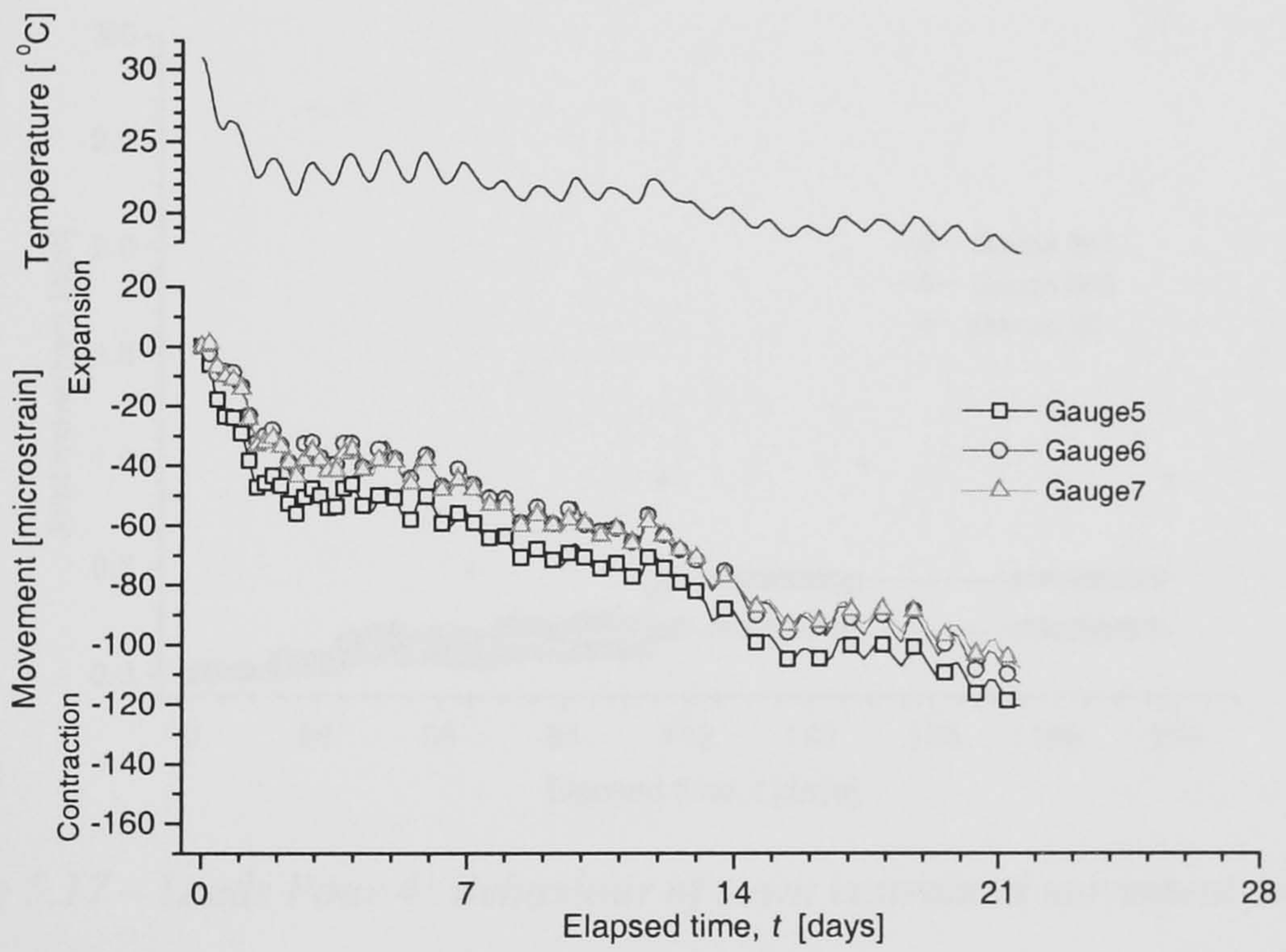

Figure 5.14 - Chepstow Pour 13: Behaviour of embedment strain gauges

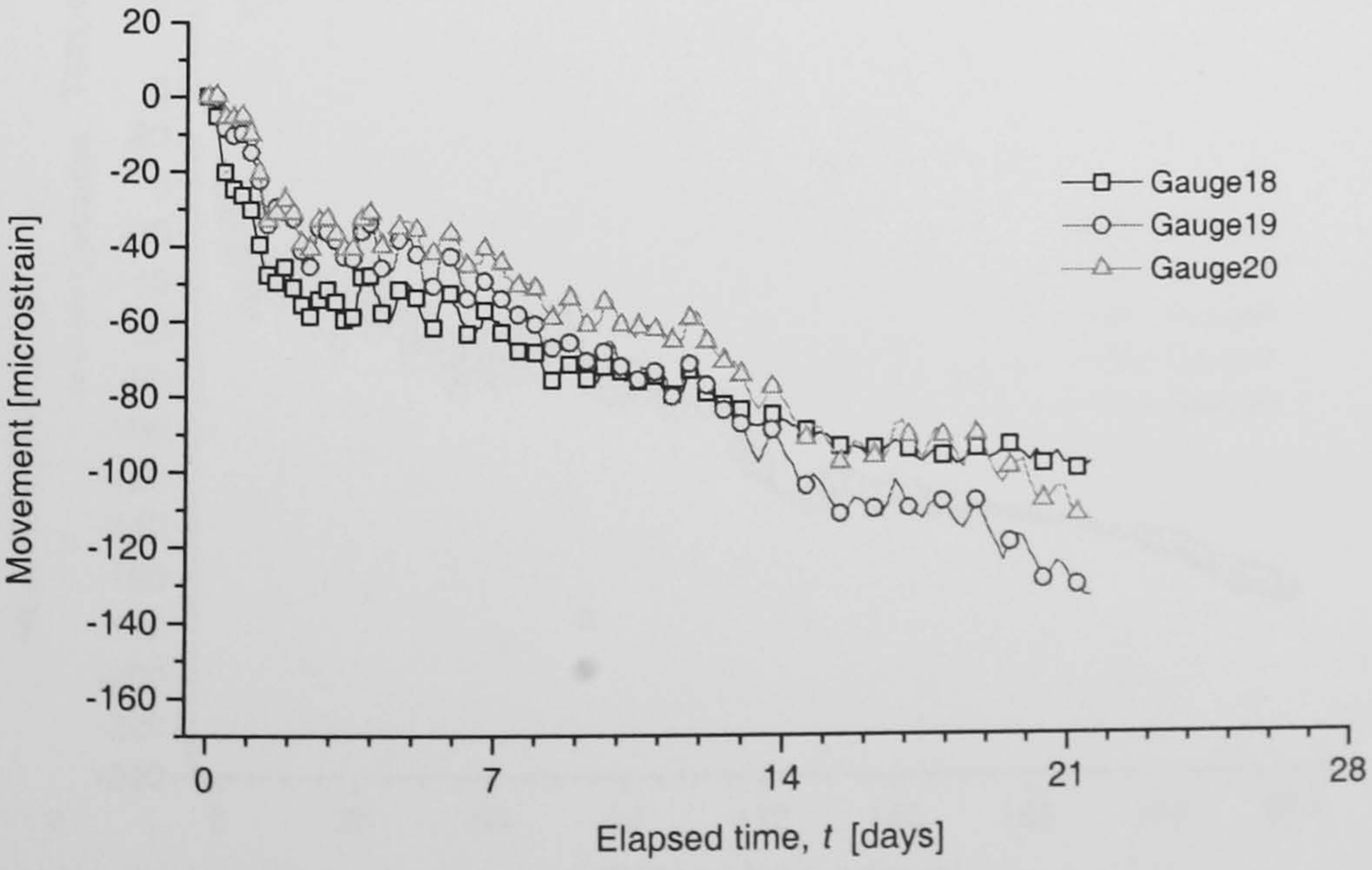

Figure 5.15 - Chepstow Pour 13: Behaviour of sawn restrained movement joints

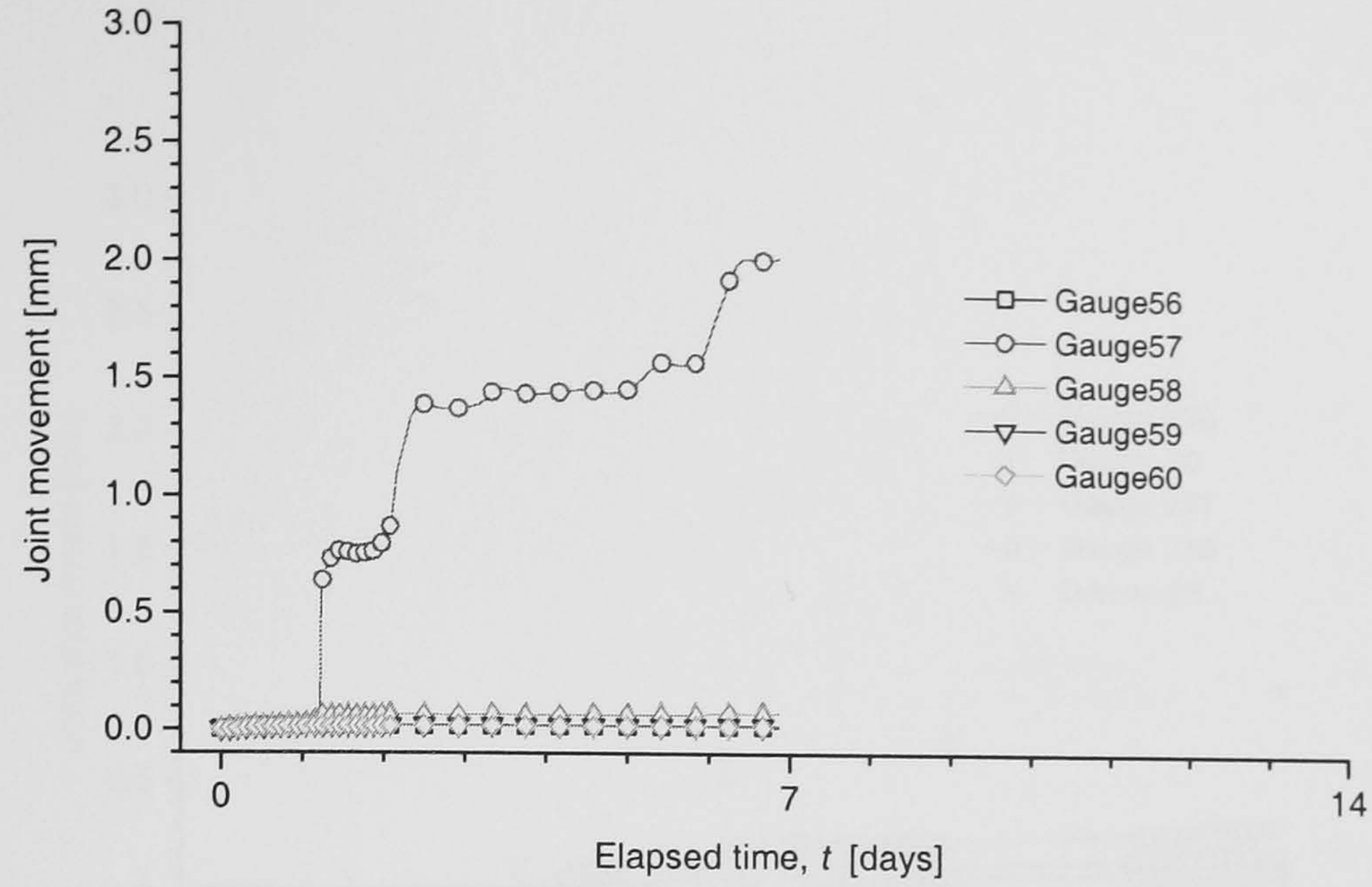

Figure 5.16 - Daventry Pour 8: Behaviour of sawn restrained movement joints

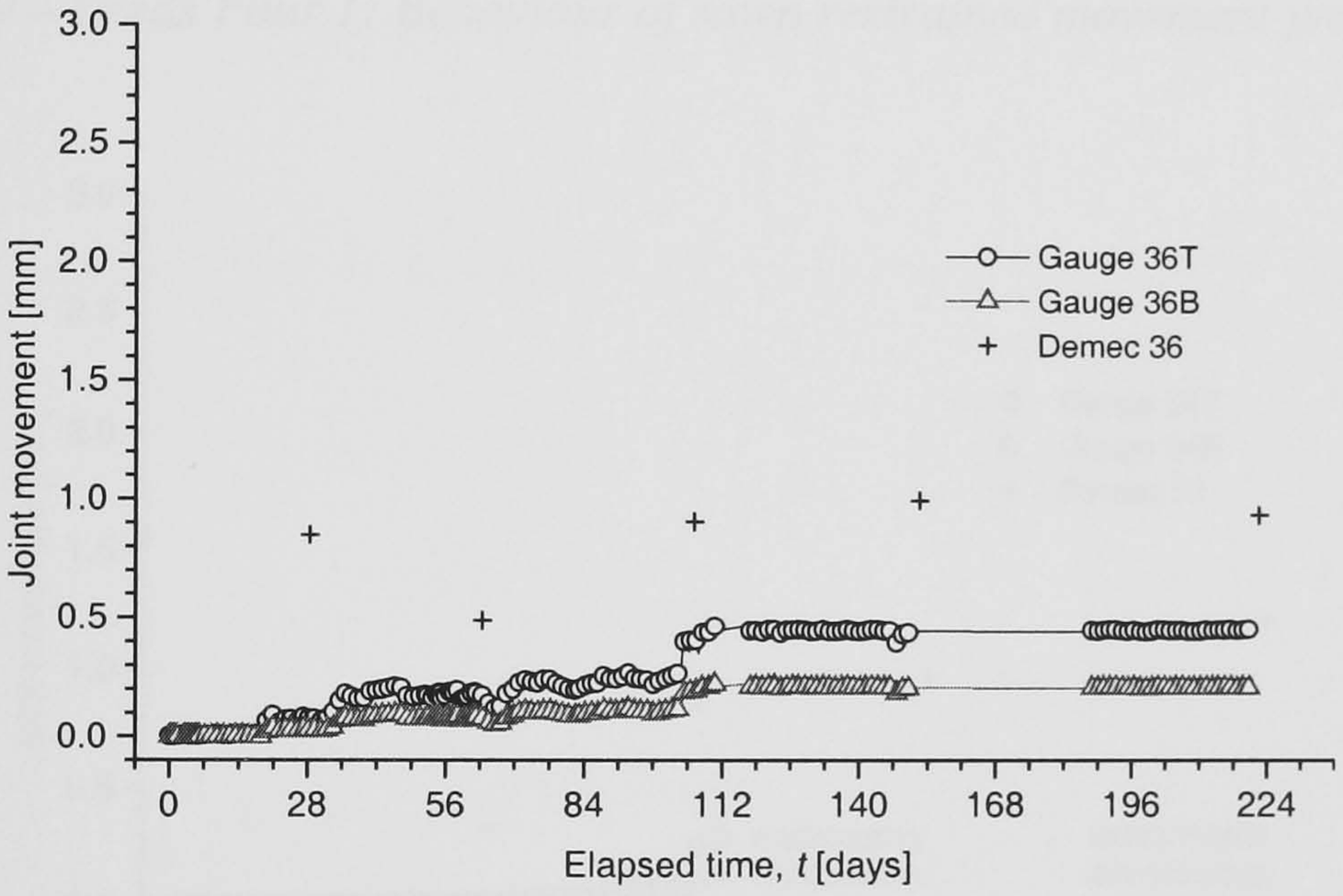

Figure 5.17 – Leeds Pour 4: Behaviour of sawn restrained movement joint 36

Figure 5.18 - Leeds Pour 1: Behaviour of embedment strain gauges

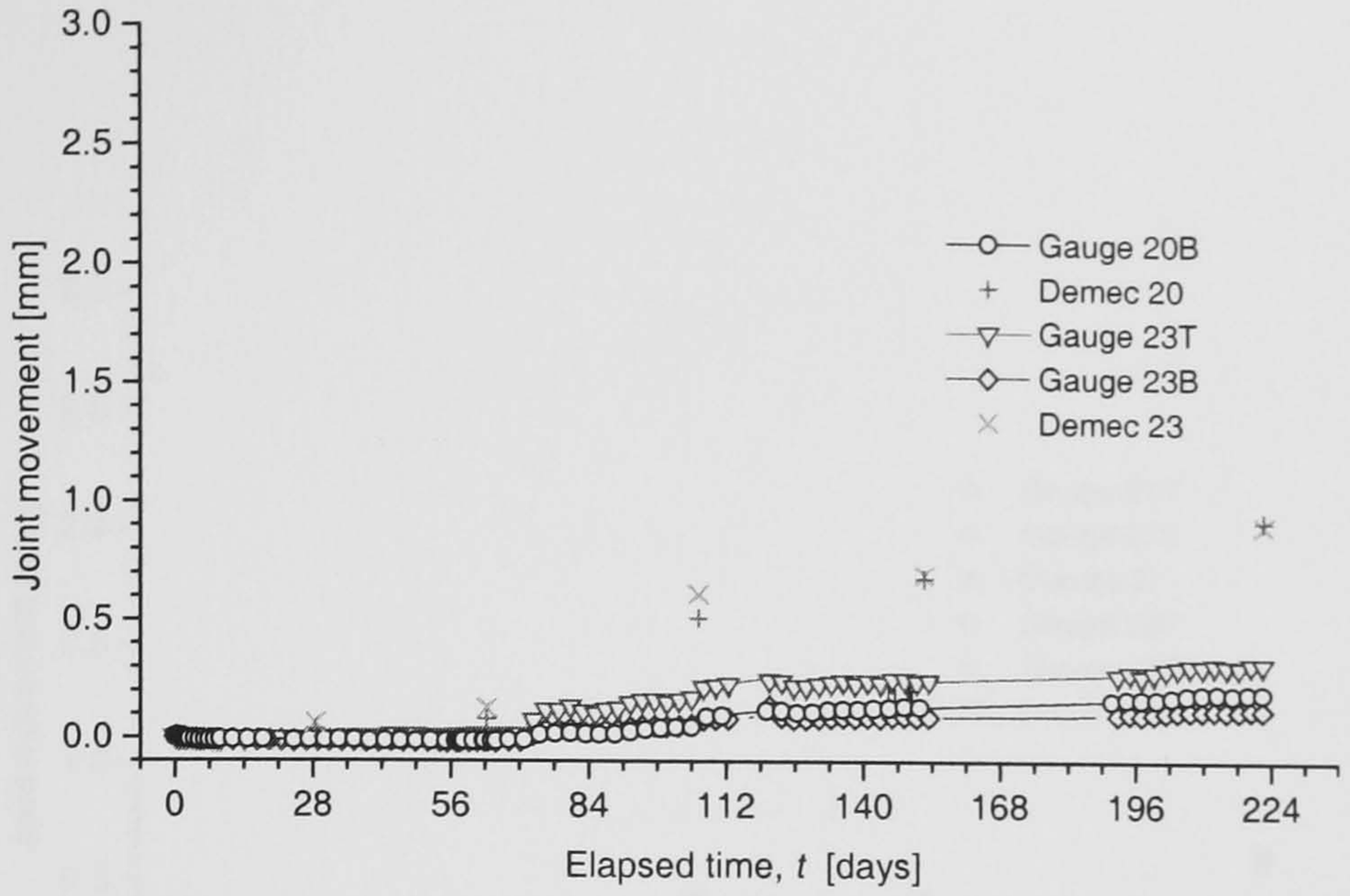

Figure 5.19 – Leeds Pour 1: Behaviour of sawn restrained movement joints 20 & 23

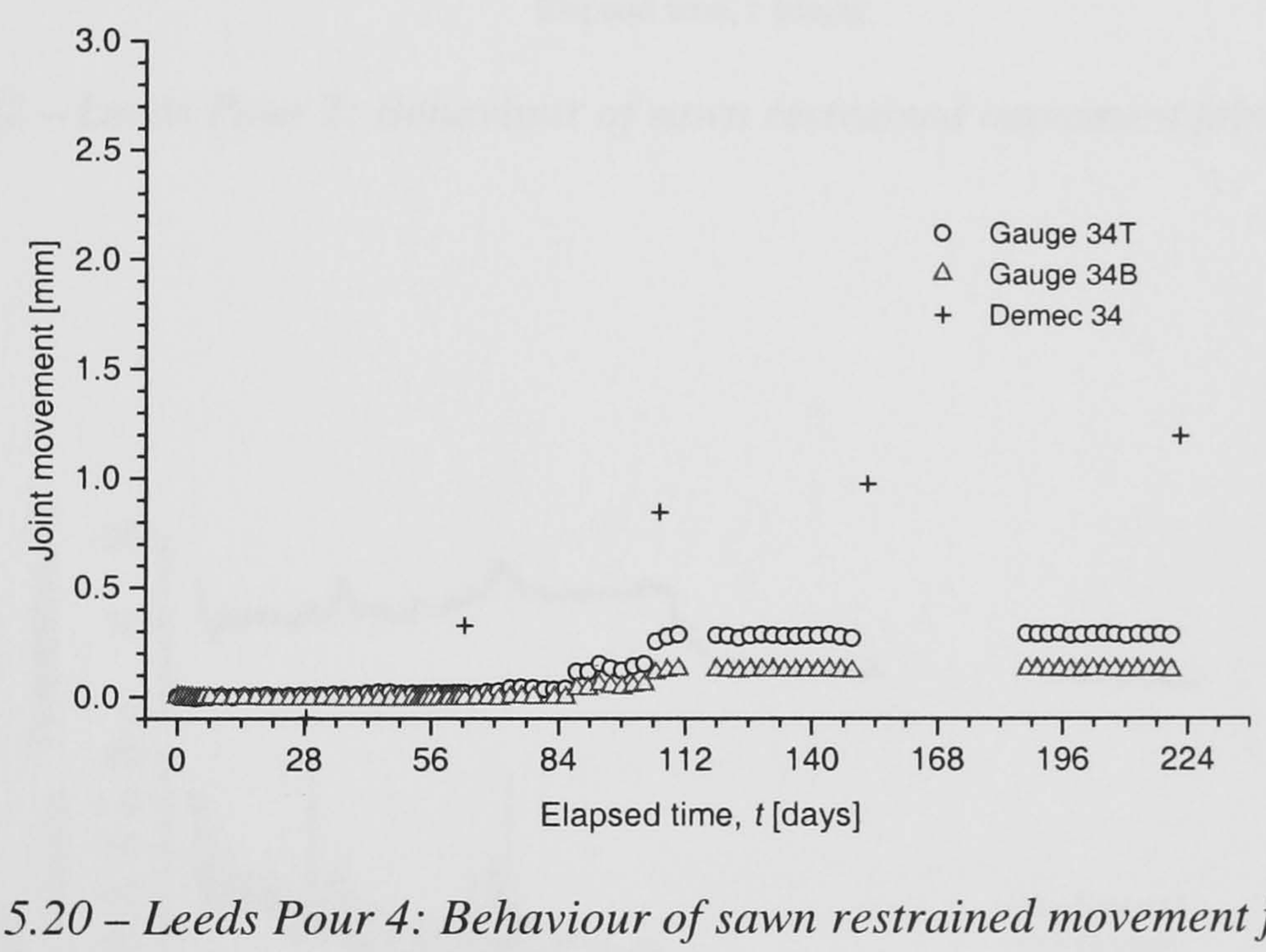

Figure 5.20 – Leeds Pour 4: Behaviour of sawn restrained movement joint 34

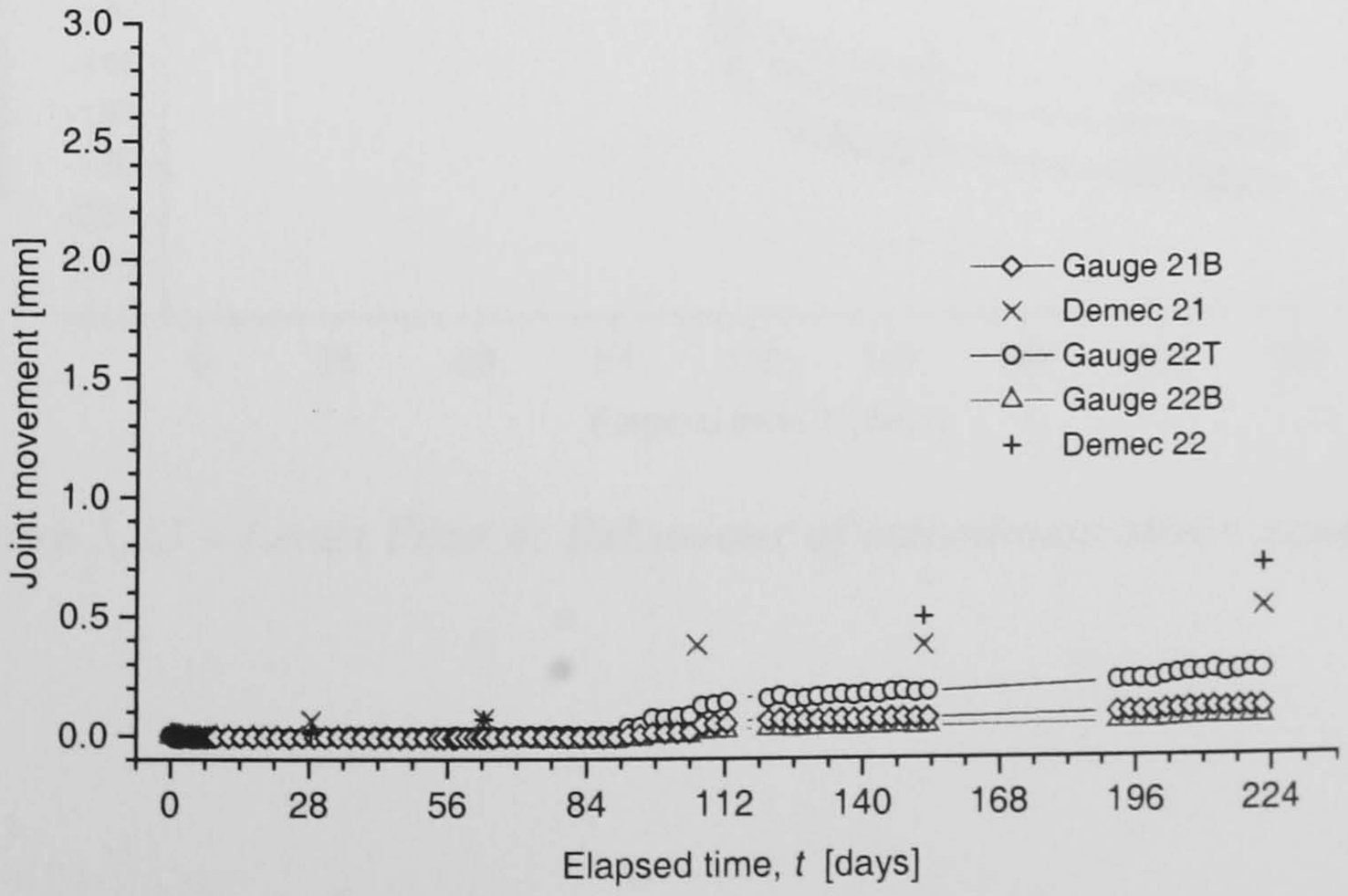

Figure 5.21 – Leeds Pour 1:Behaviour of sawn restrained movement joint 21 & 22

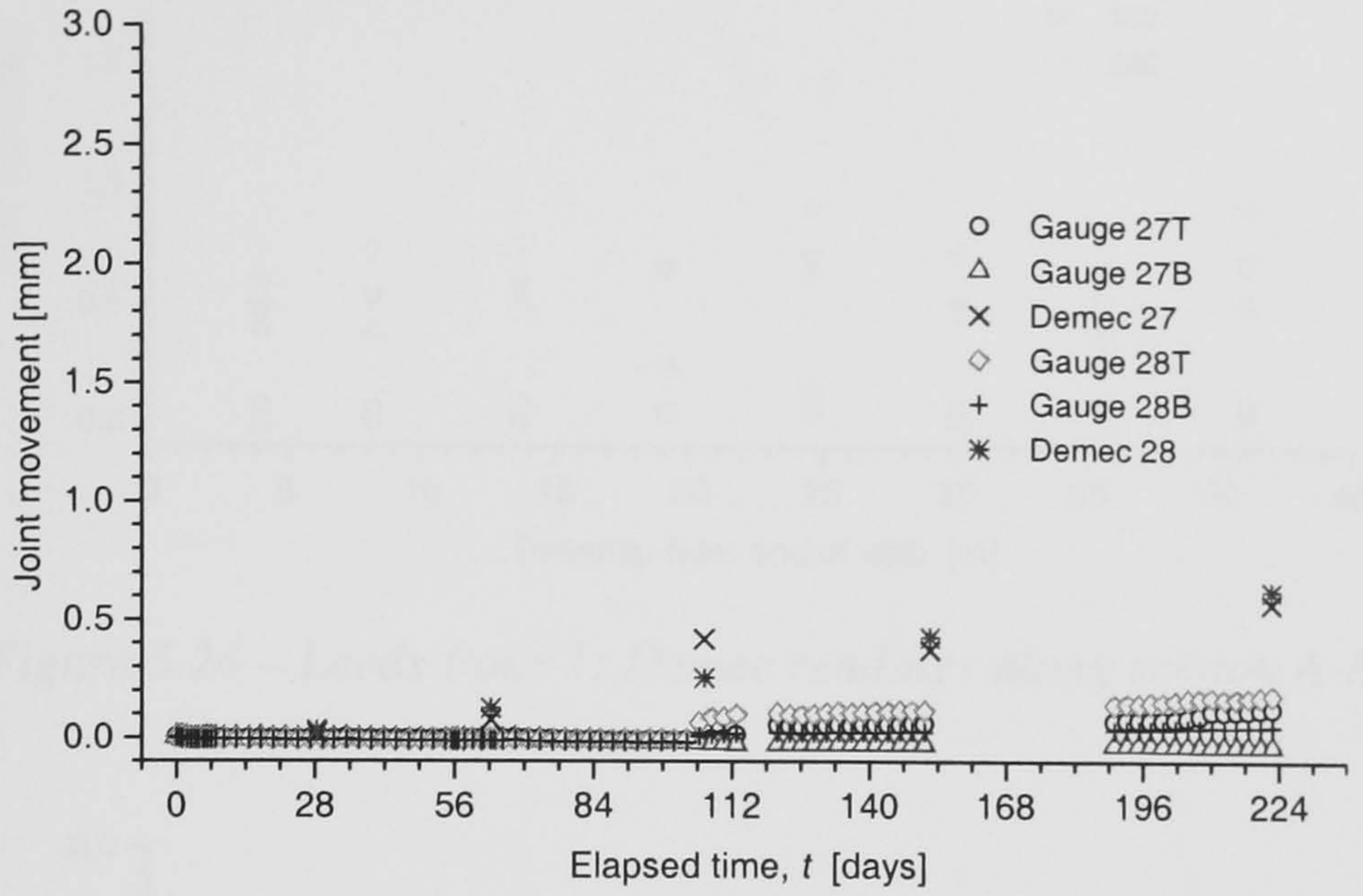

Figure 5.22 – Leeds Pour 2: Behaviour of sawn restrained movement joints 27 & 28

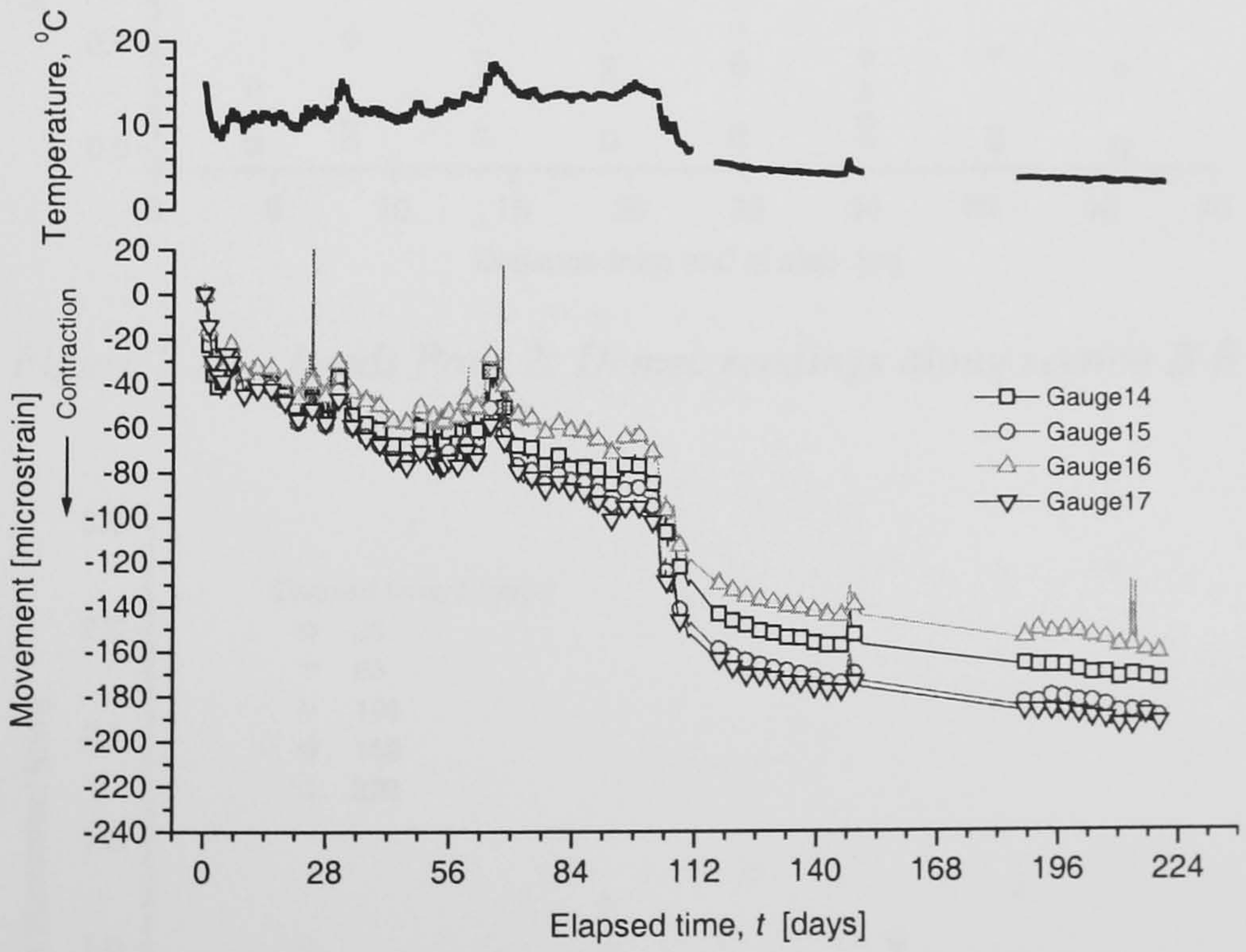

Figure 5.23 – Leeds Pour 4: Behaviour of embedment strain gauges

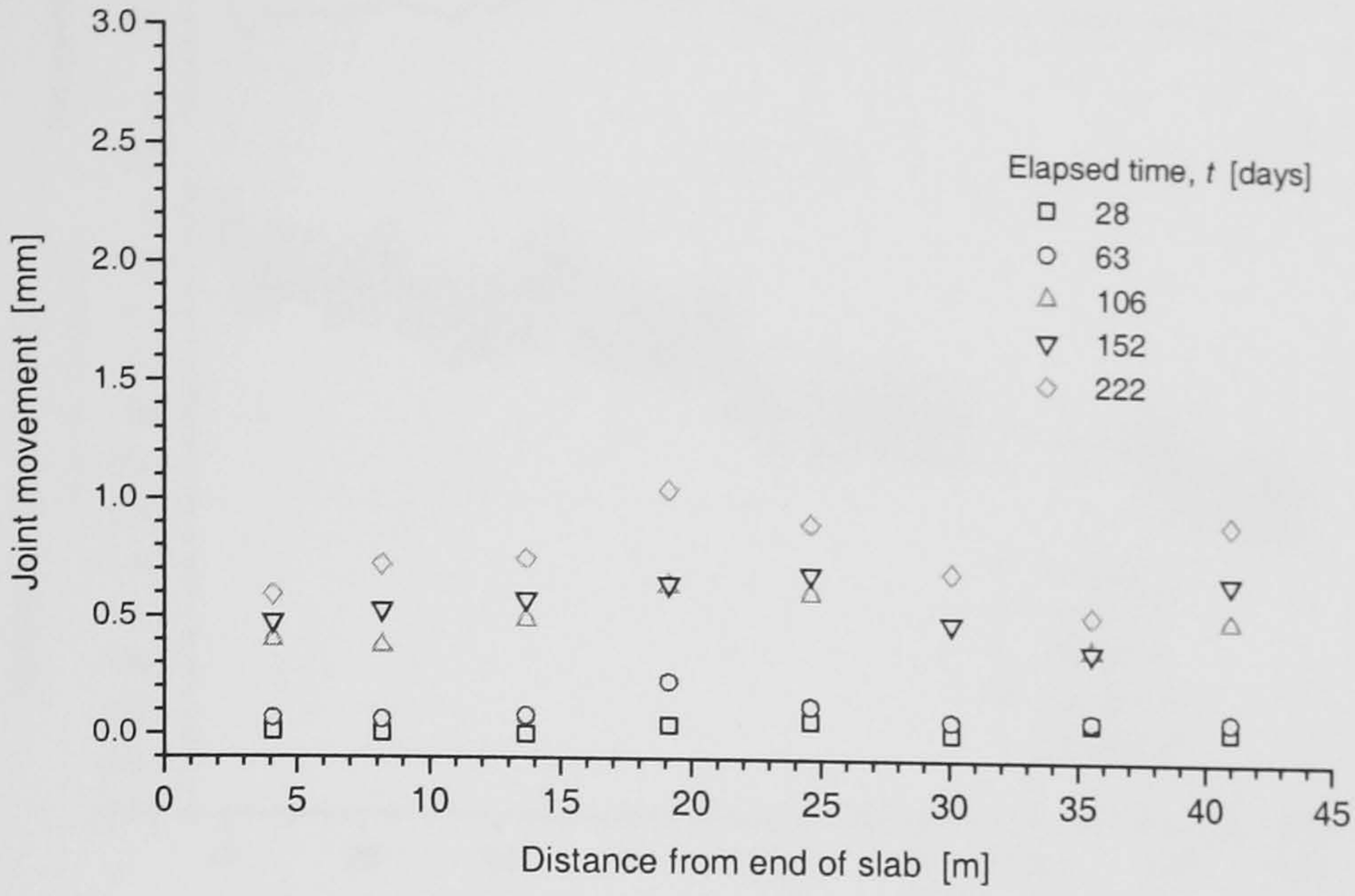

Figure 5.24 – Leeds Pour 1: Demec readings along section A-A

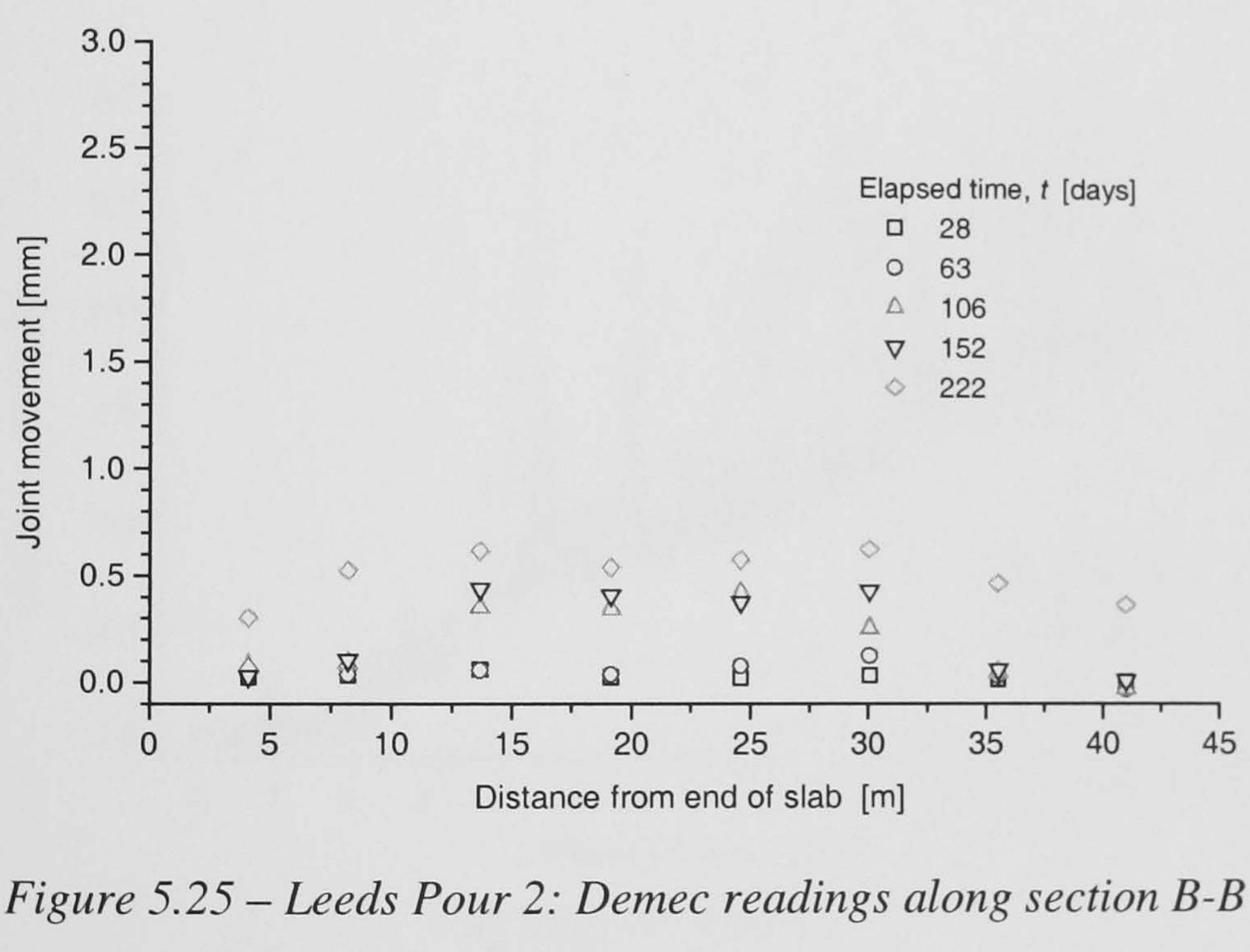

Figure 5.25 – Leeds Pour 2: Demec readings along section B-B

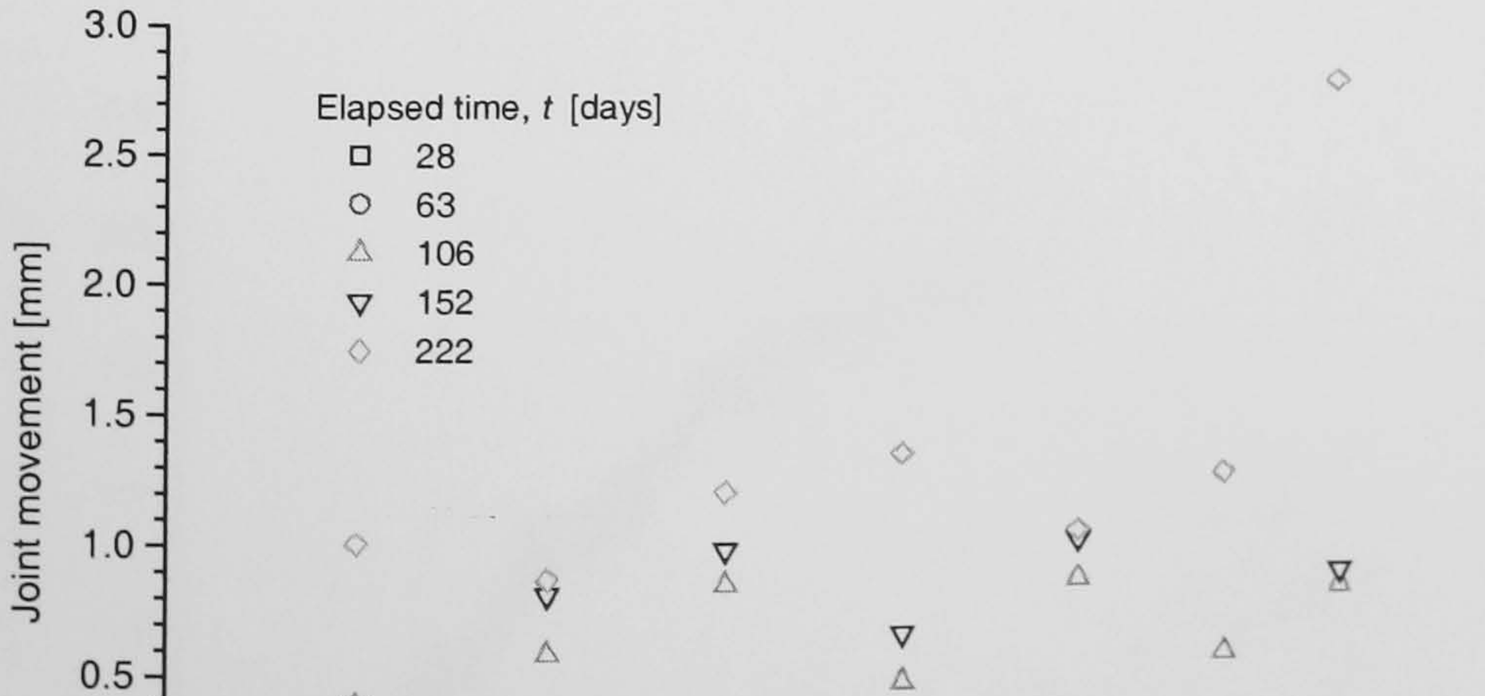

Figure 5.26 – Leeds Pour 4: Demec readings along section C-C

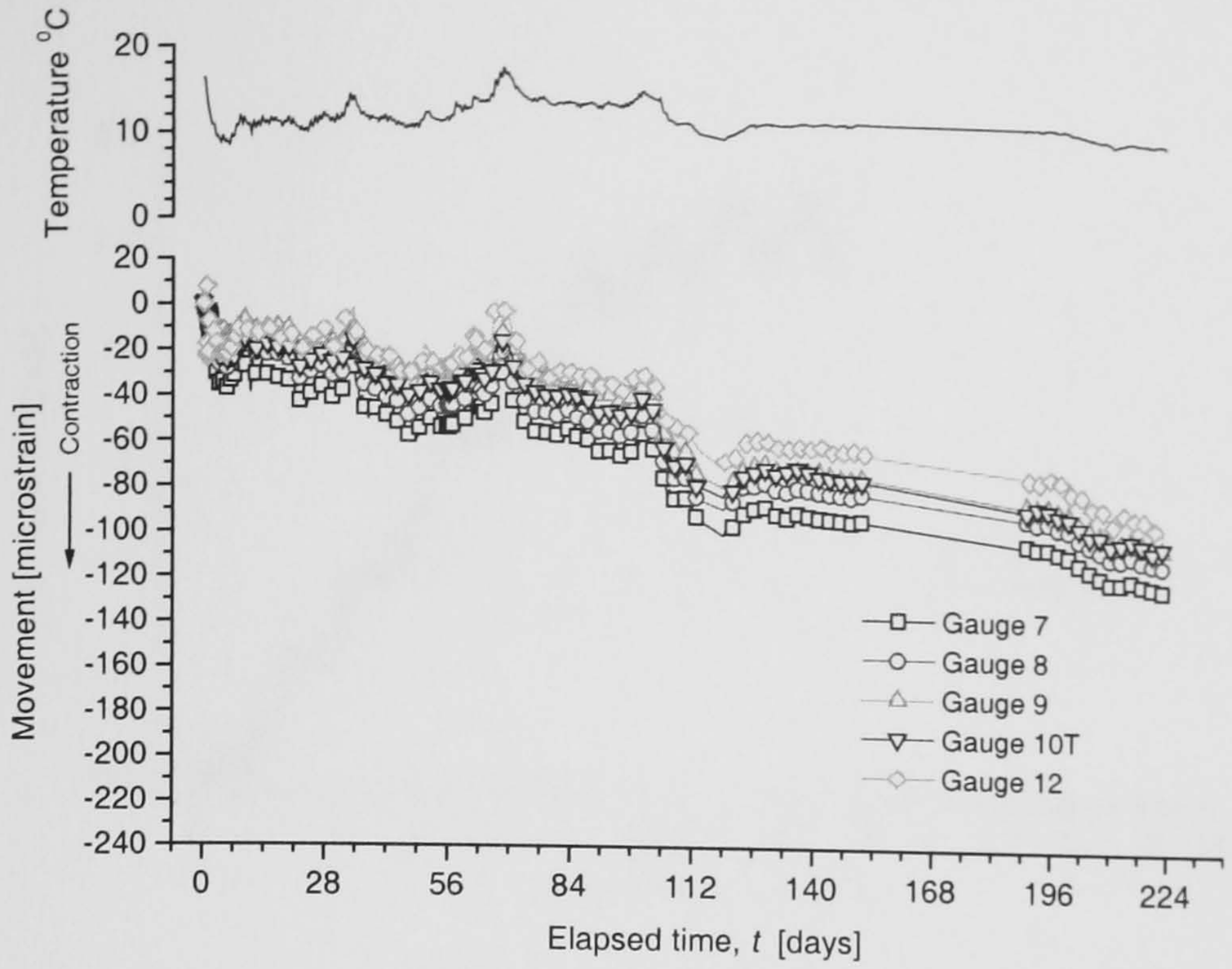

Figure 5.27 – Leeds Pour 2: Behaviour of embedment strain gauges

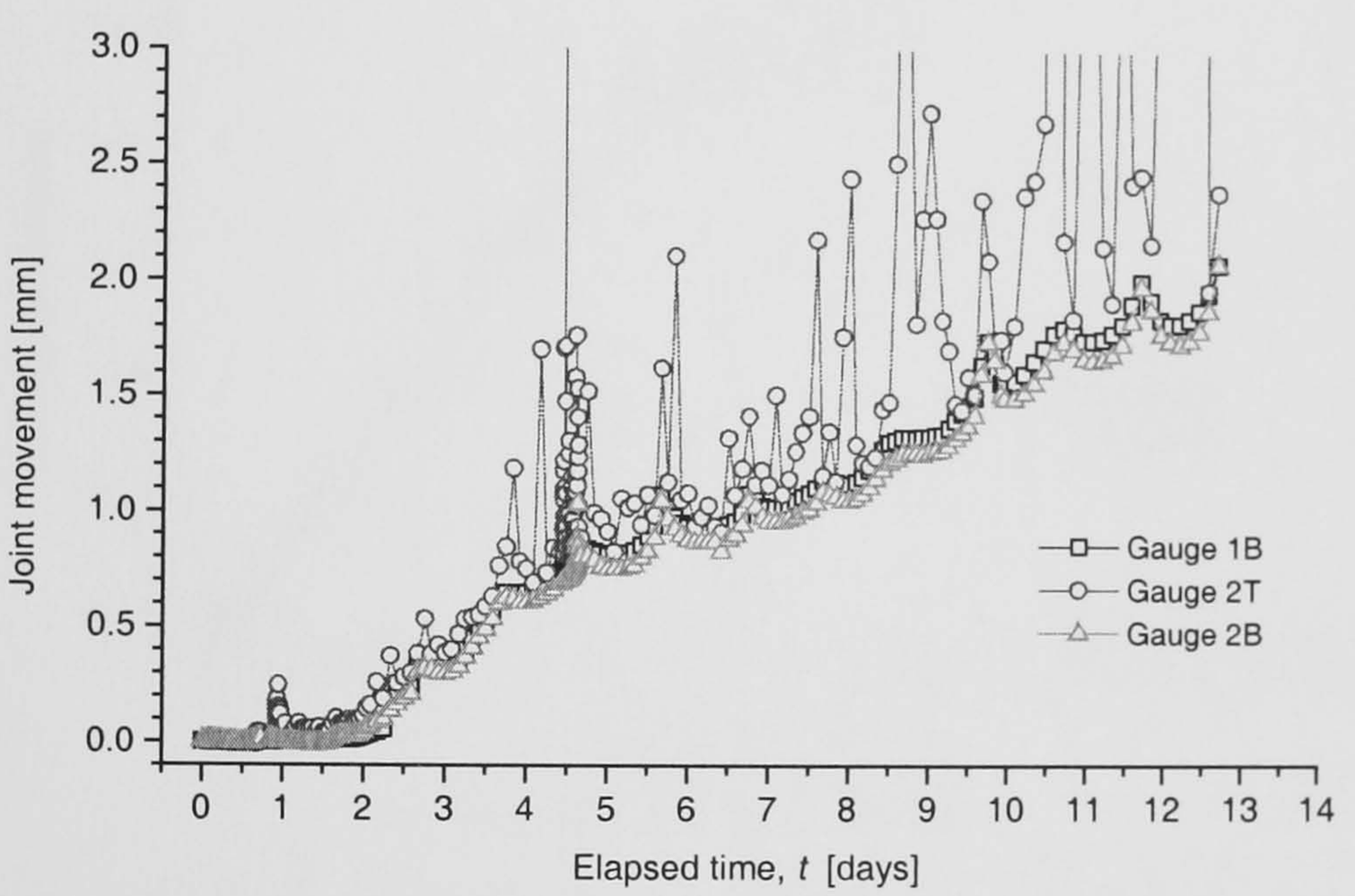

a) Edge of Pour 7

b) Edge of Pour 9

Figure 5.28 – Marston: Measured movement from the slab edges

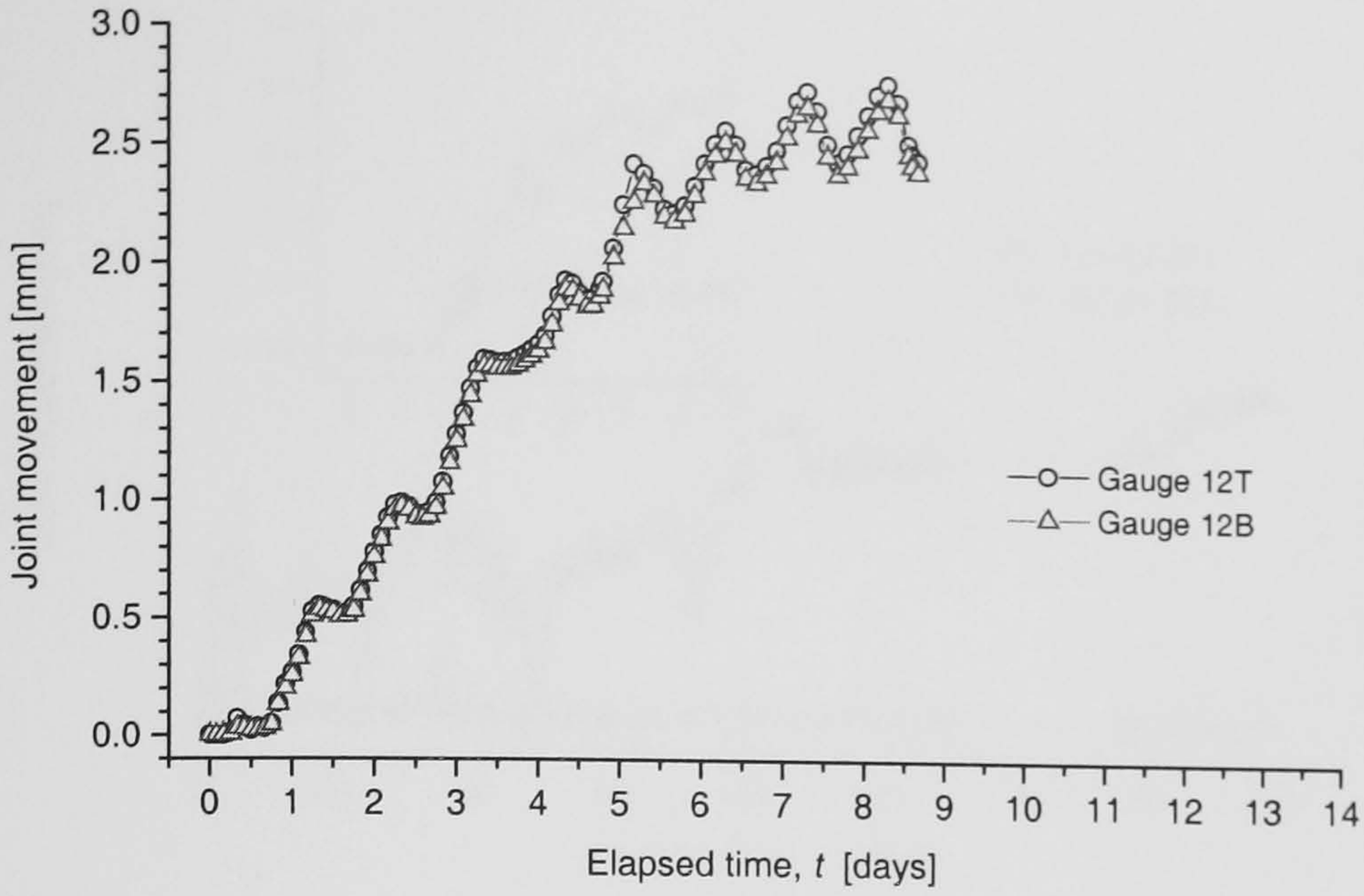

a) Between Pours 6 and 9

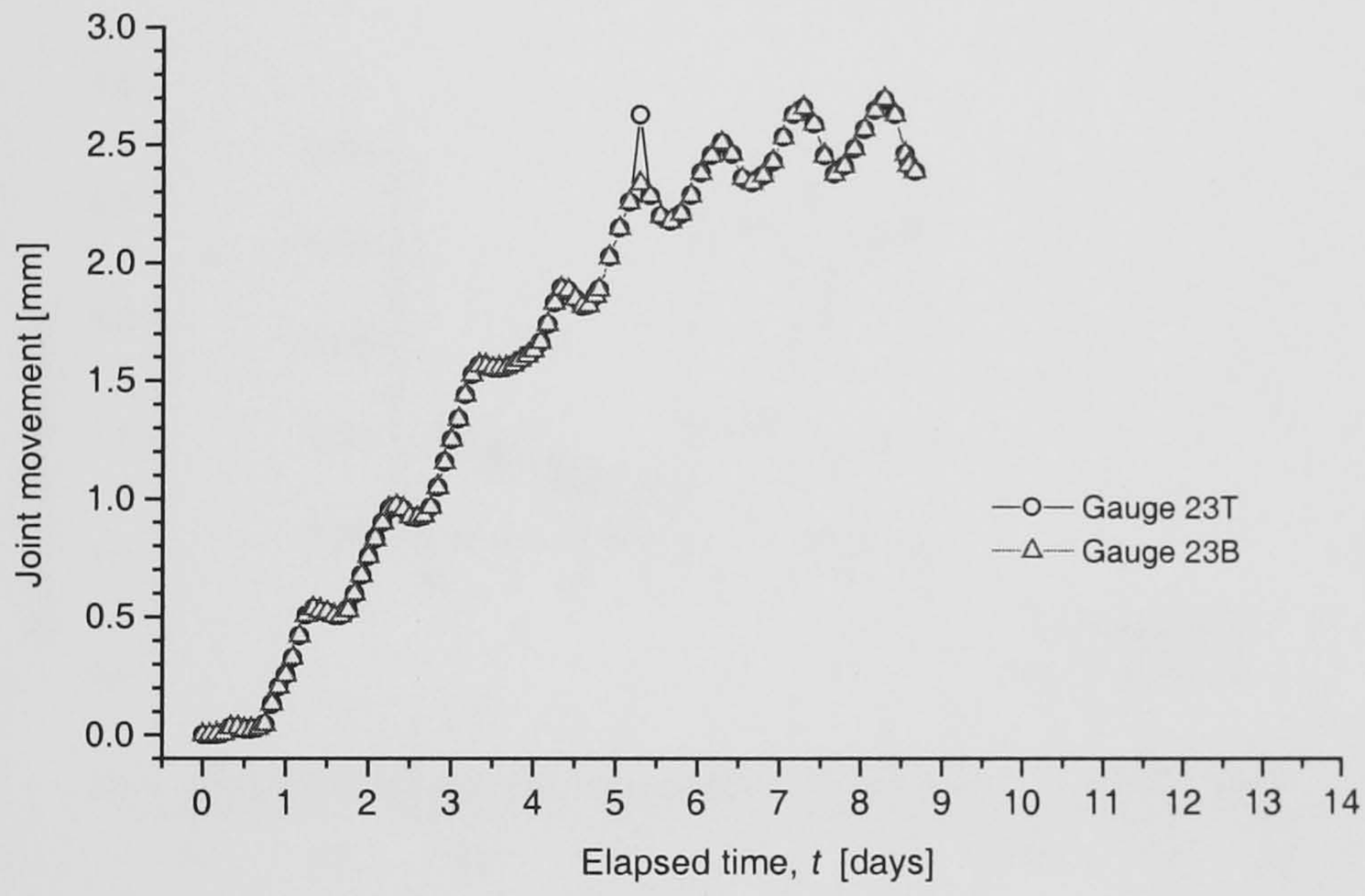

b) Between Pours 7 and 9

Figure 5.29 – Marston: Measured movement at the day joints

Figure 5.30 – Bedford: Comparison of joint movements from each side of the central pour

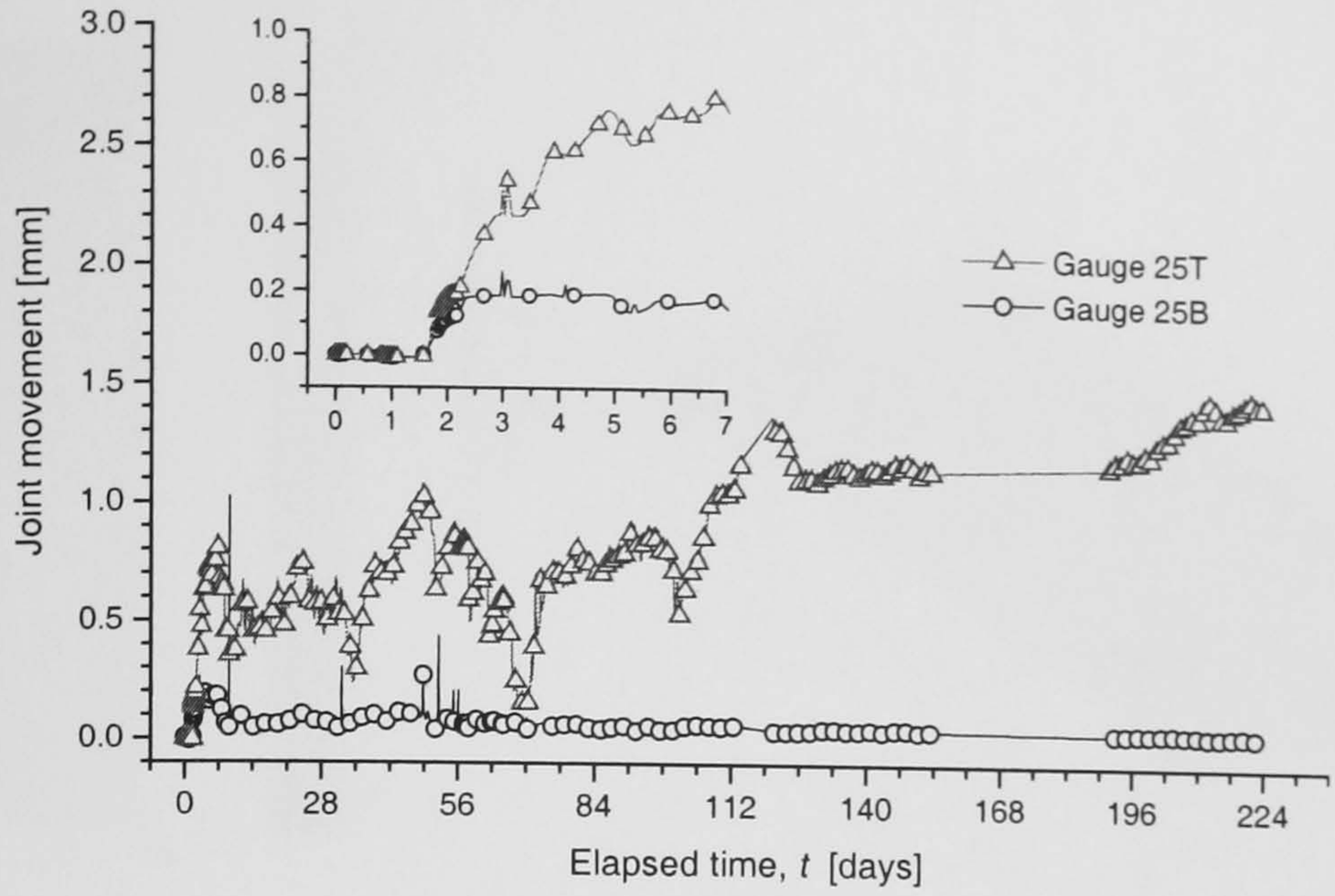

Figure 5.31 - Leeds: Behaviour of the formed free movement joint between pours one and two

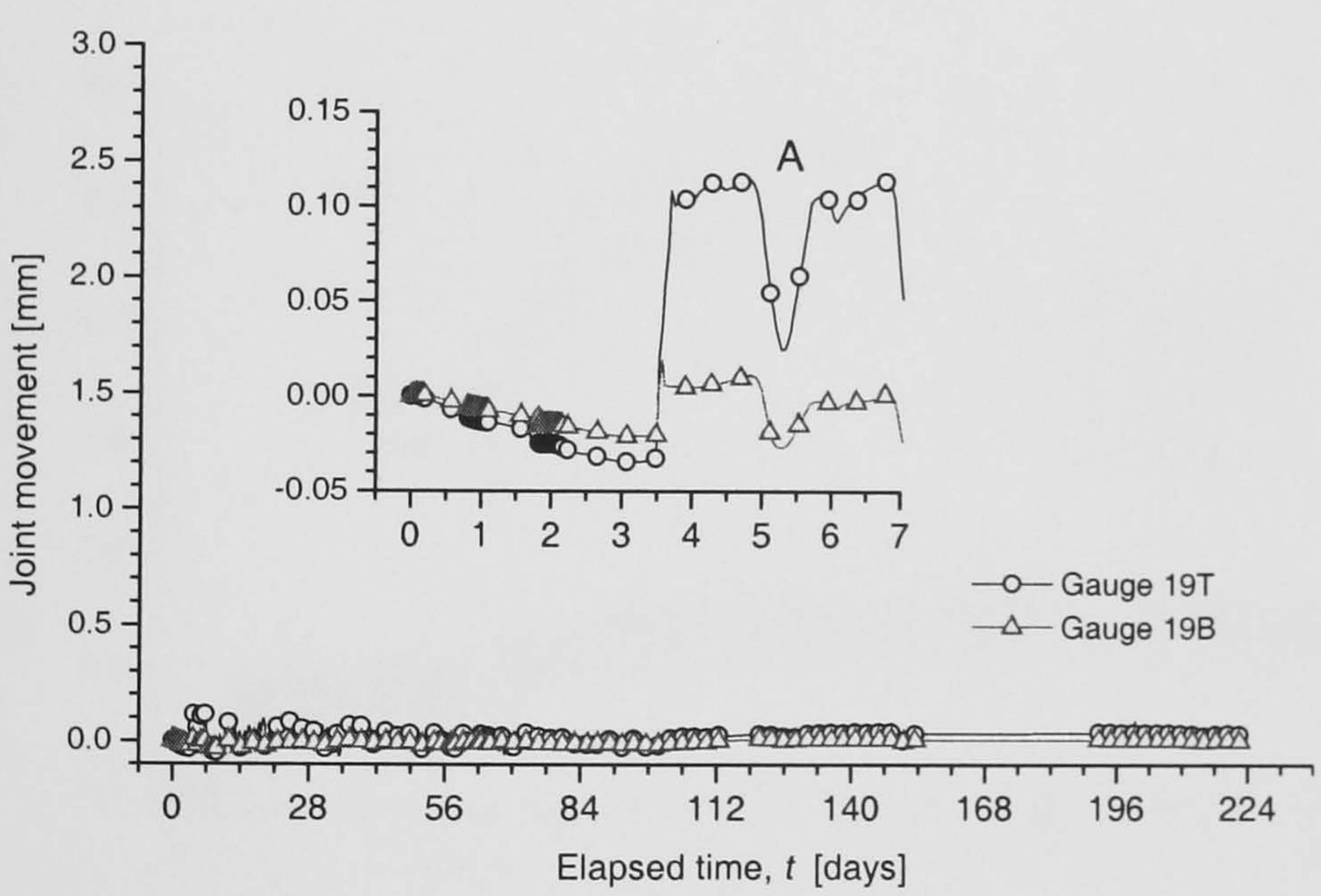

Figure 5.32 - Leeds: Behaviour of the formed free movement joint between pours one and four

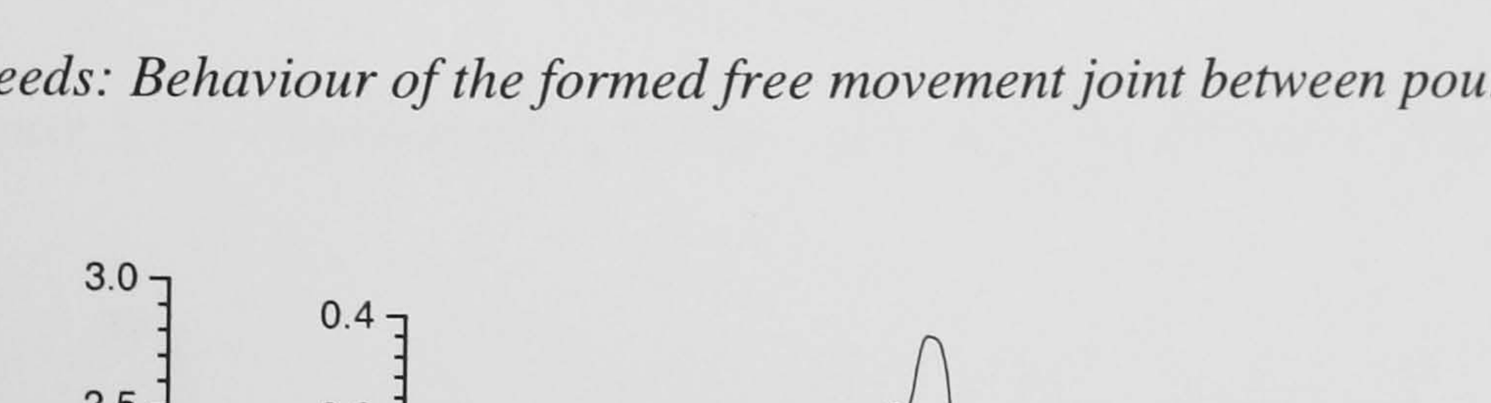

Figure 5.33 - Leeds: Behaviour of the formed free movement joint between pours two and four

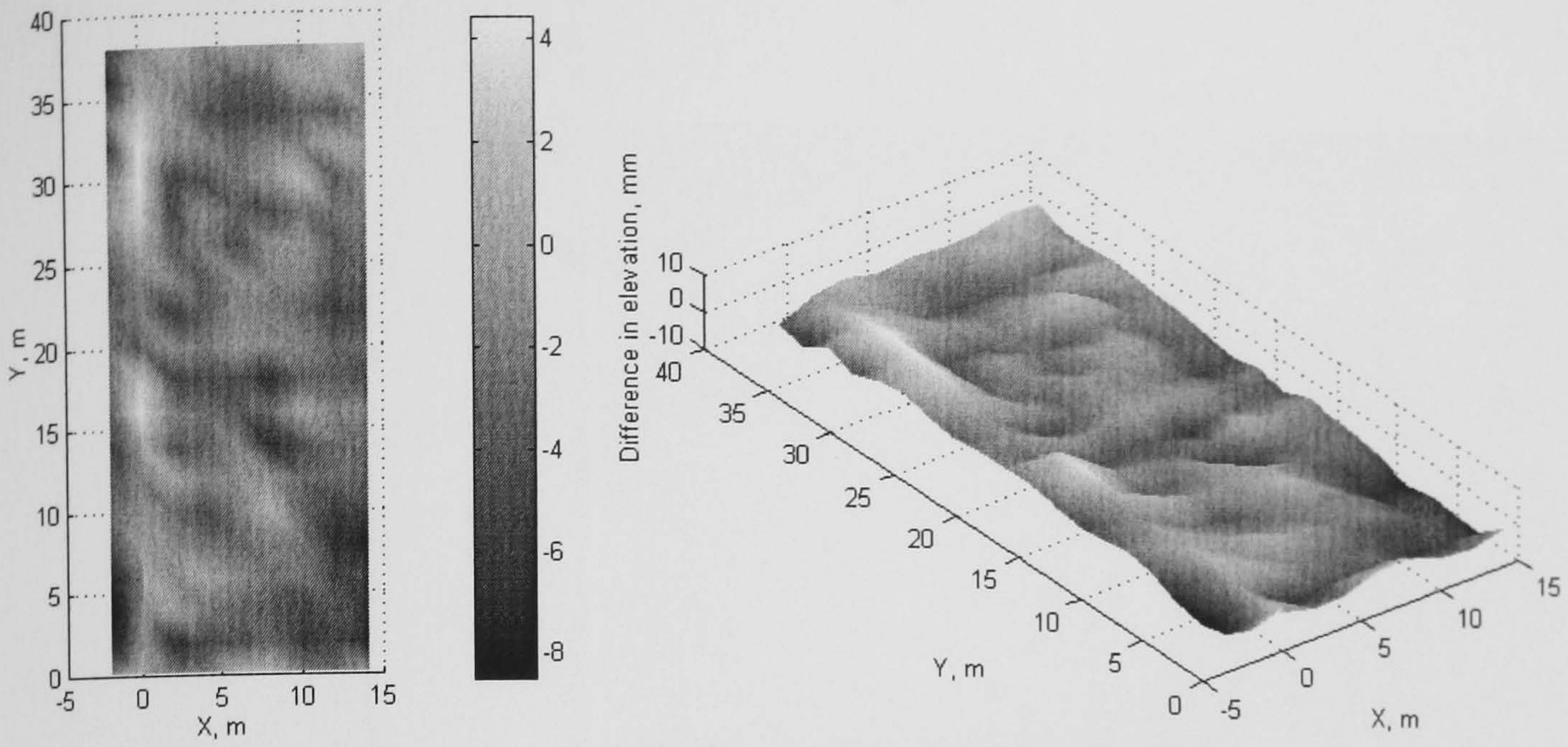

Figure 5.34 - Leeds Pour 2: Precision level survey 1 month after construction

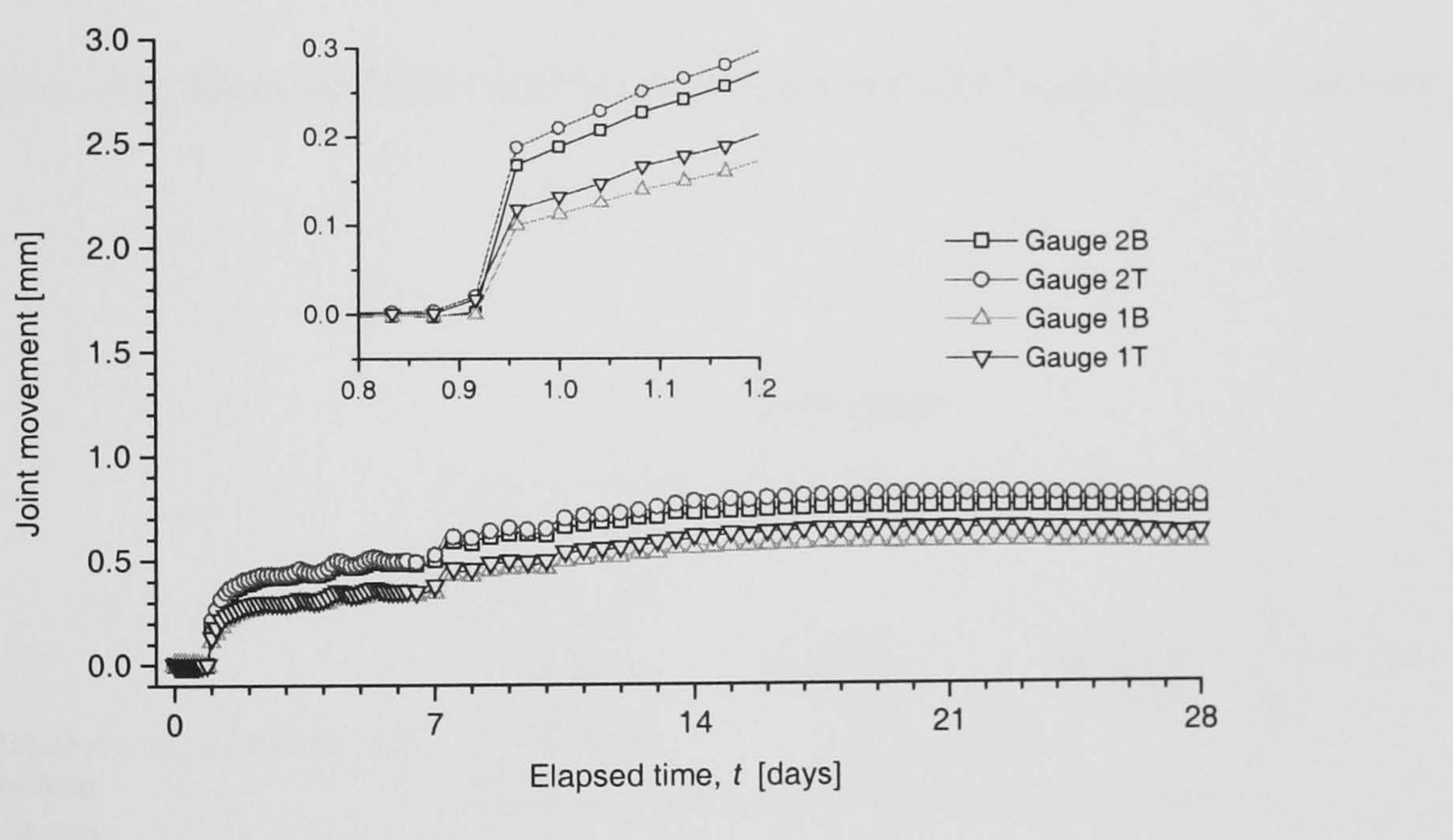

Figure 5.35 – Northampton: Long strip free movement joint behaviour

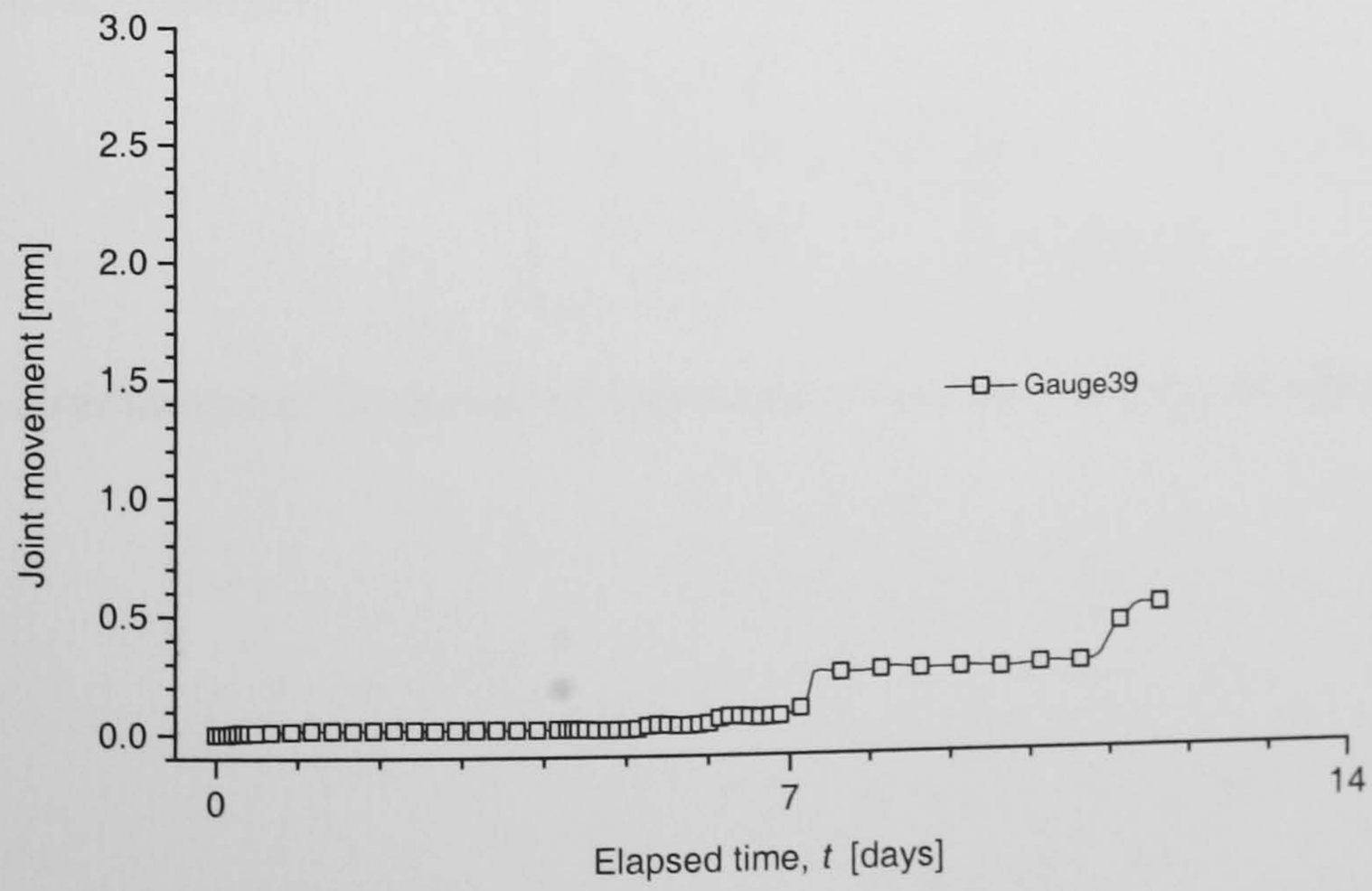

Figure 5.36 - Daventry: Pour 5 Sawn free movement joint behaviour

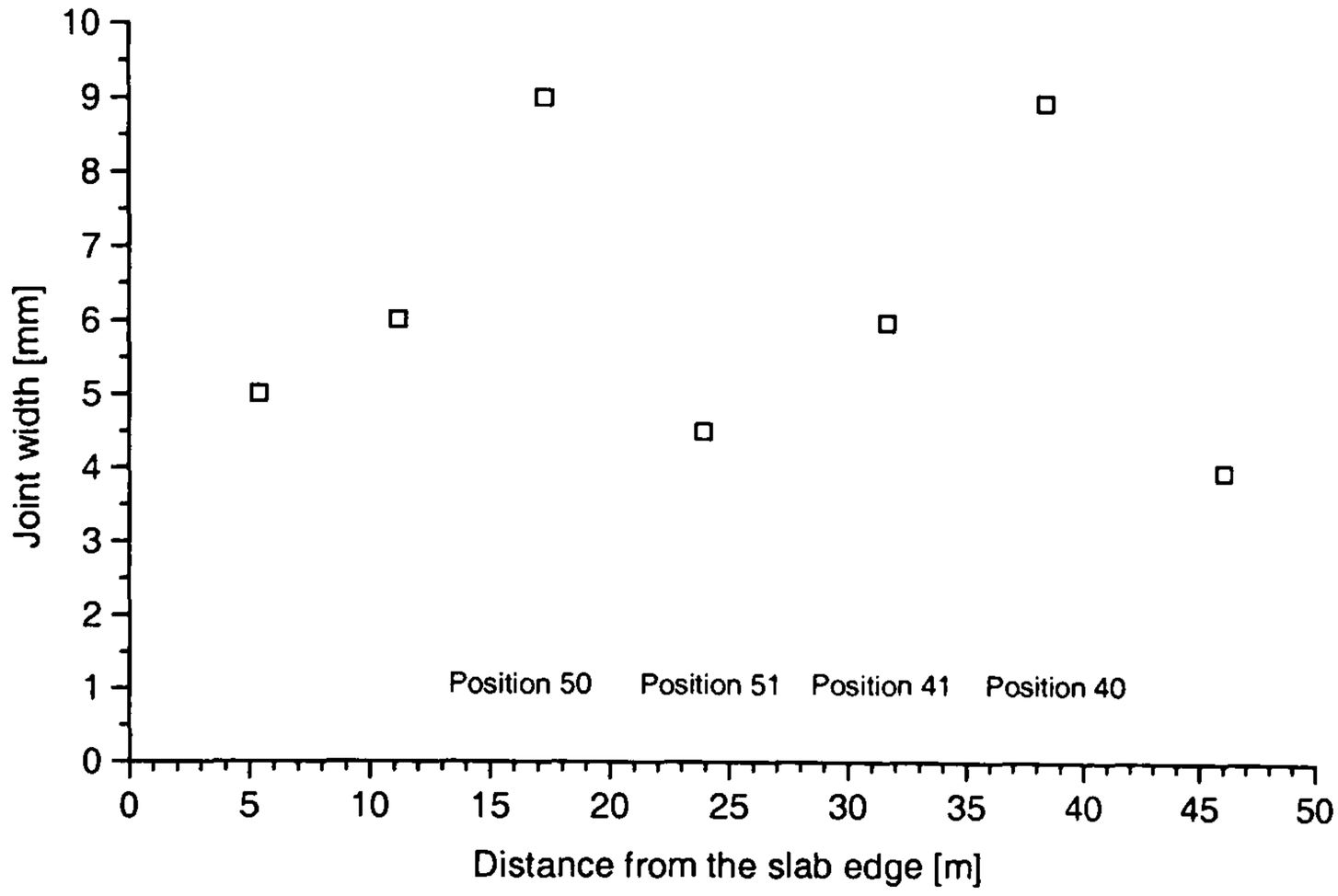

Figure 5.37 - Daventry: Measured joint widths along section B-B 15 months after construction

Incremental contractions are given for the following time periods:
τ = 3, 7, 14 and 28 days.

Gauge positions are as shown in Figure 4.1
Only one gauge was installed at position 7 so this has been shown on both plots.

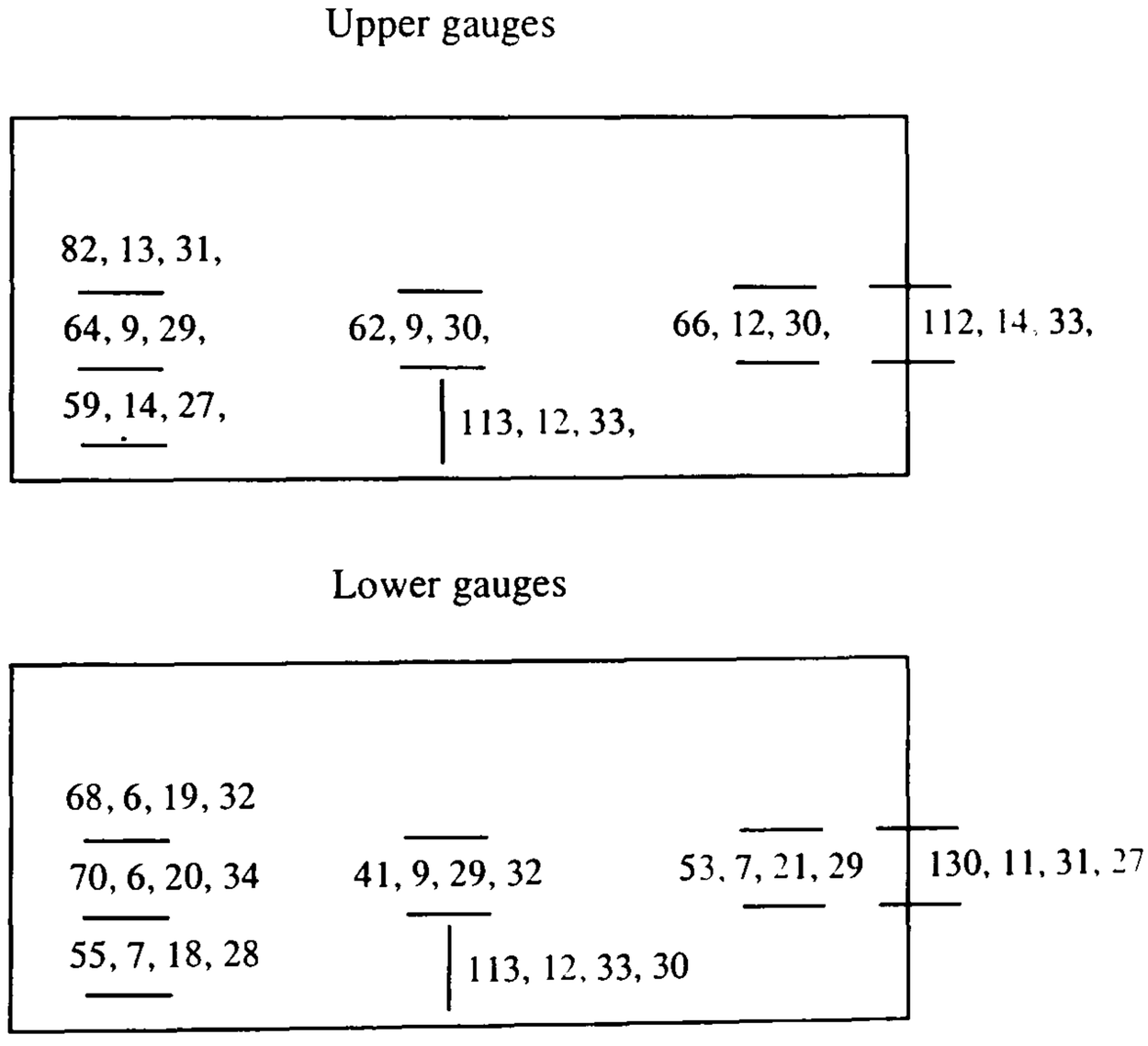

Figure 5.38 - Northampton: Incremental contraction over the first month after construction

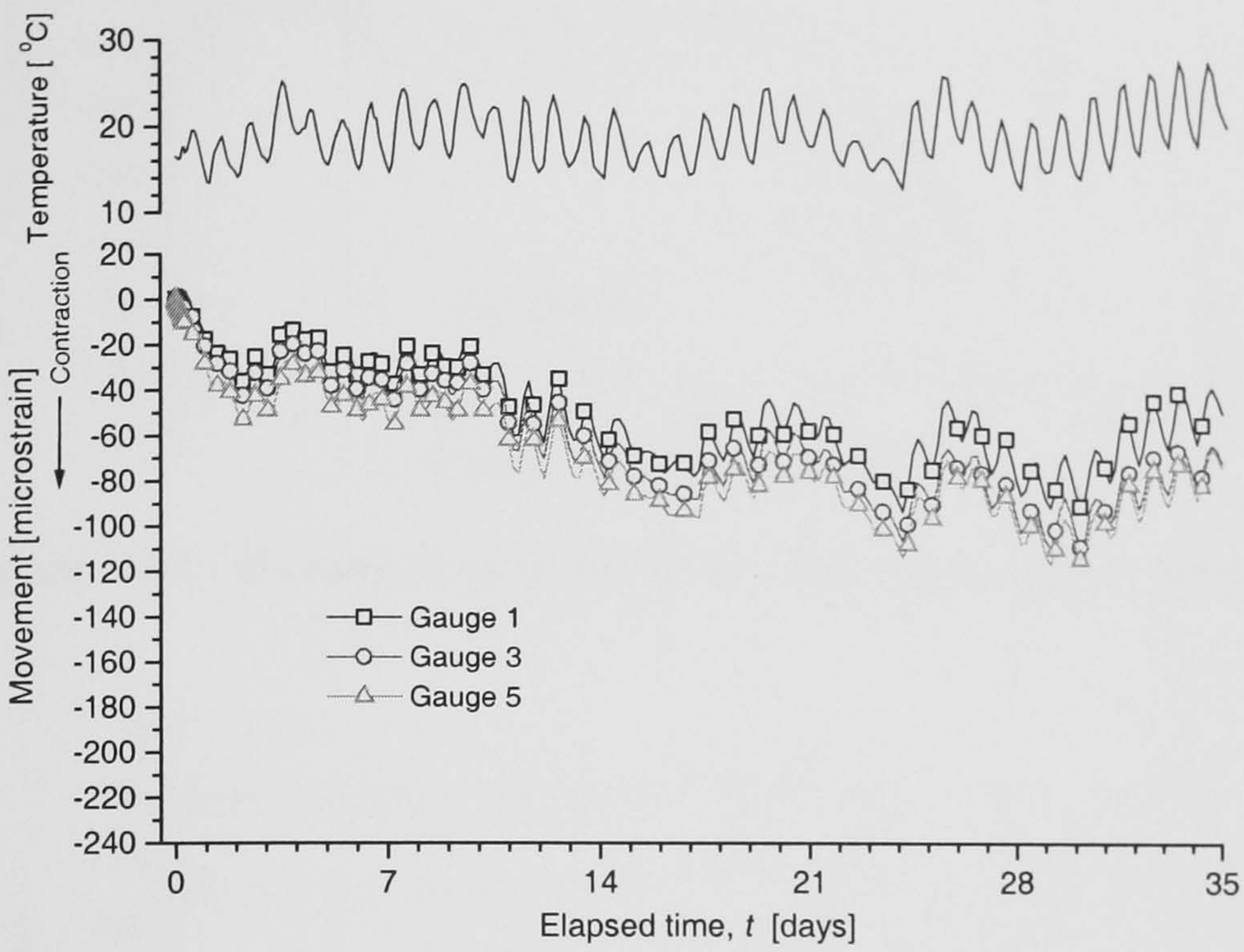

a) Down the length of the building

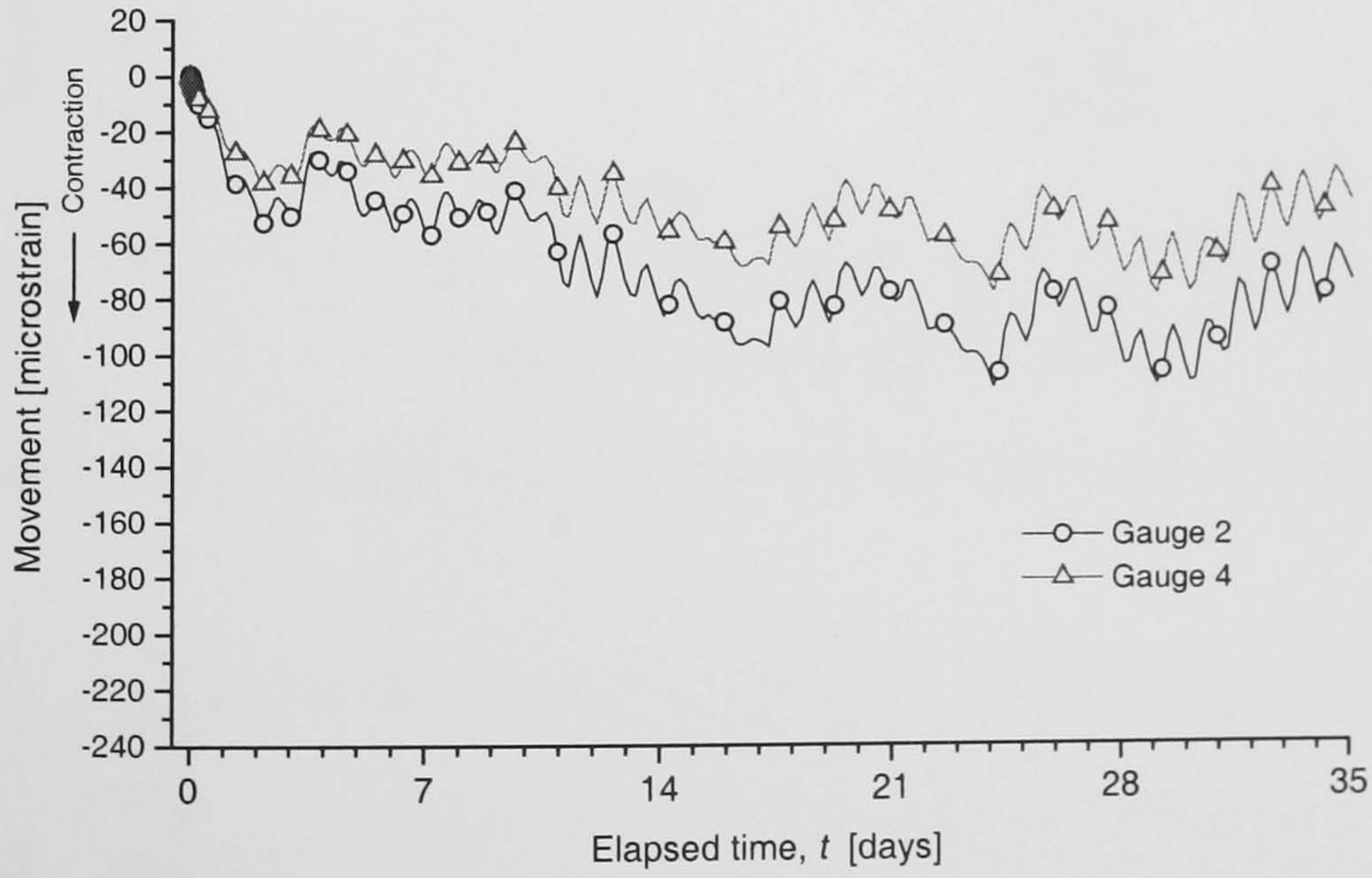

b) Across the building

Figure 5.39 – Bedford Pour 2: Measured movement from the embedment strain gauges

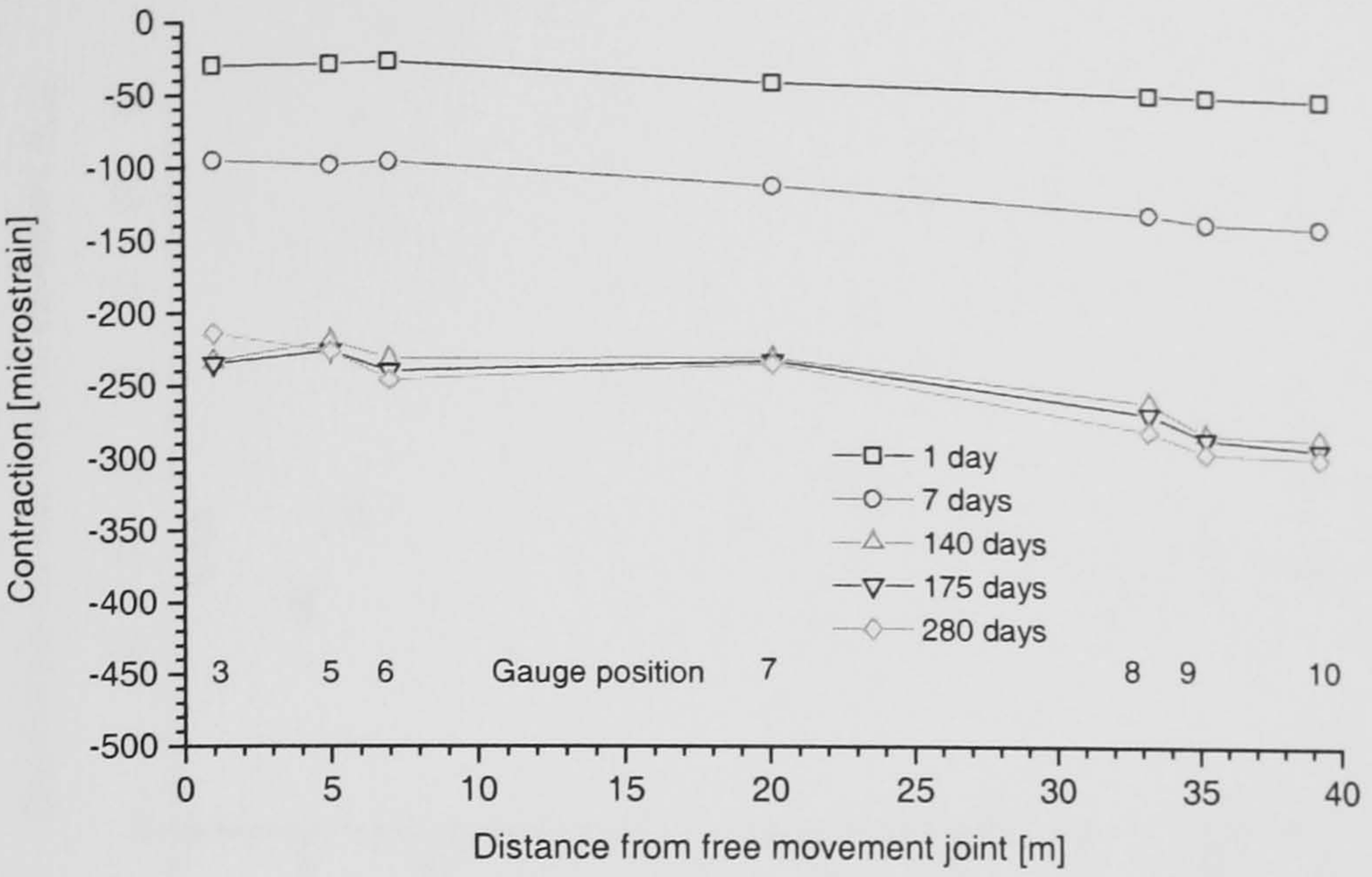

Figure 5.40 – Marston Pour 6: Mid-slab contraction against position

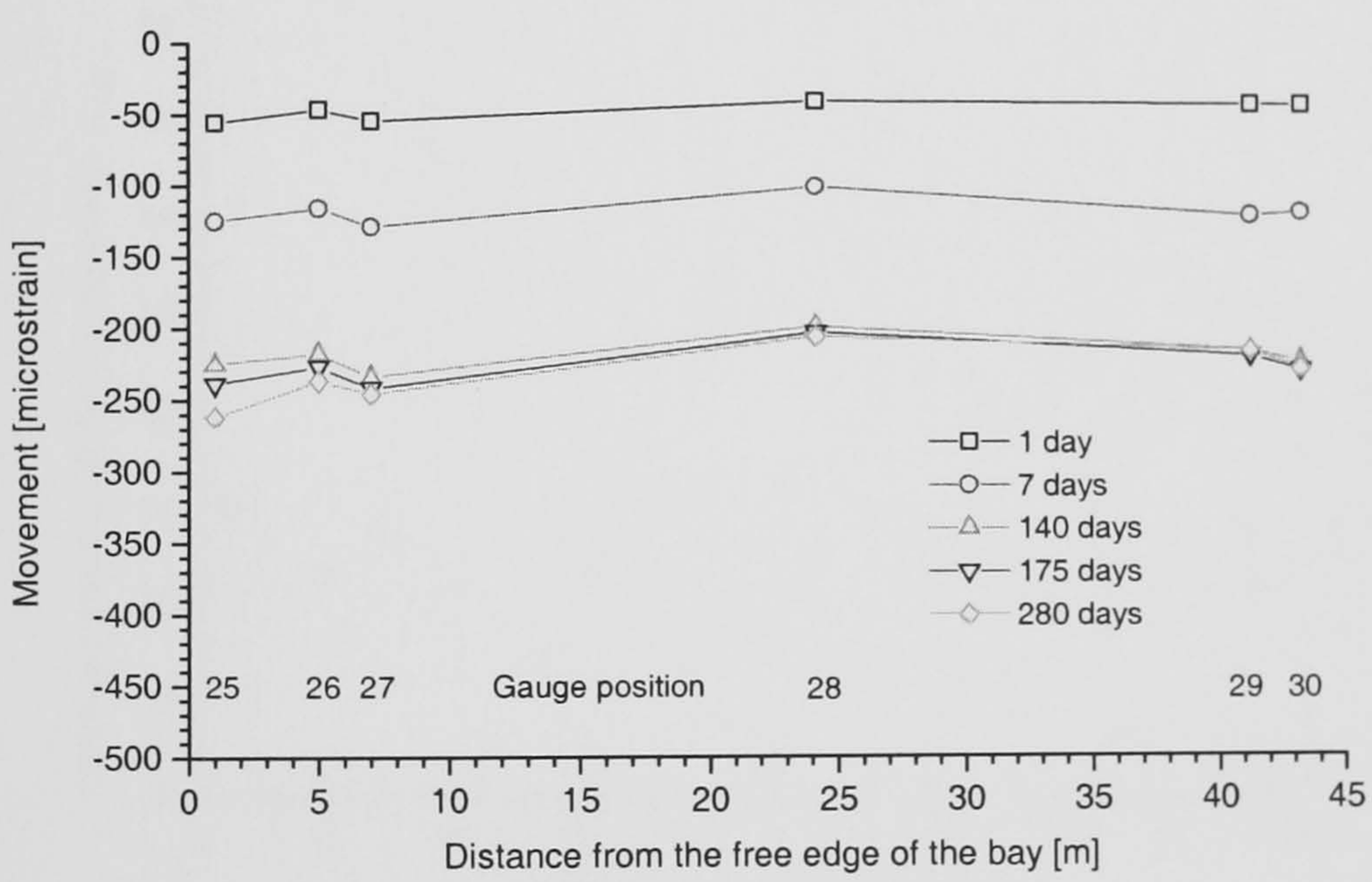

Figure 5.41 – Marston Pour 7: Mid-slab contraction against position

Figure 5.42 – Marston Pour 9: Mid-slab contraction against position

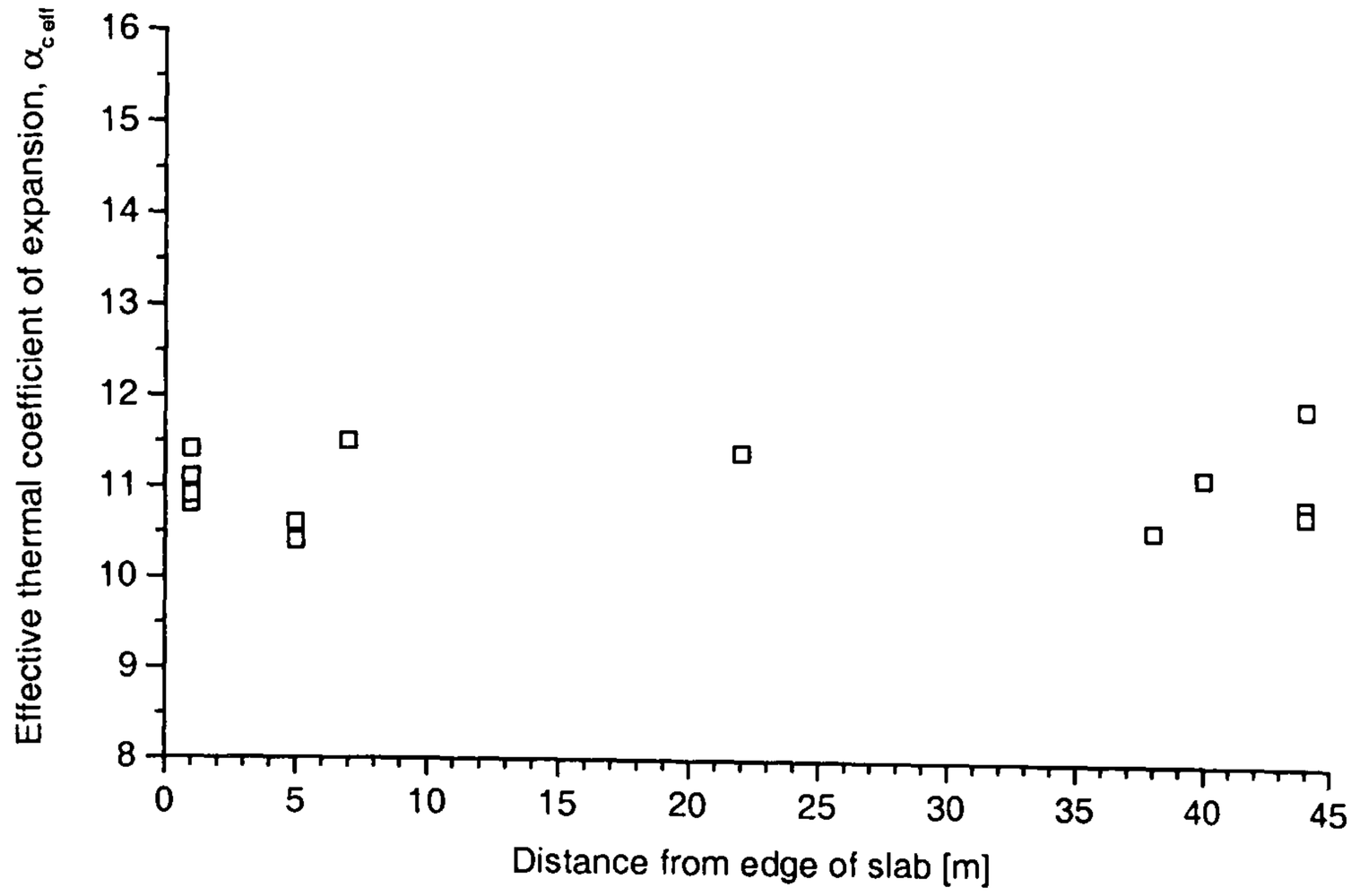

a) Pour 6

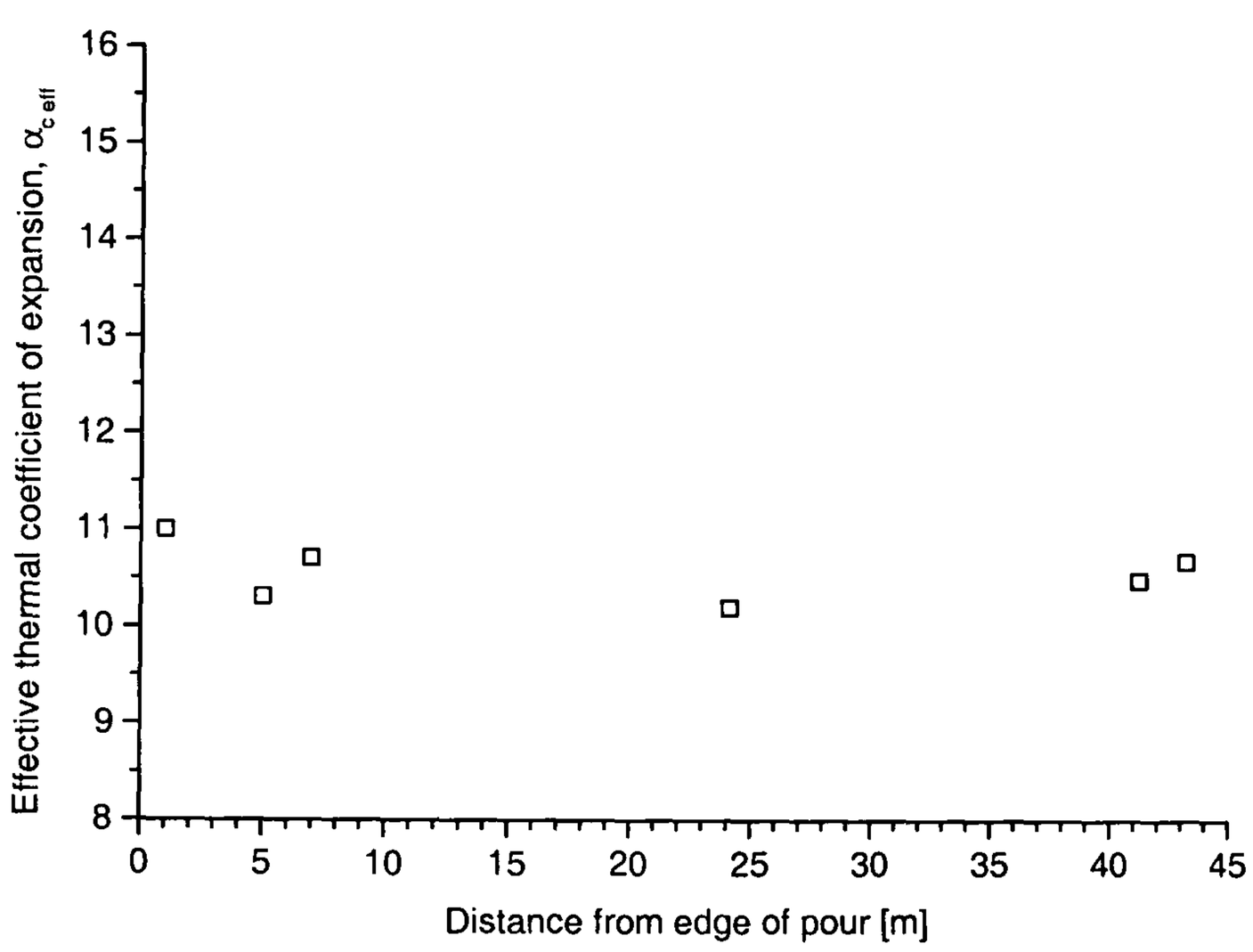

b) Pour 7

c) Pour 9

Figure 5.43 - Marston: Variation of the thermal coefficient of expansion

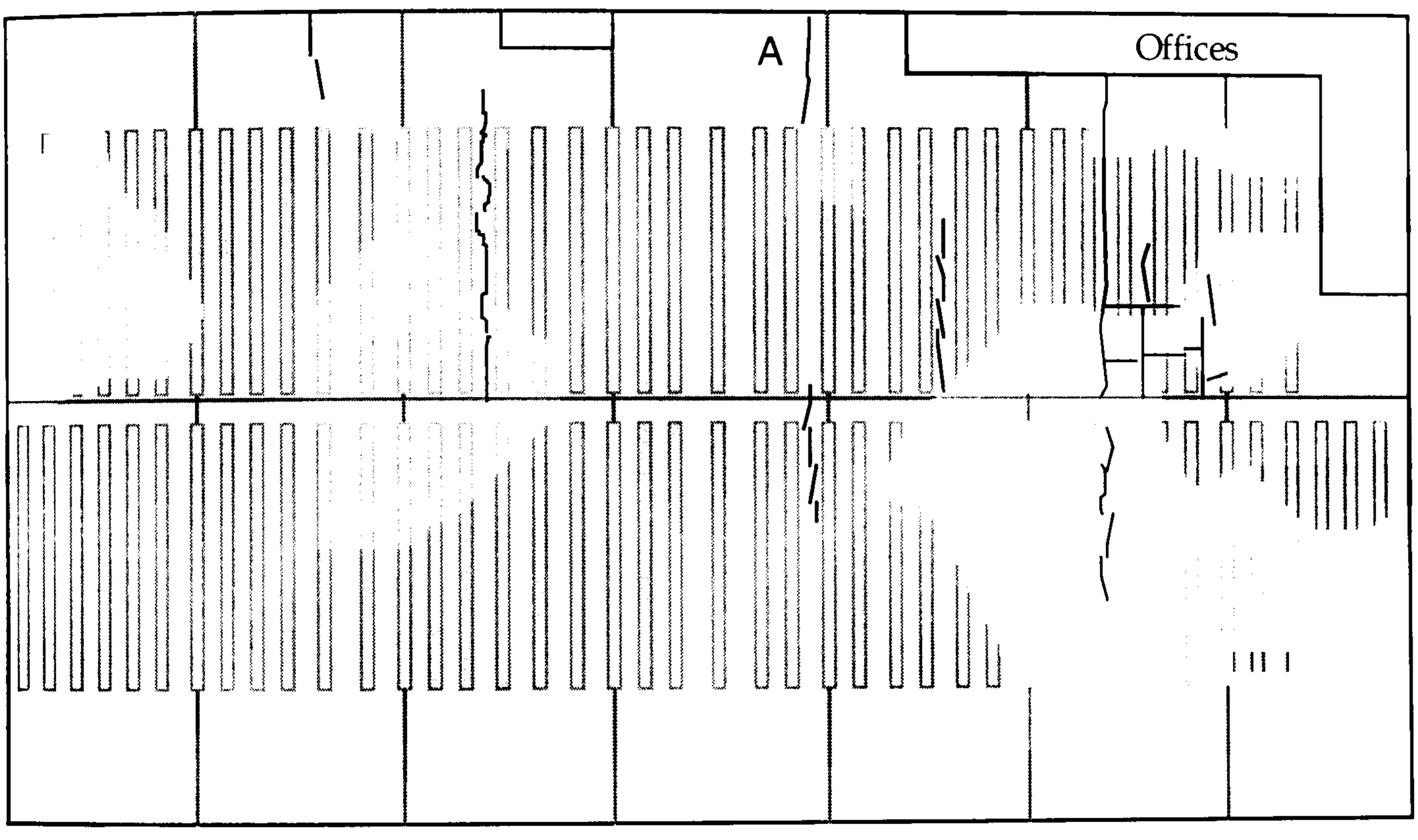

Figure 5.44 – Chepstow: Crack locations as at 19th November 1999

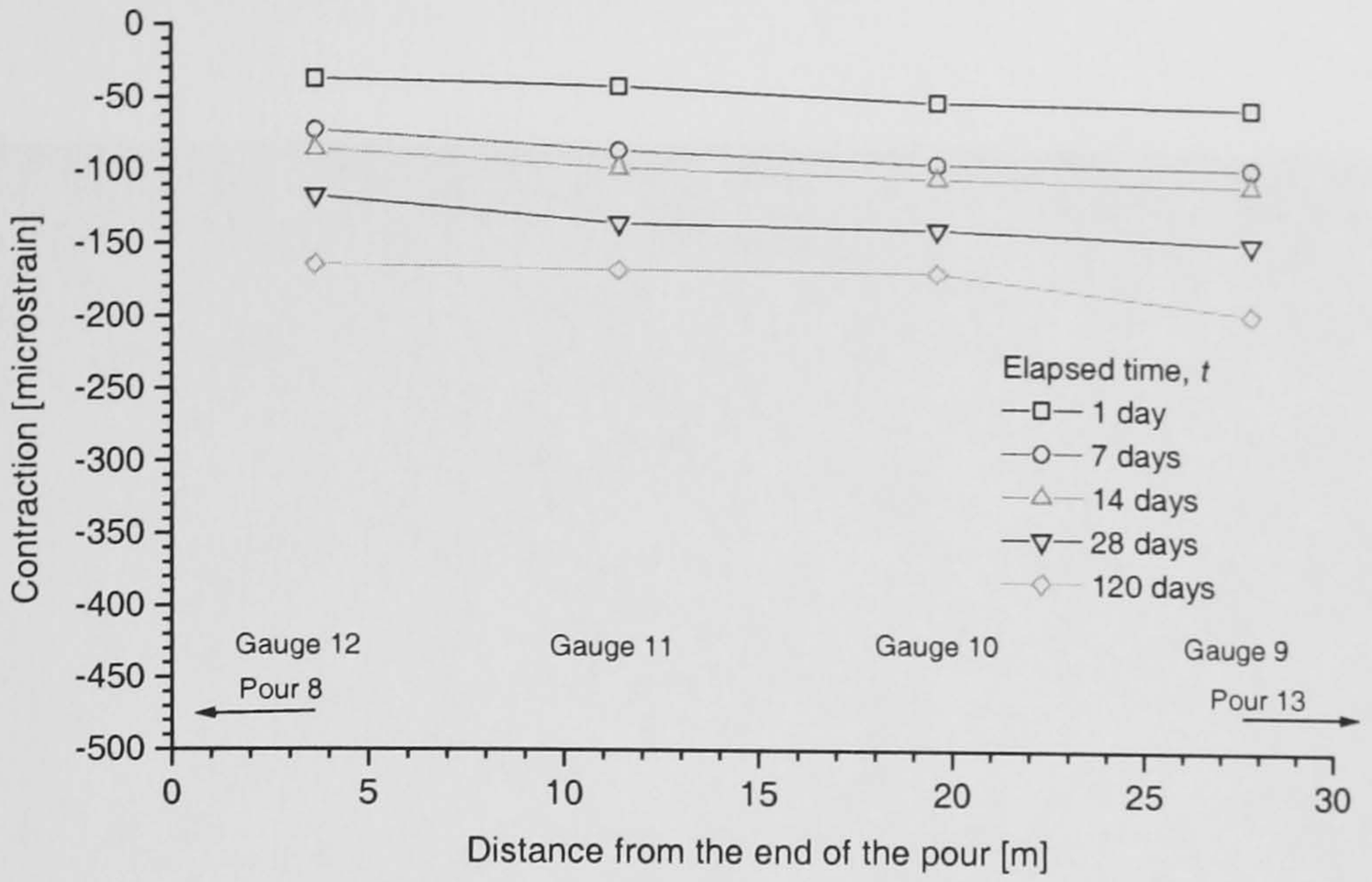

a) Pour 10

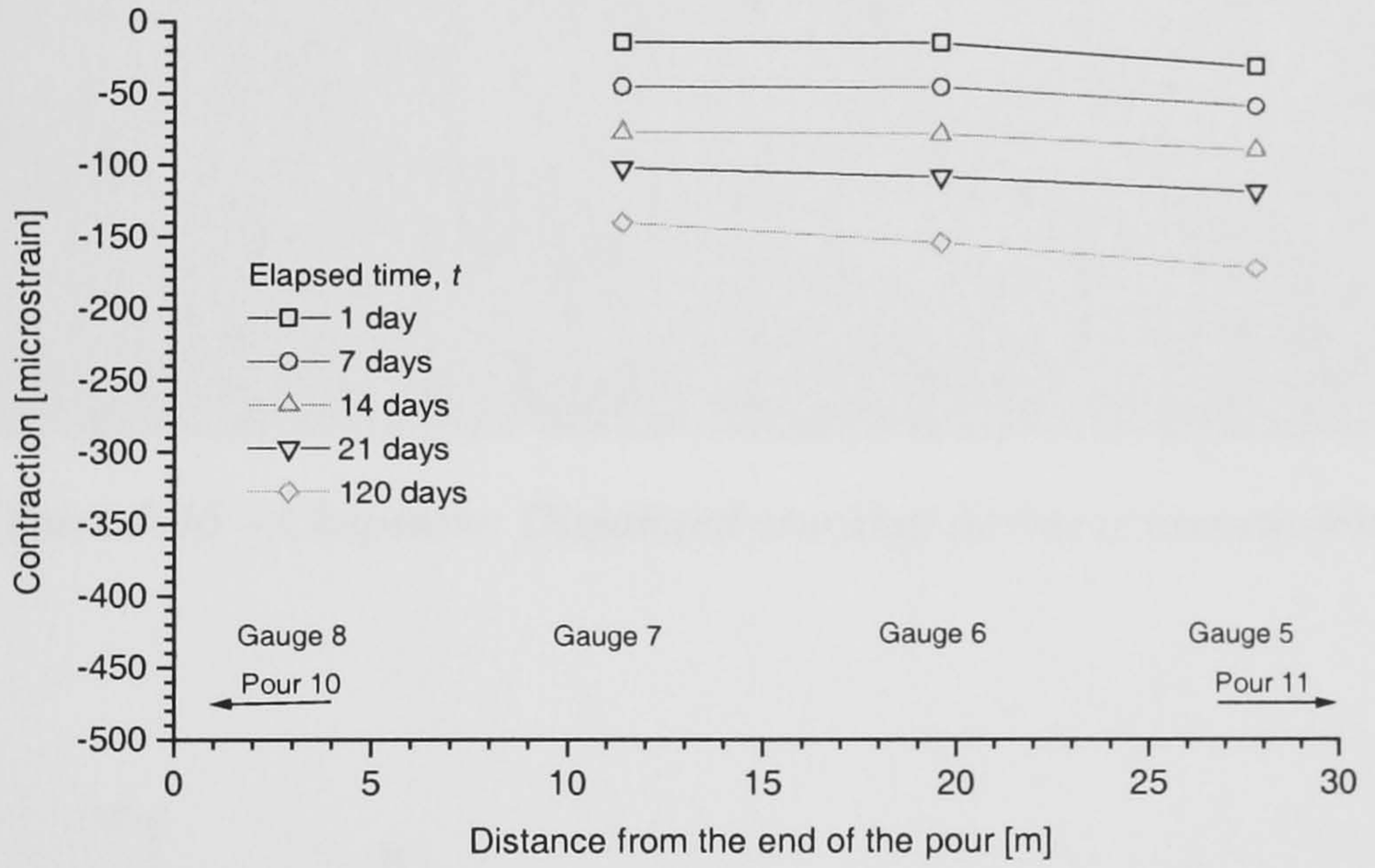

b) Pour 13

c) Pour 11

Figure 5.45 - Chepstow: Concrete contraction with location

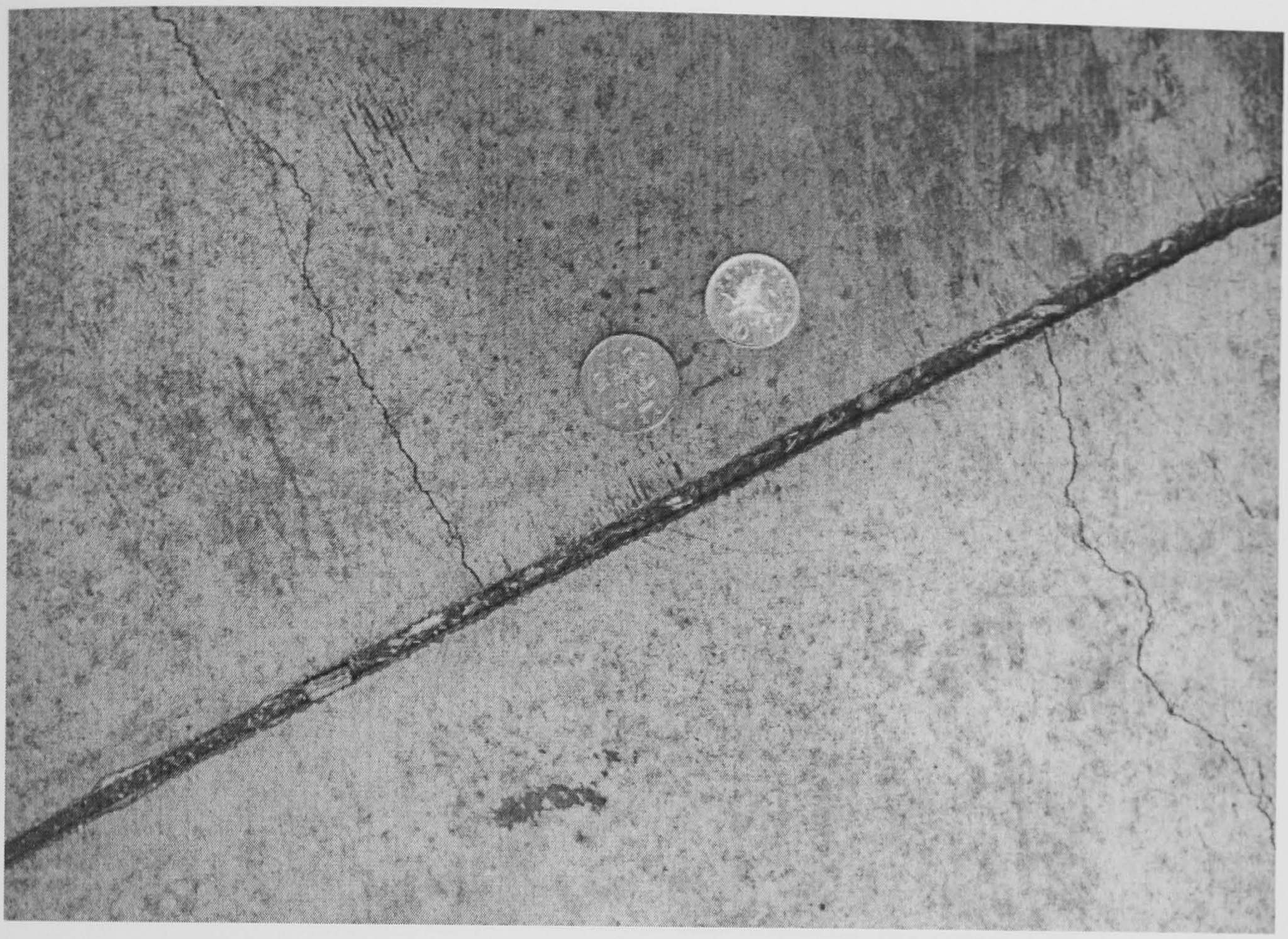

Figure 5.46 – Chepstow: Disjointed cracking across a saw-cut joint

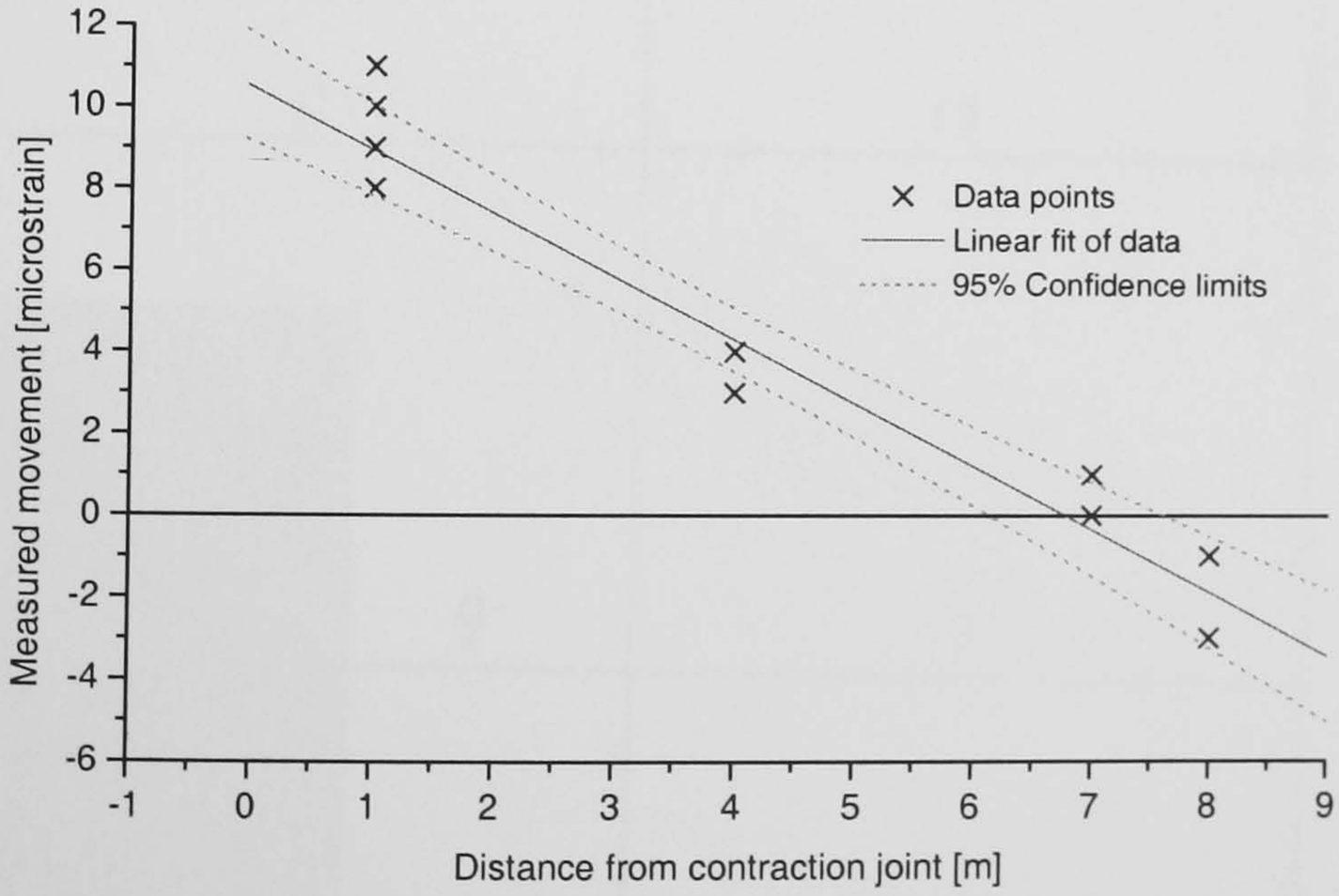

Figure 5.47 – Northampton: Measured strain changes at the first opening of the fm joint

Date:...24/2/00.....

Readings taken by:...D. Spendlove.....

All measurements in mm

Notes:

Figure 5.48 - Marston: Joint width measurements 140 days after construction

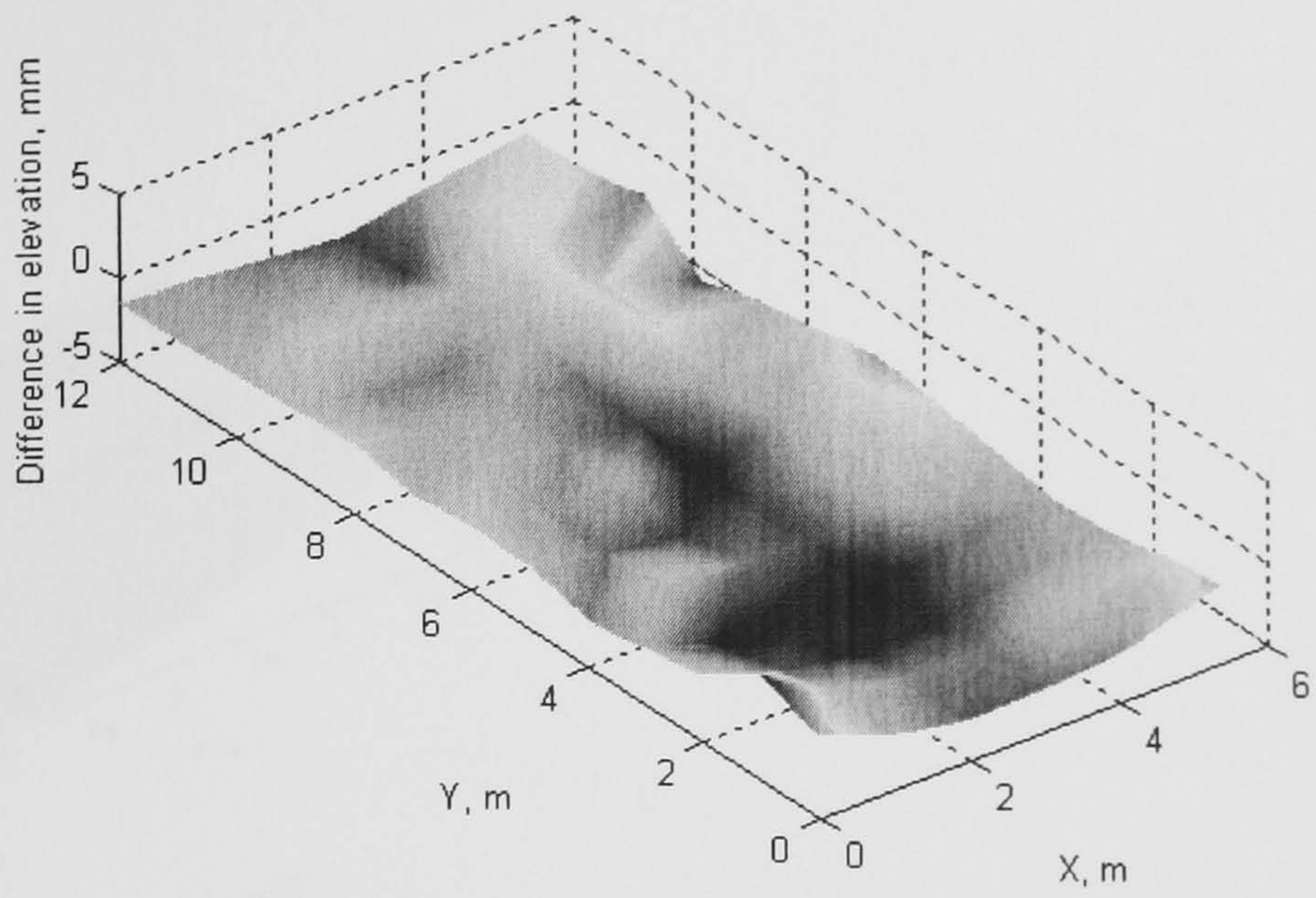

Figure 5.49 – Northampton: Precision level survey results 24 hours after construction

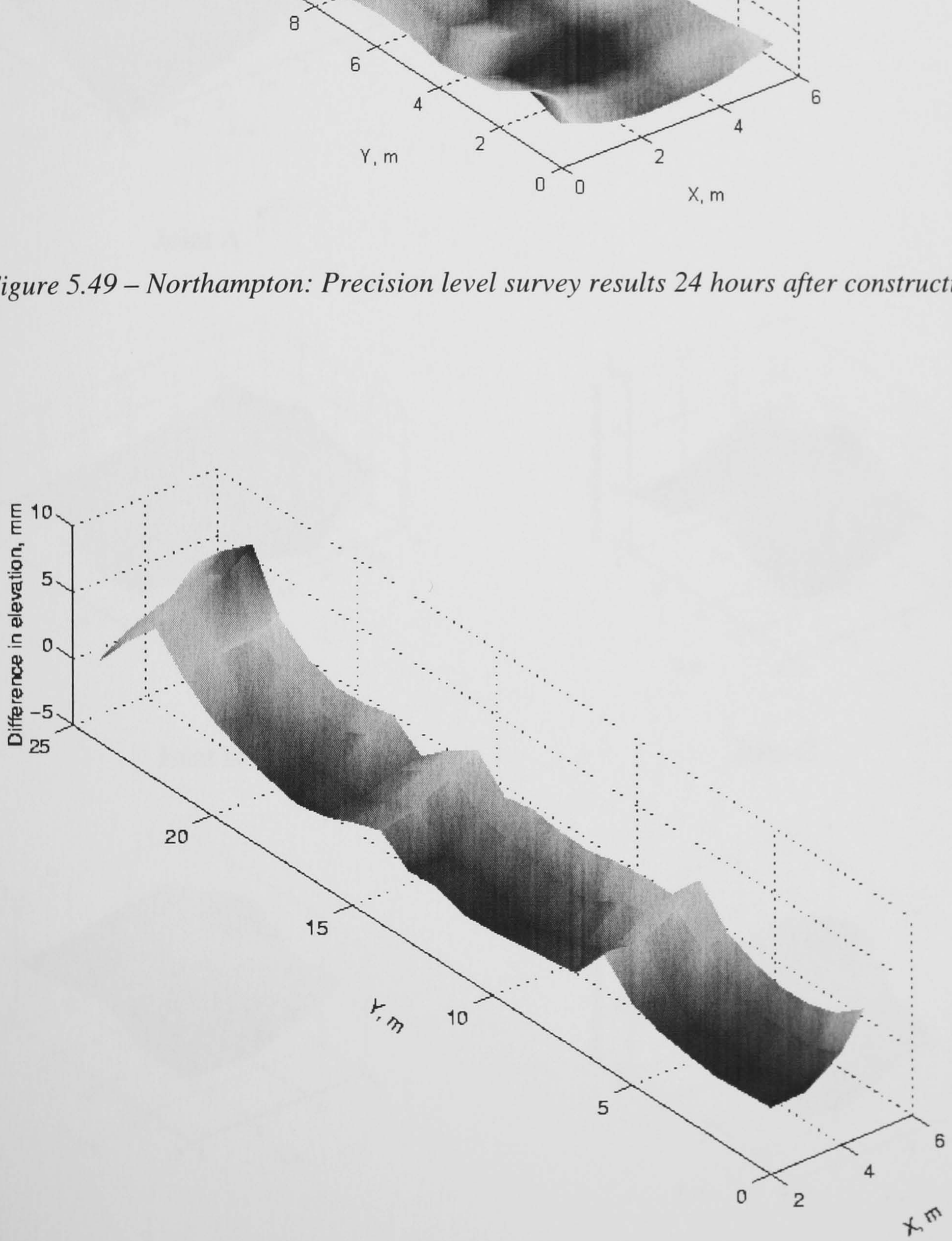

Figure 5.50 – Northampton: Surface profile of the long strip slab 10 months after construction

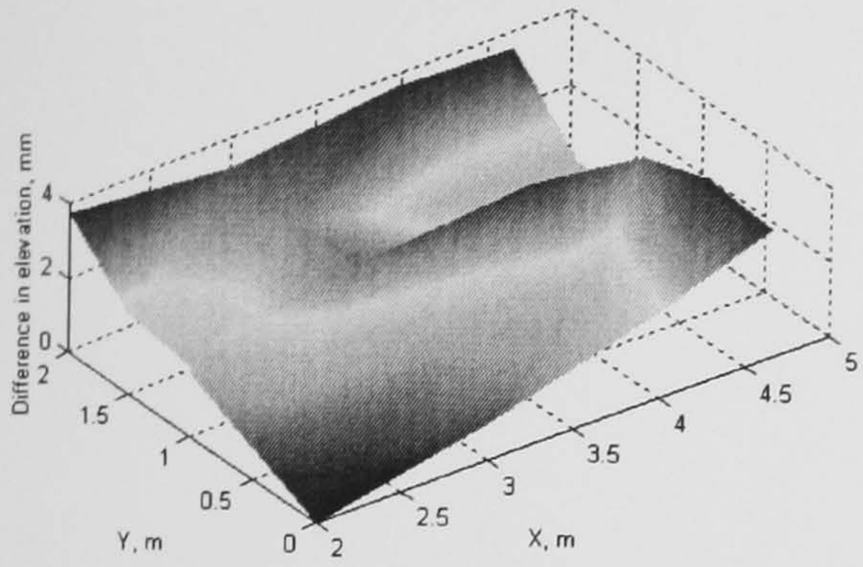

Joint A

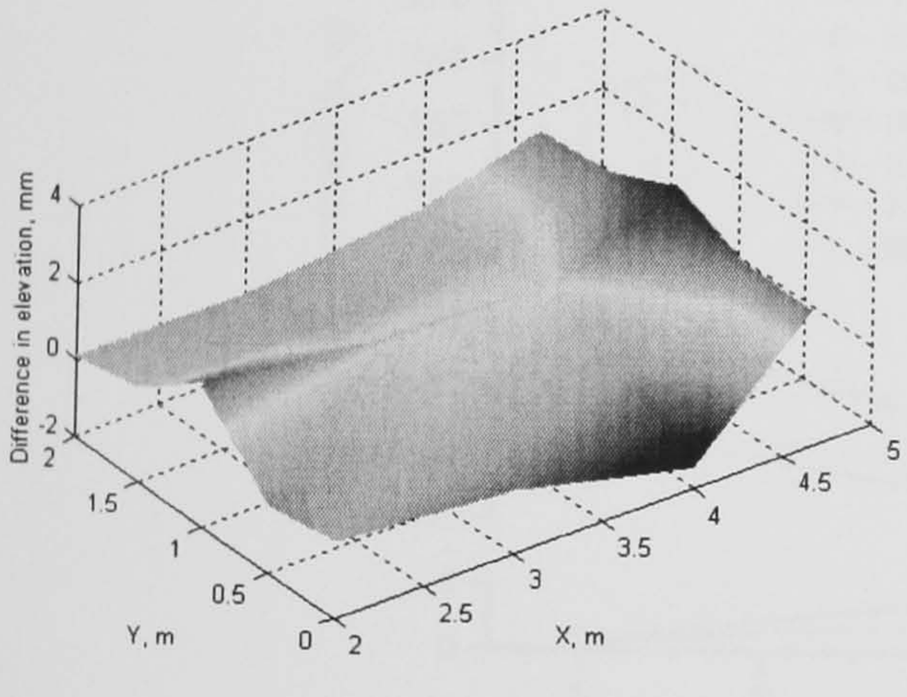

Joint B

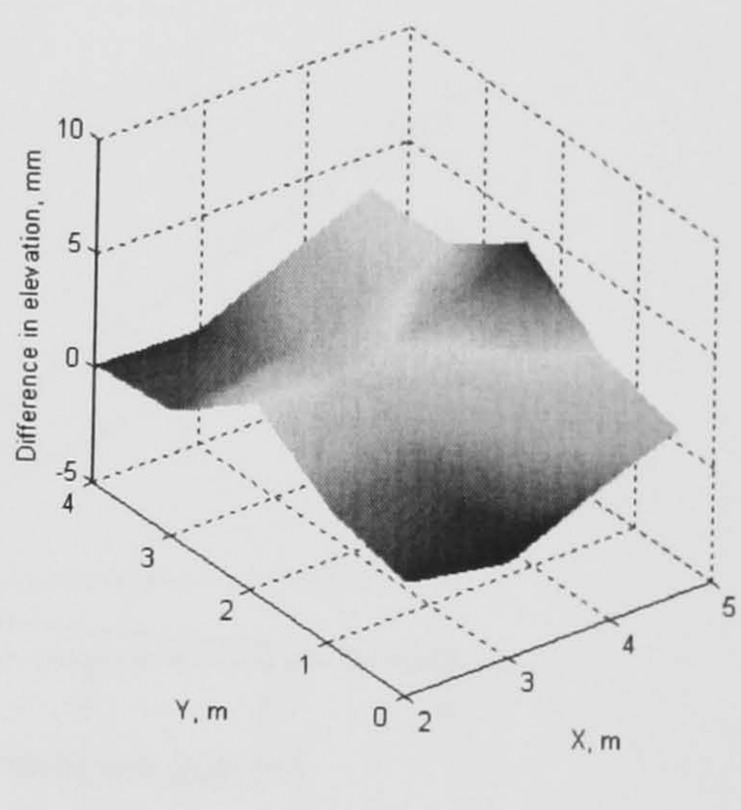

Joint C

Joint D

Joint E

Figure 5.51 – Northampton: Slab profiles near to joints 10 months after construction

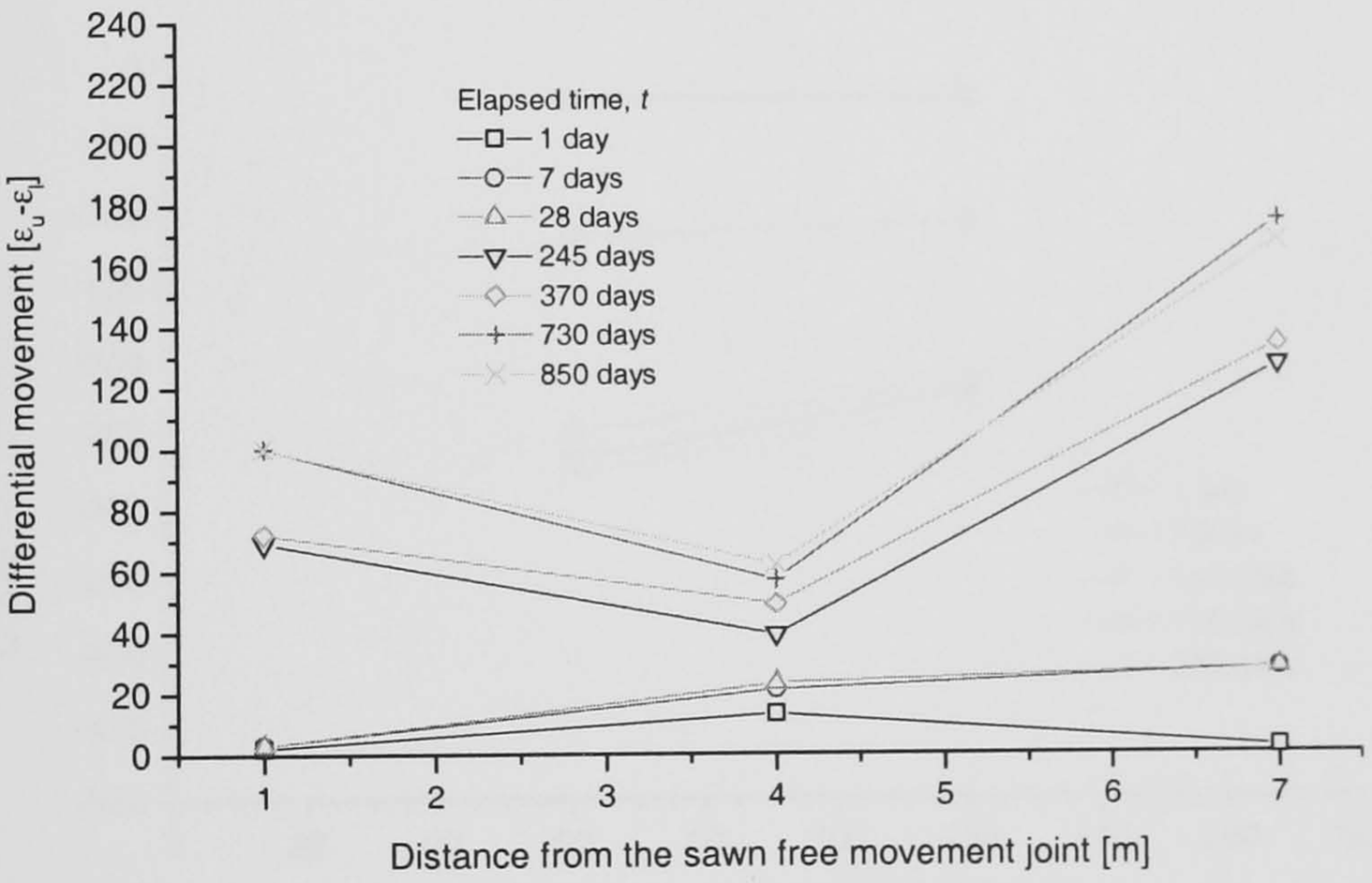

Figure 5.52 - Northampton: Differential movement with time

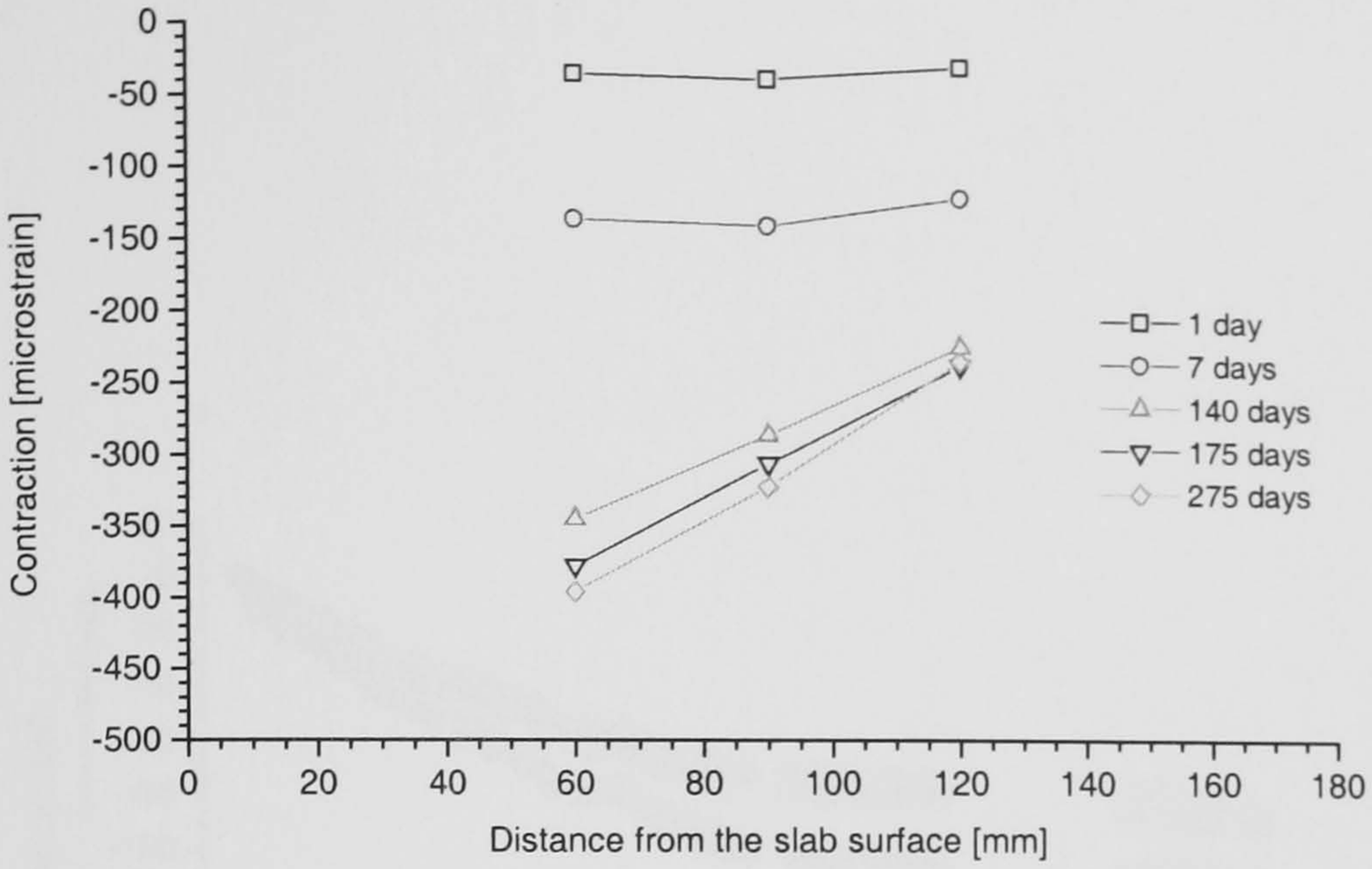

a) left-hand edge

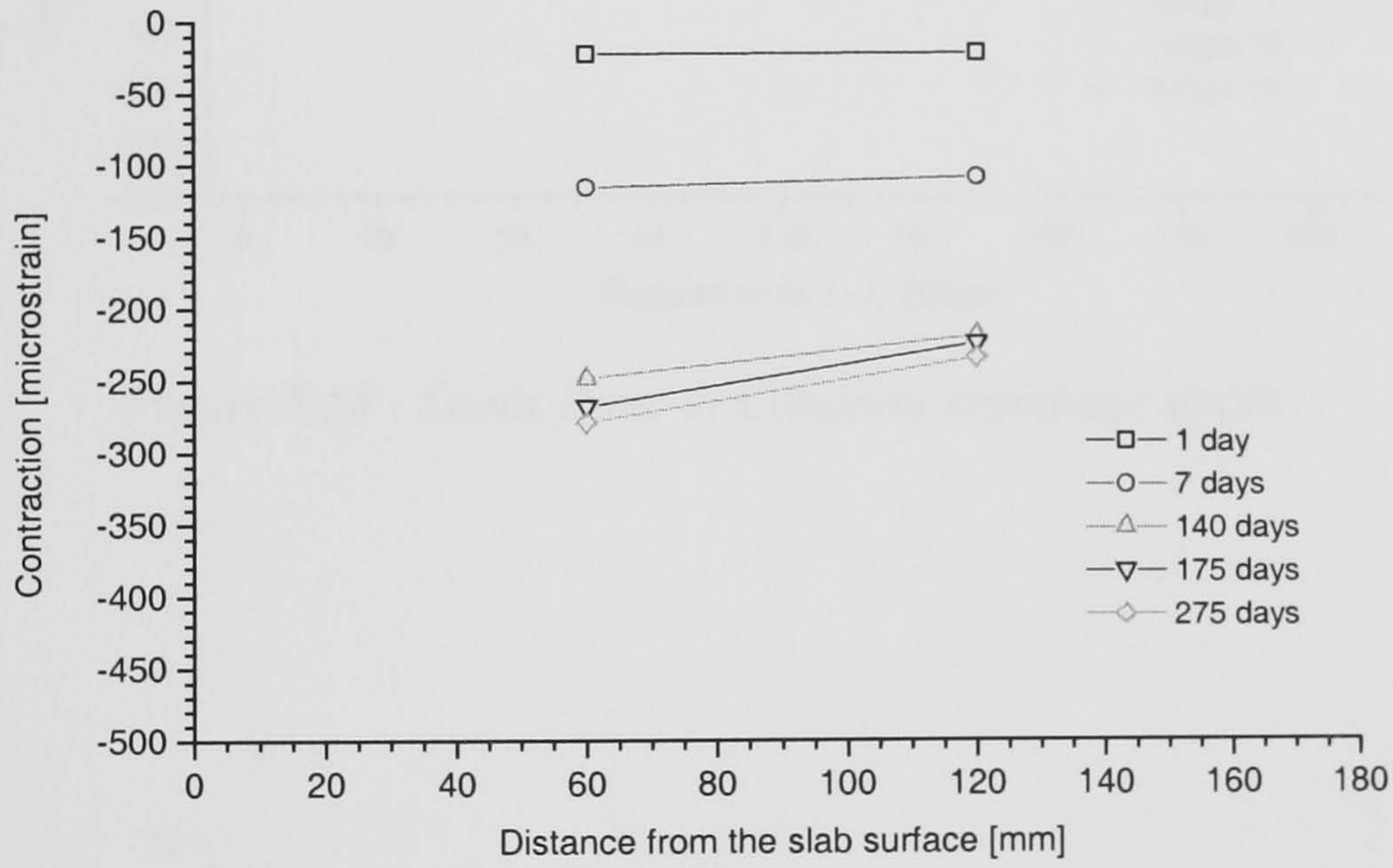

b) mid-slab

c) right-hand edge

Figure 5.53 - Bedford 2 Pour 9: Warping movement from a jointless large area pour

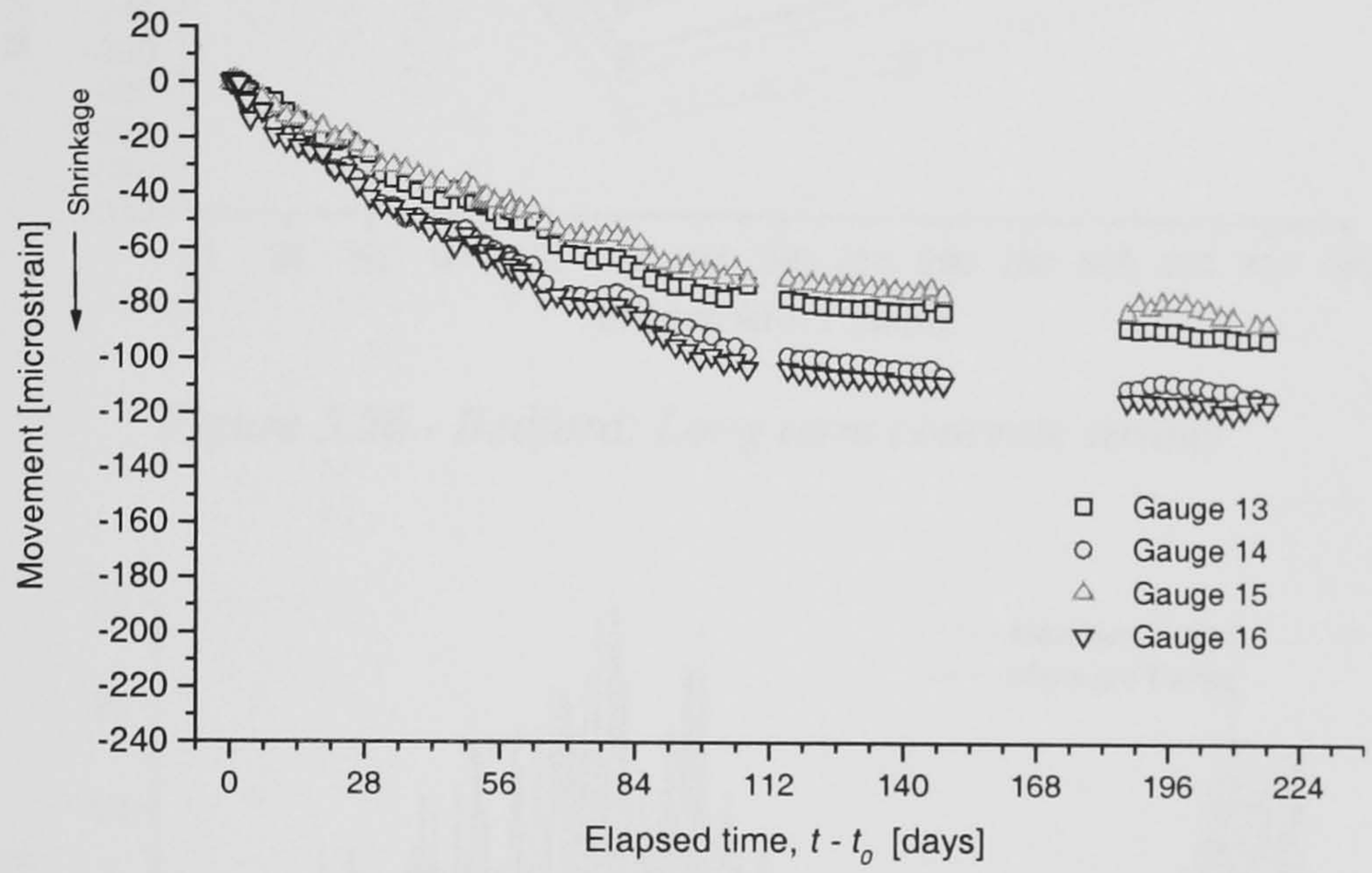

Figure 5.54 - Leeds Pour 4: Concrete shrinkage strain

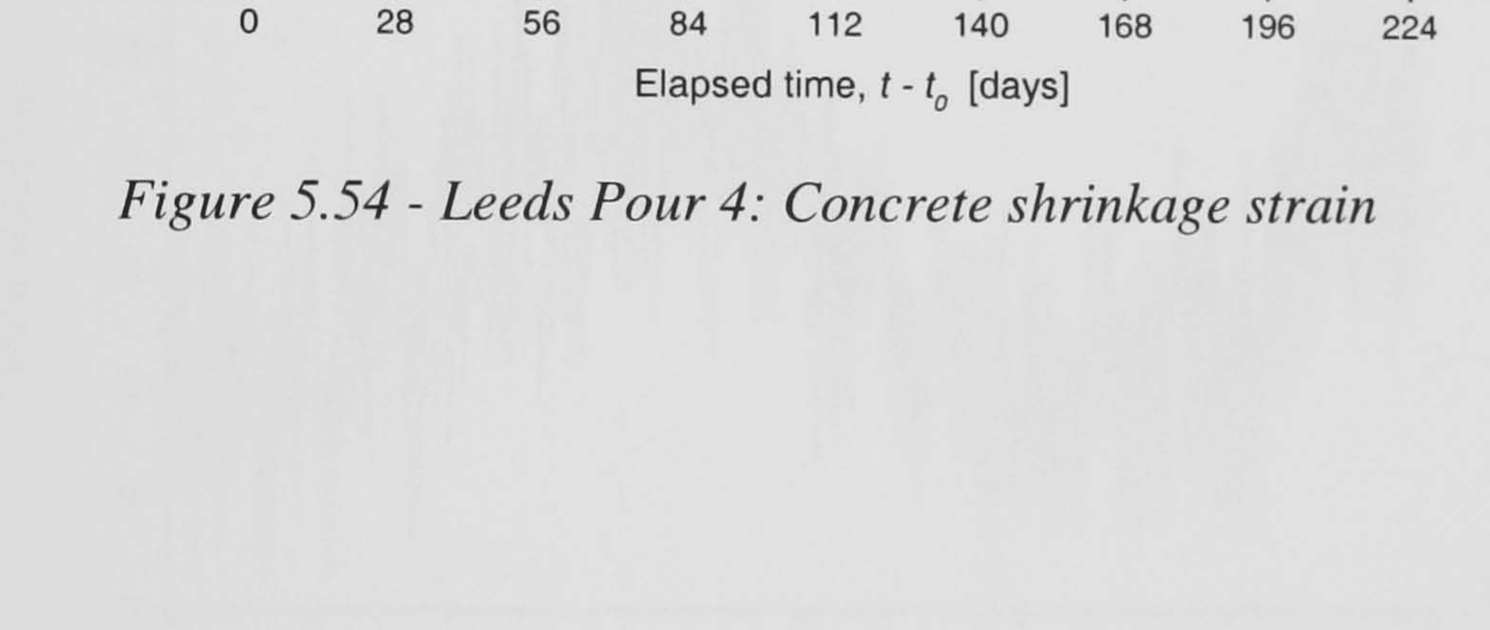

Figure 5.55 - Leeds Pour 1: Concrete shrinkage strain

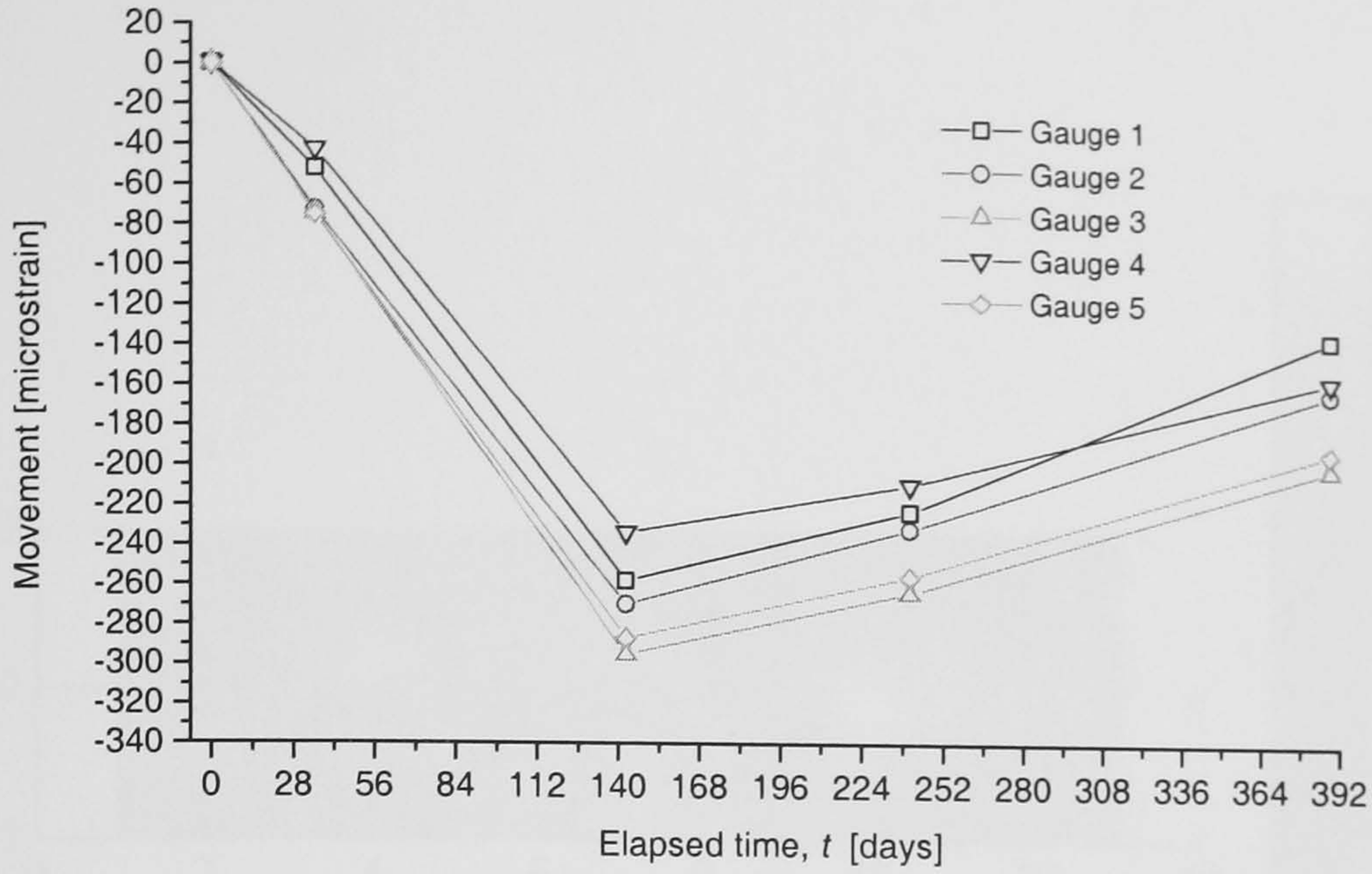

Figure 5.56 - Bedford: Long term concrete strains

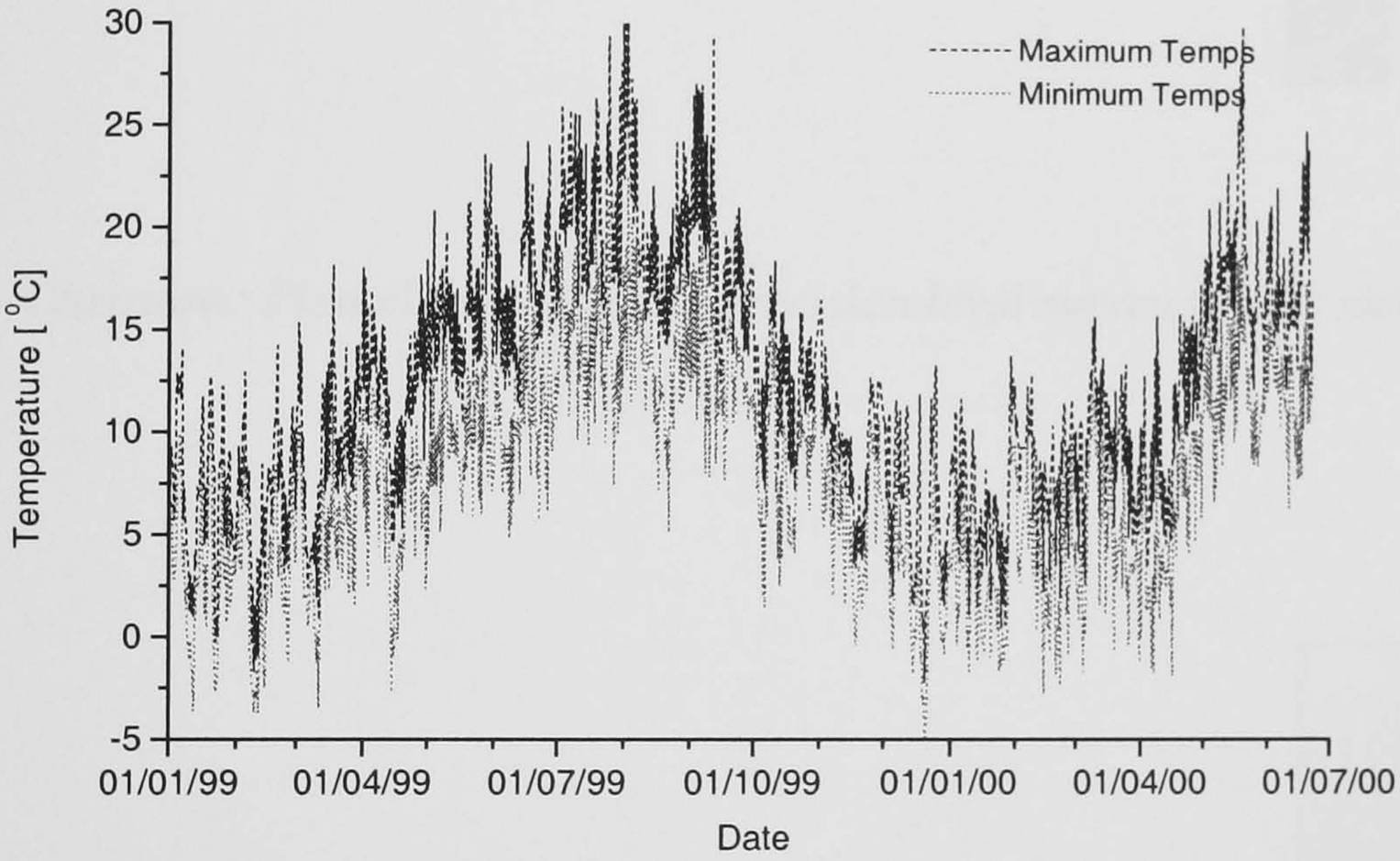

Figure 5.57 - Bedford: Ambient temperature from Bedford Saws (Data courtesy of the BADC)

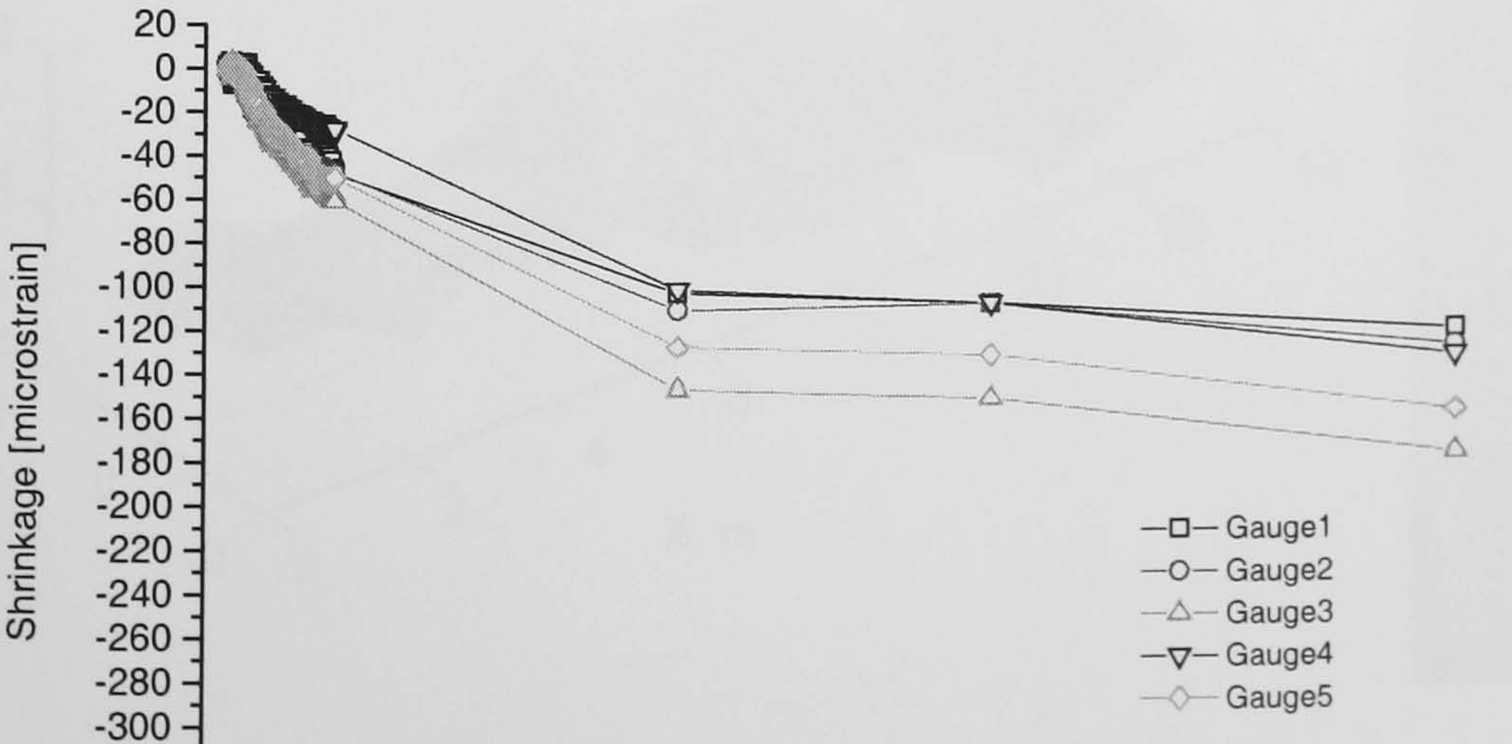

Figure 5.58 - Bedford: Long term shrinkage strains

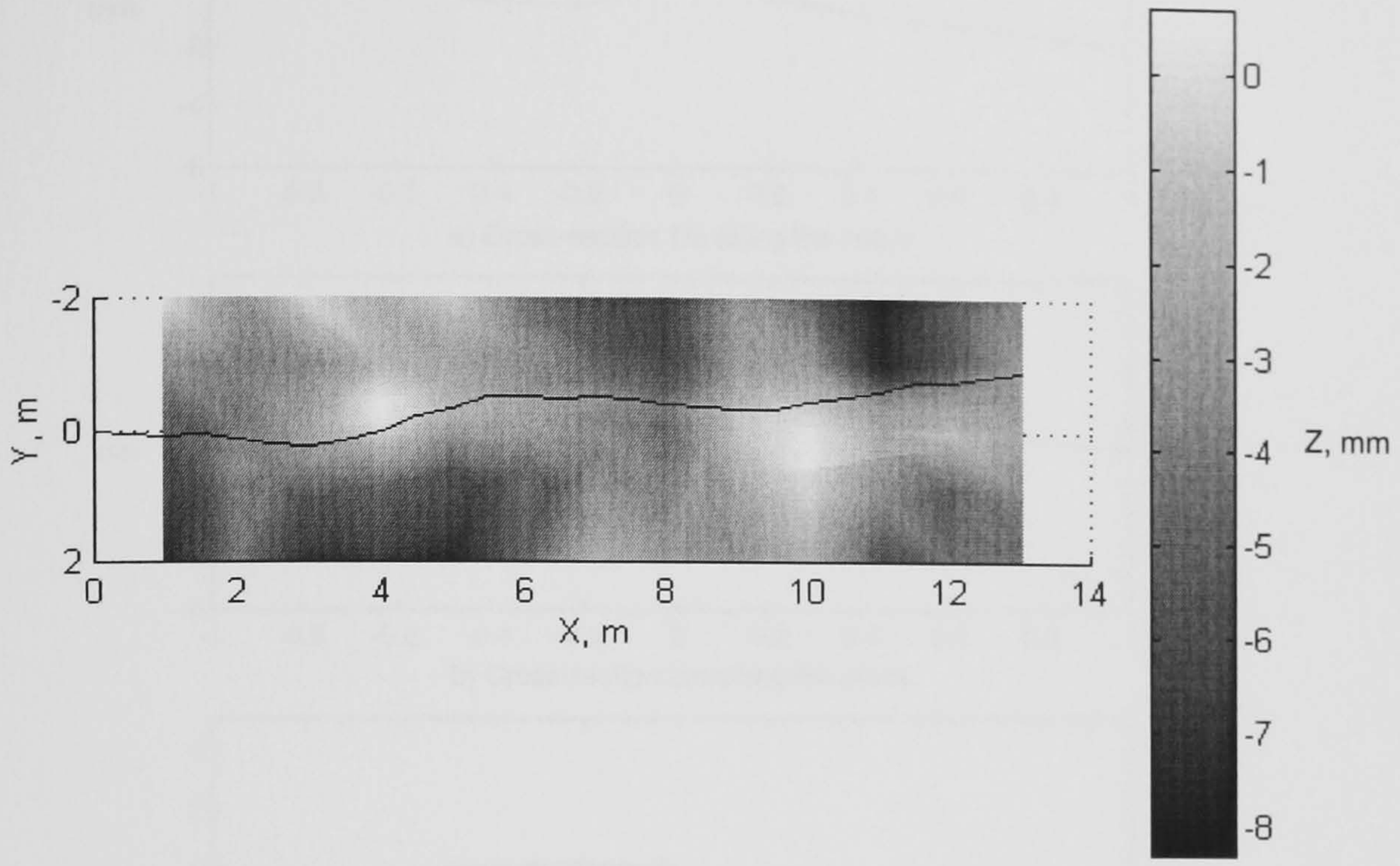

Figure 5.59 – Chepstow: Plan elevation of the precision level survey results showing crack A

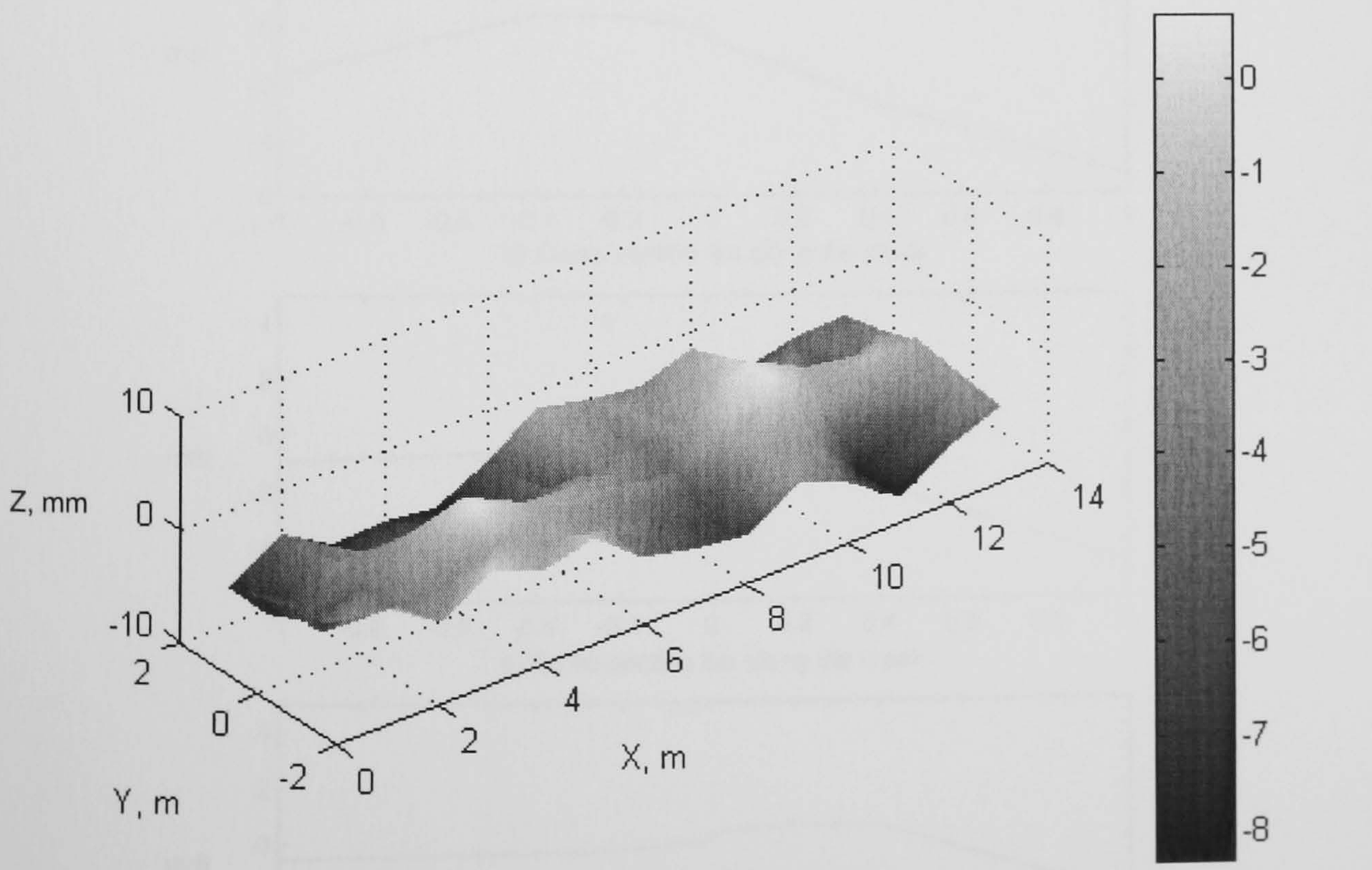

Figure 5.60 – Chepstow: 3D plot of the slab around crack A

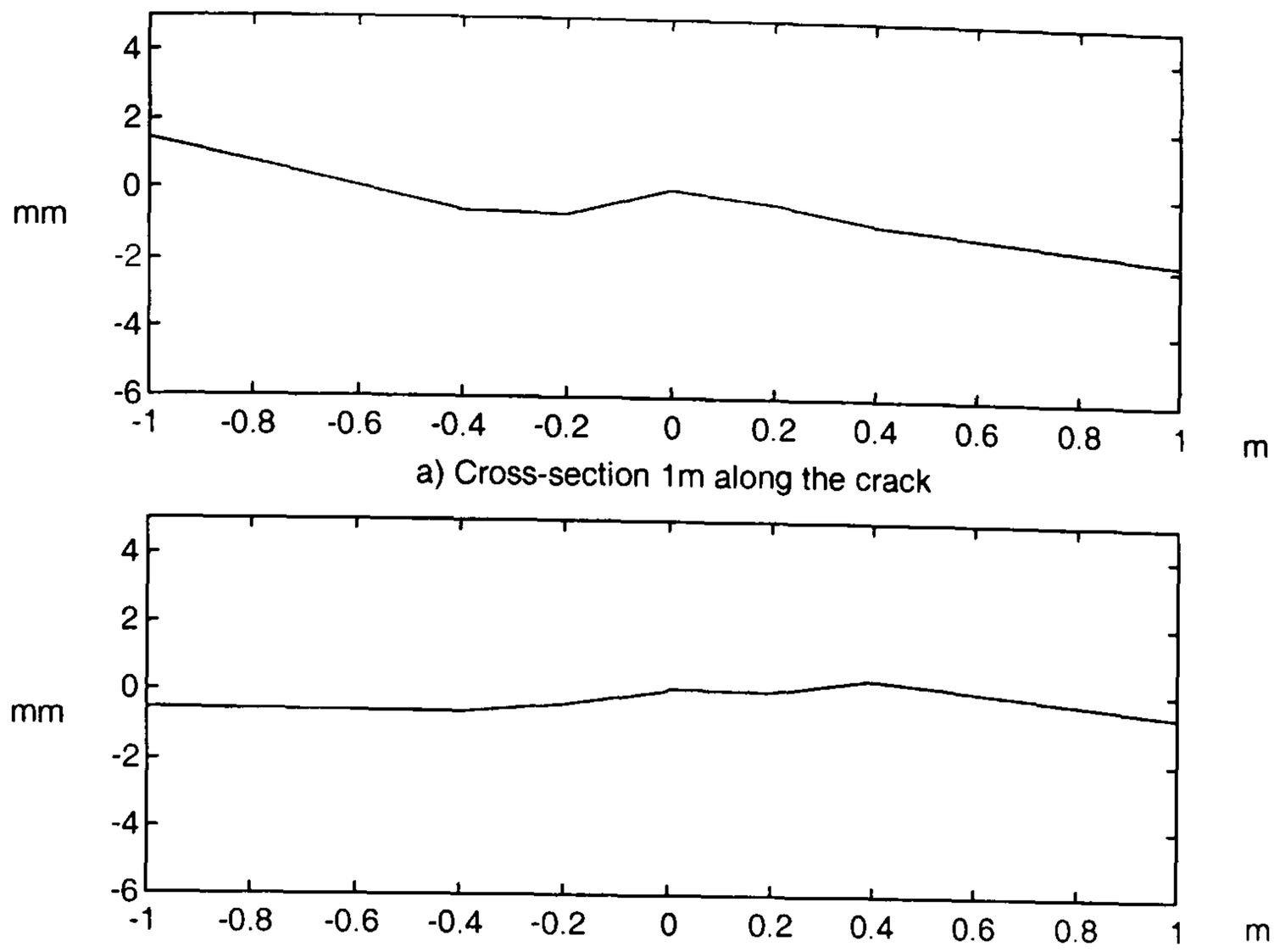

a) Cross-section 1m along the crack

b) Cross-section 2m along the crack

c) Cross-section 3m along the crack

d) Cross-section 4m along the crack

e) Cross-section 5m along the crack

f) Cross-section 6m along the crack

Figure 5.61 – Chepstow: Sectional views across crack A

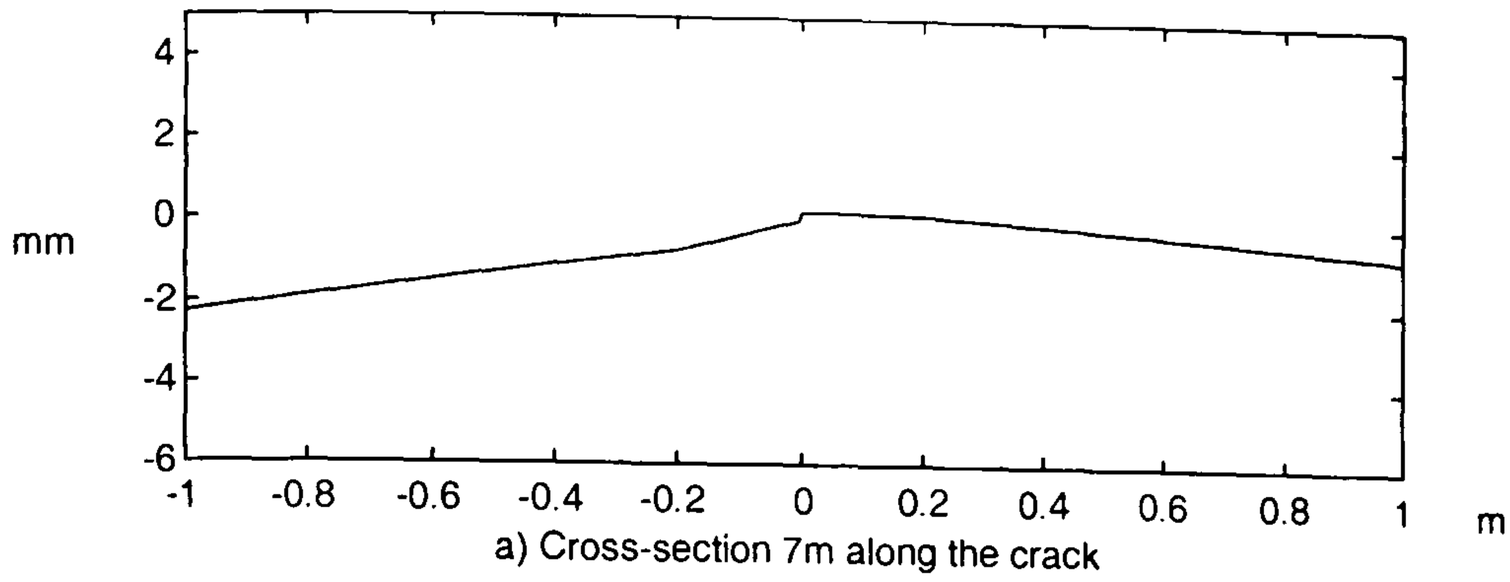

a) Cross-section 7m along the crack

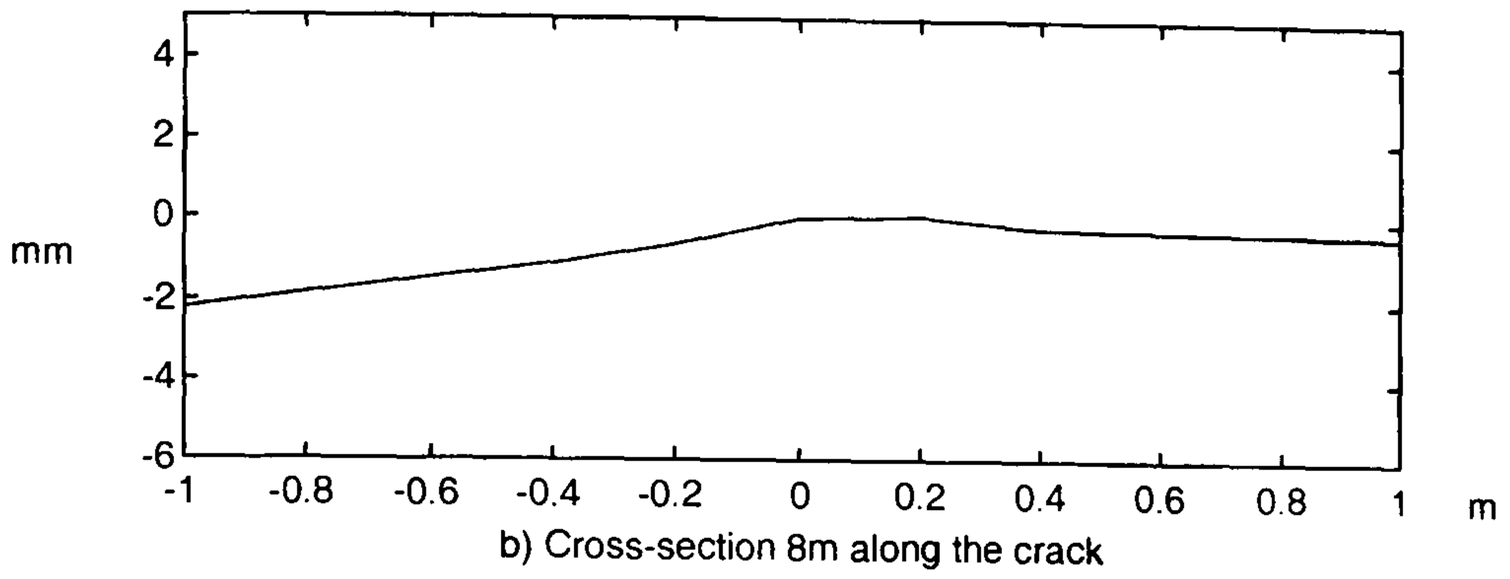

b) Cross-section 8m along the crack

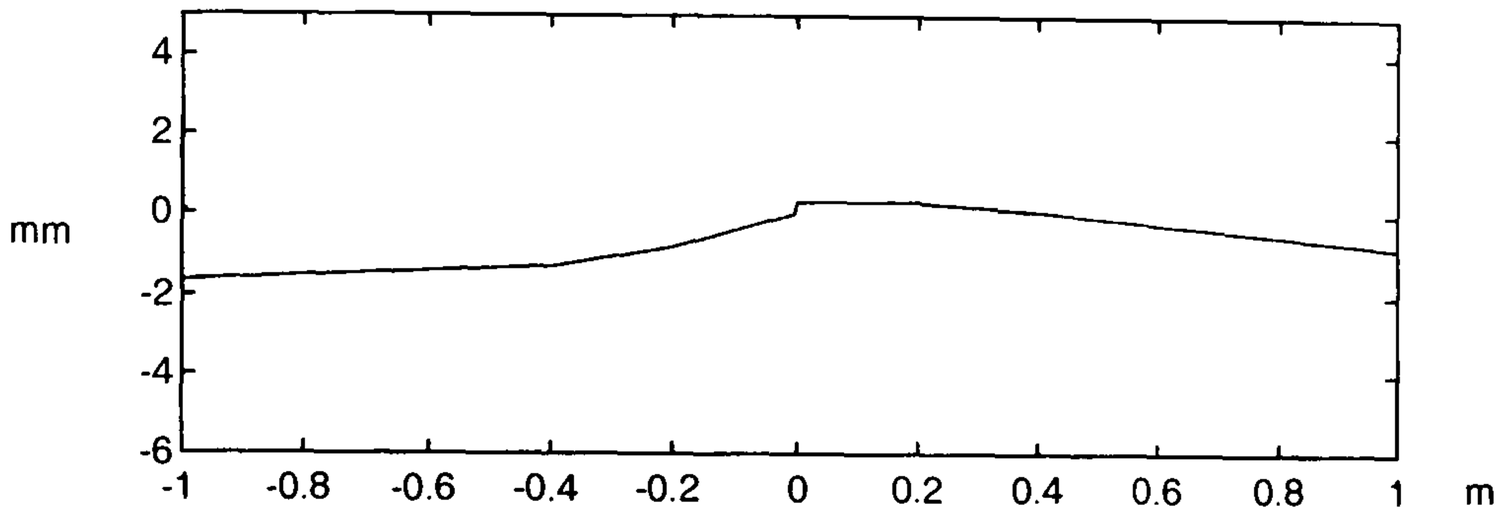

c) Cross-section 9m along the crack

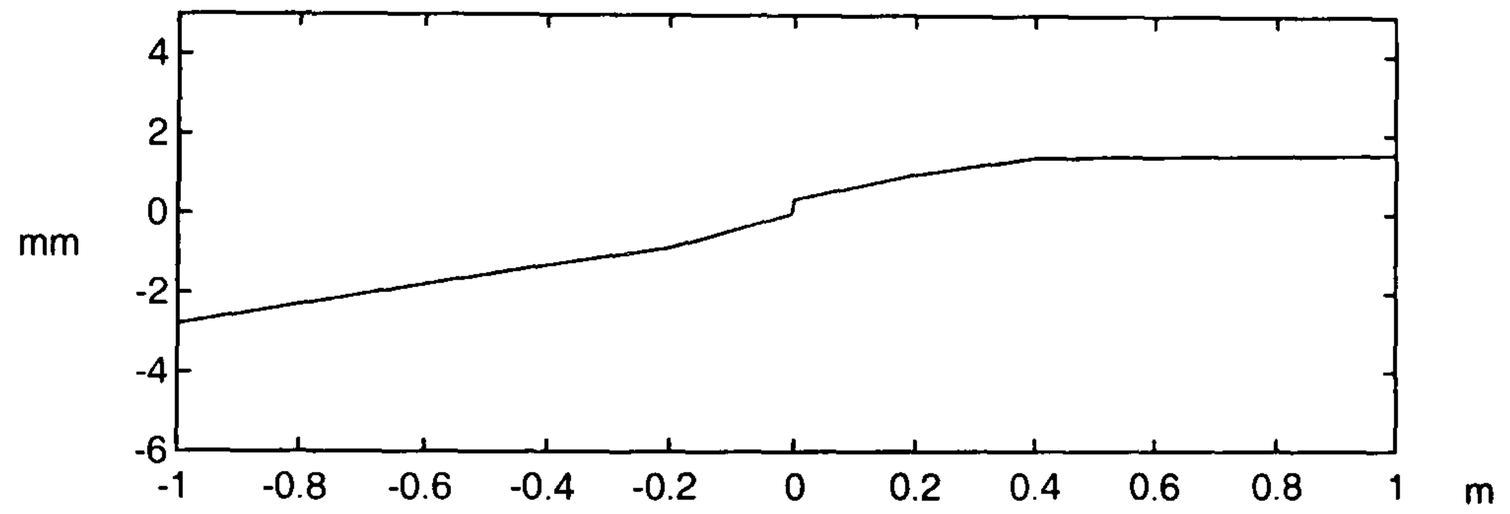

d) Cross-section 10m along the crack

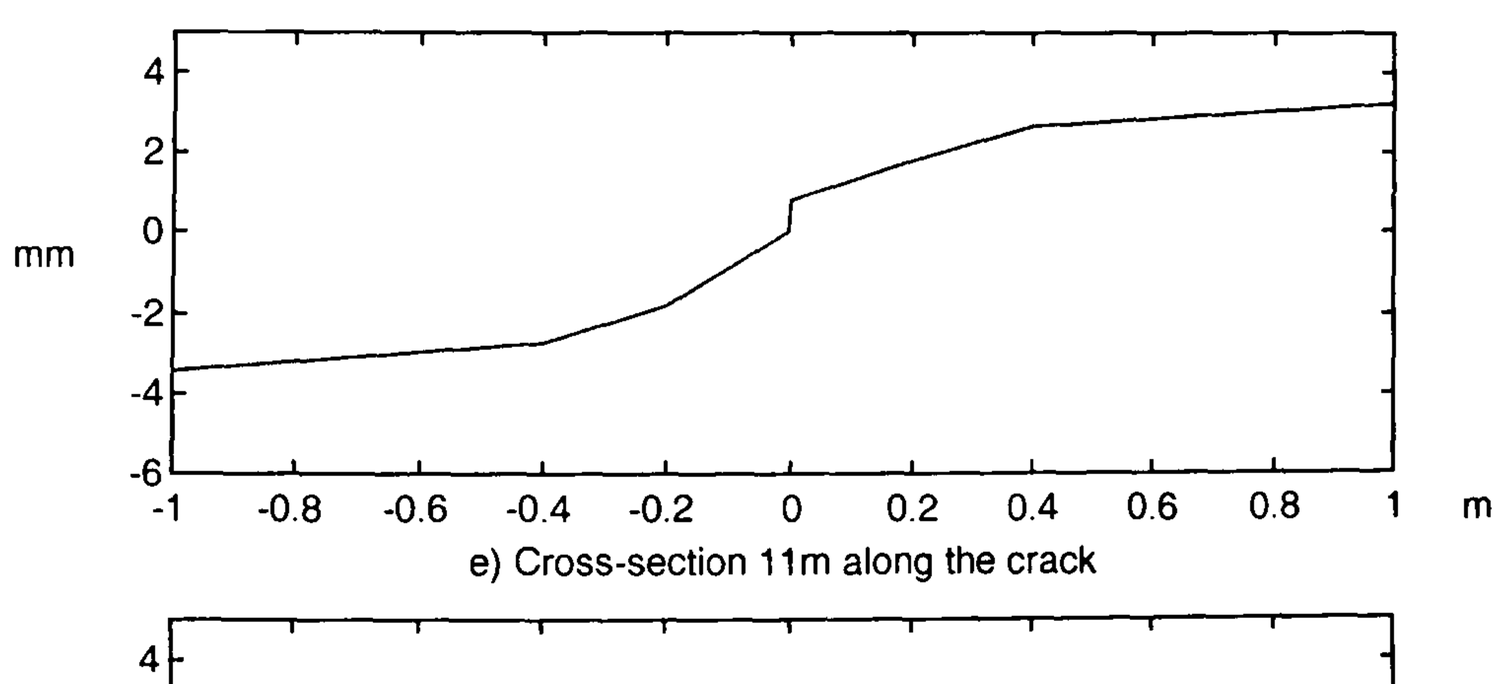

e) Cross-section 11m along the crack

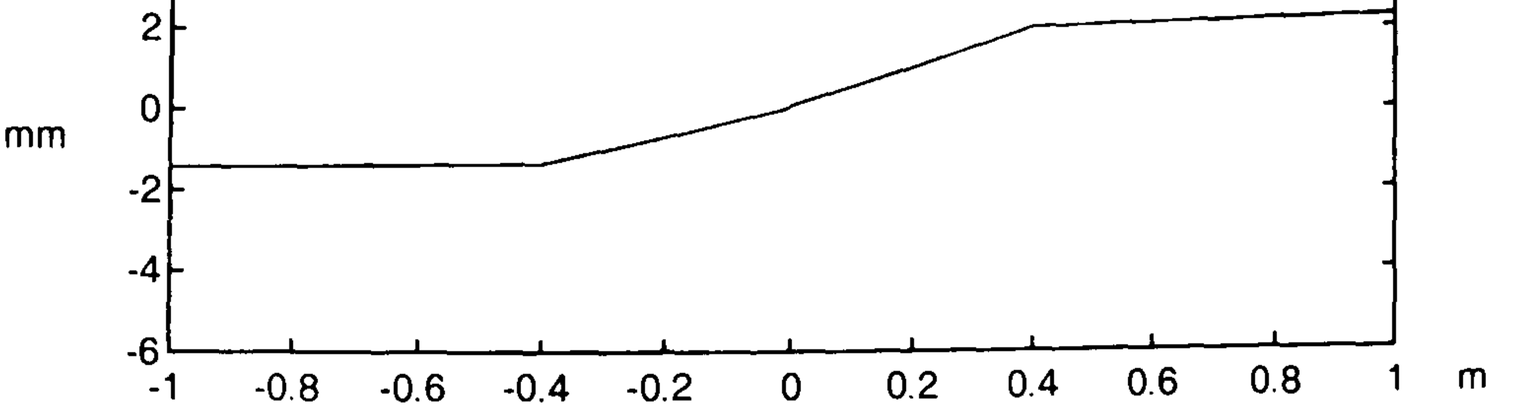

f) Cross-section 12m along the crack

Figure 5.62 – Chepstow: Sectional views across crack A

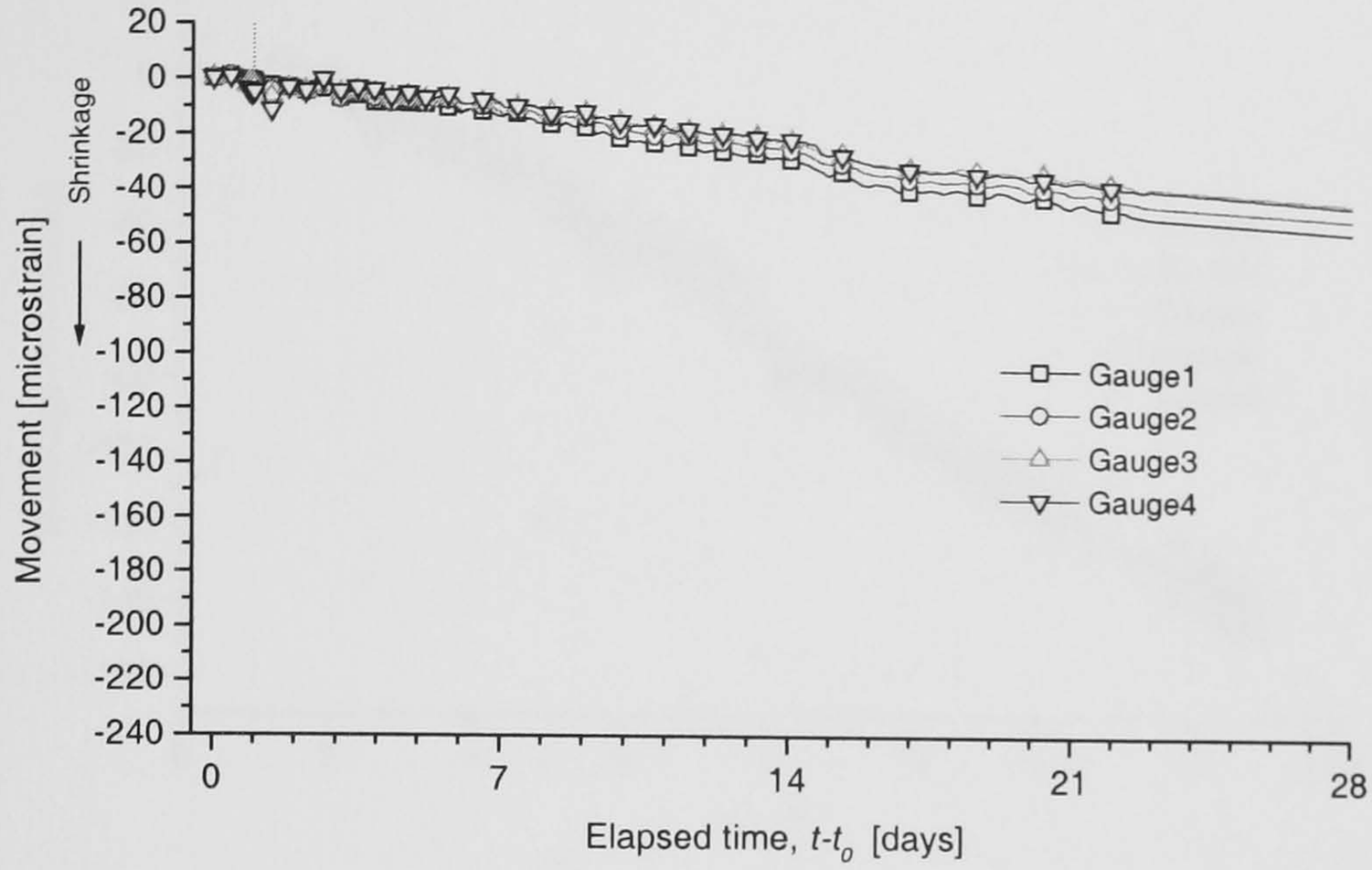

Figure 5.63 - Chepstow Pour 11: Concrete shrinkage strain

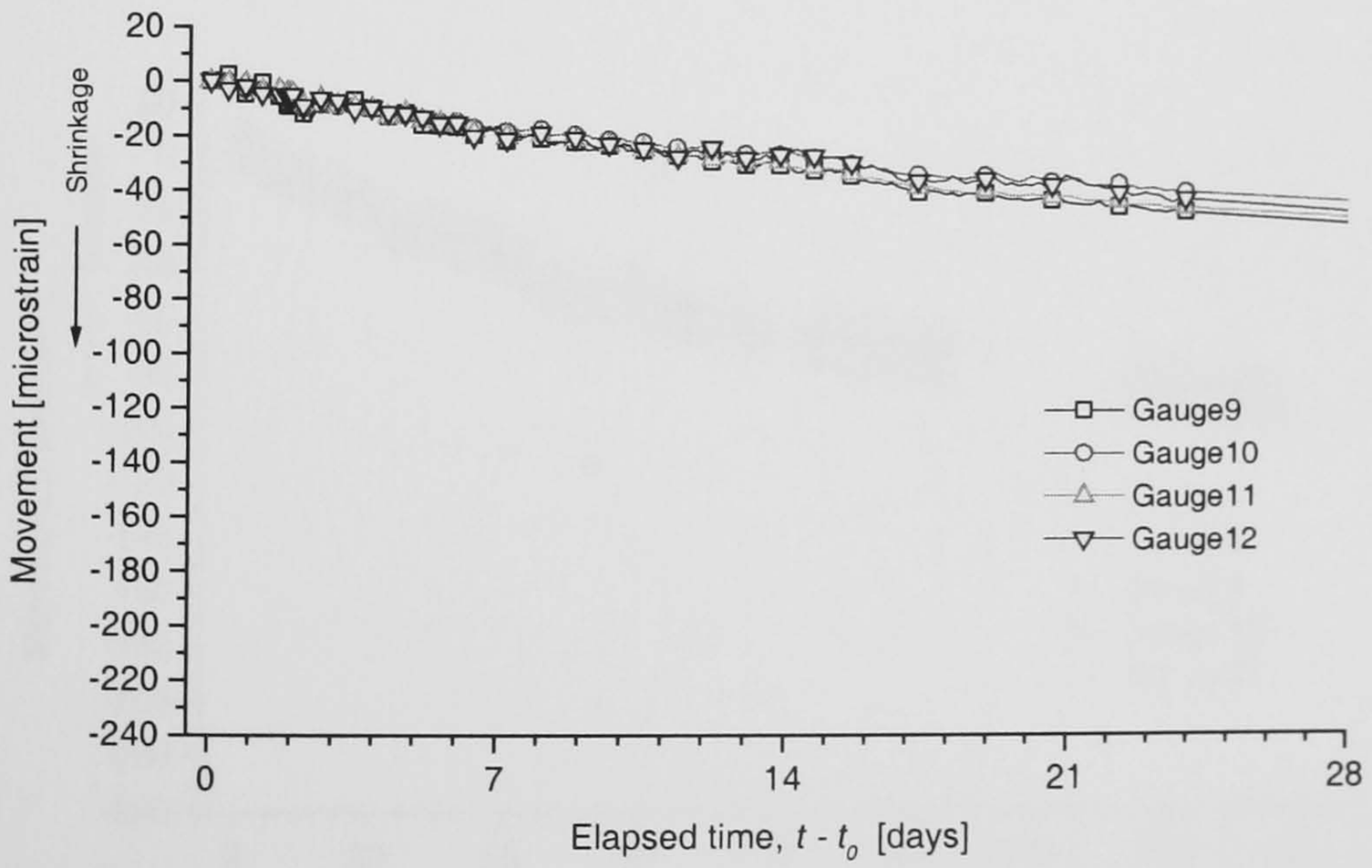

Figure 5.64 - Chepstow Pour 10: Concrete shrinkage strain

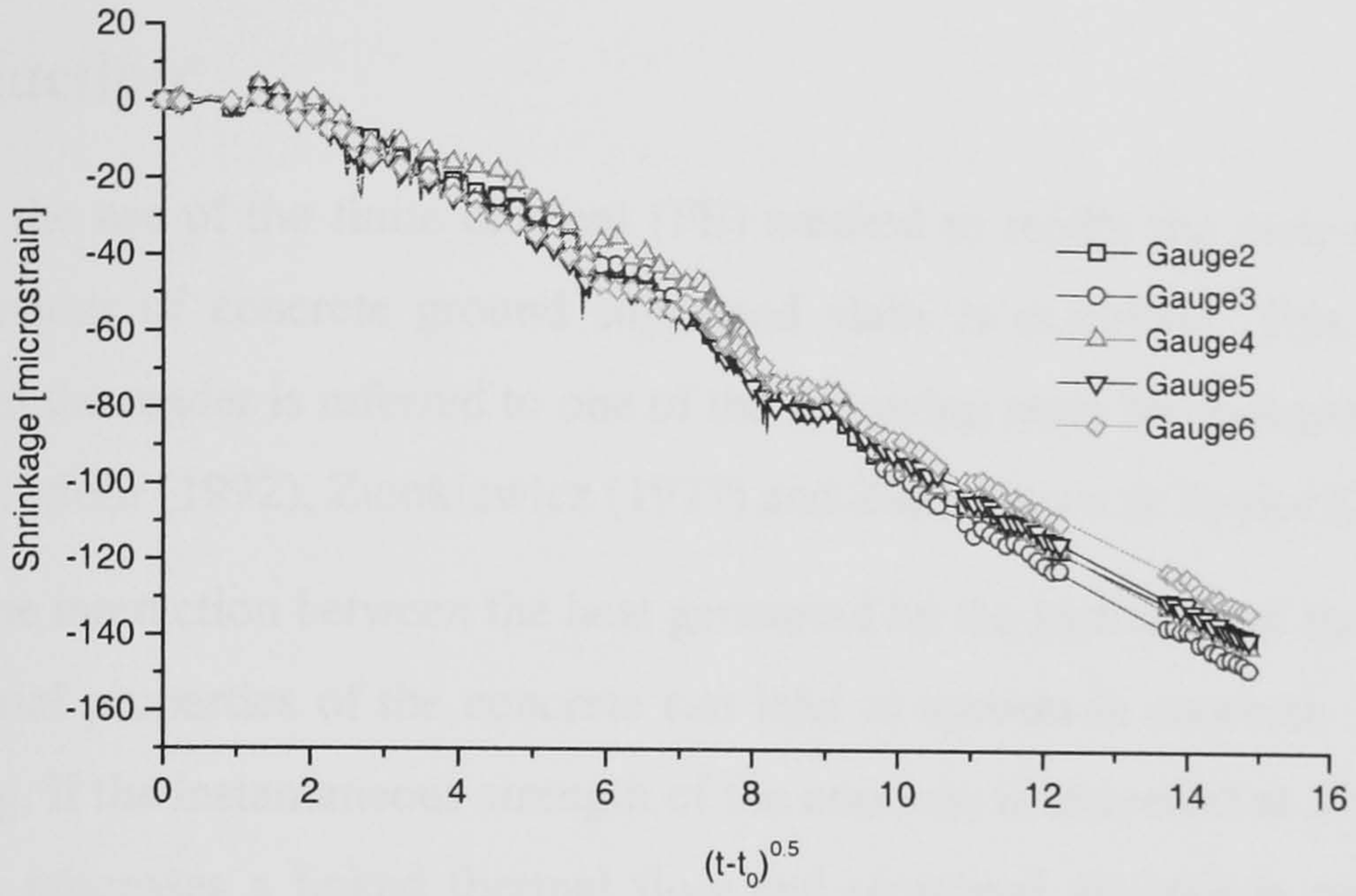

Figure 5.65 – Leeds Pour 1: Drying shrinkage behaviour

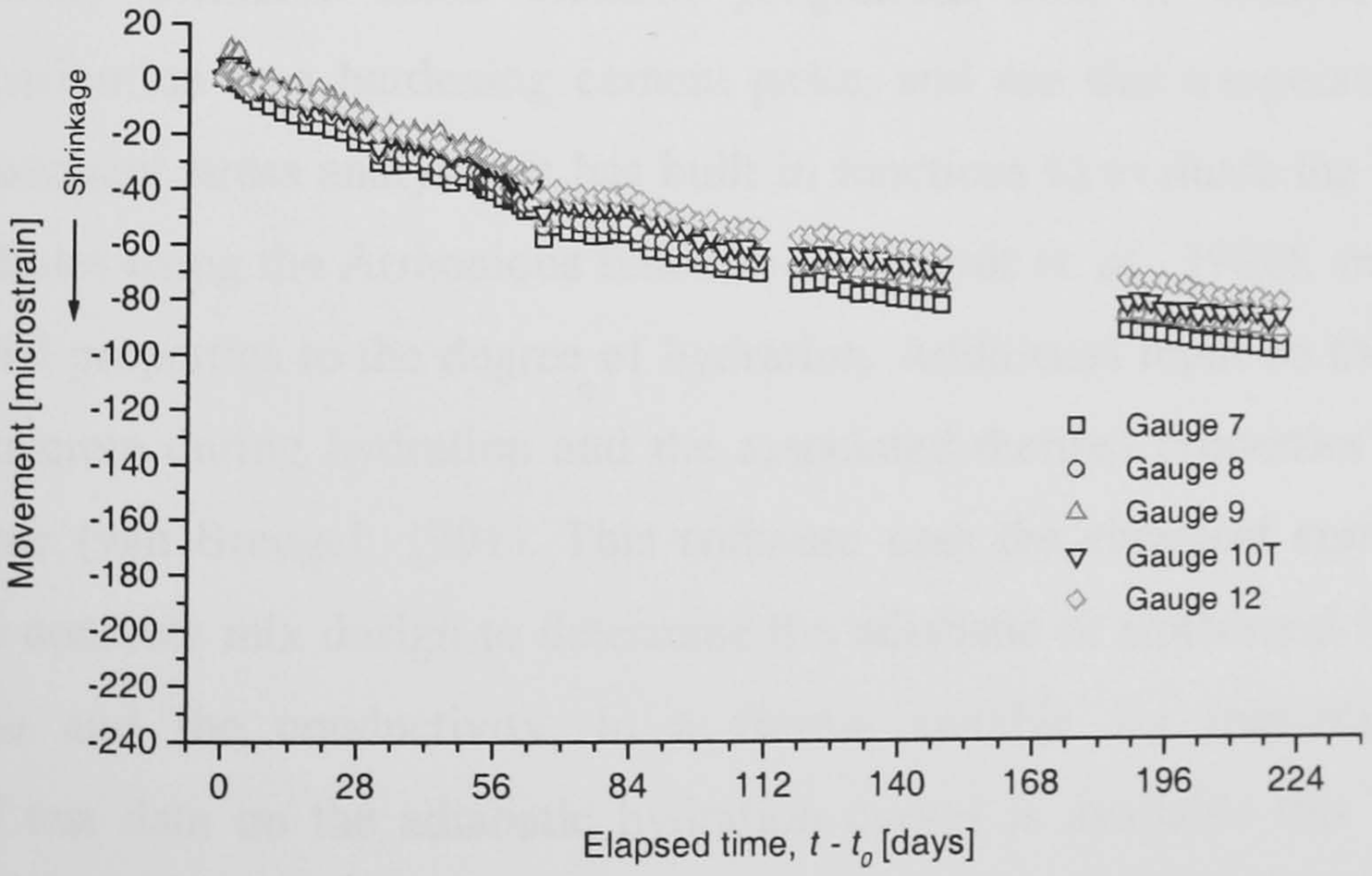

Figure 5.66 - Leeds Pour 2: Concrete shrinkage strain

6. Finite element modelling

6.1. Introduction

In this chapter the use of the finite element (FE) method to model the early-age thermal and structural behaviour of concrete ground supported slabs is described. This method is well documented and the reader is referred to one of the following texts for background information – Bathe (1982), Mohr (1992), Zienkiewicz (1977) and Zienkiewicz & Taylor (2000).

At early ages the interaction between the heat generated by the hydration of the cement and the changing material properties of the concrete can lead to tension in concrete. This in turn can lead to cracking, if the instantaneous strength of the concrete is exceeded at any point. In order to model these processes a linked thermal flow and structural analysis is required, with the outputs from the thermal analysis used as the inputs for the structural analysis.

The Diana finite element software (de Witte, 1999) was chosen for this analysis as it specialises in the early age analysis of concrete. This software has been developed by TNO Building and Construction Research in Holland since the 1970's, and still appears to be the only commercially available finite element programme able to analyse the early-age temperature distribution in a hardening cement paste, and use this temperature field as the input for a subsequent stress analysis. It has built in functions to evaluate the heat evolved as the cement hydrates using the Arrhenious function (Reinhardt *et. al.*, 1982), and can relate the concrete material properties to the degree of hydration. Additional input on the adiabatic heat evolution in concrete during hydration and the associated thermal properties can be derived using Hymostruc (van Breugel, 1991). This software uses the chemical composition of the cement and the concrete mix design to determine the adiabatic or isothermal hydration curve, the capacitance and the conductivity, in a format suitable for importing into Diana. Additionally if test data on the adiabatic hydration curves is available this can be used to further calibrate the output. Unfortunately, most tests carried out in the UK by the cement manufacturers are either isothermal or semi-adiabatic, making the data unsuitable for use with Hymostruc. Therefore, the calculated adiabatic hydration curves used in the finite element analyses were based on the average chemical composition data supplied by the manufacturers for the various plants around the UK.

Although structurally the system could be simplified to a slab resting on a frictional boundary (Pettersson, 1998), this would fail to account for the thermal interaction of the slab and the

supporting layers during hydration. For this reason, the sub-base and subgrade were modelled along with the slab. Equivalently meshed domains were required for both parts of the analysis to allow the transfer of data, although the structural elements had to be of higher order than the flow elements to maintain compatibility of the transferred thermal strains.

The data transfer was done automatically by the flow-stress module in Diana, which switched between 4 node quadratic elements for the thermal analysis and 8 node quadratic elements for the structural analysis. Compatibility in the boundary conditions was ensured by selecting the relevant group of elements for each analysis.

6.2. Thermal modelling

Thermal modelling was carried out to assess whether the thermal conditions within a hydrating concrete slab could be accurately predicted using published sources of material data. Critical parameters were the convection coefficients for the air-slab boundary, the material thermal properties, the adiabatic temperature rise and the ambient temperature (Truman et. al., 1991). Temperature readings were obtained from each of the slabs under investigation, with sensors at different depths in the slab in some cases. The slab at Leeds also had a thermocouple array extending down through the sub-base and into the subgrade to monitor the temperatures down to 800mm below the surface of the slab.

Tomlinson (1946a) showed that for a slab subjected to simple harmonic heating and cooling, as an approximation to the diurnal temperature changes, the daily temperature variation at a depth of 14in. (360mm) was 10% of that at the surface, whilst the variation was negligible by a depth of 25in. (635mm). Pufahl *et. al.* (1990) showed that 12ft (3.6m) was the depth at which soil temperatures were stable, although they were considering the annual behaviour in an outdoor, exposed location. Rees *et. al.* (1995) modelled a depth of 1.5m below the slab bottom when looking at annual thermal changes under a building slab in the UK.

At early ages the air-slab boundary conditions remain similar to the simple harmonic approximation. However, the slab also acts as an additional heat source as the cement hydrates. Truman *et. al.* (1991) analysed two 9ft (2.75m) high concrete lifts founded on soil layers 10ft (3m) and 20ft (6m) thick showing that the difference in temperature at the bottom of the concrete lift was less than 1%. The site data collected from Leeds shows that a temperature variation of several degrees occurred 800mm below the slab surface during the first couple of days after construction (Figure 5.7c), although as the slab thickness, and hence the heat generated, is significantly less than that considered by Truman *et. al.* a subgrade thickness of 1.6m topped by a sub-base between 150 and 200mm thick was modelled.

As with any thermal diffusion problem, the rate of change of temperature decreases with increasing distance from the heat source, making the model less sensitive to changes as the distance from the heat source is increased. Because of this the nodal spacing was gradually increased in order to minimise the computational effort required.

The relationship between element size and time step duration can limit the model accuracy in a diffusion problem, with Truman *et. al.*(1991) identifying the following relationship between the capacitance (C), conductivity (k), element size (ΔL) and step size (Δt):

$$\Delta t > \left(\frac{\rho \cdot C}{6k}\right)\Delta L^2 \qquad \text{equation 6.1}$$

There is no mention of this relationship in the Diana manuals, though the element sizes determined according to this relationship are generally not limiting in the case of ground supported slabs. For a 1 hour time step the concrete and sub-base elements could be up to 0.16m in size. However, in order to reproduce the thermal profile through the slab and sub-base the elements had to be much smaller than this. In fact, six elements were used in the slab, with a further six elements through the thickness of the sub-base, giving a maximum nodal separation of 0.038m in the direction of heat transfer (Figure 6.1).

The maximum element size used in the subgrade was determined as 0.2m by substituting the 4 hour time step used from 48 hours after construction until the end of modelling at 784 hours into equation 6.1. At earlier times the theoretical maximum element size of 0.1m for the 1 hour time step was exceeded, but not until almost 1m below the slab bottom. The larger element size at these lower depths at early ages was justified as site data had demonstrated that the temperature at a depth of 0.6m below the slab bottom did not alter during the first 24 hours. To further test the sensitivity of the model to the element size the nodal separations at all locations was halved. This was found to a have negligible effect on the predicted thermal profile.

Verification of the thermal model was carried out by comparing the results from the FE analysis with the data from Leeds, as temperature data was collected from the sub-base and the subgrade in addition to the slab (See Chapter 4.4).

The concrete material data was determined by Hymostruc, whilst the remaining material and air-slab boundary coefficients were varied within the ranges found in the literature in order to match the behaviour of the instrumented slab. The slab temperature was found to be sensitive to all of the material properties of the subgrade and sub-base, with increases in conductance and reductions in capacitance reducing the maximum slab temperature and vice-versa. The rate at which the slab cooled and the maximum temperature achieved were also affected by the convection coefficient chosen for the air-slab boundary.

In order to save time whilst carrying out this parametric study, the modelled domain was reduced to 2 elements wide with insulated boundaries at both edges to prevent horizontal heat flow. This approximation to a 1-D diffusion problem was reasonable because the slab under consideration was approximately 40m square in plan and only 225mm thick.

The material properties used in the first and the most accurate runs of the Leeds thermal model are shown below (Table 6.1), although the reader is referred to Chapter **2.7.10** for the sources of these values.

The output from the most accurate model can be seen in Figure 6.2 where very good agreement is seen between the measured and predicted temperatures at all times from 48 hours after construction. Up until this time the main difference arises in the prediction of the timing of the maximum temperature; with the maximum temperature recorded on site occurring approximately 11 hours later than that predicted by the model. Similar differences between model predictions and experimental data were found by de Borst and van den Boogaard (1994). However, they concluded that errors during the first 2 days were insignificant, so long as agreement during the cooling phase, when cracking was likely, was good.

Table 6.1 - Material properties for the first thermal finite element model

Material property		Initial value	Best value
Concrete	Specific heat capacity (J/kg.K)	Automatic[1]	Automatic[1]
	Conductivity (W/m.K)	1.76	1.76
	Density (kg/m^3)	2400	2400
Sub-base	Specific heat capacity (J/kg.K)	750	930
	Conductivity (W/m.K)	0.93	2.22
	Density (kg/m^3)	2000	2000
Subgrade	Specific heat capacity (J/kg.K)	1886	2000
	Conductivity (W/m.K)	1.2	1.5
	Density (kg/m^3)	2098	1500
Air – slab interface (W/m^2.K)		8.3	8.3
Slab – sub-base interface (W/m^2.K)		173	173
Sub-base – subgrade interface (W/m^2.K)		173	173

[1] Specific heat capacity is automatically determined according to the degree of hydration based on the output from Hymostruc.

Lachemi and Aitcin (1995) demonstrated with a finite element model that reducing the initial concrete temperature delayed and reduced the peak temperature. Although the measured initial concrete temperature was used in the current model, the degree of the delay which relates to the hydration behaviour of the cement, based solely it's chemical composition, has been underestimated. The fit of the model could probably have been improved had test data on the

adiabatic hydration curve for the concrete been available to input into Hymostruc. However, the intention was to asses the accuracy of the model without resorting to laboratory determinations of all of the material parameters.

Once the model had been calibrated against the data from Leeds it was further validated by comparison with the other instrumented sites. For these comparisons the material properties for the sub-base and subgrade were kept as previously determined leaving the only variables as the physical dimensions of the slab and the concrete parameters. In each case the measured site ambient temperatures were input to determine the rate of heat loss across the air-slab interface and the concrete parameters were determined using Hymostruc, according to the mix design and the chemical composition of the cement.

The comparison between the finite element predicted temperatures and the measured temperatures for the long strip slab (Figure 6.3) and the second large area pour (Figure 6.4) show good agreement at different times. The Northampton model initially under predicts the maximum temperature but gives very good agreement at later ages, whilst the Bedford model gives very good agreement during hydration with reduced accuracy as the slab aged. The overall fit of the data could be improved by adjusting the material parameters (for example by increasing the conductivity of the sub-base under the large area pour). However, this would negate the effort to assess the suitability of this technique as a design tool.

The impact of the site conditions can be demonstrated with reference to the data from Chepstow. The boundary coefficient for the air-slab interface controls the rate of heat exchange across the discontinuity in accordance with the mixed boundary formulation of equation 6.2 (Diana Non-linear Analysis Manual, de Witte, 1999)

$$qn = K(\phi - \phi_E) \qquad \text{equation 6.2}$$

where **qn** is the specific flux vector in direction **n** outwards normal to the boundary, K is the boundary conduction coefficient and ϕ and ϕ_E are the free boundary and environmental potentials respectively.

As an industrial floor is not exposed to direct sunlight and is distant from the roof of the building, radiative contributions will be small. Thermal exchange across the air-slab boundary is primarily achieved through convection, which is very sensitive to the air movement across the slab surface. Under still air conditions losses occur through natural convection; however, increases in air speed over the surface of the slab can lead to forced convection conditions resulting in much higher rates of heat loss. CIBSE in Table A3.4 (1999) gives the convection coefficient for losses upwards from a horizontal surface in still air as 4.3 $W.m^{-2}K^{-1}$, whilst Thelandersson *et. al.* (1998) proposed boundary coefficients of 7.7 and 13.5 $W.m^{-2}K^{-1}$ for air movement of 0.5 ms^{-1} and 2.0 ms^{-1} respectively. Figure 6.5 shows output from the Chepstow

finite element model demonstrating how the maximum temperature and the rate at which heat is lost to the environment are directly affected by this coefficient. The site data is from bay 10, which was constructed before the end wall and part of the nearest side wall had been completed, resulting in measured daily average wind speed movements in excess of 1.0 ms^{-1}.

Once the excess heat due to hydration has been lost to the environment the thermal changes in the slab are driven solely by the daily ambient temperature change. Because the thermal differential between the slab surface and the air is much smaller than during early hydration, the sensitivity to the air movement is much reduced resulting in very little variation between the different model predictions and good agreement with the measured temperature (Figure 6.6).

The Bedford, Chepstow and Leeds floor slabs were all constructed before the cladding had been completed, resulting in higher average daily wind speeds than the other sites. All three sites required the increased convection coefficients for the air-slab interface to get agreement between the model predictions and the site data.

Once the air-slab boundary coefficients had been corrected to represent the site conditions the good agreement between the site data and the model predictions indicates that the material properties determined from the parameter study of the Leeds data can be applied with good accuracy in models of other locations.

This finding allows the impact of this change in environmental conditions to be assessed. Exposing the slab to moving air reduces the maximum temperature in the hydrating concrete, which is beneficial, as it reduces the thermal contraction potential of the slab. More worrying is the more rapid drop in temperatures back to ambient levels. This occurs at a time when the concrete is still weak in tension and will increase the likelihood of cracking.

Once the initial heat of hydration has been lost the temperature variation in the slab, which is driven by the diurnal ambient temperature variation becomes much smaller. Figure 6.9 shows how over a 24 hour period the slab surface temperature varies by about 0.8°C, whilst there is no variation at a depth of 0.4m. The temperatures at lower depths are generally influenced only by seasonal temperature variations, though fluctuations lasting at least several days can have some impact.

6.3. Structural modelling

The structural modelling of the slab-ground system is a complex undertaking involving highly non-linear and time dependant material behaviour, the full analysis of which lies beyond the scope of this thesis. However, several models have been developed to allow comparison with the collected data.

A comparison of the stresses in a pavement subjected to wheel loads determined by a full 3D model and those from 2D plane strain and plane stress analyses was undertaken at the University of Texas (Kim *et. al.*, 2000). The plane stress model was found to give very good agreement with the full 3D analysis, whilst the plane strain model over-predicted the stresses by more than 15%. The only area where significant discrepancies between the 3-D and the plane stress approaches arose was in the strip 0.25m from the edge of the highway pavement. As this free-edge condition generally only exists at the very edges of industrial floors this limitation is not considered significant.

Eierle & Schikora (1999) used a plane strain analysis to assess the effects of restraint on concrete at early ages. Thermal problems are not well suited to plane strain implementation as the assumption of infinite thickness in the z-direction means that thermally induced stresses will always be greatest in this direction. To avoid this problem they had to make the tensile strength of the interfaces between the elements smaller than the tensile strength of the elements themselves.

In order to reduce the computational time required, and because of the similarities between the 3-D and the plane stress results, the 2-D plane stress simplification has been used here to model the structural behaviour of industrial ground floor slabs.

Initially models with constant material properties exposed to uniform and differential temperature changes were analysed. This allowed an initial assessment of how the slab could be expected to behave and allowed comparison, for example, of critical lengths under given thermal gradients with those determined from theory.

An 8m long, 160mm thick slab with an elastic modulus of 25 GPa resting on a sub-base with linear stiffness moduli (units, stress per unit length) k and k_s of 50 MN/m^3 (CBR 7.5%) and 250 MN/m^3 for the normal and shear directions respectively. A coefficient of friction of 1.0 was modelled. Because of symmetry only half of the structure needed to be input, with horizontal restraint applied to the centre line of the model. This model was first analysed with a negative temperature differential of 4°C applied to the slab – equivalent to a thermal gradient of 0.25 °C/cm - which gives a theoretical critical length according to Pettersson (equation 2.60) of 2.332m. The initial and deformed shape of the finite element model can be seen in Figure 6.10, showing the length of curled slab to be around 1.33m – a critical length of 2.66m, although some of this length has settled into the sub-base. The upwards movement of the corner node was 0.13mm, compared to a maximum vertical movement according to Rollings (equation 2.64) of 0.17mm. However, Rollings assumed a slab, resting on a rigid support. If the settlement of the slab into the sub-base is accounted for, the finite element model predicts a total movement of 0.15mm.

The maximum warping restraint stresses according to Pettersson (equation 2.67) were ±0.59 N/mm^2, whilst the finite element model predicts ±0.61 N/mm^2 – a difference of around 3%.

The model was then analysed with uniform temperature drops applied to the slab. Because of the high shear stiffness of the slab/sub-base interface a temperature change of 2°C was able to cause slipping for much of the slab. As the temperature drop was increased to 10°C in steps of 2°C the shear stress distribution along the interface can be seen in Figure 6.11. This shows how the shear stress increases linearly up to the point where slipping occurs; the reduction in shear stress as the distance from the line of symmetry increases is due to the redistribution of the ground pressure under the slab (Figure 6.12). This differs slightly from the stress distribution along the interface assumed in equation 2.1, where the shear restraint is assumed to be uniform and at the limiting value of 3.77 kN/m^2 at all points. However, the sum of the restraint is the same. With an applied temperature drop of 10°C, all elements bar that next to the line of symmetry had slipped. At this point the FE model predicted a tensile stress at mid-depth on the line of symmetry of the slab of 0.09 N/mm^2, which is the same as that predicted according to equation 2.1. Kiamco (1997) questioned the validity of this approach, given that the restraint is applied to the bottom face of the slab. This results in a much larger tensile stress at the bottom of the slab and a compressive stress at the slab surface. However, Pettersson (1998) demonstrated that because of the redistribution of the ground pressure under the slab, the maximum tensile restraint in a slab longer than 10m can be treated as centrically applied. Figure 6.13 shows a slight stress differential still exists at the line of symmetry for this 8m long slab, but there is no compressive stress as predicted by Kiamco.

The comparisons presented here demonstrate that very good agreement is obtained between the simple theoretical approximations and the more thorough finite element analyses for warping and longitudinal restraint. They also demonstrate that the stresses resulting from a differential strain change in the slab – such as caused by drying shrinkage – are greater than those caused by a uniform change of similar magnitude – such as caused by seasonal thermal effects. Additionally, whereas the stresses from the differential change are uniform for much of the slab length, those due to the uniform change increase with the distance from the free end.

Further structural models have been developed for comparison with the site data. These models do not present a new approach in the modelling of early-age concrete. Rather the approach proposed by de Borst and van den Boogaard (1994) is further developed by the addition of maturity dependant tensile strength, before being applied to the problem of the early age behaviour of ground supported floor slabs. Furthermore, the impact of changing the shear stiffness of the slab/sub-base interface and the inclusion of drying shrinkage has been analysed.

The temperatures, moisture state and material properties as a function of time or maturity were input to the structural model which aimed to predict the stresses in a 16m long section of slab. This represents the distance between the free movement joints in the instrumented long-strip slab at Northampton. Because of the symmetry of the joint arrangements, with free movement joints at either end of the 16m panel and a restrained movement joint mid-way along it's length, only 8m of the slab had to be modelled.

The constitutive material properties used in the finite element model cannot account for plastic shrinkage effects. However, Turton (1989) stated that plastic shrinkage cracking was not a problem for industrial ground floors in the UK. If the rate of moisture loss is not excessive (see Chapter 2.7.7) the assumption that the concrete begins to set in a stress free state seems reasonable (ACI Committee 207, 1987).

The development of the concrete elastic modulus was modelled by de Borst (1989) and de Borst and van den Boogaard (1994) amongst others using an empirical function (equation 6.3).

$$E_c(t) = E_0 \int_0^{r(t)} \left(\frac{T_0 + T(t)}{273} \right)^7 \cdot \left(1 - e^{\frac{-\beta(t-\tau)}{\left(\frac{T_0 + T(t)}{273}\right)^6}} \right) \mathrm{d}r(t) \qquad \textbf{equation 6.3}$$

where T_0 is the offset temperature relative to which the temperatures $T(t)$ are given, β is a delay factor, which was left at the default of 0.075 and E_0 was the initial concrete stiffness, which depended on the amount and type of cement in the concrete (van den Bogert *et. al.*, 1987; de Borst & van den Boogaard, 1994). E_0 is supposed to be defined in Reinhardt *et. al.* (1982), but no reference to equation 6.3 could be found in this paper and, despite personal correspondence with the authors of several of the papers and the suppliers of the software, it has not been possible to confirm this relationship. For this reason, the time-dependant elastic stiffness has been modelled using the maturity relationship proposed by De Schutter and Tearwe (1996) and discussed in Chapter 2.7.3 The start value of $r_0 = 0.22$ was determined according to equation 2.22 as the water/cement ratio for the Northampton floor was 0.47. Using the concrete maturity calculated in the thermal flow analysis, this gives an approximate age of 12 hours before the concrete material properties begin to evolve. This age was adopted by Eierle and Schikora (1999) who began their analyses from this time. The present study could not adopt this off-set start time because of the choice of the double power law to model the viscoplastic creep behaviour of the concrete as described in Chapter 2.7.5. Diana uses a Taylor series expansion for this function making it suitable for the analysis of early age concrete, but the series must be continuous from $t = 0$. The calculated values of the parameters ϕ_1, m and n for the concrete mix used in Northampton were 4.113, 0.295 and 0.182 respectively.

The development of the tensile strength of the concrete was modelled in a similar way to the elastic modulus using the maturity relationship given in Chapter 2.7.2.

Although the Poisson's ratio of concrete has been found to vary at early ages (Chapter 2.7.4), this material property cannot be related to the concrete maturity in Diana and has been left constant at 0.2.

Interface elements were used to model the structural interface between the slab and the sub-base. This allowed the shear stiffness of the interface to be adjusted, based on values determined by Pettersson (1998) and Timms (1963), to reflect the true behaviour of a compacted hardcore covered by a polythene slip membrane. Interface elements also allowed a coefficient of friction to be specified. However, the model became unstable when this was done, preventing convergence. This was believed to be due to ill conditioning of the stiffness matrix due to the large difference in stiffness between the concrete and the adjacent interface elements at very early ages. The omission of the friction cut-off to the shear stresses should not affect the results for the 16m section of slab as Petersson (1998), and Timms (1963) both demonstrated that a movement of around 1.2mm is required before limiting friction is reached. This means that a joint would have to open by more than 2.4 mm before limiting friction had been exceeded by the slab on both sides. The site data showed that the sawn free movement joint opening was less than 1.0mm after 28 days indicating that the slab movement on both sides of the joint was still being restrained by friction, thereby showing that this was a reasonable simplification for the model.

There is a large degree of variation in the shear stiffness parameters determined from laboratory testing. Because the true frictional behaviour is not bilinear, different methods are possible for assigning the value of the shear stiffness. Three different values have been used in the models - two as reported in Pettersson (1998); namely 10 MN/m^3 and 240 MN/m^3, representing flexible and stiff friction respectively, and 24 MN/m^3 as found by Timms (1963).

Varying the shear stiffness of the slab/sub-base interface had little effect on the slab movement; the change in interface stiffness between 10 and 24 MN/m^3 reduced the slab movement by less than 6%, and increasing the shear stiffness to 240 MN/m^3 only reduced the movement by 20%, although with each increase in the shear stiffness the difference between the top and bottom movement increased (Figure 6.14). All of the models over predicted the joint movement, even using the 4m active length found in the analysis of the site data. This is because less than a day following construction the stiffness of the concrete is higher than that of the interface – even with the stiff friction value. Therefore, as the concrete movement at early ages is thermally and hygrally driven the difference in interface shear stiffness will affect the restraint stresses in the slab, but will not prevent it from moving.

Although the Diana finite element software includes drying shrinkage models from various design codes the shrinkage data has been input in tabular form, having been determined externally according to the B3 drying shrinkage model (Bazant and Baweja, 1995a, b & c). This model was used as it allowed the dependence on the concrete composition as well as the environmental conditions to be accounted for, and had also shown good agreement with the site data. As with the other code provisions, this provides predictions of the mean shrinkage in a cross-section. Although this is suitable for determining the long-term behaviour of a structure where the interaction of different elements is considered, this approach does not allow the deformation and resultant stress profile in an individual section to be modelled.

As the slab was cast on an impermeable membrane the moisture loss is essentially one dimensional towards the surface. Therefore, because of the low hygral conductivity of concrete at early ages the strain measured by the embedment gauges at the bottom of the slab should not include much drying shrinkage. Figure 6.15 compares the measured and calculated strains for the top and bottom gauges at positions 5, 6 and 8, which are respectively 1m, 4m and 7m from the sawn free movement joint. Clearly the movement from the upper gauge is under predicted; however, good agreement is obtained with the readings from the bottom gauge. By comparison Figure 6.16 shows the results of the models run with drying shrinkage, where the agreement with the upper gauges is now much better.

This demonstrates that although it has not been possible to carry out a combined hygral and thermal diffusion analysis, the results from the models with and without shrinkage give good agreement with the site data for the top and bottom of the slab respectively. Although an oversimplification, this demonstrates that analyses may be performed using these two assumed moisture states to give reasonable predictions of the expected contraction from the top and bottom of the slab.

Because of the good agreement between the strains predicted by the finite element model and the site data, it is believed that the differences between the predicted and measured joint opening presented earlier are related to the distribution of the movement between the joints. As was demonstrated in Chapter 5.4.1 the joints in an industrial floor do not open evenly. This uneven opening is believed to be caused by localised variations in restraint leading to differing lengths of slab affecting the movement at each joint. Unfortunately, because it was not possible to collect movement data from the other joints in the long strip slab during the first 28 days, and no strain gauges were embedded in the next panel this cannot be verified.

The restraint stresses in the slab as it ages for positions 5, 6 and 8 are shown in Figure 6.17. During the first 2 days the initial temperature drops lead to tension in the bottom of the slab and compression in the top of the slab. This is more noticeable at position 5 as the movement at this location is greatest. The maximum calculated temperature during hydration was at mid-

depth in the slab, and this leads to the greatest thermal contraction on cooling. After 3 days, as the slab temperature reached ambient levels, the highest tensile stresses are at mid-depth in the slab, although a further non-uniform stress distribution due to the eccentric frictional restraint is apparent at position 5.

The effects of the eccentric restraint can be seen to reduce as the distance from the free end of the slab increases, with there being little apparent difference between positions 6 and 8. This is as predicted by Pettersson (1998) and demonstrated previously with the simplified model of a slab subjected to a uniform temperature change.

The stress distributions discussed so far do not take account of the non-uniform drying shrinkage in the slab. Thomlinson (1940a & b) and Pettersson (1998) both found that the stresses arising from these non-uniform strain changes were normally significantly larger than those resulting from uniform strain changes.

The stress distribution in a 260mm thick floor resting on a sub-base with a modulus of sub-base reaction k = 50 MN/m^3 (CBR = 7.5%) and exposed to an ETG of 1.1 °C/cm, as measured in the long strip slab at Northampton after 370 days, is shown in Figure 6.18. This stress distribution has been calculated using frictional interface elements and the gap criteria to prevent tensile restraint to vertical movement. An age adjusted elastic modulus of 9.8 GPa was used to allow for creep effects. This assumes the curling began one week after the slab was constructed and took the whole year to develop the strain gradient.

The maximum tensile stress of 1.59 N/mm^2 is very similar to the value of 1.49 N/mm^2 calculated in Chapter 5.4.5 based on the differences in strain gradients from near to the joints and midway between them. The frictional restraint is shown to reduce the compressive stress in the slab bottom to 1.28 N/mm^2 (Figure 6.19). The predicted vertical movement produced by the strain gradient is 1.7 mm, which compares to measured mean vertical movement of 3.6 mm and 2.7 mm for the restrained movement joint and the free movement joint as determined by precision level surveys. This predicted movement is based purely on the elastic deformation of the sub-base and takes no account of the long-term settlement which will occur under the slab and increase the magnitude of the deformations. This can be demonstrated by reducing the subgrade modulus in the model – a value of 10 MN/m^3 (CBR = 1%) gives a vertical differential movement of 2.1 mm. This change in subgrade modulus changes the warping restraint stresses in the slab by less than 1%.

6.4. Summary

In this chapter the development of several finite element models for predicting the behaviour of concrete industrial floor slabs has been discussed. It has been shown that using the material

properties in the literature and data supplied by the cement manufacturers it has been possible to model accurately the temperature changes both in the slab, and in the underlying layers during the first 28 days after construction.

The models have allowed the impact of the ambient conditions at early ages to be assessed. Increased air movement has been demonstrated to reduce the maximum temperature in the slab slightly, but, more significantly, this accelerates the rate at which the temperatures returned to ambient levels. As this occurs at a time when the concrete is still gaining in strength this will lead to an increased risk of cracking.

Simple structural models have demonstrated that a full FE analysis is not required to determine the effects of differential strain gradients on a slab. Petersson (1998) and Rollings (1993) offer equations which give very good agreement with the finite element predictions of slab movements and restraint stresses.

The eccentricity of the frictional restraint in industrial floors has been shown to be negligible away from the end sections of a slab. Given that the frictional restraint increases with distance from the free end, and generally only becomes significant with joint spacing > 10m, this eccentricity can safely be ignored in design.

The finite element models indicate that the maximum tensile stresses at early ages may actually be at mid-depth in the slab. For this reason the crack control reinforcement in industrial ground floors may also be better placed at mid-depth, rather than in the slab bottom. Not only would this reinforcement be in the most highly stressed part of the slab, making it *proactive* (in the words of Kiamco, 1997) in controlling the spread of cracks but, because of the reduced cover to the top of the slab, this would also improve its effectiveness in controlling crack widths.

The finite element model of the long strip slab exposed to an ETG of 1.1 °C/cm over a period of a year predicted stresses which were very similar to those calculated from the site data. The close agreement between the finite element models and the simplified expressions means that good agreement would also, therefore, be obtained from the simplified approaches. This indicates that designers could now make some allowance for the intrinsic stresses in a slab resulting from warping restraint.

The stresses resulting from a uniform contraction have been shown to be significantly less than those which result from a differential contraction. This means that in the longer term, when warping and frictional restraint are accounted for, it is likely that the maximum tensile stresses in a slab will occur at the slab surface.

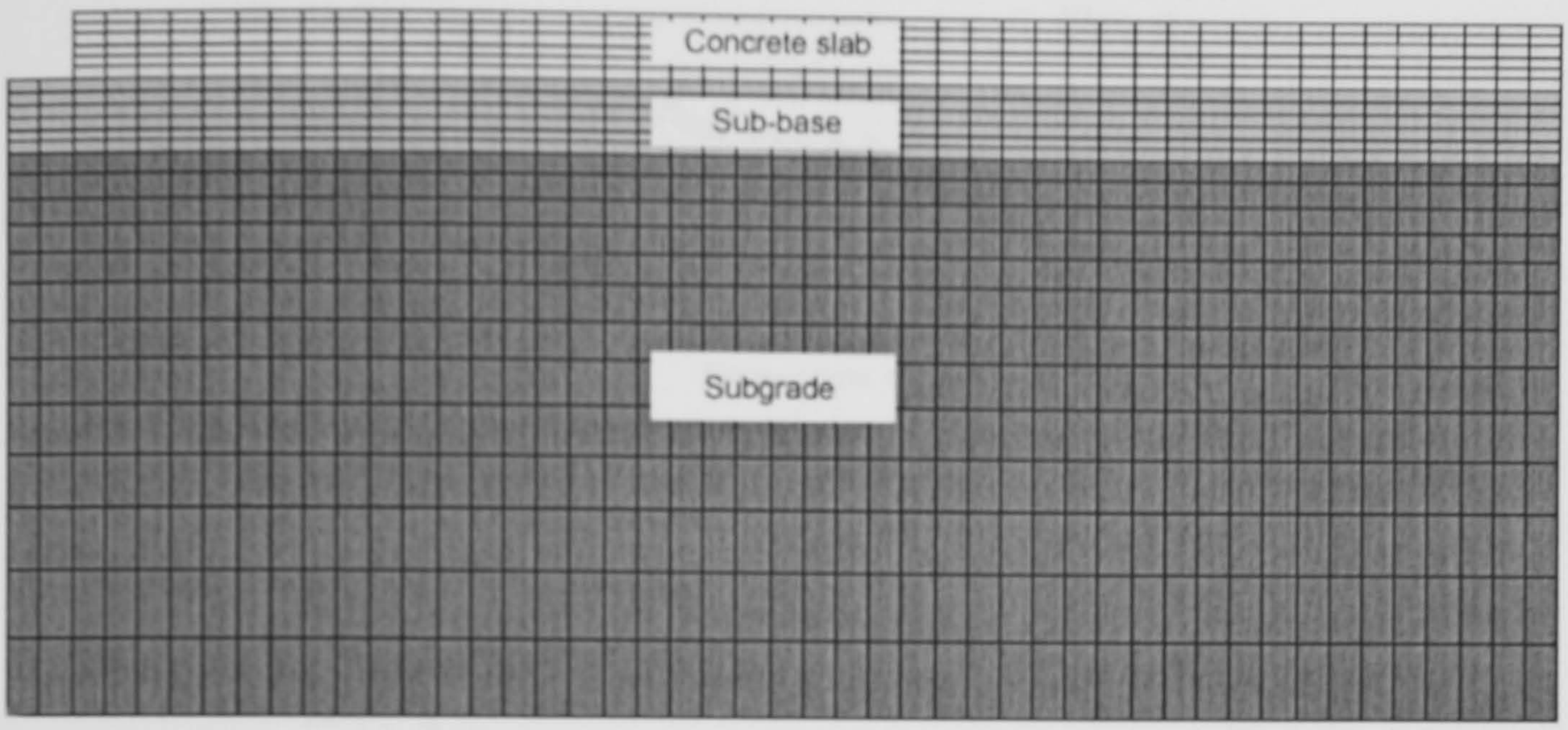

Figure 6.1 – A finite element model of the slab-ground system.

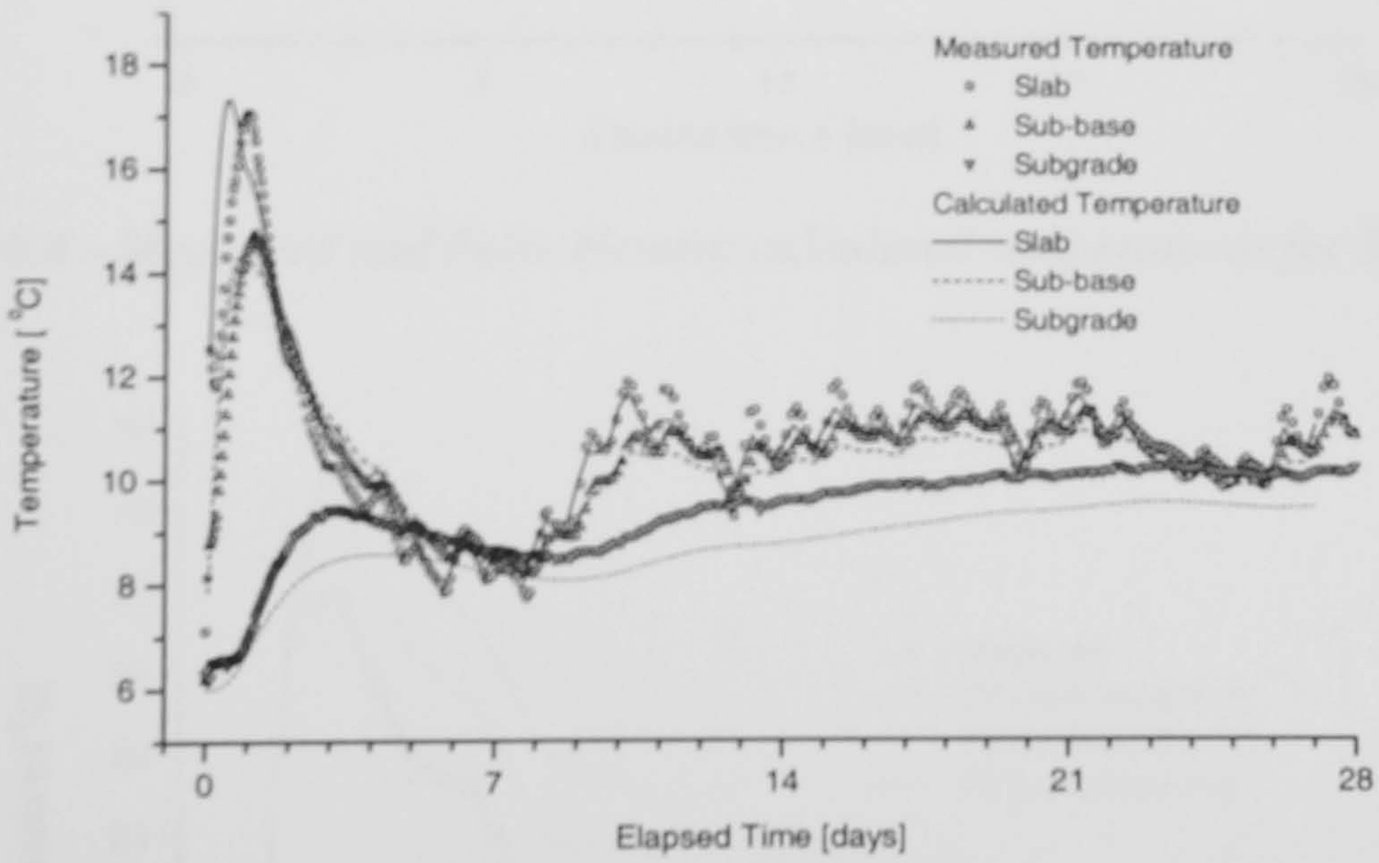

Figure 6.2 – Leeds: Comparison of the best model with measured data

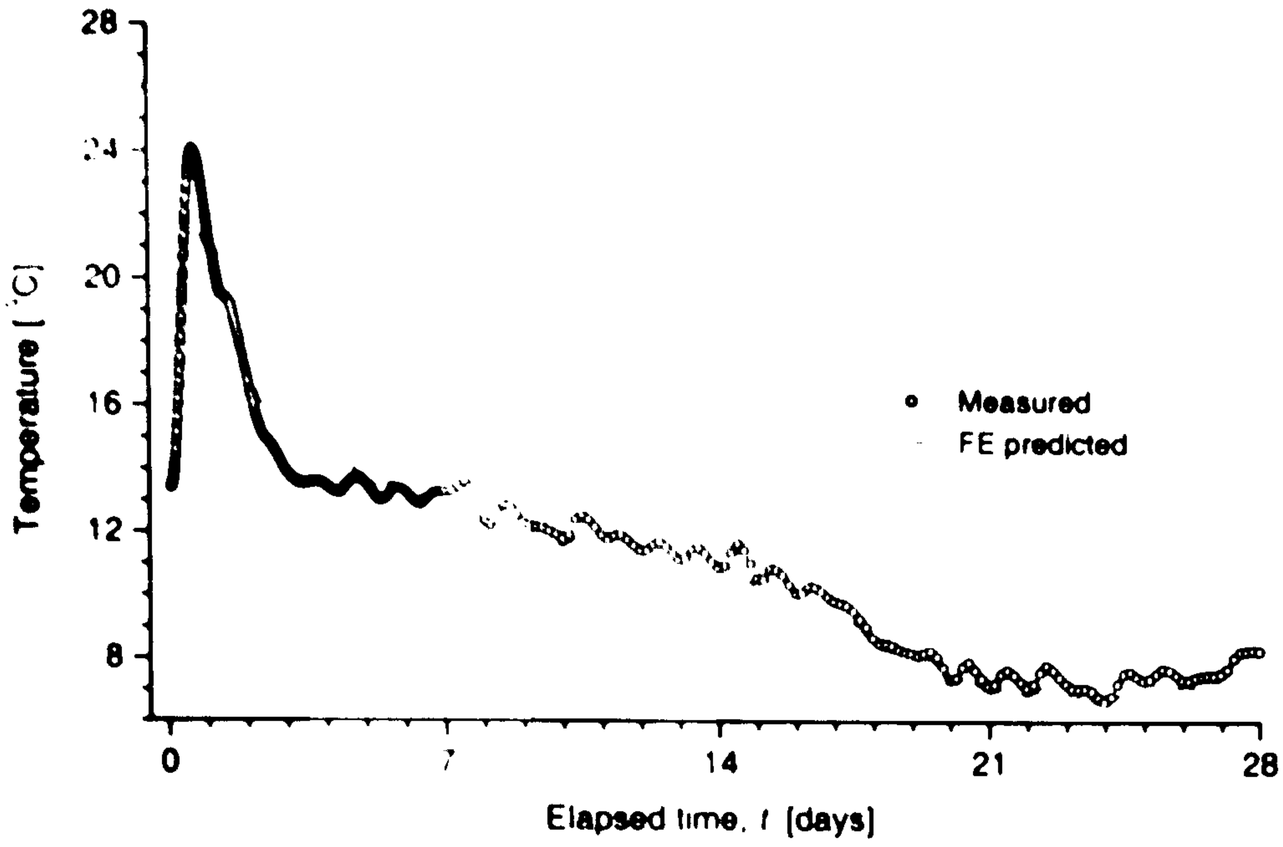

Figure 6.3 - Measured and finite element calculated slab temperatures for Northampton

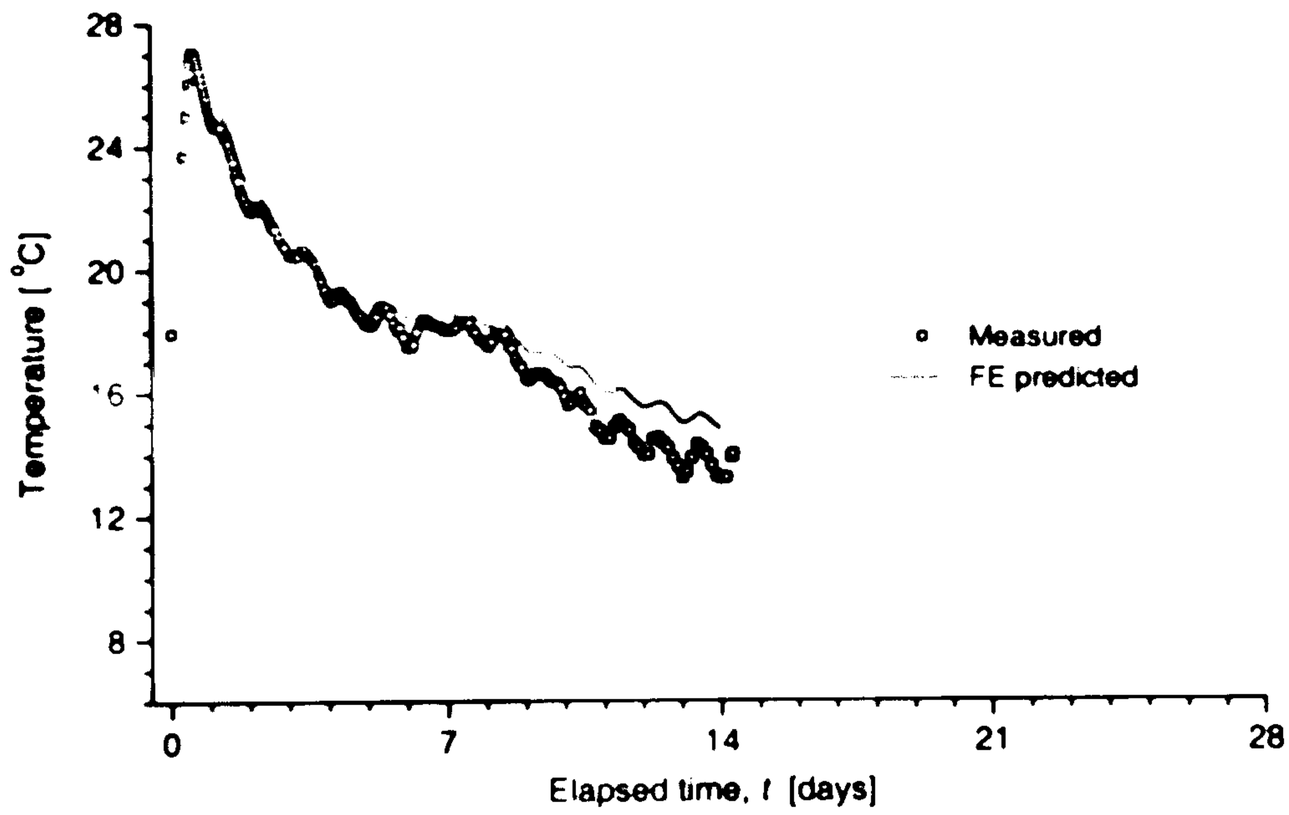

Figure 6.4 - Measured and finite element calculated temperatures for Marston

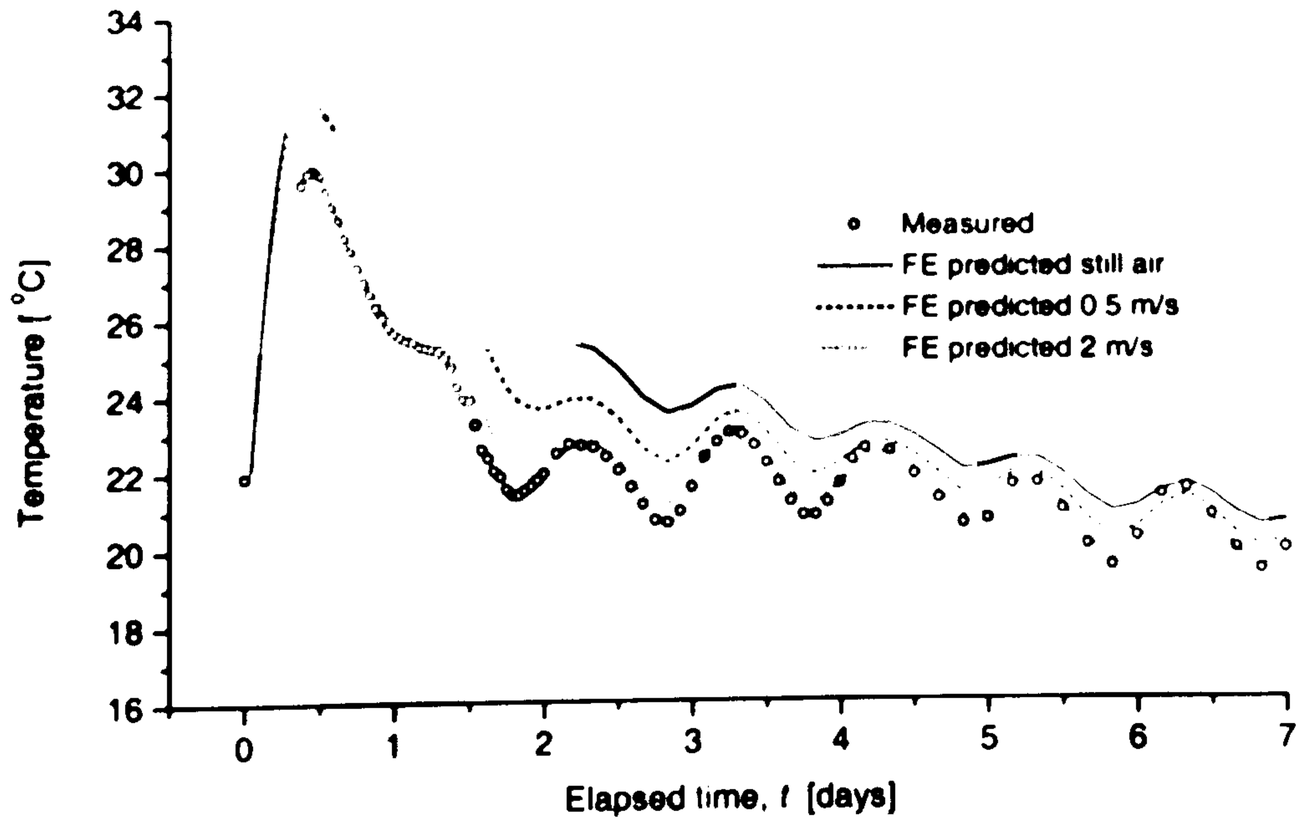

Figure 6.5 – Comparison of early-age measured and predicted temperatures from Chepstow

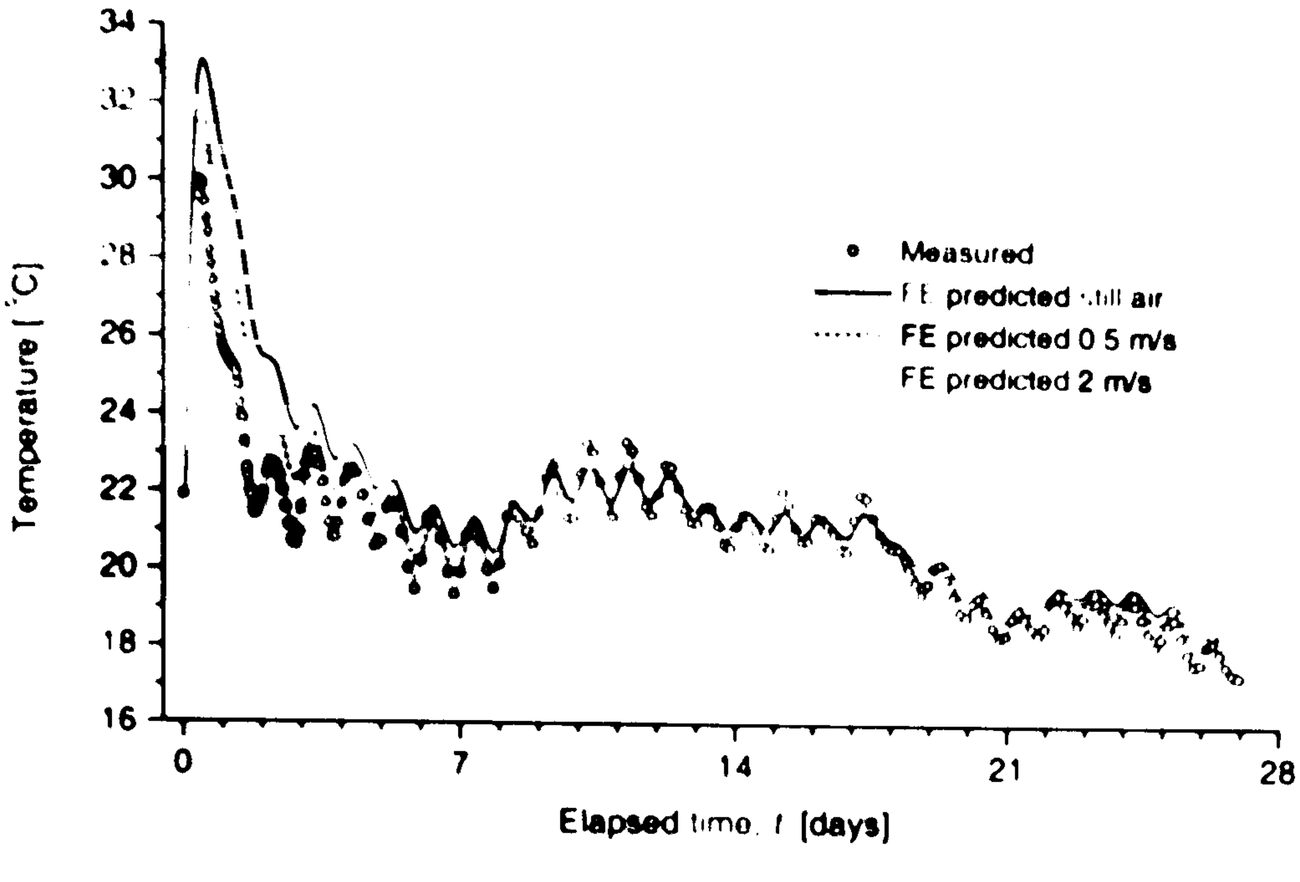

Figure 6.6 Theoretical and measured temperatures from Chepstow

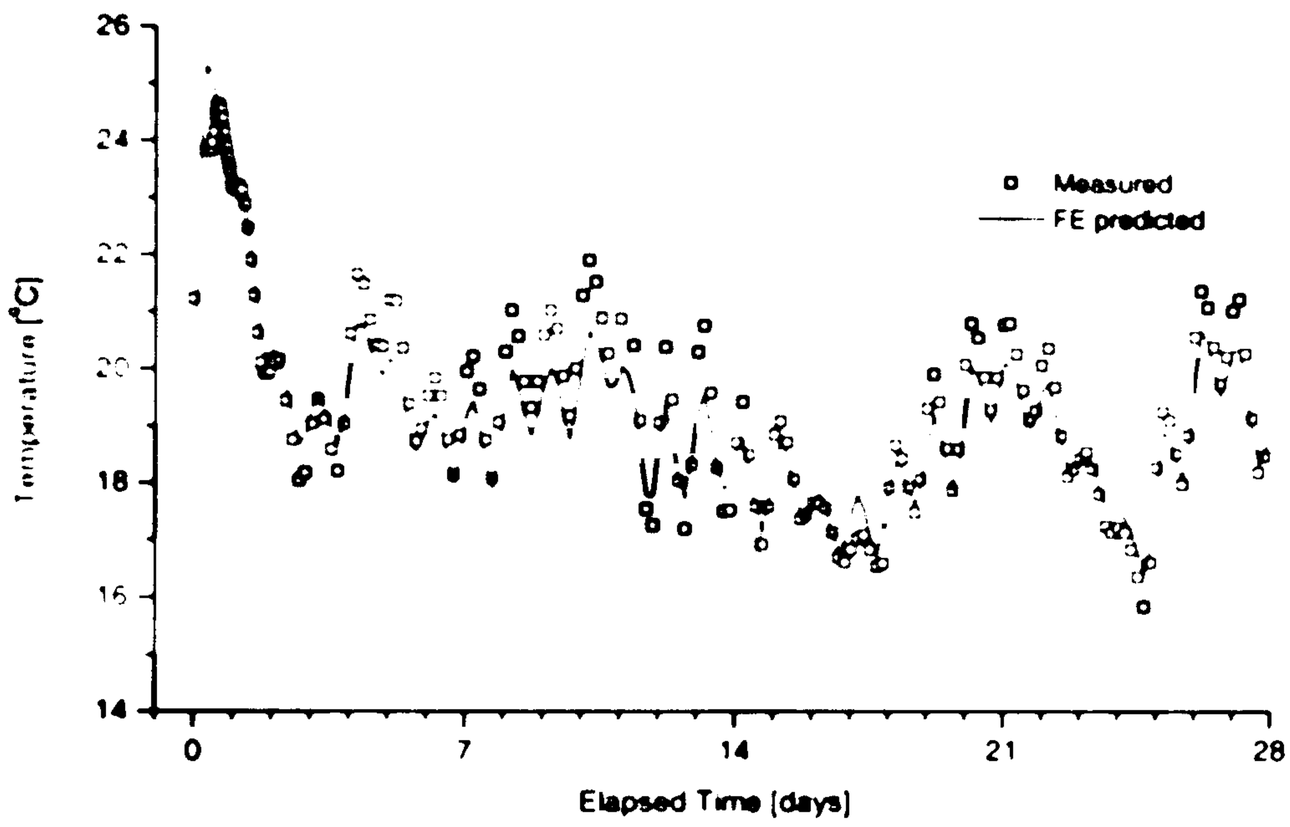

Figure 6.7 - Comparison of finite element and predicted temperatures for Bedford

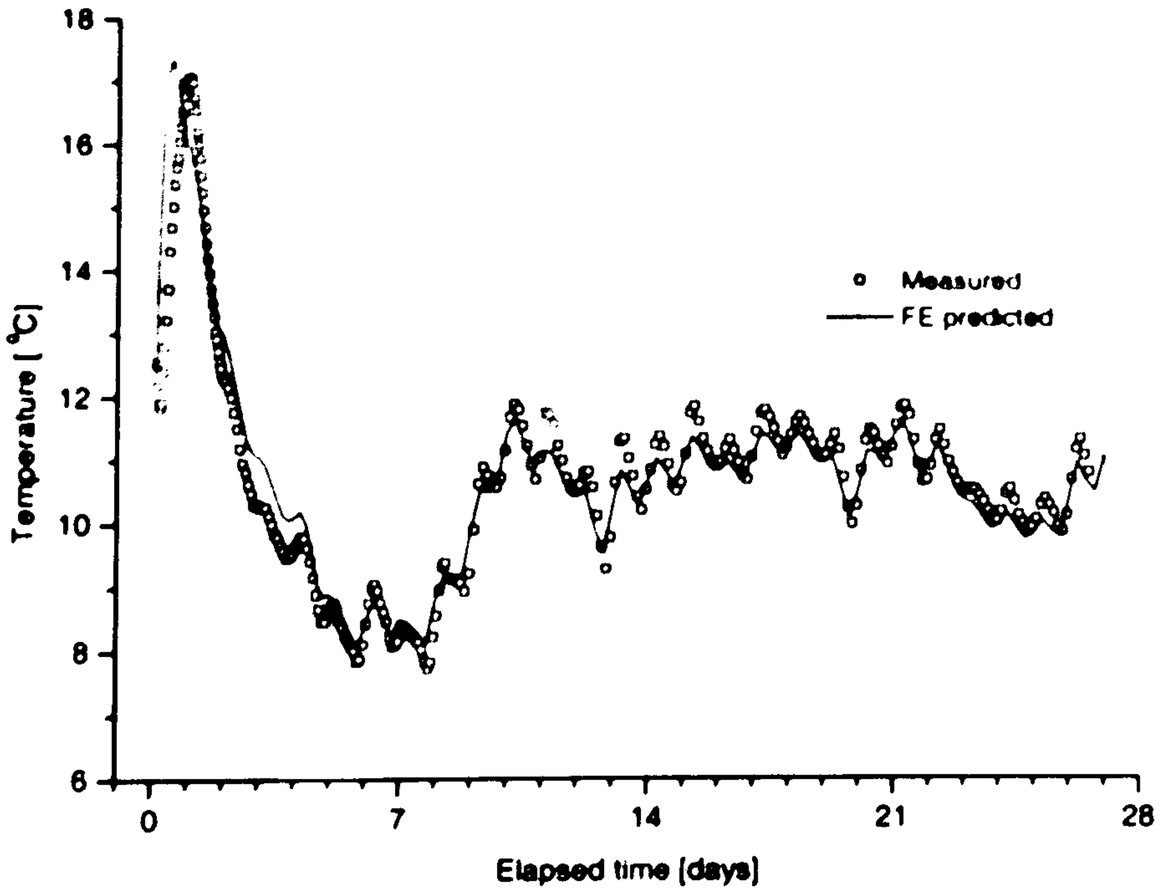

Figure 6.8 - Comparison of finite element and measured temperatures from Leeds

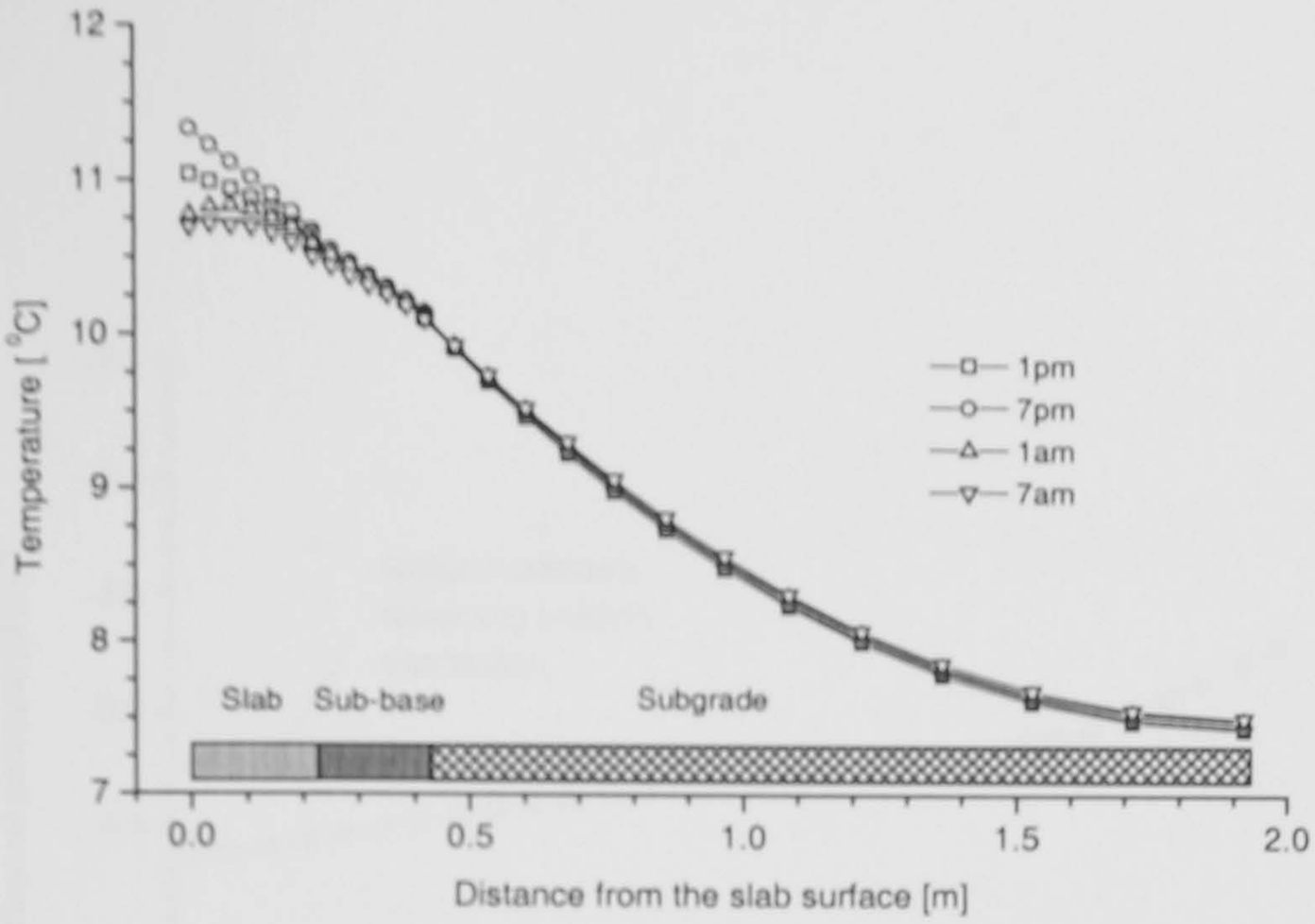

Figure 6.9 - Thermal profile through the slab system

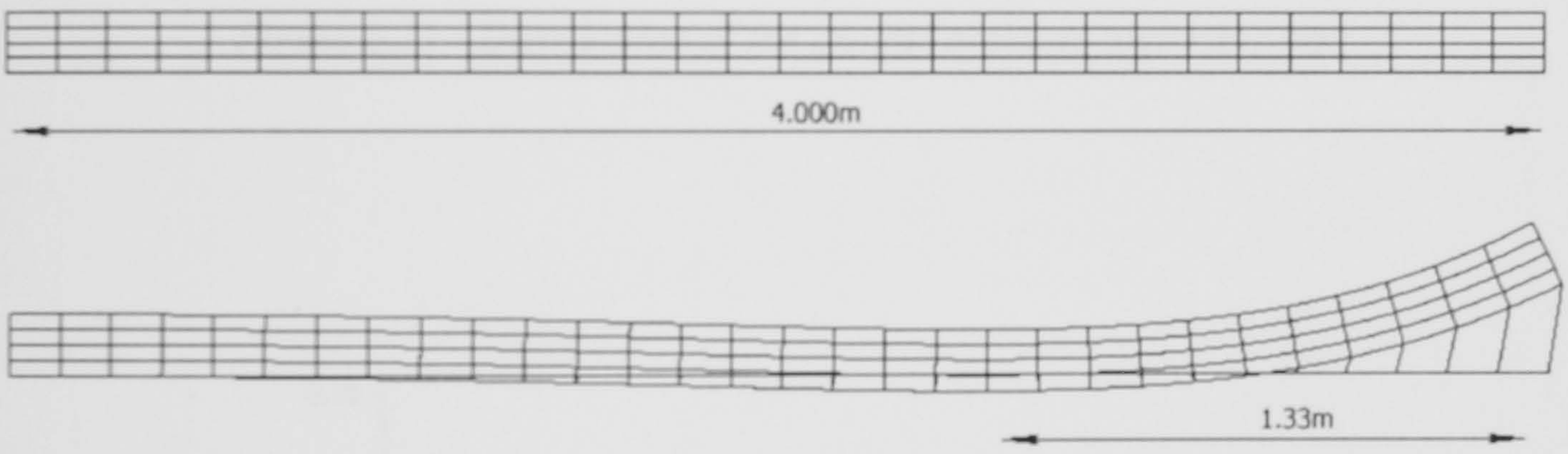

Figure 6.10 – Deformed shape of a finite element model of a slab exposed to a negative thermal gradient

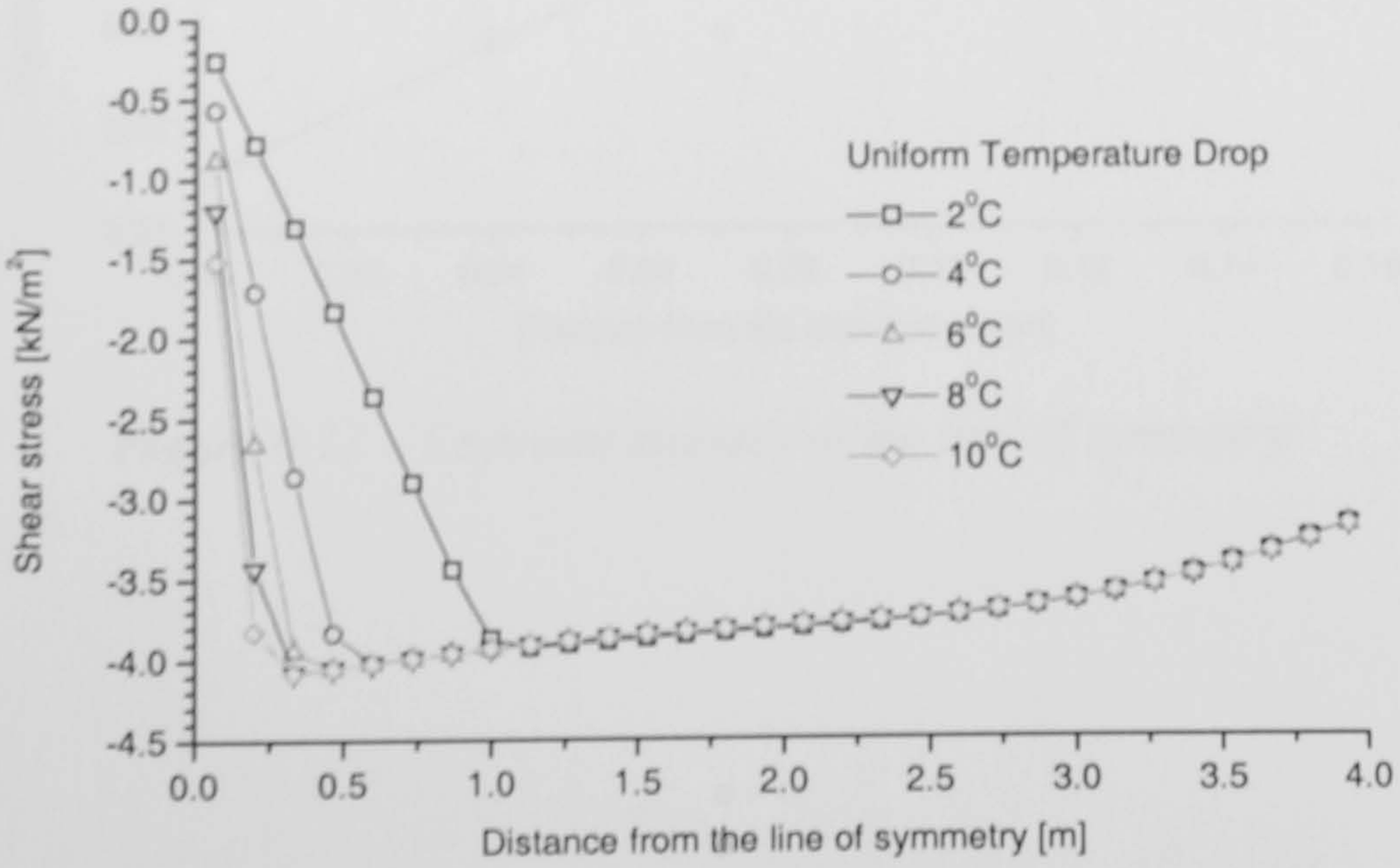

Figure 6.11 - Shear stress distribution along the slab/sub-base interface

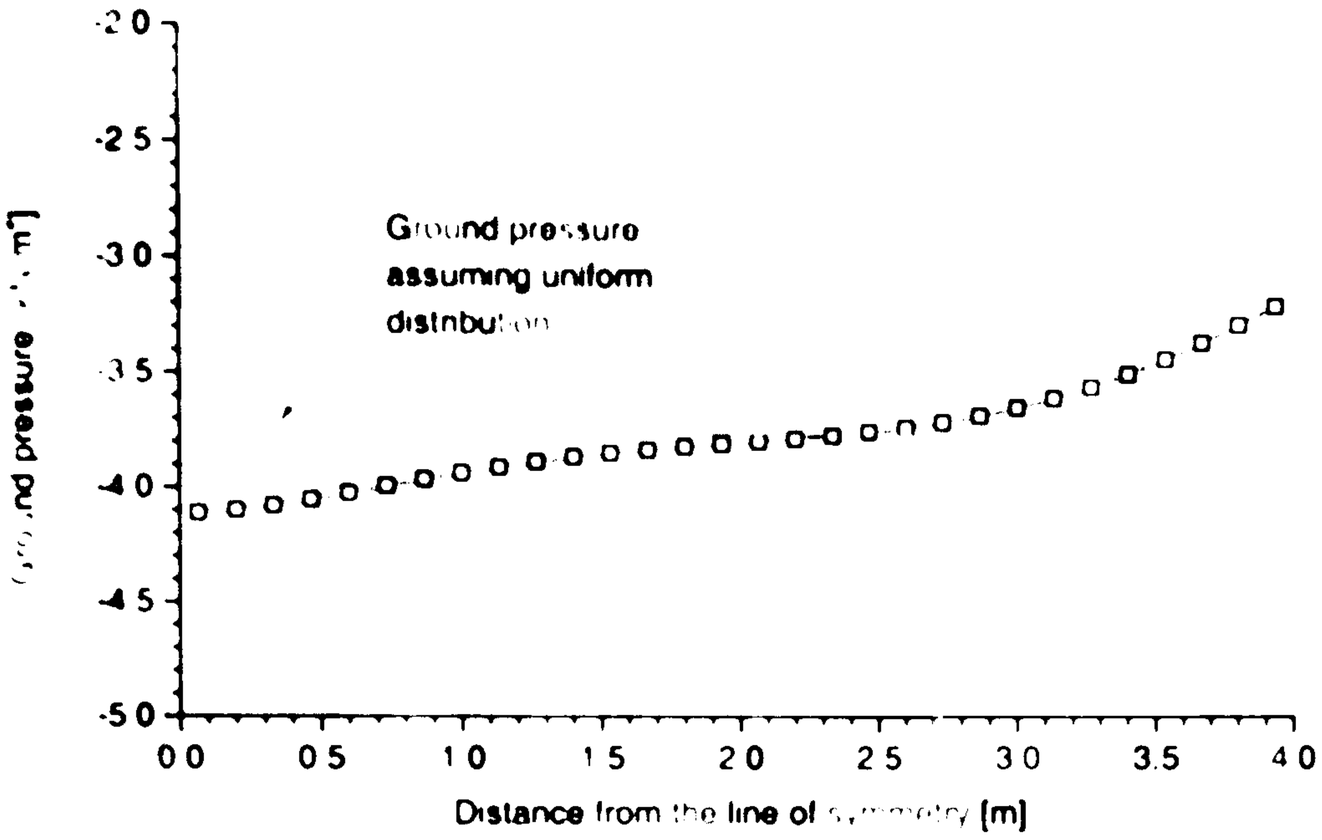

Figure 6.12 - Distribution of the ground pressure under the slab

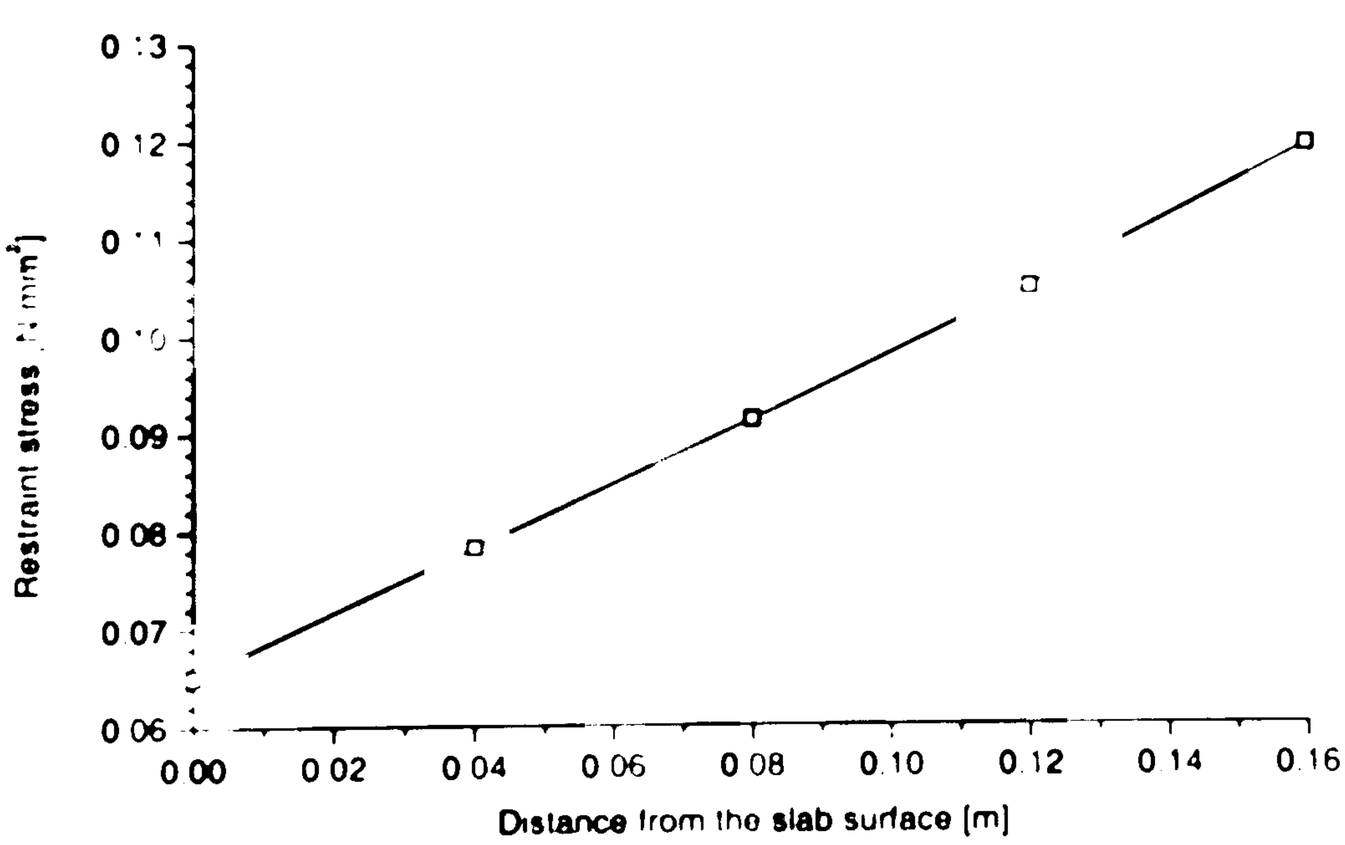

Figure 6.13 Restraint stresses at the line of symmetry

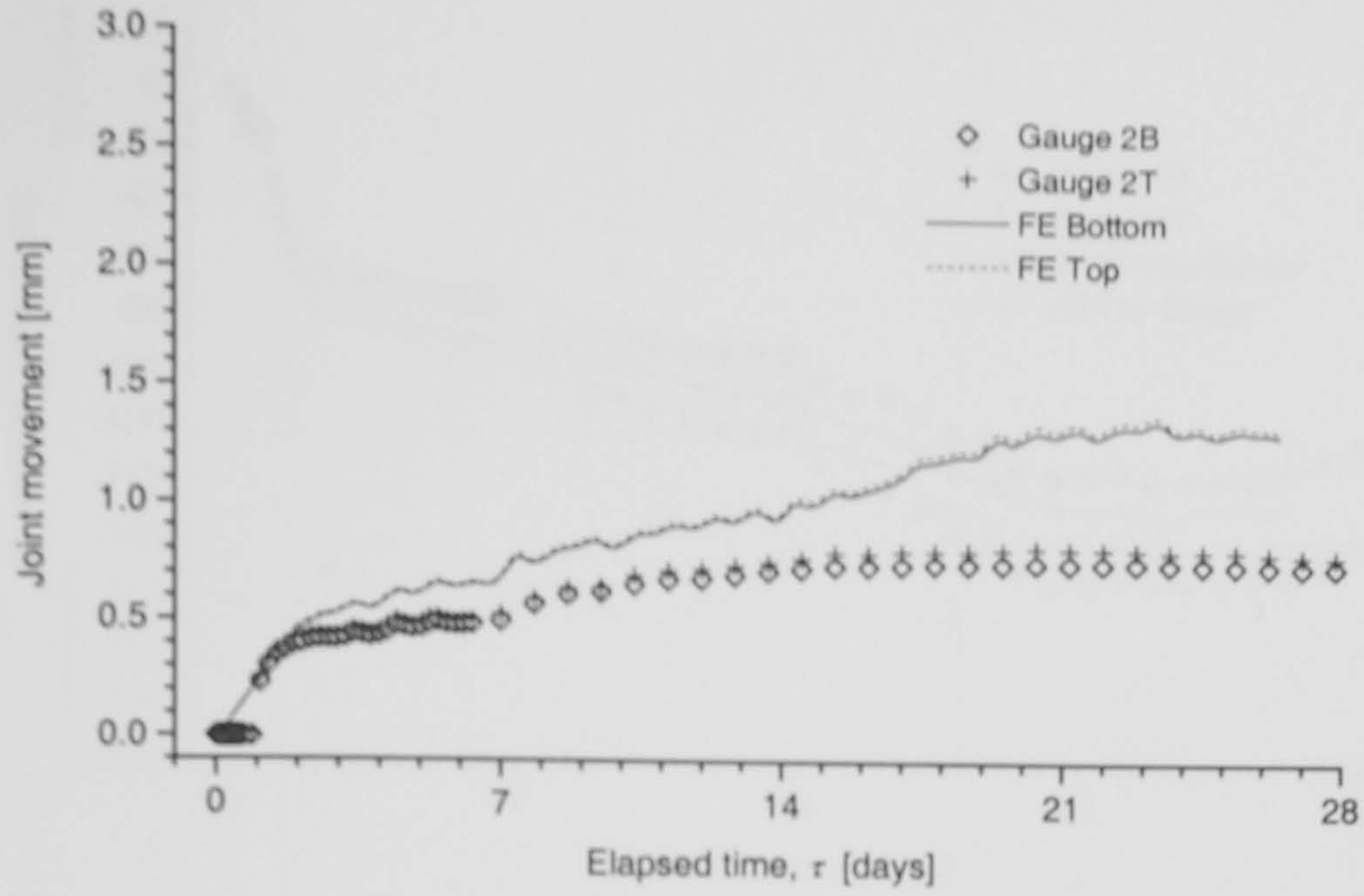

a) Interface shear stiffness, k_s = 10 MN/m^3

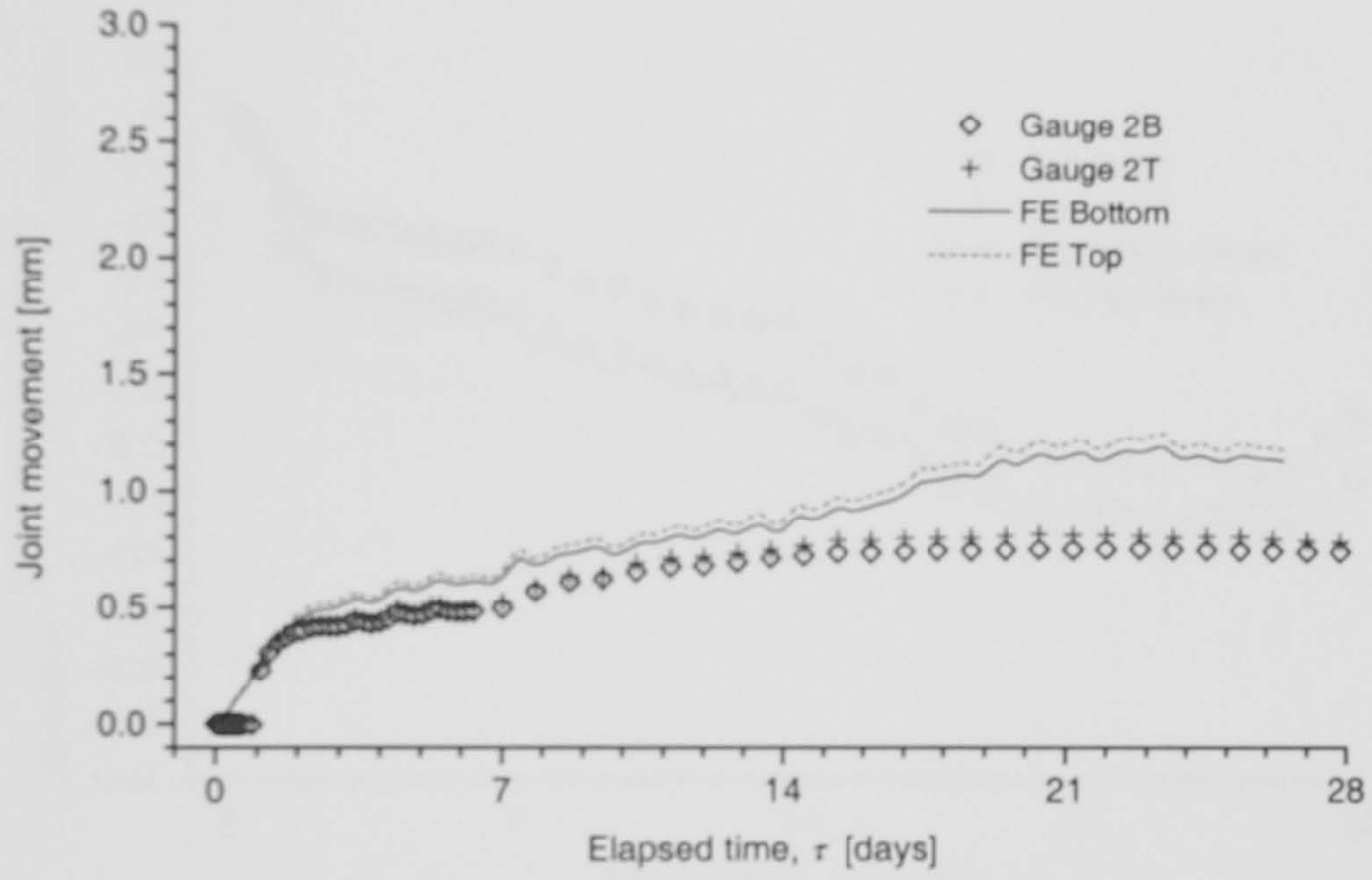

b) Interface shear stiffness, k_s = 24 MN/m^3

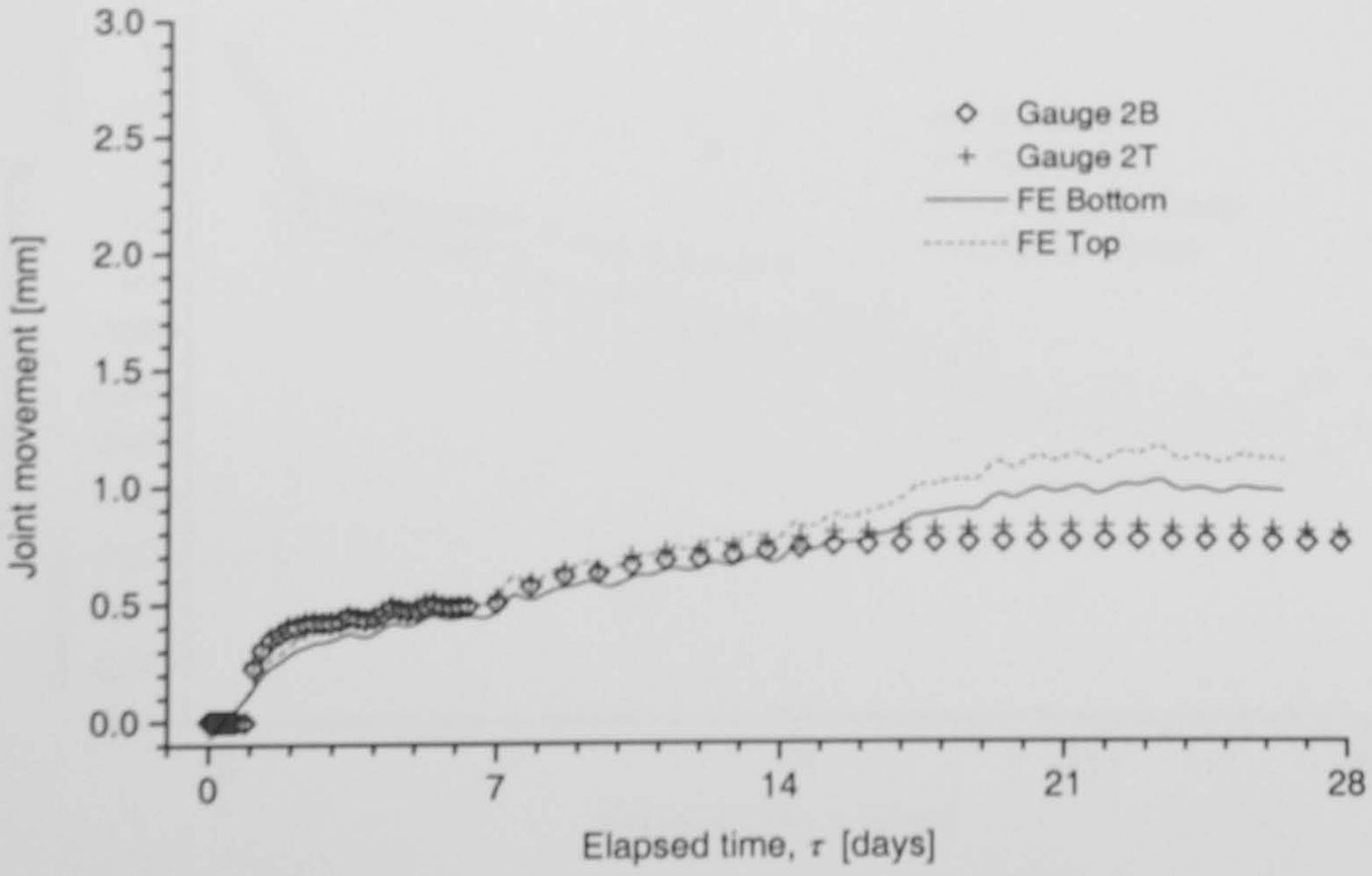

c) Interface shear stiffness, k_s = 240 MN/m^3

Figure 6.14 – Northampton: Comparison of the joint movement from the finite element model and the site data for position 2

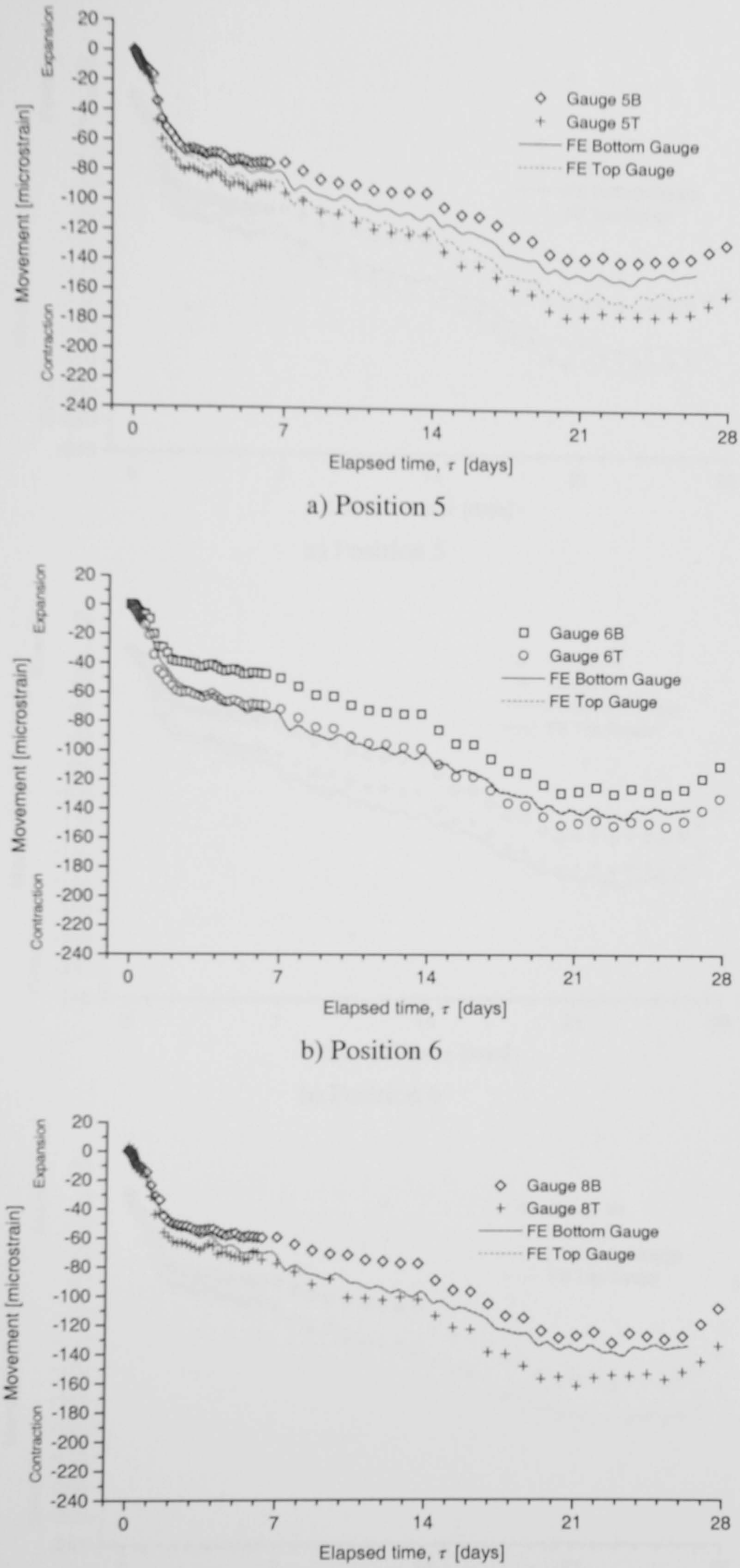

a) Position 5

b) Position 6

c) Position 8

Figure 6.15 – Northampton: Comparison of strains from the finite element model without drying shrinkage and the site data (Interface shear stiffness, $k_s = 24\ MN/m^3$)

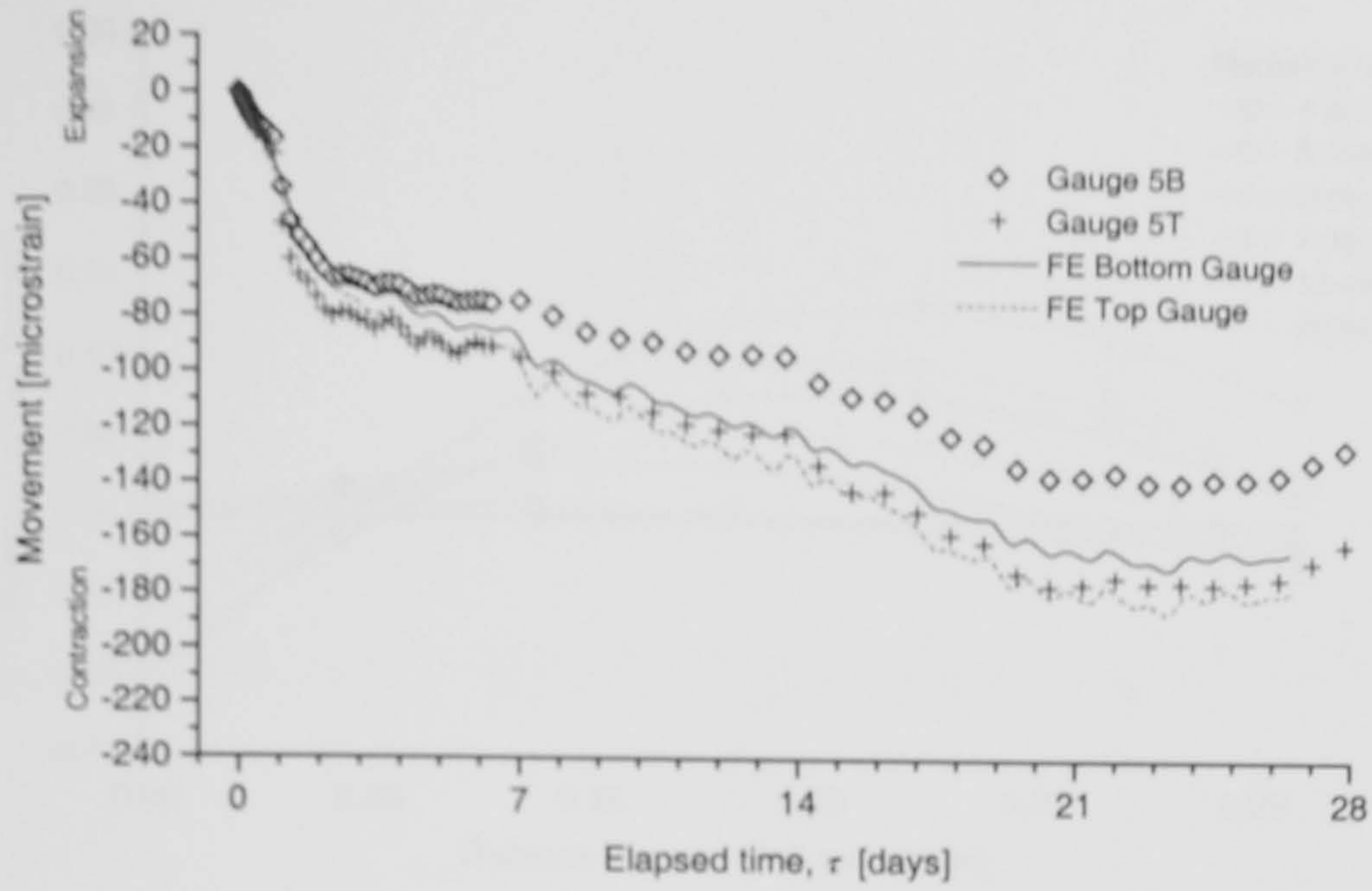

a) Position 5

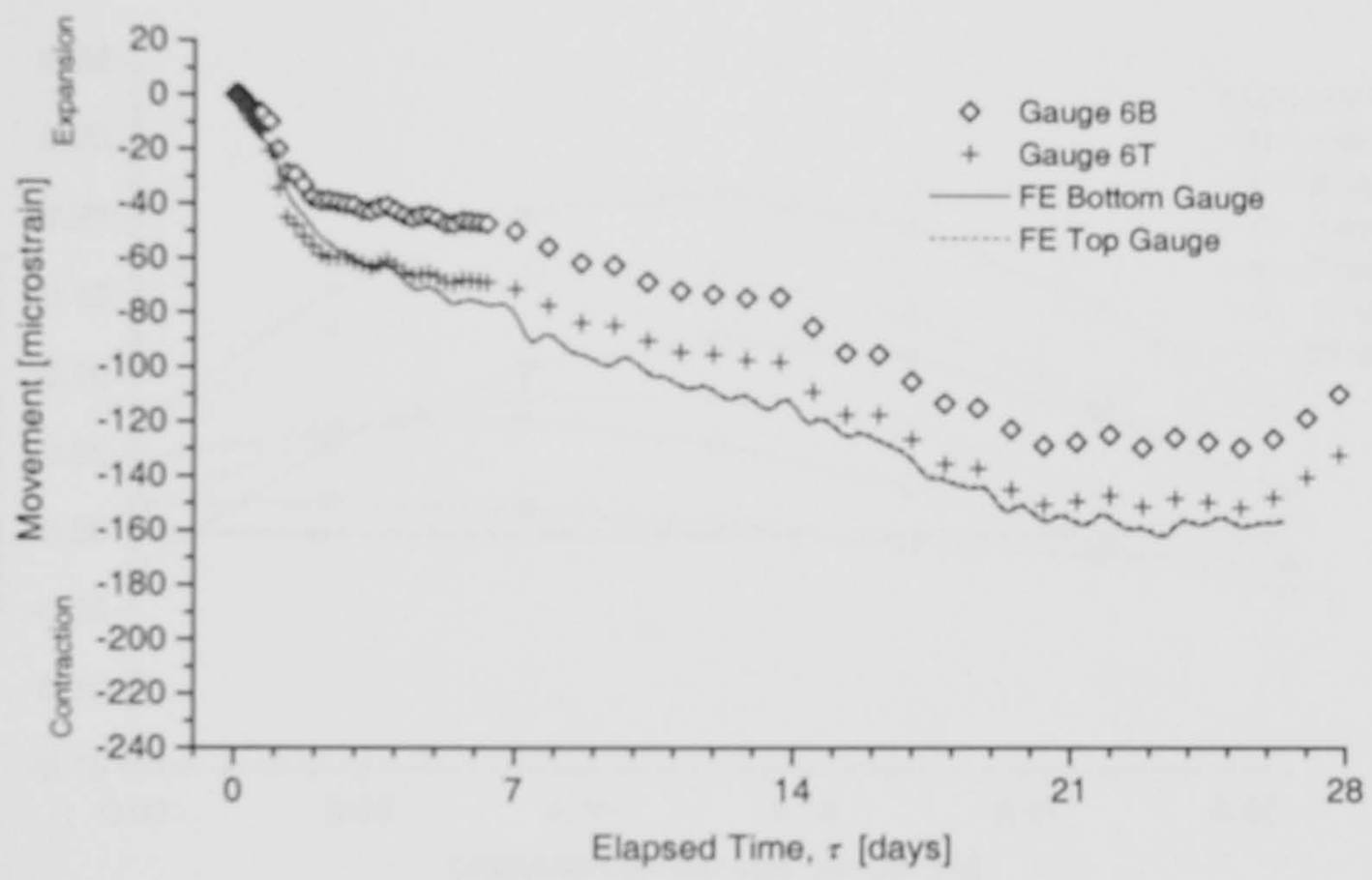

b) Position 6

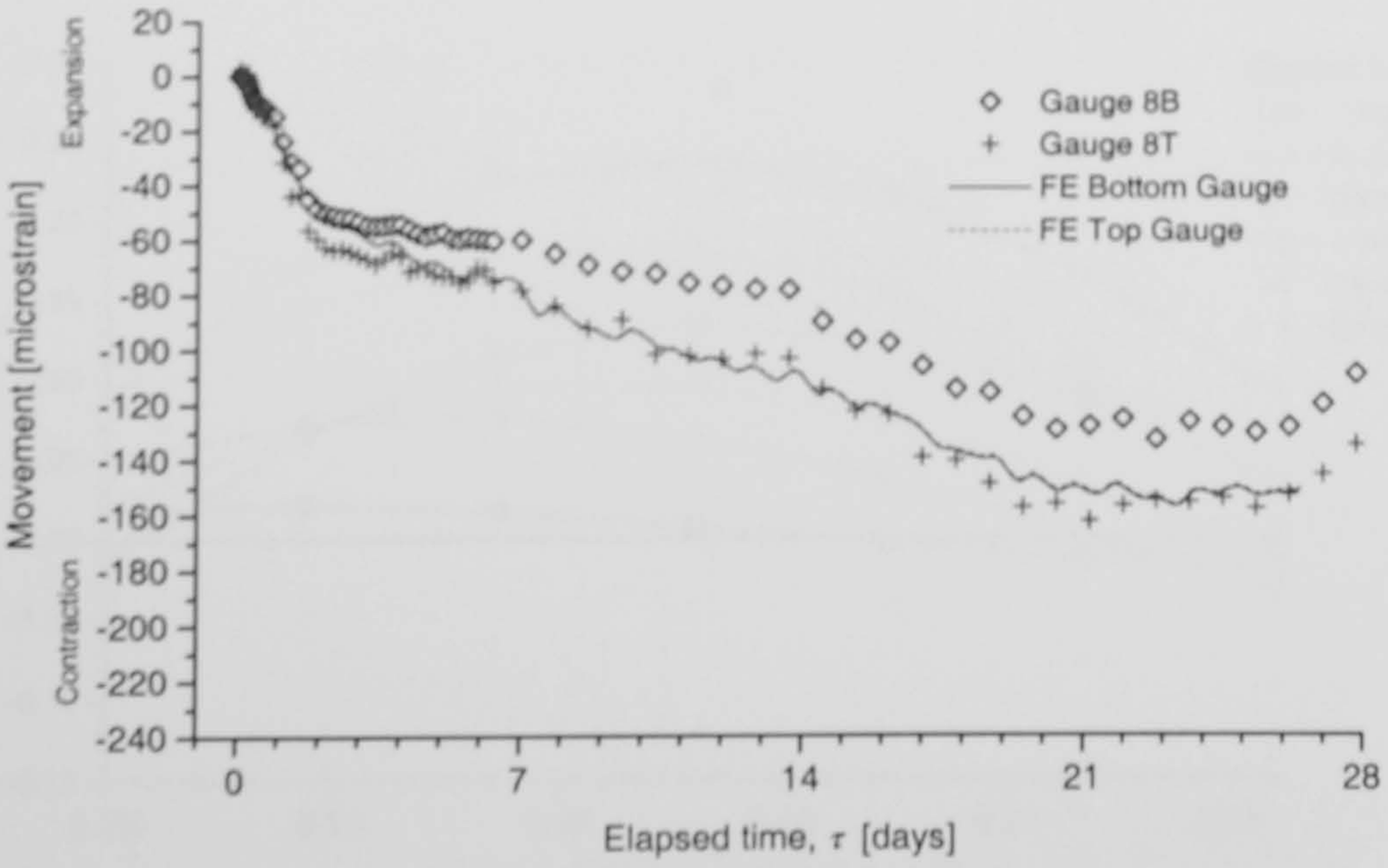

c) Position 8

Figure 6.16 – Northampton: Comparison of strains from the finite element model with drying shrinkage and the site data (Interface shear stiffness, $k_s = 24\ MN/m^3$)

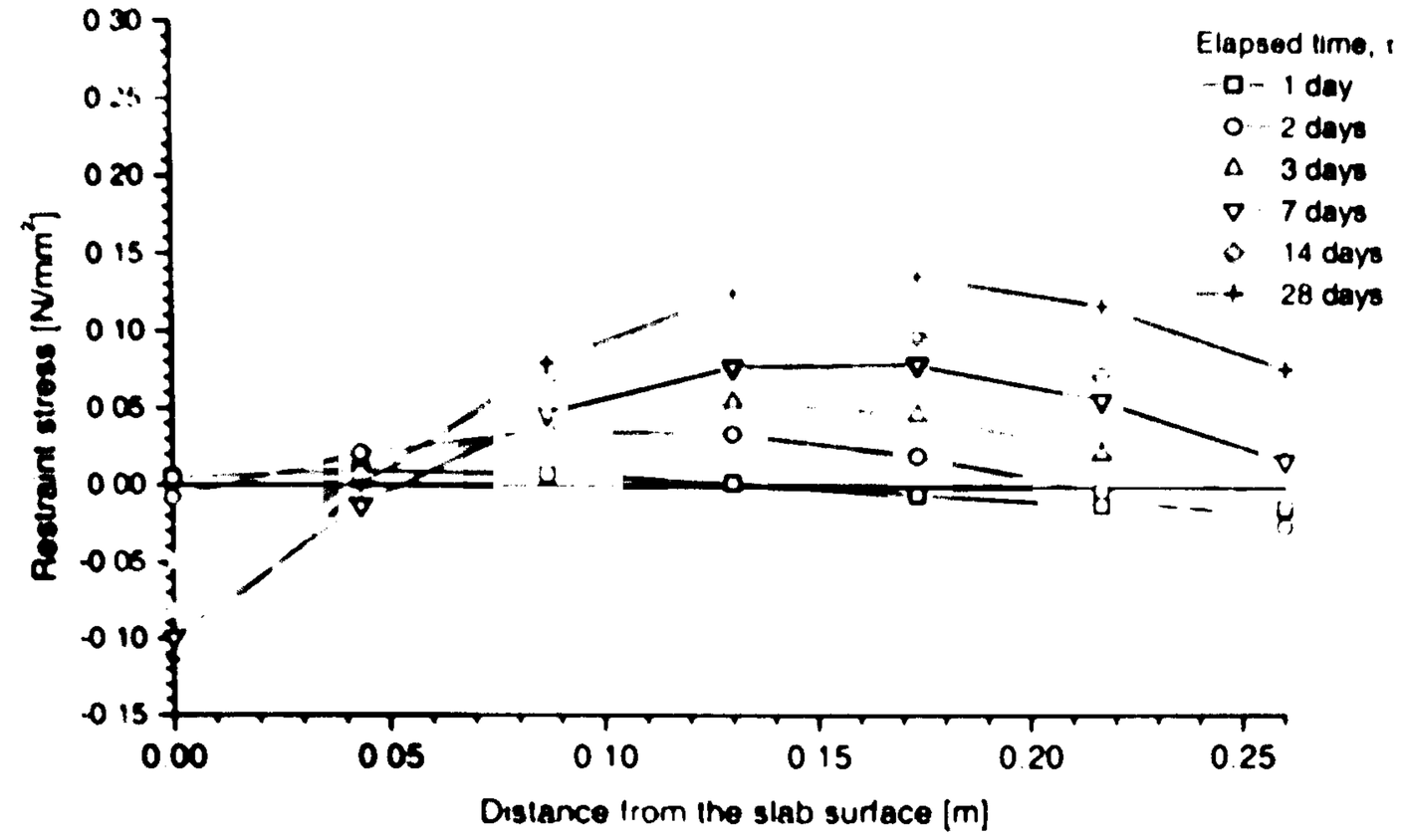

a) Position 5

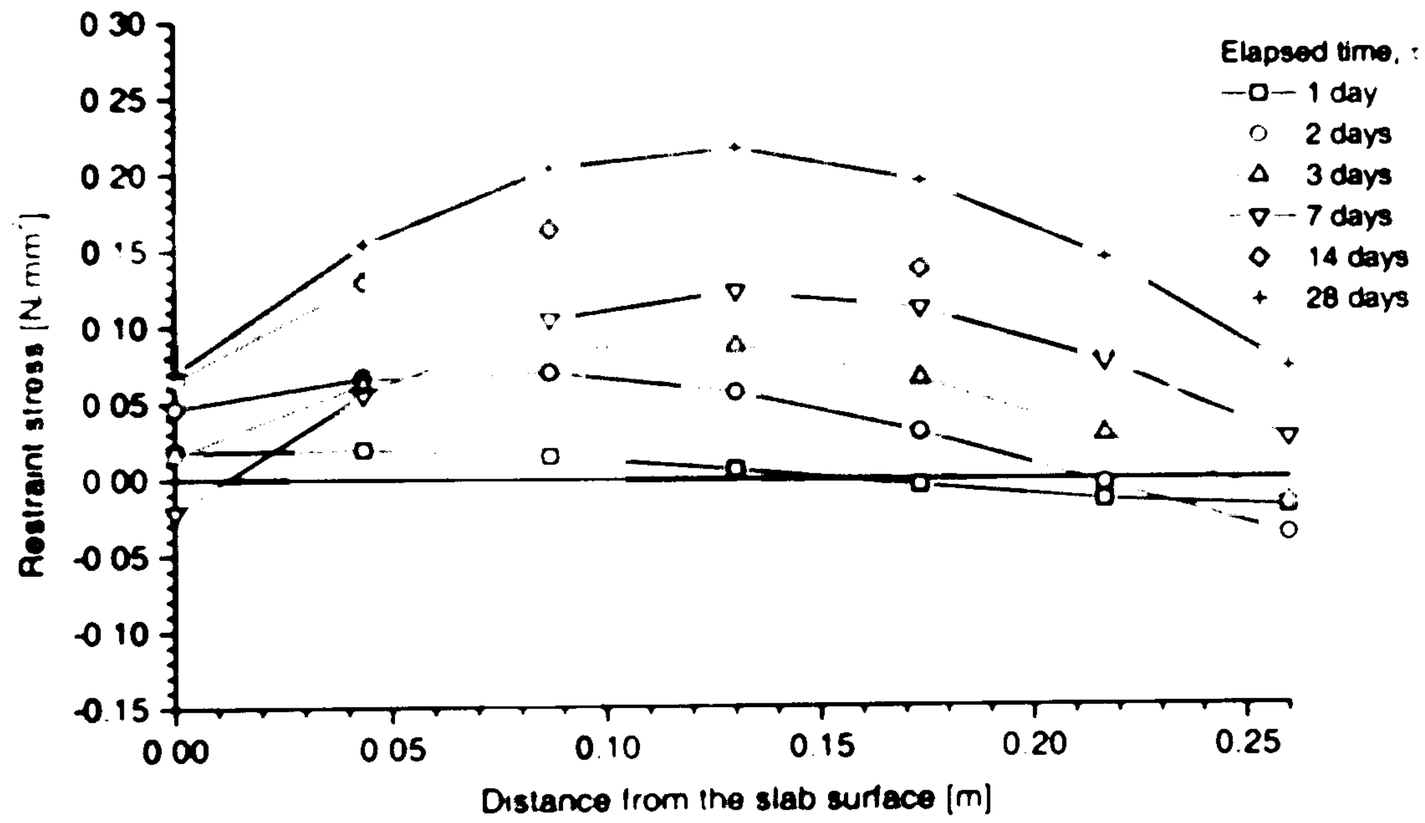

b) Position 6

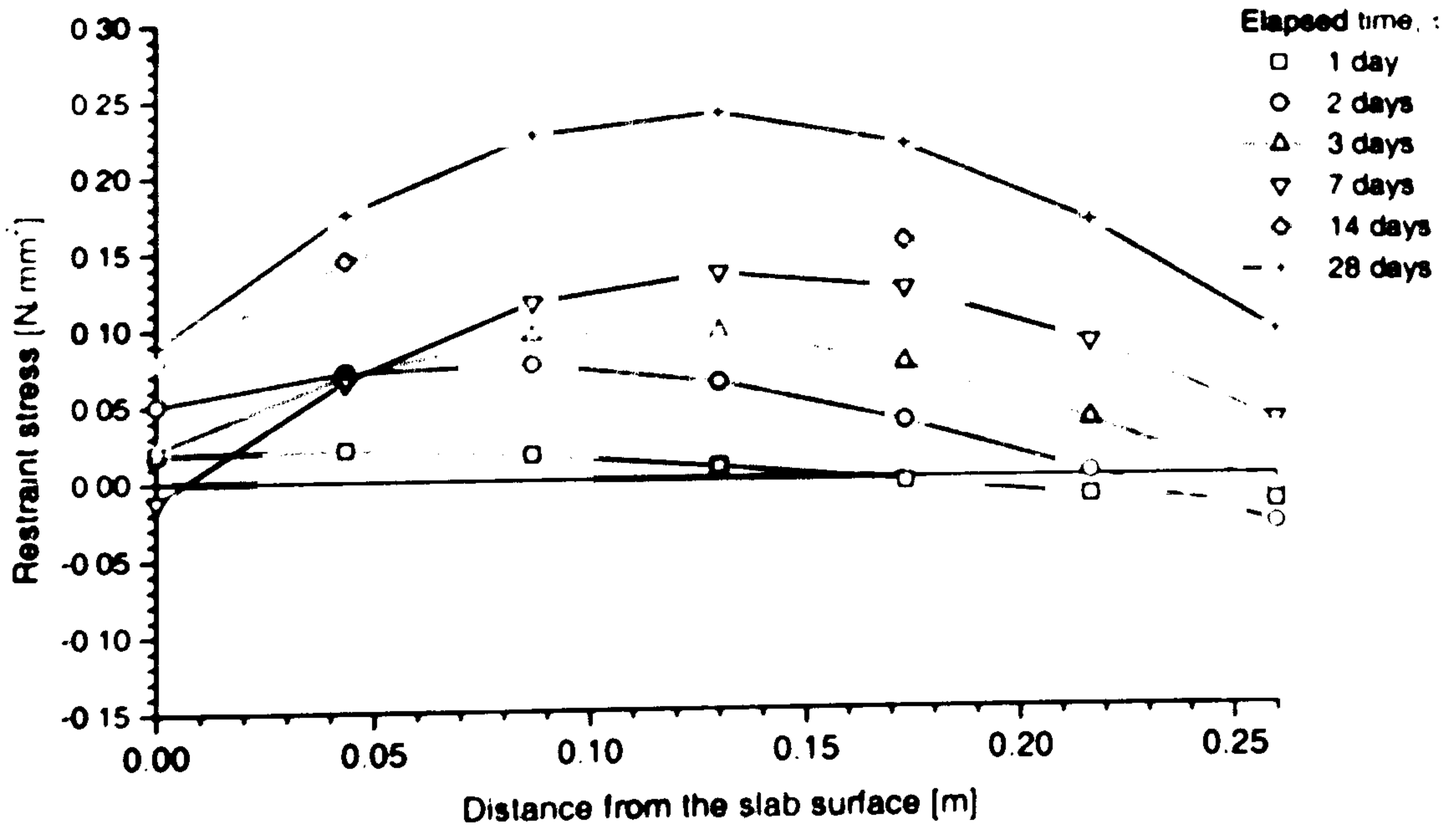

c) Position 8

Figure 6.17 – FE model of Northampton: Theoretical stress distribution in the slab

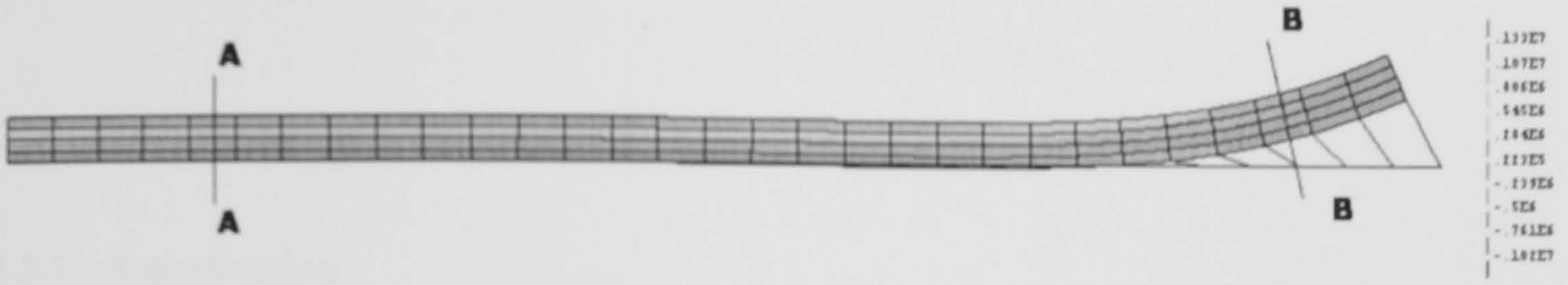

Figure 6.18 - FE model of Northampton: Warping stresses

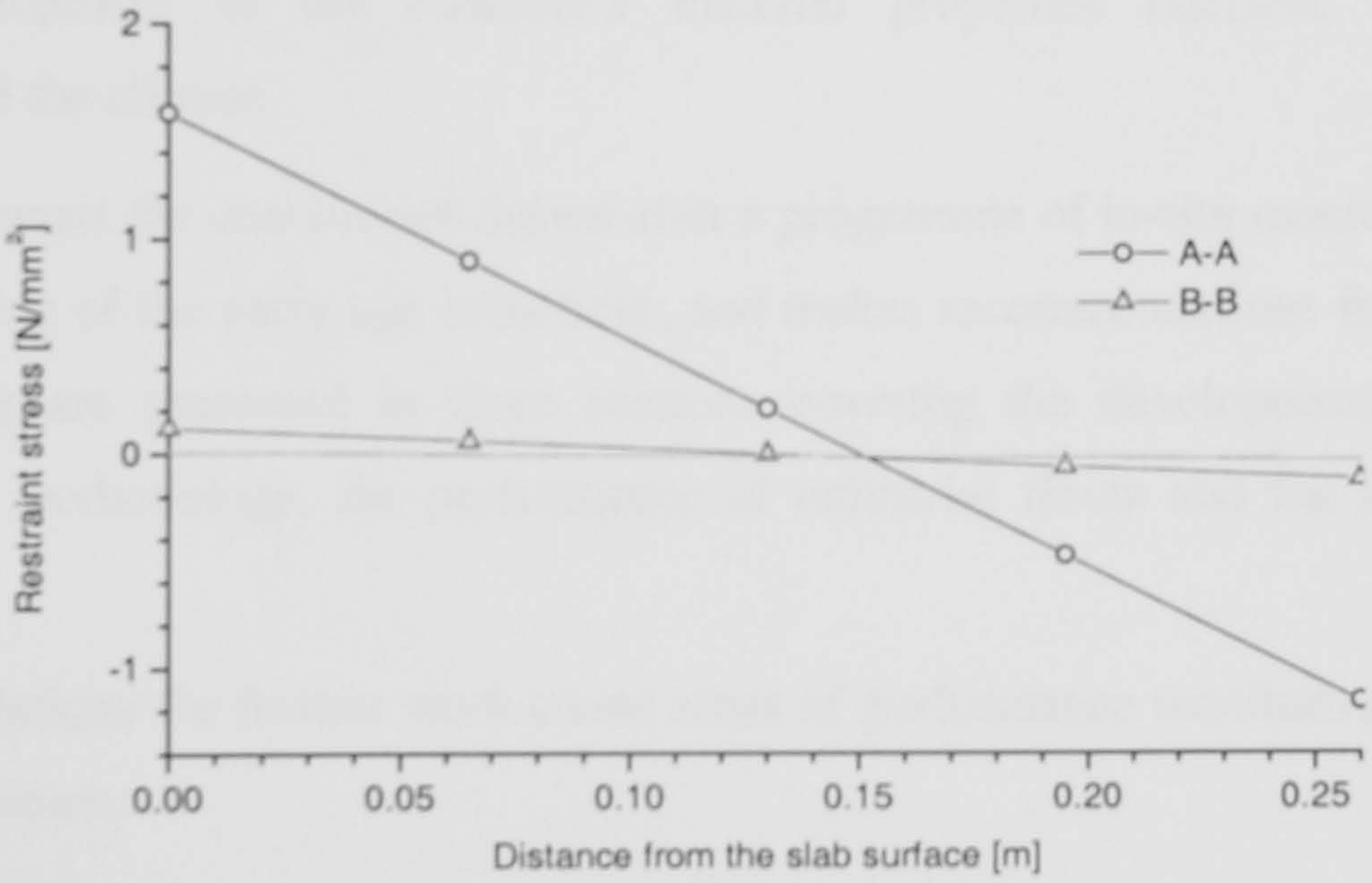

Figure 6.19 - FE Model of Northampton: Stress distributions

7. Conclusions and recommendations for further work

7.1. Conclusions

7.1.1. Introduction

Very little research has been published on the behaviour of concrete industrial ground floor slabs, explaining why the majority of the detail design guidance is empirically based. This research set out to monitor the early-age behaviour of concrete industrial floors, and the influence of the construction parameters, in order to improve our understanding of how the early-age development of the concrete's material properties interacts with the joint arrangement and the climate.

This chapter presents the conclusions drawn after a programme of in-situ monitoring and finite element modelling of the early-age behaviour, and makes recommendations for further study. The conclusions are presented in three sections covering the development of the in-situ instrumentation methodology, the performance of industrial floors and the implications for designers.

The recommendations for further work cover areas of performance monitoring and improved modelling techniques.

7.1.2. Instrumentation methodology

Field monitoring of new floor constructions was one of the main objectives of the research. This has been successfully carried out and, following the instrumentation and early-age monitoring of floor slabs in six buildings, an instrumentation methodology has been developed which could be applied to any concrete structure. The main activities involved in a structural instrumentation were identified as falling into the following four categories:

- Planning – identify the key locations for instrumentation and suitable sensor types
- Pre-site preparation – design, construct and test the wiring loom and logger program
- On-site instrumentation – locate and protect cabling and logger before installing sensors
- Performance monitoring – automated monitoring; periodic site visits for data collection

Planning

The instrumentation in the slabs was used to measure the magnitude and the timing of the concrete contraction at different depths and distances from joints, and the associated joint movements. The placement of these sensors was varied in order to try and establish the effects of the different construction methods and the ambient conditions.

Pre-site preparation

The detailed design of the floor was often only finalised around two weeks before construction commenced on site, and in some cases changes in site programmes reduced this time even further. This lead to the adoption of standard datalogger set-ups, and the use of an interface box. These allowed the neat termination of all of the cables coming out of the slab, but also facilitated the quick and easy connection and removal of the datalogger, whilst providing terminals for manual strain readings to be taken.

Grouping the gauges in clusters provided significant cost savings on cabling, whilst terminating all of the cables with crimp connectors speeded the connection of gauges on site, and allowed separate transportation to site, reducing the possibility of damage occurring at this stage.

To illustrate the work involved in producing the wiring loom, an average installation with 60 strain gauges used approximately 14 gauge clusters connecting the strain gauge leads to the multi-core cable. Each cluster box contained 24 different coloured wires requiring connection. The interface boxes contained around 300 different wires to be correctly connected to link the multi-core cables to the datalogger through 6 25-way RS232 connectors. The production of a spreadsheet to allow the identification of all of the wires connecting each of the strain gauges back to the datalogger was essential. This simplified the development of each wiring loom and also enabled testing of the completed wiring loom and logger program before transportation to site.

On site

Due to the nature of the site environment, installing instrumentation in an industrial floor requires a methodology which is quick, so as not to impede the rapid rate of construction, and robust, to ensure that instrumentation failure does not prevent the collection of data.

For the strain readings to be meaningful the accurate positioning of the gauges is essential. This was achieved by mounting the gauges on reinforcement chairs, which were then taped or tied down to prevent subsequent movement. Although the acrylic barrelled strain gauges had not been used outside of the laboratory before they were found to be suitable for site use. As with the newly developed 254mm long steel embedment and joint gauges, the concrete must be placed around the gauges and not allowed to fall directly on them, as this was found to

cause damage. The gauges for monitoring across day joints were a useful development and open up many new possibilities for monitoring across construction joints in all kinds of structures.

The simplest and most successful way to protect the multi-core cable from damage from trafficking before and during construction was found to be to bury it in the sub-base. The cables linking the gauges to the cluster boxes had to be taped to the slip membrane to prevent them moving as the concrete was placed. Movement of the cables was found to risk the loss of data either through broken connections or damage caused when the joints were saw-cut.

Marking the gauge location after embedment was found to be important as this reduced the risk of accidental damage when site personnel required access around the instrumentation before the floor was finished.

Monitoring

A sample frequency of 30 minutes during the first 2 days after construction was found to be adequate to measure all changes occurring in the slab. As the slab temperature dropped back to ambient levels the sample frequency was reduced to every hour, before reducing further to every 2 hours from 1 week after construction. For long-term monitoring, readings every 4 hours were found to give sufficient information about the slab behaviour. Manual readings from all of the strain gauges were taken on all subsequent site visits, whilst precision level surveys of the slab surface profile were undertaken where possible (subject to permission from the client).

This instrumentation and data collection regime has allowed information, not only on the early age behaviour of the slab, but also on the long-term performance to be collected. This instrumentation will remain as a useful source of performance data in the future.

7.1.3. Data interpretation

The main aim of the research was to gain a better understanding of the early-age behaviour of concrete industrial floors, and how this would affect their performance at later ages. The collected data has allowed a better insight into the early-age behaviour (during the first 28 days after construction), but has also allowed the impact of longer term influences, such as drying shrinkage and seasonal temperature changes to be studied. The main behavioural trends and the factors which influence them, as identified in Chapters 5 and 6, are now summarised.

The site data demonstrated a definite link between the concrete delivery temperature and the elapsed time before the maximum temperature was achieved, although no correlation was found with the maximum temperature. This agreed with previous work by Lachemi and Aïtcin (1997). The influence of air movement across the top of the slab was highlighted by

comparisons between the finite element models and the site data. In all cases where the building was not weather tight during construction, a higher thermal transfer coefficient was needed for the air/slab interface in the models in order to give agreement with the site data. This had the effect of slightly reducing the maximum slab temperature and increasing the rate at which the temperature returned to ambient levels as hydration slowed. It is this rapid temperature drop whilst the concrete is still relatively green that increases the risk of cracking.

As a result of these thermal losses to the air, and the ground under the slab, the maximum measured temperature was found to be at mid-depth in the slab, whilst horizontal thermal gradients were also found near the edges of concrete cast against previous pours. Temperature drops of 10°C were commonly measured during the first 3 to 4 days following construction.

Long-term readings showed how seasonal temperature changes significantly affect the measured strains in all floors, with a similar change being observed as the temperature was dropped in the chill store at Leeds. As several of the instrumented floors were constructed in unheated buildings, seasonal temperature variations in excess of 15°C were recorded. This equates to an annual periodic thermal movement potential of 150 μstrain, or around 33% of the commonly specified ultimate free drying shrinkage of the floor.

The site data showed that all of the joint movements were thermally triggered, though the time period following construction before movement was triggered varied. The sawn restrained movement joints in large area pours were found to behave inconsistently. Some joints opened and became dominant, whilst other joints did not open at all. In some cases the joint opening was sufficient to lose aggregate interlock. The comparison of surface readings from the Demec pips and measurements from the joint gauges showed that the joint width was non-uniform; the surface measurements could over-estimate the joint width lower down in the slab by more than 1mm. Therefore, any load transfer that is calculated on the basis of surface joint width measurements should be used as a minimum value.

Precision level survey data, in addition to embedment strain readings, showed that the vertical movement close to sawn restrained movement joints was greater than close to sawn free movement joints. This confirms that the sawn restrained movement joints do appear to release some of the warping stresses as assumed by TR34 (1994). The difference in behaviour of the two joint types has been attributed to the higher bending stiffness of the dowel bars crossing the free movement joints. The finite element models and simplified equations (Eisenmann & Leykauf, 1990) in Chapter 6 have shown close agreement over the deformed shape and resulting stresses for concrete slabs subjected to non-uniform contraction, which results from thermal and hygral gradients. They show how the movement occurs over a critical length near to the free end of the slab, as was also shown to be the case near to the joints in the long strip

slab. The precision level surveys conducted after differential contraction had occurred showed how most of the vertical movement was concentrated within about 1m of the joints.

Readings from the embedment strain gauges showed that differential contraction had taken place near to the edges of the large area pours, and close to the joints in the long strip. These equated to equivalent temperature gradients (ETG) of up to 1.48 °C/cm in the long strip slab and 2.02 °C/cm in the large area pour. Contrasting this differential movement with that at the points furthest from the joints gave the magnitude of the warping restraint. This was found to be significant in both floors; in the long strip it amounted to 0.74 °C/cm, whilst in the large area pour the difference between the edge and the middle of the pour was 1.51 °C/cm.

This warping restraint will have lead to restraint stresses which, even allowing for creep, could have exceeded 2 N/mm^2 in both floor types. This has been confirmed with a finite element model of the long strip slab, which was subjected to the same maximum differential gradient as was measured on site after 370 days. The resulting restraint stresses were almost identical to those determined using the site data.

The variation in measured strains (and hence restraint stresses) was noticeably larger in the floors at Bedford and Chepstow, where cracking was observed. At Bedford, details leading to external restraint reduced the measured contraction across the building, where cracking has occurred, whilst the cracking at Chepstow seems to have resulted from a combination of restrained thermal contraction and warping combined with load induced stresses.

Even in the large area pours the frictional restraint did not significantly alter the contraction behaviour, as has been confirmed by the finite element models. Changes in the interface stiffness from 10 MPa to 24 MPa were found to have little effect on the concrete contraction, or on the resultant stresses. The highest shear stiffness, 240 MPa, did significantly reduce the concrete contraction, and increase the restraint stresses. However, this is outside the expected range of stiffnesses for a concrete slab cast on a slip membrane.

Simplifications had to be made in the finite element models of ageing concrete; most notably the use of uniform concrete drying shrinkage strain and the omission of limiting friction for the shear restraint on the slab/sub-base interface. However, good agreement between the predicted and measured strains for the long strip slab was obtained at distances of 1m, 4m and 7m from the free movement joint. Models with and without drying shrinkage gave good agreement with site readings from the upper and lower embedment gauges respectively. This could be expected at early ages as the drying shrinkage will only have affected the upper parts of the slab.

The B3 model (Bazant, 1995) was found to over- predict the drying shrinkage for the thinnest floor – the 160mm thick jointless floor at Bedford. However, the predictions for the thicker

floors showed good agreement with the measured drying shrinkage. As expected the thinner slabs were found to shrink more than the thicker slabs, whilst the addition of a shrinkage-reducing admixture in the second pour at Leeds seemed to reduce the concrete shrinkage and the joint movement compared to the other pours.

The structural finite element models showed that whilst there was a stress differential between the top and bottom faces of the slab due to the eccentricity of the frictional restraint as suggested by Kiamco (1997), its effects were localised and only affected the ends of slabs. For the most part the frictional restraint resulted in a uniform tensile stress in the slab sections.

Stresses due to warping restraint were shown to be more significant than those due to longitudinal restraint, confirming Pettersson's findings (1997) that warping restraint is significant in industrial floors, whilst the eccentricity of frictional restraint is not.

For this reason, when the long-term non-uniform drying of the slab is considered, it is expected that **the resultant intrinsic stress field in the slab due to frictional and warping restraint would have tensile stresses in the top face, and compressive stresses in the bottom of the slab.**

7.1.4. Implications for design

The behaviour of the day joints in the instrumented jointless floors, and the joints in the long strip slab was as expected – i.e. the restrained joints remained closed, whilst the movement joints opened. However, there was no consistency in the behaviour of the restrained movement joints in the jointed large area pours. Some joints were found to open whilst others remained closed, and even where all joints opened a few joints became dominant. The design ethos (TR34, 1994) behind this floor type seems anomalous. Joint spacing is determined to keep the width within acceptable limits based on an assumed concrete contraction and assuming all joints open equally. Nominal fabric reinforcement placed in the bottom of the slab with 50mm cover is laid over the whole area as a continuous mat. TR34 (1994) states that this fabric weight should not be greater than A142 because heavier fabric may not allow the sawn induced joints to open, and this could result in cracking away from the joints. Site data has shown that this is not the case - joints do not open equally – leading to possible loss of load transfer and an increased risk of damage to the joint arris on the wider joints. It cannot be stated that the joints in the middle of the pours always open widest as several joints at the edges of pours have also opened widely.

Additionally, in light of the finite element model results, the current recommendation in TR34 (1994) to place the reinforcement in the bottom of the slab in large area pours may need reconsidering. Reinforcement placed at mid-slab depth would be in the part of the slab which

has higher tensile stresses at early ages and, because of the reduced cover, would be more effective in controlling the surface width of any cracks that do occur.

The design guidance for nominally reinforced jointed large area pours should be reconsidered. Crack control reinforcement may be better placed at mid-depth in the slab, and engineers should be warned of the possibility of the loss of load transfer at sawn restrained movement joints resulting from uneven opening and dominant joints.

Additionally, where possible pour sequences should avoid infill bays, as these will be exposed to greater restraint at an early age, which increases the likelihood of cracking.

Although TR34 (1994) states that the sawn restrained movement joints are to be used to relieve warping stresses, no guidance is given on the likely magnitude of these stresses, or on suitable joint spacings in order to release them. Losberg (1978) and Eisenmann and Leykauf (1990) provide methods which allow the calculation of the warping restraint stresses, and Pettersson (1998) shows how they can be expected to vary with location.

Site data has shown how curling occurs close to the joints as predicted, whilst the magnitude of the curling also appears to be affected by the joint type. Although the number of joints surveyed is small, dowelled free movement joints were consistently found to experience less vertical movement than sawn free movement joints, which indicates that the sawn restrained movement joints are indeed allowing the release of warping stresses.

It is not possible to place joints close enough in a floor to release the warping stresses at all locations, and even were this possible the end user would be left with a very uneven floor. For this reason floors should be designed allowing for reasonable warping stresses, whilst the number of sawn restrained movement joints should be reduced in order to improve the flatness of the floor.

The warping stresses will depend on the concrete stiffness, the floor thickness and the differential gradient it is exposed to. Restraint equal to equivalent temperature gradients (ETG) of up to 1.5 °C/cm has been found in the large area pours, although the reduced joint spacing and increased thickness in the long strip slab gave a smaller ETG of 0.74 °C/cm.

Greater joint spacing will make it more likely that all of the joints will open, and the provision of dowel bars across the joints would serve the dual purpose of controlling the vertical deflection and ensuring load transfer should the joint width exceed 1mm. Both of which should improve the serviceability of the floor.

The current design method, whereby the detail design and the structural design are carried out separately, is flawed and should be modified. The intrinsic stresses in a slab

from frictional restraint, and more importantly warping restraint, must be included in the structural design calculation since they can reduce the load capacity of the slab.

It has been shown that the effects of restrained drying shrinkage and temperature change combined with applied loading can be sufficient to cause cracking in a floor, where individually these would not cause concern. Current design guidance does not account for the effects of these intrinsic stresses in a slab when carrying out the structural design, even though they could account for more than 30% of the strength of the slab.

The intrinsic stresses arising from warping restraint are generally larger than those due to frictional restraint, leaving the slab with the greatest tensile stresses at the top surface. Because this intrinsic stress distribution is the reverse of that caused by loading, taking account of these stresses in design could in some cases actually increase the capacity of floor slabs in service (Sargious & Ghali, 1986).

Furthermore both theory (Meyerhof, 1962) and testing (Beckett, 1990 & 1999) have shown that there is a significant difference between the load required to cause cracking in a slab and it's ultimate capacity. As the initial cracking in a slab under a point load is in the bottom face, this will not have any significant serviceability implications for the end user. Therefore, not only is the formation of cracks in the bottom of a slab under point loading not critical to the serviceability of the floor, but the intrinsic stresses from warping restraint may actually increase the load capacity of the slab giving a greater factor of safety. **As a result, the current method, where intrinsic stresses are not considered, should give conservative designs for this loading.**

In contrast cracking on the surface of a slab can have immediate serviceability implications and can leave the client thinking that the slab has failed, even if the cracks are not significant as far as the structural integrity of the floor is concerned. In aisles between racking and uniformly loaded areas and adjacent to line loads a hogging moment failure of the floor is possible, with the load at which this will occur being reduced by the intrinsic stresses. **For this reason the intrinsic stresses due to restraint should be included when designing the slab for applied hogging moments.**

7.2. Recommendations for further work

7.2.1. Introduction

This research has developed and used a successful in-situ monitoring technique to gather performance data on industrial ground floor slabs. This has allowed the development and calibration of finite element models of the early-age slab behaviour. However, this work has

highlighted the need for the further investigation of aspects of the performance of industrial floors, as well as possibilities for the further development of the finite element modelling.

7.2.2. Site Instrumentation

A reliable in-situ instrumentation method has been developed as part of this research, and six floors have been instrumented. Conclusions have been drawn based on the collected data, however, this is still quite limited. Further performance monitoring of industrial floors is required, as the data which this generates will allow more weight to be given to any recommendations.

Measurements have shown that the longitudinal restraint appears larger than can be predicted using the current frictional restraint theory. Testing has been done on flat slabs restrained on flat sub-bases (Timms, 1958; Pettersson, 1998) to determine the shear stiffness of the interface and the coefficient of friction which determines when sliding occurs. This is an idealised condition which will not always be achieved in practice. For this reason further research is required on the effects of imperfections in the sub-base levels on the movement of the floor slab. This must include the effects of ruts, as caused by trafficking an insufficiently strong sub-base.

The precision level surveys and the differential movement measured by the embedment strain gauges has indicated that there is a difference in the curling behaviour of the floors, which can be related to the joint types. Further research should be carried out into this possible relationship as this has long-term serviceability implications for the end user of an industrial floor.

7.2.3. Finite element modelling

The finite element models presented in this research only analysed the first 28 days following construction of the slabs. Further research could investigate the long-term influences of seasonal temperature changes and drying shrinkage. This will also require the discrete analysis of the spatially varying hygral profile, rather than the simplification to the uniform time-dependant variable assumed in this early-age analysis.

Although good agreement was obtained between the finite element model and the site data, this only looked at a 16m long section of a 64m long slab. Furthermore, the simplification to a 2-D plane stress analysis neglected the edge restraint provided by the adjacent slabs. Further work could look at entire bays, with phased analysis methods allowing the duration of construction to be accounted for, whilst 3-D analysis would allow all of the restraint to be analysed, although the computing time required could be significant.

There is also still much scope for further development of the models to increase their realism. For example, the use of spatially variable, as well as time dependant, material properties would allow the statistically significant variation in the concrete's strength to be accounted for. This would remove the symmetry in the response of the model to all forms of restraint, and provide a more natural prediction of stress distributions.

The slab/sub-base interface behaviour had to be simplified for the early-age models. Because of the choice of model size to look at the behaviour of the long strip slab the frictional limiting shear stress was not reached. However, if longer slabs were analysed this would not necessarily be the case. Further work is required on the implementation of this frictional response in conjunction with the changing material properties, especially at early ages. One possibility would be the adoption of a different creep model, allowing the adoption of a non-zero start time for the analysis. This would avoid the ill conditioning produced by the large difference in stiffness between the frictional interface and the immature concrete during the first 12 hours after construction, whilst still allowing the restraint to the thermal contraction of the concrete to be modelled.

8. References

- ACI Committee 116 (1978): *Cement and Concrete Terminology*, SP-19(78), American Concrete Institute, Farmington hills, Michigan, 50 pages. Cited in Ytterberg, 1980b.
- ACI Committee 207 (1987): *Mass concrete*, Technical Report ACI 207-1R-87, American Concrete Institute, Farmington Hills, Michigan. 44 pages.
- ACI Committee 209 (1982): *Prediction of Creep, Shrinkage and Temperature effects in concrete structures*, Technical Report ACI 209R-82, American Concrete Institute, Farmington Hills, Michigan.
- ACI 305R-96 (1996): Hot Weather Concreting, *ACI Manual of Concrete Practice Part 2*. American Concrete Institute, Farmington Hills, Michigan.
- ACI 318-89 (Revised 1992): Building Code Requirements for reinforced concrete, *ACI Manual of Concrete Practice Part 3: Use of concrete in buildings – Design, Specifications and Related Topics*. American concrete Institute, Farmington Hills, Michigan. 345 pages.
- Ahlvin, R.G. (1991): *Origin of developments for structural design of pavements*, Technical Report GL-91-26, U.S. Army Corps of Engineers, Waterways Experiments Station, Vicksburg, MS.
- Aïtcin, P.C., Neville, A.M. and Acker, P. (1997): Integrated view of shrinkage deformation, *Concrete International*. Vol.**19**, No.9, pp. 35-41.
- Al-Nasra, M. and Wang, L.R.L. (1994): Parametric study of slab-on-grade problems due to initial warping and point loads, *ACI Structural Journal*. Vol. **91**, No. 1 (March-April), pp. 198-210.
- Al-Nasra, M. (1997): Finite element analysis of floor slabs under warping effect, *Engineering Structures*. Vol. **19**, No. 7, pp. 533-539.
- Alavizadeh-Farhang, A. and Silfwerbrand, J. (1998): Combined mechanical and thermal loading on plain and steel fibre reinforced concrete pavements. In: *8th International Symposium on Concrete Roads. 13th - 16th September 1998*. 1st ed. Theme I - Quality Assurance and Specifications. ATIC, Lisbon, pp. 151-157.
- Andrade, C., Sarr¡a, J. and Alonso, C. (1999): Relative humidity in the interior of concrete exposed to natural and artificial weathering, *Cement and Concrete Research*. Vol. **29**, No. 8, pp. 1249-1259.

- Armaghani, J.M., Larsen, T.J. and Smith, L.L. (1987): Temperature response of concrete pavements, *Transportation Research Record*, No. **1121**, pp. 23-33.
- Austin, S.A., Robins, P.J. and Bishop, J.W. (1998): Behaviour and design of concrete industrial ground floors, *Concrete*, Vol. 32, No. 6, pp. 8-10. (Invited)
- Austin, S.A., Robins, P.J. and Bishop, J.W. (1999): Techniques for the early-life in-situ monitoring of concrete industrial ground floor slabs. In: *Specialist techniques and materials for concrete* construction – Proceedings of the International Conference held at Dundee University on 8th to 10th October, 1st Ed. (Eds. Dhir, R.K. and Henderson, N.A.) Thomas Telford, London, pp 317-329.
- Austin, S.A. and Bishop, J.W. (2000): Monitoring of concrete industrial ground floor slabs, *Seminar on Developments in Industrial Concrete Ground Floors*, 31st October 2000, Aston University, England.
- Austin, S.A., Robins, P.J. and Bishop, J.W. (2001):In-situ instrumentation of concrete industrial ground floor slabs. Submitted to *The Structural Engineer*.
- Ayotte, É., Massicote, B., Houde, J. and Gocevski, V. (1997): Modelling the thermal stresses at early ages in a concrete monolith, *ACI Materials Journal*, Vol. **94**, No. 6 (Nov-Dec), pp. 577-587.
- Barenberg, E.J. and Zollinger, D.G. (1990): Validation of concrete pavement responses using instrumented pavements, *Transportation Research Record*, No. **1286**, pp. 67-77.
- Barnbrook, G. *et. al.* (1994): *Technical Report 34: Concrete Industrial Ground Floors - A guide to their Design and Construction*, Second ed. The Concrete Society, Slough, 145 pages.
- Bathe, K.-J. (1982): *Finite element procedures in engineering analysis*, Prentice Hall, London.
- Bazant, Z.P. (1970): Constitutive equations for concrete creep and shrinkage based on thermodynamics of multiphase systems, *Materials and Structures*, Vol **3**, pp. 3-36.
- Bazant, Z.P. (1971): Thermodynamic theory of deformations of concrete with explanation of drying creep, *American Concrete Institute Special Publication*, No. **27**, pp.411-421.
- Bazant, Z.P. (1972a): Thermodynamics of hindered absorption and its implications for hardened cement paste and concrete. *Cement and Concrete Research*, Vol. **2**, pp. 1-16.
- Bazant, Z.P. (1972b): Thermodynamics of interacting continua with surfaces and creep analysis of concrete structures. *Nuclear Engineering and Design*, Vol. **20**, pp. 477-505.

- Bazant, Z.P. (1972c): Prediction of concrete creep effects using the age effected modulus method, *ACI Journal*, Vol. **69**, pp. 212-217.
- Bazant, Z.P. (Ed): *Mathematical Modelling of Creep and Shrinkage*. John Wiley and Sons, Chichester. 1988. 459 pages.
- Bazant, Z.P. and Baweja, S. (1995a): Creep and shrinkage prediction model for analysis and design of concrete structures - model B3, *Materials and Structures*. Vol. **28**, No. 28, pp. 357-365.
- Bazant, Z.P. and Baweja, S. (1995b): Justification and refinements of Model B3 for concrete creep and shrinkage. 1 Statistics and sensitivity, *Materials and Structures*. Vol. **28**, pp. 415-430.
- Bazant, Z.P. and Baweja, S. (1995c): Justification and refinements of model B3 for concrete creep and shrinkage. 2 Updating and theoretical basis, *Materials and Structures*. Vol. **28**, pp. 488-495.
- Bazant, Z.P. and Carol, I. (Eds.): *Creep and Shrinkage of Concrete – Proceedings of the Fifth International RILEM Symposium*, Barcelona, Spain. E & FN Spon, London. 1993. 934 pages.
- Bazant, Z.P., Dougill, J., Huet, C., Tsubaki, T and Wittman, F. (1988): Material models for Structural Creep Analysis. In: *Mathematical Modelling of Creep and Shrinkage of Concrete*. John Wiley and Sons, Chichester. 1988. 459 pages.
- Bazant, Z.P. and Kim, J.-K. (1991): Consequences of diffusion theory for shrinkage of concrete, *Materials and Structures*. Vol. **24**, pp. 323-326.
- Bazant, Z.P. and Najjar, L.J. (1972): Nonlinear water diffusion in nonsaturated concrete, *Materials and Structures*. Vol. **5**, pp. 3-20.
- Bazant, Z.P. and Osman, E. (1976): Double power law for basic creep of concrete, *Materials and Structures*. Vol. **9**, No. 49, pp. 3-11.
- Bazant, Z.P., Osman, E. and Thonguthai, W. (1976): Practical formulation of shrinkage and creep of concrete, *Materials and Structures*. Vol. **9**, No. 54, pp. 395-406.
- Bazant, Z.P. and Panula, L. (1978a): Practical formulation of time-dependant deformations of concrete. Part I: Shrinkage, *Materials and Structures*. Vol. **11**, No. 65, pp. 307-316.
- Bazant, Z.P. and Panula, L. (1978b): Practical formulation of time-dependant deformations of concrete. Part II: Basic creep, *Materials and Structures*. Vol. **11**, No. 65, pp. 317-328.

- Bazant, Z.P. and Panula, L. (1978c): Practical formulation of time-dependant deformations of concrete. Part III: Drying creep, *Materials and Structures*. Vol. **11**, No. 66, pp. 415-424.

- Bazant, Z.P. and Panula, L. (1978d): Practical formulation of time-dependant deformations of concrete. Part IV: Temperature effect on basic creep, *Materials and Structures*. Vol. **11**, No. 66, pp. 424-434.

- Bazant, Z.P. and Wittman, F.H. (Eds): *Creep and Shrinkage in Concrete Structures*, John Wiley and Sons. Chichester. 1982. pp.87-108.

- Beckett, D. (1990): Comparative tests on plain, fabric reinforced and steel fibre reinforced concrete ground slabs. *Concrete*, Vol. 24, No. 3, pp. 43-45.

- Beckett, D. (1999): Corner and edge loading on concrete industrial ground floors reinforced with steel fibres. *Concrete*, Vol. 77, No , pp.22-24.

- Bhatti, M.A., Molinas-Vega, I. and Stoner, J.W. (1998): Nonlinear analysis of jointed concrete pavements, *Transportation Research Record*. No. **1629**, pp. 50-57.

- Bishop, J.W. (1998): Behaviour and Design of Concrete Industrial Ground Floors, *Concrete Day '98*, Concrete Society and the ACIFC, June 1998, Brunel University.

- Bloom, R. and Bentur, A. (1995): Free and Restrained Shrinkage of Normal and High-Strength Concrete, *ACI Materials Journal*. Vol. **92**, No. 2, pp. 211-217.

- Bodocsi, A., Minkarah, I.A. and Arudi, R.S. (1993): Analysis of horizontal movements of joints and cracks in Portland Cement concrete pavements, *Transportation Research Record*. No. **1392**, pp. 43-52.

- van den Bogert, P.A.J., de Borst, R. and Nauta, P. (1987): Simulation of the mechanical behaviour of young concrete. In: *Proceedings of the IABSE Colloquium on Computational Mechanics of Reinforced Concrete Structures: Advances and Applications*. Delft University Press, Delft, pp. 339-347.

- de Borst, R. (1989): Thermal stresses. In: *Fracture Mechanics of Concrete Structures*. 1st ed. (Ed: Elfgren.L) Chapman and Hall, London, pp. 148-154.

- de Borst, R., van den Boogaard, A.H. (1994): Finite element modelling of deformation and cracking in early-age concrete, *ASCE Journal of Engineering Mechanics*, Vol. **120**, No. 12, pp. 2519-2534.

- Boulay, C. and Paties, C. (1993): Mesure des déformations du béton au jeune âge, *Materials and Structures*. Vol. **26**, pp. 307-311.

- van Breugal, K (1980): Artificial cooling of hardening concrete, Delft.

- van Breugel, K. (1982): Development of temperature and properties of concrete as a function of the degree of hydration. In: *Proceedings of International Conference on Concrete of Early Ages*, Paris, 6-8 April 1982. Edition Anciens ENCP ed. (Ed: Rilem) Association Amicale des Engenieurs, Paris, pp. 179-185.

- van Breugel, K. (1991): Simulation model for development of properties of early age concrete. In: *Quality Control of Concrete Structures - Proceedings of the Second International RILEM/CEB Symposium, Ghent, June 1991*. RILEM Proceedings 14. (Eds: Taerwe, L. and Lambotte, H.) E & FN Spon, London, pp. 139-151.

- van Breugel, K. (1998): Prediction of temperature development in hardening concrete. In: *Prevention of Thermal Cracking in Concrete at Early Ages*. (Ed: Springenschmid, R.) E & FN Spon, London, pp. 51-75.

- Brüll, L. and Komlos, K. (1982): Early shrinkage of hardening cement pastes. In: *Fundamental Research on Creep and Shrinkage of Concrete*. (Ed: Wittman, F.H.) Martinus Nijhoff Publishers, The Hague, pp. 239-248.

- Byfors, J. (1980): *Plain concrete at early ages*. Swedish Council for Building Research. 464 pps.

- Comité Europeén du Beton/Federation Internationale de la Precontrainte (CEB-FIP, 1978): International Recommendations for the Design and Construction of Concrete Structures. Third Ed. Cement and Concrete Association, London.

- CEB-FIP Model Code 1990 (1993). Comité Euro-International du Beton.

- Chandler, J.W.E (1982): Design of Floors on Ground, *Technical Report 550*, Slough, Cement and Concrete Association, 22 pages.

- Channakeshava, C., Barzeger, F. and Voyiadjis, G.Z. (1993): Nonlinear FE analysis of plain concrete pavements with dowelled joints, *Journal of Transportation Engineering*. Vol. **119**, No. 5 (September/October), pp. 763-781.

- Choubane, B. and Tia, M. (1995): Analysis and verification of thermal-gradient effects on concrete pavements, *Journal of Transportation Engineering*. Vol. **121**, No. 1 (Jan/Feb), pp. 75-81.

- CIBSE (1999): *CIBSE Guide, Volume A – Design Data*. 6th ed. The Chartered Institute of Building Services Engineers, London.

- Crawford, R.A. and Anderson, D.W. (1963): Construction of a continuously reinforced pavement in South Dakota, *Highway Research Record*. Vol. **60**, pp. 154-168.

- Darter, M. (1976): *Design of zero-maintenance plain jointed concrete pavements*, Vol. 1, *Development of design procedures*, University of Illinois, Urbana, 1976.
- Davids, W.G., Turkiyyah, G.M. and Mahoney, J.P. (1998): EverFE - Rigid pavement three-dimensional finite element analysis tool, *Transportation Research Record*. No. **1629**, pp. 41-49.
- Eierle, B. and Schikora, K. (1999): Computational modelling of concrete at early ages using Diana. *Diana World*, No. 2, Diana Analysis bv, Delft. pp7-8.
- Eisenmann, J. and Leykauf, G. (1990): Simplified calculation method of slab curling caused by surface shrinkage. In: *2nd International Workshop on the Theoretical Design of Concrete Pavements*. 1st ed. Vol. 5. (Ed: PIARC Committee on Concrete Roads - Cembureau) Centre ROW, Ede, pp. 185-197.
- Emborg, M. (1998): Development of mechanical behaviour at early ages. In: *Prevention of Thermal Cracking in Concrete at Early Ages*. (Ed: Springenschmid, R.) E & FN Spon, London, pp. 76-148.
- Eymard, R. (1994): Allowing for the creep of concrete in a finite-element structural calculation, *Computers & Structures*. Vol. 53, No. 4, pp. 921-928.
- Faraggi, V., Jofr, C. and Kraemer, C. (1987): Combined effect of traffic loads and thermal gradients on concrete pavement design, *Transportation Research Record*. No. **1136**, pp. 108-118.
- FHWA (Federal Highway Administration, 1996): Implementation Program on High Performance Concrete – Guidelines for Instrumentation of Bridges. U.S. Department of Transportation, August 1996. http://hpc.fhwa.dot.gov/instruments.htm
- First European Conference on Smart Structures and Materials - Glasgow 12-14 May 1992. 1st ed., SPIE Volume 1777. (Eds: Culshaw, B., Gardiner, P.T. and McDonach, A.) The European Optical Society, The International Society for Optical Engineering and the Institute of Physics Publishing, Bristol.
- Friberg, B.F. (1940): Design of dowels in transverse joints of concrete pavements, *Transactions, ASCE*. Vol. **105**, pp. 1076-1095.
- Friberg, B.F. (1954): Frictional resistance under concrete pavements and restraint stresses in long reinforced slabs, *Proceedings of the Highway Research Board*. Vol. **33**, pp. 167-184.

- Fwa, T.F., Shi, X.P. and Tan, S.A. (1996): Use of Pasternak foundation model in concrete pavement analysis, *Journal of Transportation Engineering*, Vol. **122**, No. 4 (July/August), pp. 323-328.
- Gilbert, R.I. (1988): *Time Effects in Concrete Structures*. Elsevier, Amsterdam. 321pp.
- Goldbeck, A.T. (1919): Thickness of concrete slabs, *Public Roads*, Vol. **1**, No. 12.
- Grzybowski, M. and Shah, S.P. (1989): Model to predict cracking in fibre reinforced concrete due to restrained shrinkage. *Magazine of Concrete Research*. Vol. **41**, No. 148, pp. 125-135.
- Gulden, W. and Brown, D. (1985): Establishing load transfer in existing jointed concrete pavements, *Transportation Research Record*, No. **1043**, pp. 23-32.
- Hannant, D. (1994): Fibres in industrial ground-floor slabs, *Concrete*. Vol. **28**, No. 1, pp. 16-19.
- Hansen, W. and Almudaiheem, J.A. (1987): Ultimate Drying Shrinkage of Concrete - Influence of Major Parameters, *ACI Materials Journal*. Vol. 84, May-June, pp. 217-223.
- Hauggaard-Nielsen, A.B. (1997): *Mathematical Modelling and Experimental Analysis of Early Age Concrete. Ph.D. Thesis*, Department of Structural Engineering and Materials, Technical University of Denmark, DK-2800 Lyngby, Denmark. 145 pps.
- Hillerborg, A (1975): Kompendium i byggnadsmateriallära, FK1, *Dictionary of Building Materials*. Lund Institute of Technology, Sweden. In Swedish. Cited in Thelandersson *et. al.* (1998).
- Hulsey, J.L. and Powell, D.T. (1993): Rational weather model for highway structures, *Transportation Research Record*, No. **1392**, pp. 54-64.
- Ioannides, A.M., Thompson, M.R. and Barenberg, E.J. (1985): Westergaard solutions reconsidered, *Transportation Research Record*. No. **1034**, pp. 13-23.
- Ioannides, A.M. and Korovesis, G.T. (1990): Aggregate Interlock: A Pure-shear load transfer mechanism, *Transportation Research Record*. No. **1286**, pp. 14-24.
- Ioannides, A.M., Lee, Y.-H. and Darter, M.I. (1990): Control of faulting through joint load transfer design, *Transportation Research Record*. No. **1286**, pp. 49-56.
- Ioannides, A.M. and Khazanovich, L. (1998): General formulation for multilayered pavement systems, *Journal of Transportation Engineering*. Vol. **124**, No. 1(Jan/Feb), pp. 82-90.

- H.M. Jennings and Y. Xi, Microstructurally based mechanisms for modelling shrinkage of cement paste at multiple levels (Principal lecture), in: *Creep and Shrinkage of Concrete*, eds. Bazant and Carol. pp. 85-102.
- Jiang, J. and Mirza, F.A. (1997): Nonlinear analysis of reinforced concrete slabs by a discrete finite element approach, *Computers & Structures*. Vol. **65**, No. 4, pp. 585-592.
- Jonasson, J.-E. (1982): Analyses of shrinkage in concrete. In: *Fundamental Research on Creep and Shrinkage of Concrete*. (Ed: Wittman, F.H.) Martinus Nijhoff Publishers, The Hague, pp. 259-268.
- Jonasson, J.-E. and Emborg, M. (1996): Hett2DL & TempStre. Quoted in: Hauggaard-Nielsen, A.B. (1997): *Mathematical Modelling and Experimental Analysis of Early Age Concrete*. Ph.D. Thesis, Department of Structural Engineering and Materials, Technical University of Denmark, DK-2800 Lyngby, Denmark. 145 p.
- JSCE – SF4: *Method of test for flexural strength and flexural toughness of steel fibre reinforced slabs*. Japan Society of Civil Engineers.
- Kasai, Y. et al. (1971): Tensile properties of early age concrete. In: *Proceedings of the 1971 International Conference on Mechanical Behaviour of Materials*. Vol. 4. pp. 288-299.
- Kasai, Y., Matsui, I. and Yokoyama, K. (1982): Volume change of concrete at early ages. In: *Proceedings of International Conference on Concrete of Early Ages*, Paris, 6-8 April 1982. Edition Anciens ENCP ed. (Ed: Rilem) Association Amicale des Engénieurs, Paris, pp. 51-56.
- Kelley, E.F. (1939): Application of the results of research to the structural design of concrete pavements, *Journal of the American Concrete Institute, Proceedings* Vol. **35**, No. 6, pp. 437-464.
- Khan, A.A., Cook, W.D. and Mitchell, D. (1998): Thermal properties and transient thermal analysis of structural members during hydration, *ACI Materials Journal*. Vol. **95**, No. 3(May-June), pp. 293-303.
- Kiamco, C. (1997): A Structural Look at Slabs on Grade, *Concrete International*. Vol. **19**, No. 7 (July), pp. 45-49.
- Kim, J.K. and Lee, C.S. (1998): Prediction of differential drying shrinkage in concrete, *Cement and Concrete Research*, Vol. **28**, No. 7, pp. 985-994.

- Kim, S.-M., Won, M. and McCullough, B.F. (1998): Numerical modelling of continuously reinforced concrete pavement subjected to environmental loads, *Transportation Research Record*. No. **1629**, pp. 76-89.

- Kim, S.-M., Won, M.C and McCullough, B.F. (2000): *Three dimensional nonlinear finite element analysis of continuously reinforced concrete pavements*. Centre for Transportation Research, The University of Texas at Austin, Austin, Texas. 75pps.

- Knapton, J. (1999): *Single pour industrial floor slabs*, Thomas Telford Limited, London, 176pps.

- Kohler, M.A., Nordensen, T.J. and Fox, W.E. (1955): Evaporation from pans and lakes, *Research Paper* No. 38, U.S. Dept. of Commerce, Washington.

- Kovler, K. (1994): Testing system for determining the mechanical behaviour of early age concrete under restrained and free uniaxial shrinkage, *Materials and Structures*. Vol. **27**, No. 170, pp. 324-330.

- Kunt, M.M. and McCullough, B.F. (1990): Evaluation of the sub-base drag formula by considering realistic sub-base friction values, *Transportation Research Record*. No. **1286**, pp. 78-83.

- Lachemi, M. and Aïtcin, P.-C. (1997): Influence of ambient and fresh concrete temperatures on the maximum temperature and thermal gradient in a high performance concrete structure, *ACI Materials Journal*. Vol. **94**, No. 2 (March/April), pp. 102-110.

- Lachemi, M., Bois, A.-P., Miao, B., Lessard, M. and Aïtcin, P.-C. (1996): First Year Monitoring of the First Air-Entrained High-Performance Bridge in North America, *ACI Structural Journal*. Vol. **93**, No. 4 (July-August), pp. 379-386.

- Lang, F.C. (1941): Temperature and moisture variations in concrete pavements, Highway Research Board Proceedings, Vol. **21**, Washington, D.C., pp. 260-271. Cited in Liang & Niu (1998).

- Leonards, G.A and Harr, M.E (1958): Analysis of concrete slabs on ground, *Journal of Soil Mechanics*, ASCE, No. SM3, pp. 35-58.

- Li, G., Zhao, Y., Pang, S.-S. and Li, Y. (1999): Effective Young's modulus estimation of concrete, *Cement and Concrete Research*. Vol. **29**, No. 9, pp. 1455-1462.

- Liang, R.Y. and Niu, Y.Z. (1998): Temperature and curling stress in concrete pavements: analytical solutions, *Journal of Transportation Engineering*. Vol. **124**, No. 1 (Jan/Feb), pp. 91-100.

- Loo, Y.H., Peterson, J.S., Swaddiwudhipong, S. and Tam, C.T. (1995): Application of the layering method on large concrete pours, *Magazine of Concrete Research*. Vol. **47**, No. 172, pp. 209-217.

- Losberg, A. (1960): Structurally reinforced concrete pavements, *PhD Thesis*, Chalmers Technical University, Goteborg, Sweden.

- Losberg, A. (1978): Pavements and slabs on grade with structurally active reinforcement, *ACI Journal*. Vol. **75**, No. 66, pp. 647-657.

- Mandel, E.D., Burns, N.H. and McCullough, B.F. (1990): Prestressed concrete pavement: Instrumentation, behaviour, and analysis of horizontal movements, *Transportation Research Record*. No. **1286**, pp. 38-48.

- McDonald, D.B. and Roper, H. (1993): Accuracy of Prediction Models for Shrinkage of Concrete, *ACI Materials Journal*. Vol. **90**, No. 3, pp. 265-271.

- Menzel,C.A. (1954): Causes and prevention of crack development in plastic concrete, *Portland cement association annual meeting*. pp. 130-136.

- Meyerhof, G.G. (1962): Load Carrying Capacity of Concrete Pavements, *Journal of the Soil Mechanics and Foundations Division* - Proceedings of the ASCE 88 (June), pp. 89-116.

- Minkarah, I., Cook, J.P. and McDonough, J.F. (1981): Magnitude of horizontal movements in jointed concrete pavements, *Transportation Research Record*. No. **821**, pp. 61-67.

- Mirambell, E. (1990): Temperature and stress distributions in plain concrete pavements under thermal and mechanical loads. In: 2nd International Workshop on the Theoretical Design of Concrete Pavements. 1st ed. Vol. 5. (Ed: PIARC Committee on Concrete Roads - Cembureau) Centre ROW, Ede, pp. 121-135.

- Mohr, G.A. (1992): *Finite elements for solids, fluids and optimization*. Oxford University Press, Oxford.

- Nagataki, S. (1970): Shrinkage and shrinkage restraints in concrete pavements, *ASCE Structural Journal*, ST7, pp. 1333-1358.

- Nagy, A (1997): Simulation of thermal stress in reinforced concrete at early ages with a simplified model, *Materials and Structures*, Vol.30, No. , pp. 167-173.

- Neville, A.M. (1995): *Properties of Concrete*. 4th ed. Longman Group Limited, Harlow. 844 pps.

- Neil, F.R. (1996): *ICE Design and Practice Guide – Concrete Industrial Ground Floors.* Thomas Telford Publishing, London. 41 pages.
- National Cooperative Highway Research Program, NCHRP Report 372 (1995): *Support under Portland Cement Concrete Pavements.* National Academy Press, Washington, D.C. 50 pages.
- Nishizawa, T., Fukudu, T., Matsuno, S. and Himeno, K. (1997): Curling stress equation for transverse joint edge of a concrete pavement slab based on finite element method analysis, *Transportation Research Record.* No. **1525**, pp. 35-43.
- Older, C. (1924): Highway research in Illinois, *ASCE Transactions*, Vol. **87**.
- Oluokun, F.A. (1991): Prediction of concrete tensile strength from its compressive strength: Evaluation of existing relations for normal weight concrete, *ACI Materials Journal*, Vol. **88**, No. 3(May-June), pp. 302-309.
- Oluokun, F.A., Burdette, E.G. and Deatherage, J.H. (1991a): Elastic modulus, Poisson's ratio and compressive strength relationships at early ages, *ACI Materials Journal.* Vol. **88**, No. 1 (Jan/Feb), pp. 3-10.
- Oluokun, F.A., Burdette, E.G. and Deatherage, J.H. (1991b): Splitting tensile strength and compressive strength relationship at early ages, *ACI Materials Journal.* Vol. **88**, No. 2 (March-April), pp. 115-121.
- Ozbeki, M.A., Kilareski, W.P. and Anderson, D.A. (1985): Evaluation methodology for jointed concrete pavements, *Transportation Research Record.* No. **1043**, pp. 1-8.
- Parrott, L.J. (1990): *A review of methods to determine the moisture conditions in concrete.* British Cement Association, Crowthorne, Berks. 28 pages.
- Perenchio, W.F. (1997): The Drying Shrinkage Dilemma, *Concrete Construction.* Vol. **42**, No. 4, pp. 379-383.
- Pernetti, M. (1998): A simplified stress evaluation method considering the loss of contact pavement -support. In: *8th International Symposium on Concrete Roads. 13th - 16th September 1998.* 1st ed. Theme I - Quality Assurance and Specifications. ATIC, Lisbon, pp. 165-177.
- Pettersson, D. (1998): Stresses in Concrete Structures from Ground Restraint. Ph.D. Thesis, Department of Structural Engineering, Lund Institute of Technology, Sweden. 113 pps.
- Philjavaara, S.E. (1982): Estimation of drying shrinkage of concrete at different relative humidities and temperature of ambient air with special discussion about fundamental

features of drying and shrinkage. In: *Creep and Shrinkage in Concrete Structures*, Eds. Bazant, Z.P. and Wittman, F.H., John Wiley and Sons. Chichester. pp.87-108.

- Pickett, G (1951): A study of stresses in the corner region of concrete slabs under large corner loads. *Concrete Pavement Design*, Portland Cement Association, Chicago. Appendix 3, pp. 77-87.

- Poblete, M., Valenzuela, R. and Salsilli, R. (1988a): Load transfer in undowelled transverse joints of PCC pavements, *Transportation Research Record*. No. **1207**, pp. 39-49.

- Poblete, M., Salshilli, R., Valenzuela, R., Bull, A. and Spratz, P. (1988b): Field evaluation of thermal deformations in undowelled PCC pavement slabs, *Transportation Research Record*. No. **1207**, pp. 217-228.

- Powers, T.C. (1968): Mechanisms of shrinkage and reversible creep of hardened cement paste. In: *The Structure of Concrete and its behaviour under load: Proceedings of an International Conference, London, September 1965*. 1st ed. Vol. 1. (Eds: Brooks, A.E. and Newman, K.) Cement and Concrete Association, London, pp. 319-344.

- Powers, T.C. and Brownyard, T.L. (1946): Studies of the physical properties of hardened portland cement paste. *Journal of the ACI*, Vol. **18**. Quoted in: Hauggaard-Nielsen, A.B. (1997): Mathematical Modelling and Experimental Analysis of Early Age Concrete. *Ph.D. Thesis*, Department of Structural Engineering and Materials, Technical University of Denmark, DK-2800 Lyngby, Denmark. 145 p.

- Pufahl, D.E., Lytton, R.L. and Liang, H.S. (1990): Integrated computer model to estimate moisture and temperature effects beneath pavements, *Transportation Research Record*. No. **1286**, pp. 259-269.

- Radocea, A. (1994): A model of plastic shrinkage. *Magazine of Concrete Research*, Vol. **46**, No. 167, pp. 125-132.

- Rajasekaran, S. and Sankarasubramanian, G. (1996): Finite Element Non-linear Analysis of Concrete Structures, *Indian Concrete Institute Bulletin*. Vol. **56**, pp. 31-37.

- Rees, S.W., Lloyd, R.M. and Thomas, H.R. (1995): A numerical simulation of measured transient heat transfer through a concrete ground floor slab and underlying substrate, *International Journal of Numerical Methods in Heat and Fluid Flow*. Vol. **5**, pp. 669-683.

- Reinhardt, H.W., Blauuwendraad, J. and Jongedijk, J. (1982): Temperature development in concrete structures taking account of state dependent properties. In: Proceedings of the International Conference on Concrete of Early Ages, Paris, 6-8 April 1982. Edition

Anciens ENCP, Vol. 1. (Ed: Rilem), Association Amicale des Engénieurs, Paris, pp. 211-218.

- Richardson, J.M. and Armaghani, J.M. (1987): Stress caused by temperature gradient in Portland cement concrete pavements, *Transportation Research Record*. No. **1121**, pp. 7-13.

- Rilem Commission 42-CEA (1981): Properties of set concrete at early ages - State of the art report, *Materials and Structures*. Vol. **14**, No.84, pp. 399-450.

- Ringo, B.C. & Anderson, R.B. (1996): *Designing floor slabs on grade*, 2nd Ed. The Aberdeen Group, Addison, Ill. 266pps.

- Rollings, R.S. (1993): Curling failure of steel-fiber-reinforced concrete slabs, *Journal of Performance of Constructed Facilities*. Vol. **7**, No. 1 (February), pp. 3-19.

- Roper, H. and Anderson, T. (1982): Laboratory and site studies of early dimensional changes and crack development. In: *Proceedings of International Conference on Concrete of Early Ages*. Paris, 6-8 April 1982. Edition Anciens ENCP ed. (Ed: Rilem) Association Amicale des Engénieurs, Paris, pp. 63-69.

- Rostasy, F.S., Gutsch, A. and Laube, M. (1993): Creep and relaxation of concrete at early ages – experiments and mathematical modelling, In: *Proceedings of the 5th International RILEM Symposium on Creep and Shrinkage of Concrete, Barcelona*. E & FN Spon, London. pp. 453-458.

- Rüsch, H., Jungwirth, D. and Hilsdorf, H.K. (1983): *Creep and Shrinkage. Their Effect on the Behaviour of Concrete Structures*. Springer-Verlag, New York.

- Sale, J.P. (1977): Rigid pavement design for airfields, *Proceedings First International Conference on Concrete Pavement Design*, Purdue University, West Lafayette, IN.

- Samman, T.A., Mirza, W.H. & Wafa, F.F. (1996): Plastic shrinkage cracking of normal and high strength concrete: A comparative study. *ACI Materials Journal*, V.93, No. 1, pp.36-40.

- Saraf, C.L. and McCullough, B.F. (1986): Controlling longitudinal cracking in concrete pavements, *Transportation Research Record*. No. **1043**, pp. 8-13.

- Sargious, M. and Ghali, A. (1986): Stresses in prestressed and non-prestressed pavements and slabs on grade due to differential shrinkage and creep, *ACI Journal*. Vol. **83**, No. 5, pp. 772-776.

- Schrader, E.K. (1987): *A solution to cracking caused by dowels and tie bars*. (Unpublished) 18 pages. Cited in Ytterberg, 1987c.

- de Schutter, G. and Taerwe, L. (1995): Specific heat and thermal diffusivity of hardening concrete, *Magazine of Concrete Research*. Vol. **47**, No. 172, pp. 203-208.
- de Schutter, G. and Taerwe, L. (1996): Degree of hydration based description of mechanical properties of early age concrete, *Materials and Structures*. Vol. **29**, pp. 335-344.
- Scott, R.H. and Gill, P.A.T. (1987): Measurement of internal concrete strains using embedment strain gauges, *Magazine of Concrete Research*. Vol. **39**, No. 139, pp. 109-112.
- Shaeles, C.A. and Hover, K.C. (1988): Influence of mix proportions and construction operations on plastic shrinkage cracking in thin slabs, *ACI Materials Journal*. Vol. **85**, November-December, pp. 495-504.
- Shahawy, M.A. and Arockiasamy, M. (1996a): Field instrumentation to study the time-dependent behaviour in Sunshine Skyway Bridge. I, *Journal of Bridge Engineering*. Vol. **1**, No. 2, pp. 76-86.
- Shahawy, M.A. and Arockiasamy, M. (1996b): Field instrumentation to study the time-dependent behaviour in Sunshine Skyway Bridge. II, *Journal of Bridge Engineering*. Vol. **1**, No. 2, pp. 87-97.
- Shimomura, T. and Maekawa, K. (1997): Analysis of the drying shrinkage behaviour of concrete using a micromechanical model based on the micropore structure of concrete. *Magazine of Concrete Research*, Vol. **49**, No. 181, pp. 303-322.
- Spigolon, S.J. (1963): Behaviour of experimental continuously reinforced concrete pavements in Mississippi, *Highway Research Record*. Vol. **60**, pp. 140-153.
- Springenschmid, R. and Breitenbücher, R. (1998): Influence of constituents, mix proportions and temperature on cracking sensitivity of concrete. In: *Prevention of Thermal Cracking in Concrete at Early Ages*. (Ed: Springenschmid, R.) E & FN Spon, London, pp. 40-50.
- Tabatabaie, A.M. (1978): *Structural analysis of concrete pavement joints*, PhD Thesis. Univeristy of Illinois, Urbana, Illinois.
- Taplin, J.M. (1959): A method for following the hydration reaction in Portland cement paste. *Aust. J. Appl. Sci.*, Vol. **10**, No 3. pp. 329-345. Cited in Byfors, 1980.
- Teller, L.W. and Sutherland, E.C. (1936): The structural design of concrete pavements, *Public Roads*, Vol. **17**, No. 7.

- Teller, L.W. and Sutherland, E.C. (1943): The Structural design of concrete pavements, Part 5, An experimental study of the Westergaard analysis of stress conditions in concrete pavements of uniform thickness, *Public Roads*, Vol. **23**, No. 8.

- Thelandersson, S., Alemo, J. and Nagy, A. (1998): Cracking in concrete structures due to imposed strains with regard to design of reinforcement, *Materials and Structures*. Vol. **31**, No. 211. Aug-Sep, pp. 442-450.

- Thompson, M.R., Dempsey, B.J., Hill, H. and Vogel, J. (1987): Characterizing temperature effects for pavement analysis and design, *Transportation Research Record*. No. **1121**, pp. 14-22.

- Timms, A.G. (1963): Evaluating subgrade friction-reducing mediums for rigid pavements, *Highway Research Record*. Vol. **60**, pp. 28-38.

- Tomlinson, J. (1940a): Temperature variations and consequent stresses produced by daily and seasonal temperature cycles in concrete slabs, *Concrete & Constructional Engineering*. Vol.**35**, No.6 (June), pp. 298-307.

- Tomlinson, J. (1940b): Temperature variations and consequent stresses produced by daily and seasonal temperature cycles in concrete slabs, *Concrete & Constructional Engineering*. Vol.**35**, No.7 (July), pp. 352-360.

- TR 34: Concrete Industrial Ground Floors – A guide to their design and construction (2002). 3rd Edition. Currently under revision. Concrete Society, Crowthorne.

- Trost, H (1967): Auswirkungen des Superpositionsprinzips auf Kriech- und Relaxations-Probleme bei Beton und Spannbeton, *Beton- und Stahlbetonbau*. Vol. **62**, No. 10, pp. 230-238. No. 11, pp. 261-269.

- Truman, K.Z., Petruska, D., Ferhi, A. and Fehl, B. (1991): Non-linear, incremental analysis of mass-concrete lock monolith, *Journal of Structural Engineering*, Vol. **117**, pp. 1834-1851.

- Turton, C.D. (1989): Discussion on paper 'Influence of mix proportions and construction operations on plastic shrinkage cracking in thin slabs' by Shaeles *et. al.* (1988). *ACI Materials Journal*. V.**86**, pp.531-532.

- Turton, C.D. et. al. (1992): *Technical Report 22: Non-structural cracks in concrete*. Third ed. The Concrete Society, Slough. 48 pages.

- Uno, P.J. (1998): Plastic shrinkage cracking and evaporation formulas, *ACI Materials Journal*. Vol. **95**, No. 4(July/August), pp. 365-375.

- Venkatasubramanian, V. (1963): Temperature Variation in a cement concrete pavement and the underlying subgrade, *Highway Research Record*. Vol. **60**, pp. 15-27.

- Voorschriften Beton – TGB 1990 (Regulations for concrete. Structural requirements and calculation methods). Technical Report NEN 6720, Nederlands Normalisitie Instituut, 1995.

- Walker, W.W. and Holland, J. A. (1998): Plate Dowels for Slabs on Ground, *Concrete International*. Vol. **20**, No. 7.

- Wang, C. and Dilger, W.H. (1995): Modelling of the development of heat of hydration in high-performance concrete. In: *Advances in Concrete Technology - Proceedings of Second CANMET/ACI International Symposium*, Las Vegas, Nevada, USA, 1995. (Ed: Malhotra, V.) American Concrete Institute, Detroit, Michigan, pp. 73-82.

- Wang, Y., Li, V.C. and Backer, S. (1990): Experimental determination of tensile behaviour of fiber reinforced concrete, *ACI Materials Journal*. Vol. **87**, No. 5, pp. 461-468.

- Water Loss Investigations: Lake Hefner Studies, Technical Report. *Geological Survey Circular* 229, 1952.

- Westergaard, H.M. (1926): Stresses in concrete pavements computed by theoretical analysis, *Public Roads*, Vol. **7**, No 2, pp. 25-35.

- Westergaard, H.M. (1928): Spacing of dowels, *Highways Research Board, Proceedings*. Vol. **8**. pp. 154-158.

- Westergaard, H.M (1929): Analysis of stresses in concrete pavements caused by variations in temperature, *Public Roads*, Vol. **10**, No. 3.

- de Witte, F.C. (Ed.): Diana Finite Element Analysis, Online User's Manual – Release 7.2, TNO Building and Construction Research, 1999.

- Wittmann, F.H. (Ed.): *Fundamental Research on Creep and Shrinkage of Concrete*, Martinus Nijhoff Publishers, The Hague, 1982. 528 pages.

- Wittmann, F.H. (1982): Creep and shrinkage mechanisms. In: Creep and Shrinkage in Concrete Structures. Eds. Bazant, Z.P. and Wittman, F.H., John Wiley and Sons. Chichester. pp.129-161.

- Wright, H.D. and Lloyd, R.M. (1992): Monitoring the performance of real building structures. In: *First European Conference on Smart Structures and Materials* - Glasgow 12-14 May 1992. 1st ed. SPIE Volume 1777. (Eds: Culshaw, B. et al.) The European

Optical Society. The international Society for Optical Engineering and the Institute of Physics Publishing, Bristol BS1 6NX, England.

- Ytterberg, R.F. (1987a): Shrinkage and Curling of Slabs on Grade: Part 1 - Drying Shrinkage, *Concrete International*. Vol. 9, No. 4 (April), pp. 22-31.

- Ytterberg, R.F. (1987b): Shrinkage and Curling of Slabs on Grade: Part 2 - Warping and Curling, *Concrete International*. Vol. 9, No. 5 (May), pp. 54-61.

- Ytterberg, R.F. (1987c): Shrinkage and Curling of Slabs on Grade: Part 3 - Additional Suggestions, *Concrete International*. Vol. 9, No. 6 (June), pp. 72-81.

- Ziegeldorf, S., Müller, H.S., Plöhn, J. and Hilsdorf, H.K. (1982): Autogeneous shrinkage and crack formation in young concrete. In: *Proceedings of International Conference on Concrete of Early Ages*, Paris, 6-8 April 1982. Edition Anciens ENCP ed. (Ed: Rilem) Association Amicale des Engénieurs, Paris, pp. 83-88.

- Zienkiewicz, O.C. (1977): *The Finite Element Method*, 3rd Edition, McGraw-Hill, London. 787pps.

- Zienkewicz O.C. and Taylor, R.L. (2000): *The Finite Element Method*, Volume 2: Solid Mechanics, 5th Edition. Butterworth Heinemann, Oxford, 459 pps.

- Zollinger, D.G. and Barenberg, E.J. (1990): Mechanistic Design Considerations for punchout distress in continuously reinforced concrete pavements, *Transportation Research Record*. No. **1286**, pp. 25-37.

- Zollinger, D.G. et al. (1993): Fracture Toughness of Concrete at Early Ages, *ACI Materials Journal*. Vol. **90**, No. 5 (September-October), pp. 463-471.

Appendix A.

Strain gauge information

GAGE TECHNIQUE
STRUCTURAL INSTRUMENTATION ENGINEERS

Vibrating Wire Strain Gauges
Transport & Road Research Laboratory Type
Types T/E/A & T/E/S For Measuring Internal Strains in Concrete

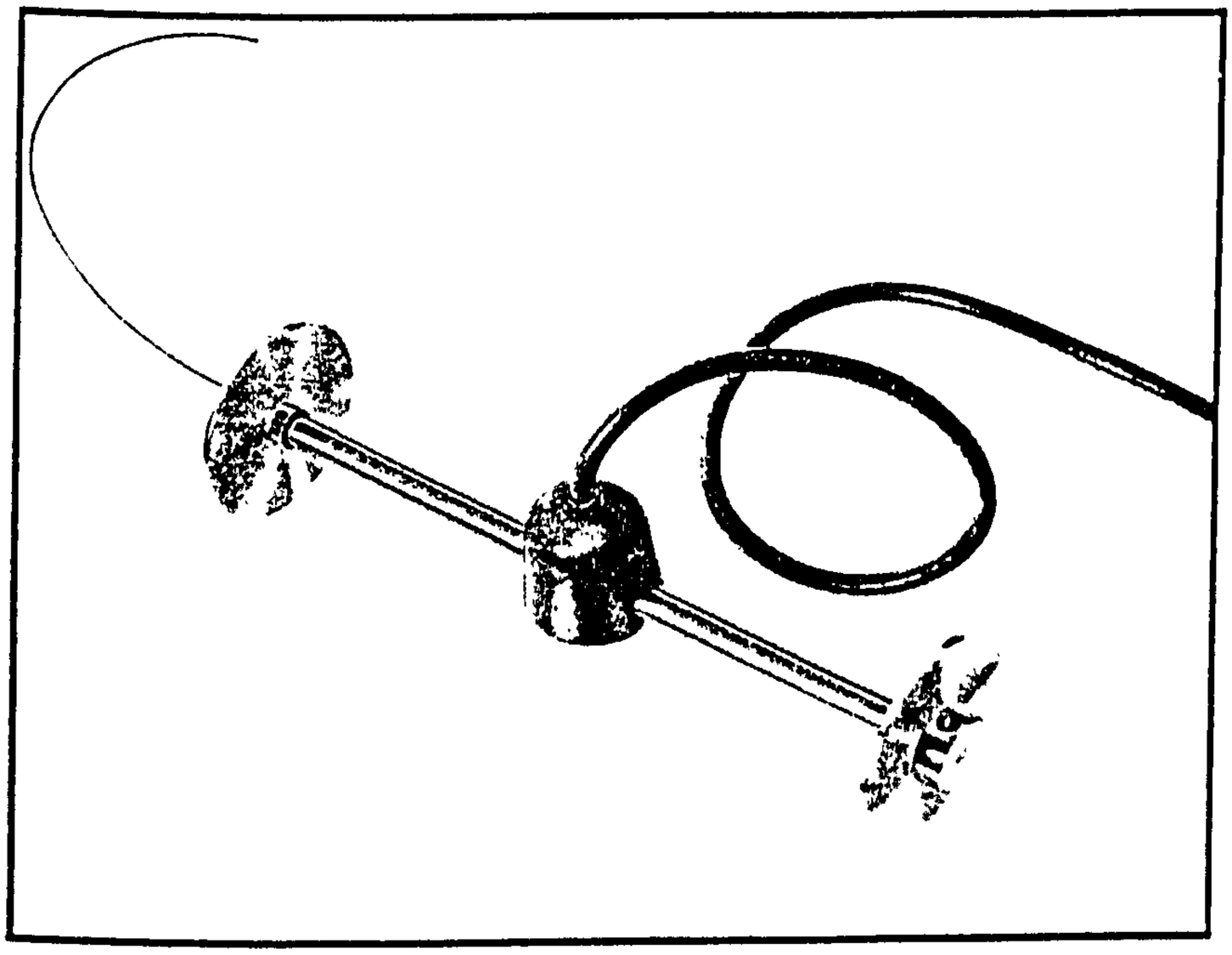

The Transport and Road Research Laboratory of the Department of the Environment measure internal strains in concrete by embedding vibrating wire strain gauges in the structure in single or multi-axis configurations. The gauges designed and used by the Laboratory are now offered by Gage Technique Limited with full TRRL approval, and incorporate the latest modifications and improvements to the basic designs.

Gauges of this type have been used extensively in concrete and steel box girder bridges, flyovers, motorways, strong floors, roof struts, concrete dams, pressure vessels and silos, turbine rafts, cast in-situ piles, driven piles, retaining walls, tunnel linings, gas and fuel pipes, coal mines, concrete caissons, and reservoirs.

Two types of gauge are supplied, each differing only in regard to the material of the enclosing tube. In one, type T/E/A, developed originally by Potocki, acrylic plastic is used. In the other, type T/E/S, introduced by Tyler, a stainless steel tube is employed. The acrylic gauge, being highly compliant on the axis of the strain, is particularly useful in measuring the characteristics of concrete during the early stages of curing. The stainless steel version is more robust and is more frequently used for strain investigations on site.

Each gauge contains a high tensile steel wire in tension between two end flanges and enclosed in either the acrylic or steel tube. A plucking coil is positioned at the centre of the tube and in close proximity to the wire. A current fed to the coil pulses the wire which then oscillates in an exponentially decaying half-wave mode along its length. The coil meantime acts as a pickup device and the voltage induced in it has the same frequency and amplitude characteristics as the oscillating wire.

When the gauge is embedded in concrete the strain resulting from the stresses developed in the concrete alters the natural frequency of oscillation of the wire. The strain in the concrete is proportional to the square of the frequency of oscillation of the wire and the gauge thus provides a sensitive system for measuring internal strains.

The signal from the coil is coupled to external measuring equipment via a flexible cable. By careful placing of gauges during the casting phase it is possible to record the complete strain history of the structure at one single remote reading console.

For measuring long term, slowly varying strains, gauges of vibrating wire type are preferable to other forms, having excellent long term stability — better than 10 microstrain per year — combined with simple installation and ease of monitoring. Tests on the gauges at the Transport and Road Research Laboratory confirm the repeatability of gauge factor, eliminating the necessity for individual calibration of gauges before use.

The gauges may be cast in direct though it is more usual to pre-briquette them before placement, using concrete of the same mix as that used in the structure.

The acrylic gauge, type T/E/A, was first employed by the TRRL in the Hammersmith Flyover, London. The steel tube version, type T/E/S has been used extensively both in the United Kingdom and abroad. Both the Medway bridge and the River Aire bridge have been instrumented with this gauge.

Because the signal output from the gauge is a frequency analogue of the strain it is measuring, no deterioration of strain translation occurs with time. It is not unusual therefore to find that instrumentation specifications, when defining gauge performance, stipulate a working life for such gauges of up to thirty years.

A temp. measuring version of the Type T/E/S/5.5 may also be supplied. This is denoted by Type Ref. T/E/S/T/5.5.

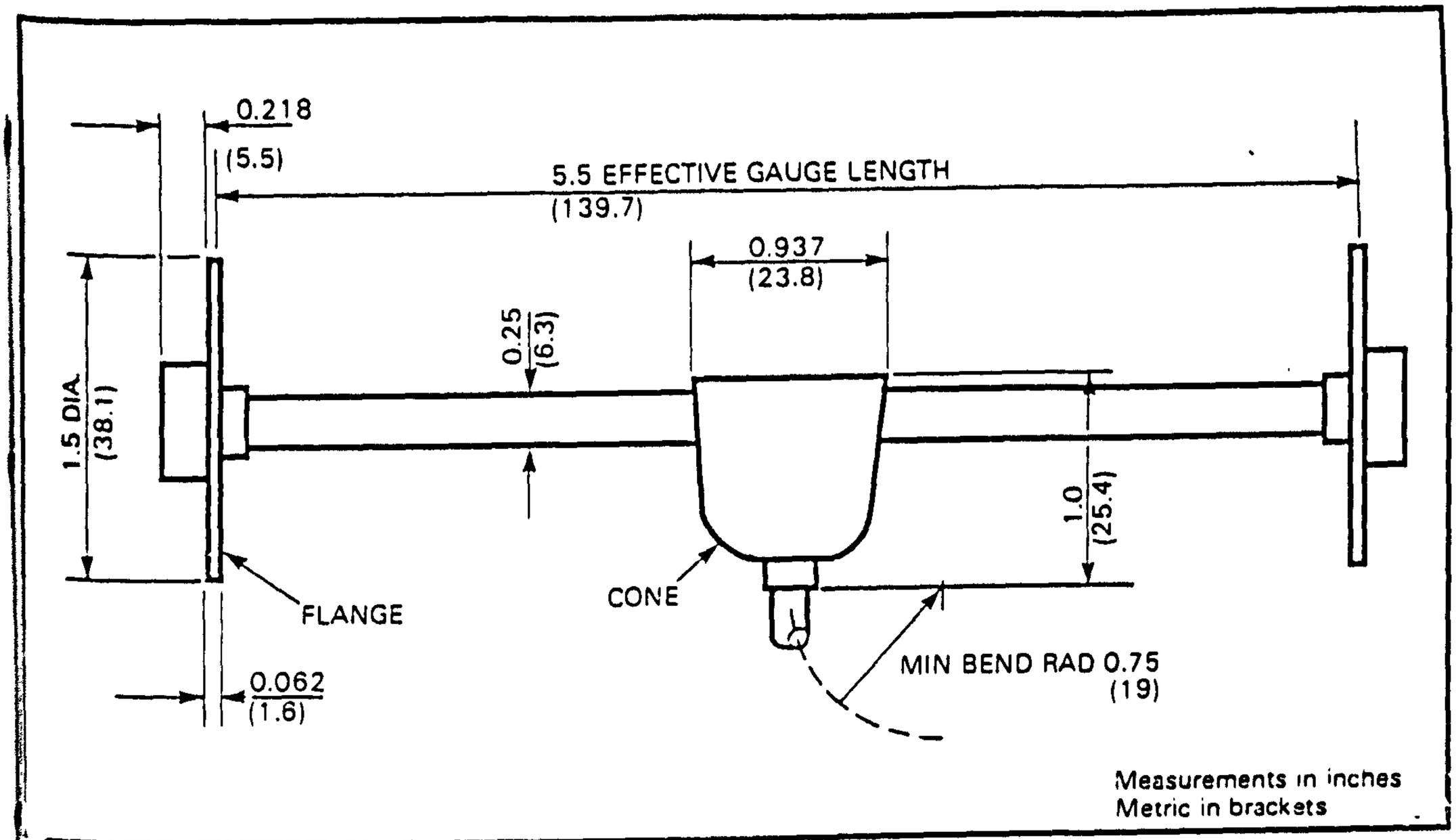

Measurements in inches
Metric in brackets

ECHNICAL SPECIFICATION
or T/E/A and T/E/S Gauges

uge Factor:
3.0 x 10^{-1} microstrain per frequency².

uge Equation:
$\delta s = 3.0 \times (f_1^2 - f_2^2) \times 10^{-1}$
icrostrain where δs is strain change.
f_1 is datum frequency in Hertz.
f_2 is frequency after loading in Hertz.

Note. Positive sign indicates compressive strain; negative sign tensile strain.

uge Length:
5.5 inches (140mm).

ain Range:
Greater than 3,000 microstrain.

solution attainable:
0.5 microstrain.

Resistance:
00 ohms nominal
(9.2 ± 0.5 on T/E/S/T).

cal Energising Voltage:
4v positive pulse, 10-20 milli-conds.

cal Datum Freq.:
00 Hertz.

perature Coeff:
T.C. of wire 11 x 10^{-6} per degree Centigrade.

perature Range:
T/E/A up to 50°C. T/E/S up to 75°C.

necting Cable:
Type 1C, screened coaxial type, terminated in coaxial connector.

le Length:
Unless order at extra cost, ndard lead length of 2 m. of cable is fitted.

re Stress:
At 800 Hertz, corresponding wire ss is 26 tons/sq. in. Wire T.S. is approx. 150 tons/sq. in.

Supply and Use:
Gauges are usually supplied unsealed and untensioned to allow setting to optimum range for strain range predicted. T/E/S can be supplied tensioned and sealed at extra cost, to customer's specification. For maximum protection gauge can be pre-cast in briquette before embedment in structure.

GAGE TECHNIQUE LIMITED
P O. BOX 30. TROWBRIDGE.
WILTSHIRE. BA14 8YD ENGLAND
TEL. (0225) 761652/3
FAX. (0225) 766290

Model 4200/4210/4202
Embedment type

Vibrating Wire Strain Gages

- For direct embedment in concrete.
- Rugged design.
- Waterproof.
- Highly sensitive.
- Long-term stability.
- Suitable for long cable lengths.

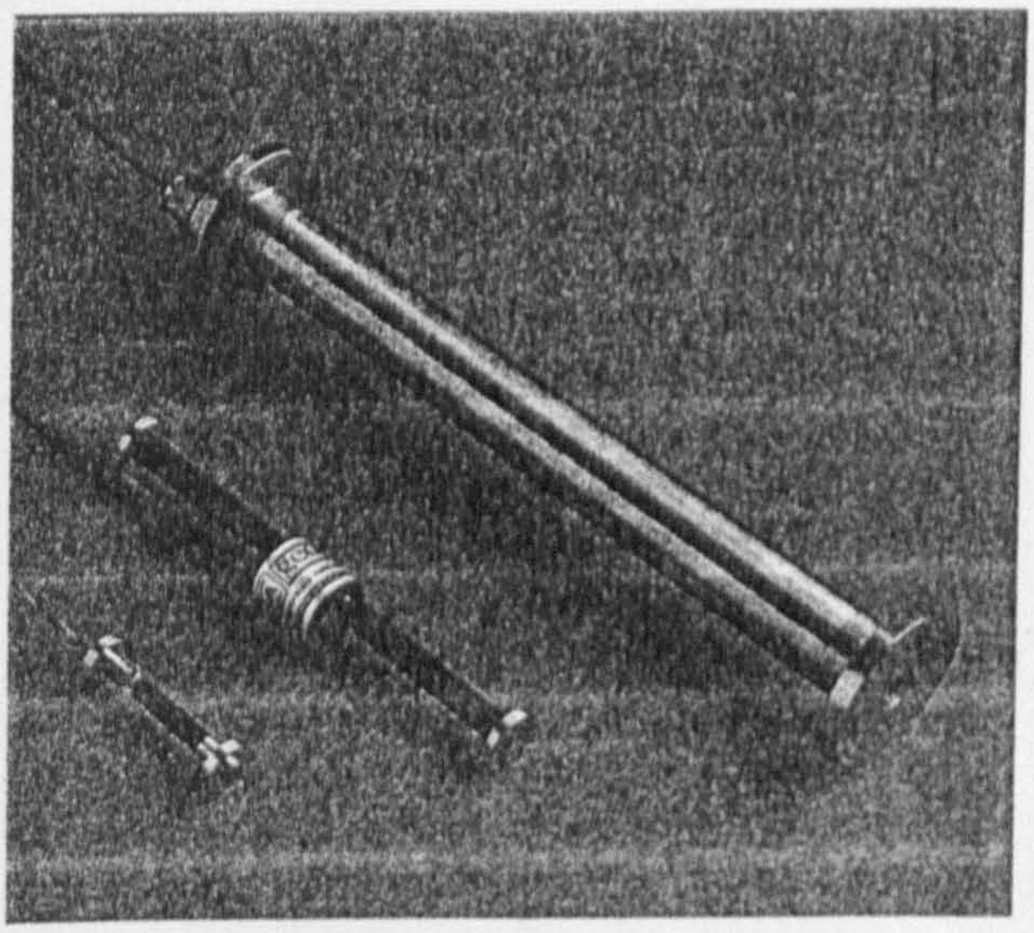

The Models VCE-4200, VCE-4210 and VCE-4202 Vibrating Wire strain Gages are designed for direct embedment in concrete. The VCE-4200 is six inches long and is commonly used for strain measurements in foundations, piles, bridges, dams, containment vessels, tunnel liners etc. The VCE-4210 is 10 inches long and is designed for use in mass concrete with coarse aggregates. It is extra rugged to resist bending, and has large flanges to provide greater engagement area. The VCE-4202 is designed for laboratory use and/or where there are space limitations.

The gages may be positioned either by means of wires wrapped around the body or by attachment to a rosette which will hold the gage at a predetermined orientation in the concrete. (One type of rosette is shown overleaf)

Strains are measured using the vibrating wire principle: A length of steel wire is tensioned between two end blocks that are embedded directly in concrete. Deformations (i.e. strain changes) of the concrete mass, will cause the two end blocks to move relative to one another, thus altering the tension in the steel wire. The tension is measured by plucking the wire and measuring its resonant frequency of vibration using an electromagnetic coil.

The Model GK-403 Readout Box, used in conjunction with the Vibrating Wire Strain Gage, will provide the necessary voltage pulses to pluck the wire and will convert the resulting frequency reading directly into strain units by means of an internal microprocessor. The strain reading is displayed on a 5-digit LCD.

The advantage of the vibrating wire strain gage over more conventional electrical resistance (or semiconductor) types lies mainly in the use of a frequency, rather than a voltage, as the output signal from the strain gage. Frequencies may be transmitted over long cable lengths without appreciable degradation caused by variations in cable resistance, contact resistance, or leakage to ground. Vibrating wire gages also have excellent long-term zero stability. For measurement of dynamic strains (up to 100 Hz) autoresonant versions are available.

Where 'no-stress' strain gages are required, a sheet steel container is available which is lined with styrofoam. This container isolates the section of concrete around the gage from the rest of the concrete so that no stresses can fall on the gage, yet apart from this it experiences the same environmental conditions as adjacent gages, and thus provides a measure of effects due to temperature, moisture, autogenous growth etc.

The strain gages are provided with thermistors encapsulated in the plucking coil. The thermistor enables temperatures to be measured. Over-voltage protection can be provided in the gage and this can be supplemented by gas tube surge arrestors at the terminal box location.

Installation procedures are fully explained in manuals supplied with the gages.

Model VCE-4200

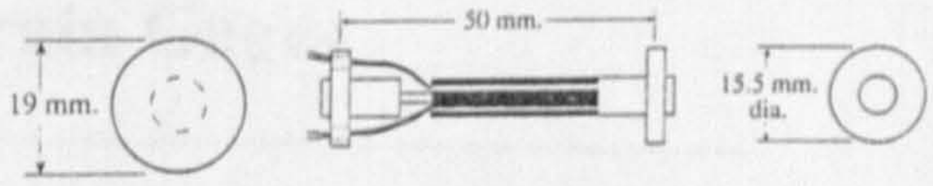

Model VCE-4202

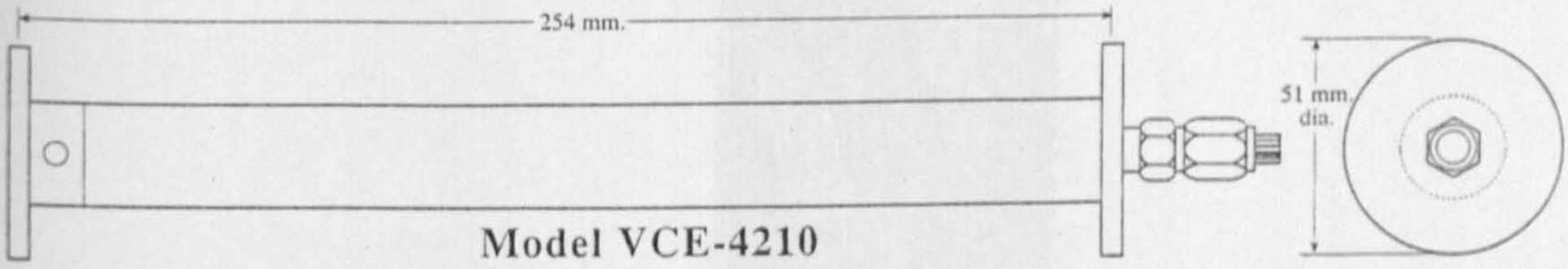

Model VCE-4210

SPECIFICATIONS

Model no.	VCE-4200	VCE-4210	VCE-4202
Method of attachment:	embedment	embedment	embedment
Active gage length: mm. (inches)	153 (6)	250 (10)*	2 (50)
Maximum strain range: microstrain	3000	3000	3000
Sensitivity: microstrain	1.0	0.5	1.0
Temperature range: °C	-20 to +80	-20 to +80	-20 to +80
Thermal coefficient of expansion: ppm/°C	12.0	12.0	12.0
Coil resistance: ohms	150	180	180
Cable types:	4-cond. shielded 22 awg		
Typical frequency datum: Hz	800	2600	2600

*Other lengths available.

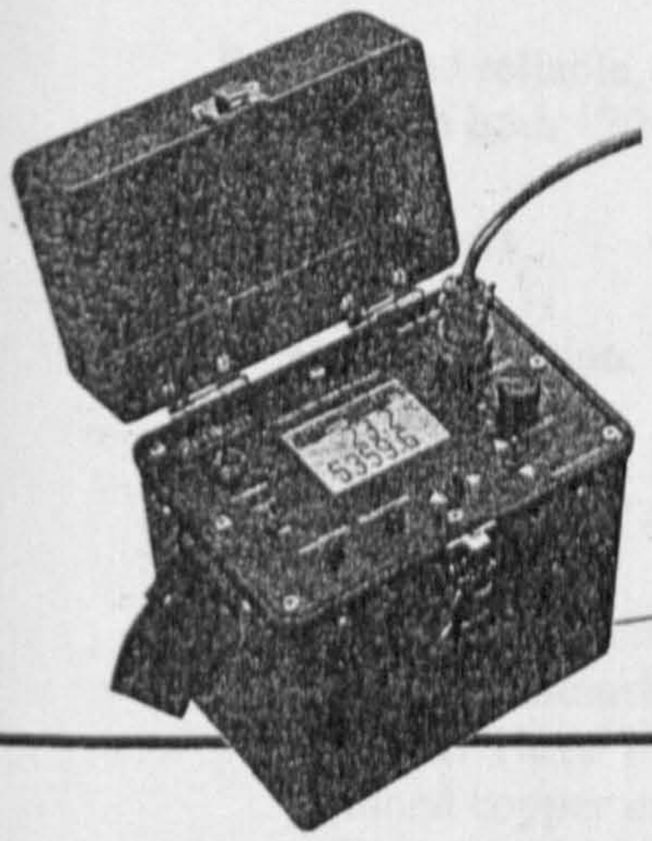

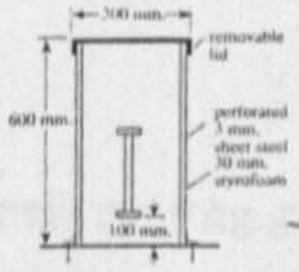

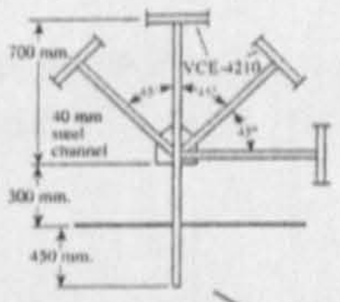

Ordering Information:

Specify:

1. Model number.
2. Cable length.
3. Accessories required.

Accessories:

1. Strain gage rosette.
2. 'No stress-strain' enclosure.
3. Readout Box Model GK-403.
4. Terminal boxes.
5. Thernistor readout box.

geokon incorporated

For further information contact us . . . .

48 SPENCER STREET
LEBANON, NH 03766 USA
TEL: 603/**448-1562**
FAX: 603/448-3216

Embedment Strain Gages

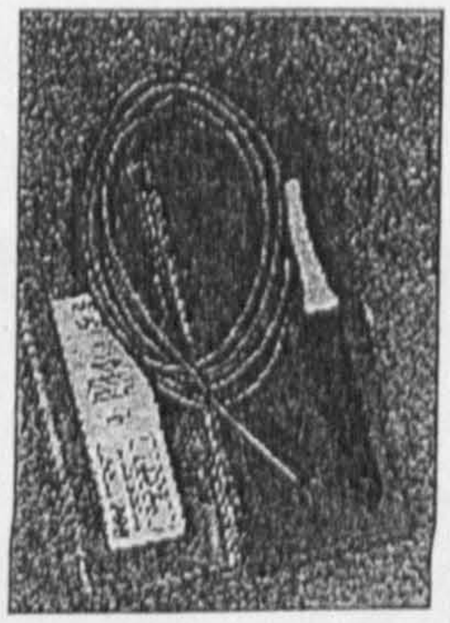

The EGP-Series Embedment Strain Gage is specially designed for measuring mechanical strains inside concrete structures. The sensing grid, constructed of a nickel-chromium alloy (similar to Karma), has an active gage length of 4 in (100 mm) for averaging strains in aggregate materials. A rugged 5-in (130-mm) outer body of proprietary polymer concrete resists mechanical damage during pouring, minimizes reinforcement of the structure, and provides protection from moisture and corrosive attack. The grid, cast within the polymer concrete to ensure maximum strain sensitivity, is self-temperature-compensated to minimize thermal output when installed in concrete structures. Each gage incorporates a heavy-duty 10-ft (3-m) cable with 22-AWG (0.643-mm diameter) leadwires; a three-wire construction to the sensing grid helps minimize temperature effects in the instrumentation leads. Special lengths of preattached cable will be quoted upon request. Micro-Measurements M-LINE accessory cable 322-DJV is available for adding cable length in the field.

Rugged and reliable, Micro-Measurements EGP-Series Strain Gages are available in both 120-ohm (EGP-5-120) and 350-ohm (EGP-5-350) resistances.

Specifications

- **Construction**. Strain sensing grid cast in a sturdy, water-resistant material.
- **Sensing Grid**. Nickel-chromium alloy on polyimide backing. Active gage length of 4 in (100 mm) nominal. Grid resistance of 120 or 350 ohms, ±0.8%.
- **Outer Body**. Proprietary polymer concrete. 5 x 0.7 x 0.4 in (130 x 17 x 10 mm) nominal.
- **Cable**. Three 10-ft (3-m) leads of 22-AWG (0.643-mm dia.) stranded tinned copper in 0.015-in (0.4-mm) thick PVC insulation. Nominal cable diameter of 0.2 in (5 mm). (Other lengths quoted upon request.)
- **Temperature Range**. The normal usage range is +25 to +125 deg F (-5 to +50 deg C). Extended range is -25 to +150 deg F (-30 to +60 deg C).

Appendix B.

Concrete mix designs and further site information

Table B.1 – Northampton: Location of strain gauges and their types

Slab position	Gauge type	Free length z [m]	Gauge position		
			Top	Middle	Bottom
1	TES/10	-	X		X
2	TES/10	-	X		X
3	TES/5.5	1.000	X		X
4	TEAB/5	1.000	X		X
5	4200X	1.000	X		X
6	TEAB/5.5	4.000	X	X	X
7	TEAB/5.5	5.600		X	
8	TEAB/5.5	7.000	X		X
9	TEAB/5.5	8.000	X		X

Table B.2 – Chepstow: Location of strain gauges and their types

Slab position	Gauge type	Free* length z [m]	Gauge position			Slab position	Gauge type	Free length z [m]	Gauge position		
			Top	Middle	Bottom				Top	Middle	Bottom
1	TEAB	3.268		X		14	TES			X	
2	TEAB	4.100		X		15	TES			X	
3	TEAB	4.100		X		16	TES			X	
4	TEAB	3.650		X		17	TES/m			X	
5	TEAB	4.100		X		18	TES			X	
6	TEAB	4.100		X		19	TES			X	
7	TEAB	4.100		X		20	TES			X	
8	TEAB	3.650		X		21	TES			X	
9	TEAB	4.100		X		22	TES/m			X	
10	TEAB	4.100		X		23	TES			X	
11	TEAB	4.100		X		24	TES			X	
12	TEAB	3.650		X		25	TES			X	
13	TES			X		26	TES			X	

* The free lengths are calculated assuming that all of the joints open

Table B.3 – Leeds: Location of strain gauges and their types

Slab position	Gauge type	Free length z [m]	Gauge position			Slab position	Gauge type	Free length z [m]	Gauge position		
			Top	Middle	Bottom				Top	Middle	Bottom
1	TES/m	-	X		X	19	TEAB	5.00		X	
2	TES/m	-	X		X	20	TEAB	1.00	X		X
3	TEAB	1.00	X		X	21	TEAB	1.00		X	
4	TEAB	1.00	X		X	22	TES/m	-	X		X
5	TEAB	5.00	X		X	23	TES/m	-	X		X
6	TEAB	7.00		X		24	TEAB	1.00	X		X
7	TEAB	20.1		X		25	TEAB	1.00		X	
8	TEAB	7.00		X		26	TEAB	5.00		X	
9	TEAB	5.00	X		X	27	TEAB	7.00		X	
10	TEAB	1.00	X		X	28	TEAB	24.12		X	
11	TEAB	1.00	X		X	29	TEAB	7.00		X	
12	TES/m	-	X		X	30	TEAB	5.00		X	
13	TEAB	1.00	X		X	31	TES/m	-	X		X
14	TEAB	1.00		X		32	TES/m	-	X		X
15	TEAB	5.00	X		X	33	TEAB	1.00		X	
16	TEAB	7.00		X		34	TEAB	1.00	X		X
17	TEAB	20.1	X		X	35	TEAB	5.00	X		X
18	TEAB	7.00		X		36	TEAB	7.00		X	

Table B.4 – Bedford: Location of strain gauges and their types

Slab position	Gauge type	Free length z [m]	Gauge position			Slab position	Gauge type	Free length z [m]	Gauge position		
			Top	Middle	Bottom				Top	Middle	Bottom
1	TEAB	14.97		X		8	TES	-		X	
2	TEAB	10.10*		X		9	TES/m	-		X	
3	TEAB	14.97		X		10	TES/m	-		X	
4	TEAB	19.45*		X		11	TES	-		X	
5	TEAB	7.485		X		12	TES	-		X	
6	TES/m	-		X		13	TES/m	-		X	
7	TES	-		X							

* As the slab was tied to the walls and the dock levellers at the slab edge this is not really a free length, rather the distance from the edge of the pour.

Table B.5 – Daventry: Location of strain gauges and their types

Slab position	Gauge type	Free* length z [m]	Gauge position			Slab position	Gauge type	Free length z [m]	Gauge position		
			Top	Middle	Bottom				Top	Middle	Bottom
1	TEAB	3.820		X		31	TEAB	3.150		X	
2	TEAB	2.373		X		32	TEAB	3.750		X	
3	TEAB	2.373		X		33	TEAB	3.750		X	
4	TEAB	2.373		X		34	TEAB	3.750		X	
5	TEAB	2.373		X		35	TEAB	3.750		X	
6	TEAB	1.669		X		36	TES			X	
7	TEAB	3.338		X		37	TES			X	
8	TEAB	1.669		X		38	TES			X	
9	TEAB	2.570		X		39	TES			X	
10	TEAB	3.350		X		40	TES			X	
11	TEAB	2.567		X		41	TES			X	
12	TEAB	2.570		X		42	TES			X	
13	TEAB	2.580		X		43	TES			X	
14	TEAB	2.580		X		44	TES			X	
15	TEAB	3.750		X		45	TES			X	
16	TEAB	3.820		X		46	TES			X	
17	TEAB	2.373		X		47	TES			X	
18	TEAB	2.373		X		48	TES			X	
19	TEAB	2.373		X		49	TES			X	
20	TEAB	2.373		X		50	TES			X	
21	TEAB	1.669		X		51	TES			X	
22	TEAB	3.338		X		52	TES			X	
23	TEAB	1.669		X		53	TES			X	
24	TEAB	2.570		X		54	TES			X	
25	TEAB	3.350		X		55	TES			X	
26	TEAB	2.567		X		56	TES			X	
27	TEAB	2.570		X		57	TES			X	
28	TEAB	2.580		X		58	TES			X	
29	TEAB	2.580		X		59	TES			X	
30	TEAB	3.750		X		60	TES			X	

* The free lengths are calculated assuming all joints open

Table B.6 – Marston: Location of strain gauges and their types

Slab position	Gauge type	Free length z [m]	Gauge position			Slab position	Gauge type	Free length z [m]	Gauge position		
			Top	Middle	Bottom				Top	Middle	Bottom
1	TES/m	-	X		X	19	TEAB	5.00		X	
2	TES/m	-	X		X	20	TEAB	1.00	X		X
3	TEAB	1.00	X		X	21	TEAB	1.00		X	
4	TEAB	1.00	X		X	22	TES/m	-	X		X
5	TEAB	5.00	X		X	23	TES/m	-	X		X
6	TEAB	7.00		X		24	TEAB	1.00	X		X
7	TEAB	20.1		X		25	TEAB	1.00		X	
8	TEAB	7.00		X		26	TEAB	5.00		X	
9	TEAB	5.00	X		X	27	TEAB	7.00		X	
10	TEAB	1.00	X		X	28	TEAB	24.12		X	
11	TEAB	1.00	X		X	29	TEAB	7.00		X	
12	TES/m	-	X		X	30	TEAB	5.00		X	
13	TEAB	1.00	X		X	31	TES/m	-	X		X
14	TEAB	1.00		X		32	TES/m	-	X		X
15	TEAB	5.00	X		X	33	TEAB	1.00		X	
16	TEAB	7.00		X		34	TEAB	1.00	X		X
17	TEAB	20.1	X		X	35	TEAB	5.00	X		X
18	TEAB	7.00		X		36	TEAB	7.00		X	

Table B.7 - Leeds: Concrete mix design

MIX DESCRIPTION	MIN CC	MAX W/C	AGG	CEMENT TYPE	BLEND	CEMENT	SSD BATCH WEIGHTS (KG/M3) AGGREGATES			FREE W/C
							2A	3B	3A	
A C40 28D DAYS	330	.55	20-5MM	PC	100MM	PC				
						360	1137	295	446	.54
B C40 28D DAYS	330	.55	20-5MM	PC	75MM	PC	2A	3B	3A	
PUMP MIX						360	1022	327	493	.54
C C40 28D DAYS	330	.55	10MM	PC	75MM	PC	2C	3B	3A	
10MM						390	1012	311	468	.55
D C30 28D DAYS	330	.55	10MM	PC	75MM	PC	2C	3B	3A	
10MM						390	1012	311	468	.55

MATERIAL SUPPLIERS

CEMENT & REPLACEMENTS		AGGREGATES							
CODE	SUPPLIER	WORKS	CODE	SIZE	TYPE	SUPPLIER	QUARRY	CODE	TYPE
PC			2A	20-5MM	LIMESTNE				
			2C	10MM	LIMESTNE				
			3B	FINES					
			3A	SAND					

THESE MIXES ARE DESIGNED TO COMPLY WITH THE REQUIREMENTS OF B.S.5328 (UNLESS OTHERWISE AGREED WITH THE CUSTOMER), CONDITIONS OF SALE. WE TRUST THE ABOVE INFORMATION MEETS WITH YOUR APPROVAL.

Table B.8 - Northampton: Concrete mix design

MATERIAL		*TYPE & SIZE*	
Cement	*1*	PC42.5N	BS 12
	2	GGBS	BS 6699
Coarse Aggregate	*3*	20-5mm	BS 882 T3
	4		
Sand	*5*	Grade M	BS 882 T4
	6		
Admixture 1	*7*		
Admixture 2	*8*		
MIX SPECIFICATION	*ref.*	BS 5328 Design	BS 5328 Design
Grade		C40	C40
Cement Type/Blend		PC	PB
Max. Agg. Size mm		20	20
Min. Cement Content kg/m³		350	350
Max. Free W/C Ratio		0 48	0.48
Target Slump mm		75	75
Air Content % (± 2%)		N/A	N/A
MIX DESIGN (kg/m³ ssd)	*1*	370	230
	2		155
	3	1067	1058
	4		
	5	783	748
	6		
(litres/m³)	*7*		
(litres/m³)	*8*		
Design free W/C Ratio		0.47	0 47

Table B.9 - Daventry: Concrete mix design

Please find below the proposed ...

We trust these to be satisfactory; however, should you have any queries, please contact us

MIX DESCRIPTION :	C40							
COMMENTS :	PUMP MIX							
AGG. SIZE :	20							
CEMENT TYPE :	P/FA-A							
SLUMP (mm) :	125							
MIN CEMT. CONT. :	325							
MAX. W/C RATIO :	0.55							
SULFATE CLASS :	-							

DESIGN SATURATED SURFACE DRY MASSES FOR ONE CUBIC METRE (UNITS kg)

CEMENT KGS. :	370							
% BLEND :	10							
AGG. ONE :	1032							
AGG. TWO :	780							
AGG. THREE :	-							
AGG. FOUR :	-							
W/C RATIO :	0.54							
ADD MIX. ONE :	1.11							
ADD MIX.TWO :	-							

MATERIAL	SUPPLIER & SOURCE	MATERIAL	SUPPLIER & SOURC
PC Class 42 SN		BLEND - P F A	
Agg 1-20>5mm Granite		Add Mix 1 - Super plas	
Agg 2 - W C S			

Table B.10 - Marston: Concrete mix design

MIX DETAILS

MIX DESIGNATION	READYMIX EASYFINISH C40
MINIMUM STRENGTH	40 N/mm2 at 28 days
MINIMUM SPECIFIED CEMENT CONTENT	325 kg/m3
MAXIMUM SPECIFIED FREE W/C RATIO	0.55
AGGREGATE SIZE	20mm
WORKABILITY	125mm

MATERIALS

CEMENT	BS 12 : 1996 PC Class 42.5 N
CEMENT REPLACEMENT	BS 6699:1992 GGBS
COARSE AGGREGATE	BS 882 : 1992
FINE AGGREGATE	BS 882 : 1992
ADMIXTURE	Readymix EasyFinish incorporates an advanced high efficiency finishing admixtu complying with BS 5075

ADDITIONAL INFORMATION

Quality Assurance	Readymix EasyFinish is a quality assured product designed in accordance with BS 5328.
ASR Control	Alkali level less than 3.5 Kg/m3.
Chloride Control	Chloride level less than 0.4%
Drying Shrinkage	Less than 0.04%

Variation in the above material sources are advised where required in accordance with BS 5328

Signed

Area Technical Manager

Registered
Registered
Coldharbo
Surrey TW2

Table B.11 - Chepstow: Concrete mix design

MATERIALS	DESCRIPTION	SUPPLIER	SOURCE
CEMENT	PC 42.5N		
REPLACEMENT	PFA		
LIMESTONE	20mm AGGREGATE		
LIMESTONE	10mm AGGREGATE		
DREDGED SAND	SAND BS 882 'M'		
DARACEM 55	WRA		

SPECIFICATION		
Mix No	1	2
MIX/GRADE	C40Nmm²	C40Nmm²
MAX AGG SIZE	20mm	20mm
CEMENT TYPE	P/FA32.5N	P/FA32.5N
TARGET SLUMP	100mm	100mm
MIN CEMENT	335	335
MAX CEMENT		
MAX W/C	0.55	0.55
MAX A/C		

SSD MIX DESIGN Kg/CUBIC METRE		
CEMENT	260	235
REPLACEMENT	115	100
COARSE AGG(1)	657	648
COARSE AGG(2)	439	432
FINE AGG(1)	805	883
FINE AGG(2)		
FINE AGG %	42.3	44.9
FREE WATER	171	156
W/C RATIO	0.46	0.46
A/C RATIO	5.06	5.85
ADMIXTURE(1)		WRA
DOSE RATE(1)		400mL/100Kgs
ADMIXTURE(2)		
DOSE RATE(2)		

Table B.12 - Bedford: Concrete mix design

MIX DESCRIPTION :	C40							
AGG. SIZE :	PUMP MIX							
CEMENT TYPE :	P/B							
SLUMP (mm) :	100							
MIN CEMT. CONT. :	325							
MAX. W/C RATIO :	0.55							
SULFATE CLASS :	-							

DESIGN SATURATED SURFACE DRY MASSES FOR ONE CUBIC METRE (UNITS kg)

CEMENT KGS. :	370							
% BLEND :	30							
AGG. ONE :	736							
AGG. TWO :	316							
AGG. THREE :	741							
AGG. FOUR :	-							
W/C RATIO :	0.53							
ADD MIX. ONE :	-							
ADD MIX.TWO :	-							

MATERIAL	SUPPLIER & SOURCE	MATERIAL	SUPPLIER & SOURC
PC Class 42 5N		BLEND - GGBS	
Agg 1-20mm Gravel			
Agg 2-10mm Gravel			
Agg 3 - W C S			

Table B.13 - Bedford cube test results

	7 day	28 day	56 day	
24/06/99	28.5	43.5	cubes tested at 4, 7 & 28 day	
	24	36	so none left to do 56 day	
	25.5	37	compliance testing	
	30	36.5		
		36.5		
		38		
		44		
		39		
			28 day mean strength	38.8125
			Standard deviation	3.195281
28/06/99	28.5	43.5	41.5	
	26	39.5		
	27.5	35.5	42	
	25.5	37.5		
		43		
		44.5		
		30	45	
		42.5		
			28 day mean strength	39.5
			Standard deviation	4.964157
29/06/99	34	52.5		
	30.5	50		
	37	44.5		
	34.5	47		
		49.5		
		47		
		52		
		53		
			28 day mean strength	49.4375
			Standard deviation	3.05237

Table B.14 - Marston cube test results

	28 day		
22/09/99	48.5		
	57.5		
	46.5		
	49.5		
		28 day mean strength	50.5
		standard deviation	4.830459
23/09/99	53		
	52.5		
	49.5		
	44.5		
		28 day mean strength	49.875
		standard deviation	3.902456
27/09/99	57		
	60.5		
	55.5		
	57		
		28 day mean strength	57.5
		standard deviation	2.12132

Table B.15 - Northampton cube test results

	7 day	28 day
23/03/98	30.5	44.5
	34.0	46.0
		29.5
		44.0
	28 day mean strength	41.0
	standard deviation	7.7

Table B.16 - Chepstow cube test results

	28 day		
21/07/99	47.5		
	53.5		
	49.0		
		28 day mean strength	50.0
		standard deviation	3.1
22/07/99	41.0		
	49.5		
	45.5		
		28 day mean strength	45.3
		standard deviation	4.3
26/07/99	40.0		
	40.0		
	39.5		
		28 day mean strength	39.8
		standard deviation	0.3

Table B.17 - Daventry cube strength results

	7 day	28 day		
26/03/99	50.0	58.5		
	48.5	57.5		
	45.0	55.0		
	50.5	56.5		
	46.5	53.0		
		50.5		
		58.0		
		57.5		
		56.5		
		55.0		
			mean 28 day strength	55.8
			standard deviation	2.5
31/03/99	43.5	53.5		
	42.0	50.5		
	43.5	56.5		
	35.0	49.5		
	41.0	54.0		
			mean 28 day strength	53.6
			standard deviation	2.7

Met Office station details

British Atmospheric Data Centre

Name: BEDFORD SAWS Locate on map
Geographic area: BEDFORDSHIRE
Latitude (decimal degrees): 52.225 (Original Met Office value = 52.217)
Longitude (decimal degrees): -0.464 (Original Met Office value = -0.467)
Grid ref: TL 049597 (504.9km East, 259.7Km North of National grid origin)
Grid ref type: Ordnance Survey
Postcode: MK44 2
Elevation: 85 meters
Time zone: 0
Drainage stream: OUSE
Hydrological area ID: 330
Station start date: 01-01-1956
Station end date: Current
BADC data directory /badc/ukmo-surface/data/united_kingdom/bedfordshire/bedford_saws

Measurements made:

Station code	Message type *(i)*	Message start date	Message end date	Data held at BADC (years)
DCNN 3440	ESAWRADT	01-06-1993	Current	1993-2000
DCNN 3440	DRADR35	01-01-1993	Current	-
DCNN 3440	ESAWSOIL	01-09-1993	Current	1995-2000
DCNN 3440	NCM	01-01-1987	Current	1991-2000
ICAO EGSV	METAR	01-11-1996	Current	-
RAIN 174063	NCM	01-01-1992	Current	1991-2000
RAIN 174063	SREW	01-01-1992	Current	1994-2000
WIND 344001	HWND6910	01-02-1992	Current	1992-1998
WIND 344001	ESAWWIND	01-09-1993	Current	1997-2000
WMO 03560	SREW	01-01-1994	Current	1994-2000
WMO 03560	NCM	01-01-1987	Current	1991-2000
WMO 03560	ESAWWIND	01-09-1993	Current	1997-2000
WMO 03560	SYNOP	01-01-1987	Current	1987-2000
WMO 03560	ESAWSOIL	01-09-1993	Current	1995-2000
WMO 03560	ESAWRADT	01-01-1995	Current	1993-2000

Please report any problems with this page to:

Met Office station details

British Atmospheric Data Centre

Name:	CHURCH LAWFORD SAWS Locate on map
Geographic area:	WARWICKSHIRE
Latitude (decimal degrees):	52.358 (Original Met Office value = 52.367)
Longitude (decimal degrees):	-1.330 (Original Met Office value = -1.333)
Grid ref:	SP 456736 (445.6km East, 273.6Km North of National grid origin)
Grid ref type:	Ordnance Survey
Postcode:	CV23 9
Elevation:	107 meters
Time zone:	0
Drainage stream:	AVON
Hydrological area ID:	542
Station start date:	01-01-1983
Station end date:	Current
BADC data directory	/badc/ukmo-surface/data/united_kingdom/warwickshire/church_lawf

Measurements made:

Station code	Message type *(i)*	Message start date	Message end date	Data held at BADC (years)
DCNN 4448	ESAWRADT	01-09-1993	Current	1995-2000
DCNN 4448	DRADR35	01-01-1993	Current	1995-1996
DCNN 4448	ESAWSOIL	01-09-1993	Current	1995-2000
DCNN 4448	NCM	01-01-1983	Current	1991-2000
RAIN 448621	NCM	01-01-1992	Current	1991-2000
RAIN 448621	CLMSPN	01-01-1961	01-12-1990	-
RAIN 448621	SREW	01-01-1992	Current	1994-2000
WIND 444801	HWND6910	01-03-1992	Current	1992-1998
WIND 444801	ESAWWIND	01-09-1993	Current	1997-2000
WMO 03544	SREW	01-01-1994	Current	1994-2000
WMO 03544	NCM	01-01-1983	Current	1991-2000
WMO 03544	ESAWWIND	01-09-1993	Current	1997-2000
WMO 03544	SYNOP	01-01-1983	Current	1983-2000
WMO 03544	ESAWSOIL	01-09-1993	Current	1995-2000
WMO 03544	ESAWRADT	01-09-1993	Current	1995-2000

Met Office station details

British Atmospheric Data Centre

Name:	LEEDS W C Locate on map
Geographic area:	WEST YORKSHIRE
Latitude (decimal degrees):	53.800 (Original Met Office value = 53.800)
Longitude (decimal degrees):	-1.559 (Original Met Office value = -1.567)
Grid ref:	SE 290339 (429km East, 433.9Km North of National grid origin)
Grid ref type:	Ordnance Survey
Postcode:	LS3 1
Elevation:	64 meters
Time zone:	0
Drainage stream:	AIRE
Hydrological area ID:	272
Station start date:	01-01-1984
Station end date:	Current
BADC data directory	/badc/ukmo-surface/data/united_kingdom/west_yorkshire/leeds_w_c

Measurements made:

Station code	Message type *(i)*	Message start date	Message end date	Data held at BADC (years)
DCNN 4055	NCM	01-11-1985	Current	1985-2000
DCNN 4055	MODLERAD	01-01-1997	Current	1996-2000
DCNN 4055	DRADR35	01-01-1997	Current	-
ICAO EGRY	METAR	Current	Current	-
RAIN 076074	NCM	01-11-1985	Current	1985-2000
RAIN 076073	WADRAIN	01-01-1992	Current	1992-1998
RAIN 076073	CLMSPN	01-01-1961	01-12-1990	-
RAIN 076074	SREW	01-01-1994	Current	1994-2000
WIND 405501	HWND6910	01-01-1987	Current	1987-1998
WIND 405501	ESAWWIND	01-06-1993	Current	1997-2000
WMO 03347	SYNOP	01-01-1984	Current	1985-2000
WMO 03347	SREW	01-01-1994	Current	1994-2000
WMO 03347	NCM	01-11-1985	Current	1985-2000
WMO 03347	ESAWWIND	01-06-1993	Current	1997-2000

Please report any problems with this page to:
BADC support

Met Office station details

British Atmospheric Data Centre

Name:	PENHOW Locate on map
Geographic area:	GWENT
Latitude (decimal degrees):	51.610 (Original Met Office value = 51.617)
Longitude (decimal degrees):	-2.847 (Original Met Office value = -2.850)
Grid ref:	ST 413906 (341.3km East, 190.6Km North of National grid origin)
Grid ref type:	Ordnance Survey
Postcode:	NP6 3
Elevation:	100 meters
Time zone:	0
Drainage stream:	COASTAL
Hydrological area ID:	560
Station start date:	01-01-1992
Station end date:	Current
BADC data directory	/badc/ukmo-surface/data/united_kingdom/gwent/penhow

Measurements made:

Station code	Message type *(l)*	Message start date	Message end date	Data held at BADC (years)
DCNN 8562	DLY3208	01-01-1992	Current	1992-2000
RAIN 481255	DLY3208	01-01-1992	Current	1992-2000
RAIN 481255	CLMSPN	01-01-1961	01-12-1990	-

Please report any problems with this page to:
BADC support

Met Office station details

British Atmospheric Data Centre

Name:	MOULTON PARK Locate on map
Geographic area:	NORTHAMPTONSHIRE
Latitude (decimal degrees):	52.272 (Original Met Office value = 52.267)
Longitude (decimal degrees):	-0.878 (Original Met Office value = -0.883)
Grid ref:	SP 765644 (476.5km East, 264.4Km North of National grid origin)
Grid ref type:	Ordnance Survey
Postcode:	NN2 7
Elevation:	127 meters
Time zone:	0
Drainage stream:	BRAMPTON
Hydrological area ID:	320
Station start date:	01-01-1976
Station end date:	Current
BADC data directory	/badc/ukmo-surface/data/united_kingdom/northamptonshire/moulton

Measurements made:

Station code	Message type *(i)*	Message start date	Message end date	Data held at BADC (years)
DCNN 4364	CLMSN	01-01-1961	01-12-1990	-
DCNN 4364	DLY3208	01-06-1976	Current	1976-2000
RAIN 160109	CLMSPN	01-01-1961	01-12-1990	-
RAIN 160109	DLY3208	01-01-1977	Current	1976-2000

Please report any problems with this page to:
BADC support

Met Office station details

British Atmospheric Data Centre

Name:	WOBURN Locate on map
Geographic area:	BEDFORDSHIRE
Latitude (decimal degrees):	52.013 (Original Met Office value = 52.017)
Longitude (decimal degrees):	-0.595 (Original Met Office value = -0.583)
Grid ref:	SP 964360 (496.4km East, 236Km North of National grid origin)
Grid ref type:	Ordnance Survey
Postcode:	MK43 0
Elevation:	89 meters
Time zone:	0
Drainage stream:	OUZEL
Hydrological area ID:	330
Station start date:	01-01-1882
Station end date:	Current
BADC data directory	/badc/ukmo-surface/data/united_kingdom/bedfordshire/woburn

Measurements made:

Station code	Message type *(i)*	Message start date	Message end date	Data held at BADC (years)
DCNN 3414	HSUN3445	01-01-1980	Current	1981-1992, 1994-1999
DCNN 3414	CLMSN	01-01-1961	01-12-1990	-
DCNN 3414	DLY3208	01-01-1959	Current	1956-1999
RAIN 172601	DLY3208	01-01-1899	Current	1899-1929, 1931-1932, 1934-1999
RAIN 172601	CLMSPN	01-01-1961	01-12-1990	-

Please report any problems with this page to:
BADC support

Appendix C.

Bedford detail survey results

Bedford **Crack survey results**

Date: 18/4/99 Readings taken by: J. Bishop

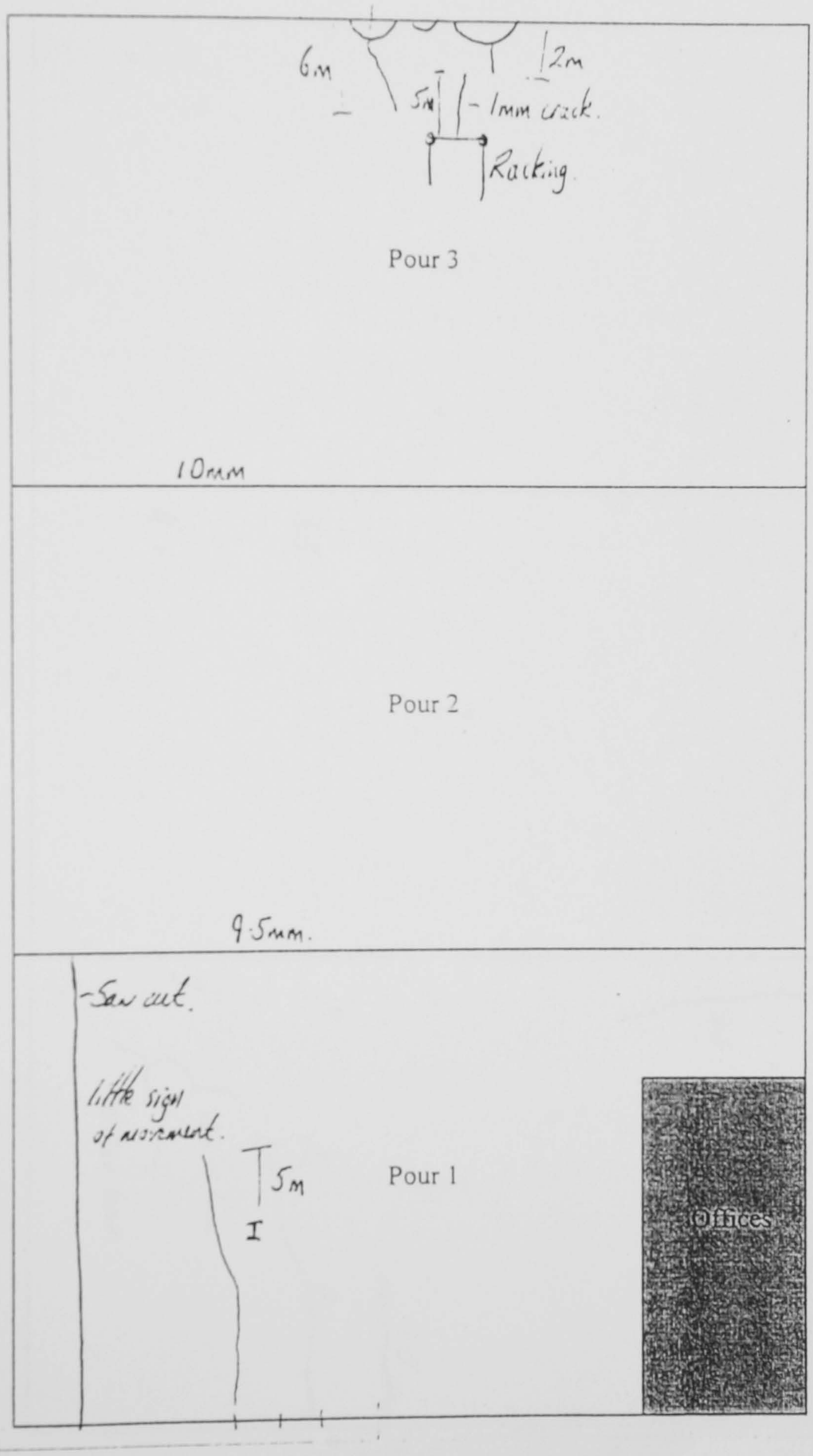

Notes: Some cracking generally originating near doors and at corners surrounding clerk (wells or manholes.

All cracks to be repaired

Bedford **Crack survey results**

Date: 26/2/00 Readings taken by: T. Sandhu

Pour 3

4 3.5

Pour 2

3 0.5

Pour 1

Alc + lamn. Manhole cover.

1 1

2 0.5

Offices

Notes: Cracks in pour 3 seen before now repaired.
Cracks in pour 1 repaired but since cracked further. (Repaired sections not opened again though)

Bedford **Crack survey results**

Date: 21/7/2000 Readings taken by: J. Bishop

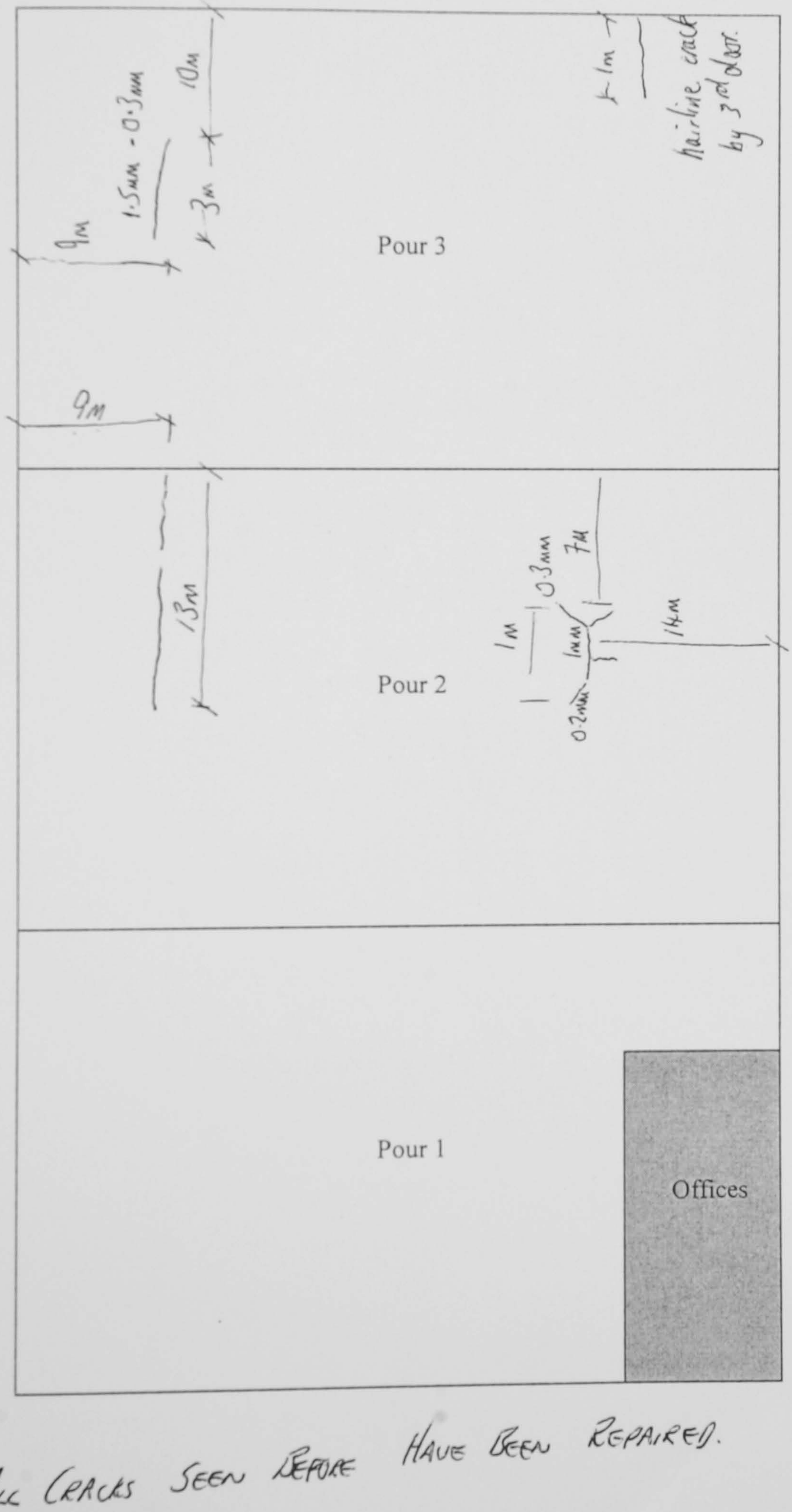

Notes: ALL CRACKS SEEN BEFORE HAVE BEEN REPAIRED.

NOT TO SCALE.